REACTOR

CHAPTER 4

TABLE OF CONTENTS

Section	Title	Page
4.0	REACTOR	4.1-1
4.1	SUMMARY DESCRIPTION	4.1-1
4.2	FUEL SYSTEM DESIGN	4.2-1
4.2.1	DESIGN BASES	4.2-1
4.2.2	MECHANICAL DESIGN DESCRIPTION	4.2-33
4.2.3	DESIGN EVALUATION	4.2-46
4.2.4	TESTING AND INSPECTION PLAN	4.2-72
4.2.5	ON-LINE FUEL SYSTEM MONITORING	4.2-73
	REFERENCES	4.2-75
4.3	NUCLEAR DESIGN	4.3-1
4.3.1	DESIGN BASES	4.3-1
4.3.2	DESCRIPTION	4.3-3
4.3.3	ANALYTICAL METHODS	4.3-21
4.3.4	CHANGES	4.3-35
	REFERENCES	4.3-36
4.4	THERMAL AND HYDRAULIC DESIGN	4.4-1
4.4.1	DESIGN BASES	4.4-1
4.4.2	DESCRIPTION OF THERMAL AND HYDRAULIC DESIGN OF THE REACTOR CORE	4.4-4
4.4.3	DESCRIPTION OF THE THERMAL AND HYDRAULIC DESIGN OF THE REACTOR COOLANT SYSTEM (RCS)	4.4-15
4.4.4	EVALUATION	4.4-17
4.4.5	TESTING AND VERIFICATION	4.4-34
4.4.6	INSTRUMENTATION REQUIREMENTS	4.4-34
4.4.7	THERMAL AND HYDRAULIC DESIGN EVALUATIONS FOR CE-16 AREVA FUEL	4.4-36
	REFERENCES	4.4-39

Section	Title	Page
4.5	REACTOR MATERIALS	4.5-1
4.5.1	CONTROL ELEMENT DRIVE STRUCTURAL MATERIALS	4.5-1
4.5.2	REACTOR INTERNALS MATERIALS	4.5-5
	REFERENCES	4.5-12
4.6	FUNCTIONAL DESIGN OF REACTIVITY CONTROL SYSTEMS	4.6-1
4.6.1	INFORMATION FOR CEA CONTROL SYSTEMS	4.6-1
4.6.2	EVALUATIONS	4.6-1
4.6.3	TESTING AND VERIFICATION	4.6-1
4.6.4	INFORMATION FOR COMBINED PERFORMANCE OF REACTIVITY SYSTEMS	4.6-2
4.6.5	EVALUATIONS OF COMBINED PERFORMANCE	4.6-2
	REFERENCES	4.6-3

REACTOR

CHAPTER 4

LIST OF TABLES

Table	Title	Page
4.2-1	MECHANICAL DESIGN PARAMETERS	T4.2-1
4.2-2	ABSORBER MATERIALS - THERMAL AND PHYSICAL PARAMETERS	T4.2-5
4.2-3	TENSILE TEST RESULTS ON IRRADIATED SAXTON CORE III CLADDING	T4.2-6
4.2-4	POOLSIDE FUEL INSPECTION PROGRAM SUMMARY	T4.2-7
4.2-5	COMPARISON OF POISON MATERIAL CONTENT FOR FULL-LENGTH CEAs (5 ELEMENT)	T4.2-8
4.2-6	ST. LUCIE 2 CYCLE 2 CLADDING COLLAPSE PREDICTIONS	T4.2-9
4.2-7	ST. LUCIE UNIT 2 TYPICAL VALUES OF REACTIVITY WORTHS AND ALLOWANCES FOR THE HOT ZERO POWER (HZP) END-OF-CYCLE (EOC) STEAM LINE BREAK (SLB) ACCIDENT, %Δρ	T4.2-10
4.2-8	ST. LUCIE UNIT 2 TYPICAL REACTIVITY WORTH OF CEA REGULATING GROUPS AT FULL POWER, %Δρ	T4.2-11
4.2-9	DELETED	T4.2-12
4.2-10	MECHANICAL DESIGN PARAMETERS - CURRENT CYCLE	T4.2-13
4.3-1	NUCLEAR DESIGN CHARACTERISTICS	T4.3-1
4.3-2	EFFECTIVE MULTIPLICATION FACTORS AND REACTIVITY DATA	T4.3-3
4.3-3	COMPARISON OF CORE REACTIVITY COEFFICIENTS WITH THOSE USED IN SELECTED SAFETY ANALYSES	T4.3-4
4.3-4	REACTIVITY COEFFICIENTS	T4.3-5
4.3-5	WORTHS OF SEQUENTIALLY WITHDRAWN CEA GROUPS	T4.3-6
4.3-6	REACTIVITY DEFECTS BETWEEN HOT FULL POWER (HFP) AND HOT ZERO POWER (HZP) AT EOC-4	T4.3-7
4.3-7	COMPARISON OF CALCULATED CEA WORTHS AND REQUIREMENTS (%Δρ) OF EOC4 FOR STEAM LINE BREAK (SLB) ANALYSES	T4.3-8
4.3-7(a)	COMPARISON OF CALCULATED CEA WORTHS AND REQUIREMENTS (%Δρ) FOR CEA EJECTION ANALYSES	T4.3-9
4.3-8	COMPARISON OF RADIAL PEAKING FACTORS FOR VARIOUS RODDED CONFIGURATIONS AT BOC AND EOC	T4.3-10

Table	Title	Page
4.3-9	CALCULATED VARIATION OF THE AXIAL STABILITY INDEX DURING THE FIRST CYCLE (hr^{-1})	T4.3-11
4.3-10	MAXIMUM FAST FLUENCE GREATER THAN 1 MeV (n/cm^2)	T4.3-12
4.3-11	CONTROL ELEMENT ASSEMBLY SHADOWING FACTORS	T4.3-13
4.3-12	FUEL ROD DESCRIPTION	T4.3-14
4.3-13	RESULT OF ANALYSIS OF CRITICAL UO_2 SYSTEMS	T4.3-15
4.3-14	RESULTS OF ANALYSIS OF PuO_2-UO_2 FUELED LATTICES	T4.3-16
4.3-15	REACTION RATES	T4.3-17
4.3-16	BEGINNING OF CYCLE, ZERO POWER UNRODDED CHARACTERISTICS	T4.3-18
4.3-17	COMPARISON OF MEASURED AND CALCULATED CONTROL ROD WORTH BOC, HOT ZERO POWER	T4.3-19
4.3-18	COMPARISONS OF CALCULATED AND MEASURED CEA WORTHS	T4.3-20
4.3-19	AT-POWER ISOTHERMAL TEMPERATURE COEFFICIENTS	T4.3-21
4.3-19a	COMPARISONS OF MEASURED AND CALCULATED PSEUDO-POWER COEFFICIENTS AT VARIOUS EXPOSURES	T4.3-22
4.3-20	DELETED	T4.3-23
4.3-21	AXIAL XENON OSCILLATIONS	T4.3-24
4.3-22	DENSIFICATION CHARACTERISTICS	T4.3-25
4.3-23	RADIAL PIN POWER CENSUS	T4.3-26
4.3-24	DELETED	T4.3-27
4.3-25	DELETED	T4.3-28
4.3-26	ST. LUCIE UNIT 2 CYCLE 2 FULL LENGTH CEA DROP DATA (HFP, EQUILIBRIUM XENON)	T4.3-29
4.4-1	THERMAL AND HYDRAULIC PARAMETERS	T4.4-1
4.4-2	COMPARISON OF THE DEPARTURE FROM NUCLEATE BOILING RATIOS COMPUTED WITH DIFFERENT CORRELATIONS	T4.4-4
4.4-3	REACTOR COOLANT FLOWS IN BYPASS CHANNELS	T4.4-5
4.4-4	REACTOR VESSEL BEST ESTIMATE PRESSURE LOSSES AND COOLANT TEMPERATURES	T4.4-6

Table	Title	Page
4.4-5	DESIGN STEADY STATE HYDRAULIC LOADS ON VESSEL INTERNALS AND FUEL ASSEMBLIES	T4.4-7
4.4-6	RCS VALVES AND PIPE FITTINGS PRESSURE BOUNDARY VALVES	T4.4-8
4.4-7	RCS FLOWRATES	T4.4-11
4.4-8	REACTOR COOLANT SYSTEM GEOMETRY	T4.4-12
4.4-9	SAFETY INJECTION LINE LENGTHS AND SIZES	T4.4-14
4.4-10	REACTOR COOLANT SYSTEM COMPONENT THERMAL AND HYDRAULIC DATA	T4.4-17
4.4-11	ST. LUCIE UNIT 2 THERMAL HYDRAULIC PARAMETERS AT FULL POWER	T4.4-20
4.6-1	POSTULATED EVENTS REQUIRING OPERATION OF TWO OR MORE REACTIVITY CONTROL SYSTEMS	T4.6-1

REACTOR

CHAPTER 4

LIST OF FIGURES

Figure	Title	
4.1-1	Reactor Vertical Arrangement	
4.1-2	Reactor Core Cross Section	
4.2-1	Circumferential Strain vs Temperature	
4.2-2	Design Curve for Cyclic Strain Usage of Zircaloy - 4 at 700°F	
4.2-3	Control Element Assembly (5-element)	
4.2-4	Control Element Assembly (4-element)	
4.2-5	Intentionally Deleted	
4.2-6	Fuel Assembly	
4.2-6a	AREVA CE-16 HTP™ Fuel Assembly	EC287528
4.2-7	Fuel Spacer Grid	
4.2-8	Guardian Grid and Debris Resistant Fuel Rod Design	
4.2-8a	Guardian Grid Fuel Rod Design	
4.2-8b	Comparison of Urania Rod Assembly Features	
4.2-9	Guardian Grid and Debris Resistant Burnable Absorber Rod Design	
4.2-9a	Modified Lower End Cap	
4.2-9b	Lower End Cap with Guardian Grid	
4.2-9c	Comparision of Gadolinia Rods for Regions M, P, and R	
4.2-9d	AREVA Fuel Rod Assemblies	EC287528
4.2-10	Control Element Assembly Locations	
4.2-11	Flow Channel Extensions	
4.2-12	4 Element CEA Shroud Flow Bypass Insert	
4.2-13	Spacer Grid Location in St. Lucie 2	
4.2-14	St. Lucie Unit 2 Cycle 2 CEA Bank and Subgroup Designations	
4.2-15	Positioning of Poison Fingers in Lead Bank	
4.3-1	Fuel Management Pattern	

Figure	Title
4.3-2a	Planar Average Power Distribution - 0 MWDT/T, Full Power, Cycle 1
4.3-2b	Planar Average Power Distribution - 0 MWD/T, Zero Power Cycle 1
4.3-3a	Planar Average Power Distribution - 50 MWD/T, Full Power, Cycle 1
4.3-3b	Planar Average Power Distribution - 50 MWD/T, Zero Power, Cycle 1
4.3-4a	Planar Average Power Distribution - 13200 MWD/T, Full Power, Cycle 1
4.3-4b	Planar Average Power Distribution - 13200 MWD/T, Zero Power Cycle 1
4.3-5	Planar Average Power Distribution - BOL, Cycle 1, Full Power, Bank 6 Inserted
4.3-6	Planar Average Power Distribution - 50 MWD/T, Cycle 1, Bank 6 Inserted, Full Power
4.3-7	Planar Average Power Distribution - 13200 MWD/T, Cycle 1, Bank 6 Inserted, Full Power
4.3-8	Planar Average Power Distribution - BOL, Cycle 1, PLRS Inserted, Full Power
4.3-9	Planar Average Power Distribution - 50 MWD/T, Cycle 1, PLRS Inserted, Full Power
4.3-10	Planar Average Power Distribution - 13200 MWD/T, Cycle 1, PLRS Inserted, Full Power
4.3-11	Planar Average Power Distribution - BOL, Cycle 1, Bank 6 and PLRS Inserted, Full Power
4.3-12	Planar Average Power Distribution - 50 MWD/T, Cycle 1, Bank 6 and PLRS Inserted, Full Power
4.3-13	Planar Average Power Distribution - 13200 MWD/T, Cycle 1, Bank 6 and PLRS Inserted, Full Power
4.3-14	Axial Power Distribution, BOC-1, Unrodded
4.3-15	Axial Power Distribution, 3000 MWD/T, Cycle 1, Unrodded
4.3-16	Axial Power Distribution, 6000 MWD/T, Cycle 1, Unrodded
4.3-17	Axial Power Distribution, 9000 MWD/T, Cycle 1, Unrodded
4.3-18	Axial Power Distribution, EOC-1, Unrodded
4.3-19	Planar Average Power Distribution - 50 MWD/T, Cycle 2, Full Power
4.3-20	Planar Average Power Distribution - 6000 MWD/T, Cycle 2, Full Power
4.3-21	Planar Average Power Distribution - 8630 MWD/T, Cycle 2, Full Power
4.3-22	Planar Average Power Distribution - 50 MWD/T, Cycle 3, Full Power

Figure	Title
4.3-23	Planar Average Power Distribution - 6000 MWD/T, Cycle 3, Full Power
4.3-24	Planar Average Power Distribution - 10469 MWD/T, EOC, Cycle 3, Full Power
4.3-25	Daily Reactor Power Maneuvering Near Beginning of Cycle (100% to 35% to 100% Power)
4.3-26	Daily Reactor Power Maneuvering Near End of Cycle (100% to 35% to 100% Power)
4.3-27	Daily Reactor Power Maneuvering Near the Beginning of Cycle (100% to 50% to 100% Power)
4.3-28	Daily Reactor Power Maneuvering Near the End of Cycle (100% to 50% to 100% Power)
4.3-29	Daily Reactor Power Maneuvering Near the Beginning of Cycle (2-Hour Ramps)
4.3-30	Daily Reactor Power Maneuvering Near the End of Cycle (2-Hour Ramps)
4.3-31a	$F^N Q$ Type equation here.Versus Time For A Load Following Transient (Sheet 1 of 3)
4.3-31b	$F^N Q$ Versus Time For A Load Following Transient (Sheet 2 of 3)
4.3-31c	$F^N Q$ Versus Time For A Load Following Transient (Sheet 3 of 3)
4.3-32a	$F^N R$ Versus Time For A Load Following Transient (Sheet 1 of 3)
4.3-32b	$F^N R$ Versus Time For A Load Following Transient (Sheet 2 of 3)
4.3-32c	$F^N R$ Versus Time For A Load Following Transient (Sheet 3 of 3)
4.3-33	Normalized Power Distribution with an Unshimmed Assembly Used in DNB Analyses
4.3-34	Fuel Temperature Coefficient Versus Effective Fuel Temperature
4.3-35	Moderator Temperature Coefficient Versus Moderator Temperature At BOC-1
4.3-36	Moderator Temperature Coefficient Versus Moderator Temperature At EOC-1
4.3-37	Moderator Density Coefficient Versus Moderator Density
4.3-38	Fuel Temperature Contribution to Power Coefficient Versus Power at EOC-1
4.3-39	CEA Bank Identification
4.3-40	Typical Power Dependent CEA Insertion Limit
4.3-41	Integral Worth Versus Withdrawal at Zero Power EOC-1
4.3-42	Integral Bank Worth vs. Withdrawal From Bank – 6 Inserted 60%, Equilibrium Xenon, EOC-1

Figure	Title
4.3-43	Reactivity Difference Between Fundamental and Excited States of a Bare Cylindrical Reactor
4.3-44	Expected Variation of the Azimuthal Stability Index with Exposure
4.3-45	Axial Stability Control Using PLCEAS
4.3-46	Rod Shadowing Effect Versus Rod Position For Rod Insertion and Withdrawal Transient At Palisades
4.3-47	Typical Shape Annealing Function, Two Subchannel
4.3-48	Geometry with Full and Partial Azimuthal Symmetry
4.3-49	Comparison of Measured and Calculated Shape Annealing Correction For Palisades
4.3-50	Typical Temperature Defect Versus Reactor Inlet Temperature
4.3-51	Comparison of Calculated and Measured Plutonium to Uranium Mass Ratio In the Asymptotic Neutron Spectrum For Yankee
4.3-52	Plutonium Isotopic Composition Versus Fuel Depletion In the Asymptotic Spectrum For Yankee
4.3-53	Critical Boron Reactivity Depletion of Palisades
4.3-54	Critical Boron for Maine Yankee
4.3-55	Critical Boron for Omaha
4.3-56	Millstone Unit 2 Power Coefficients
4.3-57	A Divergent Axial Oscillation in an EOC Core With Reduced Power Feedback (α=0.96 x 10^{-4} $\Delta\rho$/KW/FT)
4.3-58	Damping Coefficient Versus Reactivity Difference Between Fundamental and Excited State
4.3-59	Limiting Integral Radial Pin Power Distribution
4.3-60	Limiting Single Gap Power Peaking and Associated Rod Location Relative to the Gap Location
4.3-61	Augmentation Factor Versus Axial Position
4.3-62	Excore Detector Locations
4.3-63	Deleted
4.3-64	Deleted
4.3-65	Deleted

EC287528

Figure	Title
4.3-66	Deleted
4.3-67	Deleted
4.3-68	Deleted
4.4-1	Core Wide Planar Power Distribution For Sample DNB Analysis
4.4-2	Rod Radial Power Factors in Hot Assembly For Sample DNB Analysis
4.4-3	Typical Axial Power Distributions
4.4-4	Average Void Fractions and Qualities at the Exit of Different Core Regions
4.4-5	Axial Distribution of Void Fraction and Quality in the Subchannel Adjacent to the Rod with Minimum DNBR
4.4-6	Reactor Vertical Arrangement Showing Bypass Flow Paths
4.4-7	Isometric View of the Reactor Coolant System
4.4-8	Deleted
4.4-9	Deleted
4.4-10	Temperature Control Program
4.4-11	Reactor Stations
4.4-12	Sensitivity of Minimum DNBR to Small Changes in Reactor Coolant Conditions
4.6-1	Reactor Vessel Closure Head Plan View CEDM Layout

EC287528

4.0 REACTOR

4.1 SUMMARY DESCRIPTION

This chapter was originally prepared to describe the Cycle 1 core. Much of the original text is retained in the update for historical information, however, current cycle information has been added to the text. Physical changes where applicable, are reflected in the text. Where information is no longer applicable it is identified as Cycle 1.

The reactor is of the pressurized water (PWR) type using two reactor coolant loops. A vertical cross-section of the reactor is shown in Figure 4.1-1. The reactor core is composed of 217 fuel assemblies and 91 control element assemblies (CEAs). The fuel assemblies are arranged to approximate a right circular cylinder with an equivalent diameter of 136 in. and an active length of 136.7 in. The fuel assembly, which provides for 236 fuel rod positions, consists of five zircaloy guide tubes welded to spacer grids and is closed at the top and bottom by end fittings. The guide tubes each displace four fuel rod positions and provide channels that guide the CEAs over their entire length of travel. In selected fuel assemblies, the central guide tube houses incore instrumentation.

The fuel is low enriched UO_2 in the form of ceramic pellets and is encapsulated in prepressurized Zircaloy tubes that form a hermetic enclosure. Gadolinia dispersed in UO_2 pellets is also used as a burnable absorber in the bounding cycle introduced in the Cycle 12 core design. In addition, Erbia dispersed in UO_2 pellets is assumed as a burnable absorber for the bounding cycle.

The reactor coolant enters the upper section of the reactor vessel, flows downward between the reactor vessel wall and the core barrel, passes through the flow skirt where the flow distribution is equalized, and into the lower plenum. The coolant then flows upward through the core, removing heat from the fuel rods, exits from the reactor vessel and passes through the tube side of the vertical U-tube steam generators where heat is transferred to the secondary system. The reactor coolant pumps return the coolant to the reactor vessel.

Figure 4.1-2 shows the reactor core cross section and certain dimensional relations between fuel assemblies, fuel rods, and CEA guide tubes.

The reactor internals support and orient the fuel assemblies, control element assemblies, incore instrumentation, and guide the reactor coolant through the reactor vessel. The reactor internals also absorb static and dynamic loads and transmit the loads to the reactor vessel flange. They will safely perform their functions during normal operating, upset, emergency, and faulted conditions. The internals are designed to safely withstand forces due to dead weight, handling, temperature and pressure differentials, flow impingement, vibration, and seismic acceleration. All reactor components are considered seismic Category I for seismic design. The design of the reactor internals limits deflection where required by function. The stress values of all structural members under normal operating and expected transient conditions are not greater than those established by Section III, Subsection NG, of the ASME Code. The effect of neutron irradiation on the materials concerned is included in the design evaluation. The effect of accident loadings on the internals is included in the design analysis.

Reactivity control is provided by two independent systems - the control element drive system and the Chemical and Volume Control System (CVCS).

The control element drive system controls short term reactivity changes and is used for rapid shutdown. The CVCS compensates for long term reactivity changes and can make the reactor subcritical without the benefit of the control element drive system. Design of the core and the Reactor Protective System prevents fuel damage limits from being exceeded for any single malfunction in either of the reactivity control systems.

The standard control element assemblies consist of five poison rods assembled in a square array, with one rod in the center. The rods are connected to a spider structure that couples to the control element drive mechanism (CEDM) shafting. There are 91 CEAs.

The CEAs are positioned by magnetic jack control element drive mechanisms mounted on the reactor vessel head.

The maximum reactivity worth of the CEAs and the associated reactivity addition rate is limited by system design to prevent sudden large reactivity increases. The design restraints are such that reactivity increases do not result in violation of the fuel damage limits, rupture of the reactor coolant pressure boundary, nor disruption of the core or other internals sufficient to impair the effectiveness of emergency cooling.

Boric acid dissolved in the coolant is used as a neutron absorber to provide long term reactivity control. In order to reduce the boric acid concentration required at beginning-of-life operating conditions, and thus reduce the initial magnitude of the moderator temperature coefficient, burnable poison rods are provided in certain fuel assemblies. The poison is boron carbide dispersed in alumina pellets, $UO_2Gd_2O_3$ pellets, and $UO_2Er_2O_3$ pellets. The pellets are clad in Zircaloy, Zirlo™, or M5® tubing to form rods that are similar to the fuel rods. EC287528

The bounding cycle reload process encompasses a wide range of fuel management strategies so as to allow flexibility in future core designs. The fuel management schemes considered include 18 to 24 month fuel cycles and the use of gadolinia and erbia burnable poison in the fuel rods.

The bounding cycle nuclear design bases will include the following:

1. The design for each cycle shall permit operation within the Technical Specifications for St. Lucie Unit 2 Nuclear Plant, as proposed and addressed in the Safety Analysis Report.

2. The cycle specific loading pattern shall be designed to achieve power distributions and control rod activity worths according to the following constraints:

    a. The peak Linear Heat Rate (LHR) and the peaking factors shall not exceed the TS/COLR limits in any single fuel rod through the cycle under nominal full power operating conditions.

    b. The scram worth of all rods minus the most reactive rod shall exceed the shutdown margin requirements, including PDIL.

The neutronic design methods to be used to ensure the above requirements will be those previously approved by the NRC.

The nuclear design of the core ensures that the combined response, of all reactivity coefficients in the power operating range, to an increase in reactor thermal power yields a net decrease in reactivity.

Control element assemblies are moved in groups to satisfy the requirements of shutdown, power level changes, and operational maneuvering. The control system is designed to produce power distributions that are within the acceptable limits of overall nuclear heat flux factor (F_Q) and departure from nucleate boiling ratio (DNBR). The Reactor Protective System and administrative controls ensure that these limits are not exceeded.

Axial xenon oscillations, should they occur, can be manually controlled by a variety of methods, including RCS boration/dilution, RCS temperature, and CEAs, using information provided by the nuclear detectors.

The core also contained two plutonium 238-beryllium neutron sources for initial and subsequent start-up through Cycle 5. The sources have been removed from the core and are stored in the spent fuel pool within a spent fuel assembly CEA guide tube. Irradiated fuel from previous cycles is now used as the neutron source.

Fuel assembly design is discussed in Section 4.2; nuclear design of the core is discussed in Section 4.3; and the thermal and hydraulic design is discussed in Section 4.4. CEDM and reactor internals materials are discussed in Section 4.5 (the design of these components is discussed in Subsections 3.9.4 and 3.9.5). The functional design of the reactivity control systems is discussed in Section 4.6.

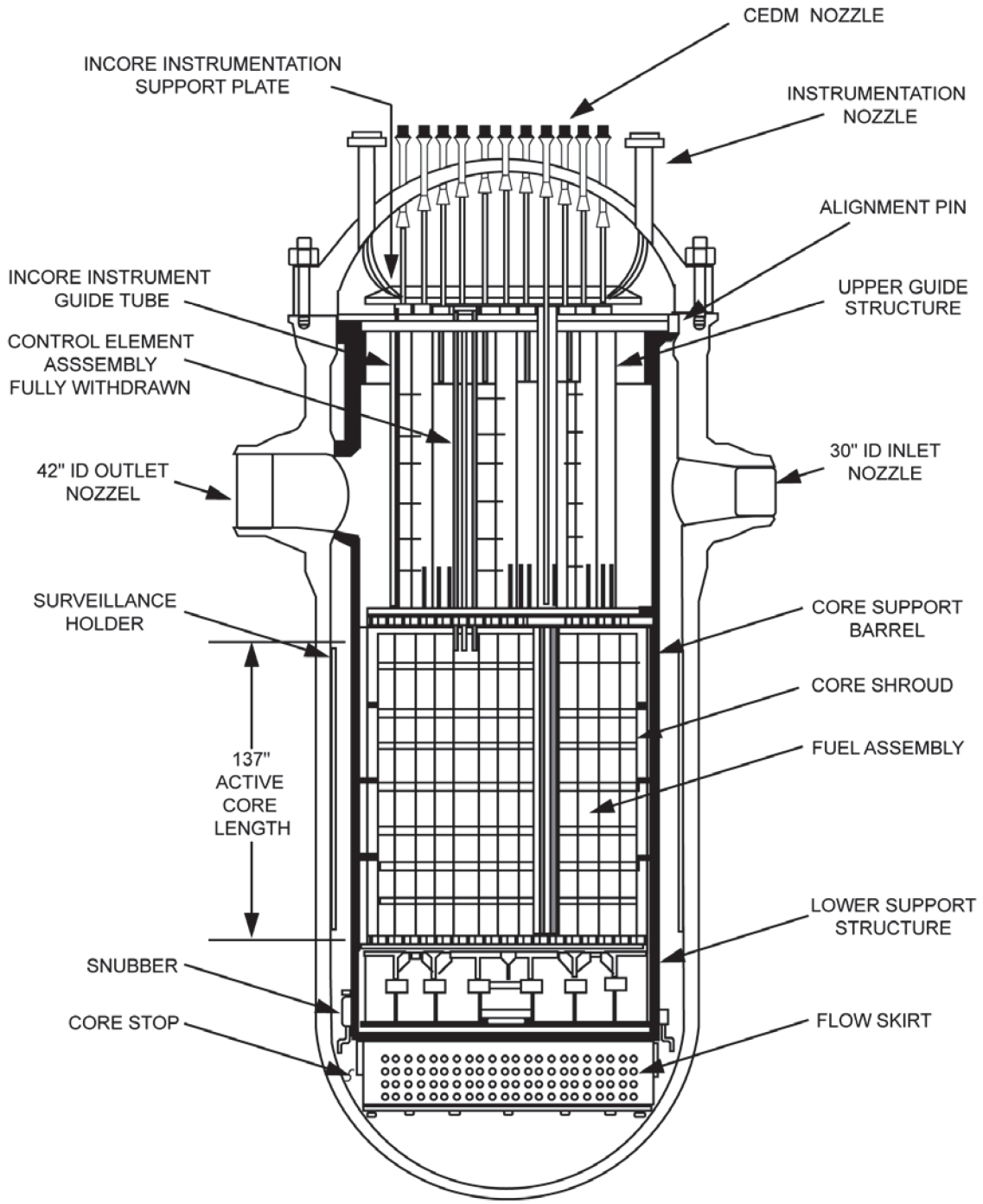

FLORIDA POWER & LIGHT COMPANY
ST. LUCIE PLANT UNIT 2

REACTOR VERTICAL ARRANGEMENT

FIGURE 4.1-1

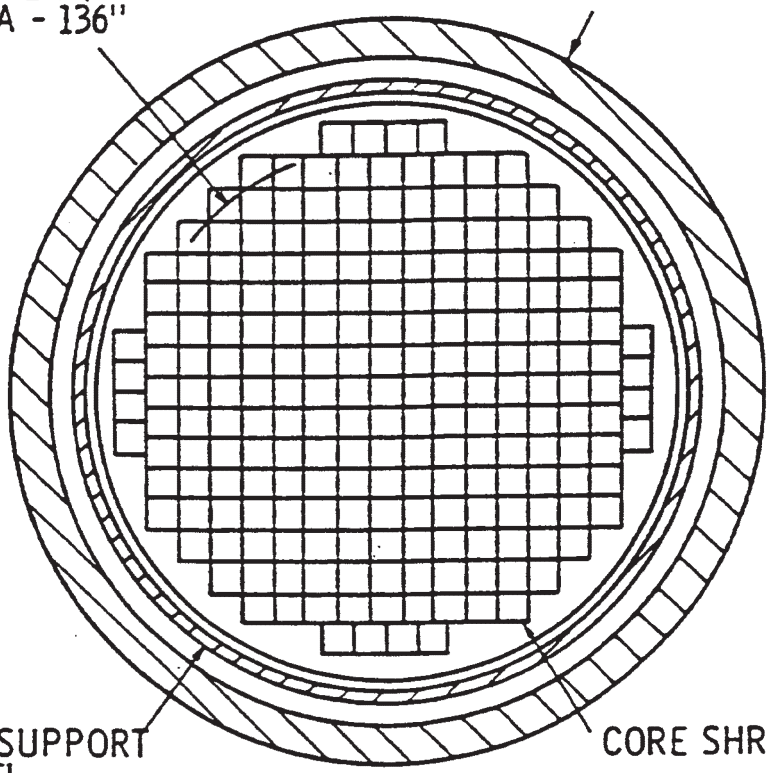

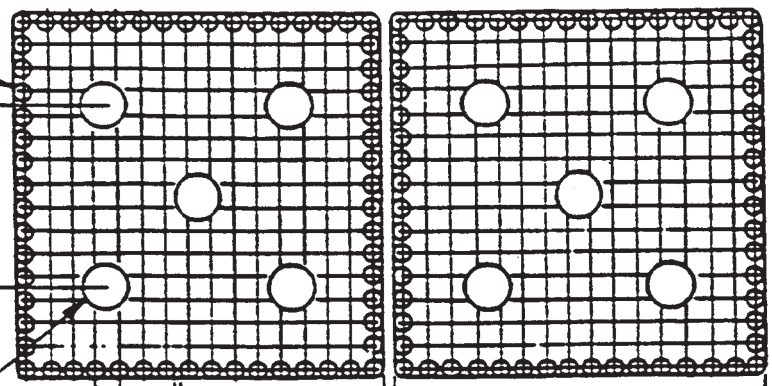

FLORIDA POWER & LIGHT
ST. LUCIE PLANT UNIT 2

REACTOR CORE CROSS SECTION

FIGURE 4.1-2

4.2 FUEL SYSTEM DESIGN

4.2.1 DESIGN BASES

The St. Lucie Unit 2 UFSAR has been revised to incorporate current Cycle reload information. Historical information pertaining to Cycle 1 and Cycle 2 has been retained.

St. Lucie Unit 2 will begin with transition from Westinghouse 16x16 Standard Value Added Fuel starting with Cycle 23. The Westinghouse 16x16 Standard Value Added fuel assembly design has been evaluated for the mixed core condition for dimensional compatibility (i.e. core fit-up/clearance, handling interfaces, component elevations, etc.), fuel assembly performance (i.e. criteria related to fuel assembly pressure drop), and loadings associated with Seismic/LOCA events. The Westinghouse 16x16 Standard Value Added Fuel continues to satisfy applicable fuel assembly mechanical design criteria in mixed core loadings with AREVA fuel. EC287528

Historical information has been retained. See Section 4.2.1.6 for the discussion related AREVA CE-16 HTP™ fuel design.

4.2.1.1 Fuel Assembly

Commencing with Cycle 17 (Region X), the 16x16 CE HID-1L fuel assembly will incorporate ZIRLO™ clad fuel rods. No other changes to the fuel assembly will occur.

ZIRLO™ is an advanced zirconium-based alloy, developed to enhance fuel performance and achieve extended fuel discharge burnup. The alloy provides a significant improvement in fuel rod and fuel assembly component corrosion resistance and dimensional stability under irradiation.

Chemical Properties

The chemical composition of the clad with the ZIRLO™ alloy in the St. Lucie Unit 2 Cycle 17 fuel assemblies are similar to that of Zircaloy-4 or OPTIN except for slight reductions in the tin (Sn) and iron (Fe) content, the elimination of chromium (Cr), and the addition of a nominal amount of niobium (Nb). This composition change and associated materials structure refinements are responsible for the improved corrosion resistance as compared to that of the standard Zircaloy-4, improved Zircaloy-4 or OPTIN components. The physical and mechanical properties of ZIRLO™ are comparable or better than those of Zircaloy-4 or OPTIN; however, the temperature at which the metallurgical phase change occurs differs, as discussed in Reference 95.

Nominal Composition of ZIRLO™ and Zircaloy-4 Cladding

Element	Zircaloy-4 (wt %)	Improved Zircaloy-4 (wt %)	OPTIN (wt %)	ZIRLO™ (wt %)
Tin (Sn)	1.2 -1.7	1.2 -1.45	1.2 -1.44	0.9 -1.1
Iron (Fe)	0.18 - 0.24	0.18 - 0.24	0.18 - 0.24	0.09 - 0.13
Chromium (Cr)	0.07 - 0.13	0.07 - 0.13	0.07 - 0.13	---
Niobium (Nb)	---	---	---	0.8 - 1.2
Zirconium (Zr)	Balance	Balance	Balance	Balance

Demonstration Programs

ZIRLO™ alloy corrosion resistance has been evaluated in long-term, out-of-pile tests over a wide range of temperatures (up to 680°F in water and up to 932°F in steam tests). Additional tests have also been conducted in lithiated water environments at temperatures of 680°F.

The improved corrosion resistance of ZIRLO™ cladding under irradiation has also been demonstrated. Beginning in the early 1970s in the BR-3 Test Reactor Demonstration Program, fuel rods containing cladding fabricated from ZIRLO™ alloy were irradiated at linear power levels of up to 17 kW/ft to rod average burnups of 68 GWD/MTU (i.e., peak pellet burnups of approximately 80 GWD/MTU). Post-irradiation examinations have demonstrated that ZIRLO™ alloy exhibited a reduction in corrosion rate and improved dimensional stability as compared to Zircaloy-4 rods having similar power histories, which were irradiated as controls in the same assemblies.

Beginning with Region N, the fuel incorporates the GUARDIAN™ fuel assembly design to screen and entrap debris. The Guardian design employs a redesigned bottom spacer grid that provides positive axial restraint to the rods and added screening features. The fuel rods have shorter, circumfrentially grooved lower end caps. The elevation of the spacer grid has been decreased, and its springs interface with the end cap grooves to provide added resistance to axial movement due to flow forces. The mechanical design of the Guardian grid offers improved resistance in entrapping debris while improving resistance to fretting when compared to the previous 16x16 Inconel spacer grid assembly design. In particular, with grid cells positioned in a square array, the Guardian grid can effectively entrap debris without affecting the function of the circulating pumps since the size of the containment strainer perforated plate hole size is smaller than the major openings between the Guardian grid and the OD of the rod assemblies. The elevations of all other grids and the two end fittings are unchanged with respect to those in prior reloads. The rod length is also the same, although its internal volume has been increased due to the shorter lower end cap. Both the Guardian spacer grid and its predecessor design allow for removal and replacement of rods.

The Guardian bottom grid continues to be made from Inconel 625 material, and it is attached to the LEF casting by the same welding technique as in the previous design. The hydraulic resistance of the bottom grid is increased due to its proximity to the LEF plate, and by its debris-screening features. Other changes incorporated into the fuel assembly design starting with Region N include increased thickness for the UEF flow plate and hold down plate. This results in more compression of the hold down springs during operation (their design is not changed), helping to maintain the margin to lifting of the Guardian assembly with its increased pressure drop.

The mechanical design criteria, as documented in the original FSAR, that are used to evaluate fuel assembly performance are unchanged for all fuel regions. In comparison to the previous regions, the difference in weight between a Region N fuel assembly and the fuel assemblies from prior regions of fuel is approximately 20 pounds. This additional increase in fuel assembly weight is from the heavier pellets beginning with the Region N fuel and gad rod assemblies.

The fuel assemblies are required to meet design criteria for each design condition listed below to assure that the functional requirements are met. Except where specifically noted, the design bases presented in this section are consistent with those used for previous designs.

a) Non Operation and Normal Operation

Condition I situations are those which are planned or expected to occur in the course of handling, initial shipping, storage, reactor servicing and power operation (including maneuvering of the plant). Condition I situations must be accommodated without fuel assembly failure and without any effect which would lead to a restriction on subsequent operation of the fuel assembly. The guidelines stated below are used to determine loads during Condition I situations:

1) Handling and Fresh Fuel Shipping

   Loads correspond to the maximum possible axial and lateral loads and accelerations imposed on the fuel assembly by shipping and handling equipment during these periods, assuming that there is no abnormal contact between the fuel assembly and any surface, nor any equipment malfunction. Irradiation effects on material properties are considered when analyzing the effects of handling loads which occur during refueling. Additional information regarding shipping and handling loads is contained in Subsection 4.2.3.1.5.

2) Storage

   Loads on both new and irradiated fuel assemblies reflect storage conditions of temperature, chemistry, means of support and duration of storage.

3) Reactor Servicing

   Loads on the fuel assembly reflect those encountered during refueling and reconstitution.

4) Power Operation

   Loads are derived from conditions encountered during transient and steady-state operation in the design power range. (Hot operational testing, system startup, hot standby, operator controlled transients within specified rate limits and system shutdown are included in this category.)

5) Reactor Trip

   Loads correspond to those produced in the fuel assembly by control element assembly (CEA) motion and deceleration.

b) Condition II: Upset Condition

Condition II situations are unplanned events which may occur with moderate frequency during the life of the plant. The fuel assembly design should have the capability to withstand any upset condition with margin to mechanical failure and with no permanent effects which would prevent continued normal operation. Incidents classified as upset conditions are listed below:

1) Operating basis earthquake (OBE)

2) Selected moderate frequency events

c) Condition III: Emergency Conditions

Condition III events are unplanned incidents which might occur very infrequently during plant life. Rod mechanical failure must be prevented for any Condition III event in any area not subject to extreme local conditions (e.g., in any rod not immediately adjacent to the impact surface during fuel handling accident).

The Condition III incidents listed below are included as a category to provide assurance that under the occurrence of a Condition III event, rod damage is minimal.

1) Selected infrequent events

2) Minor fuel handling accident (fuel assembly and grapple remain connected).

d) Condition IV: Faulted Conditions

Condition IV incidents are postulated events which are not expected to occur, but are analyzed anyway because of their potential for release of significant amounts of radioactive material. Mechanical fuel failures and reactor coolant system damage are permitted, but operation of the engineered safety features (ESF) and reactor protection systems to mitigate the consequences of the postulated event must not be impaired. Condition IV incidents are listed below:

1) Safe shutdown earthquake (SSE)

2) Selected limiting faults

3) Major fuel handling accident (fuel assembly and grapple are disengaged)

4.2.1.1.1 Fuel Assembly Structural Integrity Criteria

For each of the design conditions, there are criteria which apply to the fuel assembly and components with the exception of fuel rods. These criteria are listed below and give the allowable stresses and functional requirements for each design condition. Criteria for fuel rods are discussed separately in Subsection 4.2.1.2.

a) Design Conditions I and II

$P_m \leq S_m$

$P_m + P_b \leq F_s S_m$

Under cyclic loading conditions, stresses must be such that the cumulative fatigue damage factor does not exceed 0.8. Cumulative damage factor is defined as the sum of the ratios of the number of cycles at a given cyclic stress (or strain) condition to the maximum number permitted for that condition. The selected limit of 0.8 is used in place of 1.0 (which would correspond to the absolute maximum damage factor permitted) to provide additional margin in the design.

Deflections must be such that the allowable insertion time of the control element assemblies is not exceeded.

b) Design Condition III

$P_m \leq 1.5\ S_m$

$P_m + P_b \leq 1.5\ F_s S_m$

Deflections are limited to a value allowing the CEAs to trip, but not necessarily within the prescribed time.

c) Design Condition IV

$P_m \leq S'_m$

$P_m + P_b \leq F_s S'_m$

where S'_m = smaller value of 2.4 S_m or 0.7 S_u.

1) If the equivalent diameter pipe break in the LOCA does not exceed 0.5 square foot, the fuel assembly deformation shall be limited to a value not exceeding the deformation which would preclude satisfactory insertion of the CEAs.

2) For pipe break sizes greater than 0.5 square foot, deformation of structural components is limited to maintain the fuel in a coolable array. CEA insertion is not required for these events as the appropriate safety analyses do not take credit for CEA insertion.

d) Nomenclature

The symbols used in defining the allowable stress levels are as follows:

P_m	=	Calculated general primary membrane stress[(a)]
P_b	=	Calculated primary bending stress
S_m	=	Design stress intensity value as defined by Section III ASME Boiler and Pressure Vessel Code[(b)]
S_u	=	Minimum unirradiated ultimate tensile strength
F_s	=	Shape factor corresponding to the particular cross section being analyzed[(c)]
S'_m	=	Design stress intensity value for faulted conditions

The definition of S'_m as the lesser value of 2.4 S_m and 0.7 S_u is contained in the ASME Boiler and Pressure vessel Code (1974) Section III, Appendix F-1323.1

Where notes a, b and c are defined as:

(a) P_m and P_b are defined by Section III, ASME Code.

(b) With the exception of zirconium base alloys, the design stress intensity values, S_m, of materials not tabulated by the Code are determined in the

same manner as the Code. The design stress intensity of zirconium base alloys shall not exceed two-thirds of the unirradiated minimum yield strength at temperature. Basing the design stress intensity on the unirradiated yield strength is conservative because the yield strength of zircaloy increases with irradiation. The use of the two-thirds factor ensures 50 percent margin to component yielding in response to primary stresses. This 50 percent margin together with its application to the minimum unirradiated properties and the general conservatism applied in the establishment of design conditions is sufficient to ensure an adequate design.

(c) The shape factor, F_s, is defined as the ratio of the "plastic" moment (all fibers just at the yield stress) to the initial yield amount (extreme fiber at the yield stress and all other fibers stressed in proportion to their distance from the neutral axis). The capability of cross section loaded in bending to sustain moments considerably in excess of that required to yield the outermost fibers is discussed in Timoshenko.[1]

4.2.1.1.2 Material Selection

The fuel assembly grid cage structure consists of nine Zircaloy-4 spacer grids, one Inconel 625 spacer grid (at the lower end), five Zircaloy-4 guide tubes, two stainless steel end fittings, and five Inconel X-750 coil springs. Zircaloy-4 or ZIRLO™, selected for fuel rod cladding, and Zircaloy-4 for guide tubes and spacer grids, has a low neutron absorption cross section, and high corrosion resistance to reactor water environment. Also there is little reaction between the cladding and fuel or fission products. As described in Subsection 4.2.3, Zircaloy-4 has demonstrated its ability as a cladding, CEA guide tube, and spacer grid material. (Note that beginning with Region U, the top grid is also Inconel.)

The bottom spacer grid is of Inconel 625 and is welded to the lower end fitting. In this region of local inlet turbulence, Inconel 625 was selected rather than Zircaloy-4 to provide additional strength and relaxation resistance. Inconel 625 is a very strong material with good ductility, corrosion resistance and stability under irradiation at temperatures below 1000°F. The top grid is also Inconel beginning with Region U.

The fuel assembly lower end fitting is of cast 304 stainless steel (Grade CF-8) and the upper end fitting assembly consists of two cast stainless steel plates and five Type 304 stainless steel machined alignment posts. This material was selected based on considerations of adequate strength and high corrosion resistance. Also, Type 304 stainless steel has been used successfully in almost all pressurized water reactor environments, including all currently operating CE reactors.

4.2.1.1.3 Fuel Assembly Guide Tubes

All fuel assembly guide tubes are manufactured in accordance with Designation UNS No. R60804 ASTM B353-77A, Wrought Zirconium and Zirconium Alloy Seamless and Welded Tubes for Nuclear Service, with the following exceptions and/or additions:

a) Chemical Properties

Additional limits are placed on oxygen.

b) Mechanical Properties

Flare:

A section of annealed tube, between two and four inches in length shall be flared with a tool having a 60 degree included angle until the outside diameter has increased by 15 percent. The flared tube shall show no cracking when examined with the unaided eye.

c) Dimensional Requirements

Dimension	Permissible Tolerance (in.)
OD	±0.003
ID	±0.005

The fuel assembly guide tube has been changed in Batch D from a cold worked to an annealed material. The change to annealed material will result in a lower growth rate of the fuel assembly.

4.2.1.1.4 Zircaloy-4 Bar Stock

All Zircaloy-4 bar stock is fabricated in accordance with Designation UNS No. R60804, ASTM B351-73, Hot-Rolled and Cold-Finished Zirconium and Zirconium Alloy Bars, Rod and Wire for Nuclear Applications, with the following exceptions and/or additions:

a) Chemical Properties

Additional limits are placed on oxygen and silicon content.

b) Metallurgical Properties

Grain Size

The maximum average grain size is restricted.

4.2.1.1.5 Zircaloy-4 Strip Stock

All Zircaloy-4 strip stock is fabricated in accordance with Grade RA-2, ASTM B352, Zirconium and Zirconium Alloy Sheet, Strip and Plate for Nuclear Application, with the following exceptions and/or additions:

a) Chemical Properties

Additional limits are placed on oxygen and silicon content.

b) Metallurgical Properties

Grain Size:

The maximum average grain size is restricted.

c) Mechanical Properties

Bend:

Each sample shall be bent using a three point type, guided bend test fixture similar to that described in MAB-192-M, Evaluation Test Methods for Refractory Metal Sheet Material, Paragraph 5.2.2, published by Division of Engineering and Industrial Research, National Academy of Sciences, National Research Council, April 22, 1963. The sample shall be bent 180 degrees using a hand anvil with a radius equal to twice the sheet thickness. After bending, each specimen shall be liquid dye penetrant inspected to assure freedom from cracking. If cracking occurs on any part of the bend samples, the coils represented shall be rejected.

d) Coefficient of Thermal expansion

Axial direction - see Reference 2

e) Irradiation Properties:

The yield and tensile strengths are enhanced by irradiation. The stress relaxation with irradiation and operating temperatures proceeds at a rapid rate until nearly complete. The irradiation induced growth is documented.[3]

4.2.1.1.6 Stainless Steel Castings

All stainless steel castings are fabricated in accordance with Grade CF-8, ASTM A296, with the following addition:

Chemical Properties

Cobalt content is limited.

4.2.1.1.7 Stainless Steel Tubing

All stainless steel tubing is fabricated in accordance with ASTM A269, with the following addition:

Chemical Properties

Carbon content is limited on tubing to be welded. Cobalt content is limited.

4.2.1.1.8 Inconel X-750 Helical Springs

All Inconel springs are fabricated in accordance with AMS 5699E, with the following addition:

Chemical Properties

Cobalt content is limited.

Passivation prohibited.

4.2.1.1.9 Inconel 625 Bottom Spacer Grid Strip Material (and Top Grid Beginning with Region U)

Inconel spacer grid strip material is procured in accordance with the specification for nickel-chromium molybdenum columbium alloy plate, sheet, and strip, specification ASTM B443-84 and B443-93, with the following additional requirements:

a) Chemical Properties

Cobalt content is limited to one percent maximum.

b) Special Tests

A check analysis and a bend test are required.

4.2.1.1.10 Thermal Design and Fuel Performance

The thermal performance was evaluated for composite fuel pins (including burnable poison rods with gadolinia-urania or erbia-urania). A bounding analysis of the various fuel types anticipated was performed using the NRC approved FATES3B version of the fuel evaluation model, References 14, 79, 87 and 95. The fuel types include fuel pin designs currently in use or expected to be used. The analysis included urania fuel; gadolinia fuel with absorber concentrations of up to and including 8.0 weight percent gadolinia per Reference 88 (see also Reference 89); and erbia fuel with absorber concentrations of up to and including 2.5 weight percent erbia per Reference 90.

The thermal performance analysis utilized a power history that envelopes the power and burnup levels of the peak pin at each burnup interval, from beginning of cycle (BOC) to end of cycle (EOC) burnups. The burnup range analyzed was 0 to 60 MWD/kgU (References 84, 85 and 91), a range in excess of that expected for anticipated cycles. The maximum fuel rod internal pressure was verified to remain below the maximum allowable gas pressure, Reference 92. The effective power-to-centerline melt limit was also determined to be in excess of the 22.0 kw/ft value assumed as the basis for the LHR LSSS Setpoints.

4.2.1.2 Fuel Rod

Beginning with Region N, the pellet diameter has been increased by 0.0005 inches, and the geometry of the dishes and chamfers has been modified. A spherical configuration is used in place of the truncated cone dishes and a minor reduction in the chamfers has been made. The pellets are dried prior to loading to prevent hydriding of the zircaloy cladding. The pellet length-to-diameter ratio and chamfer decrease the interaction between the pellet and the cladding.

The compression spring, located at the top of the fuel pellet column, maintains the column in its proper position during handling and shipping.

The fuel and poison rod plenum provides space for axial thermal expansion of the fuel and poison column and accommodates the gaseous fission products. The greater portion of the fission gas remains in the pellet lattice and does not contribute to the rod internal pressure.

The mechanical design criteria, as documented in the original FSAR, that are used to evaluate fuel rod performance are unchanged for all fuel and poison regions.

4.2.1.2.1 Fuel Cladding Design Limits

The fuel cladding is designed to sustain the effects of steady-state and expected transient operating conditions without exceeding acceptable levels of stress and strain. Except where specifically noted, the design bases presented in this section are consistent with those used for previous core designs. The fuel rod design accounts for cladding irradiation growth, external pressure, differential expansion of fuel and clad, fuel swelling, fuel densification, clad creep, fission and other gas releases, initial internal helium pressure, thermal stress, pressure and temperature cycling, and flow induced vibrations. The structural criteria discussed below are based on the following for the normal, upset, and emergency loading combinations identified In Subsection 4.2.1.1. For a discussion of the thermal/hydraulic criteria, see Subsection 4.4.1.

a) During normal operating and upset conditions (Conditions I and II), the maximum primary tensile stress in the Zircaloy or ZIRLO™ clad shall not exceed two-thirds of the minimum unirradiated yield strength of the material at the applicable temperature. The corresponding limit under emergency conditions (Conditions III) is the material yield strength. The use of the unirradiated material yield strength as the basis for allowable stress is conservative because the yield strength of zircaloy increases with irradiation. The use of two-thirds factor ensures 50 percent margin to component yielding in response to primary stresses. This 50 percent margin, together with its application to the minimum unirradiated properties and the general conservatism applied in the establishment of design conditions, is sufficient to ensure an adequate design.

b) Net unrecoverable circumferential strain shall not exceed one percent as predicted by computations considering clad creep and fuel-clad interaction effects.

   Data from O'Donnell[4] and Weber[5] were used to determine the present one percent strain limit. O'Donnell developed an analytical failure curve for Zircaloy cladding based upon the maximum strain of the material at its point of plastic instability. O'Donnell compared his analytical curve to circumferential strain data obtained on irradiated coextruded Zr-U metal fuel rods tested by Weber. The correlation was good, thus substantiating O'Donnell's instability theory. Since O'Donnell performed his analysis, additional data have been derived at Bettis [6] [7] [8] and AECL [9] [10].

   These new data are shown in Figure 4.2-1, along with O'Donnell's curve and Weber's data. This curve was then adjusted because of differences in anisotropy, stress states and strain rates; and the design limit was set at one percent.

   The conservatism of the clad strain calculations is provided by the selection of adverse initial conditions and material behavior assumptions, and by the-assumed operating history. The acceptability of the 1.0 percent unrecoverable circumferential strain limit is demonstrated by data from irradiated Zircaloy-clad fuel rods which show no cladding failures (due to strain) at or below this level, as illustrated in Figure 4.2-1.

c) The clad will be initially pressurized with helium to an amount sufficient to prevent gross clad deformation under the combined effects of external pressure and long-term creep. The clad design will not rely on the support of fuel pellets or the holddown spring to prevent gross deformation.

d) Cumulative strain cycling usage, defined as the sum of the ratios of the number of cycles in a given effective strain range (Δ_ε) to the permitted number (N) at that range, as taken from Figure 4.2-2, will not exceed 0.8.

The cyclic strain limit design curve shown on Figure 4.2-2, is based upon the Method of Universal Slopes developed by S. S. Manson and has been adjusted to provide a strain cycle margin for the effects of uncertainty and irradiation. The resulting curve has been compared with known data on the cyclic loading of Zircaloy and has been shown to he conservative. Specifically, it encompasses all the data of O'Donnell and Langer.[12]

As discussed in Subsection 4.2.3.2.17, the fatigue calculation method includes the effect of clad creep to reduce the pellet to clad diametral gap during that portion of operation when the pellet and clad are not in contact. The same model is used for predicting clad fatigue as is used for predicting clad strain. Therefore, the effects of creep and fatigue loadings are considered together in determining end of life clad strain. Moreover, the current fatigue damage calculation method includes a factor of two which is applied to the calculated strain before determining the allowable number of cycles associated with that strain. This, in combination with the allowable fatigue usage factor 0.8 ensures a considerable degree of conservatism (see Figure 4.2-2).

e) There is no specific limit on lateral fuel rod deflection for structural integrity considerations except which is brought about through application of cladding stress criteria. The absence of a specific limit on rod deflection is justifled because it is the fuel assembly structure, and not the individual fuel rod, that is the limiting factor for fuel assembly lateral deflection.

f) Fuel rod internal pressure increases with increasing burnup and toward end of life the total internal pressure, due to the combined effects of the initial helium fill gas and the released fission gas, can approach values comparable to the external coolant pressure. The maximum predicted fuel rod internal pressure will be consistent with the following criteria.

1. The primary stress in the cladding resulting from differential pressure will not exceed the stress limits specified earlier in this section.

2. The internal pressure will not cause the clad to creep outward from the fuel pellet surface while operating at the design peak linear heat rate for normal operation. In determining compliance with this criterion, internal pressure is calculated for the peak power rod in the reactor, including accounting for the maximum computed fission gas release. In addition, the pellet swelling rate (to which the calculated clad creep rate is compared) is based on the observed swelling rate of "restrained" pellets (i.e., pellets in contact with clad), rather than on the greater observed swelling behavior of pellets which are free to expand.

The criteria discussed above do not limit fuel rod internal pressure to values less than the reactor coolant pressure, and the occurrence of positive differential pressures would not adversely affect normal operation if appropriate criteria for cladding stress, strain, and strain rate were satisfied.

g) The design limits of the fuel rod cladding, with respect to vibration considerations, are incorporated within the fuel assembly design. It is a requirement that the spacer grid intervals, in conjunction with the fuel rod stiffness, be such that fuel rod vibration, as a result of mechanical or flow induced excitation, does not result in excessive wear of the fuel rod cladding at the spacer grid contact areas. Vibration wear of any component within the fuel system design would be evaluated on the basis of the stress and strain criteria listed previously in this section.

4.2.1.2.2 Fuel Rod Cladding Properties

4.2.1.2.2.1 Mechanical Properties

a) Modulus of Elasticity

The value of Young's Modulus x 10^{-6} is specified in Reference 13.

b) Poisson's Ratio

N is the value specified in Reference 13.

c) Thermal Coefficient of Expansion

Diametral direction is the value specified in Reference 13.

d) Yield Strength

Irradiated values for Zircaloy or ZIRLO™ yield strength and ultimate strength are not used in any design calculations. This is conservative since allowable stresses would increase if irradiation were accounted for. Yield strength in the non-irradiated condition is shown on Figure 4.2-20 of Reference 13.

The cladding stress limits identified in Subsection 4.2.1.2.1 are based on values taken from the minimum yield strength curve at the appropriate temperatures. The limits are applied over the entire fuel lifetime, during conditions of reactor heatup and cooldown, steady state operation, and normal power cycling. Under these conditions, cladding temperatures and fast fluences can range from 70 to 750 F and from 0 to 1 x 10^{22} nvt, respectively.

e) Ultimate Strength

Irradiated values for Zircaloy or ZIRLO™ yield strength and ultimate strength are not used in any design calculations. This is conservative since allowable stresses would increase if irradiation were accounted for. Ultimate tensile strength in the non-irradiated condition is shown on Figure 4.2-21 of Reference 13.

f) Uniform Tensile Strain

Irradiation is assumed in the Zircaloy or ZIRLO™ strain limit since it lowers the allowable value. Any calculations involving permanent strain use this basis, unless they are a BOL situation. Uniform tensile strain in the non-irradiated condition is shown on Figure 4.2-22 of Reference 13.

Uniform tensile strain in the irradiated condition approaches one percent and remains relatively constant (Subsection 4.2.1.2.1).

g) Flare

A section of annealed tube, approximately two to four inches in length is flared with a tool having a 60 degree included angle, until the outside diameter has increased by 15 percent. The flared tube is to show no cracking when examined with the unaided eye.

h) Hydrostatic Burst Test

The cladding specification requires that two samples from each lot of cladding be subjected to room temperature hydrostatic burst tests. To be acceptable, the burst pressure must exceed a minimum value based on the cladding geometry and specified tensile properties, and the circumferential strain must equal or exceed a 12 percent prescribed minimum value.

4.2.1.2.2.2 Dimensional Requirements

a) Tube straightness is limited to 0.010 in./ft. and inside diameter and wall thickness are tightly controlled.

b) Ovality is measured as the difference between maximum and minimum inside diameters and is acceptable if within the diameter tolerances.

c) Outside diameter is specified as 0.382 ± 0.002 inches

d) Inside diameter is specified as 0.332 ± 0.0015 inches

e) Eccentricity is defined as the difference between maximum and minimum wall thickness at a cross-section, and is specified as 0.004 inches maximum.

f) Wall thickness is specified as 0.023 inches minimum (the nominal value reported in table 4.2-1 is based on the nominal OD and ID).

g) Fuel rod length tolerance is ± 0.065 inches.

It should be noted that the tolerances listed above are taken from design drawings. It is standard practice to obtain as-built cladding measurements of outside diameter, wall thickness, and ovality; and these measured values are occasionally used to reduce uncertainties in final analyses.

4.2.1.2.2.3 Metallurgical Properties

The metallurgical requirements of the fuel cladding and the fuel assembly structural members for the Batch D fuel are identical to those of the other fuel batches to be included in Cycle 2. Thus, the chemical or metallurgical 1 performance of the Batch D fuel remains unchanged from the performance of the Cycle 1 fuel.

a) Hydride Orientation

A restriction is placed on the hydride orientation factor for any third of the tube cross section (inside, middle, or outside). The hydride orientation factor, defined as the ratio of the number radially oriented hydride platelets to the total number of hydride platelets, shall not exceed 0.3. The independent evaluation of three portions of the cross section is included to allow for the possibility that hydride orientation may not be uniform across the entire cross section.

4.2.1.2.2.4 Chemical Properties

All fuel rod cladding is manufactured in accordance with designation UNS No. R60804, ASTM B353-77A, Wrought Zirconium and Zirconium Alloy Seamless and Welded Tubes for Nuclear Service, except additional limits are placed on oxygen, silicon and iron content.

4.2.1.2.3 Fuel Rod Component Properties

4.2.1.2.3.1 Zircaloy-4 Bar Stock

All Zircaloy-4 bar stock is fabricated in accordance with Designation UNS No . R60804, ASTM B351-73, Hot rolled and Cold Finished Zirconium and Zirconium Alloy Bars, Rod and Wire for Nuclear Application, with the following exception and/or additions:

a) Chemical Properties

Additional limits are placed on oxygen and silicon content.

b) Metallurgical Properties

The maximum average grain size is restricted.

4.2.1.2.3.2 Stainless Steel Compression Springs

All stainless steel springs are fabricated in accordance with AMS 5688.

4.2.1.2.4 UO_2 Fuel Pellet Properties

4.2.1.2.4.1 Chemical Composition

Salient points regarding the structure, composition, and properties of the UO_2 fuel pellets are discussed in the following subsections. Where the effect of irradiation on a specific item is considered to be of sufficient importance to warrant reflection in the design or analyses, that effect is also discussed.

a) Chemical analyses are performed for the following constituents:

1) Total Uranium
2) Carbon
3) Nitrogen
4) Fluorine
5) Chlorine and Fluorine
6) Iron
7) Thorium
8) Nickel

b) Limits are placed on the oxygen-to-uranium ratio.

c) The sum of the calcium, aluminum and silicon contents shall not exceed 300 ppm by weight.

d) The sum of the cross sections of the following impurities shall not exceed a specified equivalent thermal neutron capture cross section of natural boron:

1) Boron
2) Silver
3) Cadmium
4) Gadolinium
5) Europium
6) Samarium
7) Dysprosium

e) The total hydrogen content of finished ground pellets is restricted.

f) The nominal enrichment of the fuel pellets will be specified and shall be held within ± 0.05 wt percent U-235.

4.2.1.2.4.2 Microstructures

a) Acceptable porosity distribution will be determined by comparison of approved visual standards with photomicrographs from each pellet lot.

b) The average grain size shall exceed a specified minimum size.

4.2.1.2.4.3 Density

a) The density range of the sintered pellet after grinding shall be 94.5 - 96.5 percent of theoretical density (TD), based on an UO_2 theoretical density of 10.96 g/cm.

b) The in pile stability of the fuel is ensured by the use of an NRC-approved out of pile test during production. The details of this test, and the associated rationale, are presented in Reference 14.

c) The effects of irradiation on the density of sintered UO_2 pellets are discussed in Reference 14.

4.2.1.2.4.4 Thermal Properties

a) Thermal Expansion

The thermal expansion of UO_2 is described by the following temperature dependent equations: [15][16]

$$\% \text{ Linear Expansion} = (-1.723 \times 10^{-2}) + (6.797 \times 10^{-4}T) + (2.896 \times 10^{-7}T^2)$$

from 25C to 2200C

$$\% \text{ Linear Expansion} = 0.204 + (3 \times 10^{-4}T) + (2 \times 10^{-7}T^2) + (10^{-10}T^3)$$

above 2200C.

where T = temperature, C.

b) Thermal Emissivity

A value of 0.85 is used for the thermal emissivity of UO_2 pellets over the temperature range 800 to 2600 K.[17][18][19]

The earlier data on emissivity of UO_2 were those of Claudson and of Ehlert and Margrave, as reported by Belle[70]. Claudson reported that the emissivity decreased from 0.85 at 1000K to 0.37 at 2200K. Ehlert and Margrave measured the spectral emissivity of the polished surface of UO_2 to be approximately 0.40 in the temperature range of 2100-3000K. These determinations were made in the late 1950s by an indirect technique that compared the luminance of a tungsten filament and that of UO_2 at identical test environments. In a subsequent investigation, Cabannes, et. al., (Reference 18) directly measured the reflectance of UO_2 up to 2200K as a function of wavelength. In the visible region, the emissivity increased from 0.86 to 0.94 between 300 and 1600K. At longer wavelengths, the effect of temperature on emissivity was even less, and the value approached 1.0 at a 20 m wavelength. This increase in emissivity with temperature conflicts with the data of Claudson[70] and of Ehlert and Margrave[1] , and a source of error in the technique employed in the earlier work is discussed by Cabannes, et. al. In their opinion, the low luminance of tungsten in the temperature range of the earlier investigations is an important source of error and can easily lead to the discrepancy observed between their data and the data of Claudson and of Ehlert and Margrave.

The most recent determination of emissivity of UO_2 was done by Held and Wilder (Reference 19). Hemispherical spectral emittance of UO_2 pellets was determined in the composition range of $UO_{1.95}$ to $UO_{2.29}$, in the density range of 73 to 97 percent TD and in the temperature range of 450 to 2480K. The emittance was high in all cases and ranged from about 0.7 to 0.95. No decrease in emittance was observed with increasing temperature; instead, it increased slightly. These

authors also reviewed the earlier data and based on mechanistic considerations offered rationale for the relative insensitivity of emittance with temperature as observed in the more recent investigations.

A review of the more recent sources of emissivity data described above thus shows the values of 0.82 to 0.86 at 300K (Reference 17 and 18); 0.86 to 0.94 between 300 and 1600K (Reference 18); and a random scatter of values between 0.70 and 0.95 (Reference 19) for various temperatures (450, 1000, and 1800-2550K), densities and O/U ratios. No definitive trend, therefore, is noticed with variations in temperature, density, O/U ratio or surface finish. Based on these considerations, a value of 0.85 is used for the thermal emissivity of UO_2 pellets over the temperature range of interest of 800 to 2600K.

c) Melting Point and Thermal Conductivity

The fuel temperature required to incur melting is linearly dependent on local burnup as given by:

$$Tmelt = 5080 - [(290)\frac{(Burnup)}{50,000}]$$

where, Tmelt is in °F and burnup is in MWD/MTU. This equation is based on UO_2 melt data given by Reference 69.

The variation of the thermal conductivity of UO_2 with burnup is not explicitly treated, but is implicitly taken from the porosity relationship discussed in Subsection 2.2.5 of Reference 14.

d) Specific Heat of UO_2

The specific heat of UO_2 is described by the following temperature dependent equations.

T < 2240F

$$C_p = 49.67 + 2.2784x10^{-3}\,T - \frac{3.2432x10^6}{(T+460)^2}$$

T ≥ 2240F

$$C_p = -126.07 + 0.2621T - 1.399x10^{-4}\,T^2 + 3.1786x10^{-8}\,T^3 - 2.483x10^{-12}\,T^4$$

where:

C_p = specific heat, BTU/ft^3 – F

T = temperature, F

4.2.1.2.4.5 Mechanical Properties

a) Young's Modulus of Elasticity

The static modulus of elasticity of unirradiated fuel of 97 percent TD and deformed under a strain rate of 0.097 hr^{-1} is given by[21]:

$$E = 14.22\ (1.6715 \times 10^6 - 924.4T)$$

where;

E = modulus of elasticity in psi,
T = temperature in C in the range of 1000 to 1700 C.

b) Poisson's Ratio

The Poisson's Ratio of polycrystalline UO_2 has a value of 0.32 at 25 C based on Reference 66. The same reference notes a 10 percent decrease in value over the range of 25 to 1800 C. Assuming the decrease is linear, the temperature dependence of the Poisson's Ratio is given by

$$v = 0.32 - 1.8 \times 10^{-5}\ (T-25)$$

where;

v = Poisson's Ratio
T = temperature in C in the range of 25 to 1800 C.

At temperature above 1800 C a constant value of 0.29 is used for Poisson's Ratio.

c) Yield Stress (not applicable)

d) Ultimate Stress (not applicable)

e) Uniform Tensile Strain (not applicable)

4.2.1.2.5 Fuel Rod Pressurization

Fuel rods are initially pressurized with helium for two reasons:

a) Preclude clad collapse during the design life of the fuel. The internal pressurization, by reducing stresses from differential pressure extends the time required to produce creep collapse beyond the required service life of the fuel.

b) Improve the thermal conductivity of the pellet to clad gap within the fuel rod. Helium has a higher coefficient of thermal conductivity than the gaseous fission products.

In unpressurized fuel, the initially good helium conductivity is eventually degraded through the addition of the fission product gases released from the pellets. The initial helium pressurization

results in a high helium to fission products ratio over the design life of the fuel with a corresponding increase in the gap conductivity and heat transfer.

The initial helium fill pressure will be 380 ± 15 psig. This initial fill pressure will be sufficient to prevent clad collapse discussed in Subsection 4.2.3.2.8 and will produce a maximum EOL internal pressure consistent with the criteria of Subsection 4.2.1.2.1. The calculational methods employed to generate internal pressure histories are discussed in Reference 14.

4.2.1.2.5.1 Capacity for Fission Gas Inventory

The greater portion of the gaseous fission products remain either within the lattice or the microporosity of the UO_2 fuel pellets and do not contribute to the fuel rod internal pressure. However, a fraction of the fission gas is released from the pellets by diffusion and pore migration and thereafter contributes to the internal pressure.

The determination of the effect of fission gas generated in and released from the pellet column is discussed in Subsection 4.2.3.2.2. The rod pressure increase which results from the release of a given quantity of gas from the fuel pellets depends upon the amount of open void volume available within the fuel rod and the temperatures associated with the various void volumes. In the fuel rod design, the void volumes considered in computing internal pressure are:

a) Fuel rod upper end plenum

b) Fuel clad annulus

c) Fuel pellet end dishes and chamfers

d) Fuel pellet open porosity

These volumes are not constant during the life of the fuel. The model used for computing the available volume as a function of burnup and power level accounts for the effects of fuel and clad thermal expansion, fuel pellet densification, clad creep, clad growth and irradiation induced swelling of the fuel pellets.

4.2.1.2.5.2 Fuel Rod Plenum Design

The fuel rod upper end plenum is required to serve the following functions:

a) Provide space for axial thermal expansion and burnup swelling of the pellet column.

b) Contain the pellet column holddown spring.

c) Act as a plenum region to ensure an acceptable range of fuel rod internal pressure.

Of these functions, listing C is expected to be the most limiting constraint on plenum length selection, since the range of temperatures in the fuel rod, together with the effects of swelling, thermal expansion, and fission gas release can, produce a wide range of internal pressure during the life of the fuel. The fuel rod plenum pressure will be consistent with the pressurization and clad collapse criteria specified in Subsection 4.2.1.2.1. It is not a formal criterion that fuel

rod internal pressure be less than the primary coolant pressure because no adverse effect has been identified which has, as its threshold, the occurrence of a net internal pressure acting on the cladding. However, the design of the fuel rod is such that the internal pressures produced during normal operation are expected to remain below the primary coolant pressure for the design life of the fuel.

4.2.1.2.5.3 Outline of Procedure Used To Size The Fuel Rod Plenum

a) A parametric study of the effects of plenum length on maximum and minimum rod internal pressure is performed. Because the criteria pertaining to maximum and minimum rod internal pressure differ, the study is divided into two sections:

1) Maximum Internal Pressure Calculation

Maximum fuel rod pressure is limited by the stress criteria. Maximum end of life pressure is determined for each plenum length by including the fission gas released, selecting conservative values for component dimensions and properties, and accounting for burnup effects on component dimensions. The primary cladding stress produced by each maximum pressure is then compared to the stress limits to find the margin available with each plenum length. Stress limits are listed in Subsection 4.2.1.2.1.

The effect of helium prepressurization on fission gas release is not considered to be directly due to the gas pressure. The important effects of prepressurization on fission gas release are the improvement in gap gas conductivity and gap conductance and the desensitization of gap conductance to gas release rates. Fuel rods with low helium prepressurization are much more responsive to even small increases in fission gas releases at high burnup. Gap conductance, in such rods significantly decreases, leading to significant increases in fuel temperature which lead to ever increasing fission gas release. This effect is well documented by Reference 1. High prepressurization with helium greatly reduces this feedback effect, and therefore, significantly changes the response of the rod. It must be concluded that an empirical burnup enhancement would be considerably different for low and high helium prepressurizations.

CE is actively seeking and examining sources of gas release data at burnups greater than 20000 MWd/MtU, for use in determining validity or extent of burnup enhanced fission gas release.

Although CE believes the method to be inappropriate, the maximum calculated EOL peak internal fuel rod pressure has been redone using the NRC burnup enhancement factor. Tolerances were biased to maximize internal pressure. Under these conditions the maximum EOL internal pressure is calculated to be less than the nominal primary system pressure.

2) Minimum Internal Pressure/Collapse Calculation

Minimum fuel rod pressure is limited by the criterion that no rod will be subject to collapse during the design lifetime. The minimum pressure history for each plenum length is determined by neglecting fission gas release, selecting a

conservative combination of component dimensions and properties, and accounting for dimension changes during irradiation, including the effects of cladding creep, cladding growth, pellet densification, pellet swelling, and thermal expansion. Each minimum pressure history is input to the cladding collapse model [22] to establish the acceptability of the associated plenum length.

b) For each plenum length, there is a resultant range of acceptable initial fill pressures. The optimum plenum length is generally considered to be the shortest which satisfies all criteria related to maximum and minimum rod internal pressure including a range sufficient to accommodate a reasonable manufacturing tolerance on initial fill pressure.

c) Additional information on those factors which have a bearing on determination of the plenum length are discussed below:

1) Creep and dimensional stability of the fuel rod assembly influence the fission gas release model and internal pressure calculations, and are accounted for in the procedure of sizing the fuel rod plenum length. Creep in the cladding is accounted for in a change in clad inside diameter, which in turn influences the fuel/clad gap. The gap change varies the gap conductance in the FATES computer code[(14)] with resulting change in annulus temperature, internal pressure, and fission gas release. In addition, the change in clad inside diameter causes a change in the internal volume, with its resulting effect on temperature and pressure. Dimensional stability considerations affect the internal volume of the fuel rod, causing changes in internal pressure and temperature. Fuel pellet densification reduces the stack height and pellet diameter. Irradiation induced radial and axial swelling of the fuel pellets decreases the internal volume within the fuel rod. In pile growth of the fuel rod cladding contributes to the internal volume. Axial and radial elastic deformation calculations for the cladding are based on the differential pressure the cladding is exposed to, resulting in internal volume changes.

   Thermal relocation, as well as differential thermal expansion of the fuel rod materials also affect the internal volume of the fuel rods.

2) The maximum expected fission gas release in the peak power rod is calculated using the FATES computer code. Rod power history input to the code is consistent with the design limit peak linear heat rate set by LOCA considerations, and therefore the gas release used to size the plenum represents an upper limit. Because of time varying gap conductance, fuel temperature and depletion, and expected fuel management, the release rate varies as a function of burnup.

4.2.1.2.6 Fuel Rod Performance

Steady state fuel temperatures are determined by the FATES computer program. The calculational procedure considers the effect of linear heat rate, fuel relocation, fuel swelling, densification, thermal expansion, fission gas release and clad deformations. The model for predicting fuel thermal performance, including the specific effects of fuel densification on increased linear heat generation rate (LHGR) and stored energy, is discussed in Reference 14.

Significant parameters such as cold pellet and clad diameters, gas pressure and composition, burnup and void volumes are calculated and used as initial conditions for subsequent calculations for stored energy during the Emergency Core Cooling System (ECCS) analysis. The coupling mechanism between FATES calculations and the ECCS analysis is described in detail in Reference 23.

Discussions of uncertainties associated with the model, and of comparative analytical and experimental results, are also included in Reference 14.

4.2.1.3 Burnable Poison Rod

4.2.1.3.1 Burnable Poison Rod Cladding Design Limits

The burnable poison rod design accounts for external pressure, differential expansion of pellets and clad, pellet swelling, clad creep, helium gas release, initial internal helium pressure, thermal stress, and flow induced vibrations. Except where specifically noted, the design bases presented in this section are consistent with those used for previous designs. The structural criteria for the normal, upset and emergency loading combinations identified in Subsection 4 2.1.1 are as follows:

a) During normal operating and upset conditions (Conditions I and II), the maximum primary tensile stress in the Zircaloy clad shall not exceed two-thirds of the minimum unirradiated yield strength of the material at the applicable temperature. The corresponding limit under emergency conditions (Condition III) is the material yield strength.

b) Net unrecoverable circumferential strain shall not exceed one percent as predicted by computations considering clad creep and poison pellet swelling effects.

c) The clad will be initially pressurized with helium to an amount sufficient to prevent gross clad deformation under the combined effects of external pressure and long term creep. The clad design will not rely on the support of pellets or the holddown spring to prevent gross deformation.

4.2.1.3.2 Burnable Poison Rod Cladding Properties

Cladding tubes for burnable poison rods are purchased under the specification for fuel rod cladding tubes. Therefore, the mechanical, metallurgical, chemical, and dimensional properties of the cladding are as discussed in Subsection 4.2.1.2.2.

4.2.1.3.3 Al_2O_3-B_4C Burnable Poison Pellet Properties

The Al_2O_3-B_4C burnable poison pellets used in CE designed reactors consist of a relatively small volume fraction of fine B_4C particles dispersed in a continuous Al_2O_3 matrix. The boron loading is varied by adjusting the B_4C concentration in the range from 0.7 to 4.0 wt% (1 to 6.0 v/o). The bulk density of the Al_2O_3-B_4C pellets is specified to be greater than 93 percent of the calculated theoretical density. Typical pellets have a bulk density of about 95 percent of theoretical. Many properties of the two-phase Al_2O_3 -B_4C mixture, such as thermal expansion, thermal conductivity, and specific heat are very similar to the properties of the Al_2O_3 major constituent. In contrast, properties such as swelling helium release, melting point, and corrosion

are dependent on the presence of B_4C. The operating centerline temperature of burnable poison is less than 1150 F, with maximum pellet surface temperatures close to 1090 F.

4.2.1.3.3.1 Thermal-Physical Properties

a) Thermal Expansion

The mean thermal expansion coefficients of Al^2O^3[24] and B_4C[25] from 0 to 1850 F are 4.9 and 2.5 in./in. F x 10^{-6}, respectively. The thermal expansion of the Al_2O_3-B_4C two-phase mixture can be considered to be essentially the same as the value for the continuous Al_2O_3 matrix since the dispersed B_4C phase has a lower expansion coefficient and occupies only 5 v/o of the available volume. The low temperature (80 to 250 F) thermal expansion coefficient of Al_2O_3 irradiated at 480, 900 and 1300 F does not change as a result of irradiation.[26] The expansion of a similar material, beryllium oxide, up to 1900 F has also been reported to be relatively unchanged by irradiation.[27] It is therefore appropriate to use the values of thermal expansion measured for Al_2O_3 [24] for the burnable poison pellets:

Temperature Range (F from 70 F to)	Linear Expansion (%)
400	0.12
600	0.23
800	0.30
1000	0.40

b) Melting Point

The melting points of Al_2O_3(3710 F)[28] and B_4C (4400 F)[29] are higher than the melting point of the Zircaloy-4 cladding. As B_4C burns up, the lithium atoms formed occupy interstitial sites randomly distributed within the B_4C lattice, rather than forming a lithium rich phase.[30] The solid solution of lithium in B_4C should not appreciably influence the melting point of the Al_2O_3 -B_4C pellets, as only a small quantity of lithium compounds (0.5 wt%) forms during irradiation. It is concluded that the melting point of Al_2O_3 -B_4C will remain considerably above the maximum 1150 F operating temperature.

c) Thermal Conductivity

The thermal conductivity of Al_2O_3-B_4C was calculated from the measured values for Al_2O_3 and B_4C using the Maxwell-Eucken relationship[31] for a continuous matrix phase (Al_2O_3) with spherical dispersed phase (B_4C) particles. Because of the high Al_2O_3 content of these mixtures and the similarity in thermal conductivity, the resultant values for Al_2O_3-B_4C were essentially the same as the values for Al_2O_3. The measured, unirradiated values of thermal conductivity at 750 F are 0.06 cal/s-cm-k for B_4C and 0.05 cal/s-cm-k for Al_2O_3.

The thermal conductivity of Al_2O_3 after irradiation decreases rapidly as a function of burnup to values of about one-third the unirradiated values.[26] The irradiated values of Al_2O_3-B_4C calculated from the above relationships are given below as a function of temperatures.[26][32]

Temperature (F)	Thermal Conductivity (cal/s-cm-k)
400	0.015
600	0.013
800	0.010
1000	0.008

d) Specific Heat

The specific heat of the Al_2O_3 -B_4C mixture can be taken to be essentially the same as pure Al_2O_3 since the concentration of B_4C is low (6.0 v/o maximum). In addition, the effect of irradiation on specific heat is expected to be small based on experimental evidence from similar materials which do not sustain transmutations as a function of neutron exposure.

The properties of specific heat and thermal expansion are closely related as they both increase with temperature (at expected operating temperatures < 1000F) primarily due to increases in lattice vibrations.[71] That is, changes in specific heat with temperature have been shown to be primarily due to the same physical processes as changes in thermal expansion with materials such as Al_2O_3 and BeO. The conclusion that the effect of irradiation on the specific heat of Al_2O_3-B_4C is small is based on measurements which show that the specific heat of BeO does not change with irradiation[72], and measurements that show the thermal expansion coefficient of Al_2O_3 does not change[73] due to irradiation. Since measurements of the thermal expansion coefficient of irradiated Al_2O_3 have shown no change due to irradiation and since specific heat and thermal expansion are both dependent upon lattice vibrations, it is expected that specific heat is also not significantly affected by irradiation.

The specific heat of the Al_2O_3-B_4C mixture can be taken to be essentially the same as Al_2O_3 since the concentration of B_4C is a maximum of 3.7 w/o B_4C, and the specific heat of B_4C at operating temperature is close to the value of Al_2O_3.

The Debye temperature of Al_2O_3 determined by measurement is about 904°K. There is no effect of the B_4C particles in the Al_2O_3 matrix on the Debye temperature.

The values for Al_2O_3 measured on unirradiated samples[35][36] are given below:

Temperature (F)	Cal/gm-F
250	0.12
450	0.13
800	0.14
1000 and above	0.15

4.2.1.3.3.2 Irradiation Properties

a) Swelling

Al_2O_3-B_4C consists of B_4C particles dispersed in a continuous Al_2O_3 matrix, which occupies more than 95 percent of the poison pellet. The swelling of Al_2O_3-B_4C depends primarily upon the neutron fluence on the continuous Al_2O_3 matrix and, secondarily, on the B^{10} burnup of the dispersed B_4C phase. Recent measurements performed on material containing about two wt% B_4C irradiated in a CE PWR to 100 percent B^{10} burnup at a fluence of 2.4 x 10^{21} nvt (E.>0.8 MeV) revealed a diametral swelling of about one percent. Pellets similar to the burnable poison used in CE reactors with up to three wt% B_4C also sustained about 100 percent B^{10} burnup. Experimental data(34) on Al_2O_3 reveal a diametral swelling of about 0.7 percent at a fluence of 2.4 x 10^{21} nvt (E>0.8 MeV). Swelling of Al_2O_3 increases linearly with fluence to 1.8 percent diametral after an exposure of 6 x 10^{21} nvt (E>0.8 MeV).

These data show that Al_2O_3-B_4C swells somewhat more than Al_2O_3 up to a burnup of 90 percent B_4C (about 2 x 10^{21} nvt, E > 0.8 MeV).

The CE design value of Al_2O_3-B_4C swelling rate for fluences less than 2 x 10^{21} is greater than the swelling rate of Al_2O_3, while after 2 x 10^{21} fluence the swelling rate for Al_2O_3-B_4C is considered equal to that of Al_2O_3.

The data and considerations presented above result in best estimate diametral swelling values at end of life (7 x 10^{21} nvt, E > 0.8 MeV) of about two percent for Al_2O_3 and from two to three percent for Al_2O_3-B_4C loading.

b) Helium Release

Experimental measurements reveal that less than five percent of helium formed during irradiation will be released.(35) These measurements were performed on Al_2O_3-B_4C pellets irradiated at temperatures to 500 F and, subsequently, annealed at 1000 F for five days. The helium release in a burnable poison rod which operated for one cycle in a CE PWR was calculated from internal pressure measurements to be less than five percent.

Review of experimental data and an analysis have shown that the maximum helium release for the St. Lucie Unit 2 poison rods will be less than nine percent. For a helium release of nine percent, the steady-state internal rod pressure remains less than system (coolant) pressure. The acceptance criterion for the clad for all pressure evaluations are those specified in Subsection 4.2.1.1(a).

4.2.1.3.3.3 Chemical Properties

a) Al_2O_3-B_4C Coolant Reaction

Should irradiated B_4C particles be exposed to reactor coolant, the primary corrosion products that would be formed are boric acid (which is soluble in water), hydrogen, free carbon and a small amount of lithium compounds. The

presence of these products in the reactor coolant would not be detrimental to the operation of the plant.

Observations of Al_2O_3/B_4C poison shims have revealed that long term exposure of this material to reactor coolant can result in gradual leaking out of Boron and eventual eroding away of the Al_2O_3 matrix. However, the rate of reaction is such that any resultant changes in reactivity are very gradual.

b) Chemical Capability

Chemical compatibility between the Al_2O_3-B_4C pellets and the burnable poison rod cladding during long term normal operation has been demonstrated by examination of a burnable poison rod from the Maine Yankee reactor. The rod had been exposed to an axial average fluence in excess of 2×10^{21} nvt (>0.821 Mev). No evidence of a chemical reaction was observed on the cladding I.D.

Short term chemical compatibility during upset and emergency conditions is demonstrated by the fact that conditions favorable to a chemical reaction between Zircaloy-4 and Al_2O_3 are not present at temperatures below 1300 F[36]. This temperature is higher than that which will occur at burnable poison pellet surfaces during Condition II and III occurrences (Subsection 4.2.1.1). The reaction between Zircaloy-4 and Al_2O_3 described by Idaho Nuclear[37] was observed to occur rapidly only at temperatures in excess of 2500F, well above the peak Zircaloy-4 temperatures expected.

4.2.1.4 Control Element Assemblies

Except where specifically noted, the design bases presented in this section are consistent with those used for previous designs.

The mechanical design of the control element assemblies is based on compliance with the following functional requirements and criteria:

a) To provide for or initiate short-term reactivity control under all normal and adverse conditions experienced during reactor startup, normal operation, shutdown, and accident conditions.

b) Mechanical clearances of the CEA within the fuel and reactor internals are such that the requirements for CEA positioning and reactor trip are attained under the most adverse accumulation of tolerances.

c) Structural material characteristics are such that irradiation induced changes to the CEA materials will not impair the functions of the reactivity control system.

4.2.1.4.1 Thermal-Physical Properties of Absorber Material

The primary control rod absorber materials consist of boron carbide pellets (B_4C) and silver indium cadmium bars (Ag-In-Cd). Refer to Figures 4.2-3 and 4.2-4 for the specific application and orientation of the absorber materials. The significant thermal and physical properties used in mechanical analysis of the absorber materials are listed in Table 4.2-2.

4.2.1.4.2 Compatibility of Absorber and Cladding Materials

The cladding material used for the control elements is Inconel Alloy 625. The selection of this material for use as cladding is based on consideration of strength, creep resistance, corrosion resistance and dimensional stability under irradiation and also upon the acceptable performance of this material for this application in other CE reactors currently in operation.

a) B_4C /Inconel 625 Compatibility

Studies have been conducted by HEDL[38] on the compatibility of Type 316 stainless steel with B_4C, under irradiation for thousands of hours at temperatures between 1300 and 1600 F. Carbide formation to a depth of about 0.004 inch in the 316 stainless steel was measured after 4400 hours at 1300 F. Similar compound formation depths were observed after ex-reactor bench testing. After testing at 1000 F, only 0.001 in./yr of penetration was measured. Since Inconel 625 is more resistant to carbide formation than 316 stainless steel, and the expected pellet/clad interfacial temperature in the standard design is below 800 F, it is concluded that B_4C is compatible with Inconel 625.

4.2.1.4.3 Cladding Stress-Strain Limits

The stress limits for the Inconel Alloy 625 cladding are as follows:

Design Conditions I and II (Non Operation, Normal Operation, and Upset Conditions)

$P_m \leq S_m$

$P_m + Pb \leq F_s S_m$

Design Conditions III (Emergency Conditions)

$P_m \leq 1.5\ S_m$

$P_m + P_b \leq 1.5\ F_s S_m$

Design Conditions IV (Faulted Conditions)

$P_m \leq S'_m$

$P_m + P_b \leq F_s S'_m$

where S'_m is the smaller of 2.4 S_m or $0.7S_u$

For definition of P_m, P_b, S_m, S'_m, S_u, and F_s, see Subsection 4.2.1.1.1. For the Inconel 625 CEA cladding, the value of S_m is two-thirds of the minimum specified yield strength at temperature.

For Inconel 625, the specified minimum yield strength is 65,000 lb/in.^{2} at 650 F.

F_s = Mp/My where Mp is the bending moment required to produce a fully plastic section and My is the bending moment which first produces yielding at the extreme fibers of the cross section. The capability of cross sections loaded in bending to sustain moments considerably in excess of

that required to yield the outermost fiber is discussed in Reference 1. For the CEA cladding dimensions, F_s = 1.33.

The strain limits for the cladding are limited to values which will permit the CEAs to trip within the allowable time.

The net unrecoverable circumferential strain shall not exceed one percent on the CEA clad (Inconel Alloy 625) considering the effects of pellet swelling and clad creep.

The values of uniform and total elongation of Inconel Alloy 625 cladding are estimated to be as follows:

Fluence (E > 1 MeV), nvt	1×10^{22}	3×10^{22}
Uniform elongation, %	3	1
Total elongation, %	6	3

4.2.1.4.4 Irradiation Behavior of Absorber Materials

a) Boron Carbide Properties

1) Swelling: The linear swelling of B_4C increases with burnup according to the relationship:

$\%\Delta L = (0.1)\ B^{10}$ Burnup, a/o

This relationship was obtained from experimental irradiations on high density (>90 percent TD) wafers[39] and pellets with densities ranging between 71 and 98 percent TD.[38][40] Dimensional changes were measured as a function of burnup, after irradiating at temperature expected in the design.

2) Thermal Conductivity: The thermal conductivity of unirradiated 73 percent dense B_4C decreases linearly with temperatures from 300 to 1600 F, according to the relationship:

$$\lambda = \frac{1\ cal/cm\text{ - }K\text{ - }s}{2.17\ (6.87 + 0.017\ T)}$$

This relationship was obtained from measurements performed on pellets ranging from 70 to 98 percent TD.

The relationship between the thermal conductivity of irradiated 73 percent TD B_4C pellets and temperature given below was derived from measured values[41] on higher density pellets irradiated to fluences out to 3×10^{22} nvt (E > 1 MeV).

$$\lambda = \frac{1\ cal/cm\text{ - }K\text{ - }s}{2.17\ (38 + 0.025\ T)}$$

where T = temperature, K

Thermal conductivity measurements of 17 B_4C specimens with densities ranging from 83 to 98 percent TD, irradiated at temperatures from 930 to 1600 F showed that thermal conductivity decreased significantly after irradiation. The rate of decrease is high at the lower irradiation temperature, but saturates rapidly with exposure.

3) Helium Release: Helium is formed in B_4C as B^{10} burnup progresses. The fraction of helium released from the pellets is important for determining rod internal gas pressure. The relationship between helium release and irradiation temperature given below was developed at ORNL[42] to fit experimental data obtained from thermal reactor irradiations.

$$\% \text{ He release} = e^{(C-185D)} e^{\frac{-Q}{RT}}$$

where:

C = Constant, 6.69 for CE pellets
D = Fractional density, 0.73 for CE pellets
Q = Activation energy constant, 3600 cal/mole
R = Gas constant, 1.98 cal/mole K
T = Pellet temperature, K

This expression becomes

$$\% \text{ He release} = 208\, e^{\frac{-1820}{T}} + 5$$

when the above parameters are substituted. In this form, design values for helium release as a function of temperature are generated. The five percent helium release allowance (the last term in the expression) was added to ensure that design values lie above all reported helium release data. Calculated values of helium release obtained from the recommended design expression lie above all experimental data points[38][43][44] obtained on B_4C pellet specimens irradiated in thermal reactors.

4) Pellet Porosity: Experimental evidence is available[45] which shows that for pellet densities below 90 percent, essentially all porosity is open at beginning of life. Irradiation induced swelling does not change the characteristics of the porosity, but only changes the bulk volume of the specimens. Therefore, the amount of porosity available at end of life is the same as that present at beginning of life.

b) Inconel 625

1) Swelling: Available information indicates that Inconel 625 is highly resistant to radiation swelling. Exposure of Inconel 625 to a fluence of 3 x 10^{22} nvt (E > 0.1 Mev) at a temperature of 400C (725F) showed no visible cavities in metallographic examinations[48] so that swelling, if any, would be very minor. Direct measurements made after exposure of Inconel 625 to a fluence 5 x 10^{22} nvt (E > 0.1 Mev) as LMFBR conditions showed no evidence of swelling.[49] Further exposure to 6 x 10^{22} nvt (E > 0.1 MeV) at 500 C (932 F) showed

essentially no swelling as measured by immersion density, but did show small cavities. Thus, Inconel 625 after fluences of 3 x 10^{22} nvt (E > 1 Mev) is not expected to swell.

2) Ductility: The ductility of Inconel 625 decreases after irradiation. Extrapolation of lower fluence data on Inconel 625 and 500 indicates that the values of uniform and total elongation of Inconel 625 after 1 x 10^{22} nvt (E > 1 MeV) are three and six percent, respectively.

3) Strength: The value of yield strength of Inconel 625 increases after irradiation in the manner typical for metals. However, no credit is taken for increases in yield strength in the design analyses above the value initially specified.

c) Silver-Indium-Cadmium Properties

1) Swelling: Measurements performed on Ag-In-Cd rods irradiated at fluences up to 6.2 x 10^{21} nvt (E > 0.6 MeV) were employed to develop the following expression to predict the volumetric swelling for silver-indium-cadmium alloy:

$$\%\Delta V = \frac{0.3\phi}{10^{21}}$$

where φ = fluence, nvt (E > 0.6 MeV).

Linear swelling is approximately one third of the volumetric swelling.

2) Thermal Conductivity: The increase in cadmium content from five to perhaps ten wt percent, and the formation of two to three wt percent tin as a result of long-term exposures, is expected to decrease the thermal conductivity from the accepted [46] unirradiated values. Published data for unirradiated Ag-Cd binary alloys shows that thermal conductivity was decreased by about 20 percent by increasing the cadmium content from 5.0 to 10.0 wt percent.[46] Since irradiated Ag-In-Cd is expected to perform in much the same fashion, similarly, the unirradiated values of thermal conductivity are decreased by 25 percent to account for irradiation.

3) Linear Thermal Expansion: The coefficient of linear thermal expansion for unirradiated Ag-In-Cd material is 12.5 x 10^{6} in/in. F over the temperature range of 70 to 930F.[47] Published data on unirradiated [46] Ag-Cd binary alloys reveal that a cadmium increase of five percent will result in about a five percent increase in thermal expansion coefficient. The small changes in indium and tin content do not influence the thermal expansion coefficient appreciably. For simplicity, irradiated values of 13.1 x 10^{-6} in./in.-F is used in all design calculations.

4) Melting Point: The melting point of unirradiated Ag-In-Cd has been measured as 1470 F ± 30°F [46] (800C ± 17C). The formation of three wt percent tin due to the transmutation of indium and the increase in cadmium content to about 10 wt percent due to the transmutation of silver may result in a small decrease in the melting point.

4.2.1.5 Surveillance Program

4.2.1.5.1 Requirements for Surveillance and Testing of Irradiated Fuel Rods

High burnup performance experience, as described in Subsection 4.2.3 has provided evidence that the fuel will perform satisfactorily under design conditions. The current core design bases do not include a specific requirement for testing of irradiated fuel rods. However, the fuel assembly design allows disassembly and reassembly to facilitate such inspections, should the need arise.

A fuel rod irradiation program has been developed to evaluate the performance of fuel rods designed for use in the 16 x 16 fuel assembly. The program includes the irradiation of six standard 16 x 16 assemblies, two each for 1, 2, and 3 cycles, respectively, in the Arkansas Nuclear One-Unit 2 reactor (AN0-2). Each assembly will contain a minimum of 50 precharacterized, removable rods distributed within the assembly to obtain a spectrum of exposure levels for evaluation purposes in the interim and terminal examinations. Interim examination of all six assemblies is planned during refueling shutdowns after each cycle.

The ANO-2 fuel rods and specific components of the fuel rods have received a detailed pre-characterization. The program calls for substantial cladding characterization to include mechanical properties, texture, hydride orientation and out of reactor low strain rate behavior. In addition to the ID and OD dimensional data normally obtained on the clad tubing material, a minimum of 300 fuel rods will be measured to obtain as loaded dimensions. Sufficient fuel rods will be profiled to obtain diameter and ovality measurements such that changes in these parameters can be tracked by similar measurements during interim inspections. Also, a random selection of approximately 100 UO_2 pellets from each lot per batch used will be characterized dimensionally and the density distribution will be determined. About one half of these pellets will be placed in known axial locations in selected fuel rods while the remainder will be set aside as archives.

A poolside non-destructive examination will be made during each of the first three refuelings at AN0-2. The six 16 x 16 assemblies with characterized rods will be removed from the reactor at each refueling and moved to the spent fuel pool for leak testing (if failed fuel is in the core) and for visual inspection. The length of the assembly and peripheral rods will be measured. During the shutdown, a target of 20 pre-characterized rods per batch will be scheduled for examination and measurement. At some time after the refueling outage, pre-characterized rods retained in discharged assemblies will be measured. A target of 100 rods will be eddy current tested after each shutdown.

A post irradiation fuel surveillance program for St. Lucie Unit 2 is planned. This program shall consist of visual inspection of a minimum of six irradiated assemblies prior to replacement of the Reactor Vessel Head at each of the first three refueling outages. The six assemblies inspected shall consist of two assemblies of each fuel type and will be from core locations which are non adjacent. Visual inspections shall consist of viewing the top and sides of each fuel assembly via an underwater TV camera or periscope.

The visual inspection will include observation with special attention to gross problems involving cladding defects, spacer grid damage and other major structural abnormalities. No special measurement devices for these affects are intended to be provided for this visual inspection.

If major abnormalities are detected during this visual inspection or if plant instrumentation indicates gross fuel failures, the fuel vendor will be informed and further inspections shall be performed, depending on the particular condition observed. The 16 x 16 fuel design enables reconstitution. Individual fuel rods and other structural components could be examined and replaced, if required.

The NRC shall be contacted regarding gross fuel failure detected by plant instrumentation or major abnormalities observed during the post irradiation inspections described above.

4.2.1.6 AREVA CE-16 HTP™ Fuel

Beginning with Cycle 23, the feed fuel is of the AREVA CE-16 HTP™ fuel design. The AREVA CE-16 HTP™ fuel consists of a 16x16 assembly configuration with M5® clad fuel rods, Zircaloy-4 MONOBLOC™ Corner Guide tubes, an Alloy 718 HMP™ spacer at the lowermost axial elevation, Zircaloy-4 HTP™ spacers in all other axial elevations, a FUELGUARD™ lower tie plate, and the AREVA reconstitutable upper tie plate. See Section 4.2.2.6 and Table 4.2-10 for AREVA fuel design details.

The mechanical design criteria for the AREVA CE-16 HTP™ fuel is performed in accordance with the USRNC-approved generic mechanical design criteria in EMF-92-116(P)(A) (References 96 and 97) in conjunction with the USNRC-approved topical report BAW-10240(P)(A) (Reference 98). Reference 98 incorporates the M5® cladding material properties that were previously approved by the USNRC in BAW-10227(P)(A) (Reference 99) into the AREVA mechanical design methodology. All mechanical design criteria are analyzed to meet the licensed fuel rod burnup limit of 62 MWd/kgU.

4.2.1.6.1 Fuel Assembly Design Bases

EC287528

- Structural Design

  The structural integrity of the fuel assemblies is assured by setting design limits on stresses and deformations due to various handling, operational, and accident loads. These limits are applied to the design and evaluation of upper and lower tie plates, spacer grids, guide tubes, holddown (reaction) springs, and locking hardware. The design bases for evaluating the structural integrity of the fuel assemblies are:

  a. Fuel Assembly Handling – Axial loads approximately 2.5 times the assembly weight.

  b. For all applied loads for normal operation and anticipated operational events - The fuel assembly component structural design criteria are established for the two primary material categories, austenitic stainless steels (tie plates) and Zircaloy (guide tubes and spacer grids). The stress categories and strength theory for austenitic stainless steel presented in the ASME Boiler and Pressure Vessel Code, Section III are used as a general guide.

  c) Loads during postulated accidents - Deflections or failure of components shall not interfere with reactor shutdown or emergency cooling of the fuel rods.

d) The fuel assembly structural component stresses under faulted conditions are evaluated using primarily the methods outlined in Appendix F of the ASME Boiler and Pressure Vessel Code, Section III.

- Fuel Rod and Assembly Growth

  The design basis for fuel rod and assembly growth is that adequate clearance shall be provided to prevent any interference which might lead to buckling or damage. Cladding and guide tube growth measurements of AREVA fuel are used in establishing the growth correlations used for calculations.

- Assembly Holddown

  The design basis for fuel assembly holddown is that the holddown (reaction) springs, as compressed by the fuel alignment plate during reactor operation, will provide a net positive downward force during steady-state operation, based on the most adverse combination of component dimensional and material property tolerances. In addition, the holddown springs are designed to accommodate the additional load associated with a flow increase transient (resulting in possible temporary uplift of the fuel assemblies), and to continue to ensure fuel assembly holddown following such an occurrence. The holddown system is also designed to assure positive holddown during pump start up under worst case flow conditions. EC287528

- Mechanical Compatibility

  The design basis for fuel assembly mechanical compatibility is that fuel assembly will have acceptable interface with plant equipment, core structures, control components, and the handling equipment through-out the design life of the fuel.

4.2.1.6.2 Fuel Rod

The fuel rod design features M5® cladding. The M5® Zirconium-alloy cladding material provides substantial margin for end of life corrosion and hydrogen content due to its very low corrosion and hydrogen pickup rate. The material has been generically reviewed and accepted by the United States Nuclear Regulatory Commission (USNRC) for use on CE fuel designs (Reference 98). The fuel rod design includes uranium dioxide fuel rods and Gadolinia bearing uranium dioxide fuel rods up to 8 w/o gadolinia concentrations (Reference 98), both with axial blankets of lower enriched uranium dioxide. Multiple uranium-235 enrichments are used within an assembly.

The fuel rod design accounts for external pressure, differential expansion of fuel and clad, fuel swelling, clad creep, fission and other gas release, initial helium pressure, thermal stress, pressure and temperature cycling and flow induced vibration. The fuel rod generic criteria based on the methodologies discussed in References 96 through 98 are provided in Section 4.2.3.5.2.

4.2.2 MECHANICAL DESIGN DESCRIPTION

This subsection summarizes the mechanical design characteristics of the fuel system and discusses the design parameters which are of significance to the performance of the reactor. A summary of mechanical design parameters for Cycle 1 is presented in Table 4.2-1. These data are intended to be descriptive of the design; limiting values of these and other parameters are

discussed in the appropriate sections. For current cycle data, see Table 4.2-10. Figures 4.2-6 and 4.2-8 show current cycle configurations for fuel assembly and fuel rods.

Beginning with Cycle 23, the feed fuel is of the AREVA CE-16 HTP™ fuel design. See Section 4.2.2.6 for the Mechanical Design Description related to this fuel design. EC287528

4.2.2.1 Fuel Assembly

The mechanical design for the Region G reload fuel is the same as that of the Region F fuel, used in St. Lucie Unit 2 Cycle 4 and described in the Reload Safety Evaluation Report of Cycle 4 Reference 81 with the exception of a minor lower end fitting change and the incorporation of a debris-resistant pin design feature. The debris-resistant design modification shifts the fuel and burnable absorber column axially upward so that debris caught by the Inconel grid interacts with a lengthened solid lower end cap instead of the fuel rod and burnable absorber rod cladding. The specific changes in the fuel design through Region M are the following:

1) Increase the overall axial length of the fuel pin by 0.70 inches, the burnable absorber pin by 0.90 inches, and the guide-tube by 0.70 inches.

2) Lengthen the lower end cap such that the end cap-to-cladding weld is below the spring at the center of the Inconel grid and above the arch at the bottom of the grid.

3) Shorten the lower end fitting by 0.70 inches, from 3.812 inches to 3.112 inches, also, move T" stanchions inward by 0.030 inches. The resulting possible encroachment on portions of the chamfers of 32 flow holes is made optionally acceptable (References 82 and 83).

4) Change the guide-tube-to-lower-end-fitting connection to accommodate the 0.70 inch reduction in lower end fitting height.

5) Reduce the height of the fuel pin plenum region by 2.03 inches, from 7.858 inches to 5.829 inches, and the burnable absorber pin plenum region by 1.83 inches, from 9.472 inches to 7.642 inches.

6) Incorporate a fuel rod plenum spring which occupies 14% of the total plenum volume (i.e., volume without the spring), compared to a plenum spring which occupied 25% of the total plenum volume for the Region F fuel.

7) Incorporate a burnable absorber rod plenum spring which occupies 5.0% of the total plenum volume (i.e., volume without the spring), compared to a plenum spring which occupied 8.8% of the total plenum volume for the Region F fuel.

The fuel assembly (Figures 4.2-6 and 4.2-13) consists of 236 fuel and poison rods, five guide tubes, 10 fuel rod spacer grids, upper and lower end fittings, and a holddown device. The outer guide tubes, spacer grids, and end fittings form the structural frame of the assembly.

The fuel spacer grids (Figure 4.2-7) are of HID-1 design (High Impact Design). They maintain the fuel rod array by providing positive lateral restraint to the fuel rod but only frictional restraint to axial fuel rod motion. The grids are fabricated from preformed Zircaloy or Inconel strips (the

bottom spacer grid material is Inconel and beginning with Region U the top grid) interlocked in an egg crate fashion and welded together. Each cell of the spacer grid contains two leaf springs and four arches. The leaf springs press the rod against the arches to restrict relative motion between the grids and the fuel rods. The perimeter strips contain features designed to prevent hangup of grids during a refueling operation.

The Zircaloy-4 spacer grids are fastened to the Zircaloy-4 guide tubes by welding, and each grid is welded to each guide tube at eight locations, four on the upper face of the grid and four on the lower face of the grid, where the spacer strips contact the guide tube surface. The lowest spacer grid (Inconel) is not welded to the guide tubes due to material differences. It is supported by an Inconel 625 skirt which is welded to the spacer grid and to the perimeter of the lower end fitting. Beginning with Region U, the top grid is Inconel. It is secured in place by ten split sleeves positioned above and below the grid. The split sleeves are welded to the guide tubes.

Specific changes in the fuel design beginning with Region N are as follows:

(See Figures 4.2-6, 4.2-8, 4.2-9, 4.2-9a & 4.2-9b)

1) The bottom spacer grid is the laser welded Guardian straight-strip design, which is a change from the previous wavy-strip Inconel TIG welded grid.

2) The lower end cap has a different design which allows it to be used in combination with the Guardian grid.

3) The upper spacer disc, which separates the pellet from the upper spring, has been removed.

4) The plenum spring design has been modified to accommodate a larger plenum length.

5) The fuel rod pellet diameter has been increased 0.0005 inches, the pellet dish volume has been reduced approximately 60%, and the pellet nominal UO_2 density has been increased from 95.25% to 95.5% of theoretical density.

6) The guide tube (GT)/lower end fitting (LEF) joint bolt and thread length have been reduced.

7) The top spacer grid design contains backup arches in all interior cells as compared to the previous design, which only contains these backup arches in peripheral locations.

8) Modifications to the upper end fitting include i) slightly thicker flow and holddown plates, ii) increased fuel assembly spring force, iii) improved chrome plating of the post, and iv) increased center post counterbore.

Specific changes in the fuel design beginning with Region U are as follows:

1) The top spacer grid is a welded Inconel 625 grid. Like the recent Zircaloy grid that it replaces, the Inconel grid has back-up arches in all cells to limit spring deflection during rod loading as well as during refueling. Inconel material relaxes

less than Zircaloy during operation and therefore provides more positive grid-to-rod interaction and enhanced resistance to fretting at this top location.

2) The Inconel top grid is secured to the guide tubes by ten Zircaloy-4 split sleeves that are positioned above and below the grid and welded to the Zircaloy-4 guide tubes.

3) The components of the upper end fitting (see Figure 4.2-6) have been modified to allow for additional fuel skeleton length change (growth) that results from sustained grid-to-rod contact at the Inconel top grid. These modifications include a change in the thickness of the flow plate, redesigned spring to increase assembly holddown force, and adjusting the length of the upper end fitting guide posts.

The Region P fuel design is used as the basis for the identification of changes in the Region R fuel design. The Region P fuel was fabricated by ABB CE prior to the acquisition of ABB CE by Westinghouse.

Prior to Batch R, fuel assembly component and subassembly production were performed at the Windsor, CT, manufacturing facility while pelletization and rod and bundle assembly were performed at the Hematite, MO, manufacturing facility. For reload fuel assemblies beginning with Batch R, urania pellets, fuel rods and fuel bundles will be assembled at Columbia, SC. Component and subassembly production will continue to be performed in Windsor.

The integration of the CE design into the Columbia fabrication process necessitated design changes. In addition, there are differences in the fabrication processes used at Columbia. Many of these changes are generic in nature and are generally applicable to all CE designs.

Design changes associated with the Batch R fuel are described in Sections 4.2.2.2 and 4.2.4.2.

The upper end fitting is an assembly consisting of two cast 304 stainless steel plates, five machined posts and five helical Inconel X-750 springs, which attach to the guide tubes to serve as an alignment and locating device for each fuel assembly and has features to permit lifting of the fuel assembly The lower cast plate locates the top ends of the guide tubes and is designed to prevent excessive axial motion of the fuel rods.

The Inconel X-750 springs are of conventional coil design having a mean diameter of 1 746 in , a wire diameter of 201 in , and 8.2 active coils Inconel X-750 was selected for this application because of its previous use for coil springs and good resistance to relaxation during operation.

The upper cast plate of the assembly, called the hold-down plate, together with the helical compression springs, comprise the holddown device. The holddown plate is movable, acts on the underside of the fuel alignment plate and is loaded by the compression springs. Since the springs are located at the upper end of the assembly, the spring load combines with the fuel assembly weight to counteract upward hydraulic forces. The determination of upward hydraulic forces includes factors accounting for flow maldistribution, fuel assembly component tolerances, crud buildup, drag coefficient and bypass flow. The springs are sized and the spring preload selected such that a net downward force is maintained for all normal and anticipated transient flow and temperature conditions. The design criteria limit the maximum stress under the most adverse tolerance conditions to below yield strength of the spring material. The maximum stress occurs during cold conditions and decreases as the reactor heats up. The reduction in stress is

due to a decrease in spring deflection resulting from differential thermal expansion between the Zircaloy fuel bundles and the stainless steel internals.

During normal operation, a spring is never compressed to its solid height. However, if the fuel assembly is loaded in an abnormal manner such that a spring is compressed to its solid height, the spring would continue to serve its function when the loading condition returned to normal.

The lower end fitting is a stainless steel casting consisting of a plate with flow holes and four support legs which also serve as alignment posts. Precision drilled holes in the support legs mate with four core support plate alignment pins, thereby properly locating the lower end of the fuel assembly.

The four outer guide tubes have a widened region at the upper end which contains an internal thread. Connection with the upper end fitting is made by passing the externally threaded end of the guide posts through holes in the lower cast flow plate and into the guide tubes. When assembled, the flow plate is secured between flanges on the guide tubes and on the guide posts. On some Batch B and all Batch C fuel assemblies, stainless steel spacer shims are located between the guide tube flanges and the flow plate to provide additional clearance between the fuel rods and the upper end fitting. The connection with the upper end fitting is locked with a mechanical crimp. Each outer guide tube has, at its lower end, a welded Zircaloy-4 fitting. This fitting has a threaded portion which passes through a hole in the fuel assembly lower end fitting and is secured by a Zircaloy-4 nut. This joint is secured with a stainless steel locking ring tack welded to the lower end fitting in four places.

The central instrumentation guide tube inserts into a socket in the upper end fitting and is fastened at the lower end fitting by a threaded portion passing through a hole in the fuel assembly lower end fitting and secured by a Zircaloy-4 nut. This joint is secured from rotation by a stainless steel locking ring tack welded to the lower end fitting in four places. The upper end fitting socket is created by the center post which is threaded into the cast flow plate and tack welded in two places.

The five guide tubes have the effect of ensuring that bowing or excessive swelling of the adjacent fuel rods cannot result in obstruction of the control element pathway. This is so because:

a) There is sufficient clearance between the fuel rods and the guide tube surface to allow an adjacent fuel rod to reach rupture strain without contacting the guide tube surface.

b) The guide tube, having considerably greater diameter and wall thickness (and also, being at a lower temperature) than the fuel rod, is considerably stiffer than the fuel rods and would, therefore, remain straight, rather than be deflected by contact with the surface of an adjacent fuel rod.

Therefore, the bowing or swelling of fuel rods would not result in obstruction of the control element channels such as could hinder CEA movement.

The fuel assembly is designed on the basis of maintaining: 1) an adequate shoulder gap between the fuel (and poison) rods and the upper end fitting and 2) sufficient clearance between the fuel assembly and the upper guide structure throughout the expected life (burnup) of the fuel

assembly. Spacer grids are designed to allow axial rod growth without introducing significant restraints that would potentially enhance fuel rod bowing.

There is no criterion for axial growth per se; however, adequate clearances are maintained on fuel assembly structural components, fuel and poison rods, control element assemblies, neutron sources, and incore instruments to ensure functionability for their respective lifetimes. Adequate clearance is evaluated on the basis that under adverse design conditions a clearance of greater than zero shall be maintained.

The fuel assembly design enables reconstitution, i.e., removal and replacement of fuel and poison rods, of an irradiated fuel assembly. The fuel and poison rod lower end caps are conically shaped to ensure proper insertion within the fuel assembly grid cage structure; the upper end caps are designed to enable grappling of the fuel and poison rod for purposes of removal and handling. Threaded joints which mechanically attach the upper end fitting to the control element guide tubes are properly torqued and locked during service, but may be removed to provide access to the fuel and poison rods.

Two Plutonium 238/Antimony/Beryllium startup sustained source assemblies were installed in the reactor through operating Cycle 5. The purpose of the neutron sources was to provide sufficient sub-critical neutron multiplication for positive indication on the out-of-core neutron detectors. Irradiated fuel assemblies reloaded into the core from previous operating cycles produce a sufficient neutron source and are now used as the startup neutron source. The startup sustained source assemblies are stored in the spent fuel pool.

Loading and movement of the fuel assemblies is conducted in accordance with strictly monitored administrative procedures and, at the completion of fuel loading, an independent check as to the location and orientation of each fuel assembly in the core is required.

Markings provided on the fuel assembly upper end fitting enable verification of fuel enrichment and orientation of the fuel assembly. The serial number is also provided on the lower end fitting to ensure preservation of fuel assembly identity in the event of upper end fitting removal.

During the manufacturing process, each fuel rod is marked in order to facilitate a means of maintaining a record of pellet enrichment, pellet lot and fuel stack weight. In addition, a quality control program specification requires that measures be established for the identification and control of materials, components, and partially fabricated subassemblies. These means provide

a method of relating an item or assembly from initial receipt through fabrication, installation, repair or modification, to an applicable drawing, specification, or other pertinent technical document.

All batches of fuel were reviewed for dimensional change using the methods described in Reference 3. All clearances were found to be adequate during Cycle 2. Inspection of other CE 16 x 16 fuel assemblies has shown, in some cases, higher rates of shoulder gap change than predicted by the correlations described in Reference 3. Therefore, any additional analyses have been performed prior to startup of Cycle 2 operation to assure that the shoulder gap clearance between fuel rods and fuel assembly end fittings is adequate and in accordance with the Facility Operating License.

4.2.2.2 Fuel Rod

The fuel rods consist of slightly enriched UO_2 cylindrical ceramic pellets, a round wire Type 302 stainless steel compression spring, and an alumina spacer disc (through Region M) located at each end of the fuel column, all encapsulated within a Zircaloy-4 or ZIRLO™ tube seal welded with Zircaloy-4 end caps. The fuel rods are internally pressurized with helium during assembly. Figure 4.2-8 depicts the fuel rod design through Region N. Beginning with Region P, the active fuel length of the fuel rods will contain pellet columns consisting of three distinct zones. The upper and lower enrichment zones, known as axial blankets, result in more efficient fuel usage and are shown in Figure 4.2-8A.

Each fuel rod assembly includes both a serial number and a visual identification mark. The serial number ensures traceability of the fabrication history of each fuel rod component. The identification mark provides a visual check on pellet enrichment batch during fuel assembly fabrication.

The fuel cladding is cold worked and stress relief annealed Zircaloy-4 or ZIRLO™ tubing 0.025 inches thick. The actual tube forming process consists of a series of cold working and annealing operations, the details of which are selected to provide the combination of properties discussed in Subsection 4.2.1.2.2.

The UO_2 pellets are dished at both ends in order to better accommodate thermal expansion and fuel swelling. The density of the UO_2 in the pellets is less than the maximum theoretical density (TD) of UO_2. However, because the pellet dishes and chamfers constitute a percentage of the volume of the pellet stack, the average density of the pellet stack is reduced even more. This number is referred to as the "stack density." Other descriptive information is:

a) Cladding I.D. roughness is less than 0.000045 inches rms.

b) Dish diameter and depth

   Chamfer width and length

c) BOL cold void volume is 1.33 $inch^3$.

d) No sorbed gases assumed in the performance analyses.

e) BOL cold shoulder gap is 2.147 inches.

f) Nominal grid spacing is 15 13/16 inches.

The compression spring located at the top of the fuel pellet column maintains the column in its proper position during handling and shipping. The alumina spacer disc at the lower end of the fuel rod reduces the lower end cap temperature, while the upper spacer disc (through Region M) prevents UO_2 chips, if present, from entering the plenum region. The fuel rod plenum which is located above the pellet column, provides space for axial thermal differential expansion of the fuel column and accommodates the initial helium loading and evolved fission gases. (See Subsections 4.2.1.2.5.1 and 4.2.1.2.5.2). The specific manner in which these factors are taken into account, including the calculation of temperatures for the gas contained within the various types of rod internal void volume, is discussed in Reference 14.

Starting with reload Batch R, urania fuel rod fabrication was moved from Hematite, MO, to the Columbia, SC, facility. Fuel rod changes that resulted from this move include:

1. In reload assemblies prior to Batch R, the fuel rod end cap to cladding tube weld is a Magnetic Force (i.e., resistance) Weld whose outer surface is subsequently machined (i.e., deflashed). Beginning with Batch R, the joint was converted to Tungsten Inert Gas (TIG) welding. The latter also utilizes a separate (TIG) seal weld to close the opening through which the rod is pressurized.

2. The upper and lower end caps were redesigned to make them compatible with the TIG welding process.

3. The cladding tube was modified to make it compatible with the TIG welding process.

4. The fuel rod spring was redesigned for compatibility with the TIG welding process.

5. The alumina spacer between the pellet stack and the lower end cap was eliminated.

6. The combined effect of redesigning the lower end cap and eliminating the alumina spacer is to lower the active fuel region by 0.355 inch. This change in core elevation is relative to the Batch P design.

7. The combined effect of redesigning the plenum spring and eliminating the alumina spacer is to increase the rod's internal void volume by 0.028 cubic inch, relative to the Batch P design.

8. Reload rods for Batches R and later are fabricated at the Columbia facility, which builds its pellet stacks directly in the cladding tubes. Their stacks are built up, 25 at a time, from a series of shorter pre-assembled segments that are fed into a like number of tubes by a vibratory feeder. Before feeding the last row of segments into the tubes, the distance from the end of the tube to the end of the pellet stack is checked with a gauge. If necessary, an appropriate number of pellets are added to or removed from each segment in the row. As before, the distance from the end of the tube to the end of the pellet stack is then checked with a gauge.

Figure 4.2-8b compares the Region P and Region R urania rod assembly features.

4.2.2.3 Integral Burnable Absorber (Fuel/Poison) Rod

Fixed integral burnable neutron absorber rods, Figure 4.2-9, are included in selected fuel assemblies to reduce the beginning-of-life moderator coefficient. They replace fuel rods at selected locations but, unlike the burnable poison rods that were used previously, do not significantly reduce the amount of uranium in the fuel assembly. Integral burnable absorber rods are mechanically similar to fuel rods except that their pellet columns consist of three distinct zones. The upper and lower zones, which are referred to as cutback regions, are made up of slightly enriched urania (UO_2) pellets. Those pellets in the central zone consist of erbia or gadolinia (Er_2O_3 or Gd_2O_3 – the burnable neutron absorber) in a matrix of slightly enriched

urania. The pellet column in an integral burnable absorber rod has the same overall length as the one in a fuel rod.

Integral burnable absorber rod assemblies incorporate a serial number similar to the one that is used on fuel rod assemblies. They are located at the bottom of a circumferential groove on the lower end cap and serve to record fabrication information for each component in the rod assembly. The visual identification mark, that was unique to the upper end cap of the burnable poison rods, is no longer used.

The region P gadolinia rods were fabricated by ABB CE prior to the acquisition of ABB CE by Westinghouse. Component and subassembly production had been performed at the Windsor manufacturing facility while rod and bundle assembly had been performed at the Hematite manufacturing facility. Following the acquisition, the Hematite operations are being consolidated at the Columbia manufacturing facility, except for gadolinia rod fabrication. The fabrication of gadolinia rods will be done at the Westinghouse Atom manufacturing facility in Vasteras, Sweden, with the completed rods shipped to the facility assembling the fuel bundles (Columbia), as was done prior to Region N.

Vasteras uses an Electron Beam (EB) end cap weld process. The use of EB welding at Vasteras was used previously for St. Lucie 2 Region M gadolinia rods. The gadolinia rods are to be supplied by Vasteras as they were for Region M. The design of the gadolinia rod has been upgraded to account for the transition, to use with the Guardian grid and to account for compatibility with the fuel rods to be manufactured at Columbia. Design upgrades include:

a. The basis for the Region R upper end cap design is the Region M design since both designs are associated with the EB weld process performed at Vasteras.

b. The basis for the Region R lower end cap design is the Region P design since both designs interface with the Guardian grid. The basis for the upper region of the lower end cap is the Region M design since both designs are associated with the EB weld process performed at Vasteras.

c. As was done with the urania rod, the lower alumina spacer disc has been eliminated from the Region R gadolinia rod design.

d. Consistent with the EB welding process, in combination with the upper and lower end cap designs for the gadolinia rod, the gadolinia rod has the same overall rod length as the urania rod.

e. The same plenum spring design will be used in both the Region R gadolinia rods and urania rods.

f. The basic steps involved with the Region R rod assembly processes at Vasteras are unchanged from those for the Region M gadolinia rods, as follows:

    1) Although the EB welding of Region R end caps represents a change relative to the “baseline” Region P fuel, the Region R end cap weld process is merely reverting back to the Vasteras process used for Region M.

    2) The Region R gadolina rod evacuation/pressurization process will be the same as that used for the Region M gadolina rods.

3) The normal Vasteras process utilizes a chemically etched bar code on the cladding tubes to provide traceability through rod fabrication. The Vasteras process also includes the stamping of a cross-referenced serial number on the lower end cap after it is welded to the cladding tube. These are the same processes as for Region M gadolinia rods.

4) The dimensioning/tolerancing of the Region R gadolinia rods is consistent with the technique used for the Region M gadolinia rods.

5) The Region R gadolinia rod design results in an increase in the nominal void volume of approximately 0.028 cubic inches.

6) The reduction in the elevation of the bottom pellet in a Region R gadolinia rod relative to a Region P gadolinia rod is 0.355 inches, due to the removal of the aluminia spacer disc and the shortening of the lower end cap. This change is the same as the elevation change for the Region R urania rods.

Figure 4.2-9c compares the Region M, P and R gadolinia rod assembly features.

4.2.2.4 Control Element Assembly Description and Design Drawings

The St. Lucie Unit 2 reactor contains a total of 91 CEAs of two different types. These are distributed among the fuel assemblies as shown in Figure 4.2-14. The five element and four element CEAs are shown on Figures 4.2-3 and 4.2-4, respectively. All five element CEAs have four control elements arranged in a 4.050 inch square array plus one element at the center of the array. The four element CEAs have their four control elements arranged in a 4.050 x 4.130 array. Each CEA interfaces with the guide tubes of one fuel assembly, with the exception of the four element CEA, which straddles two adjacent fuel assemblies. Twelve new "reduced-strength" full- length Control Element Assemblies (CEAs) will be used for Cycle 2 operation in place of existing Cycle 1 "full-strength" CEAs. Eight of these replaced "full strength" full-length CEAs will be placed in the empty part length CEA locations for use in Cycle 2 operation. The mechanical design of these "reduced strength" CEAs are identical to the initial core full-length CEAs with the exception of individual element poison material content as shown in Table 4.2-5. There are no changes in the mechanical design bases for the CEAs from those listed in the FSAR for Cycle 1. CEAs are identified by the following features:

Engraved Identification Number (on Spider)	Grooves on Control Rod
1, 2, 3, etc. (1-in. high)	None, smooth OD

The control elements of a CEA each consist of an Inconel 625 tube loaded with a stack of cylindrical absorber pellets. The absorber material consists of 73 percent TD boron carbide (B_4C) pellets, with the exception of the lower portion of the corner elements, which contain silver-indium cadmium (Ag-In-Cd) alloy cylinders.

a) CEA Cladding Dimensional Stability

Because of its high ductility and low strength, the Ag-In-Cd will not deform the CEA cladding. Buffering of the CEA following scram, which occurs when the corner element tips enter a reduced diameter portion of the fuel assembly guide

tubes, is not degraded with long term exposure of the CEA to reactor operating conditions.

b) Adequate CEA Worth

Although some reduction in CEA worth arises because of the substitution of B_4C with Ag-In-Cd, the effect is small and is accounted for.

Above the poison column is a plenum which provides expansion volume for helium released from the B_4C. The plenum volume contains a Type 302 stainless steel holddown spring, which restrains the absorber material against longitudinal shifting with respect to the clad while allowing for differential expansion between the absorber and the clad. The spring develops a load sufficient to maintain the position of the absorber material during shipping and handling.

Each control element is sealed by welds which join the tube to an Inconel 625 nose cap at the bottom, and an Inconel 625 end fitting at the top. The end fittings, in turn, are threaded and pinned to the spider structure which provides rigid lateral and axial support for the control elements. The spider hub bore is specially machined to provide a point of attachment for the CEA extension shaft.

The CEA pattern for Cycle 1 is shown in Figure 4.2-10. Each CEA is positioned by magnetic jack control element drive mechanism (CEDM) mounted on the reactor vessel closure head. The extension shaft joins with the CEA spider and connects the CEA to the CEDM. Five-element CEAs may be connected to any extension shaft depending on control requirements. Mechanical reactivity control is achieved by positioning groups of CEAs by the CEDMs.

In the outlet plenum region, all CEAs are enclosed in CEA shrouds which provide guidance and protect the CEA and extension shaft from coolant cross flow. Within the core, each element travels in a Zircaloy guide tube. The guide tubes are part of the fuel assembly structure and ensure proper orientation of the control elements with respect to the fuel rods.

4.2.2.5 CEA Configuration, Bank Worths and Shutdown Margin

The CEA configuration for Cycle 2 differs from that of the reference cycle in that the empty part length control rod drives have had full-strength full-length control rods added to them, the banks and subgroups have been reconfigured and a new lead bank has been installed which consists of 12 “reduced-strength" CEAs each consisting of 2 B_4C fingers and 3 Al_2O_3 fingers. Figure 4.2-14 shows the location of all CEAs together with bank and subgroup designations. Figure 4.2-15 shows the location and orientation of the lead regulating bank (Bank 5) "reduced strength" CEAs.

Table 4.2-7 presents a summary of CEA shutdown worths and reactivity allowances for a typical cycle zero power steam line break. The EOC zero power steam line break accident was selected since it is the most limiting zero power transient with respect to reactivity requirements, and, thus, provides the basis for establishing the Technical Specification required shutdown margin.

Table 4.2-8 shows the reactivity worths of various CEA groups calculated at full power conditions for a typical cycle.

When the extension shaft is released by the CEDM, the combined weight of the shaft and CEA causes the CEA to insert into the fuel assembly.

The lower ends of the four outer fuel assembly guide tubes are tapered gradually to form a region of reduced diameter which, in conjunction with the outer control element on the CEA, constitutes an effective hydraulic buffer for reducing the deceleration loads at the end of a trip stroke. This purely hydraulic damping action is augmented by a spring and plunger arrangement on the CEA spider. When fully inserted, five element CEAs rest on the central post of the fuel assembly upper end fitting; the four element CEA rests on the fuel assembly upper end fitting flow bypass insert assembly.

The capability of the CEAs to scram within the allowable time is demonstrated as part of the flow testing discussed in Subsection 4.2.4.4.

4.2.2.6 Mechanical Design Description (AREVA CE-16 HTP™ Fuel)

Beginning with Cycle 23, the feed fuel is of the AREVA CE-16 HTP™ fuel design. The AREVA CE-16 HTP™ fuel consists of a 16x16 assembly configuration with M5® clad fuel rods, Zircaloy-4 MONOBLOC™ Corner Guide tubes, an Alloy 718 HMP™ spacer at the lowermost axial elevation, Zircaloy-4 HTP™ spacers in all other axial elevations, a FUELGUARD™ lower tie plate, and the AREVA reconstitutable upper tie plate.

The AREVA M5® Zirconium alloy cladding has very low corrosion and hydrogen pickup rates which provides substantial margin for end of life corrosion and hydrogen content. This material has been consistently shown to provide superior corrosion resistance and growth performance in PWR fuel assemblies in Europe and the United States. This material has been generically reviewed and accepted by the USNRC for operations in PWR fuel as fuel rod cladding and structural material (Reference BAW-10240(P)(A), Revision 0, Incorporation of M5 Properties in Framatome ANP Approved Methods). Reloads with M5® cladding have been provided in the United States since 2000 with demonstrated performance to rod exposures in excess of 80 MWd/kgU.

EC287528

The FUELGUARD™ lower tie plate design uses curved vanes to provide non-line-of-sight flow paths for the incoming coolant to protect the fuel assembly from debris that may be present. This design is very efficient at preventing debris, including small pieces of wire, from reaching the fuel. This FUELGUARD™ design has been used on reloads in the United States since 1991 and on CE-14 designs since 2001.

The upper tie plate (UTP) design is the standard AREVA reconstitutable design for CE configurations. The basic configuration is the same as that used for CE-14 plants supplied by AREVA, with the heights, diameters, and position of the corner and center posts adjusted for the CE-16 lattice and to be compatible with the core plate separation at the St. Lucie Unit 2 plant. This design does not create any loose or disposable parts during reconstitution. The design has been used for AREVA CE-14 reloads in the United States since 1982. The reconstitution capabilities of the AREVA CE designs have been successfully demonstrated in CE-14 and CE-16 fuel examinations.

The cage or skeleton uses four (4) Zircaloy-4 MONOBLOC™ corner guide tubes, one (1) Zircaloy-4 center guide tube, nine (9) Zircaloy-4 HTP™ spacers, and one (1) Alloy 718 HMP™ spacer at the lowest spacer position. The HTP™ spacers are welded directly to the five guide

tubes whereas the HMP™ spacer is attached to the guide tubes by mechanically capturing the spacer between rings that are welded to the guide tubes.

The HTP™ design provides eight (8) line contacts as the interface between the fuel rod and the spacer grid. This line contact is very resistant to fuel rod failures from flow induced vibration fretting. The HTP™ design is also configured to improve heat transfer. The spring structure provides a flow path at an angle relative to the rod longitudinal direction, causing the water to swirl around the rod without creating a large pressure drop across the spacer. The HMP™ has the same line contact configuration but the channel is not angled. Since this spacer is at the lowermost position, the improved heat transfer is not necessary.

The assembly uses a MONOBLOC™ guide tube design for the corner guide tubes and a constant outer diameter and wall thickness design for the center guide tube. The MONOBLOC™ design maintains the dashpot and non-dashpot regions, but has a constant outer diameter for the full length of the tube. Therefore, the wall thickness in the dashpot region (about the bottom 14 inches of the guide tube) is increased. The MONOBLOC™ guide tube design has been used for fuel reload batches in Europe and in the United States since 1998. The first application for CE plants was for a CE-14 design in 2010. St. Lucie Unit 1 has used the MONOBLOC™ guide tube design since 2013.

See Table 4.2-10 for a summary of the AREVA fuel assembly design parameters starting with Cycle 23. Figures 4.2-6a and 4.2-9d show the AREVA fuel assembly details.

4.2.2.6.1 Fuel Assembly Material Properties

The material properties used in the design evaluations are described in this section:

EC287528

a) Upper Tie Plate (UTP):

   i. The Reaction Plate, Flow Plate, and Spring Cups (5x) are fabricated from 304L Stainless Steel.

   ii. The holddown springs (Coil springs) are fabricated from Alloy X-750 spring wire.

   iii. The Corner Posts (4x) and Center Nut are fabricated from Alloy X-750 bar.

b) Cage Assembly:

   i. The HTP™ spacer grids (9x) are manufactured from Zircaloy-4 strip.

   ii. The HMP™ spacer grid (1x) is manufactured from Alloy 718 strip.

   iii. The Corner Guide Assemblies (4x) and Center Guide Tube Assembly (1x) are manufactured from Zircaloy-4 tubing, Zircaloy-4 bar, and 304L Stainless steel bar.

c) Fuel Rod Assemblies

   i. The cladding is manufactured from M5® Zirconium alloy tubing.

   ii. The end caps are manufactured from Zircaloy-4 or M5® bar.

iii. The plenum spring is manufactured from Alloy X-750 spring wire.

iv. The fuel pellets are low enriched UO_2 or Gd_2O_3-UO_2 fuel.

d) Lower Tie Plate (LTP)

i. The Frame and Base are machined from CF3 Stainless Steel casting.

ii. The Grid Rods are manufactured from 304L Stainless Steel bar. EC287528

iii. The curved blades are manufactured from 304L Stainless Steel strips.

e) Miscellaneous Components

i. Guide Tube Wear Sleeves are formed from 304L Stainless Steel tubing with a Chrome Plated ID.

ii. Guide Tub Cap Screws are manufactured from Alloy X-750 bar.

4.2.3 DESIGN EVALUATION

References 93 and 94 apply to the St. Lucie Unit 2 design prior to Cycle 23 feed fuel. Beginning with Cycle 23, the feed fuel is of the AREVA CE-16 HTP™ fuel design. Historical information has been retained. See Section 4.2.3.5 for the Mechanical Design Evaluations related to the AREVA CE-16 HTP™ fuel design. EC287528

4.2.3.1 Fuel Assembly

4.2.3.1.1 Vibration Analyses

Four sources of periodic excitation are recognized in evaluating the fuel assembly susceptibility to vibration damage. These sources are as follows:

a) Reactor Coolant Pump Blade Passing Frequency

Precritical vibration monitoring on previous CE designed reactors indicates that peak pressure pulses are expected at the pump blade passing frequency (74 Hz), and a lesser but still pronounced peak at twice this frequency.

b) Core Support Plate Motion

Experience with earlier CE designed reactors indicates that random lateral motion of the core support plate is expected to occur with an amplitude of 0.001 to 0.002 inch and a frequency range of between two and 10 Hz.

c) Flow Induced Fuel Assembly Vibration

Flow induced fuel assembly vibration resulting from coolant flow through the fuel assembly is expected to result in vibration amplitudes of 0.004 inches or less.

d) Flow Induced Control Element Vibration

The St. Lucie Unit 2 reactor vessel internals and fuel assembly design incorporates design features that ensures that the vibration of CEAs is such as to produce no significant wear in the guide tubes.

These sources of periodic motion are not expected to have an adverse effect on the performance of the St. Lucie Unit 2 fuel assembly. For Cycle 2 all fuel assemblies installed in Control Element Assembly locations have stainless steel sleeves installed in the guide tubes in order to mitigate guide tube wear.

The capability of the 16 x 16 fuel assembly to sustain the effects of flow-induced vibration without adverse effects was demonstrated in dynamic flow tests performed in CE's TF-2 flow test facility.

4.2.3.1.2 Fuel Assembly Guide Tube

The fuel assembly guide tubes are evaluated for structural adequacy using the criteria given in Subsection 4.2.1.1 in the following areas:

a) Steady axial load due to the combined effects of axial hydraulic forces and upper end fitting holddown forces.

   For normal operating conditions, the resultant guide tube stress levels are expected to be less than 50 percent of the two thirds yield stress criterion.

b) Short term axial load due to the impact of the spring loaded CEA spider against the upper guide structure support plates at the end of a CEA trip.

   For trips occurring during normal power operation, solid impact is not predicted to occur due to the kinetic energy of the CEA being dissipated in the hydraulic buffer and by the CEA spring.

c) Short term differential pressure load occurring in the hydraulic buffer regions of the outer guide tubes at the end of each trip stroke.

   The buffer region slows the CEA during the last few inches of the trip stroke. The resultant differential pressure across the guide tube in this region gives rise to circumferential stresses which are significantly less than the stress limits in Subsection 4.2.1.1. The trip is assumed to be repeated daily. However, the resultant stress is too small to have a significant effect on fatigue usage.

To qualify the complete fuel assembly, full scale hot loop testing was conducted. The tests were designed to evaluate fretting and wear of components, refueling procedures, fuel assembly uplift forces, holddown performance and compatibility of the fuel assembly with interfacing reactor internals, CEAs and CEDMs under conditions of reactor water chemistry, flow velocity, temperature, and pressure. The test assembly was a 16 x 16 five guide tube design. The test was run for approximately 2000 hours resulting in a demonstration of the acceptability of the design.

For conditions other than normal operation, the additional mechanical loads imposed on the fuel assembly by a Safe Shutdown Earthquake (SSE), operating basis earthquake (OBE) equivalent

to one half SSE, and large break LOCA and their resultant effect on the control element guide tubes are discussed in the following subsections:

4.2.3.1.2.1 Operating Basis Earthquake (OBE)

During the postulated OBE, the fuel assembly is subjected to lateral and axial accelerations which, in turn, cause the fuel assembly to deflect from its normal shape. The method of calculating these deflections is described in Subsection 3.7.3.14. The magnitude of the lateral deflections and resultant stresses were evaluated for acceptability. The method for calculating stresses from deflected shapes is described in Reference 50. The results of the stress analysis demonstrate that the component stresses are less than the allowable values discussed in Subsection 4.2.1.1.

4.2.3.1.2.2 Safe Shutdown Earthquake (SSE)

The axial and lateral loads and deformation sustained by the fuel assembly during a postulated SSE have the same origin as those discussed above for the OBE, but they arise from initial ground accelerations twice those assumed for the OBE. The analytical methods used for the SSE are identical to those used for the OBE. The predicted component stresses were less than the allowable values discussed in Reference 50.

4.2.3.1.2.3 Loss of Coolant Accident (LOCA)

In the event of a large break LOCA, there will occur rapid changes in pressure and flow within the reactor vessel. Associated with the transient are relatively large axial and lateral loads on the fuel assemblies. As demonstrated in Reference 77, an additional safety factor on the LOCA impact loads due to a postulated pressure pulse associated with steam flashing is unnecessary. Therefore, it was not included in the analysis. The methods used for analysis of LOCA loads and stresses are described in Reference 50. The results of the LOCA analysis were that component stresses were within the limits established in Reference 50.

4.2.3.1.2.4 Combined SSE and LOCA

It is not considered appropriate to combine the stresses resulting from the SSE and LOCA events. Nevertheless, for purposes of demonstrating margin in the design, the maximum stress intensities for each individual event were derived by a square root of sum of the squares (SRSS) method. This was performed as a function of fuel assembly elevation and position, e.g., the maximum stress intensities for the center guide tube at the upper grid elevation (as determined in the analysis discussed in Subsections 4.2.3.1.2.2 and 4.2.3.1.2.3) were combined by the SRSS method. The results (Reference 76) demonstrated that the allowable stresses described in Reference 50 were not exceeded for any position along the fuel assembly, even under the added conservatism provided by this load combination.

4.2.3.1.3 Spacer Grid Evaluation

The function of the spacer grids is to provide lateral support to fuel and burnable poison rods in such a manner that the axial forces are not sufficient to buckle or bow the rods and that the wear resulting at the grid-to-clad contact points will be limited to acceptably small amounts. It is also a criterion that the grid be capable of withstanding the lateral loads imposed during the postulated seismic and LOCA events.

Fuel assemblies are designed such that the combination of fuel rod rigidity, grid spacing, and grid preload will not result in significant fuel rod deformation under axial loads, and the long-term effects of clad creep (reduction in clad OD), the reduction of grid stiffness with temperature and the partial relaxation of the grid material during operation ensure that this criterion is also satisfied during all operating conditions. Moreover, inspection of irradiated fuel assemblies from the Maine Yankee (14 x 14), Calvert Cliffs (14 x 14), Palisades (15 x 15), and Ft. Calhoun (14 x 14) reactors has not shown significant bowing of the fuel rods. In view of these factors and the similarity of these designs to the St. Lucie Unit 2 (16 x 16) design, it is concluded that the axial forces applied by the grids on the cladding will not result in a significant degree of fuel rod bow. The influence of fuel rod lateral deflection is discussed further in Subsection 4.2.3.2.5. Additional discussion of the causes for and effects of fuel rod bowing is contained in Subsection 4.2.3.2.5 and in Reference 53.

The capability of the grids to support the clad without excessive clad wear was demonstrated by out-of pile flow testing, as described above, on the standard 16 x 16 assembly design and by the results of post irradiation examination of grid-to-clad contact points in Maine Yankee fuel assemblies which showed only negligible clad wear[51].

The capability of the grid to withstand the lateral loads produced during the postulated seismic and LOCA events is demonstrated by impact testing the reference grid design both at room temperature and at operating temperature, and comparing the test results with the analytical predictions of the seismic and LOCA loads.

The Zircaloy-4 spacer grid material is of the same composition as the fuel rods and guide tubes with which it is in contact, thereby obviating any problem of chemical incompatibility with those components. For the same reason, adequate resistance to corrosion from the coolant is assured (see Subsection 4.2.3.2.3 listing A, for additional information relative to the corrosion resistance of Zircaloy-4 in the reactor coolant environment).

The Inconel-625 material used for the lowest spacer grid (and the top grid beginning with Region U) is in contact with the coolant, the 304 stainless steel lower end fitting (to which it is welded), the Zircaloy-4 or ZIRLO™ fuel rods, the poison rods, and the Zircaloy-4 guide tubes. The mutual chemical compatibility of these materials in a reactor environment has been demonstrated by CE's use of these materials in fuel assemblies that have been operated in other CE reactors and for which post irradiation examination has yielded no evidence of chemical reaction between these components. In addition, experiments have also been performed at CE on Inconel type alloys and Zircaloy-4 which showed that eutectic reactions did not occur below 2200 F, a temperature far in excess of that anticipated at the lower grid location in the event of a LOCA.

4.2.3.1.4 Dimensional Stability of Zircaloy

Zircaloy components are designed to allow for dimensional changes resulting from irradiation-induced growth. Extensive analyses of in pile growth data have been performed to formulate a comprehensive model of in pile growth[3]. The in pile growth equations are used to determine the minimum axial differential growth allowance which must be included in the axial gap between the fuel rods and the upper end fittings. For determining the necessary fuel rod growth allowance, the growth correlations for fuel rod and guide tube growth are combined statistically such that the minimum initial gap is adequate to accommodate the upper 95 percent confidence level of differential growth between fuel rods and guide tubes in the peak burnup fuel assembly. For the purpose of predicting axial and lateral growth of the fuel assembly structure

(thereby establishing the minimum initial clearance with interfacing components), the equations are used in a conservative manner to ensure adequate margins to interference are maintained. The manner in which the in pile growth equations are described in Reference 65.

4.2.3.1.5 Fuel Handling and Shipping Design Loads

Beginning with Cycle 23, the feed batch fuel is of the AREVA CE-16 HTP™ fuel design. Refer to Section 4.2.3.5.3 for the AREVA CE-16 HTP™ fuel handling and shipping design loads. The below information is retained for historical purposes. EC287528

Three specific design bases have been established for shipping and handling loads. These are as follows:

a) The fuel assembly, when supported in the new fuel shipping container, is capable of sustaining the effect of 5g axial, lateral or vertical acceleration without sustaining stress levels in excess of those allowed for normal operation. The 5g criterion was originally established experimentally, and its adequacy is continually confirmed by the presence of impact recorders, as discussed in the following paragraph.

   Impact recorders are included with each shipment which indicate if loading in excess of 5g is sustained. A record of shipping loads in excess of 5g indicates an unusual shipping occurrence in which case the fuel assembly is inspected for damage prior to releasing it for use.

   The axial shipping load path is through either end fitting to the guide tubes. A 5g axial load produces a compressive stress level in the guide tubes less than the two thirds yield stress limit that is allowed for normal condition events. The fuel assembly is prevented from buckling by being clamped at grid locations. For lateral or vertical shipping loads, the alternate spring tabs and arches see no additional deflection as a result of 5g lateral or vertical acceleration of the shipping container. In addition, the side load on the grid faces produced by a 5g lateral or vertical acceleration is less than the measured impact strength of the grids.

b) The fuel assembly is capable of sustaining a 3000 pound axial load applied at the upper end fitting by the refueling grapple (and resisted by an equal load at the lower end fitting) without sustaining stress levels in excess of those allowed for normal operation. The 3000 pound load was chosen in order to provide adequate lift capability should an assembly become lodged. This load criterion is greater than any lift load that has been encountered in service.

c) The fuel assembly is capable of withstanding a 0.125 in. deflection in any direction whenever the fuel assembly is raised or lowered from a horizontal position without sustaining a permanent deformation beyond the fuel assembly inspection envelope.

Fuel handling procedures required the use of a strongback to limit the fuel assembly deflection to a maximum of 0.125 in. in any direction whenever the fuel assembly is raised or lowered to a horizontal position. This limits the stress and strain imposed upon the fuel assembly to values well below the limits set for normal operating conditions. The adequacy of the 0.125 in. criterion

is based on the inclusion of this limitation in specifications and procedures for fuel handling equipment, which is thereby constrained to provide support such that lateral deflection is limited to 0.125 inches

4.2.3.2 Fuel Rod Design Evaluation

The evaluations discussed in this section are based on assumed fuel rod operation within certain linear heat rate limits related to avoiding excessive fuel and clad temperatures. Information concerning the bases for these limits is contained in Section 4.4.

4.2.3.2.1 Results of Vibration Analyses

Four sources of periodic excitation are recognized in evaluating the fuel rod susceptibility to vibration damage. These sources are as described in Subsection 4.2.3.1.1.

These sources of periodic motion are not expected to have an adverse effect on the performance of the fuel rod. Subsection 4.2.3.2.4 includes additional information on fuel rod response to the sources.

4.2.3.2.2 Fuel Rod Internal Pressure and Stress Analysis

A fuel rod cladding stress analysis is conducted to determine the circumferential stress and strain resulting from normal, upset, and emergency conditions. The analysis includes the calculation of cladding temperatures and rod internal pressures during each of the occurrences listed in Subsection 4.2.1.1. The design criteria to be used to evaluate the analytical results are specified in Subsection 4.2.1.2.1. Fuel rod stresses resulting from seismic events are calculated, using the methodology described in Reference 50.

Analysis of St. Lucie Unit 2 design parameters, in conjunction with review of formal calculations on other CE 16x16 fuel system designs that envelope anticipated plant operating conditions, provide assurance that all design limits will be met (Reference 75).

4.2.3.2.3 Potential for Chemical Reaction

a) Corrosion

Zircaloy-4 fuel rod tubing has been visually examined in the spent fuel pool after three reactor cycles at Ft. Calhoun, two reactor cycles at Calvert Cliffs, and reactor cycles at Millstone, St. Lucie Unit 1 and Maine Yankee. In addition oxide thicknesses were measured in the hot cell after one cycle at Maine Yankee. In all instances the oxide appearance and oxide thickness measured similar to autoclave behavior for that time and temperature.

Coolant chemistry parameters have been specified that minimize corrosion product release rates and their mobility in the Reactor Coolant System. Specifically, the precore hot functional environment is controlled (pH and oxygen) to provide a thin, tenacious, adherent protective oxide film. This approach minimizes corrosion product release and associated inventory on initial startup and subsequent operation. During operation, lithium in the RCS causes a chemical potential gradient or driving force between hot and cooler surfaces (fuel cladding and steam generator tubing, respectively) such that soluble iron and

nickel species will preferentially deposit on the steam generator surfaces. The associated pH also minimizes general corrosion product release rates from Reactor Coolant System surfaces. Moreover, the specified hydrogen concentrations range (10-50 cm^3/kg STP) insures reducing conditions in the core, thereby avoiding low solubility Fe^{3+}. Additionally, dissolved hydrogen promotes rapid recombination of oxidizing species. (Recall, oxidizing species and a fast neutron flux are synergistic prerequisites to accelerated Zircaloy-4 corrosion).

During operation lithium, dissolved oxygen, and dissolved hydrogen will be monitored at a frequency consistent with maintaining these parameters within their specifications.

Post-operational examinations of fuel cladding that has operated within these specifications, has shown no significant chemical or corrosive attack of the Zircaloy cladding.

b) External Hydriding

During operation of the reactor with exposure to high temperature, high pressure water, Zircaloy-4 cladding will react to form a protective oxide film in accordance with the following equation:

$Zr + 2H_2O\ ZrO_2 + 2H_2$

Approximately 20 percent of the hydrogen is absorbed by the Zircaloy. Based on data describe in WAPD-MRP-107, the cladding would be expected to contain up to 250 ppm hydrogen following three years of exposure.

A series of burst tests were performed on Zircaloy -2 tubes containing 340 ppm and 460 ppm of hydrogen precipitated as hydride platelets in a circumferential manner[67]. Burst tests at 660°F showed that the burst test specimens with 340 ppm had normal burst ductility of 12 percent. Therefore, hydrogen normally absorbed in Zircaloy-4 tubing will not prove deleterious to the cladding integrity.

Early work performed at AECL has shown that hydrides become ductile on heating to 390°F, and at that temperature, and in concentrations up to 250 ppm (the expected concentration after three cycles), their presence has little effect on ductility. In addition, burst tests at 600°F and 725°F for hydride concentrations between 200 and 400 ppm did not show a significant dependence between burst ductility and hydride concentration or orientation. The potential effects of hydride orientation and concentration above 725°F have not been specifically evaluated by CE; but, provided concentrations do not exceed the range tested so far, would not be expected to be significant.

c) Internal Hydriding

A number of reported fuel rod failures have resulted from excessive moisture available in the fuel. Under operation, this moisture oxidizes the Zircaloy.

The hydrogen, which was not absorbed during normal oxidation, would then be adsorbed into the Zircaloy through a scratch in the oxide film. This localized

hydrogen adsorption by the cladding would shortly result in a localized fuel rod failure. Work performed at the Institute for Atomenergi, Halden Norway, of which CE is a member, demonstrated that a threshold value of water moisture is required for hydride sunbursts to occur.[64] Through a series of in pile experiments, the level of this threshold value was established. The allowable hydrogen limit in the fuel complies with this requirement, ensuring that hydride sunbursts will not occur. The allowable CE moisture limit for fuel and poison rods is more limiting than that specified by Reference 74.

d) Crud

Crud layers on zirconium oxide films are usually porous and noninsulating. As an example, heavy, but non-insulating crud layers have been found in Yankee Rowe (WCAP-3317-6094, Yankee Core Evaluation Program, Final Report, 1971). With porous crud, water is free to flow through the crud and provide heat transfer by convection. Under these conditions, crud enhanced corrosion should not occur.

Because of rigorous water chemistry monitoring, heavy buildup of crud has not occurred in CE reactors. Water chemistry monitoring is a continuous process and should ensure no dense crud buildup.

e) Fuel Cladding Chemical Reaction

An in depth post irradiation examination has been conducted wherein fuel cladding chemical reactions were among those items studied. This study concluded that early unpressurized elements containing unstable fuel were more susceptible to stress corrosion attack than are the current design that utilizes stable fuel and pressurized cladding. By carefully monitoring the reactor coolant activity of operating reactors, it has been concluded that the current fuel designs are not susceptible to stress corrosion (or other types of corrosion) during normal plant operation. Since stress corrosion attack is the result of a combination of stresses imposed by the fuel on the cladding and the corrosive chemical species available to the cladding, irradiation programs are being pursued to define the conditions under which pellet clad interaction will damage the cladding. These programs are currently underway both at Halden and in the Pathfinder test program being conducted jointly with KWU in the Obrigheim and Petten reactors.

4.2.3.2.4 Fretting Corrosion

The phenomenon of fretting corrosion, particularly in Zircaloy clad fuel rods supported by Zircaloy spacer grids, has been extensively investigated.

Since irradiation induced stress relaxation causes a reduction in grid spring load, spacer grids must be designed for end of life conditions as well as beginning of life conditions to prevent fretting caused by flow induced tube vibrations.

Examination of Zircaloy clad fuel rods after three cycles of exposure at Ft. Calhoun, two cycles of exposure at Calvert Cliffs and one cycle of exposure at Millstone Point, Maine Yankee, and St. Lucie Unit 1 have shown little fretting and no fuel cladding perforations from the fretting. Based on the combination of the ex-reactor tests and the in-reactor surveillance of the fuel in the ANO-2, plant, St. Lucie Unit 2 is not expected to experience fretting behavior.

4.2.3.2.5 Fuel Rod Bowing

Experience has proven that any specific criterion on allowable deflections (bowing), with respect to the effects which such deflections might have on thermal hydraulic performance, is not necessary beyond the initial fuel rod positioning requirements required of the grids. This variation in spacing is accounted for in thermal-hydraulic analysis through the introduction of hot channel factors in calculating the maximum enthalpy rise in calculating DNBR. This adjustment is called the pitch, bowing, and clad diameter enthalpy rise factor, which is conservatively applied to simulate a reduced flow area along the entire channel length. The value of this factor is given in Table 4.4-1 and its application is discussed in Section 4.4.

The subject of fuel rod bowing is discussed in Reference 53.

4.2.3.2.6 Irradiation Stability of Fuel Rod Cladding

The combined effects of fast flux and cladding temperature on irradiation stability of fuel rod cladding are considered in three ways as discussed below:

a) Cladding Creep Rate

The in pile creep performance of Zircaloy-4 is dependent upon both the local material temperature and the local fast neutron flux. The functional form of the dependencies is presented in Reference 14 for gap conductance calculations, and in Reference 22 for cladding collapse time predictions.

b) Cladding Mechanical Properties

The yield strength, ultimate strength, and ductility of Zircaloy-4 are dependent upon temperature and accumulated fast neutron fluence. The temperature and fluence dependence is discussed in Subsection 4.2.1.2.2.1. Unirradiated properties were used depending upon which is more restrictive for the phenomenon being evaluated.

c) Irradiation Induced Dimensional Changes

Zircaloy-4 has been shown to sustain dimensional changes (in the unstressed condition) as a function of the accumulated fast fluence. These changes are considered in the appropriate clearances between the various core components. The irradiation induced growth correlation method is discussed in References 3 and 65.

Inspection of fuel assemblies after two cycles of operation at the Arkansas Nuclear One, Unit 2 reactor has shown higher rates of gap closure than predicted by the method described in References 3 and 65. Closure rates predicted by these References 3 and 65 may remain valid for the St. Lucie 2 fuel assemblies because of differences in the St. Lucie 2 and Arkansas designs. Nonetheless, additional shoulder gap has been provided in those fuel assemblies scheduled for three cycles of operation.

Zircaloy-4 fuel cladding has been utilized in pressurized water reactors at temperatures and burnups anticipated in current designs with no failures attributable to radiation damage.

Mechanical property tests on Zircaloy-4 cladding exposed to neutron irradiation of 4.7 x 10^{21} nvt (E>1l MeV) (estimated) have revealed that the cladding retains a significant amount of ductility (in excess of 4 percent elongation). Typical results are shown in Table 4.2-3. It is believed that the fluence of 4.7 x 10^{21} nvt (E>1 MeV) is at saturation so that continued exposure to irradiation will not change these properties.[54]

4.2.3.2.7 Cladding Collapse Analysis

A cladding collapse analyis is performed to ensure that no fuel rod in the core will collapse during its design lifetime. The clad calculation method[21] itself does not include arbitrary safety factors. However, the calculation inputs will be deliberately selected to produce a conservative result. For example, the clad dimensional data are chosen to be worst case combinations based either upon drawing tolerances or 95 percent confidence limits on as built dimensions; the internal pressure history is based on minimum fill pressure with no assistance from released fission gas; and the flux and temperature histories are based on conservative assumptions.

4.2.3.2.8 Fuel Dimensional Stability

Fuel swelling due to irradiation (accumulation of solid and gaseous fission products) and thermal expansion results in an increase in the fuel pellet diameter. The design makes provision for accommodating both forms of pellet growth. The fuel clad diametral gap is more than sufficient to accommodate the thermal expansion of the fuel. To accommodate irradiation induced swelling, it is conservatively assumed that the fuel clad gap is used up by the thermal expansion and that only the fuel porosity and the dishes on each end of the pellets are available. Thermal and irradiation induced creep of the restrained fuel results in redistribution of fuel so that the swelling due to irradiation is accommodated by the free volume (8.2 percent of the fuel volume).

For such restrained pellets, and at a total fission product induced swelling rate of 0.7 percent $\Delta V/V$ per 10^{20} fiss/cm , 0.54 percent would be accommodated by the fuel porosity and dishes through fuel creep, and 0.16 percent would increase the fuel diameter. Assuming peak burnup, this would correspond to using up a void volume equal to ~7.4 percent of the fuel volume and increasing the fuel rod diameter by a maximum of < 0.0025 inch (<0.7 percent clad strain). When these numbers were compared to the minimum available volume and the maximum allowable strain, it was concluded that sufficient accommodation volume has been provided even under the most adverse burnup and tolerance conditions.

Demonstration of the margin which exists is seen in the large seed blanket reactor (LSBR) irradiation. Two rods which operated in the B-4 loop of the MTR offer an interesting simulation for current PWR design [60][7][55]. Both rods were comprised of 95 percent theoretical density pellets with dished ends and clad in Zircaloy. The first of these, No. 79-21, was operated successfully to a burnup of 12.41 x 10^{20} fiss/cm (48,000 MWD/MTU). The second fuel pin, No. 79-25, operated successfully to 15.26 x 10^{20} fiss/cm (60,000 MWD/MTU). The linear heat rating ranged from 7.1 to 16.0 kW/ft. The wall thickness for the latter pin was 0.028 inch as compared with 0.016 inch for the former. All other parameters were essentially identical. The two rods were assembled by shrinking the cladding onto the fuel. The maximum diametral increase measured at the ridge heights for rod 79-21 was 0.005 inch, while it was less than 0.002 inch for rod 79-25. From post-irradiation examination, it was concluded that approximately 84 percent of the total fuel swelling was accommodated by the porosity and dishes, while 16 percent caused diametrical expansion of the clad and ridging at pellet interfaces. These results indicate that a

comparable irradiation of the fuel elements for the 16 x 16 fuel design would allow adequate margin for swelling accommodation.

The successful combined VBWR-Dresden irradiation of Zircaloy-clad uranium dioxide pellets provides additional confidence with respect to the design conditions for the fuel rods for this core.[56][57] Ninety-eight rods which had been irradiated in VBWR to an average burnup of about 10,700 MWd/MTU were assembled in fuel bundles and irradiated in Dresden to a peak burnup greater than 48,000 MWd/MTU. The reported maximum heat rating for these rods is 17.3 kW/ft which occurred in VBWR. Post-irradiation examination[58] revealed that diametral increases in the fuel rods ranged from 0.001 to 0.003-inch maximum. The maximum diametral change corresponds to 1.42 percent ΔV/V (or 0.12 percent ΔV/V per 10^{20} fiss/cm^3) for these 0.424-inch diameter rods. The relevant fuel parameters are listed below:

	Fuel Density (%TD)	Cold Diametral GAP(in.)	Peak Burnup (MWd/MTU)
VBWR-Dresden	95	0.004 to 0.008	>48,000
LSBR-MTR	95	0.001	50,000; 61,000
C-E design	94.75	0.007	55,000

A comparison of the design parameters above, relative to the test results, provides a demonstration of the clad strains resulting from swelling of fuel.

4.2.3.2.9 Potential for Waterlogging Rupture and Chemical Interaction

The potential for waterlogging rupture is considered remote. Basically, the necessary factors, or combination of factors, include the presence of a small opening in the cladding, time to permit filling of the fuel rod with water, and finally, a rapid power transient. The size of the opening necessary to cause a problem falls within a fairly narrow band. Above a certain defect size, the rod can fill rapidly, but during a power increase it also expels water or steam readily without a large pressure buildup. Defects which could result in an opening in cladding are scrupulously checked for during the fuel rod manufacturing process by both ultrasonic and helium leak testing. Clad defects which could develop during reactor operation due to hydriding are also controlled by limiting those factors; e.g., hydrogen content of fuel pellets, which contribute to hydriding.

The most likely time for a waterlogging rupture incident would be after an abnormally long shutdown period. After this time, however, the startup rate is controlled so that even if a fuel rod were filled with coolant, it would "bake out", thus minimizing the possibility of additional cladding rupture. The combination of control and inspection during the manufacturing process and the limits on the rate of power change restrict the potential for waterlogging rupture to a very small number of fuel rods.

The UO_2 fuel pellets are highly resistant to attack by reactor coolant in the event cladding defects should occur. Extensive experimental work and operating experience have shown that the design parameters chosen conservatively account for changes in thermal performance during operation and that coolant activity buildup resulting from cladding rupture is limited by the ability of uranium dioxide to retain solid and gaseous fission products.

4.2.3.2.10 Fuel Burnup Experience

The CE fuel rod design is based on an extensive experimental data base and by an extension of experimental knowledge through design application of CE fuel rod evaluation codes. The experimental data base includes data from CE or CE/Kraftwerk Union (KWU) joint irradiation experiments, from CE and KWU operating commercial plant performance and from many basic experiments conducted in various research reactors which are available in the open literature. Each of these information sources will be discussed below. Evidence currently available indicates that Zircaloy and UO_2 fuel performance is satisfactory to exposures in excess of 55,000 Mwd/Mtu.

a) Public Information

General fuel performance information available in the open literature has provided part of the CE fuel rod design data base. Particular experiments that have been cited in the past as key references, they include:

1) Determination of the effect of fuel cladding gap on the linear heat rate to melting of UO_2 fuel rods, conducted in the Westinghouse test reactor.

2) Shippingport Irradiation Experience

3) Saxton Irradiation Experience

4) Combined Vallecitos Boiling Water Reactor (VBWR) Dresden Irradiation.

5) Large Seed Blanket Reactor (LSBR) Rod Experience

6) Joint U.S.-Euratom Research and Development Program to evaluate central fuel melting in the Consumers Power Co. Big Rock Point Reactor.

Since the information from these programs is available in the open literature, they will not be described here. However, details as to the significance of the results to CE fuel burnup experience are presented in Reference 59.

b) CE/KWU Technical Exchange

CE entered into a technical agreement with KWU beginning in 1972 for the complete exchange of information and technology relating to pressurized water reactor systems including fuel. This agreement makes available to CE the total experience of 10 years successful operation of commercial PWR fuel in systems designed and fabricated by KWU and is most advanced of its type in the world. An essential part of this broad based exchange involves joint sponsorship of numerous fuel testing programs.

c) Operating Fuel Experience

CE and KWU have fabricated approximately 750,000 Zircaloy clad fuel rods both internally pressurized and unpressurized over the last 10 years. Of this total 460,000 rods remain in operation (~220,000 CE rods) with average burnups in excess of 36,000 Mwd/Mtu. The remaining 290,000 rods have been discharged

with average burnups to 36,000 Mwd/Mtu. Overall performance of this fuel has been excellent. The fuel rod reliability level, estimated from coolant activities is >99.98 percent. This high reliability level is continually validated by extensive poolside fuel inspection programs conducted by both CE and KWU at reactor sites during refueling shutdowns.

d) Fuel Irradiation Programs

CE is involved in diversified fuel irradiation test programs to confirm the adequacy of the CE fuel rod design bases and models by experimental means. Some of these programs involve safety related research while other programs provide confirmatory data on performance capability or evaluate design and fabrication variables or methods which may improve and extend our current knowledge of fuel rod performance. Many of the programs involved joint CE/KWU sponsorship.

Some of the key fuel performance evaluation programs that will be summarized below include:

Fuel densification experiments at the Battelle Research Reactor (BRR)

Joint CE/KWU fuel densification experiments including tests in the MZFR reactor at Karlsruhe, West Germany, and the EEI experiments in the General Electric Test Reactor (GETR).

Direct participation in the Halden Project in Norway with access to all Halden base program fuel test data.

Irradiation of special instrumented fuel rods to obtain dynamic in-reactor measurements in Halden experimental rigs.

Ramp test programs on fuel rods to evaluate fuel load-follow capabilities and the pellet clad interaction/stress corrosion phenomenon in both the Studsvik and Petten test reactors. Other in-reactor experiments have been conducted in the Obrigheim pressurized water reactor.

Irradiation of special test and surveillance assemblies in operating CE reactors.

e) CE Fuel Densification Experiments

CE has conducted several experiments which provided data on the in-reactor densification behavior of various UO_2 fuel types. These include the BRR, EEI, and MZFR densification experiments, as discussed below.

f) BRR Fuel Densification Experiment

The object of this program was to examine the in pile densification behavior of various fuel types and microstructures fabricated with and without pore formers. The non pore former fuel types had initial densities of 93 percent to 94 percent theoretical with a grain size of less than 6 microns with a large fraction of pores less than 4 microns in diameter. The pore former fuel types had initial densities of

93 percent to 95 percent and were characterized by a combination of large grain size and/or large pore size. Fuel pellets of each experimental type were irradiated in six BRR capsules at linear heat ratings between 2.8 and 4.6 kw/ft for periods of up to 1500 hours. Post-irradiation examination of the BRR results showed significant differences in the densification behavior between pore former and non-pore former fuel. The pore former fuel showed little change in density (high stability) while the non-pore former fuel densified rapidly. A trend towards increased densification with lower initial density was apparent in the non-pore former fuel. It was concluded that the UO_2 microstructure played a dominant role in the kinetics and extent of in reactor densification. Consequently, fuel exhibiting the desirable microstructural features to reduce in reactor densification (i.e., large fraction of the pore volume in the large pore size range) became part of the standard CE fuel design.

g) CE/KWU Fuel Densification Experiment (MZFR)

As a follow-on to the CE experiment in the BRR, a joint CE/KWU program has been conducted in the German MZFR to evaluate the performance of several non-densifying fuel types at higher power levels for longer times and to higher burnups.

Sixteen full length fuel rods each containing a different fuel type were irradiated at powers up to 11 kw/ft for burnups up to 4000 Mwd/Mtu. Included in these rods are UO_2 and UO_2- PuO_2 fuels most of which was fabricated using techniques intended to minimize densification. Six rods employed CE fabricated UO_2 fuels, five of which included pore former additives and one fabricated without a pore former to serve as a referencable control sample. Eight rods were fabricated using KWU experimental fuel representing a wide range of sintering times and temperatures, initial densities and enrichments. The remaining two rods were fabricated using UO_2- PuO_2 fuels of two different densities, with and without a pore former additive. Each of the fuel pellet types and fuel rods was extensively characterized prior to testing to permit comparison with similar post irradiation measurements.

The results of the post irradiation examination showed that fuel types fabricated with pore formers (similar to current production fuel) experienced significantly less in pile densification compared to those fabricated without pore formers. The data also support use of a standardized out of pile resintering test developed by CE to characterize expected in pile densification at the time of fabrication. This simulation test has been submitted to the NRC and approved for use by CE in LOCA calculations.

h) EEI Fuel Densification Experiment

The prime objective of the EEI Fuel Irradiation Test Program conducted in the General Electric Test Reactor (GETR) was to isolate and characterize the in reactor densification behavior of pore former (or stable) fuel types. CE and KWU were among eleven participants in the program.

This program entitled CE to obtain densification data on nine base program fuel pellet types with varying microstructures. An additional four fuel types were

fabricated by CE and KWU. These included CE fuel types, two with and one without a pore former additive and a KWU standard production fuel. The pellets in the program were well characterized prior to irradiation. Four of the fuel types were irradiated in one pressurized (53 atmospheres) capsule. Two of the fuel types were also irradiated in a separate nonpressurized capsule (one atmosphere). Each of the capsules contained thermocouples to continuously monitor capsule power generation during irradiation to assure that the desired operating conditions were maintained. Post irradiation examination of these test capsules confirmed that UO_2 fuel with specific ranges of microstructural characteristics, such as produced by pore former additives, are stable with respect to densification. The largest in reactor density changes occurred for those types having a combination of the smallest pore size, the largest volume percent of porosity less than four microns in the smallest initial grain size and the lowest initial density.[60]

i) Halden Program Participation

The experimental facilities and programs of the OECD Halden Reactor Project in Norway represent one of the most advanced efforts in quantifying the effects and interaction of the various design parameters of Zircaloy clad fuel rods through measurements made in reactor. CE has been a member of the Project since 1973. CE reviews the data generated by the project in considerable detail and utilizes the results in various fuel development programs.

The Halden test reactor has unique capability for measuring fuel rod operation during irradiation. This capability has been utilized by CE with specific experiments to provide information in the following areas:

Fuel densification phenomenon including measurements of the rate of fuel column shortening as a function of the initial fuel density, power level and fuel fabrication process.

Fuel clad mechanical interaction involving studies of the effects of pellet design (shape and density) and operating parameters on cladding deformation.

Modeling of fuel rod behavior with emphasis on heat transfer characteristics.

The first three test assemblies sponsored jointly by CE and KWU contained 24 well- characterized fuel rods. These assemblies included the following range of design and operating parameters:

Helium fill pressures from 22 to 35 atmospheres.

Initial fuel densities from 91-96 percent TD.

Linear heat ratings to 15 kw/ft.

U_{235} enrichments from six to 12 percent; nine rods fabricated with mixed-oxide fuel.

The objectives of these tests were to determine the dynamic changes in fuel rod internal pressure, fuel centerline temperature and fuel stack length during operation as a function of burnup. Two of these assemblies (six test rods each) were discharged from the reactor after receiving a peak burnup of ~24,000 Mwd/Mtu. The third rig (12 rods) will be evaluated to burnups in the range of 35,000-40,000 Mwd/Mtu. The objectives of a fourth six-rod test assembly were to evaluate the effects of such design variables as pellet-clad gap, fill-gas composition, and linear heat rating (to 15 kw/ft) on heat transfer characteristics. This experiment also provided gap conductance data on UO_2 and mixed- oxide fuel. This test was discharged from the reactor after reaching a peak burnup of ~4000 Mwd/Mtu.

Instrumentation used to measure fuel behavior during irradiation includes centerline thermocouples, internal pressure transducers, linear variable differential transformers (LVDTs) for fuel column length changes and flux monitors for axial and radial power profiles.

Hot cell examination of the three discharged test assemblies is in progress. Fuel column length change data obtained supports data generated by the EEI, BRR, and MZFR experiments and confirms the in reactor stability of CE pore former fuel types. In addition, the internal pressure monitors and centerline thermocouple data have confirmed the adequacy of the CE thermal performance design models

In addition, to these CE/KWU test assemblies, CE has designed and irradiated three rods in the Halden high temperature, high pressure loop to simulate PWR coolant temperature and pressure conditions. Irradiation of the third rod is still in progress to an expected burnup at discharge of approximately 4000 Mwd/Mtu. The purpose of these experiments is to distinguish the effects of pellet configuration on the formation of circumferential ridging and on the elongation of the rods. Each rod contained three pellet types with one type as a standard. This program in combination with the results of other experiments gives CE a firm basis upon which to optimize fuel rod design with respect to dimensional changes and to improve fuel performance models developed to predict rod dimensional stability.

j) Power Ramp Programs

CE and KWU are participating in the Studsvik and Pathfinder/Petten programs to evaluate fuel rod performance under ramp conditions to power levels not recently attained. These can occur either after refueling or after extended periods of low power operation or during control rod maneuvers. The effects of various fuel rod design variables on power ramp limits is also investigated as a means to further optimize design. The Petten/Pathfinder program which began in 1973 is being conducted jointly by CE and KWU in the Obrigheim PWR reactor and Petten test reactor facilities. One special test assembly has been irradiated each year since 1973 in the Obrigheim reactor. Included in this assembly, which is designed to facilitate fuel rod removal and replacement, are well-characterized segmented rods or "rodlets" which are axially connected to form a complete fuel rod. These rodlets are "pre irradiated" in the Obrigheim reactor for one, two, or three operating cycles, and then separated and irradiated in a test reactor to evaluate

performance under ramp conditions. To date, approximately 500 rodlets have been irradiated in Obrigheim. Forty three of these rodlets have been discharged and ramped in Petten. An additional 24 rodlets are being supplied to the Studsvik Overramp project for ramp testing in the R-2 reactor at Studsvik. Ramp tests on eight of these rodlets have thus far been completed at Studsvik. Post-irradiation, hot cell examination programs form an integral part of both the Petten/Pathfinder and Studsvik experiments to characterize fuel rod behavior, particularly with respect to dimensional stability and fission product release. These test programs are designed to distinguish between fuel rod power ramps which occur on start-up and those which might occur during reactor power maneuvering operations.

Operating flexibility of a plant requires that the fuel rods maintain integrity during periodic changes in power. Power cycling tests of this type have been jointly conducted by CE/KWU in Obrigheim and Petten. In the Petten test, a single unpressurized fuel rod was power cycled between nine kw/ft and 17 kw/ft at a power change rate of about three kw/ft/min. The fuel rod successfully completed 400 cycles and achieved a burnup of 8000 Mwd/Mtu. Power cycling tests were then conducted in Obrigheim on eight short pressurized and unpressurized fuel rods. The test fuel rods were attached to a control rod drive mechanism and driven from the low power to a high power position on a nominal cycle. Power changes from 50 percent to 100 percent at rates of 20 percent per minute for 880 cycles were included. After successfully completing the experiment, the test rods achieved a peak burnup of 30,000 Mwd/Mtu without substantial cladding deformation or fuel rod perforation.

k) Fuel Surveillance Programs

CE has conducted a number of a fuel surveillance programs on fuel in operating plants. Thus far, a total of 16 poolside fuel inspection programs of varying detail have been performed by CE (see Table 4.2-4). Over 368 assemblies have been visually examined, and dimensional measurements have also been obtained on a large number of these assemblies. Fuel bundle disassembly operations have been conducted either to obtain information of particular aspects of performance of interest or as part of test assembly surveillance programs. The results of the CE poolside inspection program have been used to verify fuel assembly operation and provide data in support of design. A pre- irradiation characterization has been completed on CE's first 16 x 16 fuel for Arkansas Nuclear One, Unit 2. An examination of this fuel at the spent fuel pool will extend the design verification to the 16 x 16 design which will be used for St. Lucie Unit 2.

4.2.3.2.11 Temperature Transient Effects Analysis

4.2.3.2.11.1 Waterlogged Fuel

The potential for a fuel rod to become waterlogged during normal operation is discussed in Subsection 4.2.3.2.9. In the event that a fuel rod does become waterlogged at low or zero power, it is possible that a subsequent power increase could cause a buildup of hydrostatic pressure. It is unlikely that the pressure would build up to a level that could cause cladding

rupture because a fuel pin with the potential for rupture requires the combination of a very small defect together with a long period of operation at low or zero power.

Tests which have been conducted using intentionally waterlogged fuel pins (capsule drive core at SPERT)[61][62] showed that the resulting failures did eject some fuel material from the rod and greatly deformed the test specimens. However, these test rods were completely sealed, and the transient rates used were several orders of magnitude greater than those allowed in normal operation.

In those instances where waterlogged fuel rods have been observed in commercial reactors, it has not been clear that waterlogging was the cause, and not just the result, of associated cladding failures; and CE has not observed and is not aware of any case in which material was expelled from waterlogged fuel rods or in which the fuel cladding was significantly deformed in a normal power reactor.

It is therefore concluded that the effect of normal power transients on waterlogged fuel rods is not likely to result in cladding rupture and even if rupture does occur it will not produce the sort of postulated burst failures which would expel fuel material or damage adjacent fuel rods or fuel assembly structural components.

4.2.3.2.11.2 Intact Fuel

The thermal effects of anticipated operational occurrences on fuel rod integrity are discussed in the following subsections.

a) Fuel rod thermal transient effects are basically manifested as the change in internal pressure, the changes in clad thermal gradient and thermal stresses, and the differential thermal expansion between pellets and clad. These effects are discussed in Subsection 4.2.3.2.2

b) Another possible effect of transients would be to cause an axial expansion of the pellet column against a flattened (collapsed) section of the clad. However, the fuel rod design includes specific provisions to prevent clad flattening, and, therefore, such interactions will not occur.

4.2.3.2.12 Energy Release During Fuel Element Burnout

The Reactor Protective System provides fuel clad protection so that the probability of fuel element burnout during normal operation and anticipated operational occurrences is extremely low. Thus, the potential for fuel element burnout is restricted to faulted conditions. The LOCA is the limiting event since it results in the largest number of fuel rods experiencing burnout; thus, the LOCA analysis, which is very conservative in predicting fuel element burnout, provides an upper limit for evaluating the consequences of burnout. The LOCA analysis explicitly accounts for the additional heat release due to the chemical reaction between the Zircaloy clad and the coolant following fuel element burnout in evaluating the consequences of this accident. LOCA analysis results are discussed in Section 15.6.

4.2.3.2.13 Energy Release on Rupture of Waterlogged Fuel Elements

A discussion of the potential for waterlogging fuel rods and for subsequent energy release is presented in Subsection 4.2.3.2.9.

4.2.3.2.14 Fuel Rod Behavior Effects from Coolant Flow Blockage

An experimental and analytical program was conducted to determine the effects of fuel assembly coolant flow maldistribution during normal reactor operation. In the experimental phase, velocity and static pressure measurements were made in cold, flowing water in an oversize model of a CF 14 x 14 fuel assembly in order to determine the three-dimensional flow distributions in the vicinity of several types of flow obstruction. The effects of the distributions on thermal behavior were evaluated, where necessary, with the use of a preliminary version of the TORC thermal and hydraulic code.[63] Subjects investigated included:

a) The assembly inlet flow maldistribution caused by blockage of a core support plate flow hole. Evaluation of the flow recovery data indicated that even the complete blockage of a core support plate flow hole would not produce a W-3 DNBR of less than 1.0 even though the reactor might be operating at a power sufficient to produce a DNBR of 1.3 without the blockage.

b) The flow maldistribution within the assembly caused by complete blockage of one to nine channels. Flow distributions were measured at positions upstream and downstream of a blockage of one to nine channels. The influence of the blockage diminished very rapidly in the upstream direction. Analysis of the data for a single channel blockage indicated that such a blockage would not produce a W-3 DNBR of less than 1.0 downstream of the blockage even though the reactor might be operating at a power sufficient to produce a DNBR of 1.3 without the blockage.

The results presented above were obtained through flow testing an oversize model of a standard 14 x 14 fuel assembly. Because of the great similarity in design between 16 x 16 assembly, and the earlier 14 x 14 array, these test results also constitute an adequate demonstration of the effects that flow blockage would have on the 16 x 16 assembly. This conclusion is also supported by the fact that the 16 x 16 assembly has been demonstrated to have a greater resistance to axial flow than would occur with the 14 x 14 array. The effect of the higher flow resistance to produce more rapid flow recovery, i.e., more nearly uniform flow, is analogous to the common use of flow resistance devices (screens or perforated plates) to smooth nonuniform velocity profiles in ducts or process equipment.

4.2.3.2.15 Fuel Temperatures

Steady state fuel temperatures are determined by the FATES computer program. The calculational procedure considers the effect of linear heat rate, fuel relocation, fuel swelling, densification, thermal expansion, fission gas release, and clad deformations. The model for predicting fuel thermal performance is discussed in detail in Reference 14.

Two sets of burnup and axially dependent linear heat rate distributions are considered in the calculation. One is the hot rod, time averaged, distribution expected to persist during long term operation, and the other is the envelope of the maximum linear heat rate at each axial location. The long term distributions are integrated over selected time periods to determine burnup, which is in turn used for the various burnup dependent behavioral models in the FATES computer program. The envelope accounts for possible variations in the peak linear heat rate at any elevation which may occur for short periods of time and is used exclusively for fission gas release calculations.

The power history used assumes continuous 100 percent reactor power from beginning of life. Using this history, the highest fuel temperatures occur at beginning of life. It has been shown that fuel temperatures for a given power level at any burnup are insensitive to the previous history used to arrive at the given power level.

Fuel thermal performance parameters are calculated for the hot rod. These parameters for any other rod in the core can be obtained by using the axial location in the hot rod, whose local power and burnup corresponds to the local power and burnup in the rod being examined. This procedure will yield conservatively high stored energy in the fuel rod under consideration.

The maximum power density, including the local peaking as affected by anticipated operational occurrences, is discussed in Sections 4.3, 4.4, and Chapter 15.

4.2.3.2.16 Fuel-Cladding Interaction

An analytical model to evaluate cladding response to pellet-clad interaction has been developed[68]. This analysis which is based on an advanced version of the FATES computer code, considers generalized plane-strain of a unit section of fuel and clad. All of the physical phenomena calculation methods and input variables of the present FATES program[14] are included in the new version; and in addition, models are included for elastic and plastic stresses and strains in the clad and fuel, and fuel creep. A compatible interface modeled between the fuel and clad ensures that interaction is accurately accounted for.

The treatment of power history, axial power shapes and other operating parameters is handled similar to the current FATES version with the exception that power ramp rates and cycling can be considered. The response of the fuel and clad is calculated through an iterative process, and the interaction between the fuel and clad is established.

The resulting analytical predictions of temperatures, stresses, strains and geometric configuration are thus made available for use in conjunction with operating experience and irradiation test results in demonstrating the acceptability of the various operating conditions to which the fuel may be subjected. A detailed discussion of the methods and capabilities of the pellet-clad interaction model is contained in Reference 68.

4.2.3.2.17 Cycling and Fatigue

A fatigue analysis is performed to determine the cumulative fatigue damage of fuel rods exposed to lifetime power cycling conditions. The fatigue cycle is determined by considering combinations of normally anticipated events that would produce conservative estimates of strain in the clad. Some of the major conservative assumptions are as follows:

a) Hot spot fuel radii are used in the calculations.

b) The most adverse tolerance conditions on the fuel and cladding dimensions are chosen to produce maximum interactions and hence maximum clad strains.

The chosen fatigue cycle represents daily operation at both full and reduced power. Clad strains are calculated from the primary creep rate of the clad and used to calculate the effective strain ranges. The cumulative fatigue damage fraction is determined by summing the ratios of the number of cycles at a given effective strain range to the permitted number at that range as taken from the fatigue curve presented on Figure 4.2-2.

C-E has performed analytical predictions of cladding creep collapse time for all St. Lucie Unit 2 fuel batches that will be irradiated during Cycle 2 and has concluded that the collapse resistance of all fuel rods is sufficient to preclude collapse during their design lifetime. This lifetime will not be exceeded by the Cycle 2 duration (Table 4.2-6). The collapse analysis utilized the CEPAN computer code (Reference 80) and included conservative input values of internal pressure, cladding dimensions, cladding temperature and neutron flux.

4.2.3.3 Burnable Poison Rod

4.2.3.3.1 Burnable Poison Rod Internal Pressure and Cladding Stress

A poison shim cladding analysis will be performed to determine the stress and strain resulting from the various normal, upset, and emergency conditions discussed in Subsection 4.2.1.1. Specific accounting will be made for differential pressure, differential thermal expansion, cladding creep, and irradiation induced swelling of the Al_2O_3 B_4C burnable poison material. Owing to the very low linear heat generation rates in these rods (maximum local is less than 1.5 kW/ft), the stress analyses can be accomplished using conventional strength of materials formulae, except for determining clad collapse resistance which will be done using the CEPAN computer model[22].

Analysis of St. Lucie Unit 2 design parameters, in conjunction with review of formal calculations on other CE 16 x 16 fuel system designs that envelope anticipated plant operating conditions, provide assurance that all design limits will be met (Reference 75).

The design criteria used to evaluate the analytical results are specified in Subsection 4.2.1.3.1.

4.2.3.3.2 Potential for Chemical Reaction

A discussion of possible chemical reaction between the poison material and the coolant was presented in Subsection 4.2.1.3.3.3, along with information on chemical compatibility between poison material and cladding. Since the cladding material is identical to that of the fuel rod (Subsection 4.2.1.3.2), the description of potential chemical reactions between cladding and coolant in Subsection 4.2.3.2.3 is applicable to both fuel and poison rods.

The potential for waterlogging rupture in poison rods is much lower than that in fuel rods because of the smaller thermal and dimensional changes that occur in a poison rod during reactor power increases. Refer to Subsection 4.2.3.2.9 for a discussion of the potential for waterlogging rupture in fuel rods.

4.2.3.4 Control Element Assembly

The control rod cladding has been inspected at many reactor sites during the past several years as part of the effort to track CEA performance. The only location along the length of the cladding which had measurable wear is that corresponding to the elevation where the control rod exits the fuel assembly when the CEA is in the fully withdrawn position. The maximum wear depth observed to date (8.5 years of operation in a shutdown CEA bank) is significantly less than that which would lead to violation of the stress criteria listed in Subsection 4.2.1. Based upon the similarity of the St. Lucie 2 CEA to previous CE designs, wear depth is not expected to result in any violation of specified stress or strain limits.

Control rod nose cap wear is also believed to be present since the cap can be in contact with the fuel assembly guide tube sleeves. However, the complex shape of this component makes its inspection difficult. Since the nose cap is fabricated from a solid bar of Inconel, minor wear has no impact on CEA performance.

The CEAs were originally designed for a 10 year lifetime based on estimates of neutron absorber burnup, allowable plastic strain of the Inconel 625 cladding and the resultant dimensional clearances of the elements within the fuel assembly guide tubes.

The 10 year life limit was set based on the swelling characteristics of the original 14x14 plant CEA design. The lower portion of these CEA fingers contained boron carbide pellets rather than silver-indium-cadmium slugs. These slugs do not swell significantly under neutron irradiation. CEA inspections at both St. Lucie Units 1 and 2 demonstrated that CEAs of this design are performing well and are capable of performing their intended function in excess of 10 years (Reference 86). Life limits have been developed considering the effects of clad strain, clad wear and material degradation due to fast neutron fluence.

Analysis of St. Lucie Unit 2 design parameters, in conjunction with review of formal calculations on other CE 16 x 16 fuel system designs that envelope anticipated plant operating conditions, provide assurance that all design limits will be met (Reference 75).

a) Internal Pressure

The value of internal pressure in the control elements is dependent on the following parameters:

1) Initial fill gas pressure

2) Gas temperature

3) Helium generated and released

4) Available volume including B_4C porosity

Of the absorber materials utilized in the CEA design, only the B_4C contributes to the total quantity of gas which must be accommodated within the control element. The helium is produced by the nuclear reaction ${}_0n^1 + {}_5B^{10} \rightarrow {}_3Li^7 + {}_2He^4$, and the fraction of the quantity generated which is actually released to the plenum is temperature dependent. The release of helium from the B_4C pellets is understood to be principally dependent on diffusion, as indicated by the strong temperature dependence (°K) in the equation used to calculate release fraction for St Lucie Unit 2.

$$\text{percent released} = 208e^{-1820/T} + 5$$

Calculation of helium release from B_4C pellets is based on the maximum temperatures predicted for normal operation. While it is true that several of the anticipated operational occurrences (AOOs) produce heat generation rates (in those CEAs which remain inserted) greater than the maximum predicted for normal operation, such overpower conditions never persist for more than about 60 seconds and would not be expected to raise the pellet temperature by more

than about 200 fahrenheit degrees. Temperature excursions of this magnitude and duration would not be expected to influence a diffusion controlled helium release mechanism to any appreciable extent and so are not included in the design basis for CEA internal pressure calculations.

With respect to transients which could lead to CEA plenum temperatures in excess of 1000°F, there are none. The CEA plenum is always located above the active core region, and the temperature of the gas therein is principally dependent on the temperature of the surrounding coolant and gamma heating of the plenum spring. Since none of the AOOs produces substantial increases in either the gamma heating rate in the plenum or the local coolant temperature, it is not expected that the plenum temperature would increase significantly above the normal operation range of 600°F to 700°F.

b) Thermal Stability of Absorber Materials

None of the materials selected for the control elements are susceptible to thermally induced phase changes at reactor operating conditions. Linear thermal expansion, thermal conductivity, and melting points are given in Subsection 4.2.1.4.

c) Irradiation Stability of Absorber Materials

Irradiated properties of the absorber materials are discussed in Subsection 4.2.1.4. Irradiation induced chemical transmutations are produced in both the B_4C and Ag-In-Cd. Neutron bombardment of B-10 atoms results in the production of lithium and helium. The percent of helium released is given by the expression in Subsection 4.2.1.4.

Ag-In-Cd alloy, which has an initial chemical composition of 79 wt% minimum Ag, 15 ± 0.35 wt% In, 5 ± 0.35 wt% Cd and 0.2 wt% maximum impurities, is expected to undergo small changes in composition. Formation of three wt% tin due to the transmutation of indium and an increase in cadmium content to about 10 wt% due to the transmutation of silver is expected. These affect the thermal conductivity and linear expansion characteristics of the alloy and are accounted for in the design of the control elements.

Irradiation enhanced swelling characteristics of the absorber materials are given in Subsection 4.2.1.4. Accommodations for swelling of the absorbers have been incorporated in the design of the control elements and include the following measures:

1) All B_4C pellets have chamfered edges to promote sliding of the pellets in the cladding due to differential thermal expansion and irradiation enhanced swelling.

2) Dimensionally stable Type 304 stainless steel spacers are located at the bottom of all absorber stacks adjacent to the nose cap to minimize strain at the weld joint.

3) A hole is provided in the center of the Ag-In-Cd cylinder to accommodate swelling in excess of the amount expected over the life of the control element.

d) Potential for and Consequences of CEA Functional Failure

The probability for a functional failure of the CEA is considered to be very small. This conclusion is based on the conservatism used in the design, the quality control procedures used during manufacturing and on testing of similar full-size CEA/CEDM combinations under simulated reactor conditions for lengths of travel and numbers of trips greater than that expected to occur during the design life. The consequences of CEA/CEDM functional failure are discussed in Chapter 15.

A postulated CEA failure mode is cladding failure. In the event that an element is assumed to partially fill with water under low or zero power conditions, the possibility exists that upon returning to power, the path of the water to the outside could be blocked. The expansion of the entrapped water could cause the element to swell. In tests, specimens of CEA cladding were filled with a spacer representing the poison material. All but nine percent of the remaining volume was filled with water. The sealed assembly was then subjected to a temperature of 650°F and an external pressure of 2250 lb/in.^{2} followed by a rapid removal of the external pressure. The resulting diametral increases of the cladding were on the order of 15 to 25 mils and were not sufficient to impair axial motion of the CEA, which has a 0.084 diametral clearance with the fuel assembly guide tubes. This test result, coupled with the low probability of a cladding failure leading to a waterlogged rod, demonstrates that the probability for a CEA functional failure from this cause is low.

Another possible consequence of failed cladding is the release of small quantities of CEA filler materials, and helium and lithium (from the neutron-boron reactions). However, the amounts which would be released are too small to have significant effects on coolant chemistry or rod worth.

4.2.3.5 Mechanical Design Evaluations (AREVA CE-16 HTP™ Fuel)

The mechanical design evaluations are performed using the USNRC-approved design methods and evaluated to the USNRC-approved generic design criteria (References 96 and 97). These generic criteria are consistent with the specified acceptable fuel design limits (SAFDLs) identified in Chapter 4.2 of the Standard Review Plan (Reference 100). Reference 98 incorporates the M5® cladding material properties that were previously approved by the USNRC in Reference 99 into the AREVA mechanical design methodology. All mechanical design criteria are analyzed to meet the licensed fuel rod burnup limit of 62 MWd/kgU. EC287528

The fuel analyses are broadly separated into fuel rod analyses and structural analyses. The fuel rod analyses include evaluations of the SAFDLs such as internal rod pressure, cladding creep collapse, cladding fatigue, corrosion, etc. These evaluations are dependent on the rod power and performed each cycle to assure that the actual cycle design will not result in SAFDL non-compliance. The structural analyses are typically done once to show criteria compliance for bounding plant operating conditions, but are reviewed each cycle or revised to assure continued design compliance.

4.2.3.5.1 Input Parameters and Assumptions

The input parameters used to perform the mechanical analyses included fuel design information derived from design documents, fuel assembly and component characteristics established by mechanical / hydraulic testing, plant parameters, fatigue duty cycles created using the fatigue transients provided in the UFSAR, and fuel rod power histories.

4.2.3.5.2 Mechanical Analysis Criteria Review

The USRNC-approved generic mechanical design criteria in Reference 96, as modified by the USNRC-approved topical report in Reference 98 to incorporate M5® material properties, are summarized below. These criteria are evaluated each cycle for continued compliance.

a) Fuel Assembly Mechanical Criteria

i. Guide Tube: Limits established per SRP 4.2 Appendix A and ASME Boiler and Pressure Vessel Code, Section III, Subsection NG for Normal Operation and safe shutdown earthquake (SSE) and Appendix F for SSE+LOCA.

ii. Spacer Grids: Lateral Loads less than load limit during Normal Operation and Handling.

iii. Upper and Lower Tie Plates: Limiting loads occur during handling and postulated accidents; components maintain margin to ASME criteria. EC287528

iv. Fuel Assembly Axial Irradiation Growth: The fuel assembly length shall not exceed the minimum space between the upper and lower core pates in the cold condition at End of Life (EOL) burn-up conditions.

v. Fuel Assembly Liftoff: No liftoff from core lower support during normal operations.

vi. Fuel Assembly Handling: Assembly withstands 2.5 times the weight as a static force.

vii. Structural Deformations: Maintain coolable geometry and ability to insert control rods.

b) Fuel Rod Mechanical Criteria

All of the fuel rod mechanical criteria are based on the methodologies described in Reference 96 through 98, unless otherwise noted.

i. Cladding Collapse: Sufficient plenum spring deflection and cold radial gap to prevent axial gap formation during densification.

ii. Pellet / Cladding Interaction: For M5® cladding, strain < 1% and no centerline melting for normal operation and anticipated operational occurrences and peak rod exposures up to 62 GWd/MTU.

iii. Cladding Stress: ASME Section III, Division 1, Article III-2000, in combination with the specified 0.2% offset yield strength and ultimate strength of the

unirradiated cladding. M5® stress limit based on bi-axial burst strength of cladding. In addition, buckling criteria during the limiting overpressure at BOL is verified in accordance with Reference 99.

iv. Fuel Rod Mechanical Fracturing: ASME Section III, Division 1, Article III-2000, in combination with the specified 0.2% offset yield strength and ultimate strength of the unirradiated cladding. M5® stress limit based on bi-axial burst strength of cladding.

v. Fuel Densification and Swelling: Models included in USNRC approved fuel performance codes and taken into account in the analyses.

vi. Cladding Fatigue: Cumulative usage factor (CUF) < approved limit as provided in Reference 98.

vii. Oxidation, Hydriding, and Crud Buildup: Acceptable maximum oxide thickness. For M5® cladding, best estimate oxide < approved limit as provided in Reference 98. Effects of oxidation and crud included in thermal and mechanical fuel rod analyses. Stress analysis to include metal loss due to oxidation.

viii. Fuel Rod Axial Irradiation Growth: Clearance remains between fuel rod and upper tie plate / lower tie plate at EOL hot condition. EC287528

ix. Rod Internal Pressure: Acceptable maximum internal rod pressure < approved limit as provided in Reference 98.

4.2.3.5.3 Fuel Handling and Shipping Design Loads

The AREVA CE-16 HTP™ fuel design is evaluated for shipping and handling requirements to protect the fuel during shipment and during handling activities at the reactor site. Furthermore, spacer grid interference evaluations are performed to assure spacer grid side plate strips are protected when fuel is handled adjacent to other fuel.

a) Shipping Requirements

Fuel Assemblies are currently shipped in NRC-licensed MAP-12 Shipping Containers. Evaluations are performed to assure maximum stresses and loads on the components and component connections remain below the specified minimum strength, critical buckling loads, and/or below the stress levels for Level A service defined in the ASME Code. The following requirements are imposed on fuel shipments with these containers:

i. Fuel Assembly is capable of handling a 6 g Lateral and Vertical Acceleration Load

ii. Fuel Assembly is capable of handling a 4 g Axial Acceleration Load

iii. Fuel Assembly Spacer Grids are capable of handling a 300 lbf maximum clamping force

iv. Fuel Assembly capable of a 0.060 inch maximum deflection along the length of the fuel assembly while supported by a strongback.

If any of these requirements are violated or in question during shipping, the fuel assembly is re-inspected for critical attributes prior to loading into the core.

b) Handling Requirements

The following in-plant handling limits are evaluated and imposed on the fuel assemblies to prevent damage to the components during in-plant handling:

i. Fuel Assembly withstands 2.5 times the weight as a static force. EC287528

ii. Fuel Assembly withstands a 5 g maximum lateral acceleration when the assembly is uniformly supported by a flat surface at the spacer grids and tie plates.

iii. The Fuel Assembly withstands a 400 ft-lbf maximum moment when applied at the Upper Tie Plate Assembly.

iv. When the Fuel Assembly is handled in close proximity to other fuel assemblies or fixtures, the localized drag on the fuel assembly should be less than 0.15 g about the fuel assembly weight or comply with approved handling limits to prevent spacer grid damage.

4.2.4 TESTING AND INSPECTION PLAN

Vendor product certifications, process surveillance, inspections, tests, and material check analyses are performed to ensure conformity of all fuel assembly and control element assembly components to the design requirements from material procurement through receiving inspection at the plant site. The following are basic quality assurance measures which are performed.

4.2.4.1 Fuel Assembly Quality Program

A comprehensive quality control and inspection program is established to assure that every fuel assembly and fuel assembly components meet the requirements described in the design documents. Quality control is achieved by AREVA's Fuel Management Manual that abides by ANSI/ASME NQA-1, "Quality Assurance Program Requirements for Nuclear Facilities" and 10 CFR 50 Appendix B, "Quality Assurance Criteria for Nuclear Power Plants and Fuel Reprocessing Plants" requirements. A summary of the key fuel assembly inspections and controls are listed below: EC287528

a) An enrichment verification program which covers incoming UF6 gas to completed fuel rod

b) Verification of cladding integrity by testing and inspection of each lot of tubing received

c) Inspection of fuel pellets for conformity to specification

d) Inspection of each fuel assembly for cleanliness, straightness, envelope, rod-to-rod spacing, length and fuel rod axial position, and

e) On-site inspection for fuel rod axial position, rod-to-rod spacing, and cleanliness. EC287528

4.2.4.2 Control Element Assemblies

The CEAs are subjected to numerous inspections and tests during manufacturing and after installation in the reactor. A general product specification controls the fabrication, inspection, assembly, cleaning, packaging, and shipping of CEAs. All materials are procured to AMS, ASTM or CE specifications. In addition, various CEA hardware tests have been conducted or are in progress.

During manufacturing, the following inspections and tests are performed:

a) The loading of each control element is carefully controlled to obtain the proper amounts and types of filler materials for each CEA.

b) All end cap welds are liquid penetrant examined and helium leak tested. A sampling plan is used to section and examine end cap welds.

c) Each type of control element has unique external features which distinguish it from other types.

d) Each CEA has unique serialization on the spider (see also Figures 4.2-3 and 4.2-4).

e) Fully assembled CEAs are checked for proper alignment of the neutron absorber elements using a special fixture. The alignment check ensures that the frictional force that could result from adverse tolerances is below the force which could significantly increase trip time.

In addition to the basic measures discussed above, the manufacturing process includes numerous other quality control steps for ensuring that the individual CEA components satisfy design requirements for material quality, dimensions, and process control.

After installation in the reactor, but prior to criticality, each CEA is traversed through its full stroke and tripped. A similar procedure is conducted at refueling intervals.

The required 90 percent insertion time for CEAs shall not exceed Technical Specification (TS) drop time limits.

4.2.5 ON-LINE FUEL SYSTEM MONITORING

The Primary Sampling System (Subsection 9.3.2) is used to obtain primary coolant samples and analyze them for boron concentration, fission and corrosion product concentrations, chloride concentration, reactor coolant pH and conductivity levels.

The Secondary Sampling System (Subsection 9.3.2) is used to analyze the secondary system coolant for cation conductivity, pH, hydrazine and dissolved oxygen.

The Steam Generator Blowdown System (Subsection 10.4.8) is used in conjunction with the Chemical Feed and Secondary Sampling Systems (see Subsections 9.3.2 and 10.3.5) to control the chemistry of the secondary side water and monitor the activity in the secondary side water.

Compliance with TS limits on reactor coolant radioactivity is demonstrated by laboratory analysis of grab samples at frequencies specified in the TS.

REFERENCES: SECTION 4.2

1. Timoshenko, S., Strength of Materials, Part II Chapter IX, D. VanNostrand Co., Inc., New York, 1956.

2. "High Temperature Properties of Zircaloy and UO_2 for use in LOCA Evaluation Models," Combustion Engineering, Inc., CENPD-136 (Proprietary), CENPD-136, Rev. 01 (Non-Proprietary), July 1974.

3. CENPD-198-P, "Zircaloy Growth In Reactor Dimensional Changes In Zircaloy 4 Fuel Assemblies," December 1975, Including Supplement 1, December 1977 and Supplement 2, November 1978.

4. O'Donnel, W. J., "Fracture of Cylindrical Fuel Rod Cladding due to Plastic Instability," WAPD-TM-651, April 1967.

5. Weber, J. M., "Plastic Stability of Zircaloy-2 Fuel Cladding, Effects of Radiation of Structural Metals," ASTM STP 426, Am. Soc. Testing Mats., pp 653-669, 1967.

6. Engle, J. T. and Meieran, H. B., "Performance to Fuel Rods Having 97 Percent Theoretical Density UO_2 Pellets Sheathed in Zircaloy-4 and Irradiated at Low Thermal Ratings," WAPD-TM-631, July 1968.

7. Duncombe, E., Meyer, J. E., and Coffman, W. A., "Comparisons with Experiment of Calculated Dimensional Changes and Failure Analysis of Irradiated Bulk Oxide Fuel Test Rods Using the CYGRO-1 Computer Program," WAPD-TM-583, September 1966.

8. McCauley, J. E., et al., "Evaluation of the Irradiation Performance of Zircaloy-4 Clad Test Rod Containing Annular UO_2 Fuel Pellets (Rod 79-19)," WAPD-TM-595, December 1966.

9. Notley, M. J. F., Bain, A. S., and Robertson, J. A. L., "The Longitudinal and Diametral Expansion of UO_2 Fuel Elements," AECL-2143, November 1964.

10. Notley, M. J. F., "The Thermal Conductivity of Columnar Grains in Irradiated UO_2 Fuel Elements," AECL-1822, July 1962.

11. Manson, S. S., "Fatigue: A Complex Subject - Some Simple Approximations," Experimental Mechanics, Vol. 22, No. 2, pp 193-226, July 1965.

12. O'Donnel, W. J. and Langer, B. F., "Fatigue Design Basis for Zircaloy Components." Nuc. Sci. Eng., Vol. 20, pp 1-12, 1964.

13. CESSAR-PSAR Proprietary Appendix, Docket 50-470.

14. "CE Fuel Evaluation Model Topical Report," CENPD-139-P-A (Proprietary), CENPD-139- A (Non-Proprietary), July 1974.

15. Conway, J. B., "The Thermal Expansion and Heat Capacity of UO_2 to 2200°C," CE-NMPD-TM-63-6-6.

16. Christensen, J. A., "Thermal Expansion of UO_2," HW-75148, 1962.

17. Jones, J. M., et al., "Optical Properties of Uranium Oxides," Nature, 205, 663-65, 1965.

18. Cabannes, F. and Stora, J. P., “Reflection and Emission Factors of UO_2 at High Temperatures," C. R. Acad. Sci., Paris, Ser. B.264 (1) 45-48, 1967.

19. Held, P. C. and Wilder, D. R., "High Temperature Hemispherical Spectral Emittance to Uranium Dioxide at 0.65 and 0.70m," J. Am. Cer. Soc., Vol 52, No. 4, 1969.

20. Brassfield, M. C., "Recommended Property and Reaction Kinetics Data For Use in Evaluating a Light Water Cooled Reactor Loss-of-Coolant Incident Involving Zircaloy-4 or 324-53 Clad UO_2," GEMP-482, 1968.

21. Beals, R. J., "High Temperature Mechanical Properties of Oxide Fuels," ANL-7577, April-May 1969, Page 160.

22. "CEPAN, Method of Analyzing Creep Collapse of Oval Cladding," Combustion Engineering, Inc., CENPD-187 P-A, March 1976.

23. "STRIKIN-II, A Cylindrical Geometry Fuel Rod Heat Transfer Program," Combustion Engineering, Inc., CENPD-135P (Proprietary), CENPD-135, Rev 01 (Non-Proprietary), August 1974.

24. Deverall, J. E., LA-2669 USAEC, Vol 62, 1954.

25. Rudkin, R. L., Parker, J. W., and Jenkins, R. J., ASD-TDR-62-24, Vol 1, p 20, 1963.

26. Thorne, R. P. and Howard, V. C., "Changes in Polycrystalline Alumina by Fast Neutron Irradiation," p 415, Proceedings of the British Ceramic Society, No. 7, February 1967.

27. Simnad, M. T. and Meyer, R. S., "BeO Review of Properties for Nuclear Reactor Applications," Proceedings of the Conference on Nuclear Applications of Nonfissionable Ceramics, pp 209-210, May 9-11, 1966.

28. Rason, N. S. and Smith, A. W., "NAA-SR-862," Vol 37 (AD85006), 1954.

29. Saba, W. G. and Sterret, K. F., "J. Am. Chem. Soc.," Vol. 79, pp 3637-38.

30. "Fuels and Materials Development Quarterly Progress Report," pp 38-58, ONRL-TM-3703, December 31, 1971.

31. Kingery, W. D., "Introduction to Ceramics," John Wiley & Sons, pp 486-504.

32. Toulookan, Y. S., "Thermophysical Properties of High Temperature Solid Materials," Vol 4 and 5, MacMillan.

33. Moore, G. E. and Kelley, K. K., "J. Am. Chem. Soc.," Vol 69, pp 309-16, 1947.

34. Keilholtz, G. W., Moore, R. E., and Robitson, M. E., "Effects of High Boron Burnups on B_4C and ZrB_2 Dispersions in Al_2O_3 and Zircaloy-2," BMI-1627, April 24, 1963.

35. Burian, R. J., Fromm, E. O., and Gates, J. E., "Effect of High Boron Burnups on B_4C and ZrB_2 Dispersions in Al_2O_3 and Zircaloy-2," BMI-1627, April 24, 1963.

36. Cunningham, G. W., "Compatibility of Metals and Ceramics," Proceedings of Nuclear Applications of Nonfissionable Ceramics, pp 279-289, May 1966.

37. Graber, M. J., "A Metallurgical Evaluation of Simulated BWR Emergency Core Cooling Tests," Idaho Nuclear Corporation, IN-1453, March 1971.

38. Pitner, A. L., "The WDC-l-l Instrumental Irradiation of Boron Carbide in a Spectrum-Hardened ETR Flux," HEDL-TME-73-38, April 1973.

39. Gray, R. G. and Lynam, L. R., "Irradiation Behavior of Bulk B_4C and B_4C -SiC Burnable Poison Plates," WAPD-261, October 1963.

40. "HEDL Quarterly Technical Report for October, November and December 1974," Vol 1, HEDL-TME-74-4, pp A-51 to A-53, January 1975.

41. Mahagan, D. E., "Boron Carbide Thermal Conductivity," HEDL-TME-73-78, September 1973.

42. Homan, F. J., "Performance Modeling of Neutron Absorbers," Nuclear Technology, Vol 16, pp 216-225, October 1972.

43. Pitner, A. L. and Russcher, G. E., "Irradiation of Boron Carbide Pellets and Powders in Hanford Thermal Reactors," WHAN-FR-24, December 1970.

44. Pitner, A. L. and Russcher, G. E., "A Function to Predict LMFBR Helium Release Bound on Boron Carbide Irradiation Data from Thermal Reactors," HEDL-TME-71-127, September 30, 1971.

45. HEDL-73-6, "Materials Technology Program Report for October, November, and December 1973," pp A-69 to A-72.

46. Cohen, I., "Development and Properties of Silver-Based Alloys as Control Rod Materials For Pressurized Water Reactors," WAPD-214, December 1959.

47. Tipton, C. R., "Reactor Handbook," Vol 1, Materials, Interscience, p 827, 1960.

48. "National Alloy Development Program Information Meeting," pp 39-63, TC-291, May 22, 1975.

49. "Quarterly Progress Report - Irradiation Effects on Structural Materials," HEDL-TEM-161, pp GE-5 - GE-10.

50. "Structural Analysis of Fuel Assemblies for Seismic and Loss of Coolant Accident Loadings," Combustion Engineering, Inc., CENPD-178-P, Revision 1, August 1981.

51. "Joint CE/EPRI Fuel Performance Evaluation Program, Task C, Evaluation of Fuel Rod Performance on Maine Yankee Core I," Combustion Engineering, Inc., CENPD-221, December 1975.

52. "Pressurized Water Reactor Project Period January 24, 1964 to April 23, 1964," WAPD-MRP-108.

53. "Fuel and Poison Rod Bowing," Combustion Engineering, Inc., CENPD-225-P (Proprietary), October 1976, CENPD-225-P-A (Proprietary), CENPD-225-NP-A (Non-Proprietary), June 1983.

54. Caye, T. E. "Saxton Plutonium Project, Quarterly Progress Report for the Period Ending March 31, 1972," WCAP-3385-31, November 1972.

55. Berman, R. M. Meieran, H. B., and Patterson, P., "Irradiation Behavior of Zircaloy Clad Fuel Rods Containing Dished End UO_2 Pellets," (LWBR-LSBR Development Program), WAPD-TM-629, July 1967.

56. Baroch, S. J., et al., "Comparative Performance of Zircaloy and Stainless Steel Clad Fuel Rods Operated to 10,000 MWd/MTU in the VBWR," GEAP-4849, April 1966.

57. Megerth, F. H., "Zircaloy-Clad UO_2 Fuel Rod Evaluation Program," Quarterly Progress Report No. 8, August 1969-October 1969. GEAP-10121, November 1969.

58. Megerth, F. H., "Zircaloy-Clad UO_2 Fuel Rod Evaluation Program," Quarterly Progress Report No. 1, November 1967-January 1968, GEAP-5598, March 1968.

59. San Onofre Nuclear Generating Station, Units 2 & 3, Final Safety Analysis Report, Volume-9, pages 4.2-59 - 4.2-61.

60. Brite, D. W. et al., "EEI/EPRI Fuel Densification Program Final Report," Battelle Pacific Northwest Laboratories, March 1975.

61. Stephan, L. A., "The Response of Waterlogged UO_2 Fuel Rods to Power Bursts," IDO-ITR-105, April 1969.

62. Stephan, L. A., "The Effects of Cladding Material and Heat Treatment on the Response of Waterlogged UO_2 Fuel Rods to Power Burst," IM-ITR-III, January 1970.

63. "TORC Code: A Computer Code for Determining the Thermal Margin of a Reactor Core," Combustion Engineering, Inc., CENPD-161-P, (Proprietary) July 1, 1975, CENPD-161-P- A (Proprietary), CENPD-161-NP-A (Non-Proprietary), April 1986.

64. Joon, K., "Primary Hydride Failure of Zircaloy Clad Fuel Rods," ANS Transactions, Vol 15, No. 1.

65. "Application of Zircaloy Irradiation Growth Correlations for the Calculation of Fuel Assembly and Fuel Rod Growth Allowances," Supplement 1 to CENPD-198P, (Proprietary), December 1977.

66. Marlowe, M. O., "High Temperature Isothermal Elastic Moduli of UO_2," Journal of Nuclear Materials, Vol. 33 (1969), pages 242-244.

67. Pickman, D. O., "Properties of Zircaloy Cladding," Nuclear Engineering and Design, Vol 21, No. 2 (1972).

68. "CE Thermo-Structural Fuel Evaluation Method," Combustion Engineering, Inc., CENPD-179, April 1976.

69. J. A. Christensen, et. al., "Melting Point of Irradiated Uranium Dioxide," ANS Transactions, Volume 7:2, November, 1964, P. 390.

70. Data of T. T. Claudson, T.C. Ehlert and J. L. Margrave as reported J. Belle, Editor, Uranium Dioxide Properties and Nuclear Application, US Government Printing Office, Washington, D.C., 1961, pages 196-197.

71. "Introduction to Ceramics," W.D. Kingery, John Wiley & Sons, 1960, pp 469-471.

72. Simnad, M. T., Meyer, R. A.; "BeO Review of Properties for Nuclear Reactor Applications," Proceedings of the Conference on Nuclear Applications of Nonfissionable Ceramics, May 9-11, 1966, pp 193-206.

73. Thorne, R. P., Howard, V. C.; "Changes in Polycrystalline Alumina by Fast Neutron Irradiation," pp. 441-445, Proceedings of the British Ceramic Society, No. 7, February 1967.

74. "Standard Specification for Sintered Uranium Dioxide Pellets," ASTM Standard C776-76, Part 45 (1977).

75. "St. Lucie 2 Fuel and CEA Design Summary Evaluation Report," Combustion Engineering, Inc., CEN-222(L)-P, October 1982.

76. "Final Assessment of St. Lucie 2 Fuel Structural Integrity Under Faulted Conditions," Combustion Engineering, Inc., CEN-187(L)-P, Revision 1-P, (transmitted to NRC in FP&L Letter L-82-455 dated 10/26/82).

77. "Data Transmittal for Review of SCE Fuel Structural Integrity Under Faulted Conditions," Combustion Engineering, Inc., CEN-151(S)-P, March 1981.

78. Letter, R. A. Clark (NRC) to A. E. Lundvall, Jr. (BG&E), "Safety Evaluation of CEN-161 (FATES 3)," March 31, 1983.

79. "Improvements to Fuel Evaluation Model," CEN-161(B)-P, July 1981, CEN-161 (B)-P-A (Proprietary), CEN-161(B)-NP-A (Non-Proprietary), August 1989.

80. CENPD-187, "CEPAN Method of Analyzing Creep Collapse of Oval Cladding," June 1975.

81. Letter, E. L. Trapp (C-E) to H. A. Barth (FP&L), "Final Reload Safety Evaluation (RSE) Report for St Lucie 2 Cycle 4 Operation," F2-CE-R-171, September 9, 1987, as subsequently amended.

82. Letter, E. L. Trapp (C-E) to H. A. Barth (FP&L), "50.59 Evaluation of CE's Proposed Modification to the St Lucie Unit 2 Region G Lower End Fitting," F2-CE-R-198, November 20, 1987.

83. Letter, E. L. Trapp (C-E) to H. A. Barth (FP&L), "Proposed Modification to the Lower End Fitting Design for St Lucie Unit 2 Region G," F2-CE-R-189, November 3, 1987.

84. CEN-396(L)-P (proprietary), CEN-396(L)-NP (non-proprietary),"Verification of the Acceptability of a 1-Pin Burnup Limit of 60 MWd/kg for St. Lucie Unit 2," November, 1989.

85. J. A. Norris (U.S. NRC) to J. H. Goldberg (FPL), "St. Lucie Unit 2 - Fuel Pin Burnup of 60 MWd/kg," Docket NO. 50-389, October 18, 1991.

86. PSL-ENG-SEFJ-02-006, "St. Lucie Unit 2 Control Element Assembly (CEA) Lifetime Determination."

87. “Improvements to Fuel Evaluation Model,” CEN-161(B)-P, Supplement 1-P-A (Proprietary), CEN-161(B)- P, Supplement 1-NP-A (Non-Proprietary), January 1992.

88. “C-E Methodology for PWR Core Designs Containing Gadolinia-Urania Burnable Absorbers,” CENPD-275-P, Revision 1-P, Supplement 1-P-A (Proprietary), CENPD-275-NP, Revision 1-NP, Supplement 1- NP-A (Non-Proprietary), April 1999.

89. C-E Methodology for Core Designs Containing Gadolinia-Urania Burnable Absorbers,” CENPD-275-P, Revision 1-P-A (Proprietary), CENPD-275-NP Revision 1-NP-A (Non-Proprietary), May 1988.

90. “Methodology for Core Designs Containing Erbium Burnable Absorbers,” CENPD 382-P-A (Proprietary), CENPD 382-NP-A (Non-Proprietary), August 1993.

91. “Report on the Continued Applicability of 60 MWD/kgU for ABB Combustion Engineering PWR Fuel,” CENPD 384-P (Proprietary), CENPD 384-NP (Non-Proprietary), September 1995.

92. “Fuel rod Maximum Allowable Gas Pressure,” CEN-372-P-A (Proprietary), CEN-372-NP-A (Non- Proprietary), May 1990.

93. “Verification of the Acceptability of a 1-Pin Burnup Limit of 60 MWD/KgU for Combustion Engineering 16X16 PWR Fuel,” CEN-386-P-A (Proprietary), CEN-386-NP-A (Non-Proprietary), August 1992.

94. “Extended Burnup Operation of Combustion Engineering PWR Fuel,” CENPD-269-P, Rev 1-P (Proprietary), CENPD-269-NP, Rev 1-P (Non-Proprietary), July 1984.

95. “Implementation of ZIRLO™ Cladding Material in CE Nuclear Power Fuel Assembly Designs,” CENPD-404-PA, Rev 0, November 2001.

96. EMF-92-116(P)(A), Revision 0, “Generic Mechanical Design Criteria for PWR Fuel Designs."

97. EMF-92-116(P)(A), Revision 0, Supplement 1, Revision 0(P)(A), “Generic Mechanical Design Criteria for PWR Fuel Designs.”

98. BAW-10240(P)(A), Revision 0, “Incorporation of M5 Properties in Framatome ANP Approved Methods."

99. BAW-10227(P)(A), Revision 1, “Evaluation of Advanced Cladding and Structural Material (M5) in PWR Reactor Fuel.”

100. NUREG-0800, Revision 2, "Standard Review Plan for the Review of Safety Analysis Reports for Nuclear Power Plants, LWR Edition."

101. BAW-10133(P)(A), Revision 1, and Addenda 1 and 2, "Mark C Fuel Assembly LOCA-Seismic Analysis."

102. ANP-3352P, Revision 1, “St. Lucie Unit 2 Fuel Transition License Amendment Request.”

103. ANP-3396P, Revision 0, “St. Lucie Unit 2 Fuel Transition Supplemental Information to Support LAR”

104. ML16063A121, “St. Lucie Plant, Unit No. 2 – Issuance of Amendment Regarding Transitioning to AREVA Fuel (CAC No. MF5495).

EC287528

TABLE 4.2-1

MECHANICAL DESIGN PARAMETERS

Cycle 1

Core Arrangement

Number of fuel assemblies in core, total	217
Number of CEAs	83
Number of fuel and poison rod locations	51,212
Spacing between fuel assemblies, fuel rod surface to surface, in.	0.208
Spacing, outer fuel rod surface to core shroud, in.	0.214
Hydraulic diameter, nominal channel, ft.	0.0394
Total flow area (excluding guide tubes), ft^2	54.8
Total core area, ft^2	101.1
Core equivalent diameter, in.	136
Core circumscribed diameter, in.	143
Total fuel loading, Kg U	81.7×10^3
Total fuel weight, lb UO_2	204.4×10^3
Total weight of Zircaloy, lb	59,008
Fuel volume (including dishes), ft^3	325

Fuel Assemblies*

Batch	No. of Assemblies	Enrichment (wt%) U-235	No. of Poison Rods per Assembly
A	73	1.71	0
B	80	2.28	16
C	40	2.73	0
C0	8	2.73	12
CI	16	2.73	16

Fuel Rod array square 16 x 16
Fuel Rod Pitch, in. 0.506

Spacer Grid (HID-1):

Type	Leaf spring
Material	Zircaloy-4
Number per assembly	9
Weight each, lb	1.8

Bottom Spacer Grid:

Type	Leaf spring
Material	Inconel 625
Number per assembly	1

* Current cycle values are in Table 4.2-10.

TABLE 4.2-1 (Cont'd)

Fuel Assemblies (Cont'd)

Weight each, lb	2.6
Weight of fuel assembly, lb	1303
Outside dimensions:	
Fuel rod to fuel rod, in.	7.972 x 7.972
Fuel Rod:	
Fuel rod material (sintered pellet)	UO_2
Pellet diameter, in.	0.325
Pellet length, in.	0.390
Pellet density, g/cm^3	10.38
Pellet theoretical density, g/cm^3	10.96
Pellet density (% theoretical)	94.75
Stack height density, g/cm^3	10.061
Clad material	Zircaloy-4
Clad ID, in.	0.332
Clad OD, (nominal), in.	0.382
Clad thickness, (nominal), in.	0.025
Diametral gap, (cold, nominal), in.	0.007
Active length, in.	136.7
Plenum length, in.	8.158
Control Element (CEA):	
Number	83
Absorber elements, No. per assy.	5,4
Type	Cylindrical rods
Clad Material	Inconel 625

TABLE 4.2-1 (Cont'd)

Fuel Assemblies (Cont'd)

Control Element (CEA):	
Clad thickness, in.	0.035
Clad OD, in.	0.816
Diametral gap, in.	0.009
Center Element[(a)]	
Poison material	B_4C/Ag-In-Cd
Poison length, in.	123/l2.5
Outside Elements	
Poison Material	B_4C/Ag-In-Cd
Poison Length, in.	123/12.5
B_4C Pellet	
Diameter, in.	0.737
Density, % of theoretical density	73
of 2.52 g/cm^3	
Weight % boron, minimum	77.5
Burnable Poison Rod:	
Absorber material	Al_2O_3-B_4C
Pellet diameter, in.	0.307
Pellet length, in., min	0.500
Pellet density (% theoretical), min	93
Theoretical density, Al_2O_3, g/cm^3	3.90
Theoretical density, B_4C, g/cm^3	2.52
Clad material	Zircaloy-4

[(a)] Not Applicable for Four – Element CEA

For four-element CEA configuration, see Figure 4.2-4

TABLE 4.2-1 (Cont'd)

Burnable Poison Rod (Cont'd)

Clad ID, in.	0.332
Clad OD, in.	0.382
Clad thickness, (nominal), in.	0.025
Diametral gap, (cold, nominal), in.	0.025
Active length, in.	122.7
Plenum length, in.	8.159

TABLE 4.2-2

ABSORBER MATERIALS - THERMAL AND PHYSICAL PARAMETERS

1) Boron Carbide (B_4C):

Configuration	Right cylinder	
Outside diameter in.	0.737 ±0.001	
Pellet length, in. nominal	2	
End chamfer	0.03" x 45° CHAMF	
Density gm/cc	1.84	
Weight % boron, minimum	77.5	
% open porosity in pellet	27	
Thermal conductivity (cal/cm-sec-C)	Irradiated	Unirradiated
800 F	8.3×10^{-3}	28×10^{-3}
1000 F	7.9×10^{-3}	24×10^{-3}
Melting point, F	4,440	
% thermal linear expansion	0.23% @ 1000 F	

2) Silver-Indium-Cadmium (Ag-In-Cd):

Configuration	Cylindrical bars with central hole	
O.D. in.	0.734 ± .003	
I.D. in.	1/4	
Length of bar, inches nominal	12 1/2	
Density, lbs/in^3.	0.367	
Thermal conductivity (cal/cm-sec-C)	Irradiated	Unirradiated
at 300 C	0.14	0.182
at 400 C	0.148	0.196
Melting Point, F	1,470	
Linear Thermal Expansion, m/m- F	12.5×10^{-6}	

TABLE 4.2-3

TENSILE TEST RESULTS ON IRRADIATED SAXTON CORE III CLADDING[54]

Fluence (>1 MeV) 4.7 x 10^{21} n/cm^2 (estimated)

Rod ID	Location From Bottom (in.)	Testing Temp (°F)	0.2% Yield Stress (lb/in^2 x 10^3)	Ultimate Tensile Strength (lb/$in.^2$ x10^3)	Uniform Strain In 2-in. Gage Length (%)	Total Strain In 2-in. Gage Length
BO	11-17	650	61.4	65.6	2.2	6.8
BO	26-32	650	58.1	68.9	2.4	11.3
RD	3-9	650	62.2	70.0	2.0	4.2
RD	12-18	650	60.5	65.4	1.7	5.8
MQ	12-18	675	70.4	77.4	1.9	6.1
MQ	28-34	675	66.0	75.1	1.6	6.2
FS	28-34	675	57.2	71.4	3.9	12.9
GL	12-18	675	60.5	71.5	2.4	9.3

Table 4.2-4

POOLSIDE FUEL INSPECTION PROGRAM SUMMARY

Reactor	Shutdown Date/Cycle	Cycle Average Burnup (Mwd/Mtu)	Inspection Program Scope
Palisades	August 1973/IA	6,800	Visual Exam, Gamma-Scanning, Crud Sampling
Maine Yankee	June 1974/I	10,400	Visual Exam, Sipping, Disassembly/Single Rod Exams, Crud Sampling
	May 1975/IA	4,450	Visual Exam, Sipping
	April 1977/Core 2 Cycle I	17,400	Visual Exam, Disassembly/Single Rod Exams
	July 1978/Core 2 Cycle II		Visual Exam
Ft. Calhoun	February 1975/I	9,000	Visual Exam
	October 1975/II	10,900	Visual Exam, Crud Sampling
	September 1977/III	7,700	Visual Exam
Calvert Cliffs-I	December 1976/I	17,000	Visual Exam, CE/EPRI Test Bundle Disassembly, Single Rod Exam
	January 1978/II	8,300	Visual Exam. CE/EPRI Test Bundle Disassembly, Single Rod Exam
	April 1979/II	9,500	Visual Exam, CE/EPRI Test Bundle Disassembly, Single Rod Exam
Millstone-II	November 1977/I	15,100	Visual Exam
	March 1979/II	9,200	
			Visual Exam
St. Lucie-I	July 1976/I	800	Visual Exam, Disassembly and Single Rod Exams
	March 1978/IA	12,400	Visual Exam
Calvert Cliffs - II	September 1978/I	16,200	Visual Exam

TABLE 4.2-5

COMPARISON OF POISON MATERIAL CONTENT FOR FULL-LENGTH CEAs (5 ELEMENT)

Cycle 2

	"Reduced Strength" CEAs	"Full Strength" CEAs
Poison Material	B_4C/Ag-In-Cd (2 Outer Diagonal Elements) Al_20_3/Inconel 625 (3 Elements, Center and 2 Outer Diagonals)	B_4C/Ag-In-Cd
Poison Length (inches)	123/12.5 123/13.5	123/12.5

TABLE 4.2-6

ST. LUCIE 2 CYCLE 2
CLADDING COLLAPSE PREDICTIONS

Batch	Minimum Predicted Time to Collapse (EFPH)*	EOC2 Exposure (EFPH)
B	>30,900	20,000
C	>30,900	20,000
D	>29,000	10,000

*EFPH = Effective Full Power Hours

TABLE 4.2-7

ST. LUCIE UNIT 2

Typical Values of Reactivity Worths and Allowances for the
Hot Zero Power (HZP) End of Cycle (EOC)
Steam Line Break (SLB) Accident, %$\Delta\rho$

		Typical Cycle
1.	Worth of all CEAs Inserted (Including Bias)	10.1
2.	Stuck CEA Allowance	1.7
3.	Worth of All CEAs Less Highest Worth CEA Stuck Out	8.4
4.	Zero Power Insertion Limit CEA Bite	1.8
5.	Calculated Scram Worth (Item 3 minus Item 4)	6.6
6.	Physics Uncertainty	0.5
7.	Net Available Scram Worth (Item 5 minus Item 6)	6.1
8.	Technical Specification Shutdown Margin	5.0
9.	Margin in Excess of Technical Specification	+1.1

TABLE 4.2-8

ST. LUCIE UNIT 2

Typical Reactivity Worth of CEA Regulating Groups
at Full Power, %$\Delta\rho$

Regulating CEAs	BOC	EOC
Group 5 (Lead Bank)	0.62	0.61
Group 4	0.34	0.36
Group 3	0.89	1.13

Note:

Values shown assume sequential group insertion.

TABLE 4.2-9

This table has been deleted.

TABLE 4.2-10
MECHANICAL DESIGN PARAMETERS
Current Cycle

Core Arrangement

Number of fuel assemblies in core, total	217
Number of CEAs	91
Number of fuel and poison rod locations	51,212
Spacing between fuel assemblies, fuel rod surface to surface in.	0.208
Spacing, outer fuel rod surface to core shroud, in.	0.214
Hydraulic diameter, nominal channel, ft.	0.0394
Total flow area (excluding guide tubes), ft^2	54.8
Total core area, ft^2	101.1
Core equivalent diameter, in.	136
Core circumscribed diameter, in.	143

TABLE 4.2-10 (Cont'd)

Fuel Assemblies (Cont'd) AREVA Fuel Starting with Cycle 23

EC287528

Spacer Grid (HTP™)	
Type	High Thermal Performance (HTP™)
Material	Zircaloy-4
Number per assembly	9
Weight each, lb	2.3
Bottom Spacer Grid (HMP™)	
Type	High Mechanical Performance (HMP™)
Material	Alloy 718
Number per assembly	1
Weight each, lb	2.4
Weight of Fuel Assembly, (nominal), lb	1,336
Outside dimensions:	
Fuel rod to fuel rod, inches	7.972 x 7.972
Fuel Rod	
Fuel rod material (sintered pellet)	UO_2 or combination of UO_2 and Gd_2O_3-UO_2
Pellet diameter, inches	0.3255
Pellet length, inches	0.407 (Central Zones)
	0.506 (Blanket Zones)
Pellet density, g/cm^3	10.45 (UO_2)
Pellet density (% of theoretical)	95.35
Clad material	M5® Zirconium Alloy
Clad ID, (nominal), inches	0.332
Clad OD, (nominal), inches	0.382
Clad thickness, (nominal), inches	0.025
Diametral gap, (cold, nominal), inches	0.0065
Active length, inches	136.7
Plenum length, inches	7.39

TABLE 4.2-10 (Cont'd)

Fuel Rod (Cont'd)

Control Element (CEA):	
Number	91
Absorber elements, No. per assy.	5,4
Type	Cylindrical rods
Clad material	Inconel 625
Clad thickness, in.	0.035
Clad OD, in.	0.816
Diametrical gap, in.	0.009
Center Element[(a)]	
Poison material	B_4C/Ag-In-Cd
Poison length, in.	123/12.5
Outside Elements	
Poison Material	B_4C/Ag-In-Cd
Poison Length, in.	123/12.5
B4C Pellet	
Diameter, in.	0.737
Density, % of theoretical density of 2.52 g/cm3	73
Weight % boron, minimum	77.5
Burnable Poison Rod:	
Absorber material	Al_2O_3-B_4C
Pellet diameter, in.	0.307
Pellet length, in., min	0.500
Pellet density (% theoretical), min	93
Theoretical density, Al_2O_3, g/cm^3	3.90

[(a)] = Not Applicable for Four - Element CEA

For four-element CEA configuration, see Figure 4.2-4.

TABLE 4.2-10 (Cont'd) Burnable Poison Rod (Cont'd)

Theoretical density, B_4C, g/cm3	2.52
Clad material	Zircaloy-4
Clad ID, in.	0.332
Clad OD, in.	0.382
Clad thickness, (nominal), in.	0.025
Diametral gap, (cold, nominal), in.	0.025
Active length, in.	124.7
Plenum length, in.	7.642
Gadolinium Poison Rod[b]	
Absorber Material	Gd_2O_3 (Homogeneously mixed with UO_2)
Poison Length, in.	115.7 (10.5 inches cutback length at each end with only UO_2)
Erbium Poison Rod	
Absorber material	Er_2O_3 (Homogeneously mixed with UO_2)
Poison Length, in	Erbia is not currently included in the St. Lucie Unit 2 Core Design

[b] Dimensions are the same as those for Fuel Rod

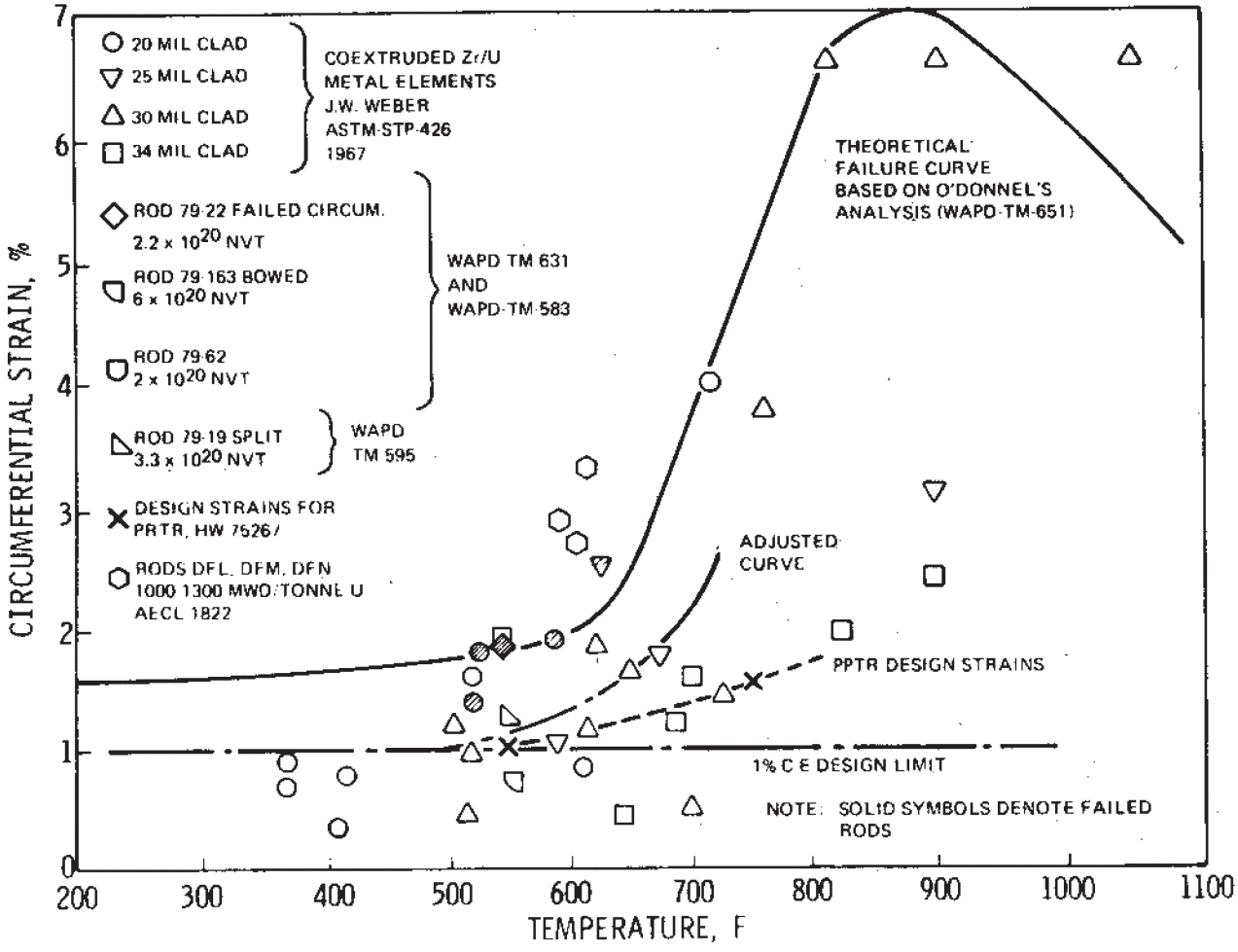

FLORIDA POWER & LIGHT COMPANY
ST. LUCIE PLANT UNIT 2

CIRCUMFERENTIAL STRAIN VS TEMPERATURE
FIGURE 4.2-1

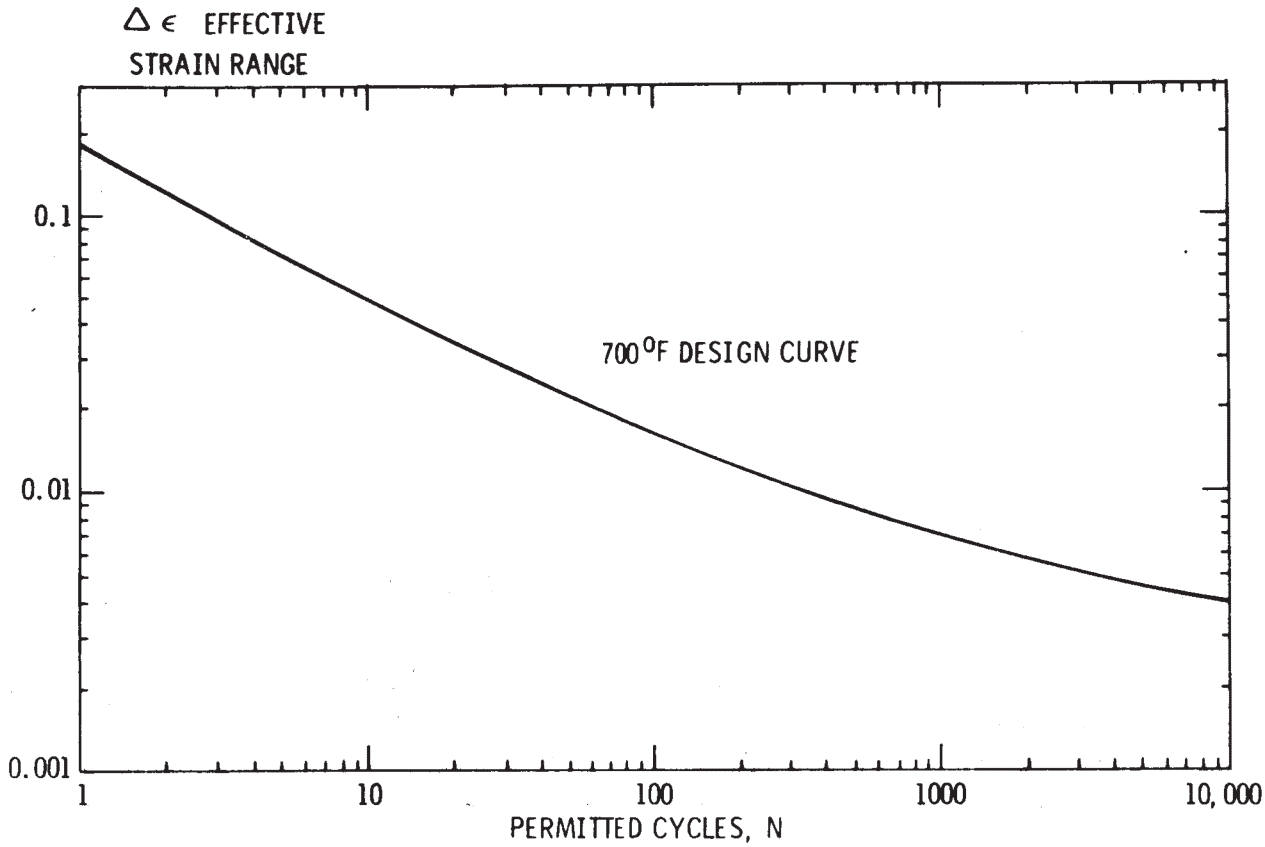

33)

FLORIDA POWER & LIGHT COMPANY
ST. LUCIE PLANT UNIT 2

DESIGN CURVE FOR CYCLIC STRAIN USAGE OF ZIRCALOY – 4 AT 700° F

FIGURE 4.2-2

Refer to Drawing
2998-20737

FLORIDA POWER & LIGHT COMPANY
ST. LUCIE PLANT UNIT 2

CONTROL ELEMENT
ASSEMBLY (5-ELEMENT)
FIGURE 4.2-3

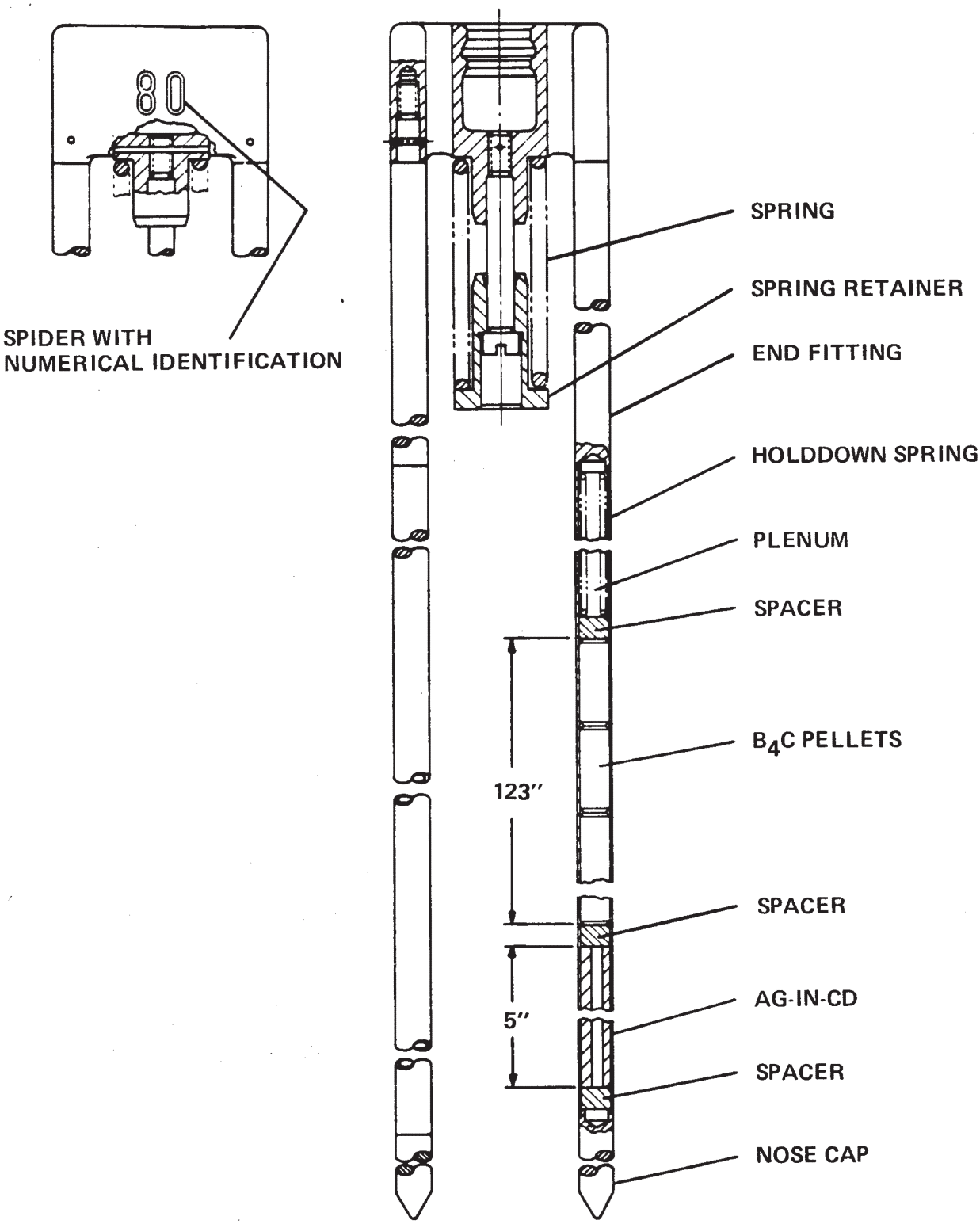

FLORIDA POWER & LIGHT COMPANY
ST. LUCIE PLANT UNIT 2

CONTROL ELEMENT
ASSEMBLY (4-ELEMENT)
FIGURE 4.2-4

FIGURE 4.2-5 HAS BEEN INTENTIONALLY

DELETED.

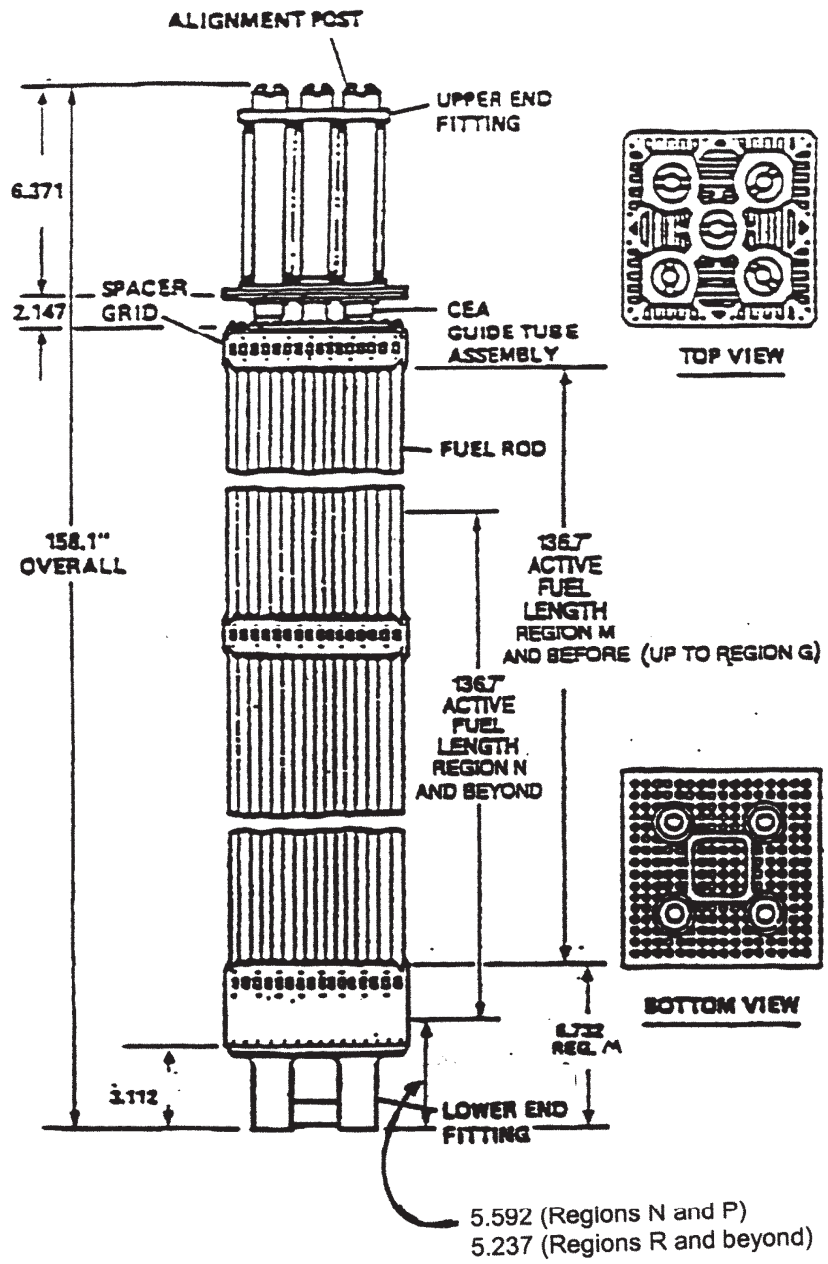

	FLORIDA POWER & LIGHT ST. LUCIE PLANT UNIT 2
Amendment No. 14 (12/01)	FUEL ASSEMBLY FIGURE 4.2-6

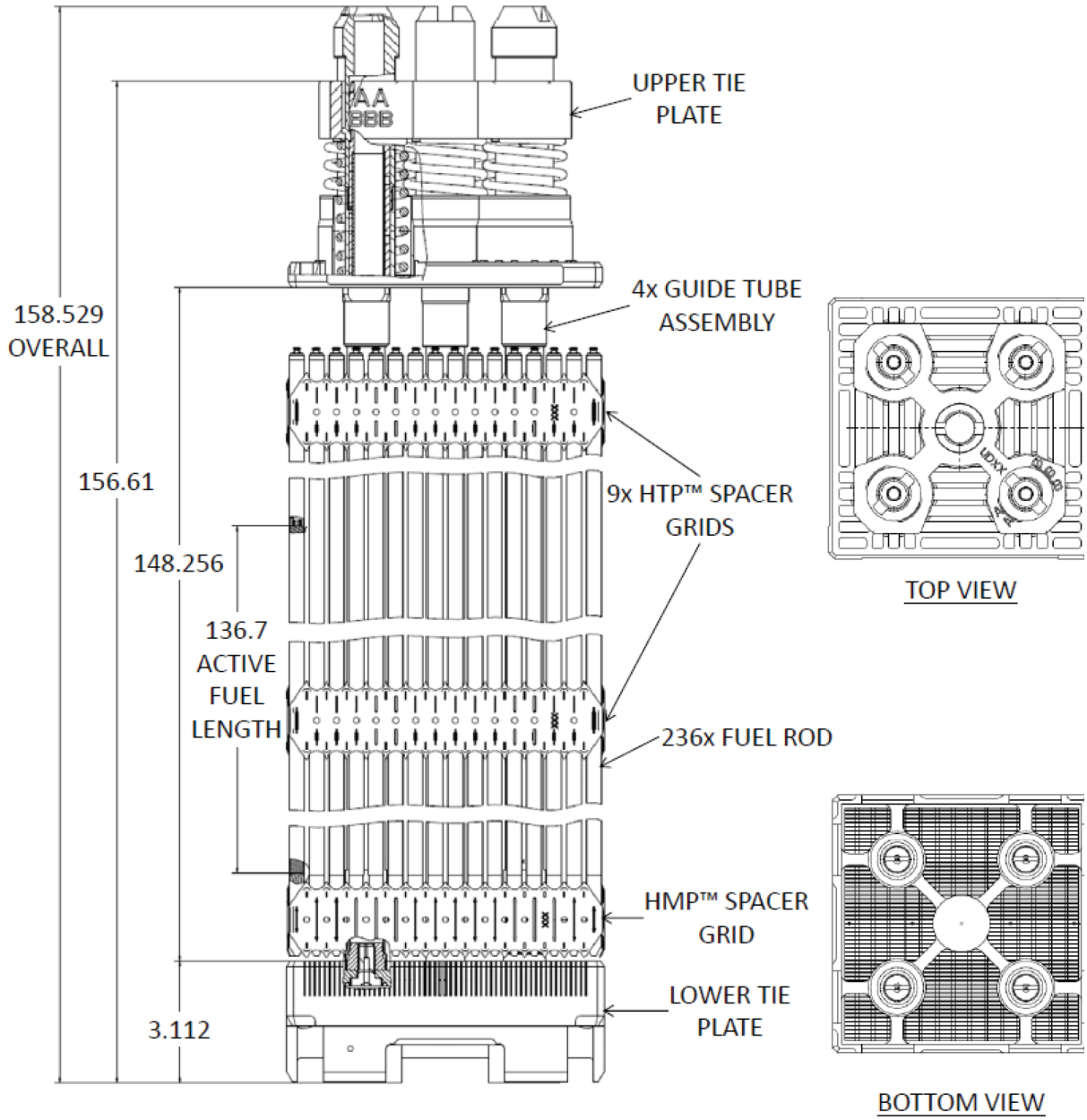

EC287528

FLORIDA POWER & LIGHT COMPANY
ST. LUCIE PLANT UNIT 2

Figure 4.2-6a
AREVA CE-16 HTP™ Fuel Assembly

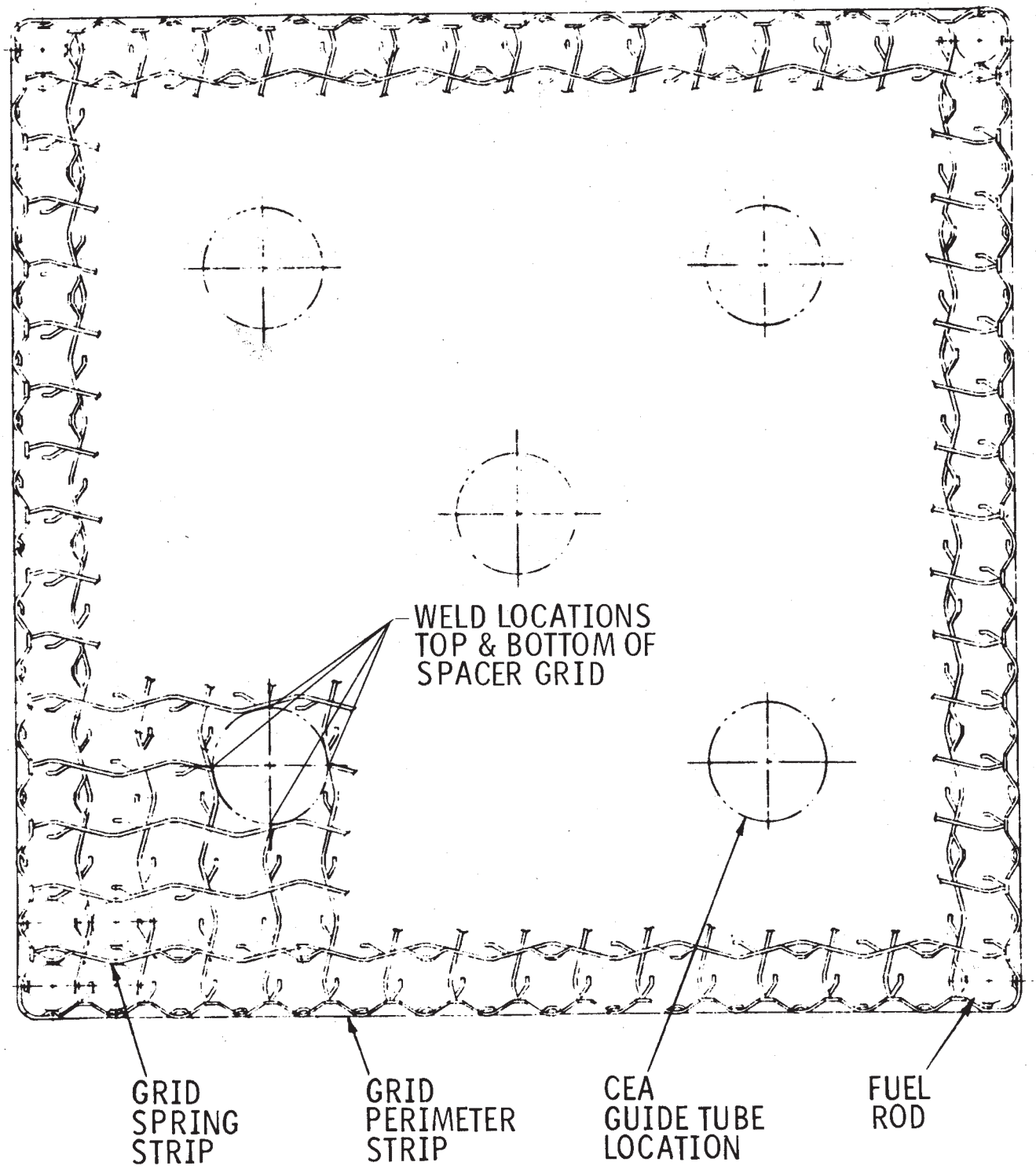

FLORIDA POWER & LIGHT COMPANY
ST. LUCIE PLANT UNIT 2

FUEL SPACER GRID

FIGURE 4.2-7

REGION N

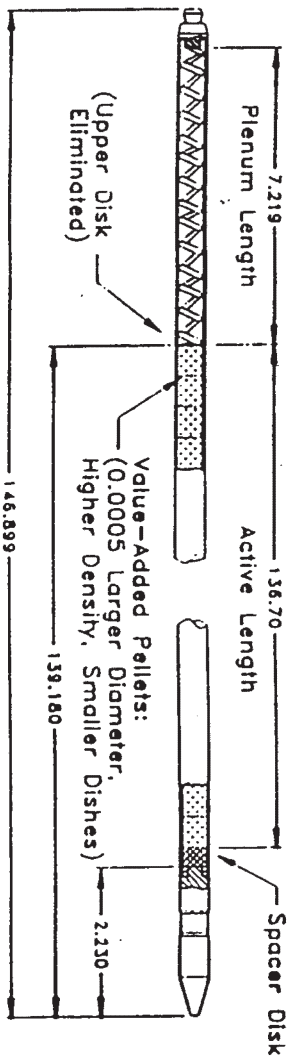

GUARDIAN GRID DESIGN

REGION G – M

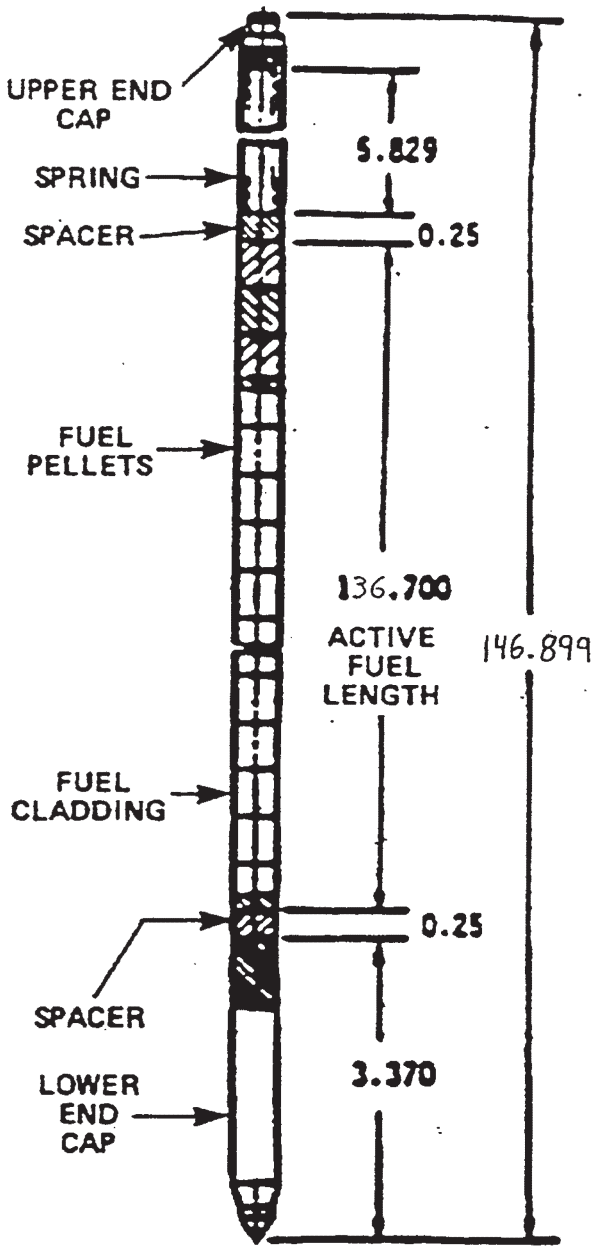

DEBRIS RESISTANT DESIGN

Amendment No. 12 (12/98)

FLORIDA POWER & LIGHT COMPANY
ST. LUCIE PLANT UNIT 2

GUARDIAN GRID AND
DEBRIS RESISTANT
FUEL ROD DESIGN

FIGURE 4.2-8

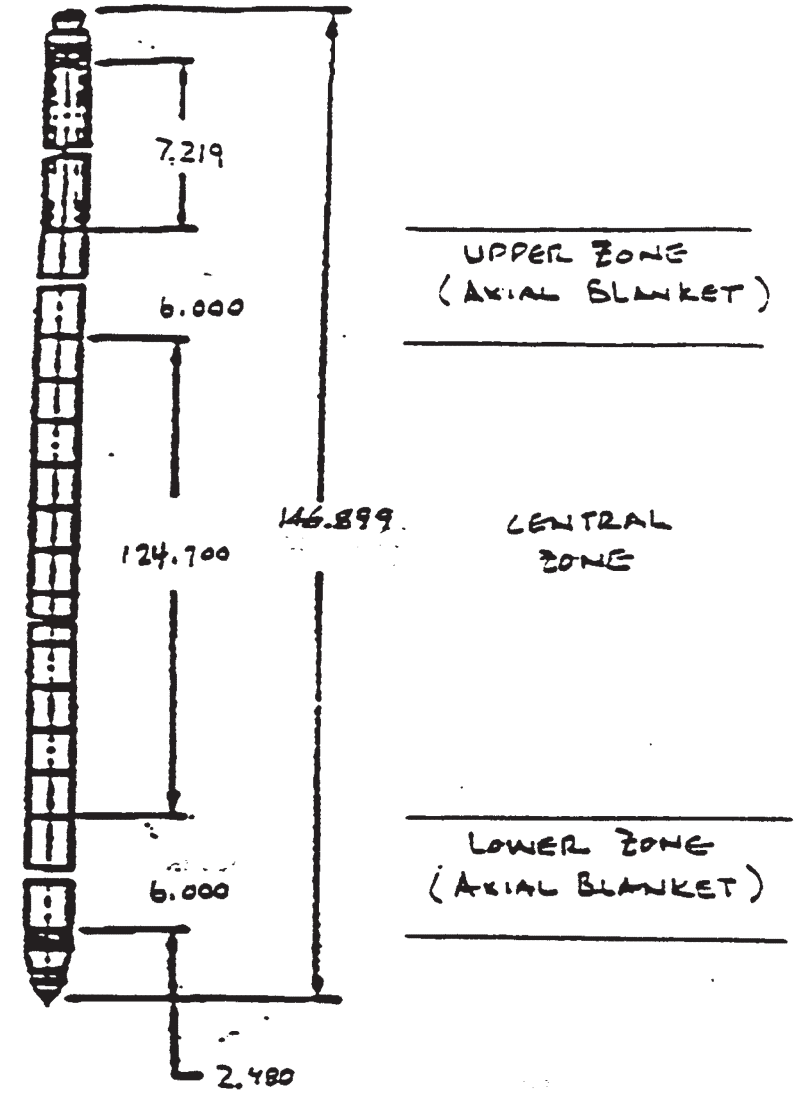

BEGINNING WITH
REGION P

GUARDIAN GRID
DESIGN

FLORIDA POWER & LIGHT
ST. LUCIE PLANT UNIT 2

GUARDIAN GRID
FUEL ROD DESIGN
FIGURE 4.2-8A

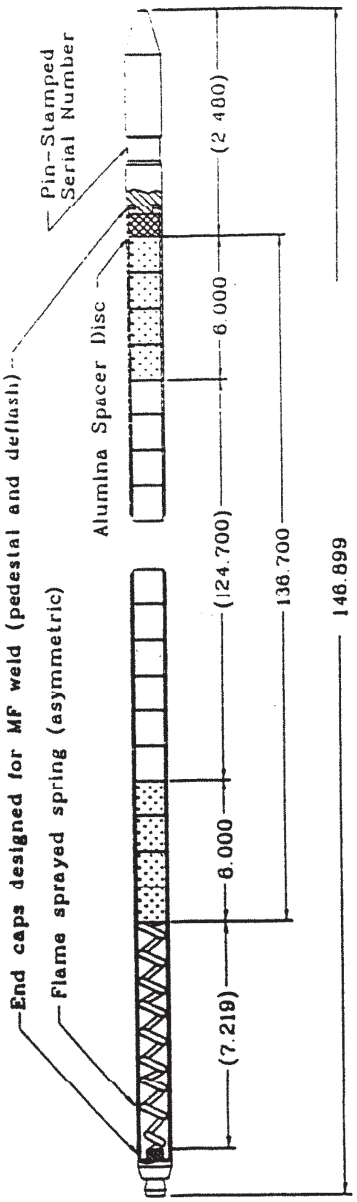

Region P Rod Assembly with MF Welds (Hematite Production)

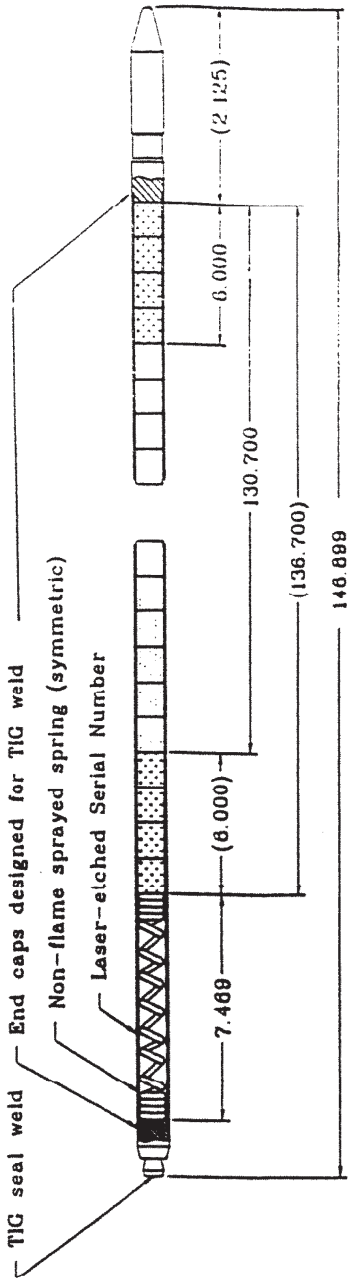

Region R Rod Assembly with TIG Welds (Columbia Production)

FLORIDA POWER & LIGHT COMPANY
ST. LUCIE PLANT UNIT 2

COMPARISON OF URANIA ROD ASSEMBLY FEATURES
FIGURE 4.2-8b

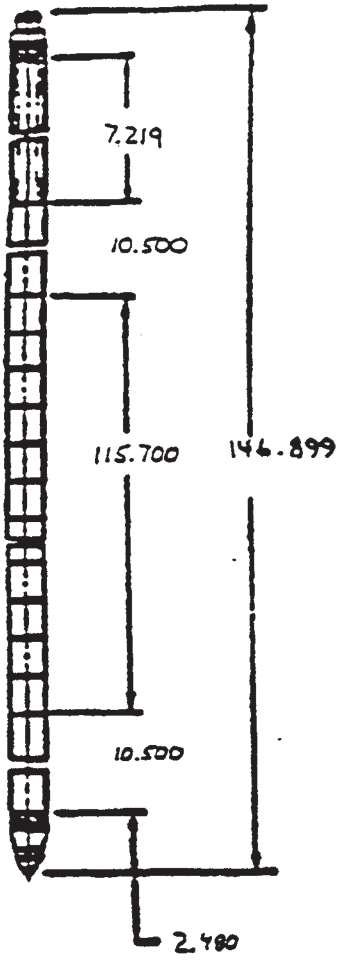

BEGINNING WITH REGION N
GUARDIAN GRID DESIGN

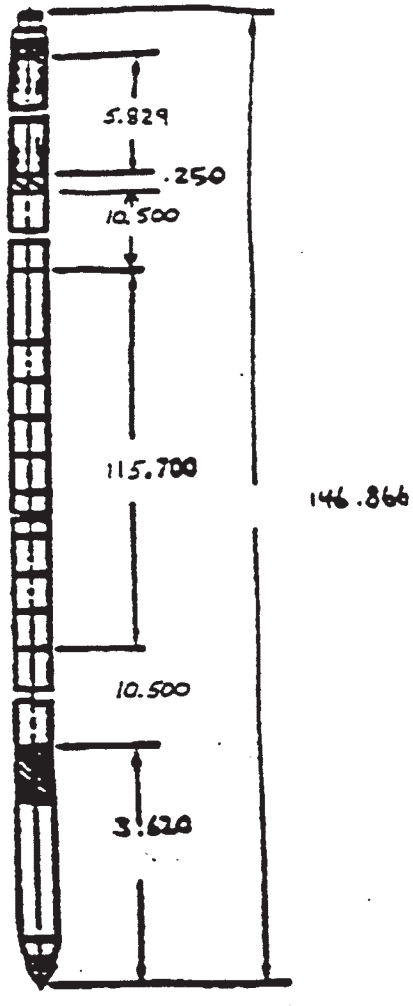

REGIONS L & M
DEBRIS RESISTANT DESIGN

FLORIDA POWER & LIGHT
ST. LUCIE PLANT UNIT 2

GUARDIAN GRID AND
DEBRIS RESISTANT
BURNABLE ABSORBER ROD DESIGN
FIGURE 4.2-9

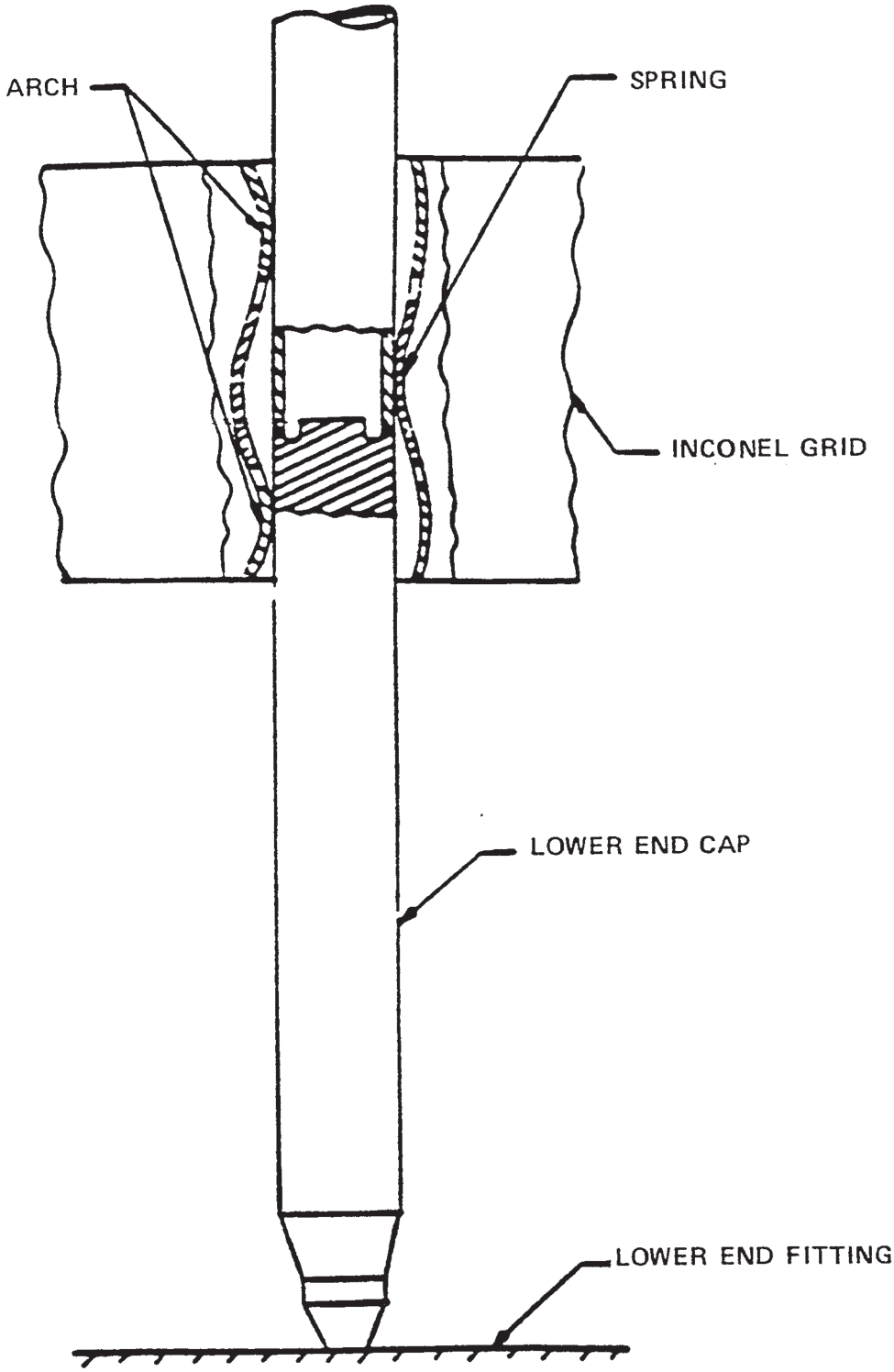

REGION G – M

FLORIDA POWER & LIGHT COMPANY
ST. LUCIE PLANT UNIT 2

MODIFIED LOWER END CAP

FIGURE 4.2-9a

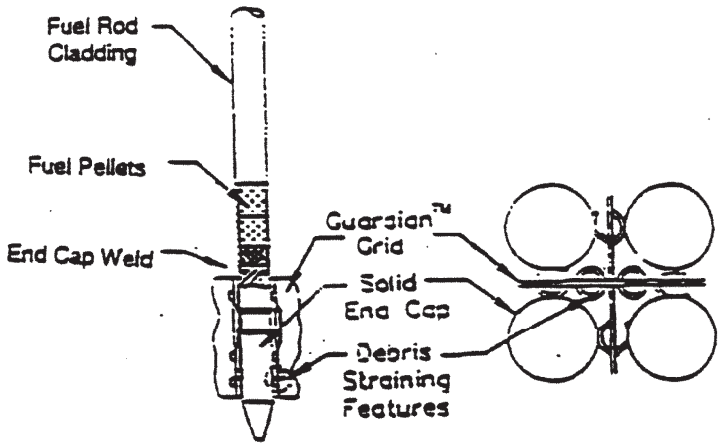

BEGINNING WITH REGION 'N'
(NO ALUMINA SPACER IN REGION 'R' AND BEYOND)

Amendment No. 14 (12/01)

FLORIDA POWER & LIGHT
ST. LUCIE PLANT UNIT 2

LOWER END CAP
WITH GUARDIAN GRID
FIGURE 4.2-9b

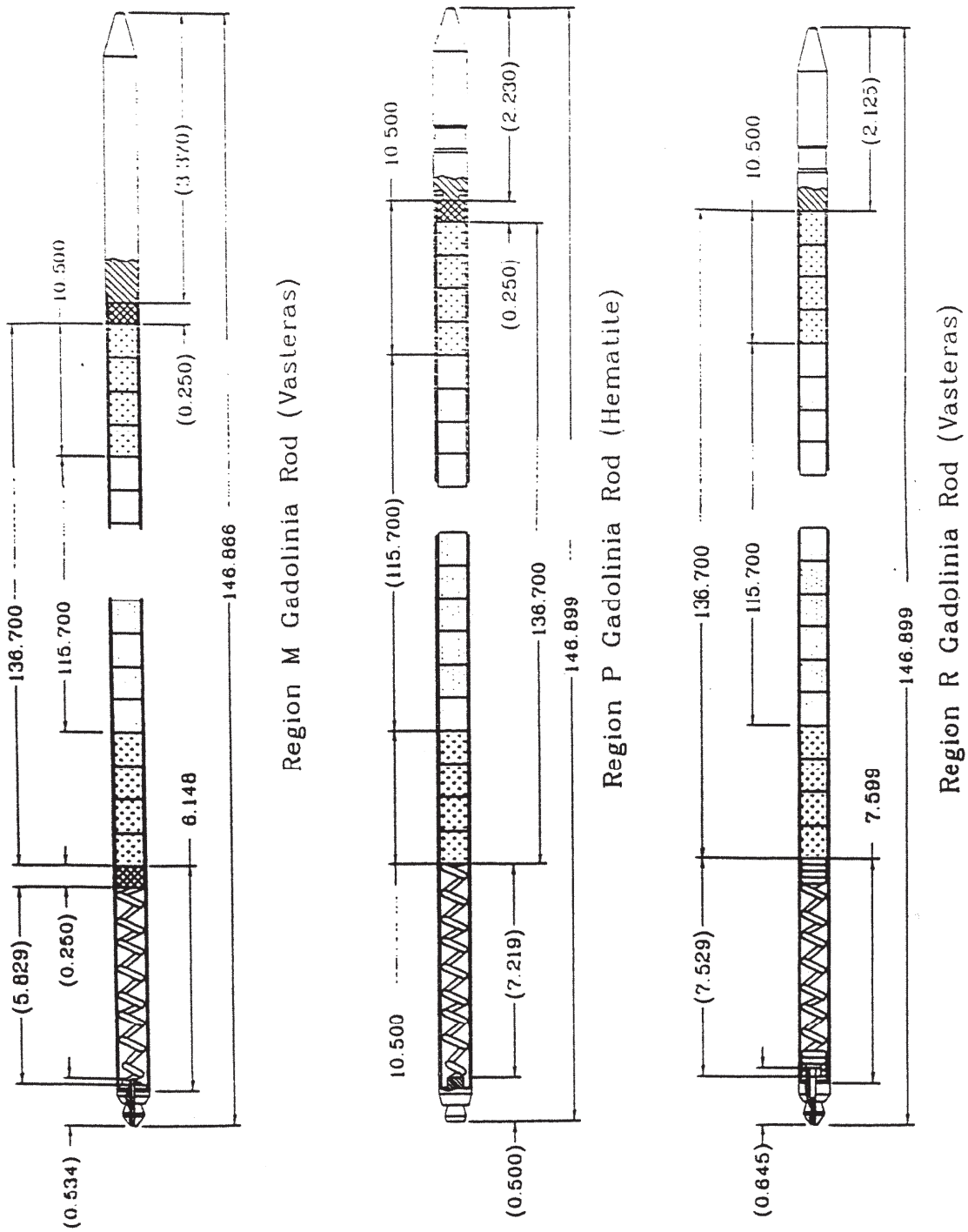

FLORIDA POWER & LIGHT COMPANY
ST. LUCIE PLANT UNIT 2

COMPARISON OF GADOLINIA RODS
FOR REGIONS M, P AND R
FIGURE 4.2-9c

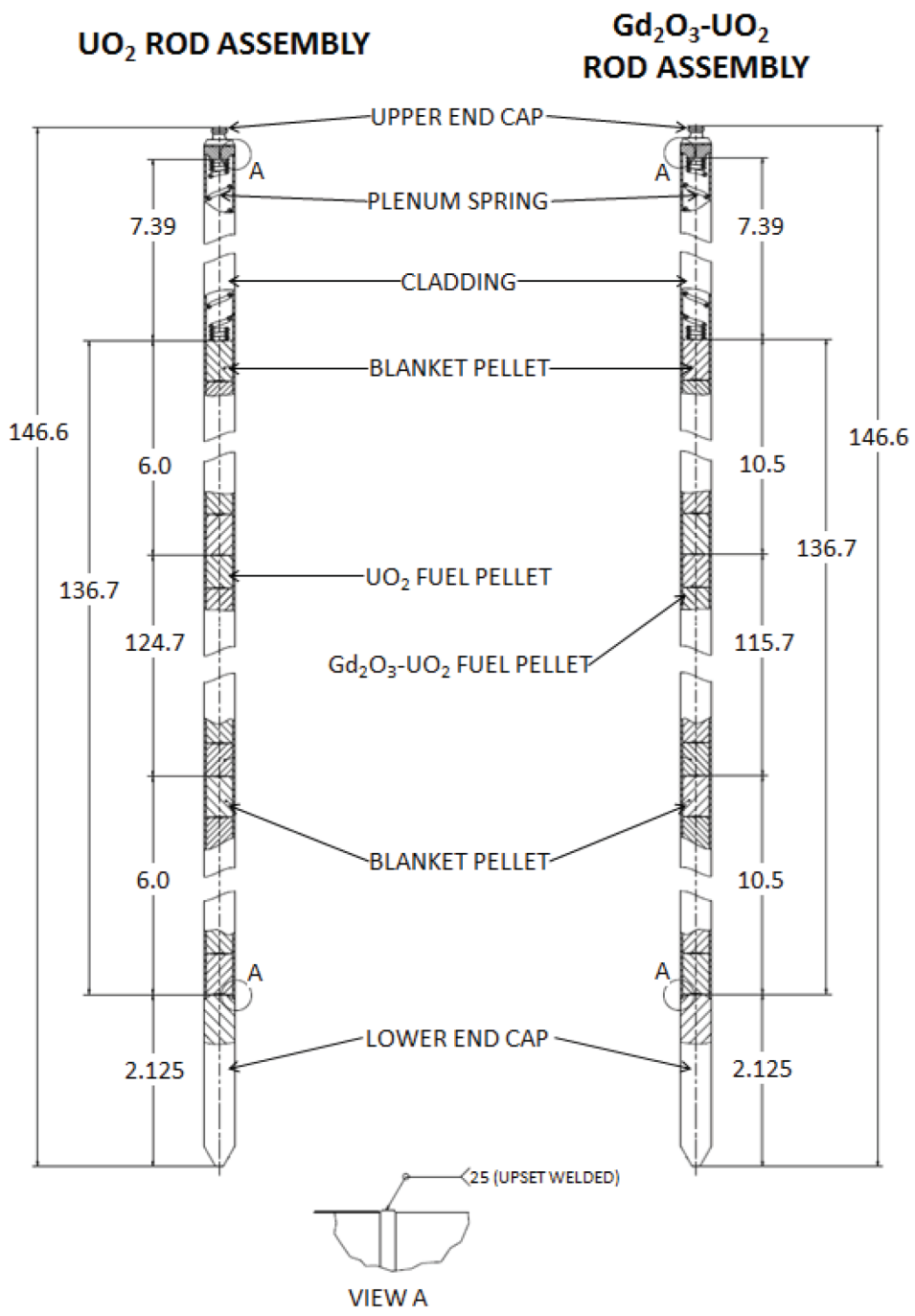

EC287528

FLORIDA POWER & LIGHT COMPANY
ST. LUCIE PLANT UNIT 2

Figure 4.2-9d
AREVA Fuel Rod Assemblies

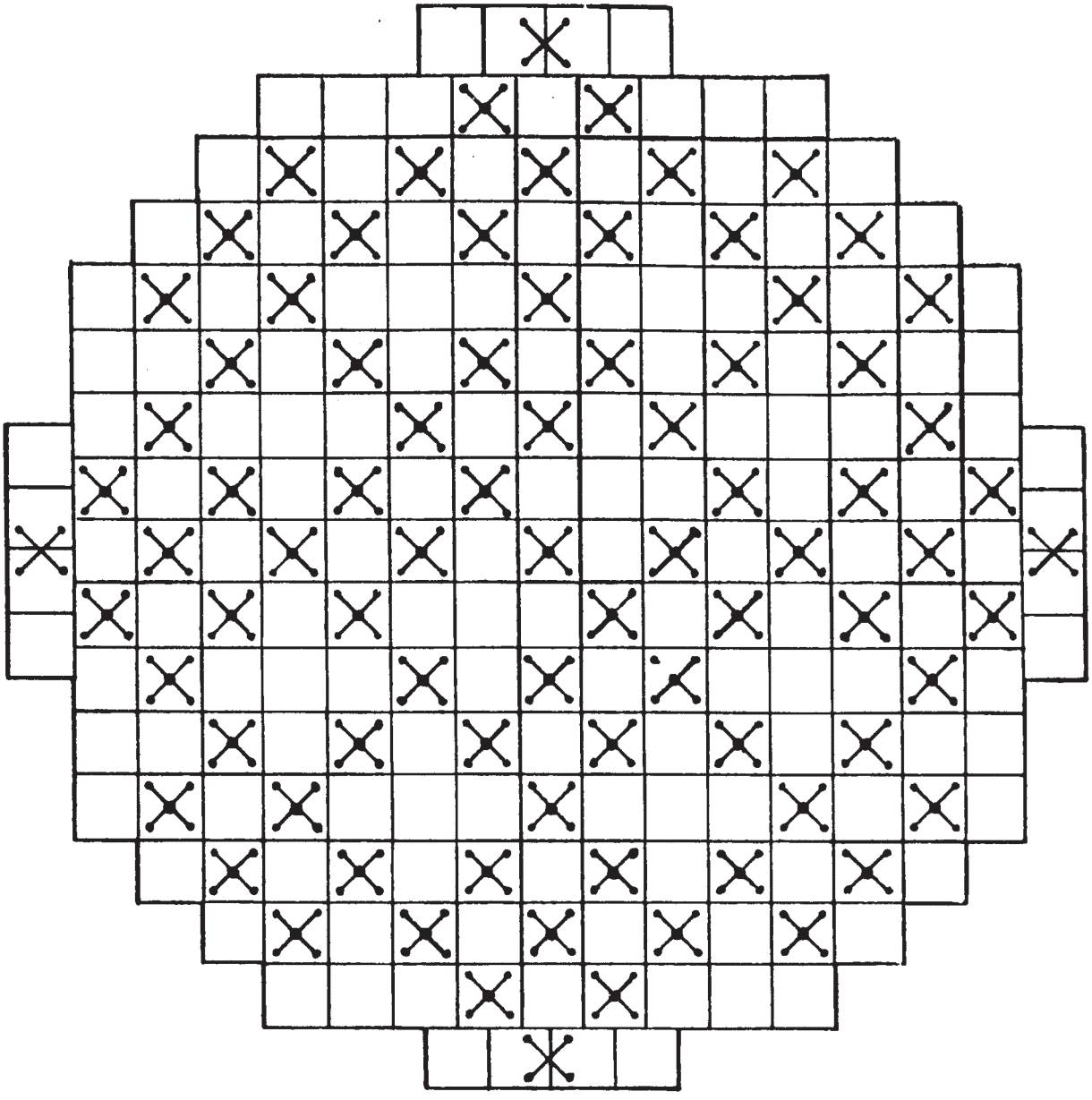

	5 ELEMENT CEA'S	79
	4 ELEMENT CEA'S	4
	TOTAL	83 CEA'S

AMENDMENT NO. 1 (4/86)

FLORIDA POWER & LIGHT COMPANY
ST. LUCIE PLANT UNIT 2

CONTROL ELEMENT ASSEMBLY LOCATIONS
FIGURE 4.2-10

CYCLE 1

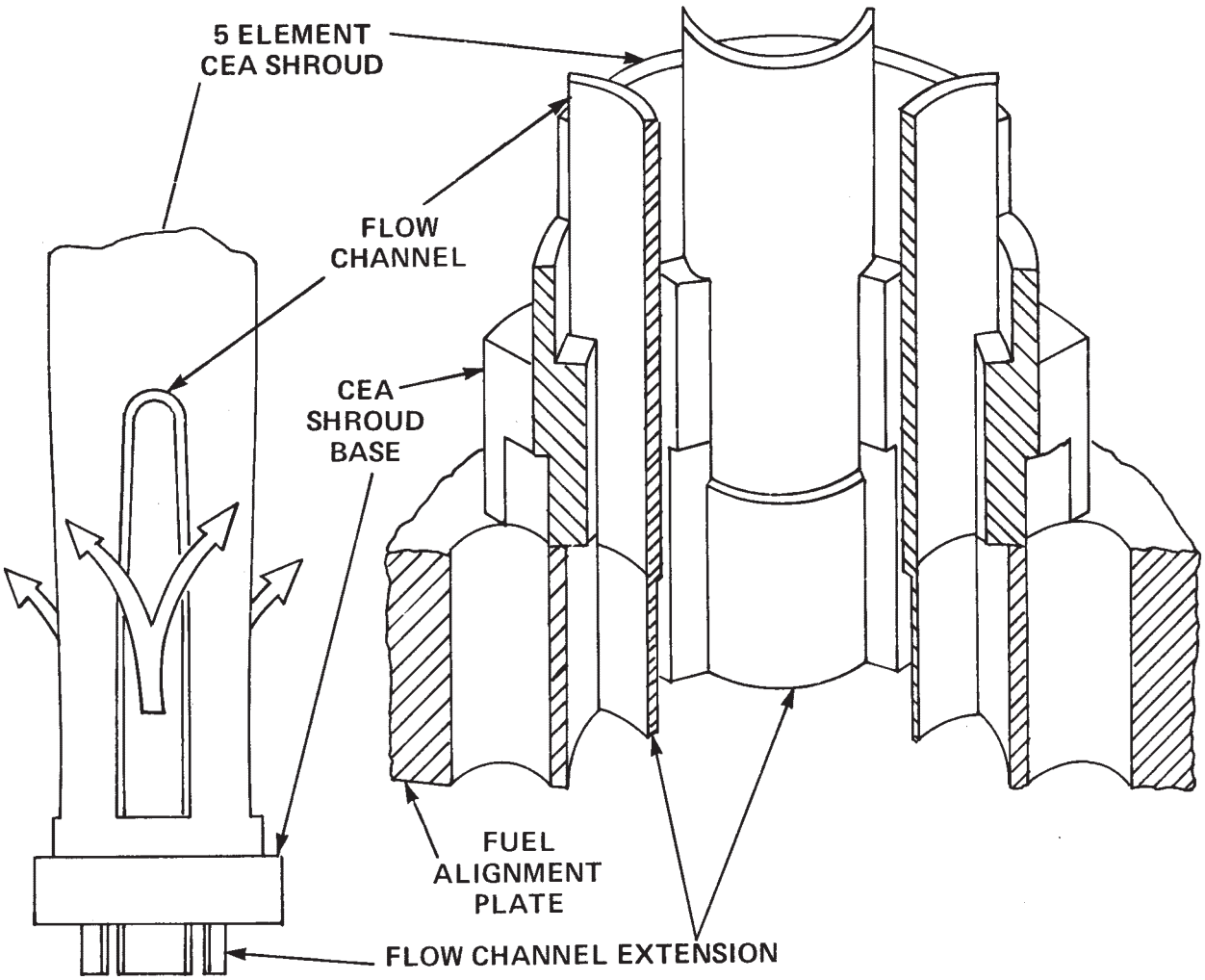

FLORIDA POWER & LIGHT COMPANY
ST. LUCIE PLANT UNIT 2

FLOW CHANNEL
EXTENSIONS

FIGURE 4.2-11

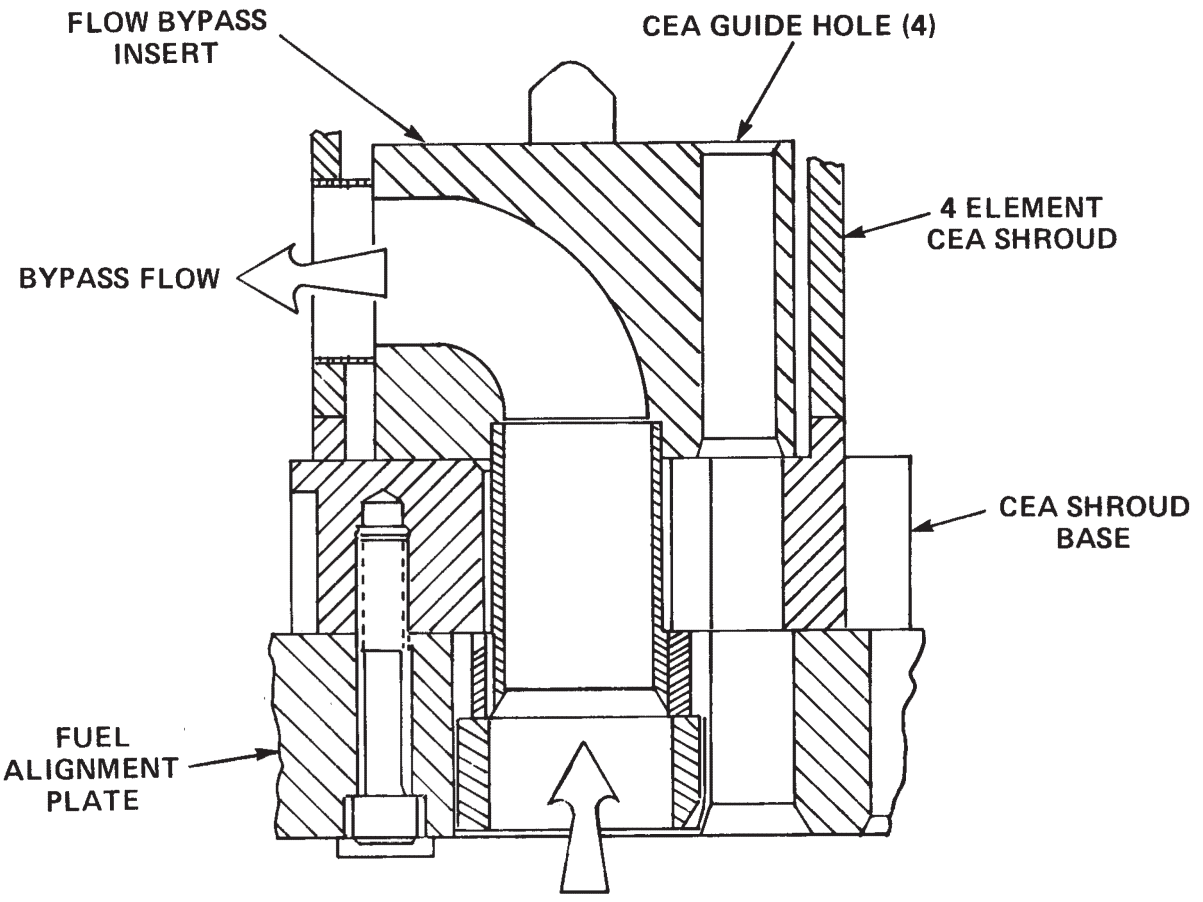

FLORIDA POWER & LIGHT COMPANY
ST. LUCIE PLANT UNIT 2

4 ELEMENT CEA SHROUD
FLOW BYPASS INSERT

FIGURE 4.2-12

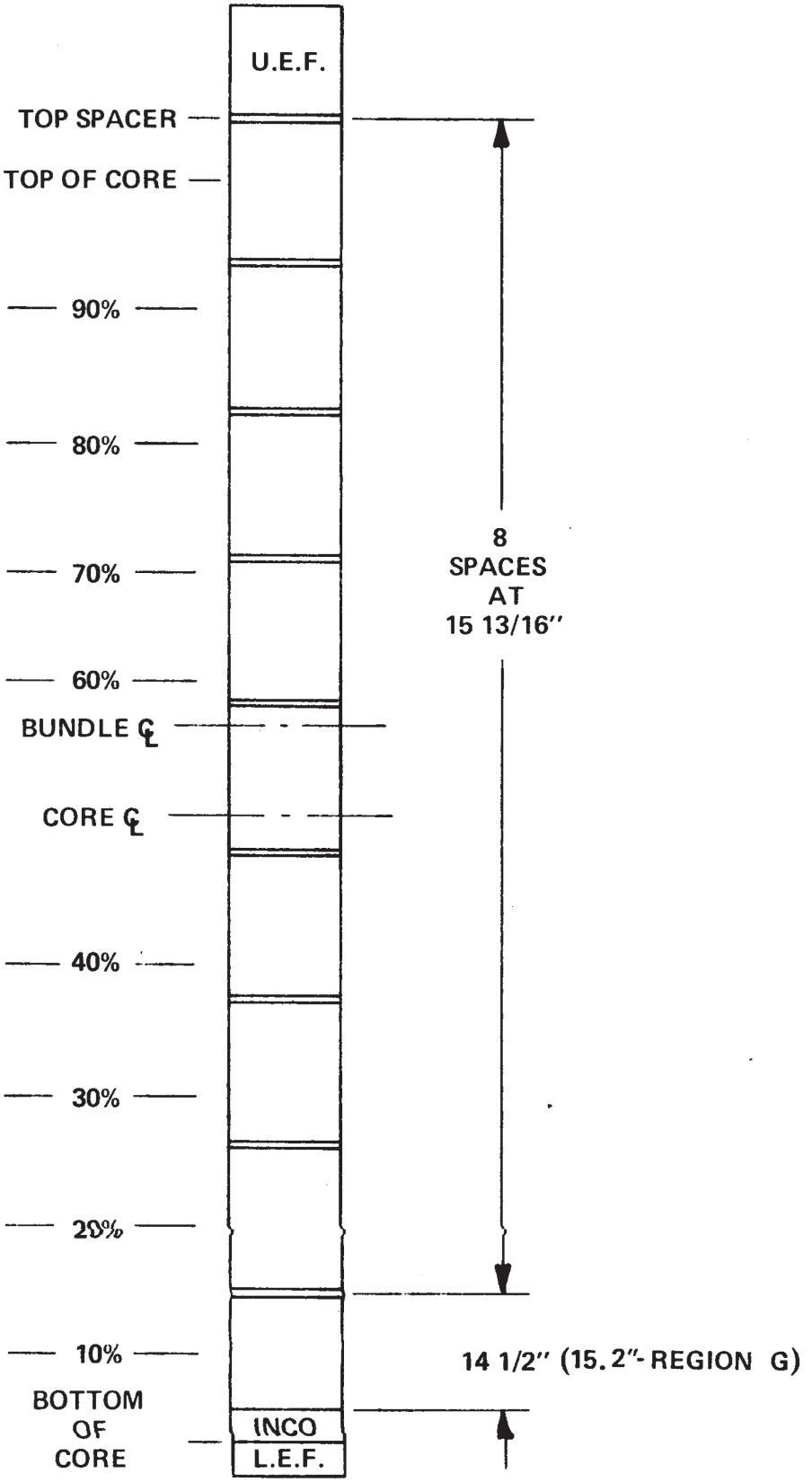

AMENDMENT NO. 5 (4/90)

FLORIDA POWER & LIGHT COMPANY
ST. LUCIE PLANT UNIT 2

SPACER GRID LOCATION IN ST. LUCIE 2

FIGURE 4.2-13

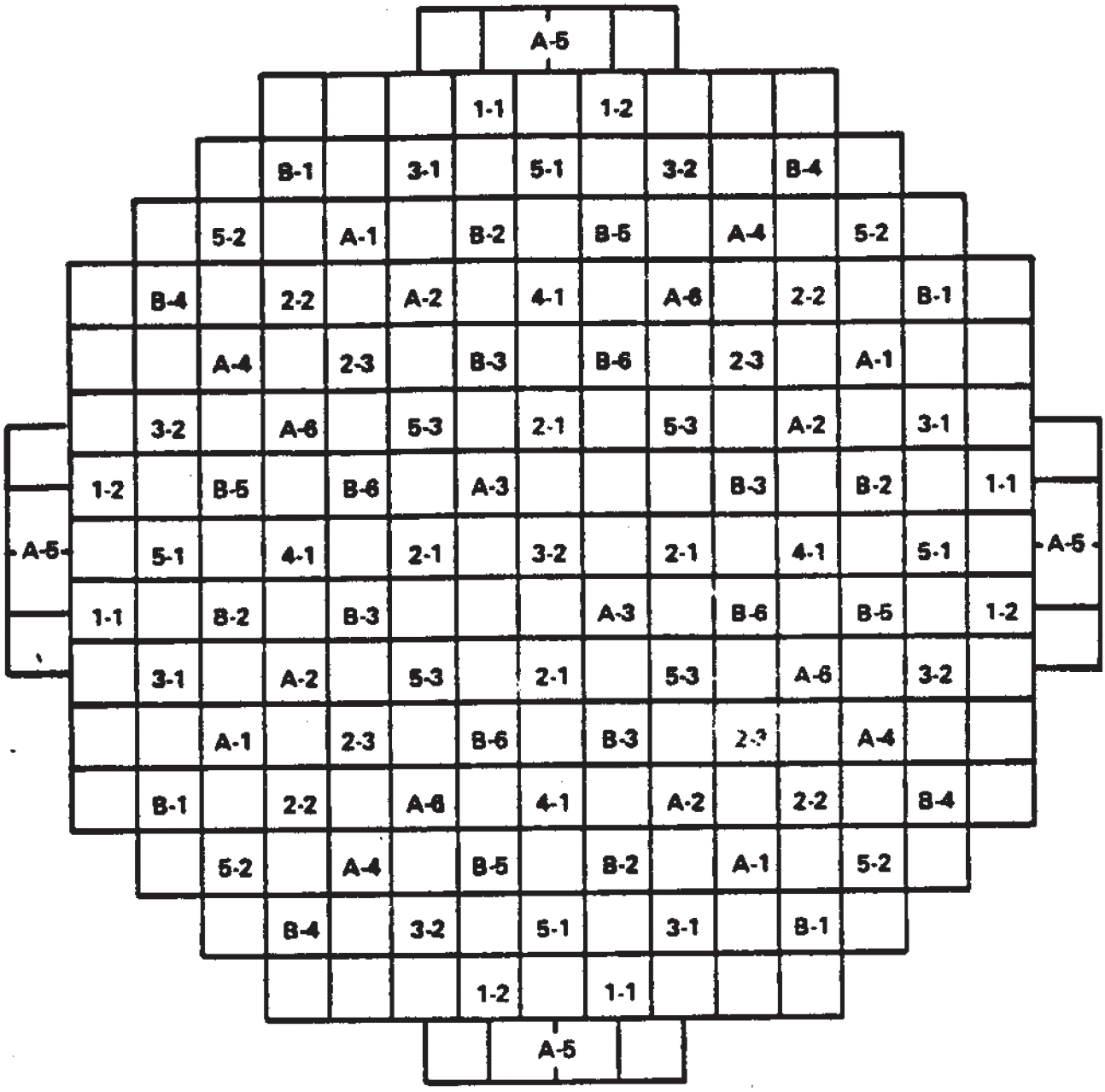

Y-Z

Y = CEA BANK DESIGNATION
Z = CEA SUBGROUP NUMBER

AMENDMENT NO. 1 (4/86)

FLORIDA POWER & LIGHT COMPANY
ST. LUCIE PLANT UNIT 2

ST. LUCIE UNIT 2 CYCLE 2
CEA BANK AND SUBGROUP DESIGNATIONS

FIGURE 4.2-14

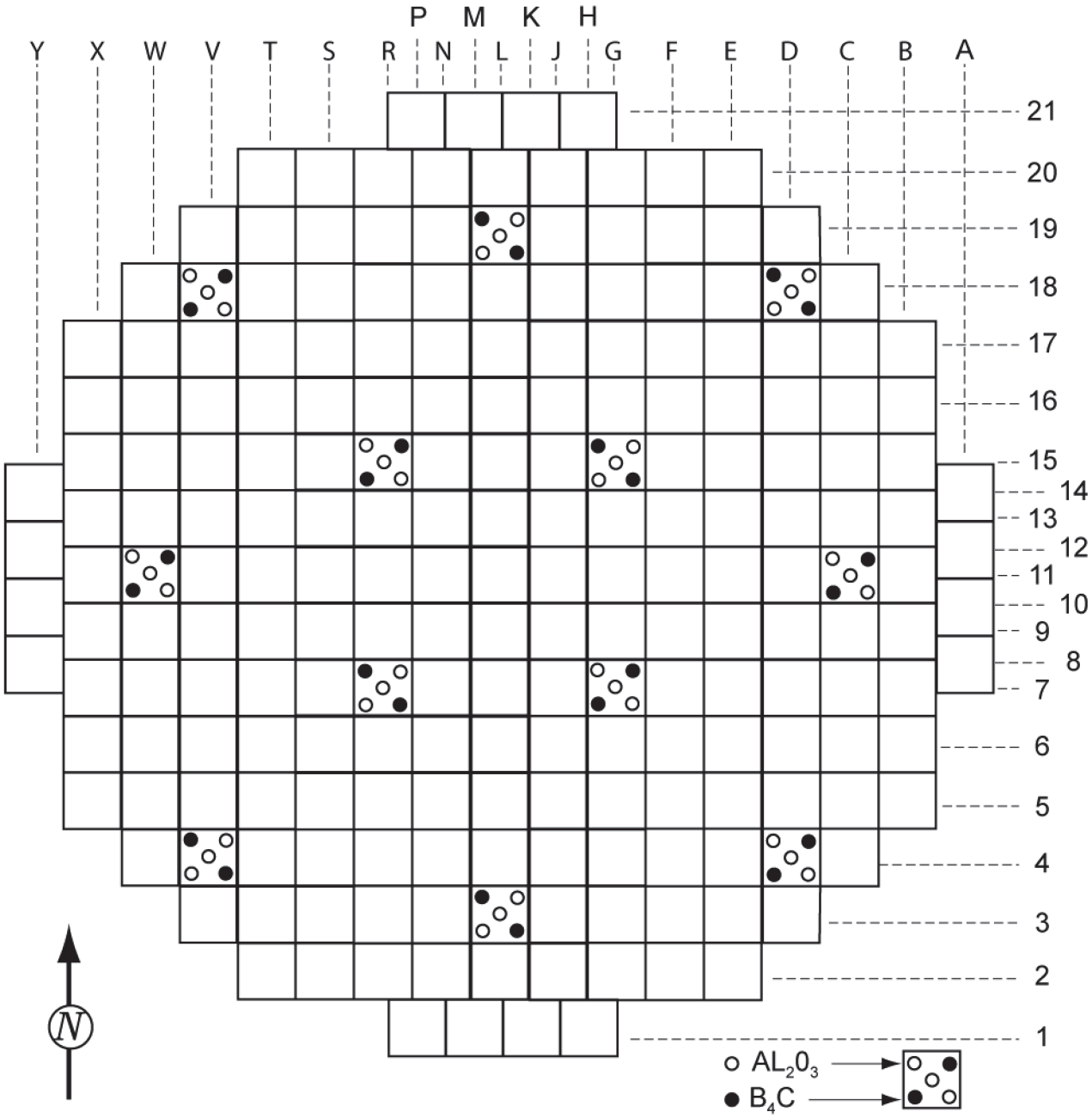

FLORIDA POWER & LIGHT COMPANY
ST. LUCIE PLANT UNIT 2

POSITIONING OF POISON FINGERS
IN LEAD BANK
FIGURE 4.2-15

4.3 NUCLEAR DESIGN

4.3.1 DESIGN BASES

Cycle specific reload typically consists of fresh, once burned and twice burned fuel assemblies for a total of 217 fuel assemblies. The safety analysis supports an end-of-cycle coastdown with a maximum reduction in the coolant inlet temperature to 535°F at full power.

The assemblies consist of non-gadolinia enriched UO_2 fuel rods and UO_2-Gd_2O_3 gadolinia burnable absorber fuel rods. The UO_2 fuel rods have central zone enrichments of 2.6 to 4.6 w/o U-235, whereas the UO_2-Gd_2O_3 rods have a central zone of 2, 4, 6, or 8 w/o UO_2-Gd_2O_3 dispersed in a lower w/o U-235 carrier. In addition, the current Cycle is continuing the use of radially zoned fuel, such that 52 rods per assembly are at a reduced enrichment.

The active fuel length of each fuel rod is 136.7 inches. The top 6 inches and the bottom 6 inches of the enriched fuel rods, which do not contain Gd_2O_3, are composed of enriched uranium (2.6 w/o U-235) axial blankets. The UO_2-Gd_2O_3 rods have an absorber length of 115.7 inches, and upper and lower enriched uranium (2.6 w/o U-235) cutback regions of 10.5 inches each.

The Cycle 23 fresh assemblies are the first feed batch of the AREVA CE-16 HTP™ fuel design.

At the reactivity end of life (end of cycle), the reactor is shut down for refueling. A portion of the fuel assemblies comprising the core are discharged, fresh fuel assemblies are added and, based on design calculations, a new core loading pattern is implemented. The core configuration following refueling operations comprises the reload core which will be operated until its respective end of reactivity life.

EC287528

Nuclear design calculations are performed for each reload core to determine a proper core loading pattern which satisfies the cycle energy and safety analysis requirements. Particular attention is paid to peaking factors and core kinetics characteristics. If core characteristics fall outside of the range of values covered by the previous nuclear design or safety analysis, those core conditions or accidents so affected are reanalyzed or evaluated for compliance with the acceptance criteria.

As part of the reload evaluation, the mechanical, nuclear, and thermal hydraulic characteristics of the reload core are assessed. Special conditions such as off-nominal operating conditions, LOCA limits, or special operational limitations are also addressed. Thus, each reload core is designed and provided with the same or better safety margins than the initial core analysis presented in this UFSAR.

4.3.1.1 Excess Reactivity and Fuel Burnup

The excess reactivity provided for each cycle is based on the depletion characteristics of the fuel and burnable poison and on the desired burnup for each cycle. The desired burnup is based on an economic analysis of the fuel cost and the projected operating load cycle for St. Lucie Unit 2. The average burnup is chosen to ensure that the peak burnup is within the limits discussed in Subsection 4.2.3.2.12. This design basis, alone with the design basis in Subsection 4.3.1.8, satisfies General Design Criterion 10.

4.3.1.2 Core Design Lifetime and Fuel Replacement Program

The core design lifetime and fuel replacement program are based on approximately 18-month refueling with approximately one third of the fuel assemblies replaced at each refueling in later cycles. The first cycle design lifetime is longer than later cycles to permit a more orderly transition to equilibrium cycle conditions.

4.3.1.3 Negative Reactivity Feedback

In the power operating range, the net effect of the prompt inherent nuclear feedback characteristics (fuel temperature coefficient, moderator temperature coefficient, and moderator pressure coefficient) tends to compensate for a rapid increase in reactivity. The negative reactivity feedback provided by the design satisfies General Design Criterion 11.

4.3.1.4 Reactivity Coefficients

The values of each coefficient of reactivity are consistent with the design basis for net reactivity feedback (Subsection 4.3.1.3), and analyses that predict acceptable consequences of postulated accidents and anticipated operational occurrences, where such analyses include the response of the Reactor Protective System (RPS).

4.3.1.5 Burnable Poison Requirements

The burnable poison reactivity worth provided in the design is sufficient to ensure that the moderator coefficient of reactivity is consistent with the design base. Burnable poisons also provide power distribution control.

4.3.1.6 Stability Criteria

The reactor and the instrumentation and control systems are designed to detect and suppress xenon induced power distribution oscillations that could, if not suppressed, result in conditions that exceed the specified acceptable fuel design limits. The design of the reactor and associated systems precludes the possibility of power level oscillations. This basis satisfies General Design Criterion 12.

4.3.1.7 Maximum Controlled Reactivity Insertion Rate

The core, control element assemblies (CEAs), Reactor Regulating System, and boron charging portion of the Chemical and Volume Control System are designed so that the potential amount and rate of reactivity insertion due to normal operation and postulated reactivity accidents do not result in:

a. Violation of the specified acceptable fuel design limits (SAFDL)

b. Damage to the reactor coolant pressure boundary

c. Disruption of the core or other reactor internals sufficient to impair the effectiveness of emergency core cooling.

This design basis, along with Subsection 4.3.1.11 satisfies General Design Criteria 25 and 28.

4.3.1.8 Power Distribution Control

The core power distribution is controlled such that, in conjunction with other core operating parameters, the power distribution does not result in violation of the limiting conditions for operation. Limiting conditions for operation and limiting safety system settings are based on the accident analyses described in Chapter 15, such that specified acceptable fuel design limits are not exceeded as a result of anticipated operational occurrences and the limits of acceptable consequences are not exceeded for other postulated accidents. This basis, along with Subsection 4.3.1.2, satisfies General Design Criterion 10.

4.3.1.9 Shutdown Margins and Stuck Rod Criteria

The amount of reactivity available from insertion of withdrawn CEAs under all power operating conditions, even when the highest worth CEA fails to insert, will provide for at least one percent shutdown margin after cooldown to hot zero power, and any additional shutdown reactivity requirements assumed in the safety analyses. This basis, along with Subsection 4.3.1.10, satisfies General Design Criteria 26 and 27.

4.3.1.10 Chemical Shim Control

The Chemical and Volume Control System (CVCS) (Subsection 9.3.4) is used to adjust the dissolved boron concentration in the moderator. After a reactor shutdown, this system is able to compensate for the reactivity changes associated with xenon decay and reactor coolant temperature decreases to ambient temperature, and it provides adequate shutdown margin during refueling. This system also has the capability of controlling, independently of the CEAs, long term reactivity changes due to fuel burnup and reactivity changes during xenon transients resulting from changes in reactor load. In particular, any xenon burnout transient may be accommodated at any time in the fuel cycle. This design basis, along with Subsection 4.3.1.9 satisfies General Design Criteria 26 and 27.

4.3.1.11 Maximum CEA Speeds

Maximum CEA speeds are consistent with the maximum controlled reactivity insertion rate design basis discussed in Subsection 4.3.1.7. Maximum CEA speeds are also discussed in Section 4.2.

4.3.2 DESCRIPTION

4.3.2.1 Nuclear Design Description

This section summarizes the nuclear characteristics of the Cycle 1 core and discusses the important design parameters that affect the performance of the core in steady state and normal transient operation. Summaries of nuclear design parameters are presented in Table 4.3-1, Table 4.3-2, and Figure 4.3-1. These data are intended to be descriptive of the first cycle design. Design limit values for these and other parameters are discussed in the appropriate sections. Discussions of methodologies within this section are written from an historic perspective and may have been superseded by newer methods as discussed in Reference 65.

Fuel enrichment and burnable poison distributions are shown on Figure 4.3-1. The other three quadrants of the core are symmetric to the displayed quadrant. Physical features of the lattice, fuel assemblies, and CEAs are described in Section 4.2.

Assembly enrichments, core burnup, critical soluble boron concentrations and worths, plutonium buildup, and delayed neutron fractions and neutron lifetime are shown in Table 4.3-1. The soluble boron insertion rates shown in this table, as discussed in Subsection 9.3.4, are sufficient to compensate for the maximum reactivity addition due to xenon burnout and normal plant cooldown. This maximum reactivity addition rate for which the CVCS will be required to compensate is given in Table 4.3-1. The maximum value occurs for an end of cycle cooldown, where the moderator temperature coefficient is most negative.

K_{eff}, reactivity, and reactivity defect data associated with the cold zero power, hot standby, hot full power without xenon or samarium, and hot full power with equilibrium xenon and samarium conditions are shown in Table 4.3-2.

For Cycle 2, the nuclear design calculations were performed using the coarse mesh code ROCS (Reference 56) and the fine mesh code PDQ (Reference 16). All cross sections were generated in accordance with the methods described in Reference 56. All fuel assembly cross sections for both coarse and fine mesh calculations were generated using the DIT assembly spectrum code (Reference 56) with appropriate corrections to account for the increased peaking that is characteristic of fuel pins adjacent to water holes in the assembly lattice. The course mesh code ROCS was used in either 2- or 3- dimensional geometry to calculate all core wide parameters and assembly relative power densities. The fine mesh code PDQ in 2-dimensional geometry was used to calculate pin peaking data.

4.3.2.2 Power Distribution

4.3.2.2.1 General

At all times during operation, it is intended that the power distribution and coolant conditions be controlled so that the peak linear heat rate and the minimum departure from nucleate boiling ratio (DNBR) are maintained within operating limits supported by the safety analyses (Chapter 15) with due regard for the correlations between measured quantities, the power distribution, and uncertainties in the determination of power distribution.

Methods of controlling the power distribution include the use of CEAs to alter the axial power distribution; decreasing CEA insertion by boration, thereby improving the radial power distribution, and correcting off optimum conditions which cause margin degradation (e.g., CEA misoperation).

4.3.2.2.2 Expected Power Distributions

Detailed core power distributions depend on CEA insertion, fuel exposure, coolant conditions, power level, soluble boron concentration, burnable poisons and fission products. Variations in the foregoing parameters are expected. However, since the core is expected to be essentially unrodded at full power throughout Cycle 1, it is possible to parameterize nominal power distributions in burnup and power level. Administrative control is provided to assure that core conditions associated with off nominal operation do not alter core composition in such a way as to negate the assumed burnup and power level dependence of the power distribution.

Normalized assembly axial power distributions are essentially the same as the core average axial power distributon during Cycle 1. This permits the separation of radial and axial components of the core power distribution during nominal Cycle 1 conditions. Separability is not possible during certain Cycle 1 transients and therefore three dimensional analyses are

required. The analysis of these transient conditions is discussed in Chapter 15. In later cycles, radial power distributions are axially dependent because of axial burn-up differences between the fuel batches. This axial dependency invalidates the simplifying assumption of separability and necessitates three dimensional analyses for most reactor states. Figures 4.3-19 through 4.3-24 provide axially averaged planar power distributions for a typical Cycle 2 and Cycle 3 fuel management scheme. The final fuel management calculations will account for the axial variation of the radial power distribution.

Power distribution variations that may result from off nominal core conditions are accounted for by the Reactor Protective System discussed in Subsection 4.3.2.2.4. Analysis of power distribution uncertainties and the results of comparisons with experimental data is discussed in Subsection 4.3.3 Startup tests, providing additional confirmation of analytical methods, are discussed in Chapter 14.

4.3.2.2.2.1 Nominal (Steady State) Power Distributions

Figures 4.3-2 through 4.3-13 and 4.3-14 through 4.3-18 show typical first cycle planar radial rodded and unrodded core average axial power distributions, respectively. They illustrate conditions expected at full power for various times in the fuel cycle as specified on the figures. It is expected that the normal operation of the reactor will be with limited CEA insertion so that these power distributions represent the expected power distribution during most of the cycle. The three dimensional peaking factor, F^nq, expected during steady state operation is then just the product of the unrodded planar radial peaking factor (F^nq) and the axial peaking factor. The maximum expected value of F^nq is 2.08 during the first cycle and, as can be seen from the above figures, occurs near the beginning of cycle for steady state, base loaded operation with no CEA insertion.

Figures 4.3-2b, 4.3-3b and 4.3-4b show zero power planar power distributions during Cycle 1. Comparison to their full power counterparts illustrates the characteristics shift of the normalized flux distribution towards the core periphery at low power levels. Additionally, Figures 4.3-19 through 4.3-24 show typical planar radial power distributions for later cycles of St. Lucie Unit 2. Based on the similarity of these radial power distributions to those in the first cycle, it is clear that no significant differences in expected power distributions between cycles should exist. The uncertainty associated with these calculated power distributions is discussed in Subsection 4.3.3.1.2.2.6.

The detailed radial power distribution within any assembly is a function of the location of that assembly within the core as well as the time in life, CEA insertion, etc. For DNB analysis, a conservatively flat local radial distribution is used to evaluate intra-assembly mixing and cross flow. This conservative distribution is shown on Figure 4.3-33; the power in the hottest rod in that assembly is assumed to be at the design limit peaking factor. Fuel management calculations are used to verify that no flatter distribution occurs in assemblies that are limiting or near limiting with respect to DNB. In Subsection 4.3.3.1.2, the accuracy of calculations of the power distribution within a fuel assembly is discussed.

4.3.2.2.2.2 Expected Transient Power Distributions

In order to illustrate the maneuvering capability available in St. Lucie Unit 2 the results of calculations of the power distributions and power peaking factors during several load following transients are discussed below. Discussions of methodologies within this section are written

from an historic perspective and may have been superseded by newer methods as discussed in Reference 65 and Reference 70.

The axial power distributions are calculated by QUIX (see Subsection 4.3.3.1.1), a one dimensional spatial flux calculation model that considers the effects of the time and spatial variations of xenon and iodine concentration, CEA position, thermal and moderator density feedback mechanisms, as well as the burnup distribution. Since QUIX does not have fuel depletion capability, axial-dependent depletion effects are included by using an axial nuclide distribution computed from one dimensional (axial) PDQ depletion calculations. Employing the separability of axial and radial power distribution components, F_q^n and F_r^n are obtained by synthesis of power distributions from two dimensional (planar) PDQ and one dimensional (axial) QUIX calculations. The QUIX model accepts values of radial peaking factors for each type of CEA bank insertion (unrodded, bank 6 inserted, etc.). These radial peaking factors are input for the appropriate core average burnup condition and are applied over the axial region of core having the specified CEA bank configuration (e.g., unrodded, bank 6 inserted, etc.). These radial peaking factors are weighted by the axial power distribution to obtain an axially integrated radial peaking factor. The value of this integrated radial peaking factor is conservatively large since the maximum of the radial peaking factors of each planar region is not, in general, expected to occur at the same fuel pin location. The magnitude of the input radial peaking factors is determined primarily by the number and location of inserted CEAs. It is evaluated at the full power condition and taken to be independent of power level.

Figures 4.3-25 through 4.3-32 show the calculated axial power distributions and associated nuclear peaking factors during a typical day of a maneuvering transient to either 50 or 35 percent of the full power conditions.

Also shown on these figures are the CEA locations during the transient. Throughout the calculation of the power distribution during these transients, it was assumed that the part length CEAs were available for control of the axial power distribution. Part length CEAs have been removed from the St. Lucie Unit 2 design; however, similar control could be obtained with full-length CEAs. Subsection 4.3.2.7 discusses xenon stability and control of axial xenon oscillations.

4.3.2.2.2.3 Power Distribution

Radial power peaks are characteristic of the major portion of the active core length between about 20 and 80 percent of the fuel height and are presented for illustrative purposes to show the assembly by assembly variations in power throughout the current cycle. EC287528

Beginning with Cycle 12, these calculations are performed using Westinghouse neutronics methodology of Reference 69.

The radial power distributions described in this section are calculated data without uncertainties or other allowances. However, single rod power peaking values do include the increased peaking that is characteristic of fuel rods adjoining the water holes in the fuel assembly lattice. For both DNB and kW/ft safety and setpoint analyses, in either rodded or unrodded configurations, the power peaking values actually used are higher than those expected to occur at any time during the cycle. These conservative values establish the allowable limits for power peaking to be observed during operation.

The range of allowable axial peaking is defined by the Limiting Conditions for Operation (LCO) of the Axial Shape Index (ASI). Within these ASI limits, the necessary DNBR and kW/ft margins are maintained for a wide range of possible axial shapes. Beginning with Cycle 15, the Westinghouse Power Distribution Methodology procedures, described in Reference 70, are employed to confirm these margins.

4.3.2.2.3 Nuclear Design Limits on Power Distribution

Specified acceptable fuel design limits (SAFDLs) require that the core power distribution does not result in either fuel centerline melting or a DNBR less than the limiting value. Assurance that SAFDLs are not exceeded is obtained through the Reactor Protective System and the Technical Specifications which enforce limiting conditions of operation (LCO). LCOs are evaluated such that the initial conditions assumed in the analysis of anticipated operational occurrences and postulated accidents are conservative with respect to allowed reactor conditions. The nuclear design limits on power distributions are, therefore, intimately related to the limiting conditions of operation.

The design limits on power distribution are as follows:

a. The limiting three-dimensional heat flux peaking factor F_q^n, was established for full power conditions at 2.59 and 2.67 for first and equilibrium cycles, respectively. For the bounding analysis introduced in Cycle 12, a value of 2.809 was used. For the extended power uprate, Fq corresponds to a peak linear heat rate of 12.5kW/foot. The lower value for the first cycle reflects the presence of burnable poison shims in the fuel lattice and a corresponding reduction in the number of fuel rods. Fn is defined in Subsection 4.4.2.2.2.1, listing C and is termed the nuclear heat flux factor or the total nuclear peaking factor.

   An F_q^n of 2.59 in combination with uncertainties and allowance on heat flux constituted one limiting combination of parameters for full power operation in the first cycle. Other combination of parameters which will result in acceptable consequences of the safety analysis do exist, e.g., a higher F_q^n is acceptable at a reduced power level.

b. The margin to the limiting minimum DNBR must be sufficient to accommodate anticipated operational occurrences. Margin to DNBR is monitored in terms of the minimum reactor coolant pressure required to assure sufficient margin. The calculated minimum reactor coolant pressure depends on core power level, axial power shape and other reactor coolant variables. (DNBR is calculated using the CE-1 DNBR correlation discussed in Section 4.4). For the bounding analysis introduced in Cycle 12, a value of 1.28 was used, consistent with Extended Statistical Combination of Uncertainties, Reference 68. Beginning with Cycle 15, Westinghouse Revised Thermal Design Procedure (Reference 71) with the ABB-NV correlation is introduced.

As was discussed in Subsection 4.3.2.2.2.1, nominal (steady state) power distributions, the maximum expected unrodded F_q^n that occurs during the first cycle at full power is 2.08. Augmenting this value by the allowances described in Subsection 4.4.2.2.2.1.d provides an upper limit on F_q^t of 2.14 which is well below the design target of 2.57. Additionally, the

calculations described in Subsection 4.3.2.7.4 show that, with proper use of the CEAs, no appreciable increase in F_q^n occurs during power maneuvering transients. In the event that the CEAs were not moved properly, the power distribution could have become unacceptable. In this case, the monitoring system would indicate that SAFDLs were being approached and would provide an audible alarm to indicate that action has to be taken to improve the core power distribution, to improve the coolant conditions or to reduce core power.

The ability of the Reactor Protective System to monitor and evaluate core conditions with respect to LCOs and SAFDLs is described in Subsection 4.3.2.2.4 and Chapter 7.

4.3.2.2.4 Power Distribution Monitoring Capability

The power distribution monitoring instrumentation employed in St. Lucie Unit 2 is similar to that provided in St. Lucie Unit 1. Flux detectors, are provided both within the active core and outside the reactor vessel. The control and maintenance of power distributions for safety considerations is entirely manageable using excore detectors. Incore detectors are used for core flow studies and for periodic calibration of excore detectors.

Subsection 4.3.3.1.1 discusses the relationship between the excore detectors and the core power distribution.

The excore detectors are used to assure that reactor conditions do not exceed SAFDL during anticipated operational occurrences. Figure 4.3-62 illustrates the placement of excore detectors in St. Lucie Unit 2. The Reactor Protective System (RPS) is provided with sufficient redundancy to permit safe operation with a limited number of failures. Allowed RPS failures are discussed in the Technical Specifications.

The Reactor Protective System continuously monitors the excore detector readings and reactor coolant variables to determine whether the plant is being operated within limits (see Section 7.2). Indications are provided to solicit operator action prior to reaching those limits. In the event that conditions reach the design limits, the RPS will automatically initiate a reactor trip. Specific setpoints for alarms, trips and rod withdrawal prohibits are discussed in Section 7.2.

The design basis of the RPS is to automatically provide a reactor trip in the event that RCS pressure or fuel performance guidelines are encountered. During certain plant transient events, the margin to fuel performance guidelines may deteriorate either in a manner that is undetected by the RPS or such that the RPS would not act before some margin loss has occurred. Because of this, the reactor must be operated such that losses in margin do not result in exceeding fuel performance guidelines before the RPS restores the reactor to a safe condition. Limiting Conditions of Operation (LCO), enforced by the Technical Specifications assure that the required initial margin exists prior to the plant transient. Power dependent insertion limits and maximum allowable azimuthal power tilt are examples of LCOs enforced by Technical Specifications. Limits on axial power shape are a function of the core operating conditions and are continuously determined and monitored by RPS as discussed in Reference 1.

RPS response times and channel calibrations are described in Section 7.2. Inputs, calculations, codes and hardware related to the RPS are described in Reference 1 and in Section 7.2. The capability of the RPS to monitor and limit power distributions is presented in Reference 1.

4.3.2.3 Reactivity Coefficients (HISTORICAL)

Reactivity coefficients relate changes in core reactivity to variations in fuel or moderator conditions. The data presented in this section and associated tables and figures was developed for Cycle 1 and illustrates the range of reactivity coefficient values calculated for a variety of operating and accident conditions. Subsection 4.3.3 presents comparisons of calculated and measured moderator temperature coefficients and power coefficients for operating reactors. The good agreement shown in that subsection provides confidence that the data presented in this section adequately characterize the St Lucie Unit 2 reactor. Table 4.3-3 presents a comparison of the reactivity coefficients calculated for St Lucie Unit 2 reactor with those used in the safety analyses described in Chapter 15. For each accident analysis, suitably conservative reactivity coefficient values are used. Since uncertainties in the coefficient values, as discussed in Subsection 4.3.3.1.2, and other conservatisms are taken into account in the safety analyses, values used in the safety analyses may fall outside the ranges in a conservative direction of the data presented in this section. A more extensive list of reactivity coefficients is given in Table 4.3-4.

The calculational methods used to compute reactivity coefficients are discussed in Subsection 4.3.3.1.1. All data discussed in subsequent paragraphs are calculated with two dimensional, quarter core nuclear models. Spatial distributions of materials and flux weighting are explicitly performed for the particular conditions at which the reactivity coefficients are calculated. The adequacy of this method is discussed in Subsection 4.3.3.1.2.

Verification of predicted power and isothermal temperature coefficients will be conducted during startup testing. (The isothermal temperature coefficient is the sum of the moderator temperature and the fuel temperature coefficients evaluated at consistent fuel and moderator temperatures). Results of these tests will support predictions of fuel and moderator temperature coefficients, moderator density and nuclear temperature coefficients and the power coefficients.

4.3.2.3.1 Fuel Temperature Coefficient

The fuel temperature coefficient is the change in reactivity per unit change in fuel temperature. A change in fuel temperature affects not only the thermal expansion of the fuel pellet, but in addition, the reaction rates in both the thermal and epithermal neutron energy regimes. Epithermally, the principal contributor to the change in reaction rate with fuel temperature is the Doppler effect arising from the increase in absorption widths of the resonances with an increase in fuel temperature. The ensuing increase in absorption rate with fuel temperature causes a negative fuel temperature coefficient. In the thermal energy regime, a change in reaction rate with fuel temperature arises from the effect of temperature dependent scattering properties of the fuel matrix on the thermal neutron spectrum. In typical PWR fuels containing strong resonance absorbers such as U-238 and Pu-240, the magnitude of the component of the fuel temperature coefficient arising from the Doppler effect is more than a factor of 10 larger than the magnitude of the thermal energy component.

Figure 4.3-34 shows the dependence of the calculated fuel temperature coefficient on the fuel temperature, both at the beginning and the end of the first cycle.

4.3.2.3.2 Moderator Temperature Coefficient

The moderator temperature coefficient relates changes in reactivity to uniform changes in moderator temperature, including the effects of moderator density changes with changes in

moderator temperature. Typically, an increase in the moderator temperature causes a decrease in the core moderator density and, therefore, less thermalization, which reduces the core reactivity. However, when soluble boron is present in the moderator, a reduction in moderator density causes a reduction in the content of soluble boron in the core, thus producing a positive contribution to the moderator temperature coefficient. In order to limit the dissolved boron concentration, burnable poison rods (shims) are provided in the form of cylindrical pellets of alumina with uniformly dispersed boron carbide particles. The number of shims for Cycle 1 is given in Table 4.3-1 and their distribution in one quadrant of the core is shown on Figure 4.3-1. The distribution is identical for the other three quadrants. The reactivity control provided by the shims is given in Table 4.3-1. This control makes possible a reduction in the dissolved boron concentration to the values given in Table 4.3-1.

The calculated moderator temperature coefficients for various core conditions at beginning and end of first cycle are given in Table 4.3-4. The moderator temperature coefficients are more negative at end of cycle because the soluble boron in the coolant is reduced. The buildup of equilibrium xenon produces a net negative change of $-.305 \times 10^{-4}$ $\Delta\rho/F$ in the moderator temperature coefficient; this change is due mainly to the concomitant reduction in critical soluble boron. The changing fuel isotopic concentrations and the changing neutron spectrum during the fuel cycle depletion also contribute a small negative component to the moderator temperature coefficient.

The dependence of the moderator temperature coefficient on moderator temperature at BOC and EOC (at constant soluble boron) is shown on Figures 4.3-35 and 4.3-36, respectively. These figures also show the expected moderator temperature coefficient at reduced power levels (corresponding to reduced moderator temperatures) based on power reductions accomplished with soluble boron only and with CEAs only. These two modes of power reduction result in the most positive and most negative moderator temperature coefficients expected to occur at reduced power levels. These figures show the expected moderator temperature coefficient for the full range of expected operating conditions and accident conditions addressed in Chapter 15. Table 4.3-3 compares expected moderator temperature coefficients with those actually used in the accident analysis.

4.3.2.3.3 Moderator Density Coefficient

The moderator density coefficient is the change in reactivity per unit change in the average core moderator density at constant moderator temperature. A positive moderator density coefficient translates into a negative contribution to the total moderator temperature coefficient, which is defined in Subsection 4.3.2.3.2. The density coefficient is always positive in the operating range, although the magnitude decreases as the soluble boron level in the core is increased. The calculated density coefficient for Cycle 1 is shown in Table 4.3-4, and curves of density coefficient as a function of density for several soluble boron concentrations are presented on Figure 4.3-37. These curves are based upon two dimensional PDO calculations and have been generated over a wide-range of core conditions, including the range of both normal operating conditions and accident conditions. The density coefficients explicitly used in the accident analyses are based upon core conditions with the most limiting temperature coefficients allowed by the technical specification.

4.3.2.3.4 Moderator Nuclear Temperature Coefficient

The moderator nuclear temperature coefficient is the change in reactivity per unit change in core average moderator nuclear temperature, at constant moderator density. The source of this

reactivity dependence is the spectral effects associated with the change in thermal scattering properties of water molecules as the internal energy, which is represented by the bulk water temperature, is changed. The magnitude of the moderator nuclear temperature coefficient is equal to the difference between the moderator temperature coefficient, defined in Subsection 4.3.2.3.2, and the moderator density coefficient, defined in Subsection 4.3.2.3.3.

4.3.2.3.5 Moderator Pressure Coefficient

The moderator pressure coefficient is the change in reactivity per unit change in Reactor Coolant System pressure. Since an increase in pressure increases the water density, the pressure coefficient is merely the density coefficient expressed in a different form. The calculated pressure coefficient at full power is shown in Table 4.3-4.

4.3.2.3.6 Moderator Void Coefficient

The anticipated occurrence of small amounts of local subcooled boiling in the reactor during full power operation results in a predicted core average steam (void) volume fraction of substantially less than one percent. Changes in the moderator void fraction produce reactivity changes that are quantified by the void coefficient of reactivity. An increase in voids decreases core reactivity, but the presence of soluble boron tends to add a positive contribution to the coefficient.

The calculated values of moderator void coefficient for Cycle 1 are shown in Table 4.3-4. Curves 1 showing void coefficient vs void content can be inferred directly from the density coefficient curves provided on Figure 4.3-37.

4.3.2.3.7 Power Coefficient

The power coefficient is the change in reactivity per unit change in core power level. All previously described coefficients contribute to the power coefficient, but only the moderator temperature coefficient and the fuel temperature coefficient contributions are significant. The contributions of the pressure and void coefficients are negligible, because the magnitudes of these coefficients and the changes in pressure and void fraction per unit change in power level are small. The contribution of moderator density change is included in the moderator temperature coefficient contribution.

In order to determine the change in reactivity with power, it is necessary to know the changes in the average moderator and effective fuel temperatures with power. The average moderator (coolant) temperature is controlled to be a linear function of power.

The core average linear heat rate is also linearly dependent on power level. The effective fuel temperature is defined as the fuel temperature that, when employed to evaluate fuel nuclear properties, results in calculated properties representative of the actual nuclear properties of fuel being considered. The effective fuel temperature is dependent on both power level and burnup. A semi-empirical relationship is used to evaluate the effective fuel temperature (TF).

$$TF = TMOD + \left[\sum_{I=0}^{2} BF(I)\ BU^{(I)}\right](LHR) + \left[\sum_{J=0}^{3} CF(J)\ BU^{(J)}\right]\ (LHR)^2 \qquad (1)$$

Where:

TF	= Effective Fuel Temperature
TMOD	= Moderator temperature
BF(I), CF(J)	= Polynomial coefficients
BU	= Burnup (MWD/T)
LHR	= Linear Heat Rate (kw/ft)

The total power coefficient at a given core power can be determined by evaluating, for the conditions associated with the given power level, the following expression:

$$\frac{d\rho}{dP} = \frac{\partial \rho}{\partial T_f} \bullet \frac{\partial T_f}{\partial P} + \frac{\partial \rho}{\partial T_m} \bullet \frac{\partial T_m}{\partial P} \qquad (2)$$

The first term of equation (2) provides the fuel temperature contribution to the power coefficient, which is shown as a function of power on Figure 4.3-38.

The first factor of the first term is the fuel temperature coefficient of reactivity discussed in Subsection 4.3.2.3.1 and shown in Figure 4.3-34. The second factor of the first term is obtained by calculating the derivative of equation (1).

The second term in equation (2) provides the moderator contribution to the power coefficient. The first factor, the moderator temperature coefficient, is discussed in Subsection 4.3.2.3.2 and shown on Figures 4.3-35 and 4.3-36. The second factor is a constant since the moderator temperature is controlled to be a linear function of power.

Since the factors $\partial p/\partial T_f$ and $\partial p/\partial T_m$ are functions of one or more independent variables (e.g., burnup, temperature, soluble boron content, xenon worth, and CEA insertion), the total power coefficient, dp/dP, also depends on these variables.

The power coefficient tends to become more negative with burnup because the fuel and moderator temperature coefficients become more negative (see Figures 4.3-34 through 4.3-36). The insertion of CEAs, while maintaining constant power, result in a more negative power coefficient, because the soluble boron level is reduced and because of the temperature dependence of CEA absorption.

The full power values of the overall power coefficient for the unrodded core at BOC and EOC are shown in Table 4.3-4.

4.3.2.4 Control Requirements

There are three basic types of control requirements that influence the design of this reactor:

a. Reactivity control so that the reactor can be operated in the unrodded, critical, full power mode for the design cycle length.

b. Power level and power distribution control so that the reactor power may be safely varied from full rated power to cold shutdown, and so that the power distribution at any given power level is controlled within acceptable limits.

c. Shutdown reactivity control sufficient to mitigate the effects of postulated accidents.

Reactivity control is provided by several different means. The amount and enrichment of the fuel and burnable poison shims are design variables that determine the initial and end of cycle reactivity for an unrodded, unborated condition. Soluble boron and CEA poisons are flexible means of controlling long term and short term reactivity changes, respectively.

Normal changes of the pH and coolant chemistry which would be expected to occur during normal operation will have no measurable effect on core reactivity. In the unlikely event that gross changes occur in core chemistry due to an abnormal operating mode, it is possible for material from other parts of the primary system to be deposited on the fuel. The small reactivity changes associated with an event of this type can easily be accommodated either through changes in the dissolved boron concentration or through changes in CEA position.

Figure 4.3-40, the power dependent CEA insertion limit curve (PDIL), specifies the allowable CEA insertion for any given power level. Figure 4.3-40 has been verified to be consistent with all aspects of the safety analysis.

The uncertainty allowances associated with each component of the shutdown margin calculation are discussed in Subsection 4.3.3, which also includes experimental confirmation of these results from operating reactors. Table 4.3-6 shows the calculational uncertainty involved in the calculation of the reactivity defect between hot full power and hot zero power at EOC4. The uncertainty allowance on moderator defect is ±l0 percent; the allowance on fuel temperature defect is ±15 percent; the allowance on rod worth is ±10 percent.

Shutdown margin requirements are largest at end-of-cycle because the MTC is the most negative at that time. Furthermore, available rod worth is less during an equilibrium cycle than for any other cycle. Consequently the data which is presented for end-of-cycle four (cycle four is the first equilibrium cycle) is the most limiting possible for a nominal 3-batch annual refueling fuel management scheme. Table 4.3-7 illustrates that even for the EOC4 case the available rod worth (after assuming that the most reactive CEA is stuck out of the core) exceeds the required reactivity worth by 1.21 percent ΔP.

The following subsections discuss the reactivity balances associated with each type of control requirement.

4.3.2.4.1 Reactivity Control at BOC and EOC

The reactivities of the unrodded core at BOC and EOC with no soluble boron are shown in Table 4.3-2. This table includes the reactivity worth of equilibrium xenon and samarium, and shows the reactivity available to compensate for burnup and fission product poisoning. Soluble boron concentrations required for criticality at various core conditions are shown in Table 4.3-1. Soluble boron is used to compensate for slow reactivity changes such as those due to burnup, changes in xenon content, etc. The reactivity controlled by burnable poison shims is also given in Table 4.3-1. At EOC, the reactivity worth of the residual poison is less than one percent, and the soluble boron concentration is near zero. The reactor is to be operated in essentially an

unrodded condition at power. The CEA insertion at power is limited by the power dependent insertion limit (PDIL) for short term reactivity changes.

4.3.2.4.2 Power Level and Power Distribution Control

The regulating CEA groups may be used to compensate for changes in reactivity associated with routine power level changes. In addition, CEAs may be used to compensate for minor variations in moderator temperature and boron concentrations during operation at power. The reactivity worth of regulating Cycle 1 CEA control groups is shown in Table 4.3-5. Soluble boron is used to maintain shutdown reactivity at cold zero power conditions. CEAs can be used to help control the core power distribution. This function includes the suppression of xenon induced axial power oscillations.

4.3.2.4.3 Shutdown Reactivity Control

The reactivity requirements of the full compliment of CEAs are determined by the power defect, the required shutdown margin and miscellaneous reactivity penalties such as CEA bite and the stuck rod worth. Table 4.3-6 presents components of the power defect. Values shown represent EOC-4 conditions. These conditions, which are the most adverse calculated through the equilibrium cycle, are expected to envelope the first and later annual cycles. Individual components of the power defect are discussed in the following subsections. No reactivity penalty is associated with xenon decay because it is controlled with soluble boron rather than CEAs.

Table 4.3-7 presents a comparison of available CEA reactivity and the various reactivity requirements. Data shown has been calculated postulating the most adverse reactor states and therefore constitutes a limiting case. Table 4.3-7 indicates that the available CEA worth is more than sufficient to meet the requirements of the steam line break analysis. It is concluded that the excess available reactivity is capable of compensating for calculational uncertainties, thus, the shutdown reactivity control provided in this design is capable of meeting all requirements. Table 4.3-7(a) presents a similar comparison for the CEA ejection events.

Subsection 4.3.3.1.2.2.2 presents comparisons between measured and calculated CEA worths. CEA worths predicted for St. Lucie Unit 2 are verified during startup testing. With the implementation of the Startup Test Activity Reduction (STAR) program, measurements of CEA worths may be skipped on a cycle specific basis with CEA worths verification being performed with an alternate method.

4.3.2.4.3.1 Fuel Temperature Variation

The increase in reactivity that occurs when the fuel temperature decreases from its full power value to its zero power value is primarily due to changes in epithermal absorption resonances. As exposure accumulates the concentrations of plutonium isotopes increase making the fuel temperature coefficient ($\Delta\rho/F$) more negative. However pellet swelling and clad creepdown associated with increasing exposure improve the heat transfer characteristics of the fuel pin and results in a lowering of the full power fuel temperature. The competing effects of a more negative fuel temperature coefficient and decreasing fuel temperature tends to minimize the burnup dependence of the fuel temperature defect.

The fuel temperature correlation used in the design of St. Lucie Unit 2 is discussed in Subsection 4.3.3.1.2.2.4. This correlation accounts for both power and burnup dependence of

fuel temperature and it is this correlation upon which the fuel temperature defect is based. The fuel temperature variation presented in Table 4.3-6 is the upper limit of the defect occurring when the overall power defect is at its maximum.

4.3.2.4.3.2 Moderator Temperature Variation

The moderator temperature variation allowance is large enough to compensate for any reactivity increase that may occur when the moderator temperature decreases from the full power value to the zero power (hot standby) value. This reactivity increase, which is primarily due to the negative moderator temperature coefficient, is largest at the end of cycle when the soluble boron concentration is near zero and the moderator coefficient is strongly negative. At beginning of cycle, when the moderator temperature coefficient is less negative, the reactivity change is smaller.

The reactivity allowance for moderator temperature variation given in Table 4.3-6 is actually the sum of two allowances. The first, and most important, is the allowance, for the moderator temperature coefficient effect. The second allowance, referred to in Table 4.3-6 as the T-H effect, is intended to cover the reactivity effects associated with the greatest expected axial flux redistribution resulting from the difference in moderator temperature profile between full and zero power, and the asymmetric axial burnup distribution at EOC.

4.3.2.4.3.3 Moderator Voids

Reducing the power level from full power to zero power causes an increase in reactivity resulting from the collapsing of steam bubbles caused by local boiling at full power. The amount of void in the core is small and is estimated to be substantially less than one percent at full power. As with the moderator temperature effect, the maximum increase in reactivity from full to zero power occurs at end of cycle, when the least amount of dissolved boron is present. The reactivity effect is small, and the allowance for this effect is shown in Table 4.3-6.

4.3.2.4.3.4 Control Element Assembly Bite

The CEA bite is the amount of CEA reactivity worth that can be inserted in the core at full power to initiate ramp changes in reactivity associated with load changes, and to compensate for minor variations in moderator temperature, boron concentration, xenon concentration, and power level. The reactivity allowance for this effect is shown in Table 4.3-7.

4.3.2.4.3.5 Part Length CEA Effects

The part length CEAs have been removed from the St. Lucie Unit 2 design. Comparison of power distributions with and without part length CEAs (Figures 4.3-2a to 4.3-13) shows that the effects of the part length CEAs on the power distributions are not significant. See Subsection 4.3.2.7.4 also.

4.3.2.4.3.6 Loss In CEA Worth

This allowance accounts for the reduction in CEA worth resulting from the shorter neutron diffusion length at zero power moderator density relative to full power moderator density. This allowance is necessary because the CEA worth presented in Table 4.3-7 was calculated at hot full power.

4.3.2.4.3.7 CEA Worth

Table 4.3-7 shows the reactivity calculated to be available using the full complement of CEAs at EOC-4. This worth is expected to approximate the minimum total worth available during plant life. The worth however, must be corrected for effects not accounted for during its calculation. These effects include:

a. Assuming that not all CEAs are available at trip and that the CEA of highest worth remains stuck in the withdrawn position.

b. Losses in available CEA worth due to partial depletion of poison in the CEAs.

c. The over prediction of available worth due to modeling CEAs as if they were B4C over their full length, neglecting the slightly weaker Ag-In-Cd tips.

4.3.2.4.3.8 Rod Worth Assumed in the SLB Analysis

This reactivity requirement is necessary to assure that the reactivity balance used in the steam line break analysis remains conservative.

4.3.2.4.3.9 Shutdown Reactivity Requirements

The shutdown reactivity requirements due to fuel, moderator, CEA losses, and voids shown in Table 4.3-6 represent reactivity inserted by a reduction from hot full power to hot zero power. These requirements are substantially less for shutdowns initiated at lower power levels. The variation in required shutdown reactivity with power level allows an equivalent reduction in required CEA worth. The resultant excess CEA worth may be used for power level changes and power shaping. The power dependent insertion limit shown on Figure 4.3-40, assures that sufficient negative reactivity, in the form of withdrawn CEAs exists to meet the power dependent shutdown requirements.

As discussed in Subsection 4.3.3, the uncertainty in worth is less than 10 percent. Even allowing for the maximum calculated errors for total CEA worth in both of the adverse directions, sufficient shutdown margin is available.

4.3.2.5 Control Element Assembly Patterns and Reactivity Worths

The locations of all CEAs are shown on Figure 4.3-39. The CEAs designated as regulating control rods are divided into five groups; the shutdown CEAs are divided into two groups. These groups are identified, for first cycle operation, on Figure 4.3-39. All CEAs in a group are withdrawn or inserted nearly simultaneously. Shutdown groups are inserted after the regulating groups are inserted and are withdrawn before the regulating groups are withdrawn. The reactivity worths of sequentially inserted CEA groups at beginning of life and end of first cycle are shown in Table 4.3-5, and the maximum rodded radial peaking factors F_r^n for these configurations are shown in Table 4.3-8.

It is expected that all CEAs will be inserted at cold shutdown conditions. The core is essentially unrodded during full power steady state operation, except for limited insertion of the first regulating group in order to compensate for variations in moderator temperature and boron concentration as described in Subsection 4.3.2.4.2. For operation with substantial CEA insertion, the relationship between power level and the maximum permitted CEA insertion is

typified in Figure 4.3-40. This figure also illustrates the regulating group insertion order (6-5-4-3-2-1) and the 40 percent fixed overlap between successive regulating groups. Compliance with the power dependent insertion limits throughout the cycle ensures that adequate shutdown margin is maintained and that the core conditions are no more severe than the initial conditions assumed in the accident analyses described in Chapter 15. Reactivity insertion rates for the safety analysis of St. Lucie Unit 2 are presented in Chapter 15.

The power dependent insertion limit is designed such that the three dimensional power peak and reactivity inserted by the ejection of any CEA will not exceed acceptable limits. Section 15.4 contains a detailed discussion of the CEA ejection analysis.

The allowable CEA misalignment from any rod group is specified in Technical Specifications. Perturbations in CEA group worth and power distributions that result from CEA misalignments are analyzed using three dimensional calculations. Uncertainties that result from allowed misalignments are included in the analysis of limiting system safety setpoints and implemented via biases applied to the parameters. Intentional misalignment of CEAs for the purpose of power shaping is not allowed.

The CEA withdrawal incident from low power is analyzed with the maximum calculated differential reactivity insertion rate resulting from a sequential CEA bank withdrawal with 40 percent overlap, including a 10 percent reactivity uncertainty. The CEA withdrawal incident from full power is analyzed from the insertion of the lead bank which maximizes the reactivity insertion and the power shape change during the CEA withdrawal. Reactivity insertion rates are calculated by a static axial model of the St. Lucie Unit 2 core. The calculated reactivity insertion resulting from the sequential CEA withdrawal is presented on Figures 4.3-41 and 4.3-42.

CEA misoperation events are discussed in Section 15.4.

The full-length CEA drop incident is analyzed by selecting the dropped CEA that maximizes the increase in the radial peaking factor. A conservatively small negative reactivity insertion is used in the accident analysis. The part length CEA subgroup drop incident is analyzed parametrically for various initial axial power shapes so that the combination of axial power shape and the inserted reactivity lead to the most adverse analyses results. A conservative reactivity insertion is used in the single PLCEA drop incident.

Selected CEA drop and withdrawal tests are conducted during startup testing. The results of these tests are compared to predictions for additional verification of the methodology employed in the CEA drop, withdrawal and ejection analysis.

The typical reactivity insertion during a reactor scram is presented in Chapter 15. This reactivity insertion is computed by static axial models at various scram CEA positions, and it is used for all accidents which are terminated by a scram, unless otherwise indicated. For the bounding analysis introduced in Cycle 12, scram reactivities are calculated as described below. The reactivity insertion is conservative since (1) an end of cycle power shape is assumed for the calculation, (2) a conservatively small shutdown worth (see Table 4.3-7) is assumed to be available, and (3) the influence of delayed neutrons on the transient power shape is neglected. The scram reactivity for other incidents, such as the loss of flow, are performed by a parametric analysis which considered various initial power shapes and the scram reactivity associated with those power shapes.

The maximum reactivity worth and planar power peaks associated with an ejected CEA event encompass the worst conditions anticipated during the current cycle and are conservative with respect to the best estimate calculated values.

The limiting dropped CEA reactivity worth and maximum increase in radial peaking factor are shown in Table 4.3-26 for Cycle 2 and the reference cycle. The values shown for Cycle 2 are the safety analysis values, which are conservative with respect to the best estimate values.

The neutronics calculation of the space-time FIESTA code[57] has been incorporated into the HERMITE code[21] for use in 1-D axial calculations. Bounding scram reactivities as a function of percent insertion are calculated using 1-D axial space-time HERMITE calculations.

4.3.2.6 Criticality of Reactor During Refueling

The soluble boron concentrations during refueling are shown in Table 4.3-1. These concentrations ensure that the k_{eff} of the core during refueling does not exceed 0.95. Technical Specifications regarding the minimum concentration of soluble boron during refueling assure that k_{eff} will not exceed 0.95.

4.3.2.7 Stability

4.3.2.7.1 General

Pressurized water reactors (PWRs) with negative overall power coefficients are inherently stable with respect to power oscillations. Therefore, this discussion will be limited to xenon induced power distribution oscillations. Xenon induced oscillations occur as a result of rapid perturbations to the power distribution which cause the xenon and iodine distributions to be out of phase with the perturbed power distribution. This results in a shift in the iodine and xenon distribution that causes the power distribution to change in an opposite direction from the initial perturbation and thus an oscillating condition is established. The magnitude of the power distribution oscillation can either increase or decrease with time. Thus, the core can be considered to be either unstable or stable with respect to these oscillations. Discussed below are the methods of analyzing the stability of the core with respect to xenon oscillations. The tendency of certain types of oscillations to increase or to decrease is calculated, and the method of controlling unstable oscillations is presented.

4.3.2.7.2 Method of Analysis

Xenon oscillations may be analyzed by two methods. The first method consists of an explicit analysis of the spatial flux solution accounting for the space-time solution of the xenon concentrations. Such a method is useful for testing various control strategies and evaluating transitional effects (such as power maneuvers). The second method consists of modal perturbation theory analysis, which is useful for the evaluation of the sensitivity of the stability to changes in the reactor design characteristics, and for the determination of the degree of stability for a particular oscillatory mode.

The stability of a reactor can be characterized by a stability index or a damping factor which is defined as the natural exponent which describes the growing or decaying amplitude of the oscillation. A xenon oscillation may be described by the following equation:

$$\phi(\bar{r},t) = \phi_o(\bar{r}) + \Delta\phi_o(\bar{r})\ e^{bt} \sin(\omega t + \delta)$$

where

$\phi(\bar{r},t)$	is the space-time solution of the neutron flux
$\phi_0(\bar{r})$	is the initial fundamental flux
$\Delta\phi_0(\bar{r})$	is the perturbed flux mode
b	is the stability index
ω	is the frequency of the oscillation
δ	is a phase shift

Modal analysis consists of an explicit solution of the stability index b using known fundamental and perturbed flux distributions. A positive stability index b indicates an unstable core, and a negative value indicates stability for the oscillatory mode being investigated. The stability index is generally expressed in units of inverse hours, so that a value of –0.01/hr would mean that the amplitude of each subsequent oscillation cycle decreases by about 25 percent (for a period of about 30 hours for each cycle).

Xenon oscillation modes in PWRs can be classified into three general types: radial, azimuthal, and axial. To analyze the stability for each oscillation mode, only the first overtone needs to be considered since higher harmonic modes decay more rapidly than the first overtone. Furthermore, since the first overtone of a radial oscillation decays more rapidly than the first overtone of an azimuthal oscillation, only the latter of these two modes will be considered in detail.

4.3.2.7.3 Expected Stability Indices

4.3.2.7.3.1 Radial Stability

A radial xenon oscillation consists of a power shift inward and outward from the center of the core to the periphery. This oscillatory mode is generally more stable than an azimuthal mode. This effect is illustrated in Figure 4.3-43, which shows that for a bare cylinder the radial mode is more stable than the azimuthal mode. Discussion of the stability for radial oscillator mode is therefore deferred to the azimuthal mode.

4.3.2.7.3.2 Azimuthal Stability

An azimuthal oscillation consists of a X-Y power shift from one side of the reactor to the other. Modal analysis for this type of oscillation is performed for a range of expected reactor operating conditions.

The expected variation of the stability index during the first cycle is shown in Figure 4.3-44. These results are obtained from analyses which consider the spatial flux shape changes during the cycle, the changes in the moderator and Doppler coefficient during the cycle, and the change in xenon and iodine fission yield due to plutonium buildup during the cycle. As is shown

on the figure, the expected stability index is no more positive than (-0.044/hr) at any time during the cycle for the expected mode of reactor operation. Comparison of predicted stability index with those actually measured on operating cores, as discussed in Subsection 4.3.3.2.3, provide a high confidence level in the prediction of azimuthal stability. Measurements of xenon spatial stability in large cores have been made[2] which provide confidence in the methods that are used to predict the azimuthal stability of this core.

4.3.2.7.3.3 Axial Stability

Axial xenon oscillations consist of a power shift toward the top and bottom of the reactor core. This type of oscillation may be unstable during the first cycle. Table 4.3-9 shows the calculated variation of the axial stability index during the first cycle. It is anticipated that control action with CEAs may be required to limit the magnitude of the oscillation. As discussed in Subsection 4.3.2.2, the axial power distribution is monitored by the RPS. Based on the measurement of the axial power distribution, the operator may move the CEAs so as to control any axial oscillations.

4.3.2.7.4 Control of Axial Instabilities

The control of axial oscillations during a power maneuver is illustrated in Figures 4.3-25 through 4.3-32. In these figures, PLCEAs are used throughout these maneuvers to limit the change in the power distribution. The difference between an uncontrolled and a controlled xenon oscillation is illustrated in Figure 4.3-45. It was assumed in the calculation of the controlled oscillation that the PLCEAs were moved in such a way as to preserve the initial shape in the core prior to the initiating perturbation. The calculations are performed at the end of the first cycle which corresponds to the expected least stable condition for axial xenon oscillations. Similar control can be obtained using full-length CEAs.

4.3.2.7.5 Summary of Special Features Required by Xenon Instability

The RPS described in Subsection 7.2.2 is designed to prevent exceeding acceptable fuel design limits and to limit the consequences of postulated accidents. In addition, a means is provided to assure that under all allowed operating modes, the state of the reactor is confined to conditions not more severe than the initial conditions assumed in the design and analysis of the protective system.

Since the reactor is predicted to be stable with respect to azimuthal xenon oscillations, no special protective system features are needed to accommodate azimuthal mode oscillations. Nevertheless, a maximum quadrant tilt is prescribed in the technical specifications along with prescribed operating restrictions in the event that the tilt is exceeded. The maximum allowed azimuthal power tilt is assumed in the setpoint analysis[1].

4.3.2.7.5.1 Features Provided for Azimuthal Xenon Effects

a. Administrative limits on azimuthal power tilt

b. Monitoring and indicating the azimuthal power tilt.

c. Accounting for the maximum allowed azimuthal power tilt in the RPS limits.

4.3.2.7.5.2 Features Provided for Axial Xenon Effects and Power Distribution Effect and Control

a. RCS boration / dilution for control of the axial power distribution, if required

b. CEAs for additional axial power distribution control, if required.

c. RCS temperature for control of axial power distribution, if required.

d. Monitoring and accounting for the axial power distribution in the RPS.

4.3.2.8 Vessel Irradiation

The design of the reactor internals and of the water annulus between the active core and vessel wall is such that for reactor operation at the full power rating and an 80 percent capacity factor over the 60-year design life of the vessel (or 48 EFPY), the vessel fluence greater than one MeV at the vessel wall will reach approximately 3.8×10^{19} n/cm^2. The calculated exposure projections beyond the end-of-cycle 19 includes a 10 percent uncertainty factor.

The maximum fast neutron fluences greater than one MeV accumulated on the vessel clad base metal interface (CBMI) and shroud inside surface are as shown in Table 4.3-10. The projection fluxes are based on a time averaged equilibrium cycle radial power distribution and an axial power distribution with a peak to average of 1.11. The calculation assumed a thermal power of 2700 MWt for cycles 1 through 19 and of 3020 MWt for cycle 20 and onwards. The models used in these calculations are discussed in Subsection 4.3.3.3.

4.3.3 ANALYTICAL METHODS

Discussions of methodologies within this section are written from an historic perspective and may have been superseded by newer methods as discussed in Reference 65.

Westinghouse physics methodology is used to generate physics inputs and characteristics based on Reference 69 (beginning with Cycle 12) and Reference 70 (beginning with Cycle 15).

Starting with Cycle 23, AREVA methods are also approved for use in generating physics inputs and characteristics based on References 76, 77, and 78. EC287528

4.3.3.1 Reactivity and Power Distribution

4.3.3.1.1 Method of Analysis (HISTORICAL)

The nuclear design analysis for low enrichment PWR cores is based on a combination of multigroup neutron spectrum calculations, which provide cross sections appropriately averaged over a few broad energy groups, and few group one, two, and three dimensional diffusion theory calculations of integral and differential reactivity effects and power distributions. The multigroup calculations include spatial effects in those portions of the neutron energy spectrum where volume homogenization is inappropriate; e.g., the thermal neutron energy range. Most of the calculations are performed with the aid of computer programs embodying analytical procedures and fundamental nuclear data consistent with the current state of the art.

Comparisons between calculated and measured data that validate the design procedures are presented in Subsection 4.3.3.1.2. As improvements in analytical procedures are developed,

and improved nuclear data become available, they will be added to the design procedures, but only after validation by comparison with related experimental data.

Few group cross sections for subregions of the core that are represented in spatial diffusion theory codes, e.g., fuel pin cells, moderator channels, structural member cells, etc., are calculated by the CEPAK lattice program. This program is the synthesis of a number of computer codes, many which were developed elsewhere; e.g., FORM,[3] THERMOS[4] and CINDER.[5] These programs are interlinked in a consistent way with inputs from differential cross-section data from an extensive library.

The microscopic data base for both fast and thermal neutron cross-section is derived from the Evaluated Nuclear Data File ENDF/B-IV. Some modifications have been applied to the U-238 resonance integral to correct for a recognized overestimation of that quantity in ENDF/B-IV.

The entire neutron spectrum is represented by 83 neutron groups between 0 and 10 MeV. Neutron leakage in a single Fourier mode is represented by either P-l or B-1 approximations to transport theory throughout this entire range. Resonance shielding is determined analytically; the Hellstrand correlation[6] is employed for U-238, with appropriate adjustments guided by Monte Carlo calculations of resonance capture in U-238 so as to provide agreement with selected measurements of the conversion ratio. Plutonium resonance integrals are determined from an intermediate resonance formulation using equivalence relationships for the lattice representation.[7]

Appropriate Dancoff correction factors are determined for uniform lattices by a three region model of the unit cell to provide a better description of the effect of scattering in the clad on resonance capture. For heterogeneous lattices, this calculation is extended to include heterogeneous by nearest neighbor approximations. Included also in the resonance shielding calculation is an appropriate account of resonance overlap effects between different uranium and plutonium isotopes. In the thermal energy range, the effects of cell environment on the spatially dependent neutron spectrum within the lattice cell can be included in those cases where such effects are important. Anisotropic scattering and temperature dependent effects associated with the hydrogenous moderator are approximated by the use of transport corrected temperature dependent scattering kernels generated by the GAKER program.[8] A major subroutine of CEPAK provides depletion calculations in the reactor cell to describe the evolution of the reactor spectrum and the appropriate cross section averages, the production of fission products, including xenon and samarium, and the production of conversion products such as plutonium isotopes. Various criticality search options are available to approximate the effects of reactivity control on the neutron spectrum and thus on the few group cross section averages over energy.

Boundary conditions and equivalent diffusion theory constants for individual elements of a CEA are calculated by the CERES program. For a one region CEA in cylindrical geometry, boundary conditions are calculated in each multi group by the method of successive generations, with capture probabilities based on the tabulations of Stuart and Woodruff.[9] Two region CEAs are transformed to fictitious homogeneous CEAs by matching extrapolation lengths on the outer surface, as defined by Kear and Ruderman.[10] The homogeneous CEAs are then treated as above. Fictitious few group diffusion parameters for use in multidimensional diffusion theory calculations are obtained using methods defined by Wachspress[11] and Henry.[12]

Effective diffusion theory constants for burnable poison rod shim cells are calculated by a sequence of programs consisting of HAMMER,[13] DTF-IV,[14] and MO-807.[15] HAMMER is

employed as a few group region-wise cross section generator for the shim cell; DTF-IV is employed in a one dimensional representation of the shim cell and environment to define relative reaction rates between shim and fuel cells; and MO-807 is employed to calculate the effective diffusion theory constants.

Static and depletion dependent reactivities and nuclide concentration, flux and power distributions in one, two, and three dimensional representations of the core are determined by a diffusion-depletion program, PDQ-X. The program is an extension of the PDQ-7[16] and HARMONY[17] programs to include the following optional capabilities:

a. Moderator and fuel temperature feedback in the three dimensional geometry option, fuel temperature feedback in two dimensional geometry

b. Poison content criticality searches as well as spatial feedback on the power distribution by fuel and moderator temperature in the one dimensional geometry option.

Approximations in the fine structure flux distribution within an assembly, resulting from the use of diffusion theory and finite mesh sizes, are corrected by normalizing the pin to box power ratio to the results of more exact multigroup transport calculations. The two dimensional integral transport code DIT[18] has been used to generate benchmark power distributions in each type of fuel assembly, which were compared to results of standard fine mesh PDQ calculations. DIT in turn was calibrated against power distributions measured in cold and hot critical experiments. This procedure resulted in the establishment of biases and uncertainties in pin peaking factors for DIT and in biases between DIT and PDQ. It was thus possible to define a set of correction factors applicable to the pin-by-pin power distributions generated by PDQ to produce the current best estimate of the radial peaking factor. Correction factors range from 1.05 in freshly loaded assemblies to 1.02 for twice burned assemblies. The detail of the procedure described above is presented in Reference 19.

For first cycle calculations a quarter core representation with reflective boundary conditions at the core centerlines is usually adequate. For cores with an asymmetric fuel loading or for the calculation of ejected rod worths, full representations are used.

The quarter core fine mesh representation described above requires about 25,000 mesh points to describe the geometry of a 217 assembly reactor core. For some applications this detail is not required. For these purposes coarse mesh calculations are constructed having only a few mesh regions per assembly (typically four). Coarse mesh calculations are capable of accurately predicting gross power distributions, core reactivity, and depletion characteristics but cannot accurately calculate pin power peaks. Cross sections for coarse mesh calculations are obtained by spatially collapsing, by batch type, the fine mesh cross sections in such a way preserve the individual reaction rates.

Coarse mesh calculations are also performed by the Reactor Operation and Control Simulator (ROCS) code[20]. This code contains a higher order nodel solution to the diffusion equation to obtain a high degree of accuracy with a low number of spatial mesh points. The axial and radial reflector regions are replaced by a node dependent boundary condition that relates the current out of the node to the average flux in the node adjacent to the boundary. The code also contains all the feedback required to correctly determine the spatial distributions of fuel temperatures and moderator density, and a number of search options.

As the size of large power reactors increases, space time effects during reactor transients become more important. In order not to penalize reactor performance unduly with overly conservative design methods, it is desirable to have the capability of performing detailed space time and static neutronics calculations for both nominal and off nominal core conditions.

The HERMITE computer code[21] has been developed to meet this objective. It solves the few-group, space and time dependent neutron diffusion equation including feedback effects of fuel temperature, coolant temperature, coolant density and control rod motion. The fuel temperature model explicitly represents the pellet, gap and clad regions of the fuel pin, in which case the governing heat conduction equations are solved by a finite difference method. Alternatively, the correlation described in Subsection 4.3.2.3.7 between fuel temperature and power can be used.

These calculations employ macroscopic or microscopic cross section data for time independent or depletion effects respectively generated by the methods described in the preceding paragraphs.

The cycle one spatial flux in the reactor core is customarily assumed to be separable into radial and axial components. Thus, the detailed spatial variations of the flux and power are obtained from the calculation of the broad group fluxes in a two dimensional calculation of a typical plane in the reactor. The calculation is corrected for axial leakage effects by the use of a group dependent buckling, which is obtained from a one dimensional core average axial calculation.

For detailed calculations of pinwise power distributions, a mesh rectangle is assigned to each pin cell. The inter-assembly water channel, the core shroud and the core barrel are each represented explicitly in standard fine mesh design calculations. In addition, water holes, shim boron cells and control rods are each represented.

In a large PWR core, the calculated power distributions are fairly sensitive to the treatment of the reflector cross sections. Terney[23] has compared transport and diffusion calculations of the albedo and shown that the latter substantially underpredicts the reflector albedos in the fast (top) group and that the power distribution is shifted toward the core center when compared to multigroup transport theory results. When the fast diffusion coefficients in the reflector are altered to make the transport and diffusion theory albedos agree, the power distributions are also brought into agreement.

In addition, Terney[23] has obtained an additional correction factor for mesh size effects that is applicable to coarse mesh problems. The use of this formula gives the correct albedos at the reflector-core interface, as well as improved power distributions for coarse mesh problems.

The HARMONY [17] scheme of cross section organization is used to input cross sections for the PDQ, ROCS, and HERMITE spacial calculations. The fuel cross sections are calculated for each assembly type as a function of exposure, soluble boron concentration, initial enrichment, moderator temperature or density and fuel temperature. The HARMONY scheme allows for any microscopic cross section to be interpolated against any of the above variables at each depletion time step. Separate cross section sets are generated for the water holes, poison rods, water channel, reflector and control rods.

The depletion of the core is accomplished by utilizing a set of linearized depletion chains specifying the coupling (neutron capture or fission or decay) between the isotopes in the chain. Except for I-135, Xe-135 and Sm-149, the fission products are added together into a single lumped fission product. The exposure intervals of the depletion calculations are usually chosen

to be 1000 MWd/T during which it is assumed that the flux and microscopic cross sections are unchanged. At the end of each exposure interval, the fluxes and cross sections are recalculated. Shorter exposure intervals are used for recalculation of cross sections, which vary rapidly with depletion, such as shim boron. The soluble boron concentration and axial leakages are modified at each exposure interval, to maintain the calculational model critical.

The local fuel temperature has a large effect upon the spatial power distribution and therefore has to be factored into the spatial calculations. This effect is included by a fuel temperature feedback, in which the local effective fuel temperature is calculated as a function of local exposure and power density as described in Subsection 4.3.3.1.2.2.4, and the cross sections are evaluated at the same conditions. This process is iterated until a converged solution is obtained between power density, fuel temperature and neutron reaction rate distributions.

The treatment of thermal hydraulic effects in the axial direction is performed by including on top of the fuel temperature dependence, a variation of the cross sections with local moderator temperature and/or density. The moderator density distribution is calculated from the inlet coolant conditions of temperature, flow and pressure, and from the enthalpy rise in the core. The heat transfer model between fuel rods and coolant covers four regimes: 1) single phase liquid, 2) two phase liquid steam, 3) super-heated steam, and 4) supercritical (pressure greater than 3208 psia). In the single phase and two phase regimes, a subcooled boiling model developed by Maurer[54] may be included in the calculation at the user's option.

Axial depletion calculations are performed by the PDQ-X code, whose results are used to supply the necessary input to the QUIX code, which generates the data required by the monitoring and control systems. In addition to the eigenvalue problem, QUIX will perform three types of search calculations to attain a specified eigenvalue; viz., a poison search CEA, region boundary search, and a moderator density dependent poison search. The effects of moderator and fuel temperature feedback on the power distribution can be treated. The program can also perform power shaping searches.

The QUIX code has the capability of simulating excore detector responses expected during operation. The calculated normalized core average power distribution is first corrected by the application of CEA shadowing factors to simulate the peripheral fuel assembly power distribution. Shape annealing factors (defined below) are then applied to the peripheral axial power distribution to simulate the integrated response of the sub-channels of the two element excore detectors.

CEA shadowing is the change in excore detector response resulting from changing the core configuration from an unrodded condition to a condition with CEAs inserted, while maintaining constant power operation. Although CEA shadowing is a function of azimuthal location, its effects is minimized by placing the excore detectors at azimuthal locations where minimum CEA shadowing occurs, CEA shadowing factors can be determined using detailed two dimensional power distributions (XY-PDQs) representing the cumulative presence of the various CEA banks and employing the shielding code SHADRAC.[24] SHADRAC calculates fast neutron and gamma ray spectra, heating, and dose rates in a three dimensional system utilizing a moments method solution of the transport equation. The core, vessel internals, vessel, and excore detector location are treated explicitly in the calculation.

Normalized CEA shadowing factors are relatively constant with burnup and power level changes made without moving CEAs. CEA shadowing factors at beginning and end of first cycle life are as shown in Table 4.3-11.

Figure 4.3-46 shows the typical behavior of the CEA shadowing factor during a CEA insertion and withdrawal sequence. QUIX simulated factors and experimentally measured CEA shadowing factors during this transient situation are shown to have quite good agreement over a significant range of CEA insertions.

Shadowing factors account for the radial effects and annealing accounts for the axial effects on the excore detector responses. Due to neutron scattering in the various regions separating the core and the excore detectors, each detector subchannel responds to neutrons from the entire length of the core and not just from the section immediately opposite the subchannel. This effect is independent of the axial power shape and the azimuthal CEA shadowing factors. Typical axial shape annealing functions, given as fractional response per percent of core height for a two subchannel system, are in Figure 4.3-47.

Shape annealing functions (SAFs) are calculated using DOT[25, 26] of the DOT-DOMINO[27]-MORSE[28] technique.

The SAF is determined from a series of fixed source calculations in which the source is given by an isotropic fission spectrum distributed uniformly, radially and axially throughout successive horizontal slices of the core. The result of each fixed source calculation is the response in each of the excore detectors from each horizontal slice of the core. These results are then normalized so that the sum over all the detectors and fixed source calculations representing the entire height of the core equals 1.0. The effect of variations in the percent of core height used for each fixed source calculation is removed and the units of the SAF converted to fractional response per percent of axial height of the core by dividing the results for each case by the respective percent of core height used for the source of that calculation. The SAF is then plotted for each excore detector as the fractional response per percent of core height versus the percent of the core height.

For cases which may be described adequately by azimuthally symmetric models (Figure 4.3-48) the response at the detector given a fixed source in some increment of the core, may be determined by first solving the Boltzmann transport equation in "RZ" cylindrical geometry for (r,z,ζ,ψ,E).

The method of discrete ordinates, DOT IIW, or DOT III, can be used to solve an approximation to this equation. The major features of the method used in both codes are as follows:

a. Energy dependence is considered using the multigroup treatment.

b. The derivative terms and spatial dependence are approximated using a finite difference technique.

c. Dependence upon the direction variables is treated using the discrete ordinates method.

d. The scattering integral is evaluated using a discrete ordinates quadrature in combination with a Legendre expansion of the scattering kernel to approximate anistropic scattering.

In some problems it is not possible to adequately model the geometry unless a three dimensional representation is used. In these cases the response of each detector is obtained by first solving the three dimensional form of the transport equation.

The current state-of-the-art in solving this equation involves the use of the Monte Carlo method and in particular the MORSE code. The major features of the MORSE code are as follows:

a. Multigroup treatment of energy dependence,

b. Combinatorial geometry representation of the problem geometry,

c. Generalized Gaussian Quadrature for the treatment of the angular distribution of group to group transfers.

The existence of partial azimuthal symmetry in the problem geometry can be employed to reduce the analysis effort. The geometry may then be divided into two overlapping parts, one with complete azimuthal symmetry and the remaining one without azimuthal symmetry. The radiation field in the symmetric portion of the geometry may then be calculated using the DOT IIW/DOT III codes and the asymmetric portion calculated using the MORSE code and a source generated along an interface between two portions of the geometry.

This source for the Monte Carlo calculations are generated for MORSE by the DOMINO code, a utility code which converts the boundary angular flux from a DOT "RZ" geometry, calculation into the appropriate format for use as a source in MORSE.

The RZ-DOTs and MORSE use P_3 scattering cross sections based on the CASK (DLC-23E) cross section set.[29]

As the annealing is determined using a flat axial shape, the resulting annealing factors, S(z), must be multiplied by the appropriate peripheral axial power shape, P(z), to obtain the total detector response.

$$D_{Lower} = \int_{o}^{H} P(z)\, S(z\ )_{lower}\, dz = lower\ detector\ response$$

$$D_{upper} \quad \int_{o}^{H} P(z)\, S(z\ )_{upper}\, dz = upper\ detector\ response$$

The shape annealing factors are purely geometric correction factors applied to the peripheral axial power distribution. As such, the effects of time in fuel cycle, transient xenon redistribution and CEA insertion, although affecting the peripheral bundle power shape, do not affect the geometric shape annealing correction factors. Figure 4.3-49 compares the peripheral axial shape index with the external shape index, inferred from detector signals at the core boundary, during a CEA and PLCEA motion test for the Palisades reactor. Shown are the results of QUIX simultations of the test as well as experimental data taken during the test.

From this curve, we can conclude that even though the axial power distribution in the core and the core periphery was changing during this transient, the relationship between the excore response and the peripheral response was not. These results justify not only the separability of CEA shadowing and shape annealing assumed in QUIX but also demonstrate that shape annealing is purely a geometric effect, independent of the peripheral axial power distribution.

The excore detector temperature decalibration effect is the relative change in detector response as a function of reactor water inlet temperature. The temperature decalibration effect is calculated utilizing SHADRAC with explicit representation of core, vessel internals, vessel, and

detector location for various reactor inlet temperatures. Typical detector temperature normalized to an inlet temperature of 548 F is as shown in Figure 4.3-50.

Final normalization of the CEA shadowing, shape annealing, and temperature decalibration constants will be accomplished during startup testing.

Beginning with Cycle 15, the Relaxed Axial Offset Control axial power distribution confirmation (Reference 70) is employed.

4.3.3.1.2 Comparisons with Experiments

The nuclear analytical design methods in use for St. Lucie Unit 2 have been checked against a variety of critical experiments and operating power reactors. In the first type of analysis, reactivity, reaction rates and power distribution calculations are performed, which leads to information concerning the validity of the basic fuel cell calculation. The second type of analysis consists of a core follow program in which power distributions, reactivity coefficients, reactivity depletion rate, and CEA worths are analyzed to provide a global verification of the nuclear design package.

4.3.3.1.2.1 Critical Experiments

Table 4.3-12 summarizes the properties of the fuel rods employed in the lattices analyzed. The enrichments, pin dimensions, and water to fuel ratios are similar to those used in pressurized power reactors. Tables 4.3-13 and 4.3-14 summarize pertinent characteristics of the lattices and the eigenvalues calculated for the uranium and mixed oxide lattices, respectively.

The average eigenvalue for the uranium oxide lattices is 1.0008 ± 0.0031 and for the mixed oxide lattices it is 1.0043 ± 0.0034.

Reaction rates were measured in some of the lattices noted in the previous subsection and are shown, along with definitions of the measured quantities, in Table 4.3-15.

Although some scatter can be seen in the differences between measured and calculated values, the average error in the prediction of reaction rates is of the order of one percent only, except for δ 25, the epicadmium to subcadmium fission rate for U235, which is consistently overestimated by seven to eight percent. This overprediction of the fast fission rate in U-235 is due to simplifying assumptions in the resonance shielding, which were shown not to affect the reactivity level of the isotopic depletion rates.

Selected CE and KRITZ critical experiments were analyzed to obtain comparisons between predicted and measured power distributions. Only those critical configurations which simulated the fuel waterhole arrangement employed in the CE fuel assembly were chosen to establish uncertainties in local power peaking factor predictions. These experiments were analyzed with standard design methodology (PDQ-CEPAK), corrected for transport effects by normalizing the power peaking factors to values predicted by two dimensional multi-group transport calculation. These analyses formed the basis for a systematic definition of correction factors applicable to local power peaking factors calculated by standard design methodology which led to our current best estimate of the fine structure power distribution within a fuel assembly.

4.3.3.1.2.2 Power Reactors

The accuracy of the calculational system in its entirety can only be assessed through the analysis of experimental data collected on operating power reactors. The data under investigation consists of critical conditions, reactivity coefficients, and rod worths measured during the startup period, and of critical conditions, power distributions, and reactivity coefficients measured throughout the various cycles.

4.3.3.1.2.2.1 Startup Data

Because of the clean core configuration prevailing during the initial zero power operation, the startup data is extremely valuable in assessing the validity of the physics design package.

The soluble boron concentration that has to be added to the moderator to bring the unrodded reactor critical is a measure of the excess reactivity present in the core to accommodate the negative reactivity insertion due to the power escalation and the fuel depletion. The boron concentrations measured in cold and hot conditions for various reactors are compared with the calculated predictions in Table 4.3-16, showing an average error of -7 ppm (calculated-measured) with a standard deviation of 13 ppm.

The isothermal temperature coefficient is the change in reactivity resulting from a unit change in moderator inlet temperature. The isothermal temperature coefficient (ITC) differs from the moderator temperature coefficient in that the ITC includes a change in fuel temperature equal to the change in inlet moderator temperature. (Fuel and moderator temperature coefficients are discussed in Subsections 4.3.2.3.1 and 4.3.2.3.2 respectively).

The result of analyses of beginning of cycle temperature coefficients is given in Table 4.3-16, showing an excellent agreement between measured and calculated values. The average error in the eight coefficients given in the table is only $-0.03 \pm 0.007 \times 10^{-4}$ $\Delta\rho/F$.

4.3.3.1.2.2.2 CEA Reactivity Worth

Comparisons were made between the predicted and measured CEA worths for individual banks inserted sequentially for the Maine Yankee, Fort Calhoun, Calvert Cliffs, Millstone, St. Lucie Unit 1 and ANO-2. (ANO-2 has the 16 x 16 fuel assembly design similar to that of St. Lucie Unit 2) reactors. Table 4.3-17 summarizes the comparison between calculation and experiment. In the evaluation of the experimental data, revised values of delayed neutron fractions published in Reference 31 were used. The comparisons demonstrate that CEA reactivity can be calculated to within seven percent of the experimental value. A comparison between calculation and measurement of ejected, stuck and dropped CEA worths is given in Table 4.3-18 for Palisades, Fort Calhoun and Maine Yankee. The differences between calculation and measurement here are approximately the same as in the individual CEA bank calculations. For these comparisons the stuck, ejected, and dropped CEA worths are calculated to within eight percent of the experimental value.

4.3.3.1.2.2.3 Depletion Calculation

Over 50 spent fuel samples from Yankee Rowe Core I were subjected to isotopic and radio-chemical analyses which were performed in the Tracerlab Laboratory at Richmond, California and by the Vallecitos Atomic Laboratory of the General Electric Company.[30] Depletion calculations were performed on the Yankee core for comparison with the above measurements.

Figure 4.3-51 compares measured and calculated values of the Pu/U mass ratio versus U-235 depletion, and Figure 4.3-52 shows a comparison for the relative isotopic composition of plutonium as a function of fractional U-235 depletion.

Comparisons of the depletion behavior of the measured and calculated critical boron concentrations for the Palisades, Maine Yankee, and Omaha reactors are shown in Figures 4.3-53, 4.3-54, and 4.3-55, respectively. These comparisons indicate good agreement for the Palisades reactor and a relatively consistent bias between calculation and measurement for the Maine Yankee and Omaha reactors of approximately 50 to 70 ppm for the range of conditions shown in the figures. Best estimate reactivity predictions for these latter two classes of reactors are currently obtained by increasing the calculated critical boron concentration by approximately 50 ppm. A prior knowledge of the expected bias between measured and calculated soluble boron concentration is factored into the design calculations and results in better estimates of these characteristics which are sensitive to the boron level such as moderator temperature coefficients, power distributions, and cycle length. The resulting difference between the best estimate predicted soluble boron concentration and measured critical soluble boron concentrations after adjustment to standard conditions is within approximately 0.4 percent reactivity, of which a significant fraction is associated with the spread in the experimental data.

4.3.3.1.2.2.4 Fuel Temperature and Power Coefficients

The power coefficient is expressed in terms of reactivity change per unit change in power. This coefficient consists mostly of two components: one results from reactivity change associated with the core coolant temperature distribution and the other, which will be discussed here, is due to the change in fuel temperature. At each power level, an equilibrium exists between the power produced in the fuel, the fuel temperature, the heat transfer between the fuel and the coolant, and the energy removed by the coolant. The fuel temperature can be calculated directly by a heat transfer calculation, or indirectly by the analysis of the reactivity effects associated with a fuel temperature change. Both approaches have been used and lead to very consistent results.

The reactivity effects attributable to the fuel temperature are due to the Doppler broadening of the cross section reasonances, mostly those of uranium U238, as well as to the change in scattering properties of the oxygen present in the fuel. The fuel temperature component of the power coefficient can be expressed as:

$$\frac{\partial \rho}{\partial \underline{P}} = \frac{\partial \rho}{\partial T} \frac{\partial T}{\partial \underline{P}}$$

The determination of the first term, $\partial\rho/\partial T$, is performed by the lattice code CEPAK, in which the Hellstrand correlation is used to calculate the Doppler broadening of U238[6] and an equivalence principle is used for the plutonium isotopes[7]. The second term, $\partial T/\partial P$ has been calculated by the FATES code[31], for a St. Lucie Unit 2 fuel pin as well as for a Millstone II fuel pin, which has different dimensions but the same fuel densification properties. FATES shows that the fuel temperature is insensitive to the pellet diameter, and therefore that the measured power coefficients $\partial P/\partial P$ at Millstone II can be used to establish the validity of the fuel temperature correlation.

The following correlation is semi empirically derived from the FATES results and the analysis of the Millstone II power coefficients.

$$T_{fuel}(F) = T_{mod} + \left(\sum_{i=0}^{2} B_i M^i\right)P + \left(\sum_{j=0}^{3} C_j M^j\right)P^2$$

P is the linear heat generation rate in the fuel in KW/ft; T_{mod} is the coolant temperature; M is the fuel exposure in MWD/T and T_{fuel} the pellet average fuel temperature used in the resonance broadening calculation. This correlation follows the evolution of the fuel temperature with power level and exposure up to 20000 MWD/T. Beyond this exposure, the fuel temperature is function of the power level only.

The coefficients B_i and C_j are determined from least squares fitting of the fuel temperature generated by FATES. For a St. Lucie Unit 2 fuel pin, the following values apply:

B_0	=	146.526	C_o	=	2.0355
B_1	=	$.8841 \times 10^{-3}$	C_1	=	$-.5121 \times 10^{-3}$
B_2	=	$-.2052 \times 10^{-6}$	C_2	=	$.5043 \times 10^{-7}$
			C_3	=	$-.1071 \times 10^{-11}$

Reactivity changes accompanying power level changes at constant average moderator temperature have been measured for both densifying and non-densifying fuel types. These measurements include effects from both fuel temperature and the distribution of moderator temperatures or the 'T-H effect'. Since the T-H effect is small compared to the fuel temperature component any uncertainty associated with the T-H effect calculation will be negligible compared to the total calculated coefficient. It follows, therefore, that agreement between measured and predicted total coefficients is essentially verification of the fuel temperature correlation.

Figure 4.3-56 compares measured and calculated results of the Millstone II coefficient versus power level at BOC 1. Table 4.3-19a presents comparisons of the same coefficient versus exposure for both Millstone II and Calvert Cliffs I. The nature of the coefficient measured and the good agreement in both power and burnup space is considered to be sound experimental support for the current fuel temperature model.

4.3.3.1.2.2.5 Isothermal Temperature Coefficients

Isothermal temperature coefficients were measured at or near full power for a number of reactors of the 133 or 217 fuel assembly design, at various core exposure throughout the cycles. The analysis of this data is a complement to the analysis of beginning of life, zero power coefficients presented earlier. The accuracy of the full power temperature coefficient predictions has a direct bearing on the prediction of most fast transients. Table 4.3-19 gives the results of the analysis and shows that with standard two dimensional calculations, the average error is $(-0.016 \pm 0.10) \times 10^{-4}$ $\Delta\rho/F$. Three dimensional calculations, performed with full feedback, led to essentially the same results, demonstrating the validity of two-dimensional calculations.

4.3.3.1.2.2.6 Core Power Distributions

The accuracy of the power distribution predictions cannot be disassociated from the accuracy of the instrumentation which is used to measure these power distributions. The instrumentation in CE reactors consists of fixed self powered rhodium detectors, whose signals are fed into a computer code system which determines a full core power distribution. The uncertainties associated with each step of this process, and the differences observed between calculated and measured three dimensional power distributions, are documented in detail in References 19 and 1 for the CECOR code and Reference 66 for the BEACON system.

4.3.3.2 Spatial Stability (HISTORICAL)

4.3.3.2.1 Methods of Analysis

An analysis of xenon induced spatial oscillations may be done by two classes of methods: time dependent spatial calculations and linear modal analysis. The first method is based on computer simulation of the space, energy, and the time dependence of neutron flux and power density distributions. The second method calculates the damping factor based on steady state calculations of flux, importance (adjoint flux), xenon and iodine concentrations, and other relevant variables.

The time dependent calculations are indispensable for studies of the effects of CEA, core margin, out of core and incore detector responses, etc., and are performed in one, two, and three dimensions with few group diffusion theory, using tested computer codes and realistic modeling of the reactor core.

The linear modal analysis methods are used to calculate the effect on the damping factors of changes in fuel zoning, enrichment, CEA patterns, operating temperature, and power levels. These methods, using information at a single point in time, are particularly suited to survey type calculations. Methods are used on the work of Randall and St. John[33] as extended by Stacey.(34) These methods are verified by comparison with time dependent calculations.

4.3.3.2.2 Radial Xenon Oscillations

To confirm that the radial oscillation mode is extremely stable, a space time calculation was run for a reflected, zoned core 11 feet in diameter without including the damping effects of the negative power coefficient. The initial perturbation was a poison worth of 0.4 percent in reactivity placed in the central 20 percent of the core for one hour. Following removal of the perturbation, the resulting oscillation was followed in four hour time steps for a period of 80 hours. The resulting oscillation died out very rapidly with a damping factor of about -0.06 per hour. When this damping factor is corrected for a finite time step size by the formula in Reference 35, a more negative damping factor is obtained indicating an even more strongly convergent oscillation. On this basis, it is concluded that a radial oscillation instability will not occur.

4.3.3.2.3 Azimuthal Xenon Oscillations

Two dimensional modal analysis techniques were used to calculate the damping factor for azimuthal oscillations, and included both the fuel temperature and moderator temperature components of the total power coefficient. These calculational techniques were used to predict the results of azimuthal oscillation tests at Maine Yankee at 75 percent power. The predicted

damping factor of -0.045 per hour for azimuthal oscillations was found to agree well with the measured value of -0.047 ± 0.005 per hour.

Measurements of the azimuthal damping factor on other (earlier) reactors near full power will further substantiate the techniques used to predict the damping factor for St Lucie Unit 2.

4.3.3.2.4 Axial Xenon Oscillations

To check and confirm the predictions of the linear modal analysis approach, numerical space time calculations were performed for both beginning and end of cycle. The fuel and poison burnup distributions were obtained by depletion with soluble boron control, so that the power distribution was strongly flattened. Spatial Doppler feedback was included in these calculations. In Figure 4.3-57, the time variation of the power distribution along the core axis is shown near end of cycle with reduced Doppler feedback. The initial perturbation used to excite the oscillations was a 50 percent insertion into the top of the core of 1.5 percent reactivity CEA bank for one hour. The damping factor for this case was calculated to be about 0.02 per hour; however, when corrected for finite time step intervals by the methods of Reference 35, the damping factor is increased to approximately +0.04. When this damping factor is plotted on Figure 4.3-58 at the appropriate eigenvalue separation for this mode at end of cycle, it is apparent that good agreement is obtained with the modified Randall-St. John prediction. This good agreement is a result of the generally antisymmetric distribution of the moderator coefficient about the core midplane, and its consequent flux and adjoint weighted integrals of approximately zero.

Axial xenon oscillation experiments performed at Omaha at a core exposure of 7000 MWd/T and at Stade at beginning of cycle and at 12000 MWd/T[36] were analyzed with a space time one dimensional axial model. The results are given in Table 4.3-21 and show no systematic error between the experimental and analytical results.

4.3.3.3 Reactor Vessel Fluence Calculation Model

In performing the discrete ordinates calculations for the St. Lucie Unit 2 reactor, plant-specific forward transport calculations were carried out using the three-dimensional flux synthesis technique described in Section 1.3.4 of Regulatory Guide 1.190[72]. For all fuel cycles, the following synthesis equation was employed:

$$\Phi(r,\theta,z) = \Phi(r,\theta) \times \Phi(r,z) / \Phi(r)$$

where $\Phi(r,\theta,z)$ is the synthesized three-dimensional neutron flux distribution, $\Phi(r,\theta)$ is the transport solution in r,θ geometry, $\Phi(r,z)$ is the two-dimensional solution for a cylindrical reactor model using the actual axial core power distribution, and $\Phi(r)$ is the one-dimensional solution for a cylindrical reactor model using the same source per unit height as that used in the r,θ two-dimensional calculation.

For this analysis, all of the transport calculations were carried out using the DORT discrete ordinates code[37] and the BUGLE-96 cross-section library[38]. The BUGLE-96 library provides a 67-group coupled neutron-gamma ray cross-section data set produced specifically for light water reactor application. In these analyses, anisotropic scattering was treated with a P_5 Legendre expansion and the angular discretization was modeled with an S_{16} order of angular quadrature. Energy and space dependent core power distributions as well as system operating temperatures were treated on a fuel cycle-specific basis.

The acceptance criterion derived from Regulatory Guide 1.190, Section 1.4.3, a vessel fluence uncertainty of 20% (1σ) for light water reactor neutron exposure evaluations, was shown to be met by comparison of aforementioned calculations with two surveillance capsules dosimetry measurements removed from the St. Lucie Unit 2 at the end of cycle 1 and 9. The least-squares dosimetry evaluations were performed with the FERRET code[73] using SNRML dosimetry cross section data[74] within an NRC-approved methodology framework[75].

4.3.3.4 Local Axial Power Peaking Augmentation

A reduction in UO_2 volume associated with fuel densification results in a shortening of the active fuel pellet stack height. If it is assumed that the reduction in the active stack length is not reflected by an equivalent increase in the length of the gas plenum but, instead, results in the formation of axial gaps within the fuel column, local power peaking is experienced in the vicinity of the fuel gaps. This arises because the decrease in neutron absorption, due to fuel removal, more than compensates for the fission loss.

Since the magnitude of the local power peaking in a given rod is a function of both the size and number of gaps in surrounding fuel rods, and the distribution of gaps within a given volume of the core cannot be defined explicitly, a statistical approach to the determination of the local peaking factor, resulting from the presence of gaps, is employed. This additional peaking due to gaps is called the augmentation factor. The augmentation factor, at any given plane, is defined as the ratio of the maximum power in that plane with the statistically expected distribution of gaps to the maximum power without gaps. The peaking augmentation factors are based on a 95 percent confidence level. That is to say, for each axial region, the augmented power is chosen so that there is a 95 percent probability that no more than one rod exceeds the augmented power.

A detailed discussion of the theoretical model, a description of the gap distribution characteristics employed in the model, the data from which these characteristics were established, and a discussion of the application of the model to the calculation of axial peaking augmentation factors are presented in Reference 31. Reference 31 describes the model in detail and gives as an example a calculation using input characteristics for a typical reactor.

Input information, which is specific to the reactor under consideration and is required for the calculation of augmentation factors, includes the fuel densification and clad growth characteristics, the radial pin power distribution, and the single gap peaking factors. The fuel densification characteristics used in the calculation of augmentation factors for St. Lucie Unit 2 are presented in Table 4.3-22. The radial pin power census used in calculation of the augmentation factors is given in Table 4.3-23. The integration of this radial pin power census into the R(x) function described in Reference 31 is illustrated here as Figure 4.3-59. Figure 4.3-60 shows the specific assignment of fuel rod locations to radial groups and gives the power peaking associated with a single gap at each of these locations used in the calculation of the limiting augmentation factors for St. Lucie Unit 2.

The axial dependent peaking augmentation factors for noncollapsed gaps are presented in Figure 4.3-61 for St. Lucie Unit 2. Augmentation factors were calculated using limiting radial pin power distributions and single gap peaking factors, and therefore can be used throughout the first cycle.

4.3.4 CHANGES

A significant amount of core operating data has been incorporated into the nuclear design methods used for the design of this reactor. Operating reactor power distributions, critical boron concentrations, reactivity coefficients, and/or control rod worths were measured on the Maine Yankee, Fort Calhoun, Calvert Cliffs, Millstone, St. Lucie Unit 1 and ANO-2 reactors. The design methodology used for St. Lucie Unit 2 is essentially identical to the methodology used in the analysis of the experimental data reported in Subsection 4.3.3.1.2. The good agreement between measured values and those predicted by the analytic methods, as described in Subsection 4.3.3, lends confidence to the methods used in the design of this reactor.

As more experimental data becomes available, the methods verification program is extended, and the results of these analyses are implemented in the design of future cores. The methodology used for the St. Lucie Unit 2 nuclear design will be continuously evaluated in light of the most recent improvements.

SECTION 4.3: REFERENCES

1. C-E Setpoint Methodology: C-E Local Power Density and DNB LSSS and LCO Setpoint Methodology for Analog Protection Systems, CENPD-199, C-E Topical Report, April 1976; Rev. 1-P-A, January 1986 and Rev. 1-P-A, Supplement 2-P-A.

2. Krebs, W. D. and Brinkman, H., Proceedings of Reaktortagung 1976, Dusseldorf, Germany, March 1976.

3. McGoff, D. J., FORM-A Fourier Transform Fast Spectrum Code for the IBM-7090, NAA-SR-Memo, September 1960.

4. Honeck, H., "THERMOS-A Thermalization Transport Theory Code for Reactor Lattice Calculations," BNL-5816, July 1961.

5. England, T. R., "CINDER-A One Point Depletion and Fission Product Program," WAPD-TM-334, Revised June 1964.

6. Hellstrand, E., Measurement of Resonance Integral, Proceedings of National Topical Meeting of the ANS., San Diego, The M.I.T. Press, February 7-9, 1966.

7. Goldstein, R., "Temperature-Dependent Intermediate Neutron Resonance Integrals," Nuclear Science and Engineering, 48, 248, 1972.

8. Honeck, H., Description of the Code GAKER, BNL Memorandum, January 6, 1964.

9. Stuart, G. W. and Woodruff, R. W., "Method of Successive Generations," Nuclear Science and Engineering, Vol 3, p 339, 1958.

10. Kear, G. N. and Ruderman, M. J., "An Analysis of Methods in Control Rod Theory and Comparison with Experiment," GEAP-3937, May 1962.

11. Wachspress, E. L., "Thin Regions in Diffusion Theory Calculations," Nuclear Science and Engineering, Vol 3, p 186, 1958.

12. Henry, A. F., "A Theoretical Method for Determining the Worth of Control Rods," WAPD-218, August 1959.

13. Suich, J. E. and Honeck, H. C., "The HAMMER System," DP-1064, January 1967.

14. Lathrop, L. D., "DFT-IV, A Fortran IV Program for Solving the Multigroup Transport Equation with Anisotropic Scattering," LA-3373, July 15, 1965.

15. Rutherford, C. N., "Mo-807 - A Diffusion Theory Fitting Program Using Fortran-IV," WAPD- TM-671, September 1967.

16. Cadwell, W. R., "PDQ-7 Reference Manual," WAPD-TM-678, January 1968.

17. Breen, R. J., et al., "HARMONY-System for Nuclear Reactor Depletion Computation," WAPD-TM-478, January 1965.

18. Jonsson, A., Rec, J.R., Singh, U. N., "Verification of a Fuel Assembly Spectrum Code Based on Integral Transport Theory," TIS-5815-1978.

19. "Evaluation of Uncertainty in the Nuclear Form factor Measured by Self-Powered Fixed In- Core Detector System," CENPD-153, C-E Topical Report, August 1974.

20. Ober, T. E., Storr, J. C., Richard, I. C., "Theory, Capabilities and Use of the Three Dimensional Reactor Operation and Control Simulator (ROCS)," Nuclear Science and Engineering, 64, pp 605-623, 1977.

21. Rohan, P. E., Wagner, S. G., Ritterbusch, S. E., "HERMITE, a Multi-dimensional Space-Time Kinetics Code for PWR Transients," CE Topical Report CENPD-188-A, July 1976.

22. "TORC, A Computer Code for Determining Thermal Margin of a Reactor Core," C-E Topical Report, CENPD-161-P-A, April 1986.

23. Terney, W. C., "Albedo Adjusted Reflector Fast Diffusion Coefficient," Transactions American Nuclear Society, 18, 312, 1974.

24. SHADRAC, "Shield Heating and Dose Rate Attenuation Calculation," G30-1365, March 25, 1966.

25. Soltesz, R. G. and Disney, R. K., "Users' Manual for the DOT-IIW Discrete Ordinates Transport Computer Code," WANL-TME-1982, December 1969.

26. "DOT III Two Dimensional Discrete Ordinates Transport Code," ORNL-TM-4280, September 1973.

27. Emmet, M. B., "Domino, A general purpose code for coupling discrete ordinates and monte carlo radiation transport calculations," ORNL-4853, July 1973.

28. Straker, E. A. et al., "MORSE CODE with Combinatorial Geometry," DNA-2860T, May 1972.

29. "Cask, 40 Group Coupled Neutron and Gamma Cross Section Data," RISC Publication DLC-23E, March 1975.

30. Chajson, L., et al., "Yankee Core Evaluation Program - Quarterly Report for the Period Ending September 30, 1963," WCAP-6056, October 1963.

31. CENPD-139, "C-E Fuel Evaluation Model Topical Report," (Chapter 3, Augmentation Factors), C-E Proprietary Topical Report, July 1, 1974.

32. "A Method of Analyzing In-Core Detector Data in Power Reactors," CENPD-145, C-E Topical Report, April 1975.

33. Randall, D. and St. John, D. S., "Xenon Spatial Oscillations," Nucleonics, 16, 3, pp 82-86, 1958.

34. Stacey, Jr., W. M., "Linear Analysis of Xenon Spatial Oscillations," Nuclear Science Engineering 30, pp 453-455, 1967.

35. Poncelet, C. G., "The Effect of a Finite Time Step Length on Calculated Spatial Xenon Stability Characteristics in Large PWR's," Trans. ANS. 10, 2, p 571.

36. Gruen, A., "Messung Physikalischer Kenngroessen an Leistungsreakoren," Atom Kernenergie, 25, 2, 1975.

37. RSICC Computer Code Collection CCC-650, “DOORS 3.2, One-, Two-, and Three Dimensional Discrete Ordinates Neutron/Photon Transport Code System,” Radiation Safety Information Computational Center, Oak Ridge National Laboratory, April 1998.

38. RSICC Data Library Collection DLC-185, “BUGLE-96, Coupled 47 Neutron, 20 Gamma-Ray Group Cross Section Library Derived from ENDF/B-VI for LWR Shielding and Pressure Vessel Dosimetry Applications,” Radiation Safety Information Computational Center, Oak Ridge National Laboratory, March 1996.

39. MORSE, General Purpose Monte Carlo Multigroup Neutron and Gamma Transport Code with Combinatorial Geometry, ORNL-4585, September, 1970.

40. Users and Programmers Manual for the GGC-3 Multigroup Cross Section Code, GA-7157, July 25, 1967.

41. J. R. Knight, F. R. Mynatt, "MUG, A Program for Generating Multigroup Photon Cross Sections," CTC-17, January 20, 1970.

42. Engeloer, T. C., et al., "Spectral Shift Control Reactor, Basic Physics Program," B & W - 1273, November 1963.

43. Clark, R. H., et al., "Physics Verification Program," Final Report B & W - 3647-3, March 1967.

44. Davidson, P. W., et al., "Yankee Critical Experiments," YAEC-94, April 1969.

45. Eich, W. J. and Rocacik, W. P., "Reactivity and Neutron Flux Studies in Multi-Region Loaded Cores," WCAP-1443, 1961.

46. Fayers, F. J., et al., "An Evaluation of Some Uncertainties in the Comparison Between Theory and Experiments for Regular Light Water Lattices, British Nuclear Engineering Society Journal, April 6, 1967.

47. Brown, J. R., et al., "Kinetic and Buckling Measurements on Lattices of Slightly Enriched Uranium and UO2 Rods in Light Water," WAPD-176, 1958.

48. Schmid, L. C., et al., "Critical Masses and Buckling of Pu 02-UO2-1120 System," ANS Transactions, 1, 216, 1964.

49. Dawson, F. D., "Plutonium Utilization Program Annual Report," BNWL-624, December 1964.

50. Leame, R. D., "PuO_2-H_2O Fueled Critical Experiments," WCAP-3726-1, July 1967.

51. Tomlinson, L., "Delayed Neutrons for Fision," UKAEA Report AERE-R-6993, Harwell, Berkshire, 1972.

52. Vukmir, A., et al, "Critical Experiments for Combustion Engineering, Inc.," WCAP 7102, April 1968.

53. "Plutonium Experiments for KWU: Part 1 Critical Experiments in Kritz," AB Atomenergi, Studsvik, Sweden.

54. G. W. Maurer, "A Method of Predicting Steady-State-Boiling Vapor Fraction in Reactor Coolant Channels," WAPD-AD-TH-556, November, 1959.

55. A. Jonsson, et al., "Evaluation of Uncertainty in the Nuclear Power Peaking Measured by the Self- Powered, Fixed InCore Detector System," CENPD-153-P, Rev. 1-P-A, May 1980.

56. CENPD-266-P-A, "The ROCS and DIT Computer Codes for Nuclear Design," April 1983.

57. CEN-133(B), "FIESTA - A One-Dimensional Two-Group Space Time Kinetics Code for Calculating PWR Scram Reactivities," November 1979.

58. CENPD-225-P-A, "Fuel and Poison Rod Bowing," June 1983.

59. Letter, E. L. Trapp (C-E) to H. A. Barth (FP&L), "50.59 Evaluation of Reconstituted St Lucie 2 Fuel Assembly D008 and Recaged Assembly D006," F2-CE-R-197, November 13, 1987.

60. Letter, E. L. Trapp (C-E) to H. A. Barth (FP&L), "Final Reload Safety Evaluation (RSE) Report for St Lucie 2 Cycle 4 Operation," F2-CE-R-171, September 9, 1987, as subsequently amended.

61. St. Lucie Unit 2 Cycle 6 Reload Safety Evaluation (RSE) Report, E. Trapp to W. Park, F2-90-035, July 6, 1990.

62. St. Lucie Unit 2 Cycle 5 Reload Safety Evaluation (RSE) Report, E. Trapp to H. Barth, F2-CE-R-280, November 22, 1988.

63. St. Lucie Unit Cycle 7 Reload Safety Evaluation (RSE) Report, E. Trapp to W. Parks, F2-92-012, February 7, 1992.

64. Letter, E. Trapp to W. Parks, "Justification for Extending Cycle 6 to 11,900 EFPH," F2-92-032, March 18, 1992.

65. Transmittal of St. Lucie Unit 2 Cycle 12 Safety Analysis Report, F2-99-140, December 15, 1999.

66. JPN-PSL-SEFJ-96-022, Rev. 1, "Evaluation of the Best Estimate Analyzer for Core Operations – Nuclear (BEACON)."

67. CEN-123 (F)-P, “Statistical Combination of Uncertainties Methodology,” Part 1, December 1979, Part 2, January 1980; and Part 3, February 1980.

68 CEN-371 (F)-P, “Extended Statistical Combination of Uncertainties,” July1989.

69. WCAP-11596-P-A, “Qualification of the PHOENIX-P/ANC Nuclear Design System for Pressurizer Water Reactors,” June 1988.

70. WCAP-10216-P-A, Rev. 1A, “Relaxation of Constant Axial Offset Control: FQ Surveillance Technical Specification,” February 1994.

71. WCAP-11397-P-A, “Revised Thermal Design Procedure,” April 1989.

72. Regulatory Guide 1.190, “Calculational and Dosimetry Methods for Determining Pressure Vessel Neutron Fluence,” U.S. Nuclear Regulatory Commission, March 2001.

73. RSICC Code Package PSR-145, “FERRET: Least-Squares Solution to Nuclear Data and Reactor Physics Problems,” Radiation Safety Information Computational Center, Oak Ridge National Laboratory, January 1980.

74. RSIC Data Library Collection DLC-178, “SNLRML: Recommended Dosimetry Cross-Section Compendium,” Radiation Safety Information Computational Center, Oak Ridge National Laboratory, July 1994.

75. WCAP-16083-NP-A, Revision 0, “Benchmark Testing of the FERRET Code for Least Squares Evaluation of Light Water Reactor Dosimetry,” May 2006.

76. EMF-96-029(P)(A), Volumes 1 and 2, "Reactor Analysis System for PWRs, Volume 1 Methodology Description, Volume 2 Benchmarking Results."

77. XN-NF-78-44(NP)(A), "A Generic Analysis of the Control Rod Ejection Transient for Pressurized Water Reactors." EC287528

78. XN-75-27(A) and Supplements 1 through 5, "Exxon Nuclear Neutronics Design Methods for Pressurized Water Reactors", Exxon Nuclear Company, Report and Supplement 1 dated April 1977, Supplement 2 dated December 1980, Supplement 3 dated September 1981 (P), Supplement 4 dated December 1986 (P), and Supplement 5 dated February 1987 (P).

TABLE 4.3-1

NUCLEAR DESIGN CHARACTERISTICS

Cycle 1

Item	Value
General Characteristics	
Fuel management	3-batch, mixed central zone
First cycle average burnup, MWd/MTU	13,187
First cycle lifetime, full power hours	10,085
U-235 enrichments, wt%	
Batch A, 73 assemblies	1.71
Batch B, 80 assemblies	2.28
Batch C, 64 assemblies	2.73
Core average	2.21
Core average H_2O/UO_2 volume ratio, first cycle, hot	2.01
Number of control element assemblies	83
Burnable Poison Rods	
Number	1,632
Material	B_4C-Al_2O_3
Worth % Δ p, at BOC	
Hot (573°F)	6.91
Cold (68°F)	5.32
Dissolved Boron	
Dissolved boron content for criticality, ppm, (CEAs withdrawn, BOC, Cycle 1)	
Cold (68°F)	901
Hot, zero power, clean, 532°F	809
Hot, full power, clean, 573°F	715
Hot, full power, equilibrium Xe	493

TABLE 4.3-1 (Cont'd)

Item	Value
Dissolved boron content (ppm) for:	
Refueling, first cycle/later cycles	1720/2150
10% subcritical, cold, first cycle (all CEAs out)	1521
10% subcritical, hot, first cycle (all CEAs out)	1559
Design maximum soluble boron addition rate required to compensate for reactivity addition due to system cooldown and xenon decay, ppm/h	360
Maximum reactivity addition rate due to system cooldown and xenon decay, % △ p/h	3.97
Boron worth, ppm/% △ p (BOC/EOC), Cycle 1	
Hot (573 F)	78/76
Cold (68 F)	62/60
Neutron Parameters	
Neutron lifetime minimum, microseconds	27.6
Delayed neutron fraction	
Beginning-of-cycle	.0073
End-of-cycle	.0054
Plutonium Buildup (at end of first cycle)	
Gms Fissile Pu (final) / Kg U (original)	4.27
GMS Total Pu (final) / KgU (original)	5.40

TABLE 4.3-2

EFFFCTIVE MULTIPLICATION FACTORS AND REACTIVITY DATA (*)

Cycle I

Condition	K_{eff}	ρ
Cold (68F), 0 MWD/T, 0 ppm	1.170	0.145
Cold (68F), at minimum refueling boron concentration (1,720 ppm)	0.883	-.132
Hot (532F), zero power, no Xe or Sm, BOC 1	1.120	0.108
Hot, full power, no Xe or Sm, 573 F	1.100	0.091
Hot, full power, equilibrium Xe	1.070	0.065
Hot, full power equilibrium Xe and Sm (reactivity available for depletion)	1.064	0.060
Reactivity decrease, hot		
Zero to full power, BOC		.0121
Fuel temperature		.0091
Moderator temperature		.0030
Reactivity decrease, hot		
Zero to fullpower, EOC		.0142
Fuel temperature		.0078
Moderator temperature		.0064

(*) No control element assemblies or dissolved boron except as noted, initial core.

TABLE 4.3-3

COMPARISON OF CORE REACTIVITY COEFFICIENTS WITH THOSE USED IN SELECTED SAFETY ANALYSES

Cycle 1

	Moderator Temperature Coefficient (Δ p/Fx10^{-4})	Doppler Coefficient
Coefficients from Table 4.3-4		
Full power		
BOC	-.74	Figure 4.3-34
EOC 1	-1.76	Figure 4.3-34
Zero power, CEAs at PDIL		
BOC	-.87	Figure 4.3-34
EOC I	-1.68	Figure 4.3-34
Coefficients used in Accident Analyses		
CEA withdrawal (full/zero power)		
Rad. Release Events	-.120/+0.080	0.85[(a)]
Peak. Pressure Events	0/N/A	0.85[(a)]
CEA misoperation (full length)		
Dropped CEA	-4.0	1.15[(a)]
CEA misoperation (part length)		
Dropped CEA	-0.5	0.85[(a)]
Loss of flow	+0.4	0.85[(a)]
CEA ejection (full/zero power)		
BOC	-0.120/+0.100	1.0 W_R/2.10 WR(b)
EOC 1	-2.88/-2.10	1.0 W_R/2.10 WR
Loss of coolant accident	(c)	1.0

(a) Nominal values of the Doppler coefficient (Δ p/ F) as a function of fuel temperature are shown in Figure 4.3-34. The numbers entered in the Doppler column of the above table are the multipliers applied to the nominal value for analysis of designated accidents.

(b) W_R is a reactivity dependent factor.

(c) A curve of reactivity vs. moderator density is used for the LOCA evaluation. The value of density coefficient used corresponds to an MTC value of +0.5 x 10^{-4} Δ p/F.

TABLE 4.3-4

REACTIVITY COEFFICIENTS

Cycle 1

Moderator Temperature Coefficient, △ p /F	
Beginning of cycle (505 ppm, soluble boron)	
Cold, 68 F	$-.800 \times 10^{-5}$
Hot, zero power, 532 F, no CEAs	$-.525 \times 10^{-4}$
Hot, full power, 573 F, no CEAs, clean, 715 ppm	$-.435 \times 10^{-4}$
Hot, full power, equilibrium Xe, no CEAs	$-.740 \times 10^{-4}$
Hot, zero power, banks 6-4 CEAs inserted	$-.870 \times 10^{-4}$
End of cycle (0 ppm, soluble boron)	
Cold, 68 F	$-.900 \times 10^{-5}$
Hot zero power, 532 F, no CEAs	-1.18×10^{-4}
Hot full power, equilibrium Xe, no CEAs	-1.76×10^{-4}
Hot zero power, rodded banks 6-4 CEAs inserted	-1.68×10^{-4}
Moderator Density Coefficient, △ p/gm/cm^3	
Hot, operating, 573 F	
Beginning of the cycle, 505 ppm soluble boron	0.020
Fuel temperature contribution to power coefficient, △ p/(kW/ft)	
Hot, zero power	-2.47×10^{-3}
Hot, full power	-1.68×10^{-3}
Moderator void coefficient △ p/% void	
Hot, operating, 573 F Beginning of cycle, 505 ppm soluble boron	-1.24×10^{-4}
Moderator pressure coefficient, △ p/psi	
Hot, operating, 573 F Beginning of cycle, 505 ppm soluble boron	0.28×10^{-6}
Overall power coefficient, △ p/(kW/ft)	
Hot, operating, 573 F beginning of cycle, 505 ppm soluble boron	-2.35×10^{-3}
End of cycle, 0 ppm soluble boron	-3.02×10^{-3}

TABLE 4.3-5

WORTHS OF SEQUENTIALLY WITHDRAWN CEA GROUPS (% △ p)

Cycle 1

	50 MWD/T, BOC 1, 505 ppm	13187 MWD/T, EOC 1, 0 ppm
Shutdown CEAs	6.51	6.62
Regulating CEAs		
Group 1	1.24	1.12
Group 2	.65	.60
Group 3	.99	1.05
Group 4	.97	.93
Group 5	.41	.45
Group 6 (lead bank)	.44	.39
	11.21	11.16

TABLE 4.3-6

REACTIVITY DEFECTS BETWEEN HOT FULL POWER (HFP)*
AND HOT ZERO POWER (HZP)** AT EOC-4
(% Δ p)

	w/o Uncertainites	w/Uncertainties
Fuel Temperature Variation (HFP $\rightarrow$ 548 F)	0.71	0.85
Moderator Temperature Variation (588 F $\rightarrow$ 548 F)	1.35	1.47
MTC Component	0.95	1.03
T-H Effect (Axial Redistribution)	0.40	0.44
Loss in CEA Worth (573 F $\rightarrow$ 548 F)	0.47	0.52
Moderator Void Collapse	0.10	0.10
Total "Power Defect"	2.63	2.94

*HFP - The nominal HFP value of Moderator Average Temperature is 573 F. In computing the Moderator Temperature Variation component, 588 F is used instead of 573 F because a larger Power Defect results. In computing Loss in CEA Worth, this need not be done because the rod worths appearing in Table 4.3-7 are based on a core average moderator temperature of 573 F.

**HZP - Uniform Temperature of 548 F

TABLE 4.3-7

COMPARISON OF CALCULATED CEA WORTHS AND REQUIREMENTS (%Δρ) OF EOC4 FOR STEAM LINE BREAK (SLB) ANALYSES

	SLB @ HFP (T_M = 573 F)				SLB @ HZP (548 F)			
Item		No Stuck CEA		With Stuck CEA		No Stuck CEA		With Stuck CEA
Calculated Total Reactivity Available at Trip		-10.20		-10.20		-7.57*		-7.57*
Penalties on Trip Reactivity								
Stuck Rod Worth			1.56		-		1.56	
CEA Bite/Deadbond	0.45		0.45		-		-	
CEA Burnup	0.10		0.10		0.10		0.10	
CEA Ag-In-Cd Tips	0.45		0.45		-		-	
Moderator Void Collapse	0.10		0.10		-		-	
Total of Penalties Taken		+1.10		+2.66		+0.10		+1.66
Reactivity Available for Trip After Penalties		-9.10		-7.54		-7.47		-5.91
Trip Worth Assumed in SLB Analysis		-7.78		-6.68		-5.00		-5.00
Excess Reactivity		-1.32		-0.86		-2.47		-0.91

*HFP Value minus "Power Defect" from Table 4.3-6 (2.63%Δρ)

TABLE 4.3-7(a)

EC287528

COMPARISON OF CALCULATED CEA WORTHS AND REQUIREMENTS (%Δρ) FOR CEA EJECTION ANALYSES HISTORICAL

Item	Ejection @ HFP		Ejection @ HZP	
Calculated Total Reactivity Available at Trip		-10.20		-7.57*
Penalties on Trip Reactivity				
Stuck plus Ejected Rod Worth	3.24		3.24	
CEA Bite/Deadbond	0.45		-	
CEA Burnup	0.10		0.10	
Ag-In-Cd Tips	0.45		-	
Moderator Void Collapse	0.10		--	
Total of Penalties Taken		4.34		3.34
Reactivity Available For Trip After Penalties		-5.86		-4.23
Trip Worth Assumed For CEA Ejection Analysis		-5.05		-1.53
Excess Reactivity		-0.81		-2.70

*HFP Value minimum "Power Defect" from Table 4.3-6 (2.63%Δρ)

TABLE 4.3-8

COMPARISON OF RADIAL PEAKING FACTORS FOR VARIOUS RODDED CONFIGURATIONS AT BOC AND EOC

Cycle 1

Configurations	Maximum Rod Radial Peaking Factor F^n_r	
	50 MWD/T, BOC, 505 ppm	13187 MWD/T, EOC, 0 ppm
Unrodded	1.36	1.36
Bank 6	1.35	1.43
PLCEA(1)	1.39	1.44
Bank 6 and PLCEA	1.46	1.52
Bank 5+6(*)	1.50	1.60
Bank 4+5+6(*)	1.56	1.57
Bank 3+4+5+6(*)	2.16	1.85
Bank 2+3+4+5+6(*)	1.76	1.79
Bank 1+2+3+4+5+6(*)	1.72	1.77

(*) No PLCEA

(1) PLCEAs have been removed from the design of St. Lucie Unit 2.

TABLE 4.3-9

CALCULATED VARIATION OF THE AXIAL STABIILITY INDEX DURING THE FIRST CYCLE* (hr^{-1})

Power Level (% of Full Power)	BOC	MOC	EOC
100	-.003	+.028	+.102
75	-	-	+.070
50	-.046	-	+.019

*Equilibrium Xenon Conditions

TABLE 4.3-10

MAXIMUM FAST FLUENCE GREATER THAN 1 MeV (n/cm ^{2})

Cycles	Cumulative EFPY	Fluence, Shroud Inside Surface	Fluence, Vessel CBMI
1	1.05	1.68E+21*	1.10E+18
2	2.17	3.35E+21	2.22E+18
3	3.40	5.12E+21	3.36E+18
4	4.55	6.78E+21	4.09E+18
5	5.84	8.64E+21	4.88E+18
6	7.19	1.02E+22	5.76E+18
7	8.40	1.16E+22	6.62E+18
8	9.78	1.28E+22	7.19E+18
9	11.01	1.42E+22	7.88E+18
10	12.46	1.59E+22	8.73E+18
11	13.77	1.74E+22	9.50E+18
12	15.29	1.88E+22	1.04E+19
13	16.58	2.03E+22	1.12E+19
14	18.01	2.18E+22	1.21E+19
15	19.16	2.30E+22	1.28E+19
16	20.41	2.43E+22	1.37E+19
17	21.73	2.57E+22	1.45E+19
18	23.14	2.72E+22	1.54E+19
19	24.46	2.86E+22	1.63E+19
20	25.87	3.04E+22	1.75E+19
21	27.28	3.24E+22	1.88E+19
22	28.69	3.44E+22	2.01E+19
--	32.00	3.90E+22	2.31E+19
--	36.00	4.47E+22	2.67E+19
--	40.00	5.03E+22	3.03E+19
--	48.00	6.16E+22	3.76E+19
--	54.00	7.01E+22	4.31E+19
--	60.00	7.85E+22	4.85E+19

Note: * denotes powers of ten, i.e., 1.68 x 10^{21}

TABLE 4.3-11

CONTROL ELEMENT ASSEMBLY SHADOWING FACTORS

Cycle 1

	BOC	EOC
Bank 6	1.11	1.09
PLCEAs[1]	1.07	1.07
Bank 6 + PLCEAs	1.20	1.17

[1] PLCEAs have been removed from the design St. Lucie Unit 2.

TABLE 4.3-12

FUEL ROD DESCRIPTION

Laboratory	Clad OD (in.)	Clad Thickness (in.)	Clad Material	Fuel Pellet OD (in.)	Fuel Density (g^2/cm^3)	Fuel Enrichment Wt % U-235	Fuel Enrichment Wt % PuO_2
B&W	0.4755	0.016	SS 304	0.440	9.46	4.020	0
B&W	0.4748	0.032	AL 6061	0.4054	10.24	2.459	0
Yankee	0.3383	0.0161	SS 304	0.3000	10.18	2.700	0
Winfrith	0.4301	0.01051	SS 304	0.3984	10.44	3.003	0
Bettis	0.453	0.028	Al	0.3830	10.53	1.311	0
Hanford	0.426	0.027	Zr-2	0.372	9.646[(a)]	0.22	1.50
Battelle N.W. Westinghouse	0.568	0.030	Zr-2	0.508	9.869[(a)]	0.72	2.20
CE-Westinghouse	0.4683	0.03145	Zr-4	0.400	10.40	2.72	0
Kritz	0.4223	0.02835	Zr-4	0.3575	10.15	3.10	0

(a) Effective fuel density

TABLE 4.3-13

RESULT OF ANALYSIS OF CRITICAL UO_2 SYSTEMS

Lattice		Wt % U-235	Pitch (in.)	H_2O/UO_2	Boron (ppm)	k_{eff}	Ref
B&W-1273	1	4.020	0.595	1.137	0	1.0012	42
	2	4.020	0.595	1.137	3390	1.0053	42
	3	4.020	0.571	0.956	0	0.9984	42
	4	2.459	0.595	1.371	0	1.0042	42
	5	2.459	0.595	1.371	1075	1.0055	42
B&W-3647	6	2.459	0.644	1.846	0	1.0027	43
	7	2.459	0.644	1.846	846	1.0044	43
	8	2.459	0.644	1.846	1536	1.0033	43
Yankee	9	2.700	0.405	1.048	0	1.0009	44
	10	2.700	0.435	1.405	0	1.0011	44
	11	2.700	0.470	1.853	0	1.0014	44
	12	2.700	0.493	2.166	0	1.0024	45
Winfrith	13(20°C)	3.003	0.520	1.001	0	1.0021	46
	14(20°C)	3.003	0.520	1.001	0	0.9994	46
	15	3.003	0.735	3.164	0		
	16	3.003	0.492	0.779	0		46
Bettis	17	1.311	0.6133(*)	1.429	0	1.0005	47
	18	1.311	0.6504(*)	1.781	0	1.0004	47
	19	1.311	0.7110(*)	2.401	0	1.0011	47
C-E-12	20	2.720	0.600	1.494	0	1.0003	52
C-E-32	21	2.720	0.600	1.494	0	1.0012	52
C-E-43	22	2.720	0.600	1.494	323	0.9978	52
C-E-53	23	2.720	0.575	1.260	0	0.9966	52
C-E-56	24	2.720	0.575	1.260	302	0.9938	52
Kritz	25	3.100	0.565	1.785	950	0.9938	53

Average calculated eigenvalue 1.0008
average error 0.0008
Standard Deviation 0.0031

Note: * Triangular pitch

TABLE 4.3-14

RESULTS OF ANALYSIS OF PuO_2-UO_2 FUELED LATTICES

Lattice	Wt % U-235	Wt/%$Pu0_2$	Pitch (in.)	H_2O/Fuel	Boron (ppm)	k_{eff}	Ref
Hanford	0.22	1.50	0.55(b)	1.099	0	0.9998	48
			0.60(b)	1.557	0	1.0026	48
			0.71(b)	2.705	0	1.0081	48
			0.80(b)	3.783	0	1.0071	48
BNWL	0.72	2.2[(a)]	0.85(b)	1.837	0	1.0058	49
			0.93(b)	2.445	0	1.0093	49
WCAP	0.72	2.2[(a)]	0.69	1.099	0	1.0019	50
			0.75	1.525	0	1.0067	50
			0.67	1.099	201	1.0013	50
			0.69	1.099	526	1.0011	50

Average calculated eigenvalue 1.0043
average error 0.0043
Standard Deviation 0.0034

Note:

(a) 7.654 Wt/% Pu-240 in Pu
(b) Triangular pitch

TABLE 4.3-15

REACTION RATES(*)

Lattice Number	Measured	Calculated	Measured	Calculated	Measured	Calculated
Babcock and Wilcox		ρ28		δ25		
1	4.12±0.31	4.38	0.254±0.006	0.292		
3	5.08±0.10	5.19	0.307±0.002	0.351		
4	2.28±0.03	2.40	0.151±0.001	0.163		
		ρ28		δ28		MCR
6	1.85±0.02	1.81	0.063±0.006	0.056	0.484±0.011	0.480
Winfrith		RCR		δ28		Pu239/U235 Fission
13	4.158±0.03	4.203	0.0845±0.0009	0.0884	1.589±0.009	1.568
14	4.293±0.047	4.311	0.0881±0.0027	0.0903	1.637±0.009	1.608
16	4.789±0.053	4.874	0.1050±0.0018	0.1056	1.661±0.009	1.633
Bettis		ρ28		δ28		δ25
17	1.43±0.01	1.40	0.078±0.004	0.078	0.089±0.002	0.091
18	1.15±0.01	1.16	0.070±0.004	0.067	0.072±0.001	0.074
19	0.9374±0.01	0.907	0.057±0.003	0.055	0.055±0.001	0.057

Note: (*) Definitions:

ρ28 = epicadmium captures in U-238/subcadmium captures in U-238
δ25 = epicadmium fissions in U-235/subcadmium fissions in U-235
δ28 = Total fissions in U-238/total fissions in U-235
MCR = captures in U-238/fissions in U-235
RCR = MCR in lattice/MCR in thermal column

TABLE 4.3-16

BEGINNING OF CYCLE, ZERO POWER UNRODDED CHARACTERISTICS

Reactor	Temperature (°F)	Critical Boron (ppm) Measured	Critical Boron (ppm) Calculated	Temperature Coefficient x 10^{-4} $\Delta\rho$/°F Measured	Temperature Coefficient x 10^{-4} $\Delta\rho$/°F Calculated
Maine Yankee Core I	260	955	952	0.18	0.08
	525	988	989	0.13	0.23
Maine Yankee Core II	525	809	799	-0.24	-0.29
Fort Calhoun	260	900	889	0.22	0.08
	525	933	911	0.26	0.21
Calvert Cliffs 1	260	1048	1062	0.20	0.14
	525	1106	1078	0.22	0.26
Millstone Unit 2	532	960	951	0.08	0.02
St. Lucie Unit 1	532	962	963	0.02	0.03
Average Error (calc-meas)		-7		-.03 x 10^{-4}	
Standard Deviation (σ_s)		13		.07 x 10^{-4}	

TABLE 4.3-17

COMPARISON OF MEASURED AND CALCULATED CONTROL ROD WORTH
BOC, HOT ZERO POWER

Rod	M.Y. Core I		M.Y. Core II		Omaha		BGF&E Unit I		BG&E Unit 1		Millstone Unit 2		St. Lucie Unit 1		ANO-2	
Bank	Meas.	Calc.	Meas.	Calc.	Meas.	Calc.	Meas.	Calc.	Meas.	Calc.	Meas.	Calc.	Meas.	Calc.	Meas.	Calc.
7	--	--	--	--	--	--	--	--	--	--	0.76	0.74	0.74	0.74	--	--
6	--	--	--	--	--	--	--	--	--	--	0.50	0.47	0.52	0.50	0.57	0.56
5	0.57	0.58	0.57	0.56	--	--	0.55	0.54	0.56	0.55	0.33	0.29	0.35	0.33	0.52	0.51
4	0.37	0.38	0.27	0.27	0.60	0.54	0.35	0.35	0.37	0.35	1.37	1.36	1.30	1.37	0.74	0.77
3	0.92	0.93	0.77	0.80	0.58	0.57	0.93	0.90	0.91	0.93	0.62	0.62	0.55	0.57	0.79	0.78
2	0.86	0.95	0.59	0.64	2.10	2.01	0.78	0.74	0.81	0.79	1.40	1.40	1.41	1.45	0.92	0.94
1	0.80	0.80	1.05	0.93	0.99	0.91	1.95	1.04	0.89	0.93	0.69	0.70	0.70	0.69	1.27	1.26
C	1.21	1.23	1.80	1.60	--	--	1.30	1.40	1.28	1.29	--	--	--	--	--	--
B	0.76	0.75	0.67	0.67	2.13	2.09	0.99	0.87	0.97	0.97	0.39	0.46	0.42	0.40	--	--
Total	5.49	5.62	5.72	5.47	6.40	6.12	5.85	5.84	5.79	5.81	6.06	6.04	5.99	6.05	4.81	4.82
$\overline{X}$ *	0.023		-0.044		-0.044		-0.002		0.003		-0.003		0.010		0.002	
q	0.038		0.073		0.037		0.074		0.032		0.086		0.041		0.024	

Average of 55 individual banks : $\overline{X}$ = -0.006 = 0.056 = 5.6% of the worth

Average of 8 total worths : $\overline{X}$ = -0.007 = 0.024 = 2.4% of the worth

Note:

* Average relative error and standard deviation (calc-meas)/meas.

TABLE 4.3-18

COMPARISONS OF CALCULATED AND MEASURED CEA WORTHS

Condition	CEA Worth Calculated	CEA Worth Measured
Ejected CEA:		
Maine Yankee		
9 CEA pattern	0.15	0.14
Omaha		
17 CEA pattern	0.29	0.28
Palisades		
9 Rod pattern	0.25	0.28
13 Rod pattern	0.71	0.67
St. Lucie 1		
13 Rod pattern	0.33	0.31
Dropped CEA:		
Maine Yankee		
Dual CEA	0.15	0.14
Omaha		
Dual (peripheral) CEA	0.14	0.15
Dual (central) CEA	0.18	0.19
St. Lucie 1		
Dual	0.14	0.14
Stuck CEA (with all other CEAs inserted):		
Maine Yankee		
Dual	1.89	2.14
Omaha		
Dual	1.57	1.46
St. Lucie 1		
Dual	2.70	3.29

Average Error (% of measured worth) = -1.20%
Standard Deviation (% of measured worth) = 8.93%

TABLE 4.3-19

AT-POWER ISOTHERMAL TEMPERATURE COEFFICIENTS

Core	Exposure (MWD/T)	Boron (PPM)	Measured	Temperature Coefficient ($x10^{-4}$ Δρ / F) Calculated 2-D	Calculated 3-D
Fort Calhoun	3000	597	-0.13	-0.29	
	8200	300	-0.97	-0.91	
Maine Yankee Core I	2000	750	0.03	-0.01	
	4400	760	0.13	0.06	
	4400	712	-0.06	-0.04	-0.04
	6500	640	-0.19	-0.19	-0.21
	9000	500	-0.47	-0.46	-0.48
	10360	420	-0.61	-0.67	-0.58
	6700	537	-0.50	-0.45	
Maine Yankee Core II	400	525	-0.93	-0.69	
	4700	521	-0.42	-0.48	
Calvert Cliffs 1	15000	83	-1.38	-1.36	
Millstone II	1100	668	-0.28	-0.46	
St. Lucie I	2500	585	-0.42	-0.48	
Average difference, $\overline{X}$ (Calc-meas)				-0.016	0.003
Standard deviation of difference, σ				0.100	0.024

TABLE 4.3-19a

COMPARISON OF MEASURED AND CALCULATED PSEUDO*-POWER COEFFICIENTS AT VARIOUS EXPOSURES

Reactor:	Calvert Cliffs Unit 1				Millstone Unit 2			
Fuel Type:**		Densifying				Non-Densifying		
	Meas.	Calc. (3D)			Meas.	Calc. (3D)		
Exposure	Total	Doppler	TH	Total	Total	Doppler	TH	Total
BOC1	-1.03	-1.09	0	-1.09	-0.76	-0.78	0	-0.78
EOC1	-0.89	-0.88	-0.04	-0.92				
BOC2	-1.02***	-0.89	-0.08	-0.97	-0.78	-0.75	-0.08	-0.83

* Coefficient measured includes fuel temperature and moderator temperature distribution effects. However, average moderator temperature changes normally associated with power level changes are excluded in both the experimental and calculational methodologies.

** All new CE fuel is of the non-densifying type.

*** Fresh fuel was of the non-densifying type.

TABLE 4.3-20 HAS BEEN DELETED

TABLE 4.3-21

AXIAL XENON OSCILLATIONS

Reactor	Exposure (MWd/T)	Period (hr) Measured	Period (hr) Calculated	Damping (hr^{-1}) Measured	Damping (hr^{-1}) Calculated
Omaha	7075	29	32	-0.027	-0.030
Stade	BOC	36	36	-0.096	-0.090
Stade	12200	27	30	-0.021	-0.019

TABLE 4.3-22

DENSIFICATION CHARACTERISTICS
(Prior to Region DD Fuel)

EC287528

Core Height	136.7 in.
Fractional Density Change	0.016
Clad Growth Allowance	5.07×10^{-3} in./in.

TABLE 4.3-23

RADIAL PIN POWER CENSUS
(Prior to Region DD Fuel)

EC287528

Pin Power Interval	Number of Pins with Power in Interval
0 - 1.00	17144
1.00 - 1.05	6360
1.05 - 1.10	8756
1.10 - 1.20	11976
1.20 - 1.30	5344

TABLE 4.3-24

This table has been deleted.

Table 4.3-25

This table has been deleted.

TABLE 4.3-26

ST. LUCIE UNIT 2 CYCLE 2
FULL LENGTH CEA DROP DATA
(HFP, EQUILIBRIUM XENON)
(Prior to Region DD Fuel)

EC287528

	Reference Cycle Safety Analysis Value	Cycle 2 Safety Analysis Value
Single Drop		
Minimum Worth (%Δρ)	0.0	0.0
Maximum Percent Increase in Radial Peaking Factor (%)	13.5	14.0
Maximum 15 Minute Xenon Redistribution Penalty (%)	5.1	4.0
Subgroup Drop		
Minimum Worth (%Δρ)	0.0	0.15
Maximum Percent Increase in Radial Peaking Factor (%)	19.4	19.0

FUEL TYPE	NO. OF ASSEMBLY	ENRICHMENT W/O	NO. OF SHIMS
A	73	1.71	0
B	80	2.28	16
C	40	2.73	0
C-	8	2.73	12
C+	16	2.73	16
D	56	3.13	0
D*	16	2.60	0
E	60	3.09	0
E*	12	2.75	0

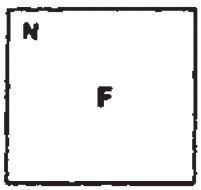

N = BOX NO.
F = FUEL TYPE

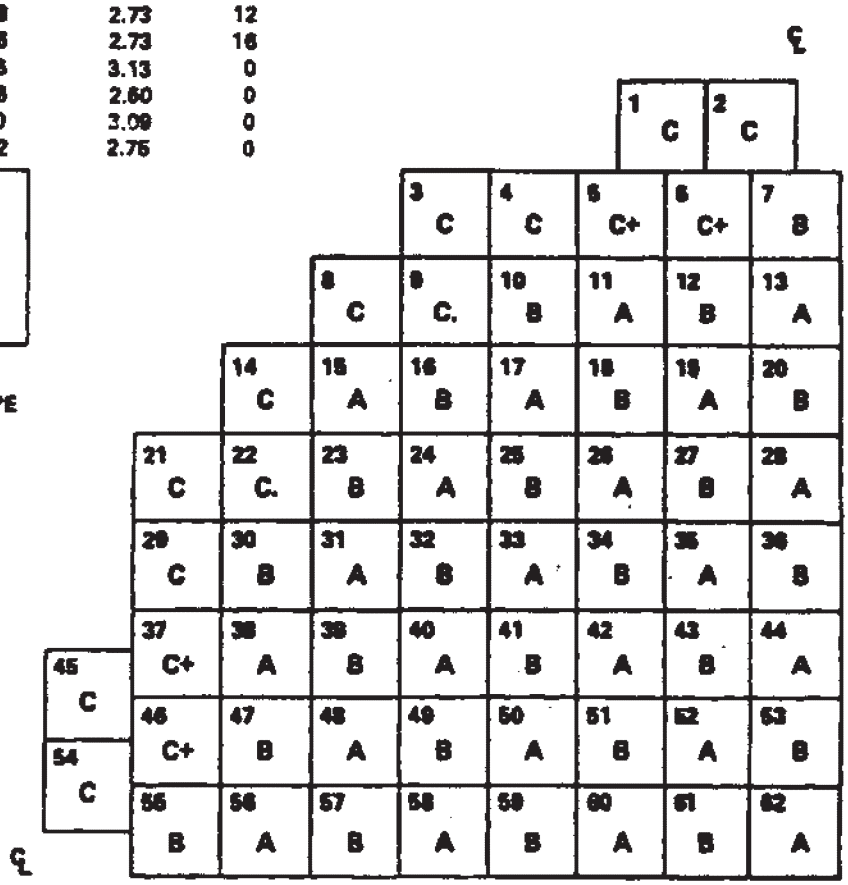

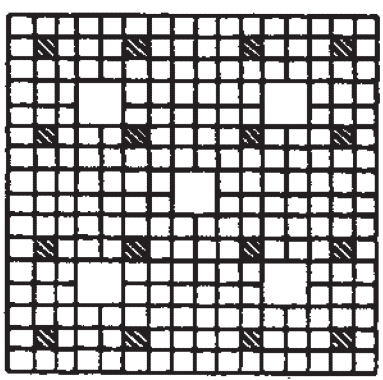

16 SHIM ASSEMBLY

FUEL PIN
SHIM PIN

SHIM PELLET	
FUEL TYPE	$gm/_{in}B^{10}$
B	0.019
C	0.010

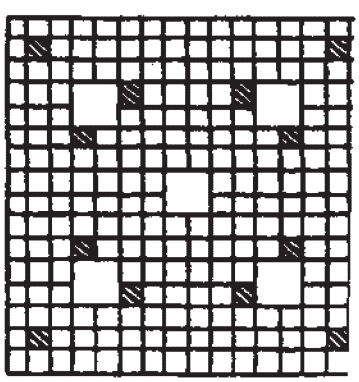

12 SHIM ASSEMBLY

AMENDMENT NO. 8 (9/93)

FLORIDA POWER & LIGHT COMPANY
ST. LUCIE PLANT – UNIT 2

CYCLE 1
FUEL MANAGEMENT PATTERN

FIGURE 4.3-1

X.XX	BOX AVERAGE (BOX POWER/CORE AVERAGE POWER)
X.XX	MAXIMUM ENTHALPY RISE FACTOR (MAXIMUM OF THE AVERAGE POWER OF 4 NEIGHBORING PINS/CORE AVERAGE POWER)
X.XX	MAXIMUM ONE-PIN FACTOR (MAXIMUM PIN POWER/CORE AVERAGE POWER)

						C 1 0.67 1.08 1.13	C 2 0.91 1.20 1.26	
				C 3 0.61 0.98 1.02	C 4 0.84 1.12 1.18	C+ 5 0.97 1.20 1.26	C+ 6 1.14 1.23 1.30	B 7 1.04 1.11 1.17
			C 8 0.68 1.03 1.07	C. 9 0.97 1.10 1.16	B 10 0.98 1.07 1.14	A 11 0.99 1.08 1.14	B 12 1.08 1.15 1.21	A 13 1.03 1.12 1.18
		C 14 0.68 1.03 1.07	A 15 0.81 0.92 0.97	B 16 0.98 1.06 1.12	A 17 0.98 1.07 1.12	B 18 1.10 1.15 1.22	A 19 1.04 1.14 1.20	B 20 1.13 1.18 1.25
	C 21 0.61 0.98 1.02	C. 22 0.97 1.10 1.16	B 23 0.98 1.06 1.12	A 24 0.97 1.07 1.12	B 25 1.09 1.15 1.22	A 26 1.05 1.15 1.20	B 27 1.15 1.20 1.27	A 28 1.08 1.17 1.23
	C 29 0.85 1.12 1.18	B 30 0.98 1.07 1.14	A 31 0.98 1.07 1.12	B 32 1.09 1.15 1.22	A 33 1.05 1.15 1.20	B 34 1.16 1.21 1.28	A 35 1.09 1.19 1.25	B 36 1.18 1.22 1.30
	C+ 37 0.97 1.20 1.26	A 38 0.99 1.08 1.14	B 39 1.10 1.15 1.22	A 40 1.05 1.15 1.20	B 41 1.16 1.21 1.28	A 42 1.10 1.20 1.25	B 43 1.19 1.24 1.31	A 44 1.11 1.21 1.27
C 45 0.67 1.08 1.13	C+ 46 1.14 1.23 1.30	B 47 1.08 1.15 1.21	A 48 1.04 1.14 1.20	B 49 1.15 1.20 1.27	A 50 1.09 1.19 1.25	B 51 1.19 1.24 1.31	A 52 1.12 1.22 1.28	B 53 1.21 1.25 1.32
C 54 0.91 1.20 1.26	B 55 1.04 1.11 1.17	A 56 1.03 1.12 1.18	B 57 1.13 1.18 1.25	A 58 1.08 1.17 1.23	B 59 1.18 1.22 1.30	A 60 1.11 1.21 1.27	B 61 1.21 1.25 1.32	A 62 1.13 1.23 1.29

FLORIDA POWER & LIGHT COMPANY
ST. LUCIE PLANT UNIT 2

PLANAR AVERAGE POWER DISTRIBUTION – 0 MWD/T, FULL POWER, CYCLE 1

FIGURE 4.3-2a

X . XX	BOX AVERAGE (BOX POWER/CORE AVERAGE POWER)
X . XX	MAXIMUM ENTHALPY RISE FACTOR (MAXIMUM OF THE AVERAGE POWER OF 4 NEIGHBORING PINS/CORE AVERAGE POWER)
X . XX	MAXIMUM ONE-PIN FACTOR (MAXIMUM PIN POWER/CORE AVERAGE POWER)

| | | |

X . XX	BOX AVERAGE (BOX POWER/CORE AVERAGE POWER)
X . XX	MAXIMUM ENTHALPY RISE FACTOR (MAXIMUM OF THE AVERAGE POWER OF 4 NEIGHBORING PINS/CORE AVERAGE POWER)
X . XX	MAXIMUM ONE-PIN FACTOR (MAXIMUM PIN POWER/CORE AVERAGE POWER)

						C 1 .65 1.03 1.08	C 2 .87 1.15 1.21	
				C 3 .60 .96 1.00	C 4 .83 1.10 1.16	C+ 5 .95 1.18 1.24	C+ 6 1.10 1.19 1.26	B 7 1.00 1.09 1.14
			C 8 .67 1.03 1.07	C. 9 .96 1.10 1.15	B 10 .97 1.07 1.13	A 11 .98 1.08 1.13	B 12 1.07 1.14 1.21	A 13 1.02 1.12 1.17
		C 14 .67 1.03 1.07	A 15 .82 .93 .98	B 16 .98 1.07 1.13	A 17 .99 1.08 1.14	B 18 1.10 1.16 1.23	A 19 1.05 1.15 1.21	B 20 1.13 1.19 1.26
	C 21 .60 .96 1.00	C. 22 .96 1.10 1.15	B 23 .98 1.07 1.13	A 24 .99 1.08 1.14	B 25 1.11 1.17 1.24	A 26 1.07 1.17 1.22	B 27 1.16 1.22 1.29	A 28 1.09 1.19 1.25
	C 29 .83 1.10 1.16	B 30 .97 1.07 1.13	A 31 .99 1.08 1.14	B 32 1.11 1.17 1.24	A 33 1.07 1.17 1.23	B 34 1.17 1.23 1.30	A 35 1.11 1.21 1.27	B 36 1.19 1.25 1.32
	C+ 37 .95 1.18 1.24	A 38 .98 1.08 1.13	B 39 1.10 1.16 1.23	A 40 1.07 1.17 1.22	B 41 1.17 1.23 1.30	A 42 1.12 1.22 1.28	B 43 1.21 1.26 1.33	A 44 1.14 1.24 1.30
C 45 .65 1.03 1.08	C+ 46 1.10 1.19 1.26	B 47 1.07 1.14 1.21	A 48 1.05 1.15 1.21	B 49 1.16 1.22 1.29	A 50 1.11 1.21 1.27	B 51 1.21 1.26 1.33	A 52 1.14 1.24 1.31	B 53 1.23 1.27 1.35
C 54 .87 1.15 1.21	B 55 1.00 1.09 1.14	A 56 1.02 1.12 1.17	B 57 1.13 1.19 1.26	A 58 1.09 1.19 1.25	B 59 1.19 1.25 1.32	A 60 1.14 1.24 1.30	B 61 1.23 1.27 1.35	A 62 1.15 1.25 1.32

FLORIDA POWER & LIGHT COMPANY
ST. LUCIE PLANT UNIT 2

PLANAR AVERAGE POWER DISTRIBUTION – 50 MWD/T, FULL POWER, CYCLE 1

FIGURE 4.3-3a

X . XX X . XX X . XX	BOX AVERAGE (BOX POWER/CORE AVERAGE POWER) MAXIMUM ENTHALPY RISE FACTOR (MAXIMUM OF THE AVERAGE POWER OF 4 NEIGHBORING PINS/CORE AVERAGE POWER) MAXIMUM ONE-PIN FACTOR (MAXIMUM PIN POWER/CORE AVERAGE POWER)

						C 1 0.68 1.10 1.15	C 2 0.92 1.22 1.29
			C 3 0.62 0.99 1.03	C 4 0.85 1.13 1.19	C+ 5 0.98 1.21 1.27	C+ 6 1.14 1.24 1.31	B 7 1.05 1.12 1.18
		C 8 0.68 1.05 1.09	C. 9 0.98 1.11 1.17	B 10 0.98 1.08 1.14	A 11 0.99 1.09 1.15	B 12 1.08 1.15 1.22	A 13 1.03 1.13 1.18
	C 14 0.68 1.05 1.09	A 15 0.82 0.93 0.98	B 16 0.98 1.06 1.13	A 17 0.98 1.08 1.13	B 18 1.09 1.15 1.22	A 19 1.04 1.14 1.20	B 20 1.12 1.17 1.24
C 21 0.62 0.99 1.03	C. 22 0.98 1.11 1.17	B 23 0.98 1.06 1.13	A 24 0.98 1.07 1.12	B 25 1.09 1.15 1.22	A 26 1.05 1.14 1.20	B 27 1.14 1.19 1.26	A 28 1.07 1.17 1.23
C 29 0.85 1.13 1.19	B 30 0.98 1.08 1.14	A 31 0.98 1.08 1.13	B 32 1.09 1.15 1.22	A 33 1.05 1.14 1.20	B 34 1.14 1.20 1.27	A 35 1.08 1.18 1.24	B 36 1.16 1.21 1.28
C+ 37 0.98 1.21 1.27	A 38 0.99 1.09 1.15	B 39 1.09 1.15 1.22	A 40 1.05 1.14 1.20	B 41 1.14 1.20 1.27	A 42 1.09 1.19 1.25	B 43 1.17 1.22 1.30	A 44 1.10 1.20 1.26
C+ 46 1.14 1.24 1.31	B 47 1.08 1.15 1.22	A 48 1.04 1.14 1.20	B 49 1.14 1.19 1.26	A 50 1.08 1.18 1.24	B 51 1.17 1.22 1.30	A 52 1.11 1.21 1.27	B 53 1.19 1.23 1.31
B 55 1.05 1.12 1.18	A 56 1.03 1.13 1.18	B 57 1.12 1.17 1.24	A 58 1.07 1.17 1.23	B 59 1.16 1.21 1.28	A 60 1.10 1.20 1.26	B 61 1.19 1.23 1.31	A 62 1.11 1.21 1.28

C 45 0.68 1.10 1.15	
C 54 0.92 1.22 1.29	

FLORIDA POWER & LIGHT COMPANY
ST. LUCIE PLANT UNIT 2

PLANAR AVERAGE POWER DISTRIBUTION – 50 MWD/T, ZERO POWER, CYCLE 1

FIGURE 4.3-3b

X.XX X.XX X.XX

BOX AVERAGE (BOX POWER/CORE AVERAGE POWER)

MAXIMUM ENTHALPY RISE FACTOR (MAXIMUM OF THE AVERAGE POWER OF 4 NEIGHBORING PINS/CORE AVERAGE POWER)

MAXIMUM ONE-PIN FACTOR (MAXIMUM PIN POWER/CORE AVERAGE POWER)

						C 1 0.60 0.95 0.97	C 2 0.76 1.02 1.06	
				C 3 0.58 0.94 0.97	C 4 0.79 1.06 1.09	C+ 5 0.99 1.21 1.26	C+ 6 1.16 1.30 1.34	B 7 1.12 1.22 1.27
			C 8 0.65 1.00 1.03	C. 9 1.02 1.21 1.26	B 10 1.09 1.19 1.24	A 11 1.00 1.07 1.11	B 12 1.19 1.24 1.30	A 13 1.05 1.08 1.13
		C 14 0.65 1.00 1.03	A 15 0.84 0.99 1.02	B 16 1.12 1.21 1.26	A 17 1.03 1.07 1.12	B 18 1.18 1.23 1.30	A 19 1.04 1.08 1.13	B 20 1.19 1.23 1.29
	C 21 0.58 0.94 0.97	C. 22 1.02 1.21 1.26	B 23 1.12 1.21 1.26	A 24 1.03 1.07 1.12	B 25 1.19 1.23 1.29	A 26 1.03 1.07 1.12	B 27 1.17 1.22 1.28	A 28 1.02 1.06 1.11
	C 29 0.79 1.06 1.09	B 30 1.09 1.19 1.24	A 31 1.03 1.07 1.12	B 32 1.18 1.23 1.29	A 33 1.03 1.07 1.12	B 34 1.16 1.21 1.27	A 35 1.01 1.05 1.09	B 36 1.14 1.19 1.25
C 45 0.60 0.95 0.97	C+ 37 0.99 1.21 1.26	A 38 1.00 1.07 1.11	B 39 1.18 1.23 1.29	A 40 1.03 1.07 1.12	B 41 1.16 1.21 1.27	A 42 1.00 1.04 1.09	B 43 1.13 1.18 1.23	A 44 0.99 1.02 1.06
C 54 0.76 1.02 1.06	C+ 46 1.16 1.30 1.34	B 47 1.19 1.24 1.30	A 48 1.04 1.08 1.12	B 49 1.17 1.22 1.28	A 50 1.01 1.05 1.09	B 51 1.13 1.18 1.23	A 52 0.98 1.02 1.06	B 53 1.11 1.15 1.21
	B 55 1.12 1.22 1.27	A 56 1.05 1.08 1.13	B 57 1.19 1.23 1.29	A 58 1.02 1.06 1.11	B 59 1.14 1.19 1.25	A 60 0.99 1.02 1.06	B 61 1.11 1.51 1.21	A 62 0.97 1.00 1.04

FLORIDA POWER & LIGHT COMPANY
ST. LUCIE PLANT UNIT 2

PLANAR AVERAGE POWER DISTRIBUTION – 13200 MWD/T, FULL POWER, CYCLE 1

FIGURE 4.3-4a

X.XX
X.XX
X.XX

BOX AVERAGE (BOX POWER/CORE AVERAGE POWER)

MAXIMUM ENTHALPY RISE FACTOR (MAXIMUM OF THE AVERAGE POWER OF 4 NEIGHBORING PINS/CORE AVERAGE POWER)

MAXIMUM ONE-PIN FACTOR (MAXIMUM PIN POWER/CORE AVERAGE POWER)

						C 1 0.66 1.04 1.07	C 2 0.84 1.13 1.17	
				C 3 0.62 1.01 1.04	C 4 0.85 1.13 1.17	C+ 5 1.06 1.29 1.34	C+ 6 1.25 1.38 1.44	B 7 1.21 1.30 1.35
			C 8 0.68 1.05 1.09	C. 9 1.09 1.27 1.33	B 10 1.14 1.23 1.28	A 11 1.04 1.09 1.14	B 12 1.23 1.30 1.36	A 13 1.08 1.13 1.18
		C 14 0.68 1.05 1.09	A 15 0.88 1.01 1.06	B 16 1.16 1.23 1.28	A 17 1.04 1.08 1.12	B 18 1.18 1.23 1.29	A 19 1.03 1.08 1.12	B 20 1.17 1.24 1.29
	C 21 0.62 1.01 1.04	C. 22 1.09 1.27 1.33	B 23 1.16 1.23 1.28	A 24 1.03 1.07 1.11	B 25 1.16 1.22 1.27	A 26 0.99 1.05 1.09	B 27 1.11 1.18 1.23	A 28 0.97 1.02 1.06
	C 29 0.85 1.13 1.17	B 30 1.14 1.23 1.28	A 31 1.04 1.08 1.12	B 32 1.16 1.22 1.27	A 33 0.98 1.04 1.08	B 34 1.08 1.15 1.19	A 35 0.93 0.98 1.02	B 36 1.05 1.11 1.15
	C+ 37 1.06 1.29 1.34	A 38 1.04 1.09 1.14	B 39 1.18 1.23 1.29	A 40 0.99 1.05 1.09	B 41 1.08 1.15 1.19	A 42 0.91 0.96 1.00	B 43 1.02 1.07 1.11	A 44 0.88 0.92 0.96
C 45 0.66 1.04 1.07	C+ 46 1.25 1.38 1.44	B 47 1.23 1.30 1.36	A 48 1.03 1.08 1.12	B 49 1.11 1.18 1.23	A 50 0.93 0.98 1.02	B 51 1.02 1.07 1.11	A 52 0.87 0.90 0.94	B 53 0.98 1.02 1.07
C 54 0.84 1.13 1.17	B 55 1.21 1.30 1.35	A 56 1.08 1.13 1.18	B 57 1.17 1.24 1.29	A 58 0.97 1.02 1.06	B 59 1.05 1.11 1.15	A 60 0.88 0.92 0.96	B 61 0.98 1.02 1.07	A 62 0.85 0.88 0.91

FLORIDA POWER & LIGHT COMPANY
ST. LUCIE PLANT UNIT 2

PLANAR AVERAGE POWER DISTRIBUTION – 13200 MWD/T, ZERO POWER, CYCLE 1

FIGURE 4.3-4b

X.XX X.XX X.XX

BOX AVERAGE (BOX POWER/CORE AVERAGE POWER)

MAXIMUM ENTHALPY RISE FACTOR (MAXIMUM OF THE AVERAGE POWER OF 4 NEIGHBORING PINS/CORE AVERAGE POWER)

MAXIMUM ONE-PIN FACTOR (MAXIMUM PIN POWER/CORE AVERAGE POWER)

						C 1 0.75 1.21 1.26	C 2 1.02 1.34 1.41
			C 3 0.69 1.10 1.14	C 4 0.94 1.24 1.31	C+ 5 1.07 1.31 1.37	C+ 6 1.24 1.34 1.42	B 7 1.13 1.20 1.27
		C 8 0.76 1.16 1.21	C. 9 1.09 1.22 1.29	B 10 1.07 1.15 1.22	A 11 1.05 1.14 1.20	B 12 1.11 1.17 1.23	A 13 1.03 1.13 1.19
	C 14 0.76 1.16 1.21	A 15 0.91 1.02 1.07	B 16 1.07 1.15 1.21	A 17 1.04 1.13 1.19	B 18 1.10 1.15 1.22	A 19 0.95 1.06 1.11	B 20 0.95 1.07 1.12
C 21 0.69 1.10 1.14	C. 22 1.09 1.22 1.29	B 23 1.07 1.15 1.21	A 24 1.04 1.13 1.19	B 25 1.12 1.17 1.23	A 26 1.01 1.10 1.16	B 27 0.94 1.05 1.11	A 28 0.57 0.68 0.71
C 29 0.94 1.24 1.31	B 30 1.07 1.15 1.22	A 31 1.04 1.13 1.19	B 32 1.12 1.17 1.23	A 33 1.04 1.14 1.19	B 34 1.09 1.15 1.21	A 35 0.95 1.04 1.10	B 36 0.94 1.05 1.11
C+ 37 1.07 1.31 1.37	A 38 1.05 1.14 1.20	B 39 1.10 1.15 1.22	A 40 1.01 1.10 1.16	B 41 1.09 1.15 1.21	A 42 1.03 1.12 1.18	B 43 1.10 1.15 1.22	A 44 1.01 1.11 1.16
C+ 46 1.24 1.34 1.42	B 47 1.11 1.17 1.23	A 48 0.96 1.06 1.11	B 49 0.94 1.05 1.11	A 50 0.95 1.04 1.10	B 51 1.10 1.15 1.22	A 52 1.06 1.15 1.21	B 53 1.14 1.19 1.26
B 55 1.13 1.20 1.27	A 56 1.03 1.14 1.19	B 57 0.95 1.07 1.12	A 58 0.57 0.68 0.71	B 59 0.94 1.05 1.11	A 60 1.01 1.11 1.16	B 61 1.14 1.19 1.26	A 62 1.07 1.17 1.23

C 45 0.75 1.21 1.26	
C 54 1.02 1.34 1.41	

FLORIDA POWER & LIGHT COMPANY
ST. LUCIE PLANT UNIT 2

PLANAR AVERAGE POWER DISTRIBUTION – BOL, CYCLE 1, FULL POWER, BANK 6 INSERTED

FIGURE 4.3-5

X . XX
X . XX
X . XX

BOX AVERAGE (BOX POWER/CORE AVERAGE POWER)

MAXIMUM ENTHALPY RISE FACTOR (MAXIMUM OF THE AVERAGE POWER OF 4 NEIGHBORING PINS/CORE AVERAGE POWER)

MAXIMUM ONE-PIN FACTOR (MAXIMUM PIN POWER/CORE AVERAGE POWER)

							C 1 0.71 1.13 1.18	C 2 0.95 1.25 1.32
				C 3 0.69 1.09 1.14	C 4 0.93 1.22 1.28	C+ 5 1.03 1.27 1.33	C+ 6 1.18 1.27 1.35	B 7 1.07 1.14 1.21
			C 8 0.77 1.18 1.22	C. 9 1.09 1.23 1.29	B 10 1.07 1.16 1.22	A 11 1.04 1.14 1.20	B 12 1.08 1.14 1.21	A 13 1.01 1.11 1.16
		C 14 0.77 1.18 1.22	A 15 0.93 1.05 1.10	B 16 1.09 1.17 1.24	A 17 1.06 1.16 1.22	B 18 1.11 1.17 1.23	A 19 0.96 1.06 1.12	B 20 0.94 1.06 1.12
	C 21 0.69 1.09 1.14	C. 22 1.09 1.23 1.29	B 23 1.09 1.17 1.24	A 24 1.07 1.17 1.23	B 25 1.15 1.20 1.27	A 26 1.03 1.13 1.19	B 27 0.95 1.06 1.13	A 28 0.58 0.69 0.72
	C 29 0.93 1.22 1.28	B 30 1.07 1.15 1.23	A 31 1.06 1.16 1.22	B 32 1.15 1.20 1.27	A 33 1.07 1.17 1.23	B 34 1.12 1.18 1.24	A 35 0.97 1.07 1.13	B 36 0.95 1.07 1.13
C 45 0.71 1.13 1.18	C+ 37 1.03 1.27 1.33	A 38 1.04 1.14 1.20	B 39 1.11 1.17 1.23	A 40 1.03 1.13 1.19	B 41 1.12 1.18 1.24	A 42 1.06 1.15 1.21	B 43 1.12 1.18 1.25	A 44 1.03 1.14 1.19
C 54 0.95 1.26 1.32	C+ 46 1.18 1.27 1.35	B 47 1.08 1.14 1.21	A 48 0.96 1.06 1.12	B 49 0.95 1.07 1.13	A 50 0.97 1.07 1.13	B 51 1.12 1.18 1.25	A 52 1.08 1.18 1.24	B 53 1.16 1.22 1.29
	B 55 1.07 1.14 1.21	A 56 1.01 1.11 1.16	B 57 0.94 1.06 1.12	A 58 0.58 0.69 0.72	B 59 0.95 1.07 1.13	A 60 1.03 1.14 1.19	B 61 1.16 1.22 1.29	A 62 1.10 1.20 1.26

FLORIDA POWER & LIGHT COMPANY
ST. LUCIE PLANT UNIT 2

PLANAR AVERAGE POWER DISTRIBUTION – 50 MWD/T, CYCLE 1, BANK 6 INSERTED, FULL POWER

FIGURE 4.3-6

X . XX
X . XX
X . XX

BOX AVERAGE (BOX POWER/CORE AVERAGE POWER)

MAXIMUM ENTHALPY RISE FACTOR (MAXIMUM OF THE AVERAGE POWER OF 4 NEIGHBORING PINS/CORE AVERAGE POWER)

MAXIMUM ONE-PIN FACTOR (MAXIMUM PIN POWER/CORE AVERAGE POWER)

						C 1 0.67 1.04 1.07	C 2 0.84 1.13 1.16
			C 3 0.67 1.07 1.10	C 4 0.89 1.18 1.21	C+ 5 1.09 1.31 1.36	C+ 6 1.25 1.37 1.43	B 7 1.20 1.28 1.34
		C 8 0.74 1.14 1.18	C. 9 1.16 1.36 1.42	B 10 1.20 1.30 1.35	A 11 1.06 1.12 1.16	B 12 1.21 1.28 1.34	A 13 1.05 1.12 1.16
	C 14 0.74 1.14 1.18	A 15 0.95 1.10 1.15	B 16 1.24 1.32 1.38	A 17 1.10 1.15 1.20	B 18 1.19 1.27 1.32	A 19 0.95 1.05 1.09	B 20 1.00 1.14 1.18
C 21 0.67 1.07 1.10	C. 22 1.16 1.36 1.42	B 23 1.24 1.32 1.38	A 24 1.11 1.15 1.20	B 25 1.22 1.30 1.35	A 26 0.99 1.07 1.12	B 27 0.96 1.09 1.13	A 28 0.56 0.73 0.76
C 29 0.89 1.18 1.21	B 30 1.20 1.30 1.35	A 31 1.10 1.15 1.20	B 32 1.22 1.30 1.35	A 33 1.02 1.09 1.14	B 34 1.09 1.17 1.22	A 35 0.86 0.93 0.96	B 36 0.89 0.98 1.02
C+ 37 1.09 1.31 1.36	A 38 1.06 1.12 1.16	B 39 1.19 1.27 1.32	A 40 0.99 1.07 1.12	B 41 1.09 1.17 1.22	A 42 0.92 0.98 1.02	B 43 1.01 1.06 1.11	A 44 0.87 0.91 0.95
C+ 46 1.25 1.37 1.43	B 47 1.21 1.29 1.34	A 48 0.95 1.05 1.09	B 49 0.96 1.09 1.13	A 50 0.86 0.93 0.96	B 51 1.01 1.06 1.11	A 52 0.89 0.92 0.96	B 53 1.01 1.05 1.10
B 55 1.20 1.28 1.34	A 56 1.05 1.12 1.16	B 57 1.00 1.14 1.18	A 58 0.56 0.73 0.76	B 59 0.88 0.98 1.02	A 60 0.86 0.91 0.95	B 61 1.01 1.05 1.10	A 62 0.89 0.92 0.96

C 45 0.67 1.04 1.07
C 54 0.84 1.13 1.16

FLORIDA POWER & LIGHT COMPANY
ST. LUCIE PLANT UNIT 2

PLANAR AVERAGE POWER DISTRIBUTION
13200 MWD/T, CYCLE 1, BANK 6 INSERTED
FULL POWER

FIGURE 4.3-7

X . XX	BOX AVERAGE (BOX POWER/CORE AVERAGE POWER)
X . XX	MAXIMUM ENTHALPY RISE FACTOR (MAXIMUM OF THE AVERAGE POWER OF 4 NEIGHBORING PINS/CORE AVERAGE POWER)
X . XX	MAXIMUM ONE-PIN FACTOR (MAXIMUM PIN POWER/CORE AVERAGE POWER)

NOTE: AS INDICATED IN SECTION 4.3.2.4.3.5 AND 15.0.3.3, THE PLRS (OR PART-LENGTH CEAS) HAVE BEEN REMOVED FROM THE ST. LUCIE 2 DESIGN.

						C 1 0.74 1.19 1.23	C 2 1.00 1.32 1.39	
				C 3 0.64 1.02 1.06	C 4 0.89 1.18 1.24	C+ 5 1.03 1.27 1.34	C+ 6 1.23 1.33 1.41	B 7 1.12 1.20 1.27
			C 8 0.69 1.06 1.09	C. 9 0.99 1.13 1.18	B 10 1.00 1.09 1.15	A 11 1.01 1.11 1.17	B 12 1.12 1.18 1.25	A 13 1.07 1.17 1.23
		C 14 0.69 1.06 1.10	A 15 0.82 0.93 0.97	B 16 0.98 1.05 1.11	A 17 0.96 1.04 1.09	B 18 1.05 1.12 1.19	A 19 1.03 1.13 1.19	B 20 1.14 1.18 1.25
	C 21 0.64 1.02 1.06	C. 22 1.00 1.13 1.18	B 23 0.98 1.05 1.11	A 24 0.94 1.03 1.08	B 25 1.01 1.06 1.12	A 26 0.84 0.88 0.90	B 27 1.09 1.16 1.23	A 28 1.06 1.15 1.21
	C 29 0.89 1.18 1.24	B 30 1.00 1.09 1.15	A 31 0.96 1.04 1.09	B 32 1.01 1.06 1.12	A 33 0.97 1.06 1.12	B 34 1.07 1.16 1.23	A 35 1.06 1.16 1.22	B 36 1.16 1.22 1.29
	C+ 37 1.03 1.27 1.34	A 38 1.01 1.11 1.17	B 39 1.05 1.12 1.19	A 40 0.84 0.88 0.90	B 41 1.07 1.16 1.23	A 42 1.07 1.17 1.23	B 43 1.19 1.25 1.33	A 44 1.12 1.23 1.29
C 45 0.74 1.19 1.23	C+ 46 1.23 1.33 1.41	B 47 1.12 1.18 1.25	A 48 1.03 1.13 1.19	B 49 1.09 1.16 1.23	A 50 1.06 1.16 1.22	B 51 1.19 1.25 1.33	A 52 1.14 1.25 1.31	B 53 1.24 1.29 1.36
C 54 1.00 1.32 1.39	B 55 1.12 1.20 1.27	A 56 1.07 1.17 1.23	B 57 1.14 1.18 1.25	A 58 1.06 1.15 1.21	B 59 1.16 1.22 1.29	A 60 1.12 1.23 1.29	B 61 1.24 1.29 1.36	A 62 1.17 1.27 1.33

FLORIDA POWER & LIGHT COMPANY
ST. LUCIE PLANT UNIT 2

PLANAR AVERAGE POWER DISTRIBUTION
BOL, CYCLE 1, PLRS INSERTED, FULL POWER

FIGURE 4.3-8

X.XX
X.XX
X.XX

BOX AVERAGE (BOX POWER/CORE AVERAGE POWER)

MAXIMUM ENTHALPY RISE FACTOR (MAXIMUM OF THE AVERAGE POWER OF 4 NEIGHBORING PINS/CORE AVERAGE POWER)

MAXIMUM ONE-PIN FACTOR (MAXIMUM PIN POWER/CORE AVERAGE POWER)

NOTE: AS INDICATED IN SECTION 4.3.2.4.3.5 AND 15.0.3.3, THE PLRS (OR PART-LENGTH CEAS) HAVE BEEN REMOVED FROM THE ST. LUCIE 2 DESIGN.

						C 1 0.70 1.11 1.16	C 2 0.94 1.24 1.30	
				C 3 0.64 1.01 1.05	C 4 0.87 1.16 1.21	C+ 5 1.00 1.24 1.30	C+ 6 1.17 1.27 1.34	B 7 1.07 1.15 1.21
			C 8 0.70 1.07 1.11	C. 9 1.00 1.12 1.19	B 10 1.00 1.09 1.15	A 11 1.01 1.11 1.16	B 12 1.11 1.17 1.24	A 13 1.06 1.16 1.21
		C 14 0.70 1.07 1.11	A 15 0.84 0.95 1.00	B 16 0.99 1.07 1.13	A 17 0.97 1.06 1.11	B 18 1.05 1.13 1.19	A 19 1.04 1.14 1.19	B 20 1.14 1.18 1.25
	C 21 0.64 1.01 1.05	C. 22 1.00 1.13 1.19	B 23 0.99 1.07 1.13	A 24 0.96 1.06 1.11	B 25 1.03 1.09 1.15	A 26 0.85 0.90 0.91	B 27 1.10 1.18 1.25	A 28 1.07 1.17 1.23
	C 29 0.87 1.16 1.21	B 30 1.00 1.09 1.15	A 31 0.97 1.06 1.11	B 32 1.03 1.09 1.15	A 33 1.00 1.09 1.14	B 34 1.09 1.18 1.25	A 35 1.08 1.18 1.24	B 36 1.18 1.24 1.31
C 45 0.70 1.11 1.16	C+ 37 1.00 1.24 1.30	A 38 0.01 0.11 0.16	B 39 1.05 1.13 1.19	A 40 0.85 0.90 0.91	B 41 1.09 1.18 1.25	A 42 1.09 1.20 1.26	B 43 1.21 1.28 1.36	A 44 1.15 1.26 1.32
C 54 0.94 1.24 1.30	C+ 46 1.17 1.27 1.34	B 47 1.11 1.17 1.24	A 48 1.04 1.14 1.19	B 49 1.10 1.18 1.25	A 50 1.08 1.18 1.24	B 51 1.21 1.28 1.36	A 52 1.17 1.28 1.34	B 53 1.26 1.31 1.39
	B 55 1.07 1.15 1.21	A 56 0.06 0.16 0.21	B 57 1.14 1.18 1.25	A 58 1.07 1.17 1.23	B 59 1.18 1.24 1.31	A 60 1.15 1.26 1.32	B 61 1.26 1.31 1.39	A 62 1.19 1.30 1.36

FLORIDA POWER & LIGHT COMPANY
ST. LUCIE PLANT UNIT 2

PLANAR AVERAGE POWER DISTRIBUTION
50 MWD/T, CYCLE 1, PLRS INSERTED
FULL POWER

FIGURE 4.3-9

X . XX	BOX AVERAGE (BOX POWER/CORE AVERAGE POWER)
X . XX	MAXIMUM ENTHALPY RISE FACTOR (MAXIMUM OF THE AVERAGE POWER OF 4 NEIGHBORING PINS/CORE AVERAGE POWER)
X . XX	MAXIMUM ONE-PIN FACTOR (MAXIMUM PIN POWER/CORE AVERAGE POWER)

NOTE: AS INDICATED IN SECTION 4.3.2.4.3.5 AND 15.0.3.3, THE PLRS (OR PART-LENGTH CEAS) HAVE BEEN REMOVED FROM THE ST. LUCIE 2 DESIGN.

						C 1 .67 1.04 1.07	C 2 .84 1.13 1.17	
				C 3 .63 1.00 1.04	C 4 .85 1.13 1.16	C+ 5 1.06 1.29 1.34	C+ 6 1.26 1.39 1.44	B 7 1.22 1.31 1.36
			C 8 .69 1.05 1.09	C. 9 1.08 1.26 1.32	B 10 1.14 1.22 1.27	A 11 1.04 1.10 1.14	B 12 1.24 1.31 1.37	A 13 1.10 1.15 1.19
		C 14 .69 1.05 1.09	A 15 .88 1.01 1.06	B 16 1.15 1.21 1.27	A 17 1.02 1.07 1.11	B 18 1.14 1.22 1.27	A 19 1.03 1.09 1.14	B 20 1.19 1.26 1.31
	C 21 .63 1.00 1.04	C. 22 1.08 1.26 1.32	B 23 1.15 1.21 1.27	A 24 1.01 1.05 1.10	B 25 1.10 1.19 1.23	A 26 .82 .93 .95	B 27 1.09 1.17 1.21	A 28 .99 1.04 1.08
	C 29 .85 1.13 1.16	B 30 1.14 1.22 1.27	A 31 1.02 1.07 1.11	B 32 1.10 1.19 1.23	A 33 .95 1.00 1.04	B 34 1.06 1.11 1.16	A 35 .95 .99 1.03	B 36 1.10 1.14 1.20
	C+ 37 1.06 1.29 1.34	A 38 1.04 1.10 1.14	B 39 1.14 1.22 1.27	A 40 .82 .93 .95	B 41 1.06 1.11 1.16	A 42 .95 .99 1.03	B 43 1.09 1.14 1.19	A 44 .96 1.00 1.04
C 45 .67 1.04 1.07	C+ 46 1.26 1.39 1.44	B 47 1.24 1.31 1.37	A 48 1.03 1.09 1.14	B 49 1.09 1.17 1.21	A 50 .95 .99 1.03	B 51 1.09 1.14 1.19	A 52 .96 1.00 1.04	B 53 1.10 1.14 1.19
C 54 .84 1.13 1.17	B 55 1.22 1.31 1.36	A 56 1.10 1.15 1.19	B 57 1.19 1.26 1.31	A 58 .99 1.04 1.08	B 59 1.10 1.14 1.20	A 60 .96 1.00 1.04	B 61 1.10 1.14 1.19	A 62 .97 1.00 1.04

FLORIDA POWER & LIGHT COMPANY
ST. LUCIE PLANT UNIT 2

PLANAR AVERAGE POWER DISTRIBUTION
13200 MWD/T, CYCLE 1, PLRS INSERTED
FULL POWER

FIGURE 4.3-10

X . XX
X . XX
X . XX

BOX AVERAGE (BOX POWER/CORE AVERAGE POWER)

MAXIMUM ENTHALPY RISE FACTOR (MAXIMUM OF THE AVERAGE POWER OF 4 NEIGHBORING PINS/CORE AVERAGE POWER)

MAXIMUM ONE-PIN FACTOR (MAXIMUM PIN POWER/CORE AVERAGE POWER)

NOTE: AS INDICATED IN SECTION 4.3.2.4.3.5 AND 15.0.3.3, THE PLRS (OR PART-LENGTH CEAS) HAVE BEEN REMOVED FROM THE ST. LUCIE 2 DESIGN.

						C 1 0.82 1.32 1.37	C 2 1.12 1.47 1.54	
				C 3 0.72 1.15 1.20	C 4 0.99 1.31 1.38	C+ 5 1.14 1.39 1.46	C+ 6 1.34 1.45 1.53	B 7 1.22 1.30 1.38
			C 8 0.79 1.21 1.26	C 9 1.13 1.26 1.33	B 10 1.11 1.18 1.25	A 11 1.08 1.19 1.25	B 12 1.15 1.23 1.30	A 13 1.08 1.20 1.25
		C 14 0.79 1.21 1.26	A 15 0.94 1.05 1.10	B 16 1.09 1.15 1.21	A 17 1.03 1.12 1.18	B 18 1.06 1.15 1.22	A 19 0.94 1.06 1.11	B 20 0.96 1.09 1.15
	C 21 0.72 1.15 1.20	C 22 1.13 1.26 1.33	B 23 1.09 1.14 1.21	A 24 1.02 1.11 1.17	B 25 1.05 1.12 1.19	A 26 0.80 0.86 0.87	B 27 0.87 0.96 1.02	A 28 0.55 0.67 0.69
	C 29 1.00 1.31 1.38	B 30 1.11 1.18 1.25	A 31 1.03 1.12 1.18	B 32 1.05 1.12 1.19	A 33 0.96 1.05 1.10	B 34 1.00 1.06 1.12	A 35 0.89 0.99 1.04	B 36 0.90 1.02 1.07
	C+ 37 1.14 1.39 1.46	A 38 1.08 1.19 1.25	B 39 1.06 1.15 1.22	A 40 0.80 0.86 0.87	B 41 1.00 1.06 1.12	A 42 0.98 1.07 1.12	B 43 1.06 1.13 1.20	A 44 0.99 1.09 1.14
C 45 0.82 1.32 1.37	C+ 46 1.34 1.45 1.53	B 47 1.15 1.23 1.30	A 48 0.94 1.06 1.11	B 49 0.87 0.96 1.02	A 50 0.89 0.99 1.04	B 51 1.06 1.13 1.20	A 52 1.04 1.14 1.20	B 53 1.13 1.19 1.26
C 54 1.12 1.47 1.54	B 55 1.22 1.30 1.38	A 56 1.08 1.20 1.25	B 57 0.96 1.09 1.15	A 58 0.55 0.67 0.69	B 59 0.90 1.02 1.07	A 60 0.99 1.09 1.14	B 61 1.13 1.19 1.26	A 62 1.08 1.17 1.23

FLORIDA POWER & LIGHT COMPANY
ST. LUCIE PLANT UNIT 2

PLANAR AVERAGE POWER DISTRIBUTION
BOL, CYCLE 1, BANK 6 AND PLRS
INSERTED, FULL POWER

FIGURE 4.3-11

X . XX
X . XX
X . XX

BOX AVERAGE (BOX POWER/CORE AVERAGE POWER)

MAXIMUM ENTHALPY RISE FACTOR (MAXIMUM OF THE AVERAGE POWER OF 4 NEIGHBORING PINS/CORE AVERAGE POWER)

MAXIMUM ONE-PIN FACTOR (MAXIMUM PIN POWER/CORE AVERAGE POWER)

NOTE: AS INDICATED IN SECTION 4.3.2.4.3.5 AND 15.0.3.3, THE PLRS (OR PART-LENGTH CEAS) HAVE BEEN REMOVED FROM THE ST. LUCIE 2 DESIGN.

							C 1 0.78 1.23 1.29	C 2 1.04 1.37 1.44
				C 3 0.73 1.15 1.20	C 4 0.98 1.29 1.35	C+ 5 1.11 1.35 1.41	C+ 6 1.27 1.37 1.46	B 7 1.16 1.24 1.30
			C 8 0.81 1.23 1.28	C. 9 1.14 1.27 1.34	B 10 1.11 1.18 1.25	A 11 1.08 1.18 1.24	B 12 1.13 1.20 1.27	A 13 1.06 1.17 1.23
		C 14 0.81 1.23 1.28	A 15 0.96 1.09 1.14	B 16 1.11 1.17 1.24	A 17 1.04 1.15 1.20	B 18 1.06 1.16 1.23	A 19 0.94 1.06 1.11	B 20 0.95 1.08 1.14
	C 21 0.73 1.15 1.20	C. 22 1.14 1.27 1.34	B 23 1.11 1.17 1.24	A 24 1.05 1.15 1.21	B 25 1.07 1.15 1.22	A 26 0.81 0.87 0.89	B 27 0.88 0.97 1.03	A 28 0.56 0.67 0.70
	C 29 0.98 1.29 1.35	B 30 1.11 1.18 1.25	A 31 1.04 1.15 1.20	B 32 1.07 1.15 1.22	A 33 0.99 1.08 1.13	B 34 1.02 1.09 1.15	A 35 0.91 1.02 1.07	B 36 0.92 1.04 1.10
	C+ 37 1.11 1.35 1.41	A 38 1.08 1.18 1.24	B 39 1.06 1.16 1.23	A 40 0.81 0.87 0.89	B 41 1.02 1.09 1.15	A 42 1.01 1.10 1.16	B 43 1.09 1.16 1.23	A 44 1.02 1.12 1.18
C 45 0.78 1.23 1.29	C+ 46 1.27 1.38 1.46	B 47 1.13 1.20 1.27	A 48 0.94 1.06 1.11	B 49 0.88 0.97 1.03	A 50 0.91 1.02 1.07	B 51 1.09 1.16 1.23	A 52 1.07 1.17 1.23	B 53 1.16 1.22 1.29
C 54 1.04 1.37 1.44	B 55 1.15 1.24 1.31	A 56 1.06 1.17 1.23	B 57 0.95 1.08 1.14	A 58 0.56 0.67 0.70	B 59 0.92 1.04 1.10	A 60 1.02 1.12 1.18	B 61 1.16 1.22 1.29	A 62 1.11 1.21 1.27

FLORIDA POWER & LIGHT COMPANY
ST. LUCIE PLANT UNIT 2

PLANAR AVERAGE POWER DISTRIBUTION
50 MWD/T, CYCLE 1, BANK 6 AND PLRS INSERTED, FULL POWER

FIGURE 4.3-12

X.XX
X.XX
X.XX

BOX AVERAGE (BOX POWER/CORE AVERAGE POWER)

MAXIMUM ENTHALPY RISE FACTOR (MAXIMUM OF THE AVERAGE POWER OF 4 NEIGHBORING PINS/CORE AVERAGE POWER)

MAXIMUM ONE-PIN FACTOR (MAXIMUM PIN POWER/CORE AVERAGE POWER)

NOTE: AS INDICATED IN SECTION 4.3.2.4.3.5 AND 15.0.3.3, THE PLRS (OR PART-LENGTH CEAS) HAVE BEEN REMOVED FROM THE ST. LUCIE 2 DESIGN.

							C 1 0.73 1.13 1.16	C 2 0.92 1.22 1.26
				C 3 0.70 1.12 1.16	C 4 0.94 1.24 1.27	C+ 5 1.15 1.38 1.44	C+ 6 1.34 1.46 1.52	B 7 1.29 1.37 1.44
			C 8 0.78 1.19 1.22	C. 9 1.20 1.40 1.46	B 10 1.24 1.33 1.39	A 11 1.10 1.16 1.21	B 12 1.26 1.36 1.41	A 13 1.10 1.18 1.23
		C 14 0.78 1.19 1.22	A 15 0.99 1.13 1.18	B 16 1.27 1.34 1.40	A 17 1.09 1.17 1.21	B 18 1.15 1.27 1.32	A 19 0.94 1.06 1.10	B 20 1.01 1.17 1.20
	C 21 0.70 1.12 1.16	C. 22 1.20 1.40 1.46	B 23 1.27 1.34 1.40	A 24 1.09 1.15 1.20	B 25 1.15 1.26 1.31	A 26 0.79 0.95 0.97	B 27 0.89 1.00 1.04	A 28 0.54 0.71 0.75
	C 29 0.94 1.24 1.27	B 30 1.24 1.33 1.39	A 31 1.09 1.17 1.21	B 32 1.15 1.26 1.31	A 33 0.94 1.02 1.07	B 34 0.99 1.06 1.10	A 35 0.81 0.87 0.91	B 36 0.86 0.95 0.99
	C+ 37 1.15 1.39 1.44	A 38 1.10 1.16 1.21	B 39 1.15 1.27 1.32	A 40 0.79 0.95 0.97	B 41 0.99 1.06 1.10	A 42 0.88 0.92 0.95	B 43 0.98 1.03 1.08	A 44 0.85 0.90 0.93
C 45 0.73 1.13 1.16	C+ 46 1.34 1.46 1.52	B 47 1.26 1.36 1.41	A 48 0.94 1.06 1.10	B 49 0.89 1.01 1.04	A 50 0.81 0.87 0.91	B 51 0.98 1.03 1.08	A 52 0.88 0.92 0.95	B 53 1.01 1.05 1.10
C 54 0.92 1.22 1.26	B 55 1.29 1.37 1.44	A 56 1.10 1.18 1.23	B 57 1.01 1.17 1.21	A 58 0.54 0.71 0.75	B 59 0.86 0.95 0.99	A 60 0.85 0.90 0.93	B 61 1.81 1.05 1.10	A 62 0.89 0.92 0.96

FLORIDA POWER & LIGHT COMPANY
ST. LUCIE PLANT UNIT 2

PLANAR AVERAGE POWER DISTRIBUTION
13200 MWD/T, CYCLE 1, BANK 6 AND
PLRS INSERTED, FULL POWER

FIGURE 4.3-13

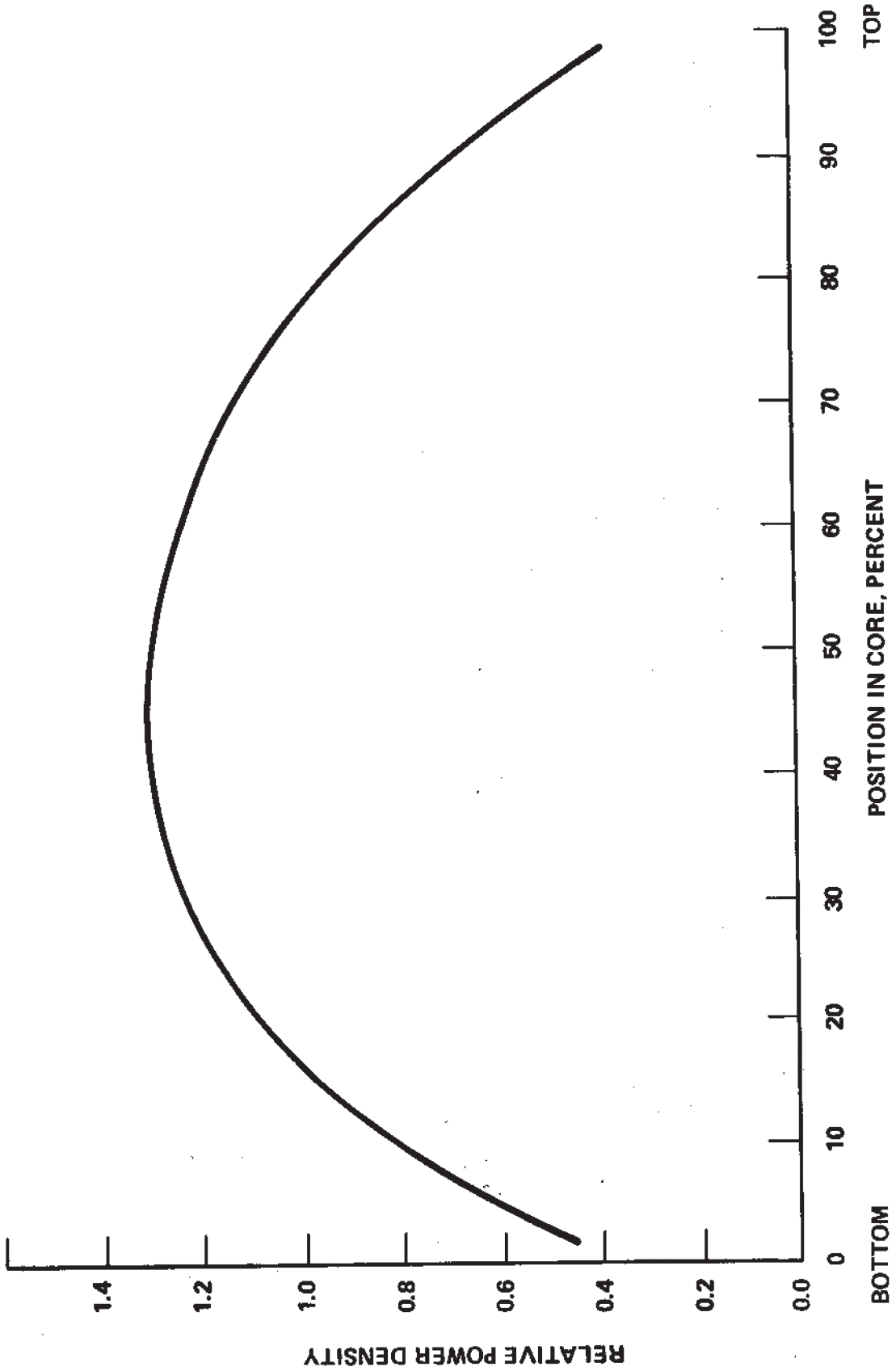

FLORIDA POWER & LIGHT COMPANY
ST. LUCIE PLANT UNIT 2

AXIAL POWER DISTRIBUTION
BOC-1, UNRODDED

FIGURE 4.3-14

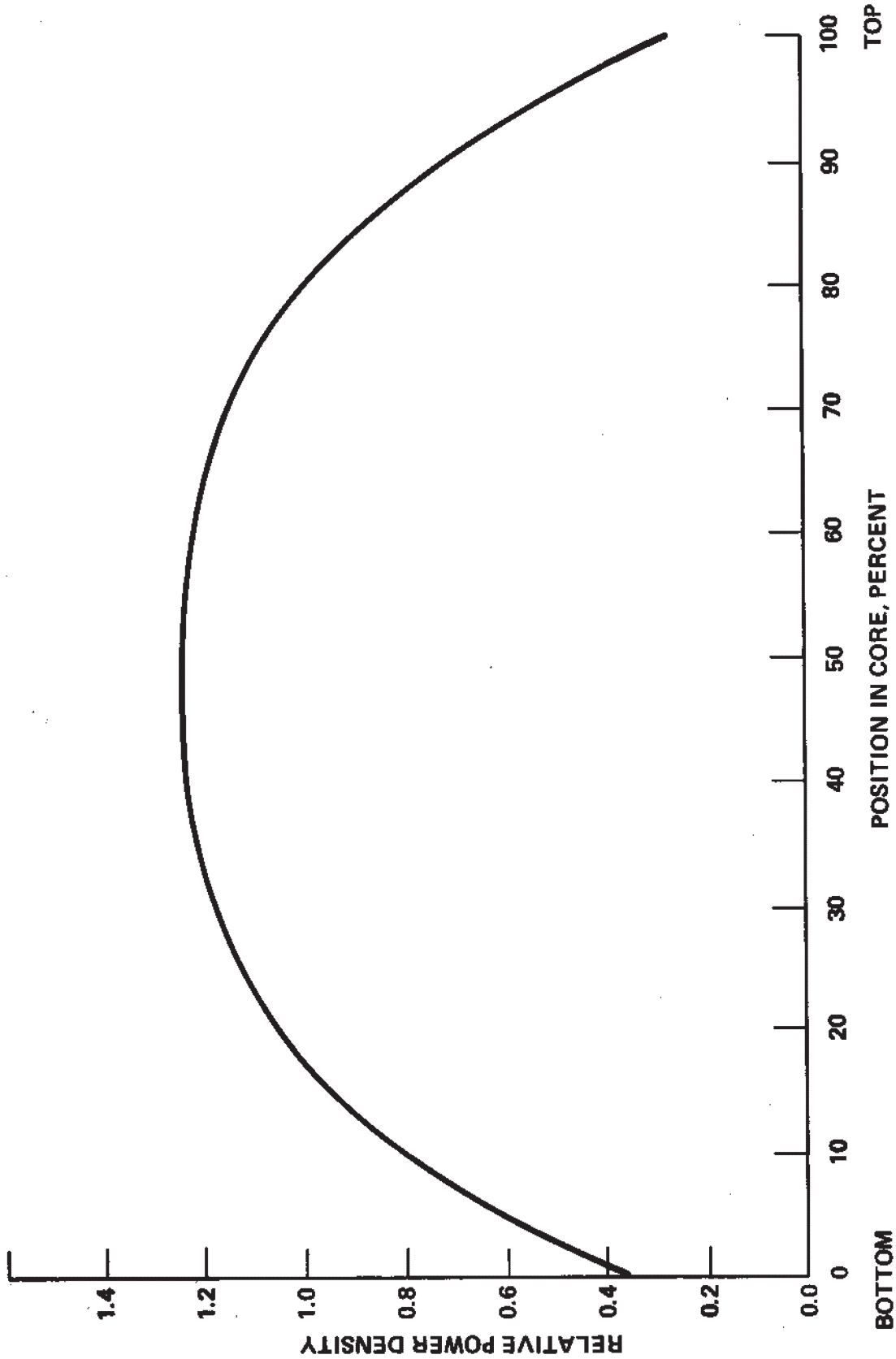

FLORIDA POWER & LIGHT COMPANY
ST. LUCIE PLANT UNIT 2

AXIAL POWER DISTRIBUTION
3000 MWD/T, CYCLE 1, UNRODDED
FIGURE 4.3-15

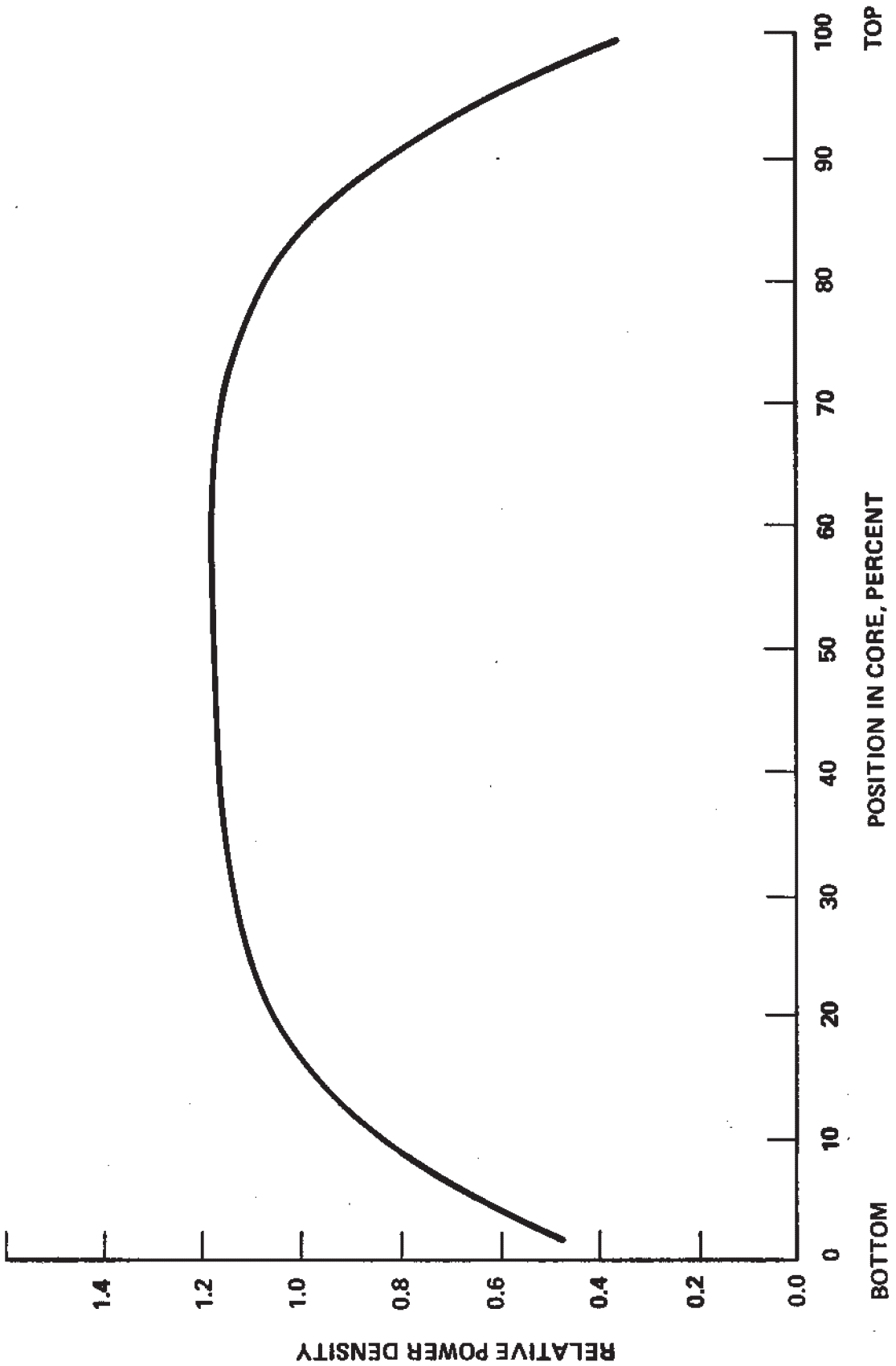

FLORIDA POWER & LIGHT COMPANY
ST. LUCIE PLANT UNIT 2

AXIAL POWER DISTRIBUTION
6000 MWD/T, CYCLE 1, UNRODDED
FIGURE 4.3-16

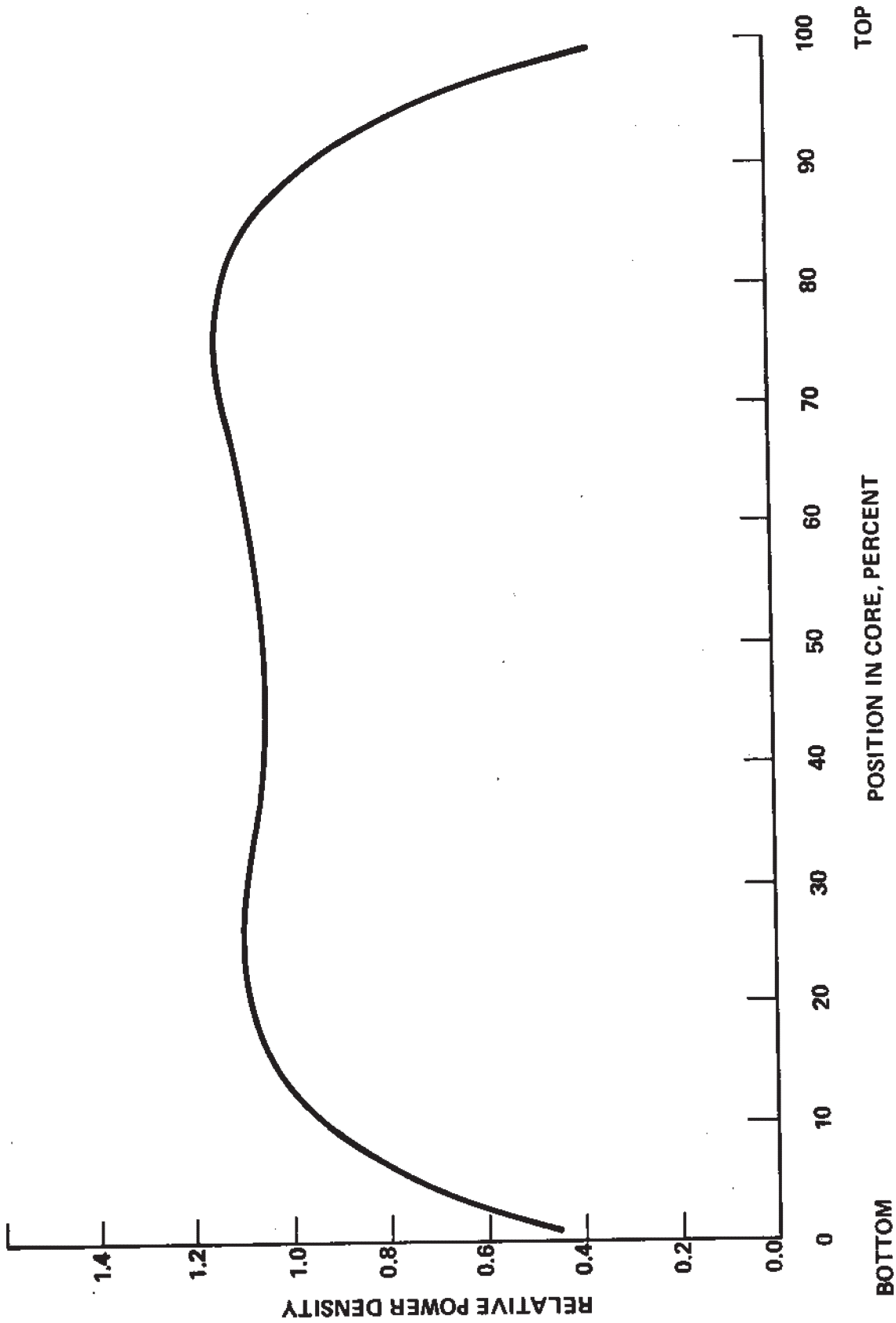

FLORIDA POWER & LIGHT COMPANY
ST. LUCIE PLANT UNIT 2

AXIAL POWER DISTRIBUTION
9000 MWD/T, CYCLE 1, UNRODDED
FIGURE 4.3-17

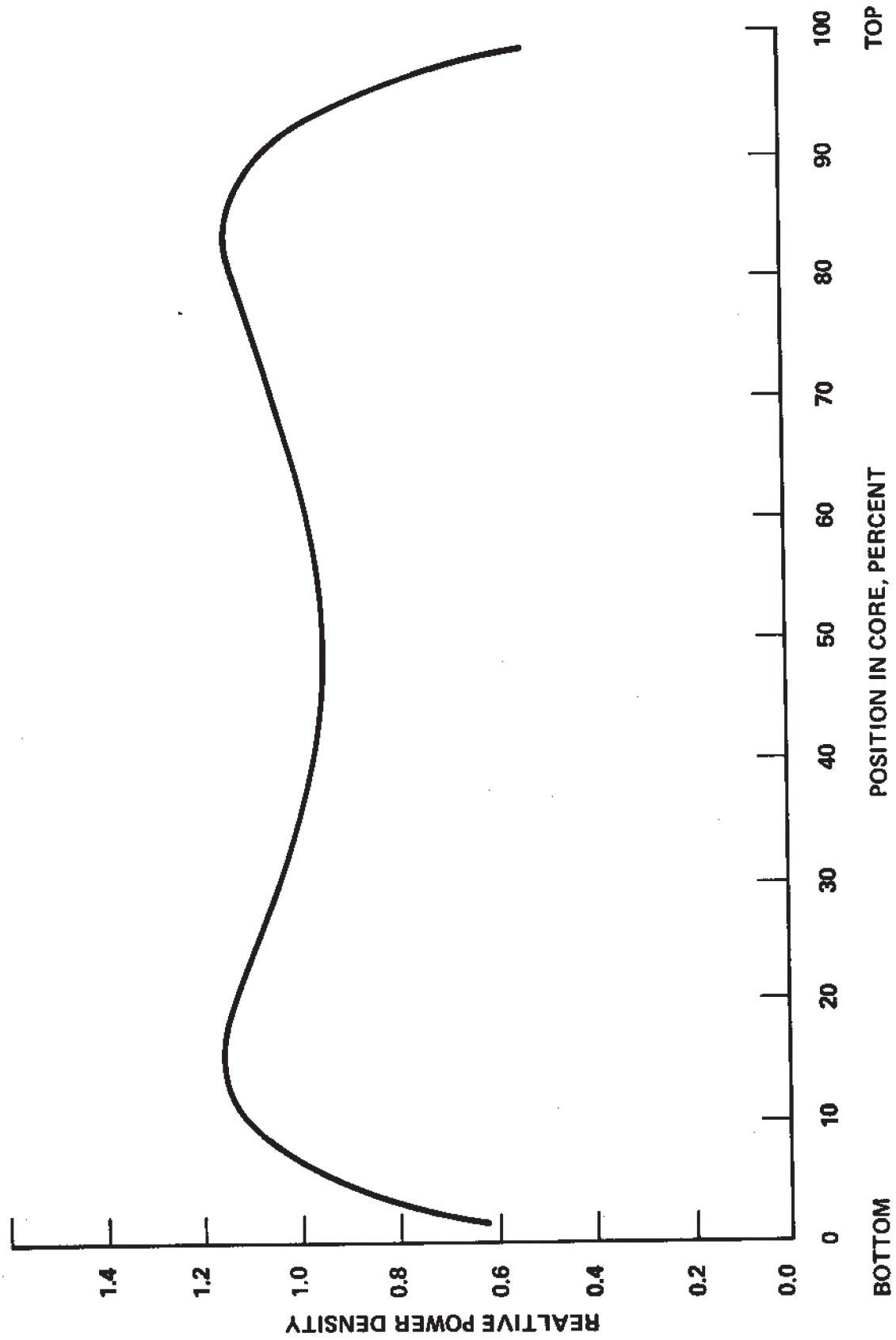

FLORIDA POWER & LIGHT COMPANY
ST. LUCIE PLANT UNIT 2

AXIAL POWER DISTRIBUTION
EOC-1, UNRODDED

FIGURE 4.3-18

X . XX	BOX AVERAGE (BOX POWER/CORE AVERAGE POWER)
X . XX	MAXIMUM ENTHALPY RISE FACTOR (MAXIMUM OF THE AVERAGE POWER OF 4 NEIGHBORING PINS/CORE AVERAGE POWER)
X . XX	MAXIMUM ONE-PIN FACTOR (MAXIMUM PIN POWER/CORE AVERAGE POWER)

						D 1 0.69 1.08 1.12	D 2 0.94 1.30 1.36	
				D 3 0.70 1.13 1.17	D 4 0.93 1.21 1.27	D 5 1.08 1.25 1.32	B 6 0.93 1.02 1.05	D* 7 1.20 1.30 1.37
			D 8 0.71 1.10 1.14	D 9 1.17 1.31 1.38	B 10 0.94 0.99 1.03	B 11 0.93 0.99 1.03	C+ 12 1.00 1.05 1.09	B 13 0.94 0.99 1.03
		D 14 0.72 1.10 1.14	B 15 0.77 0.88 0.91	C+ 16 1.03 1.14 1.19	B 17 0.96 1.05 1.08	D* 18 1.22 1.32 1.39	B 19 0.97 1.03 1.07	D* 20 1.21 1.31 1.38
	D 21 0.70 1.13 1.17	D 22 1.17 1.31 1.38	C+ 23 1.03 1.14 1.19	C 24 1.08 1.16 1.21	C 25 1.18 1.29 1.35	B 26 1.02 1.08 1.12	C 27 1.10 1.20 1.24	B 28 0.98 1.03 1.07
	D 29 0.93 1.21 1.27	B 30 0.94 1.00 1.04	B 31 0.96 1.05 1.08	C 32 1.18 1.29 1.35	B 33 1.01 1.06 1.10	C 34 1.17 1.26 1.32	B 35 0.98 1.03 1.07	C 36 1.13 1.22 1.27
	D 37 1.08 1.25 1.32	B 38 0.93 0.99 1.03	D* 39 1.22 1.32 1.39	B 40 1.02 1.08 1.12	C 41 1.17 1.26 1.32	C 42 1.12 1.18 1.24	C 43 1.10 1.19 1.24	B 44 1.00 1.04 1.08
D 45 0.69 1.08 1.12	B 46 0.93 1.02 1.05	C+ 47 1.00 1.05 1.10	B 48 0.97 1.03 1.07	C 49 1.10 1.20 1.24	B 50 0.98 1.03 1.07	C 51 1.10 1.19 1.24	B 52 0.96 1.00 1.05	C 53 1.11 1.20 1.26
D 54 0.94 1.30 1.36	D* 55 1.20 1.30 1.37	B 56 0.94 0.99 1.03	D* 57 1.21 1.31 1.38	B 58 0.98 1.03 1.07	C 59 1.13 1.22 1.27	B 60 1.00 1.04 1.08	C 61 1.11 1.20 1.26	A 62 0.85 0.88 0.92

FLORIDA POWER & LIGHT COMPANY
ST. LUCIE PLANT UNIT 2

PLANAR AVERAGE POWER DISTRIBUTION – 50 MWD/T, CYCLE 2, FULL POWER

FIGURE 4.3-19

X.XX
X.XX
X.XX

BOX AVERAGE (BOX POWER/CORE AVERAGE POWER)

MAXIMUM ENTHALPY RISE FACTOR (MAXIMUM OF THE AVERAGE POWER OF 4 NEIGHBORING PINS/CORE AVERAGE POWER)

MAXIMUM ONE-PIN FACTOR (MAXIMUM PIN POWER/CORE AVERAGE POWER)

							D 1 0.71 1.09 1.13	D 2 0.92 1.24 1.29
				D 3 0.71 1.12 1.15	D 4 0.94 1.21 1.26	D 5 1.08 1.26 1.32	B 6 0.96 1.01 1.05	D* 7 1.18 1.25 1.32
			D 8 0.74 1.12 1.16	D 9 1.16 1.30 1.37	B 10 0.97 1.02 1.06	B 11 0.96 1.01 1.04	C+ 12 1.03 1.07 1.11	B 13 0.96 1.00 1.04
		D 14 0.74 1.12 1.16	B 15 0.82 0.93 0.96	C+ 16 1.06 1.17 1.21	B 17 0.98 1.04 1.08	D* 18 1.21 1.28 1.34	B 19 0.97 1.02 1.06	D* 20 1.20 1.26 1.33
	D 21 0.71 1.12 1.16	D 22 1.16 1.30 1.37	C+ 23 1.06 1.17 1.21	C. 24 1.09 1.13 1.19	C 25 1.15 1.24 1.29	B 26 1.00 1.06 1.10	C 27 1.08 1.16 1.20	B 28 0.97 1.02 1.06
	D 29 0.94 1.21 1.26	B 30 0.97 1.02 1.06	B 31 0.98 1.04 1.08	C 32 1.15 1.24 1.29	B 33 0.99 1.03 1.08	C 34 1.12 1.21 1.26	B 35 0.97 1.01 1.05	C 36 1.11 1.18 1.23
	D 37 1.08 1.26 1.32	B 38 0.96 1.01 1.04	D* 39 1.21 1.28 1.34	B 40 1.00 1.06 1.10	C 41 1.12 1.21 1.27	C 42 1.09 1.15 1.20	C 43 1.08 1.16 1.20	B 44 1.00 1.04 1.08
D 45 0.71 1.09 1.13	B 46 0.96 1.01 1.05	C+ 47 1.03 1.07 1.11	B 48 0.97 1.02 1.06	C 49 1.08 1.16 1.20	B 50 0.97 1.01 1.05	C 51 1.08 1.16 1.21	B 52 0.96 1.00 1.04	C 53 1.09 1.18 1.23
D 54 0.92 1.24 1.29	D* 55 1.18 1.25 1.32	B 56 0.96 1.00 1.04	D* 57 1.20 1.26 1.33	B 58 0.97 1.02 1.06	C 59 1.11 1.18 1.23	B 60 1.00 1.04 1.08	C 61 1.09 1.18 1.23	A 62 0.87 0.90 0.93

FLORIDA POWER & LIGHT COMPANY
ST. LUCIE PLANT UNIT 2

PLANAR AVERAGE POWER DISTRIBUTION – 6000 MWD/T, CYCLE 2, FULL POWER

FIGURE 4.3-20

X . XX
X . XX
X . XX

BOX AVERAGE (BOX POWER/CORE AVERAGE POWER)

MAXIMUM ENTHALPY RISE FACTOR (MAXIMUM OF THE AVERAGE POWER OF 4 NEIGHBORING PINS/CORE AVERAGE POWER)

MAXIMUM ONE-PIN FACTOR (MAXIMUM PIN POWER/CORE AVERAGE POWER)

							D 1 0.71 1.09 1.12	D 2 0.92 1.21 1.26
				D 3 0.72 1.11 1.15	D 4 0.94 1.20 1.25	D 5 1.08 1.25 1.31	B 6 0.96 1.01 1.05	D* 7 1.17 1.23 1.29
			D 8 0.76 1.12 1.16	D 9 1.15 1.29 1.35	B 10 0.97 1.02 1.06	B 11 0.96 1.00 1.04	C+ 12 1.03 1.07 1.11	B 13 0.96 1.00 1.03
		D 14 0.76 1.12 1.16	B 15 0.83 0.94 0.97	C+ 16 1.06 1.17 1.21	B 17 0.98 1.03 1.07	D* 18 1.20 1.26 1.32	B 19 0.97 1.02 1.05	D* 20 1.19 1.24 1.30
	D 21 0.72 1.11 1.15	D 22 1.15 1.29 1.35	C+ 23 1.06 1.17 1.21	C. 24 1.08 1.13 1.18	C 25 1.14 1.22 1.28	B 26 1.00 1.05 1.09	C 27 1.08 1.15 1.20	B 28 0.97 1.01 1.05
	D 29 0.94 1.20 1.25	B 30 0.97 1.02 1.06	B 31 0.98 1.03 1.07	C 32 1.14 1.22 1.28	B 33 0.99 1.03 1.07	C 34 1.12 1.20 1.25	B 35 0.97 1.01 1.05	C 36 1.11 1.18 1.23
	D 37 1.07 1.25 1.30	B 38 0.96 1.00 1.04	D* 39 1.20 1.26 1.32	B 40 1.00 1.05 1.09	C 41 1.12 1.20 1.25	C 42 1.08 1.15 1.20	C 43 1.08 1.16 1.20	B 44 1.00 1.05 1.09
D 45 0.71 1.09 1.12	B 46 0.96 1.01 1.05	C+ 47 1.03 1.07 1.11	B 48 0.97 1.02 1.05	C 49 1.08 1.15 1.20	B 50 0.97 1.01 1.20	C 51 1.08 1.16 1.20	B 52 0.97 1.01 1.05	C 53 1.10 1.18 1.23
D 54 0.92 1.21 1.26	D* 55 1.17 1.23 1.29	B 56 0.96 1.00 1.03	D* 57 1.19 1.24 1.30	B 58 0.97 1.01 1.05	C 59 1.11 1.18 1.23	B 60 1.00 1.04 1.09	C 61 1.10 1.18 1.23	A 62 0.89 0.92 0.96

FLORIDA POWER & LIGHT COMPANY
ST. LUCIE PLANT UNIT 2

PLANAR AVERAGE POWER DISTRIBUTION – 8630 MWD/T, CYCLE 2, FULL POWER

FIGURE 4.3-21

X.XX	BOX AVERAGE (BOX POWER/CORE AVERAGE POWER)
X.XX	MAXIMUM ENTHALPY RISE FACTOR (MAXIMUM OF THE AVERAGE POWER OF 4 NEIGHBORING PINS/CORE AVERAGE POWER)
X.XX	MAXIMUM ONE-PIN FACTOR (MAXIMUM PIN POWER/CORE AVERAGE POWER)

							E 1 0.69 1.12 1.16	E 2 0.84 1.15 1.20
				E 3 0.68 1.13 1.17	E 4 0.93 1.22 1.28	E 5 1.10 1.32 1.38	E* 6 1.17 1.28 1.35	C, 7 0.88 0.94 0.97
			E 8 0.77 1.17 1.22	E 9 1.16 1.30 1.37	D 10 1.11 1.17 1.22	C+ 11 0.90 0.94 0.98	D* 12 0.99 1.07 1.11	C 13 0.93 0.97 1.01
		E 14 0.77 1.17 1.22	E 15 1.15 1.26 1.33	C+ 16 0.91 0.97 1.00	C 17 0.95 1.04 1.08	D 18 1.17 1.25 1.31	C 19 0.97 1.06 1.09	E* 20 1.22 1.31 1.39
	E 21 0.68 1.13 1.16	E 22 1.16 1.30 1.37	C+ 23 0.91 0.97 1.00	D* 24 0.99 1.05 1.10	D 25 1.14 1.22 1.28	C 26 0.94 1.02 1.06	D 27 1.19 1.27 1.34	B 28 0.90 0.94 0.97
	E 29 0.93 1.22 1.28	D 30 1.11 1.17 1.22	C 31 0.95 1.04 1.08	D 32 1.14 1.22 1.28	C 33 0.92 0.98 1.02	D 34 1.14 1.20 1.26	C 35 0.96 1.04 1.08	D 36 1.22 1.29 1.35
E 45 0.69 1.12 1.16	E 37 1.10 1.32 1.38	C+ 38 0.90 0.95 0.98	D 39 1.17 1.24 1.31	C 40 0.94 1.02 1.06	D 41 1.14 1.20 1.26	D* 42 1.06 1.10 1.15	D 43 1.17 1.25 1.30	C 44 0.97 1.06 1.10
E 54 0.84 1.15 1.20	E* 46 1.17 1.28 1.35	D* 47 0.99 1.07 1.11	C 48 0.96 1.06 1.09	D 49 1.19 1.27 1.34	C 50 0.96 1.04 1.08	D 51 1.17 1.24 1.30	B 52 0.86 0.94 0.97	D 53 1.13 1.18 1.24
	C 55 0.88 0.94 0.97	C 56 0.93 0.97 1.01	E* 57 1.22 1.31 1.39	B 58 0.90 0.95 0.98	D 59 1.21 1.29 1.35	C 60 0.97 1.06 1.10	D 61 1.13 1.18 1.24	B 62 0.82 0.85 0.88

FLORIDA POWER & LIGHT COMPANY
ST. LUCIE PLANT UNIT 2

PLANAR AVERAGE POWER DISTRIBUTION – 50 MWD/T, CYCLE 3, FULL POWER

FIGURE 4.3-22

X.XX
X.XX
X.XX

BOX AVERAGE (BOX POWER/CORE AVERAGE POWER)
MAXIMUM ENTHALPY RISE FACTOR (MAXIMUM OF THE AVERAGE POWER OF 4 NEIGHBORING PINS/CORE AVERAGE POWER)
MAXIMUM ONE-PIN FACTOR (MAXIMUM PIN POWER/CORE AVERAGE POWER)

						E 1 0.70 1.10 1.14	E 2 0.86 1.14 1.19	
				E 3 0.69 1.10 1.13	E 4 0.92 1.19 1.25	E 5 1.08 1.28 1.34	E* 6 1.16 1.25 1.31	C. 7 0.89 0.95 0.99
			E 8 0.78 1.14 1.19	E 9 1.13 1.26 1.33	D 10 1.09 1.14 1.19	C+ 11 0.91 0.96 0.99	D* 12 1.01 1.06 1.10	C 13 0.95 0.99 1.03
		E 14 0.78 1.14 1.19	E 15 1.13 1.24 1.30	C+ 16 0.92 0.99 1.02	C 17 0.96 1.04 1.08	D 18 1.16 1.23 1.29	C 19 0.97 1.05 1.09	E* 20 1.21 1.28 1.35
	E 21 0.69 1.10 1.13	E 22 1.14 1.26 1.33	C+ 23 0.92 0.99 1.02	D* 24 1.00 1.06 1.11	D 25 1.14 1.21 1.26	C 26 0.95 1.02 1.06	D 27 1.18 1.25 1.31	B 28 0.91 0.95 0.98
	E 29 0.92 1.19 1.25	D 30 1.09 1.14 1.19	C 31 0.96 1.04 1.08	D 32 1.14 1.21 1.26	C 33 0.94 1.00 1.03	D 34 1.13 1.19 1.24	C 35 0.96 1.03 1.07	D 36 1.19 1.26 1.32
	E 37 1.08 1.28 1.34	C+ 38 0.91 0.96 0.99	D 39 1.16 1.23 1.29	C 40 0.95 1.02 1.06	D 41 1.13 1.19 1.24	D* 42 1.05 1.09 1.14	D 43 1.16 1.23 1.28	C 44 0.98 1.05 1.09
E 45 0.70 1.10 1.14	E* 46 1.16 1.25 1.31	D* 47 1.01 1.06 1.10	C 48 0.97 1.05 1.09	D 49 1.18 1.25 1.31	C 50 0.96 1.03 1.07	D 51 1.16 1.23 1.28	B 52 0.89 0.95 0.98	D 53 1.14 1.20 1.25
E 54 0.86 1.14 1.19	C 55 0.89 0.95 0.98	C 56 0.95 0.99 1.03	E* 57 1.21 1.28 1.35	B 58 0.91 0.95 0.98	D 59 1.19 1.26 1.32	C 60 0.98 1.05 1.09	D 61 1.14 1.20 1.25	B 62 0.86 0.89 0.92

FLORIDA POWER & LIGHT COMPANY
ST. LUCIE PLANT UNIT 2

PLANAR AVERAGE POWER DISTRIBUTION – 6000 MWD/T, CYCLE 3, FULL POWER

FIGURE 4.3-23

X.XX
X.XX
X.XX

BOX AVERAGE (BOX POWER/CORE AVERAGE POWER)

MAXIMUM ENTHALPY RISE FACTOR (MAXIMUM OF THE AVERAGE POWER OF 4 NEIGHBORING PINS/CORE AVERAGE POWER)

MAXIMUM ONE-PIN FACTOR (MAXIMUM PIN POWER/CORE AVERAGE POWER)

							E 1 0.71 1.08 1.13	E 2 0.87 1.12 1.17
				E 3 0.70 1.08 1.11	E 4 0.92 1.17 1.22	E 5 1.07 1.25 1.30	E* 6 1.14 1.22 1.28	C. 7 0.90 0.96 0.99
			E 8 0.78 1.13 1.17	E 9 1.12 1.24 1.30	D 10 1.08 1.13 1.17	C+ 11 0.92 0.96 0.99	D* 12 1.01 1.05 1.09	C 13 0.96 0.99 1.03
		E 14 0.78 1.13 1.17	E 15 1.12 1.23 1.29	C+ 16 0.93 1.00 1.02	C 17 0.96 1.04 1.08	D 18 1.15 1.22 1.28	C 19 0.97 1.04 1.08	E* 20 1.20 1.25 1.32
	E 21 0.70 1.08 1.11	E 22 1.12 1.24 1.30	C+ 23 0.93 1.00 1.02	D* 24 1.01 1.06 1.11	D 25 1.14 1.20 1.25	C 26 0.96 1.02 1.05	D 27 1.17 1.24 1.29	B 28 0.92 0.96 0.99
	E 29 0.92 1.17 1.22	D 30 1.08 1.13 1.17	C 31 0.96 1.04 1.08	D 32 1.14 1.20 1.25	C 33 0.95 1.00 1.04	D 34 1.13 1.18 1.23	C 35 0.97 1.03 1.06	D 36 1.18 1.25 1.30
	E 37 1.07 1.25 1.30	C+ 38 0.92 0.96 0.99	D 39 1.15 1.22 1.28	C 40 0.96 1.02 1.05	D 41 1.13 1.19 1.23	D* 42 1.05 1.09 1.13	D 43 1.15 1.22 1.27	C 44 0.99 1.05 1.09
E 45 0.71 1.08 1.13	E 46 1.14 1.22 1.28	D* 47 1.01 1.05 1.09	C 48 0.97 1.04 1.08	D 49 1.17 1.24 1.29	C 50 0.97 1.03 1.06	D 51 1.15 1.22 1.27	B 52 0.91 0.96 1.00	D 53 1.15 1.21 1.26
E 54 0.87 1.12 1.17	C 55 0.90 0.96 0.99	C 56 0.96 0.99 1.03	E* 57 1.20 1.25 1.32	B 58 0.92 0.96 0.99	D 59 1.18 1.25 1.30	C 60 0.99 1.05 1.09	D 61 1.15 1.21 1.26	B 62 0.89 0.92 0.95

FLORIDA POWER & LIGHT COMPANY
ST. LUCIE PLANT UNIT 2

PLANAR AVERAGE POWER DISTRIBUTION – 10469 MWD/T, EOC, CYCLE 3, FULL POWER

FIGURE 4.3-24

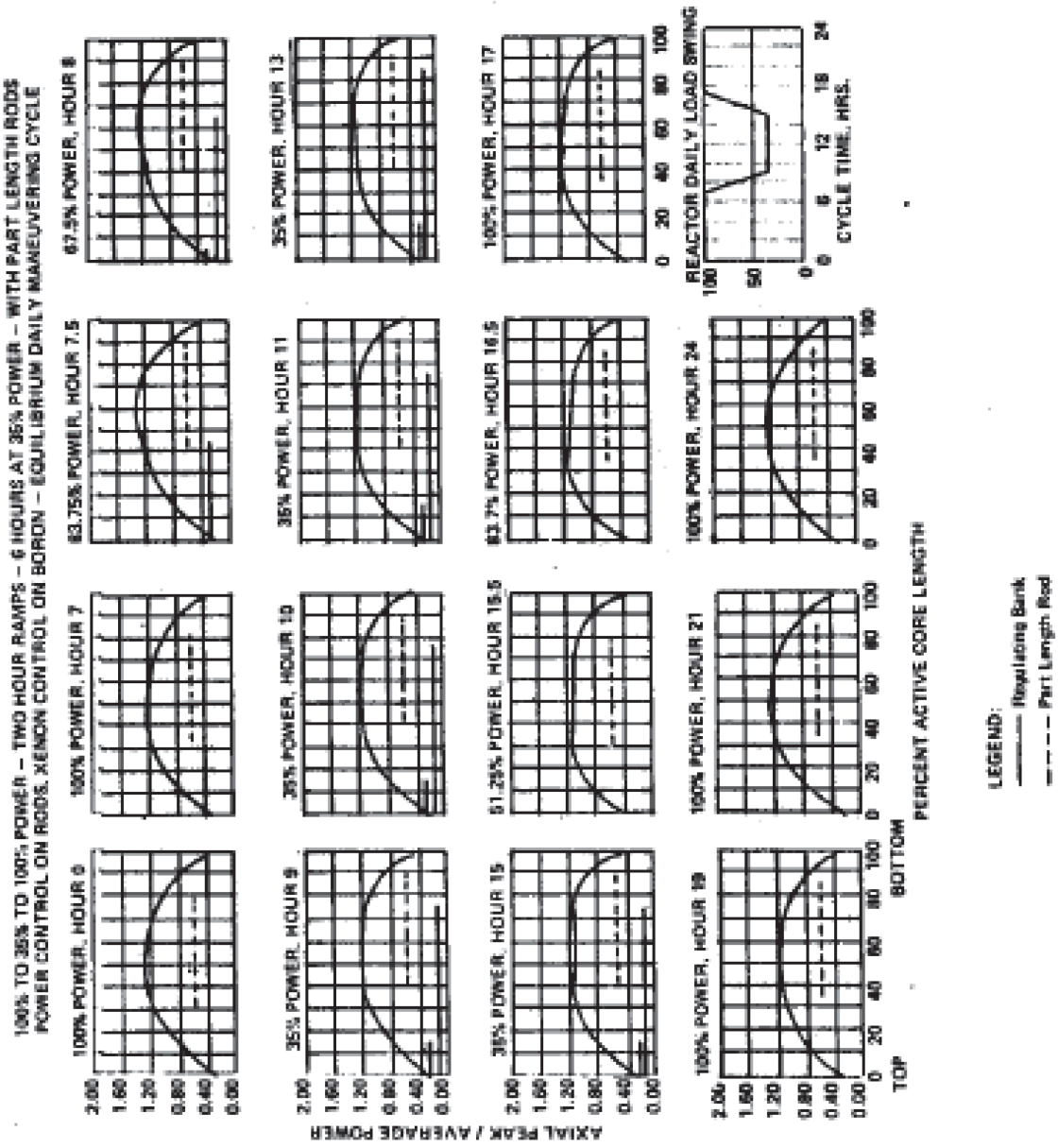

Note: As indicated in Sections 4.3.2.4.3.5 and 15.0.3.3, the part length CEAs have been removed from the St. Lucie Unit 2 design.

FLORIDA POWER & LIGHT COMPANY **ST. LUCIE PLANT UNIT 2**
DAILY REACTOR POWER MANEUVERING NEAR BEGINNING OF CYCLE (100% TO 35% TO 100% POWER) **FIGURE 4.3-25**

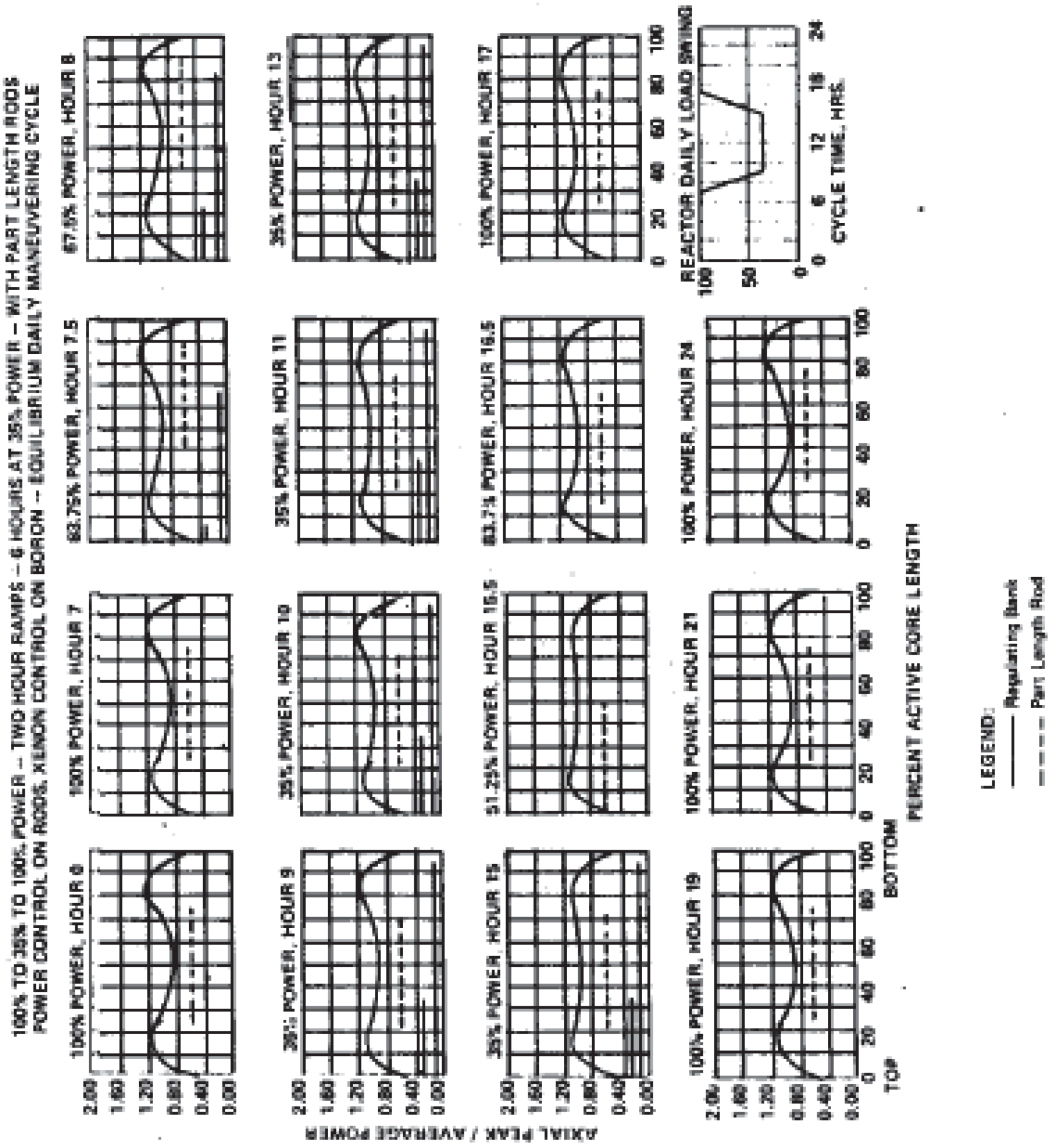

Note: As indicated in Sections 4.3.2.4.3.5 and 15.0.3.3, the part length CEAs have been removed from the St. Lucie Unit 2 design.

FLORIDA POWER & LIGHT COMPANY **ST. LUCIE PLANT UNIT 2**
DAILY REACTOR POWER MANEUVERING NEAR END OF CYCLE (100% TO 35% TO 100% POWER) **FIGURE 4.3-26**

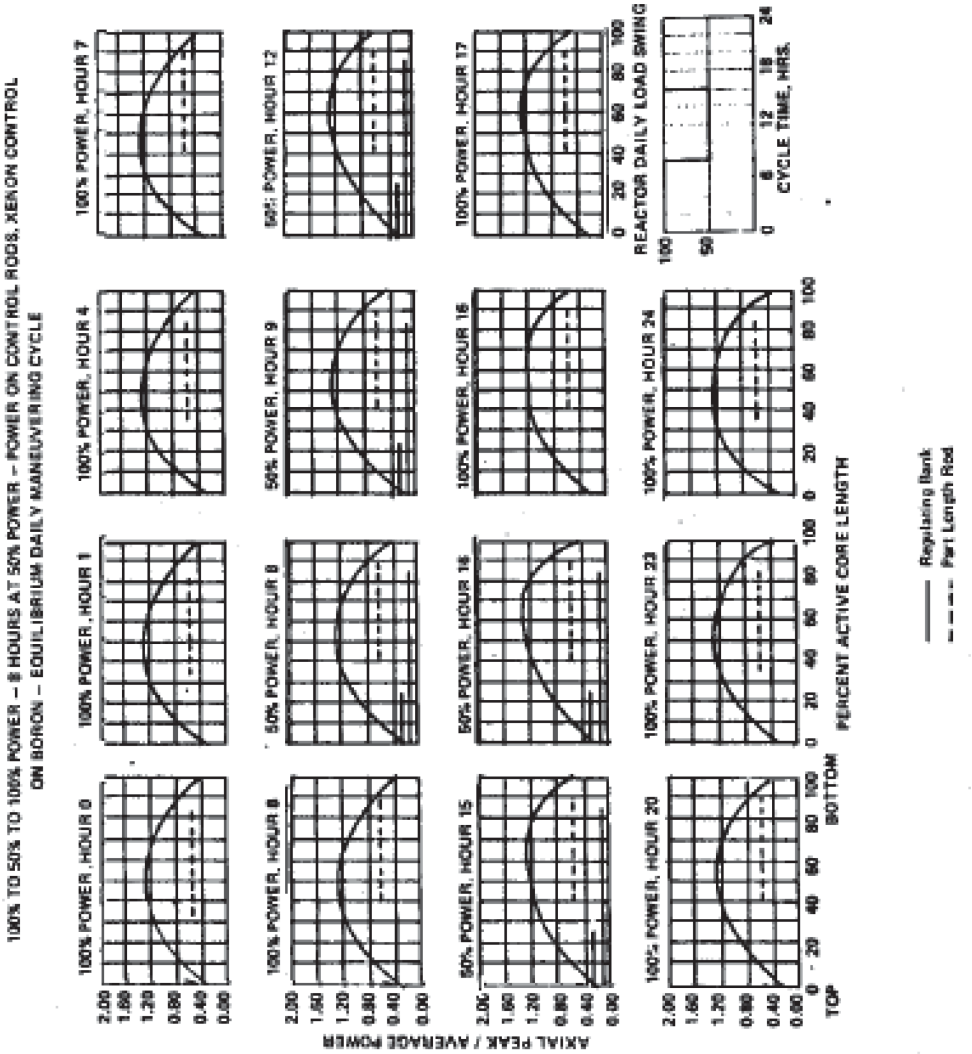

Note: As indicated in Sections 4.3.2.4.3.5 and 15.0.3.3, the part length CEAs have been removed from the St. Lucie Unit 2 design.

FLORIDA POWER & LIGHT COMPANY **ST. LUCIE PLANT UNIT 2**
DAILY REACTOR POWER MANEUVERING NEAR THE BEGINNING OF CYCLE (100% TO 50% TO 100% POWER **FIGURE 4.3-27**

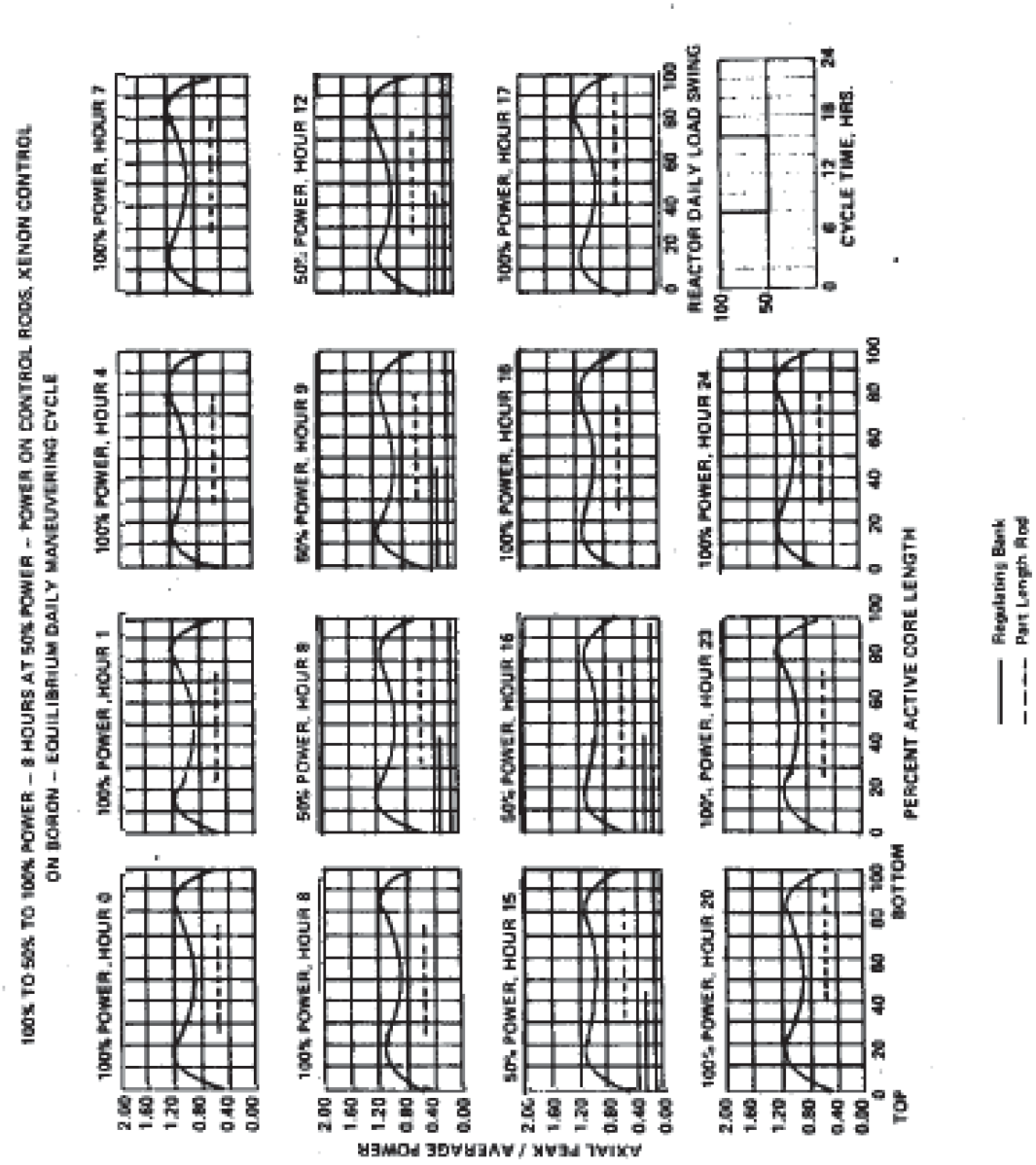

Note: As indicated in Sections 4.3.2.4.3.5 and 15.0.3.3, the part length CEAs have been removed from the St. Lucie Unit 2 design.

FLORIDA POWER & LIGHT COMPANY **ST. LUCIE PLANT UNIT 2**
DAILY REACTOR POWER MANEUVERING NEAR THE END OF CYCLE (100% TO 50% TO 100% POWER) **FIGURE 4.3-28**

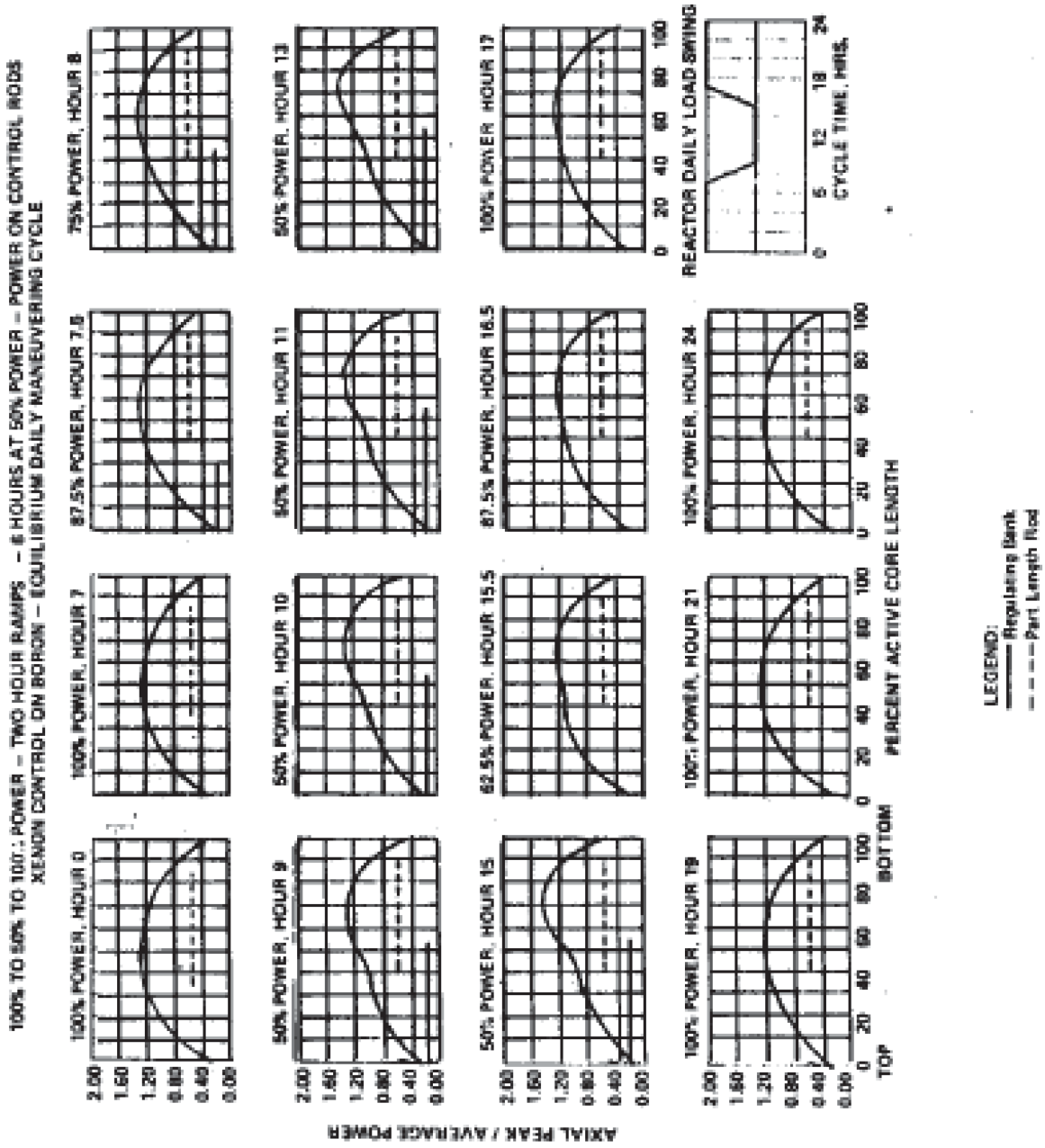

Note: As indicated in Sections 4.3.2.4.3.5 and 15.0.3.3, the part length CEAs have been removed from the St. Lucie Unit 2 design.

FLORIDA POWER & LIGHT COMPANY **ST. LUCIE PLANT UNIT 2**
DAILY REACTOR POWER MANEUVERING NEAR THE BEGINNING OF CYCLE (2-HOUR RAMPS) **FIGURE 4.3-29**

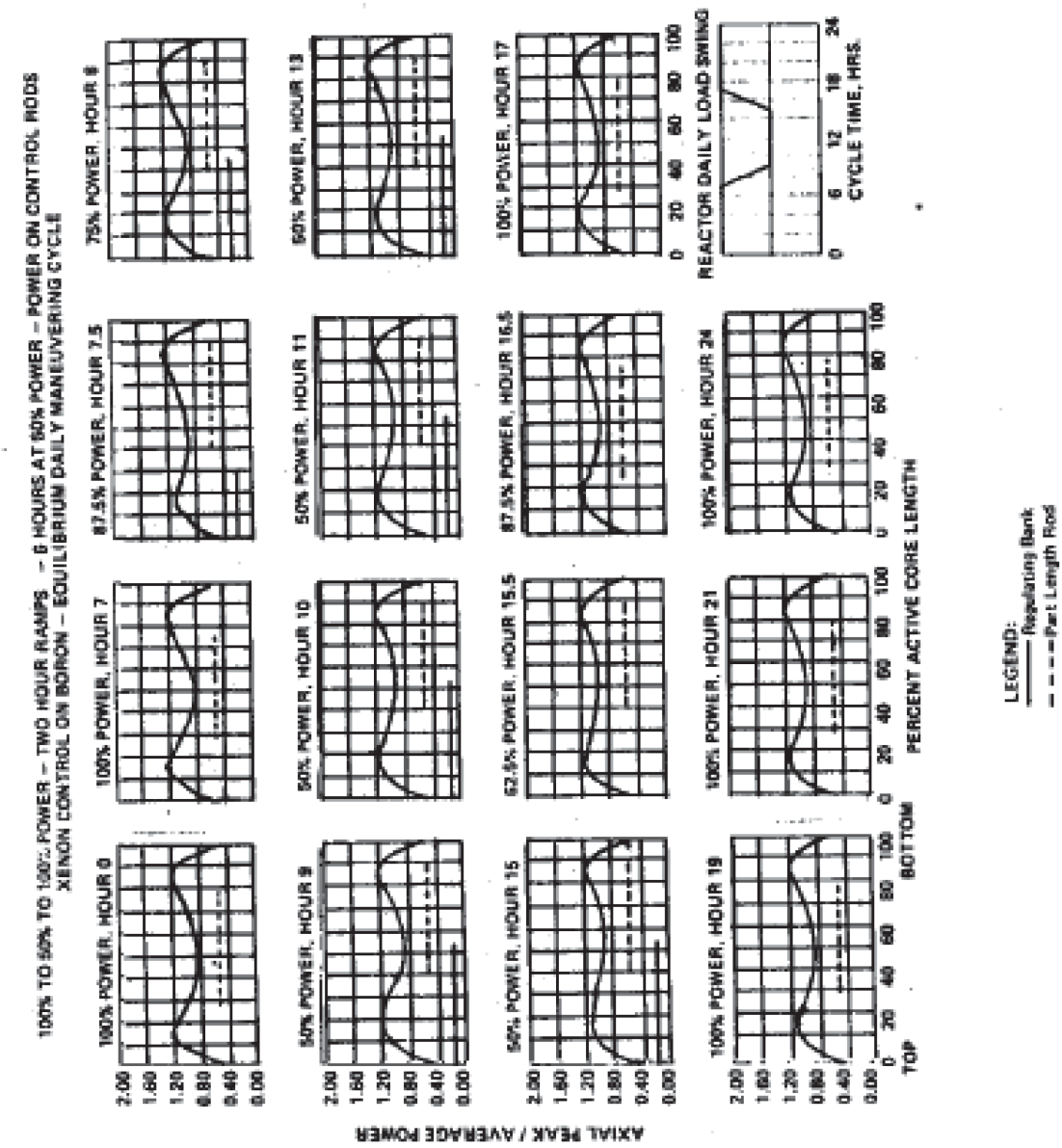

Note: As indicated in Sections 4.3.2.4.3.5 and 15.0.3.3, the part length CEAs have been removed from the St. Lucie Unit 2 design.

FLORIDA POWER & LIGHT COMPANY **ST. LUCIE PLANT UNIT 2**
DAILY REACTOR POWER MANEUVERING NEAR THE END OF CYCLE (2-HOUR RAMPS) **FIGURE 4.3-30**

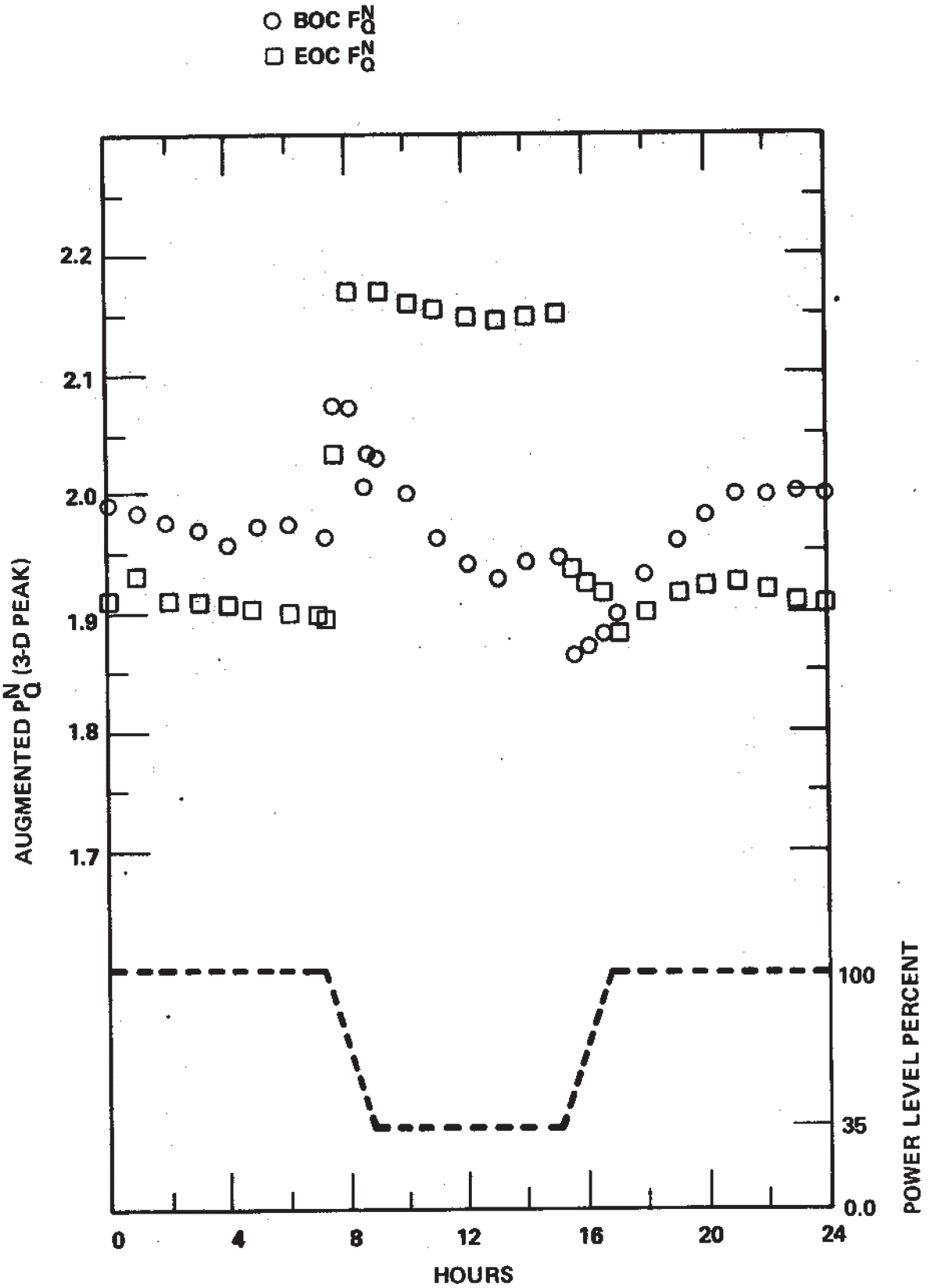

FLORIDA POWER & LIGHT COMPANY
ST. LUCIE PLANT UNIT 2

F_Q^N VS. TIME FOR A LOAD FOLLOWING TRANSIENT
SHEET 1 OF 3

FIGURE 4.3-31a

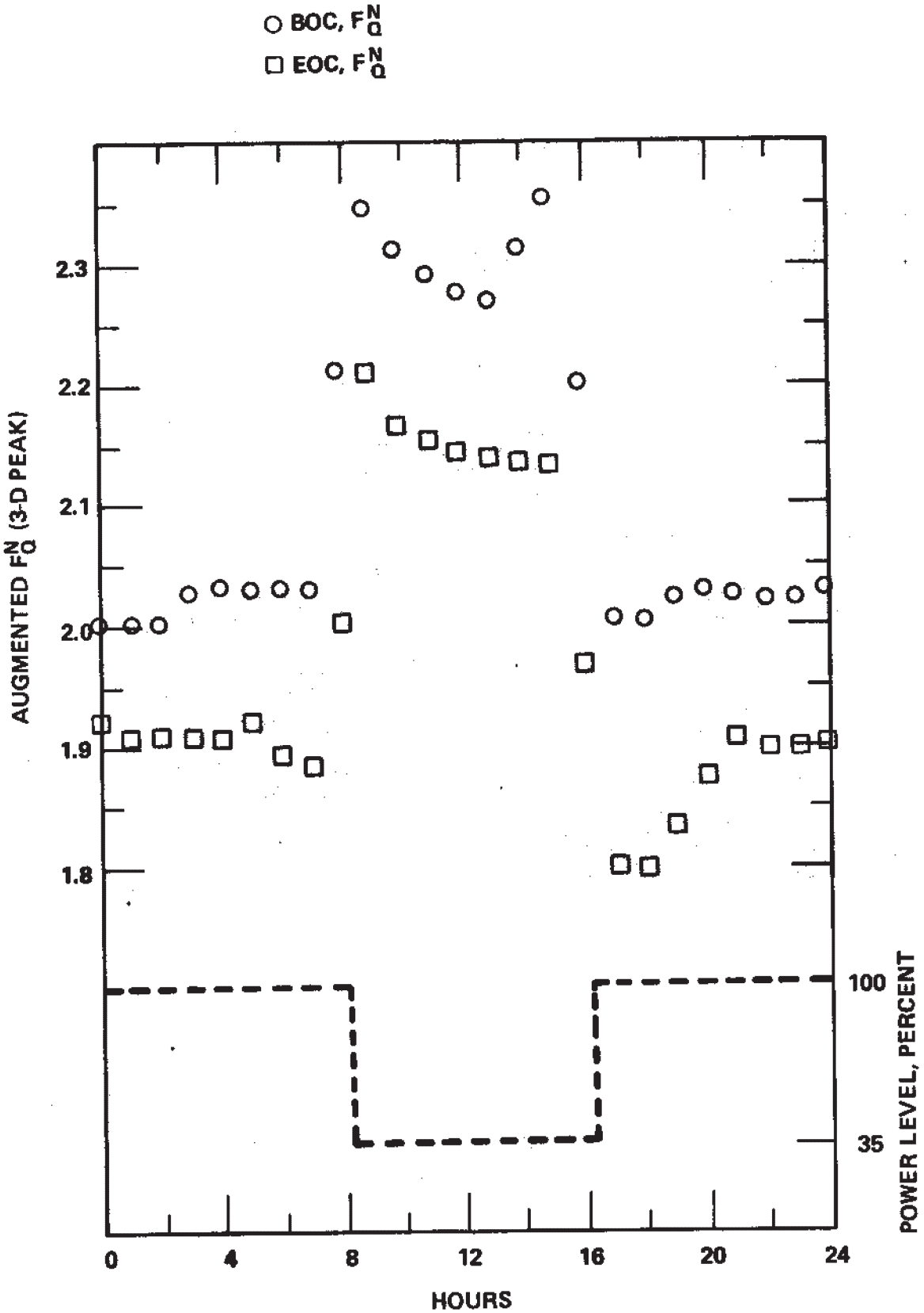

FLORIDA POWER & LIGHT COMPANY
ST. LUCIE PLANT UNIT 2

F_Q^N VS TIME FOR A LOAD FOLLOWING TRANSIENT
SHEET 2 OF 3

FIGURE 4.3-31b

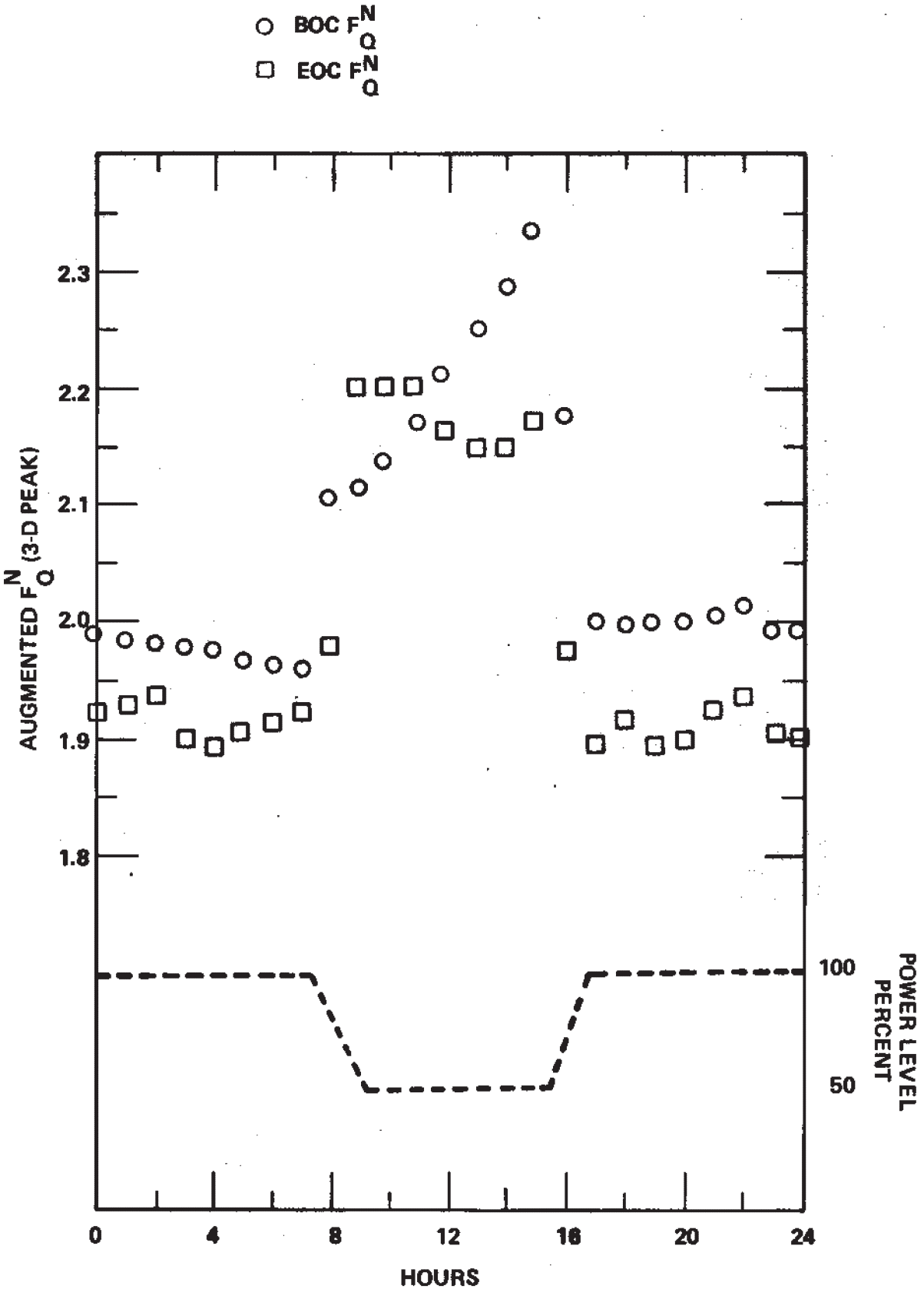

FLORIDA POWER & LIGHT COMPANY
ST. LUCIE PLANT UNIT 2

F_Q^N VS TIME FOR A LOAD FOLLOWING TRANSIENT
SHEET 3 OF 3

FIGURE 4.3-31c

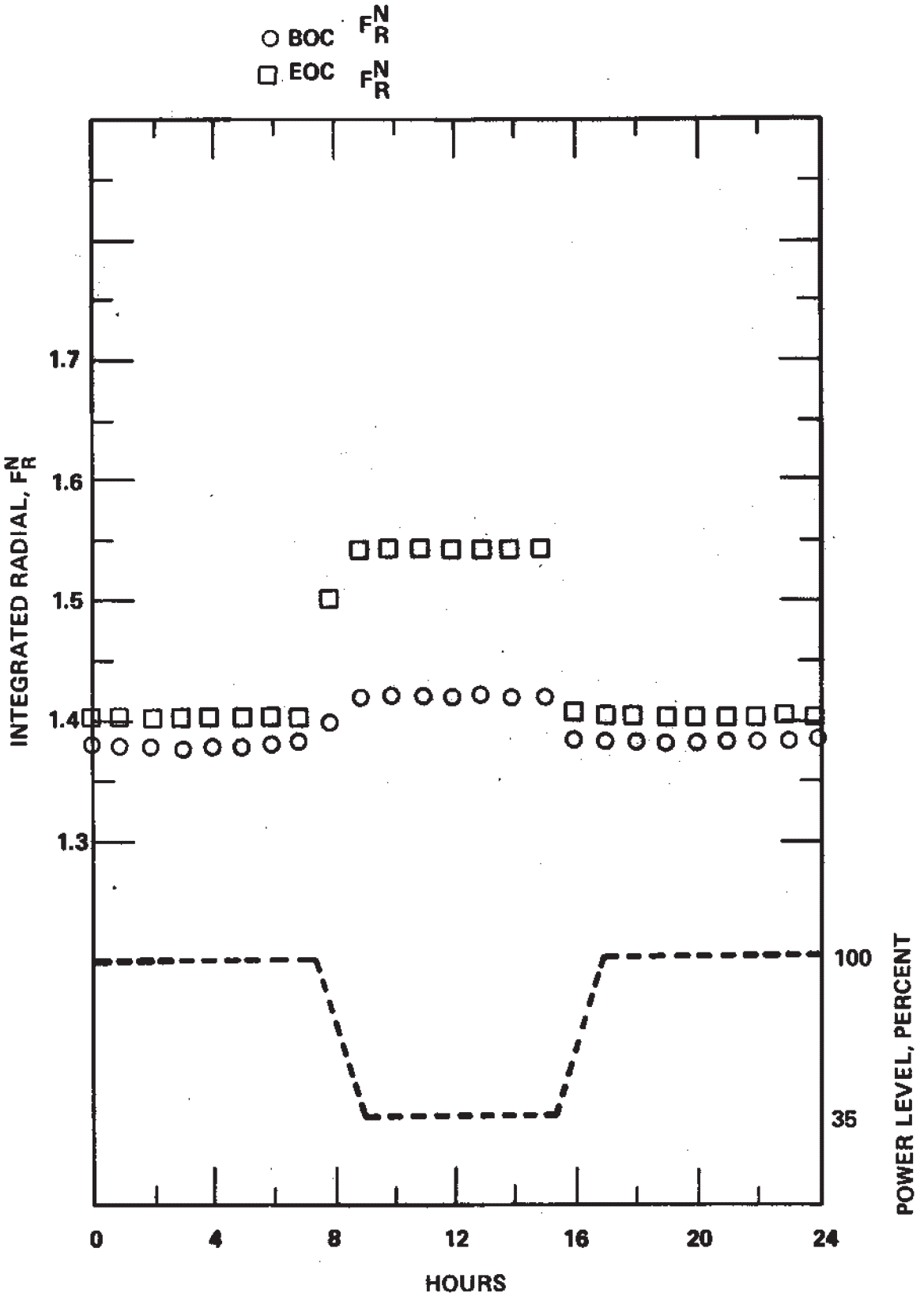

FLORIDA POWER & LIGHT COMPANY
ST. LUCIE PLANT UNIT 2

F_R^N VS TIME FOR A LOAD FOLLOWING TRANSIENT
SHEET 1 OF 3

FIGURE 4.3-32a

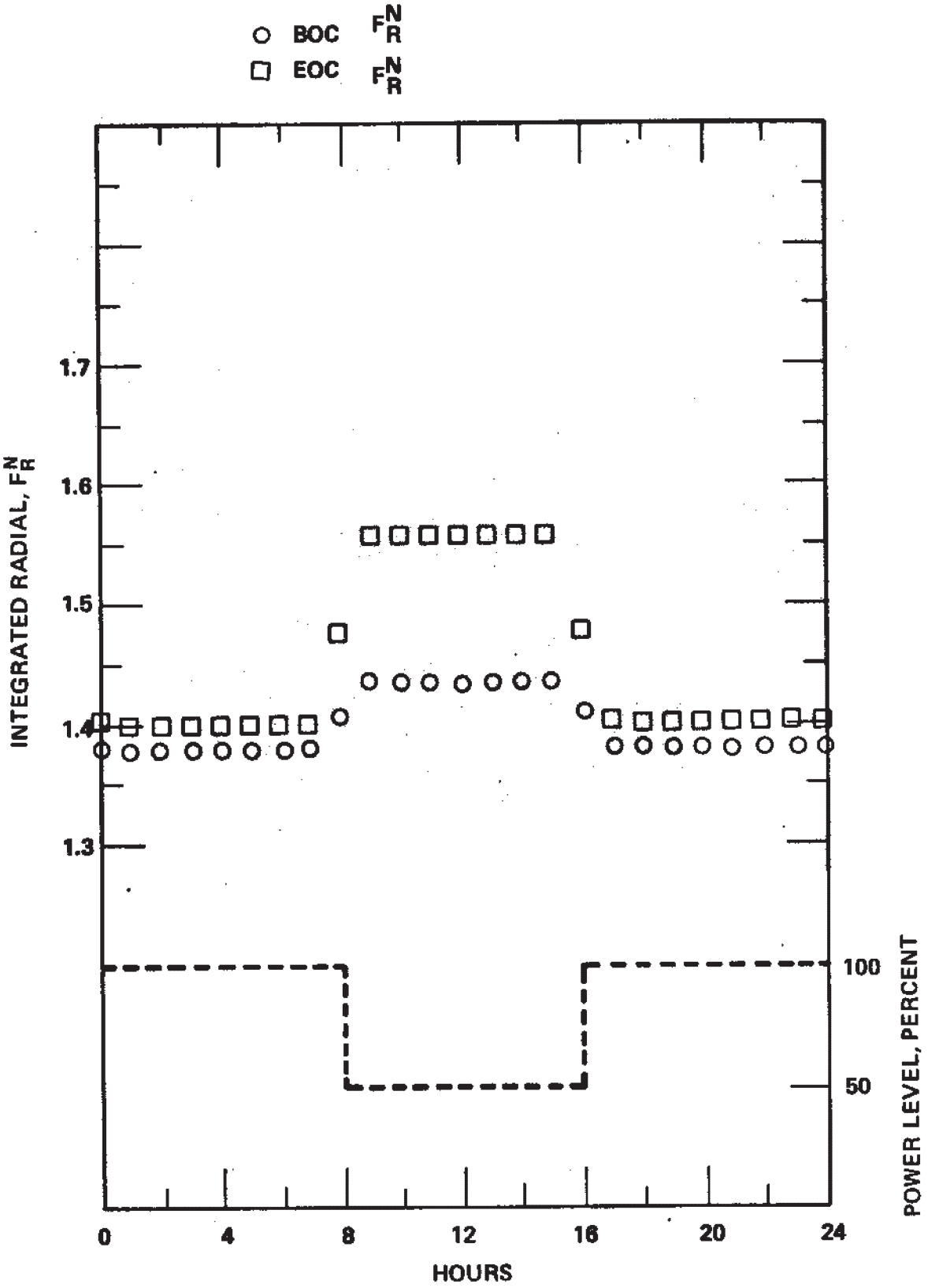

FLORIDA POWER & LIGHT COMPANY
ST. LUCIE PLANT UNIT 2

F_R^N VS TIME FOR A LOAD FOLLOWING TRANSIENT
SHEET 2 OF 3

FIGURE 4.3-32b

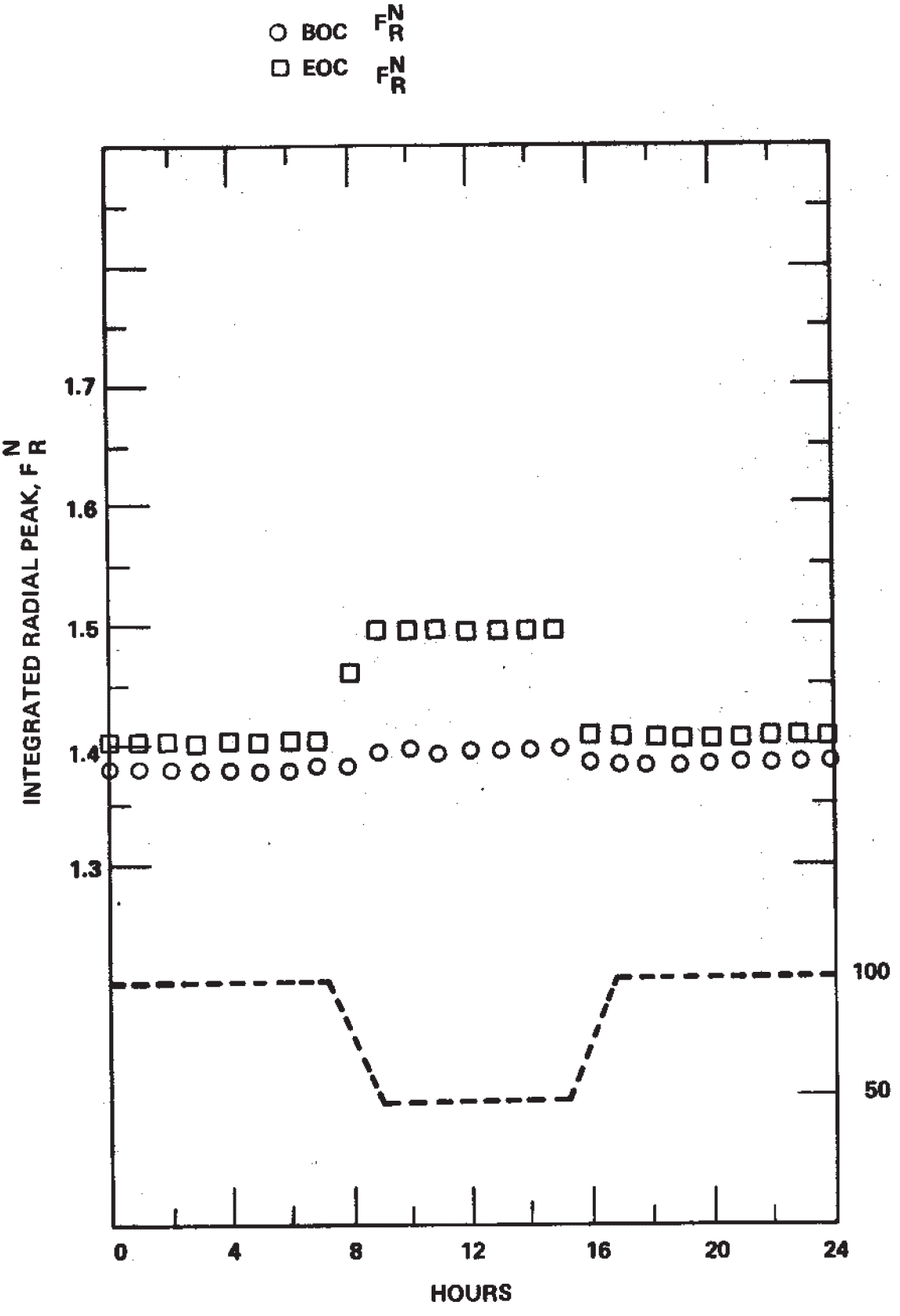

FLORIDA POWER & LIGHT COMPANY
ST. LUCIE PLANT UNIT 2

F_R^N VS TIME FOR A LOAD FOLLOWING TRANSIENT
SHEET 3 OF 3

FIGURE 4.3-32c

.953	.933	.942	.950	.950	.945	.945	.947
.933	.950	.968	.984	.987	.979	.972	.968
.942	.968	1.003	1.039	1.045	1.021	.999	.990
.950	.984	1.039			1.063	1.024	1.009
.950	.987	1.045			1.076	1.039	1.027
.945	.979	1.021	1.063	1.076	1.060	1.048	1.049
.945	.972	.999	1.024	1.039	1.048	1.068	1.094
.947	.968	.990	1.009	1.027	1.049	1.094	

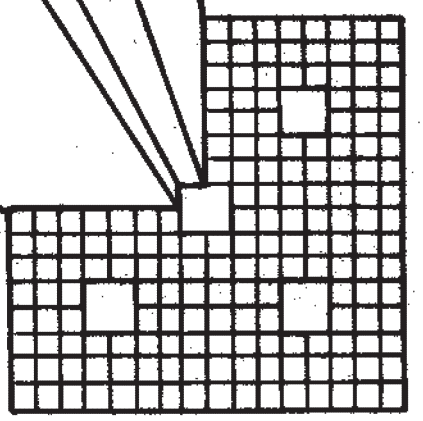

FLORIDA POWER & LIGHT COMPANY
ST. LUCIE PLANT UNIT 2

NORMALIZED POWER DISTRIBUTION WITHIN AN UNSHIMMED ASSEMBLY USED IN DNB ANALYSES

FIGURE 4.3-33

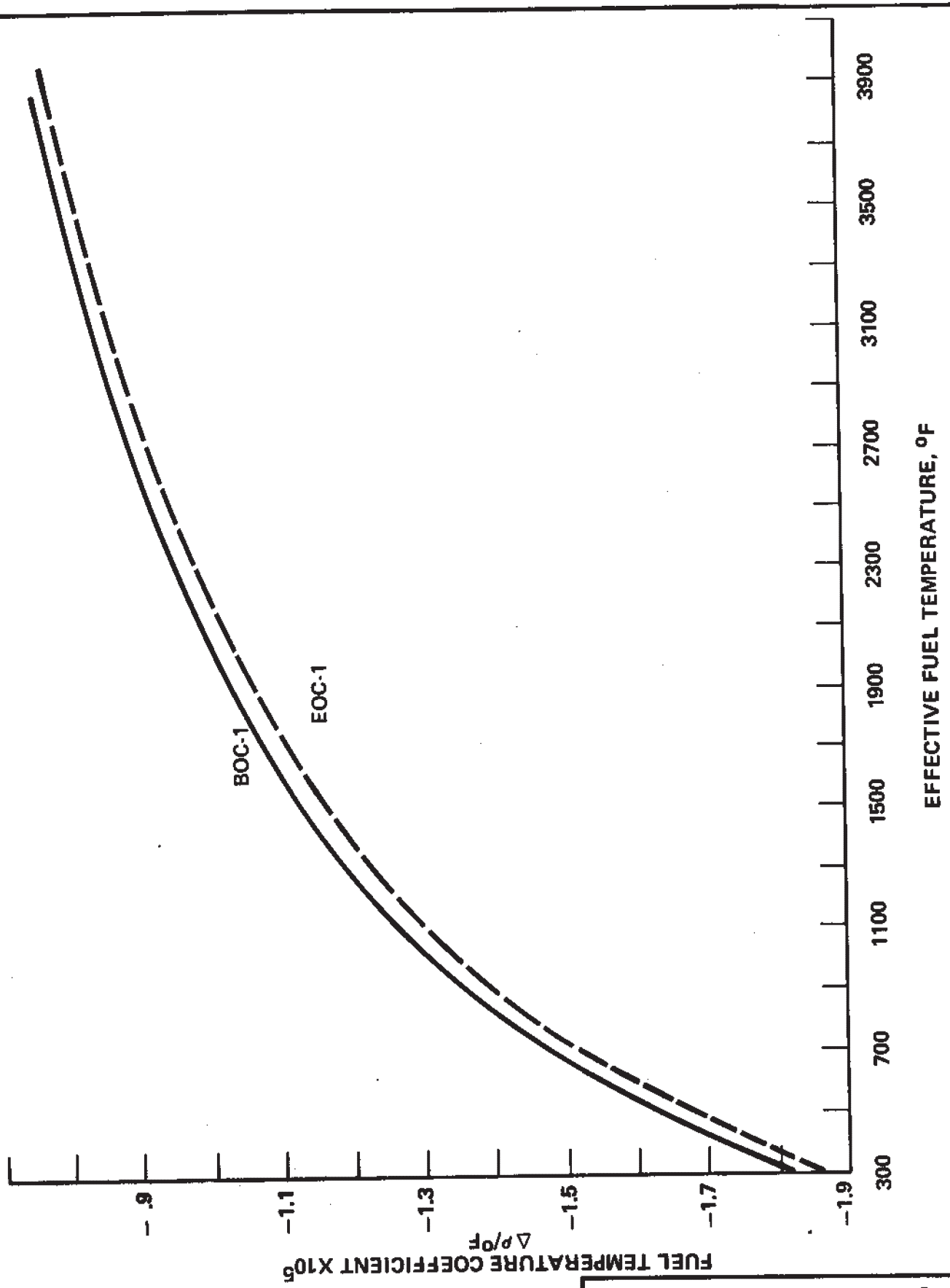

FLORIDA POWER & LIGHT COMPANY
ST. LUCIE PLANT UNIT 2

FUEL TEMPERATURE COEFFICIENT
VS EFFECTIVE FUEL TEMPERATURE
FIGURE 4.3-34

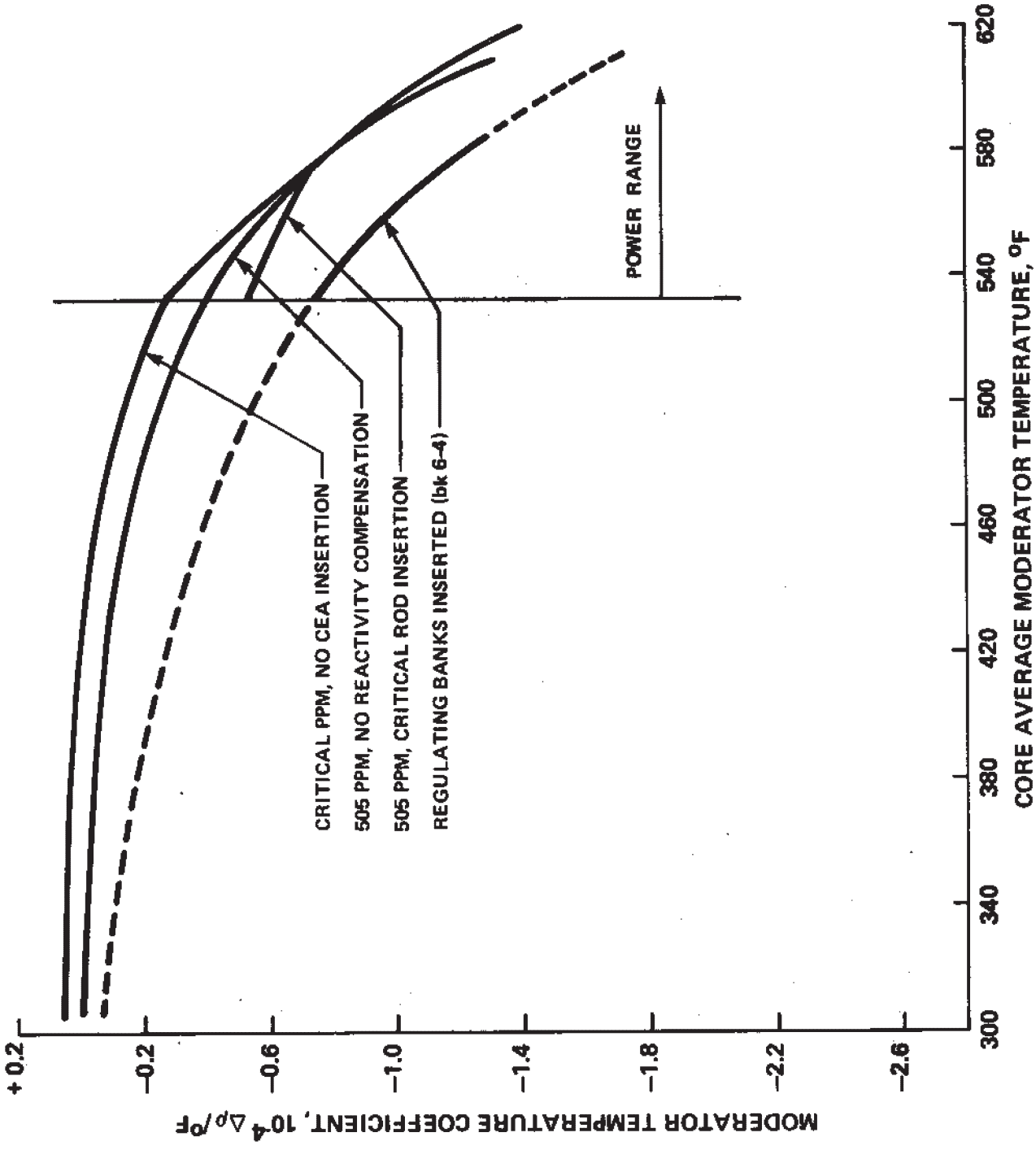

FLORIDA POWER & LIGHT COMPANY
ST. LUCIE PLANT UNIT 2

MODERATOR TEMPERATURE COEFFICIENT VS MODERATOR TEMPERATURE AT BOC-1

FIGURE 4.3-35

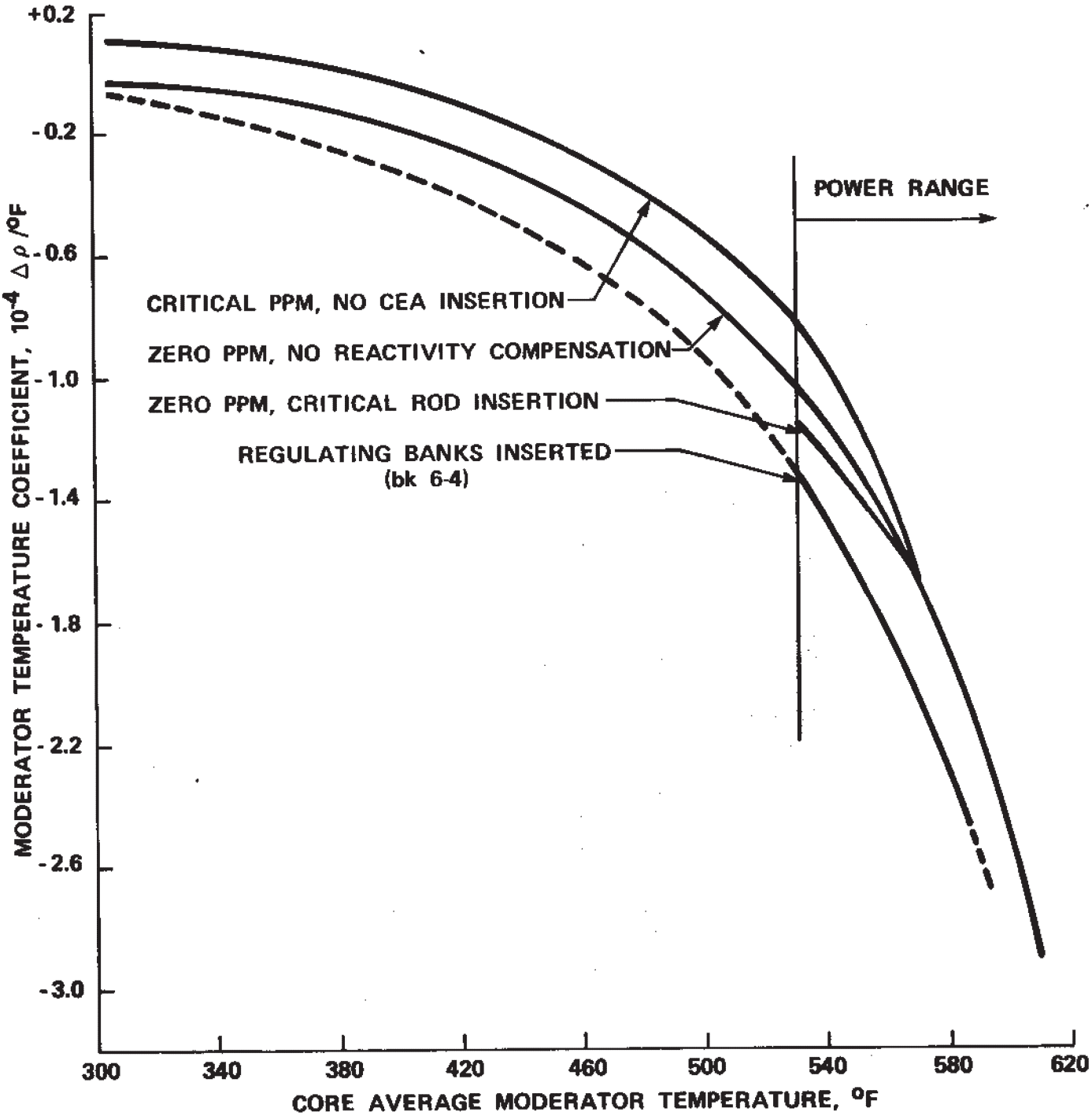

FLORIDA POWER & LIGHT COMPANY
ST. LUCIE PLANT UNIT 2

MODERATOR TEMPERATURE COEFFICIENT VS MODERATOR TEMPERATURE AT EOC-1

FIGURE 4.3-36

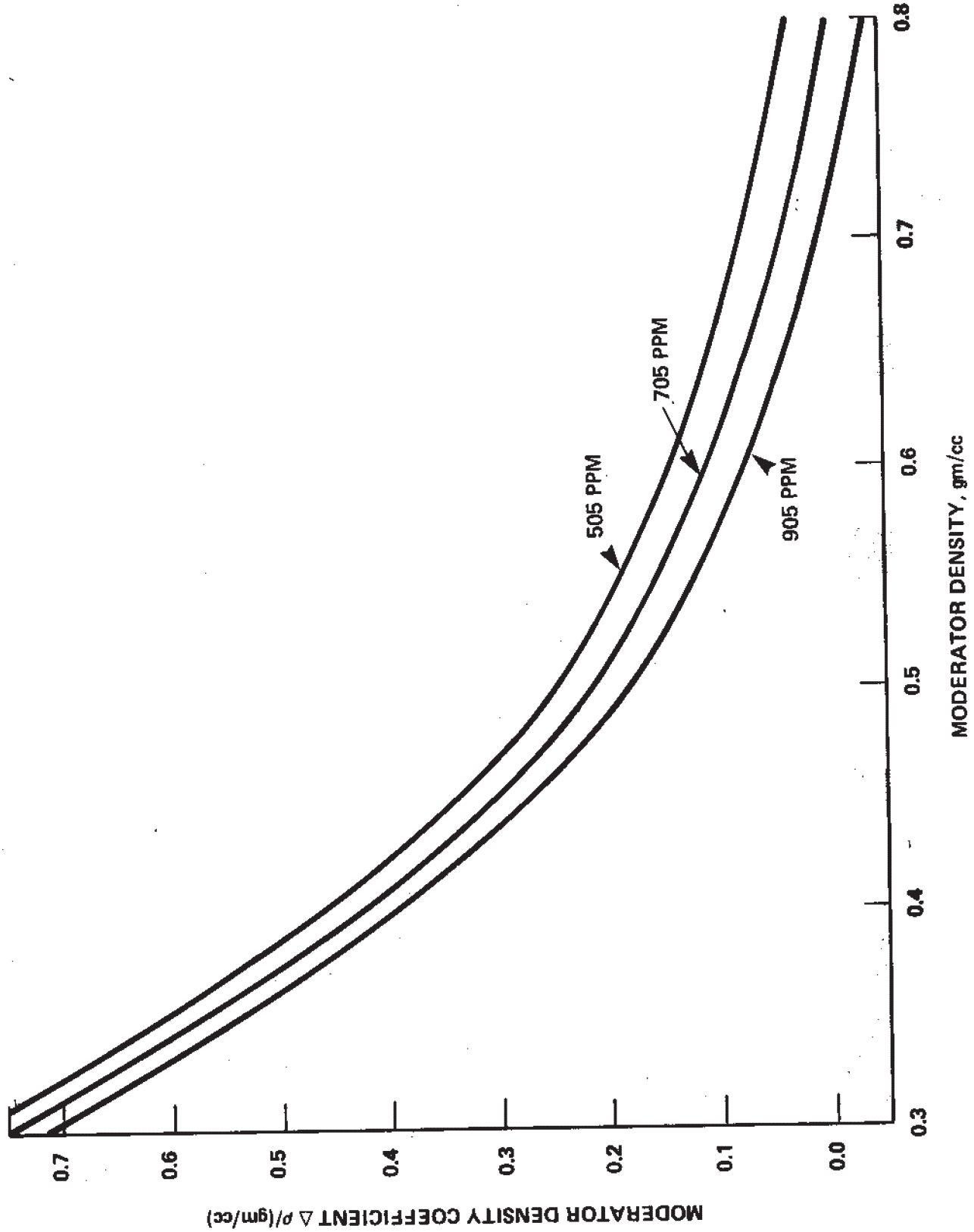

FLORIDA POWER & LIGHT COMPANY
ST. LUCIE PLANT UNIT 2

MODERATOR DENSITY COEFFICIENT
VS MODERATOR DENSITY
FIGURE 4.3-37

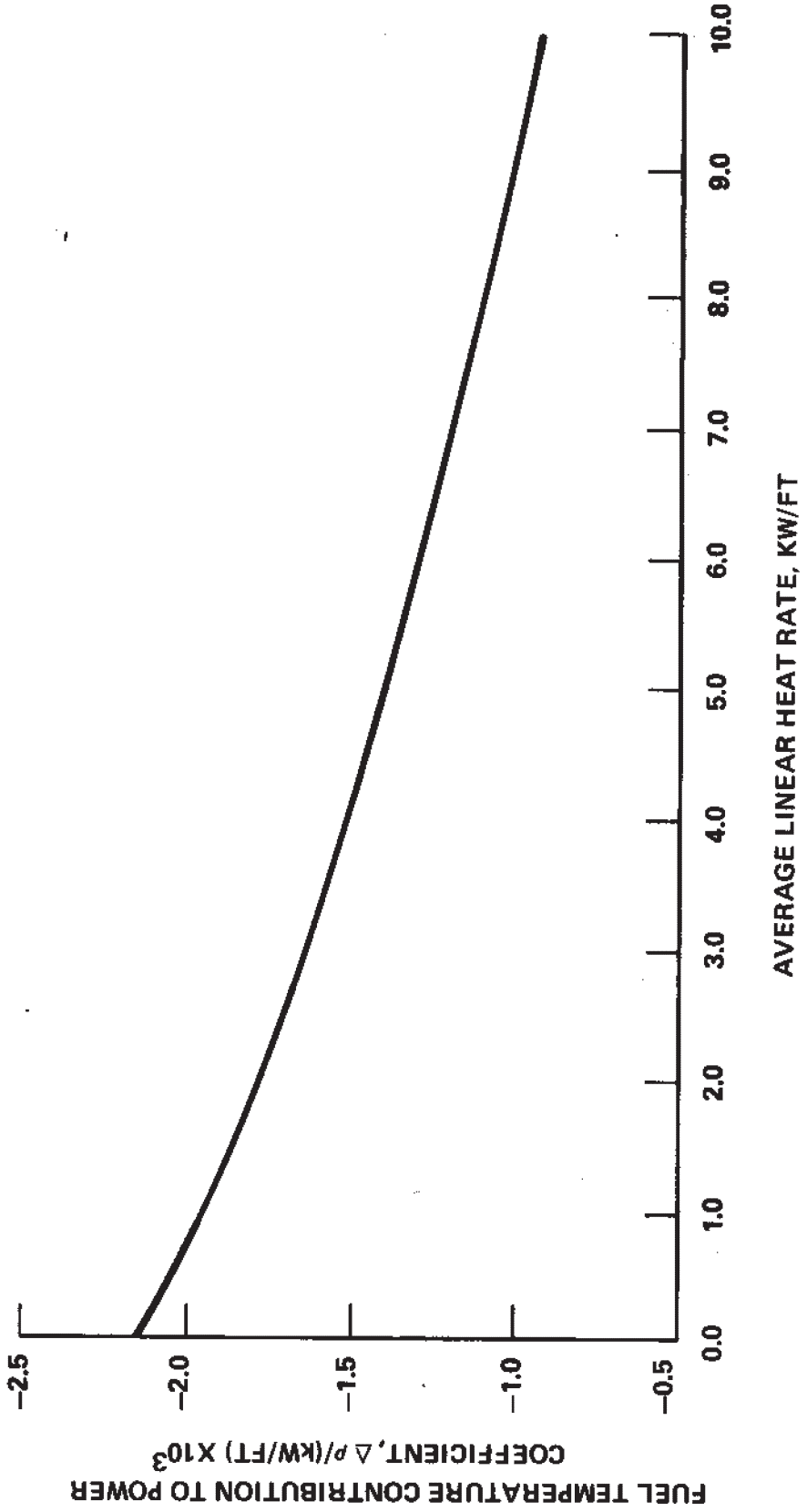

FLORIDA POWER & LIGHT COMPANY
ST. LUCIE PLANT UNIT 2

FUEL TEMPERATURE CONTRIBUTION TO POWER COEFFICIENT VS POWER AT EOC-1

FIGURE 4.3-38

6 - LEAD REGULATING BANK
5 - SECOND REGULATING BANK
4 - THIRD REGULATING BANK
3 - FOURTH REGULATING BANK
2 - FIFTH REGULATING BANK
1 - LAST REGULATING BANK
S_B - SHUTDOWN BANK B
S_A - SHUTDOWN BANK A

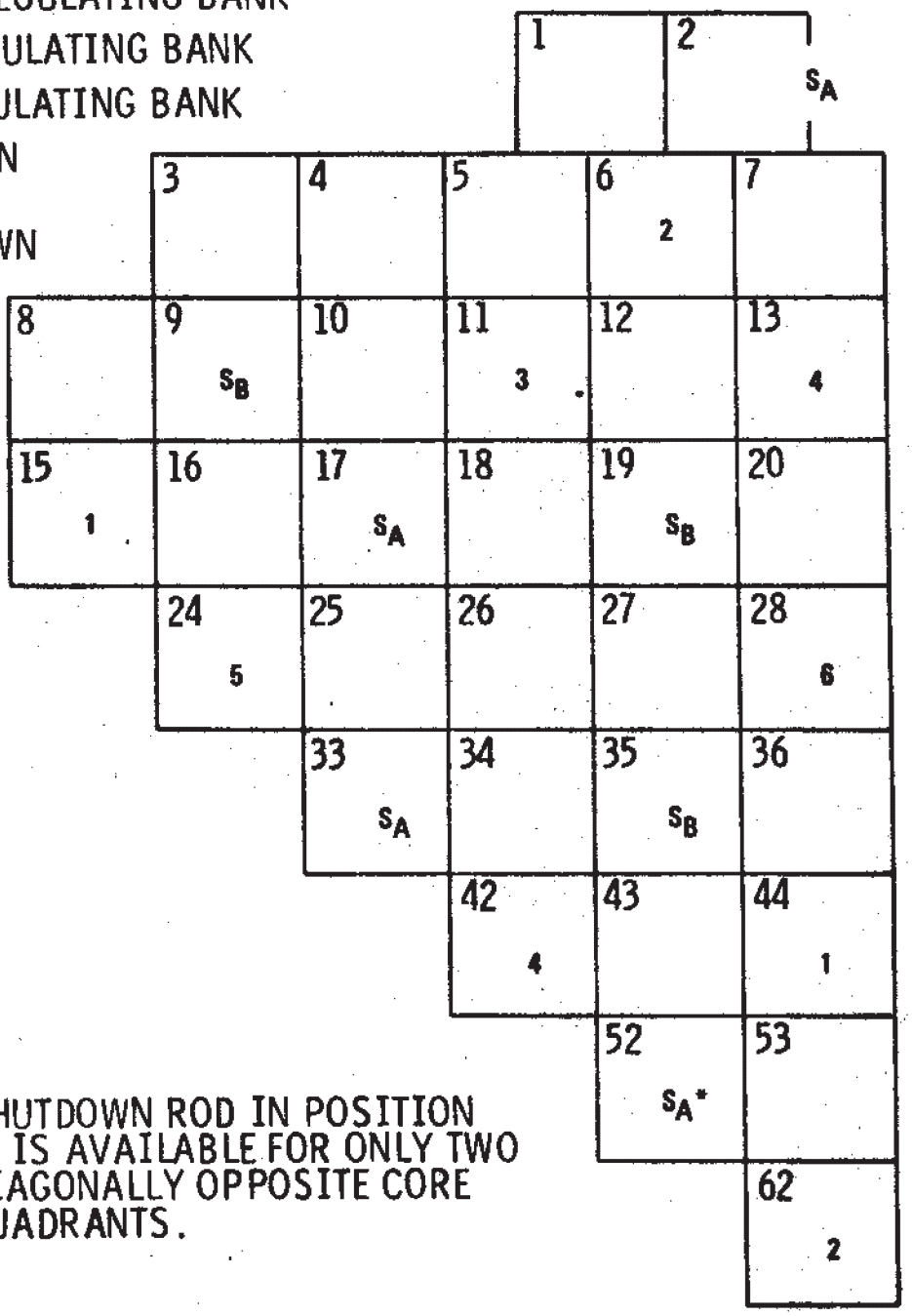

*SHUTDOWN ROD IN POSITION 52 IS AVAILABLE FOR ONLY TWO DIAGONALLY OPPOSITE CORE QUADRANTS.

FLORIDA POWER & LIGHT COMPANY
ST. LUCIE PLANT UNIT 2

CEA BANK IDENTIFICATION

FIGURE 4.3-39

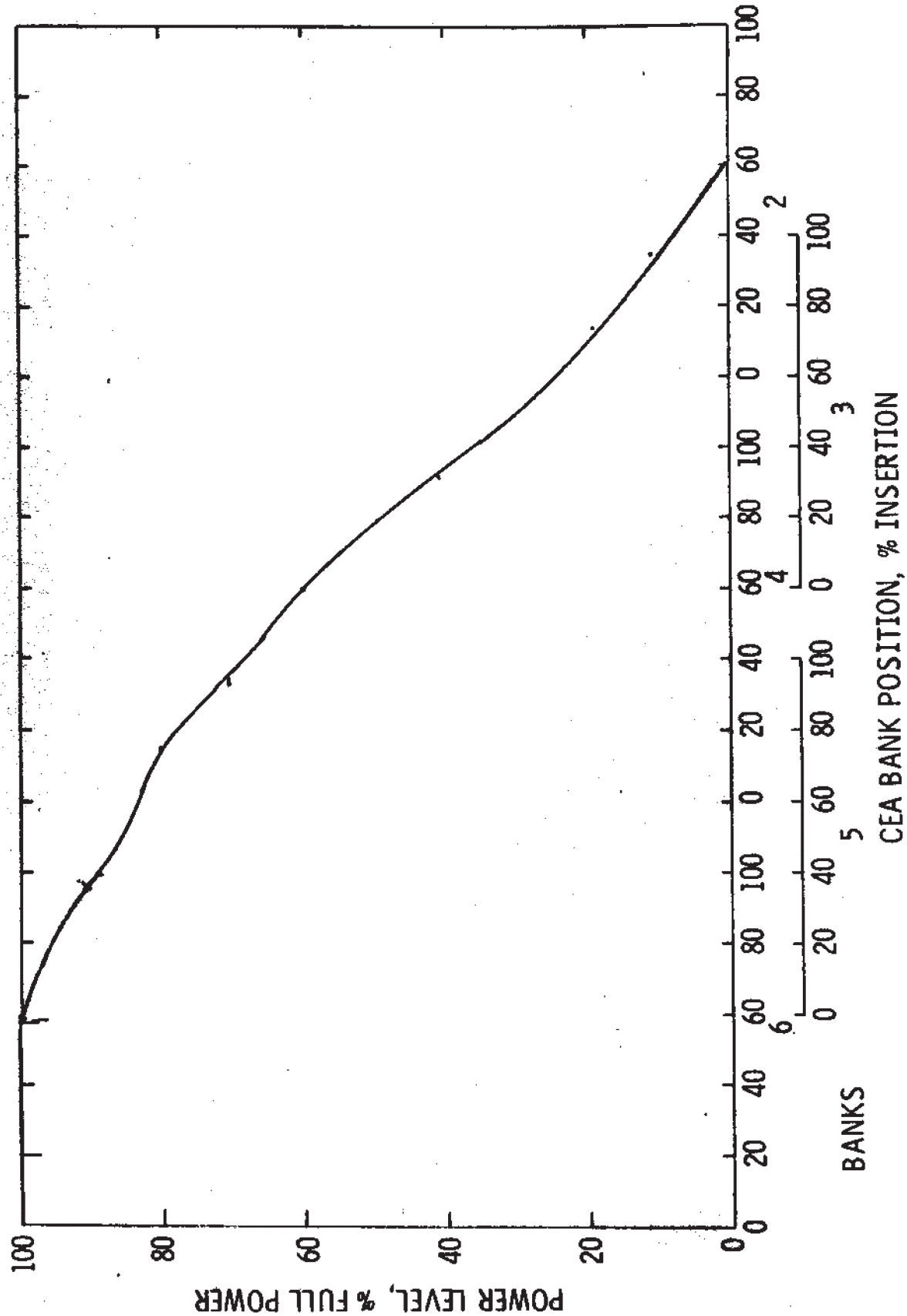

FLORIDA POWER & LIGHT COMPANY
ST. LUCIE PLANT UNIT 2

TYPICAL POWER DEPENDENT
CEA INSERTION LIMIT
FIGURE 4.3-40

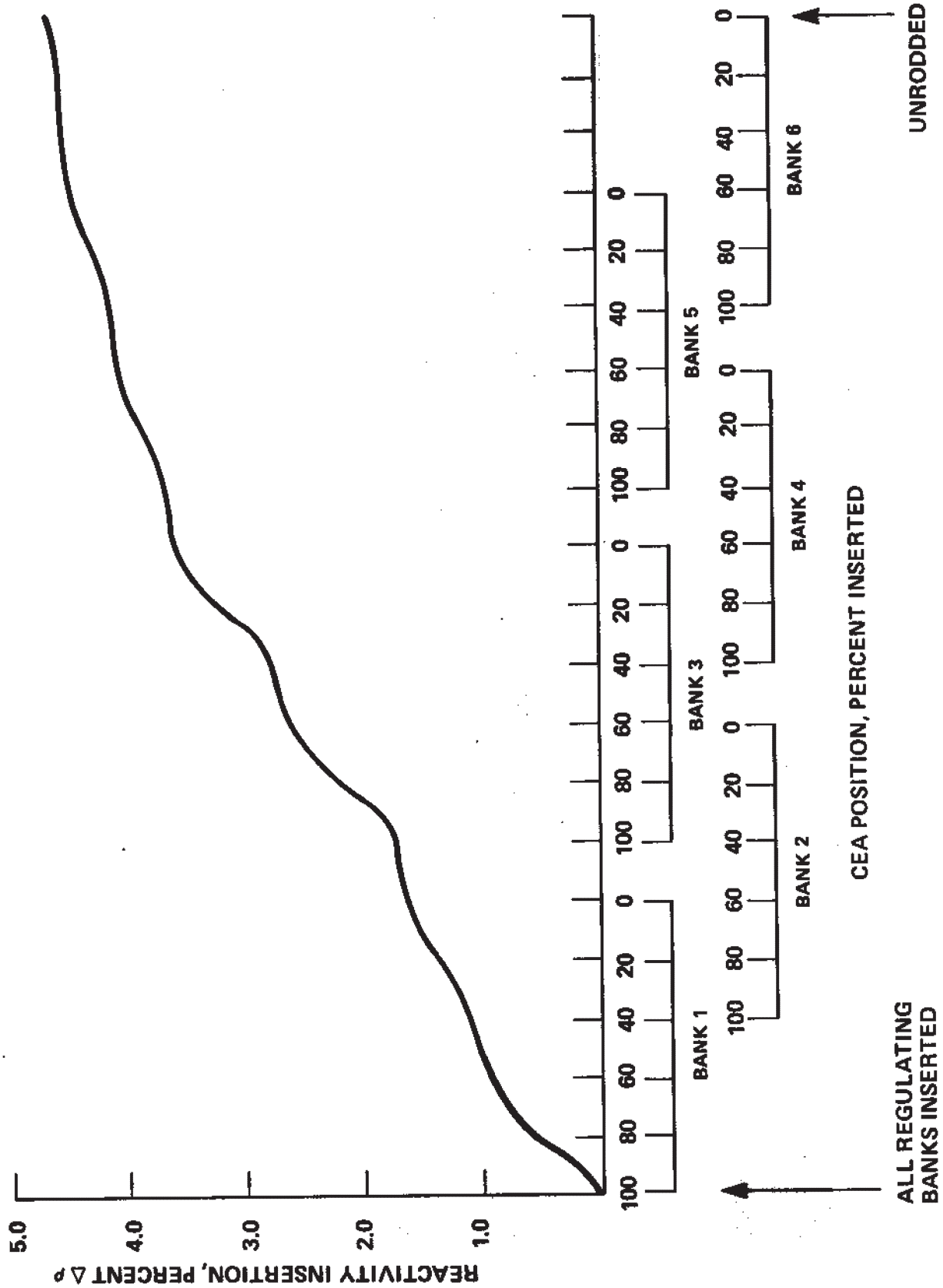

FLORIDA POWER & LIGHT COMPANY
ST. LUCIE PLANT UNIT 2

INTEGRAL WORTH VS WITHDRAWAL AT ZERO POWER, EOC-1
FIGURE 4.3-41

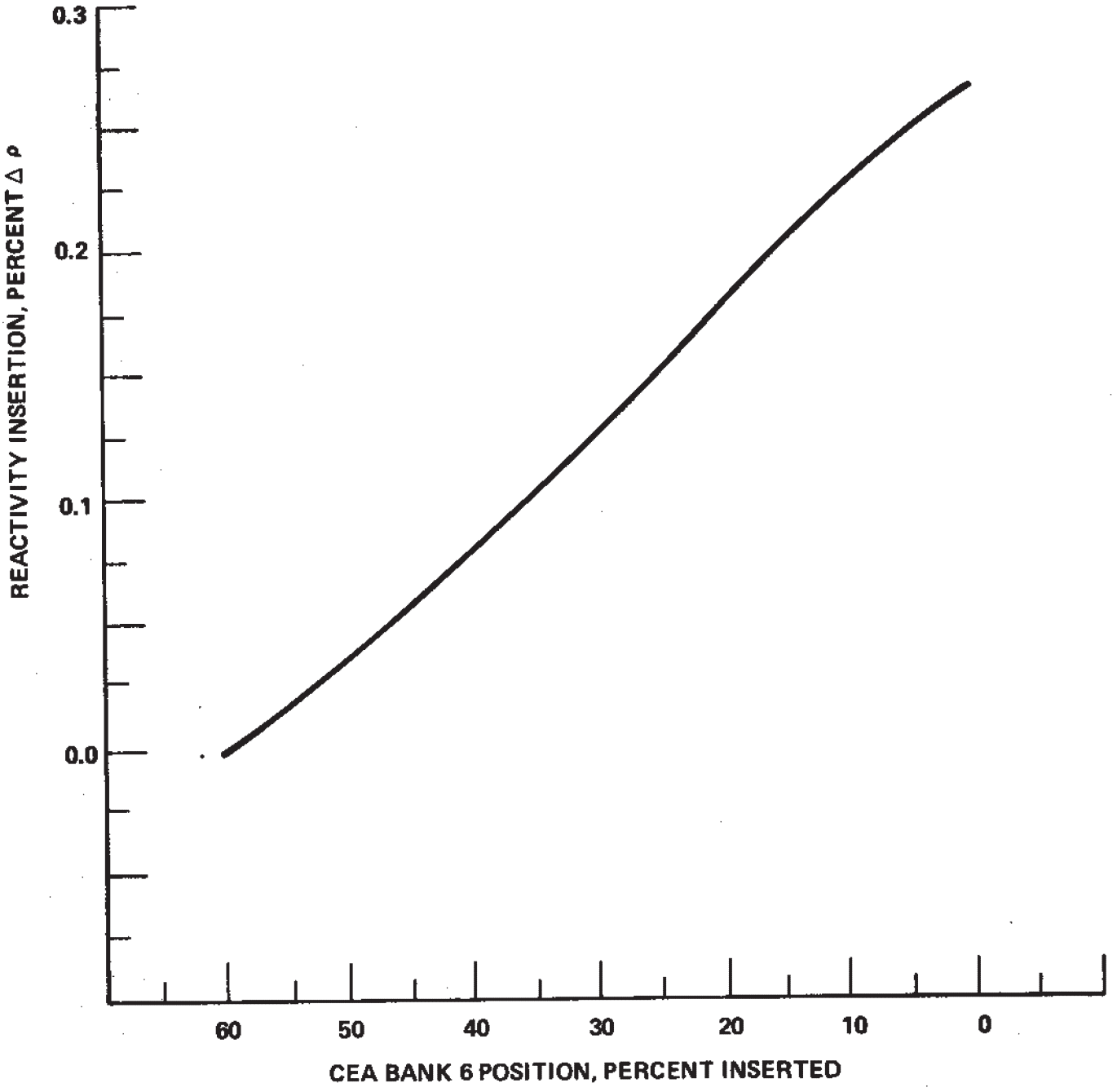

FLORIDA POWER & LIGHT COMPANY
ST. LUCIE PLANT UNIT 2

INTEGRAL BANK WORTH VS WITHDRAWAL FROM BANK – 6 INSERTED 60%, EQUILIBRIUM XENON, EOC-1

FIGURE 4.3-42

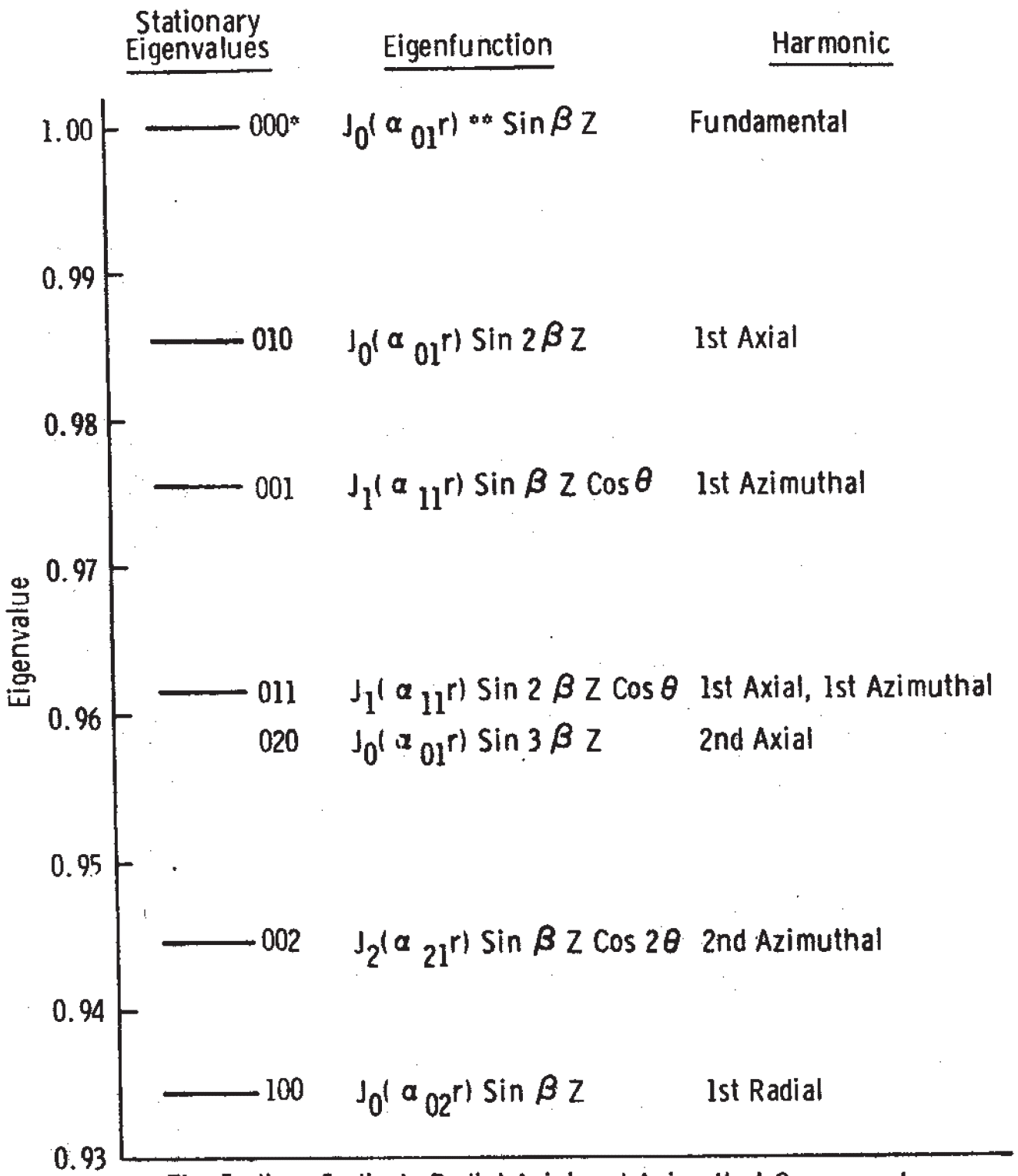

* The Indices Indicate Radial Axial and Azimuthal Components of the Separable Modes in that Order

** $_{ij}$ Indicates the jth Zero of the ith Bessel Function

FLORIDA POWER & LIGHT COMPANY
ST. LUCIE PLANT UNIT 2

REACTIVITY DIFFERENCE BETWEEN FUNDAMENTAL AND EXCITED STATES OF A BARE CYLINDRICAL REACTOR

FIGURE 4.3-43

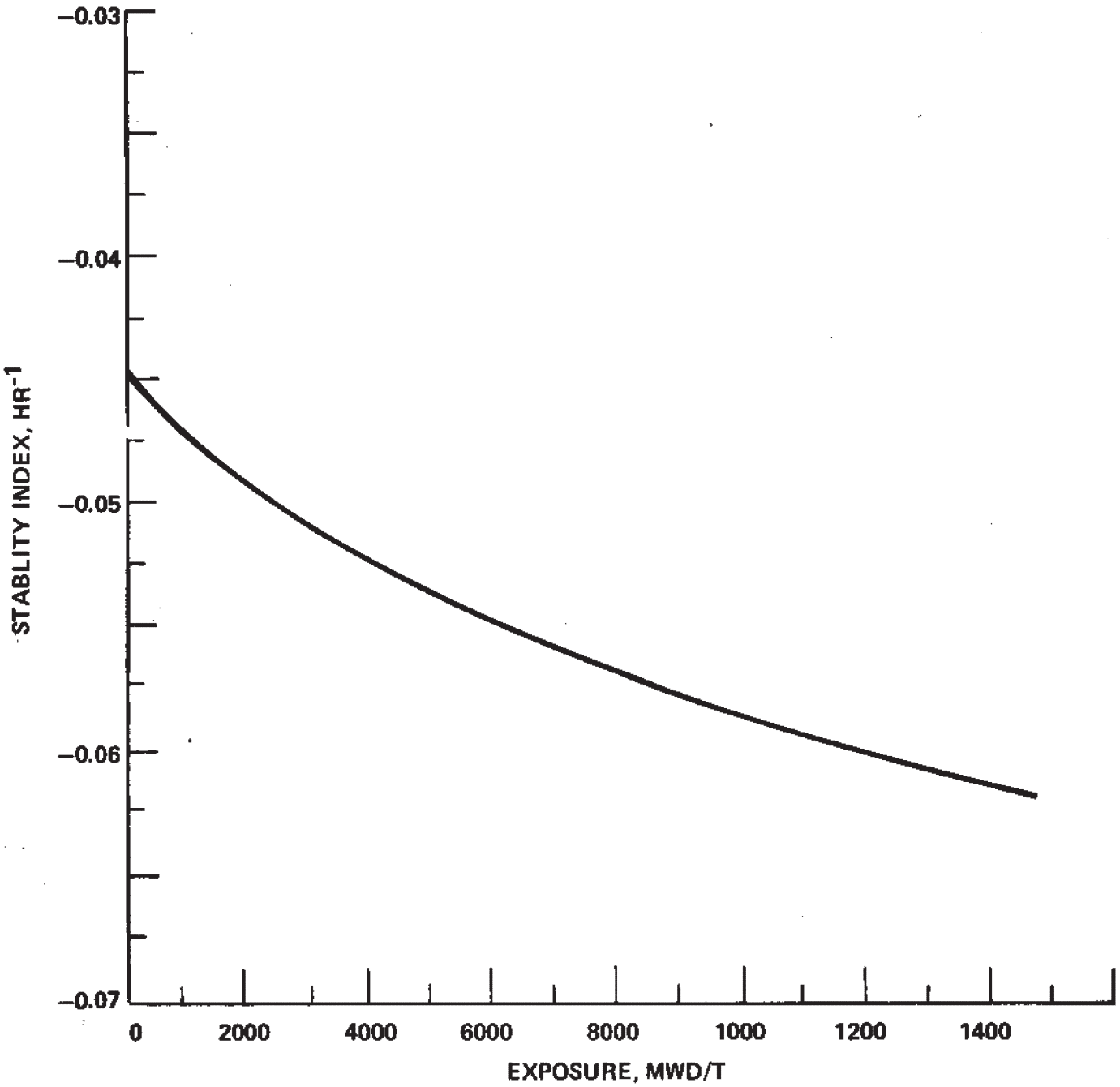

FLORIDA POWER & LIGHT COMPANY
ST. LUCIE PLANT UNIT 2

EXPECTED VARIATION OF THE AZIMUTHAL STABILITY INDEX WITH EXPOSURE

FIGURE 4.3-44

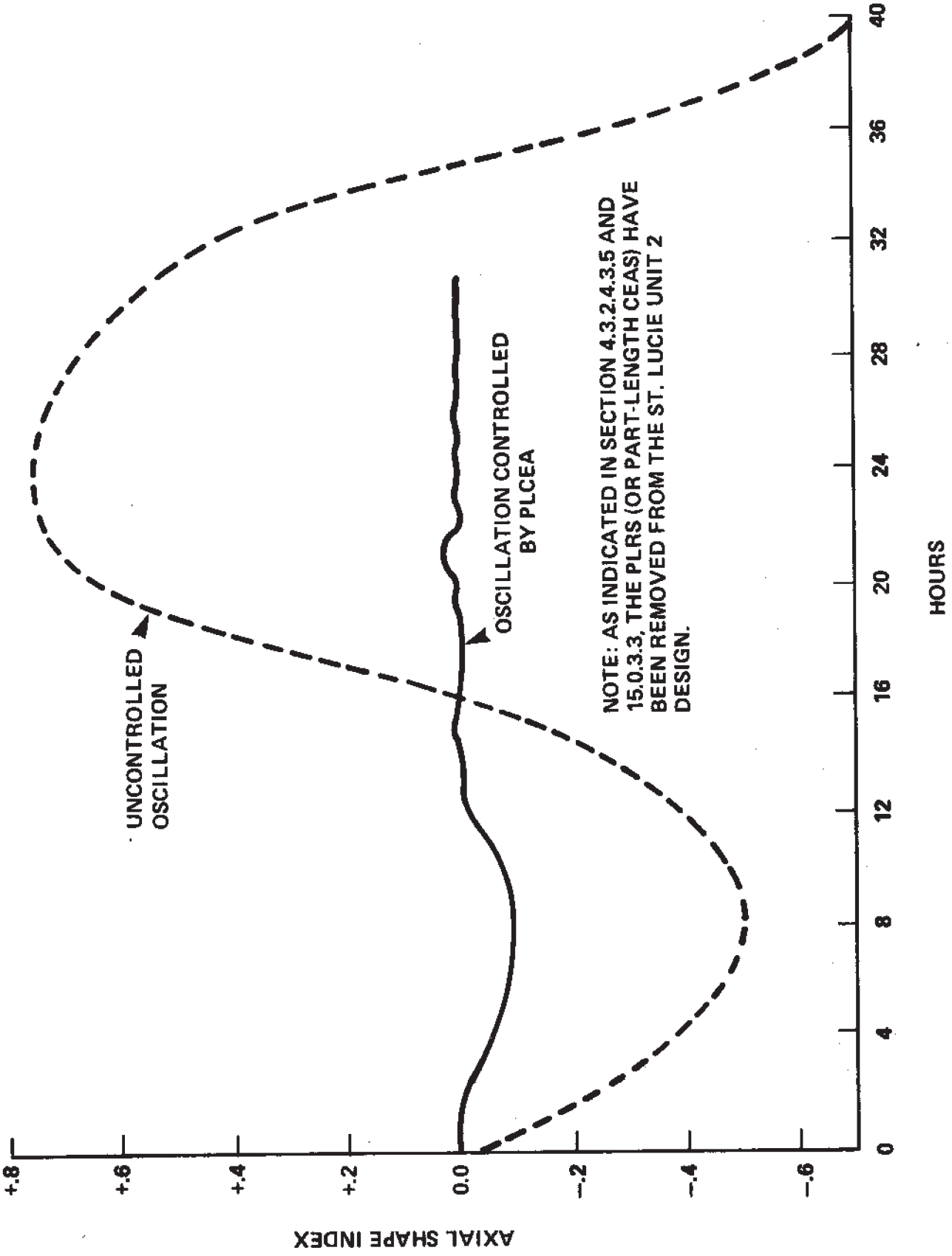

FLORIDA POWER & LIGHT COMPANY
ST. LUCIE PLANT UNIT 2

AXIAL STABILITY CONTROL USING PLCEAS

FIGURE 4.3-45

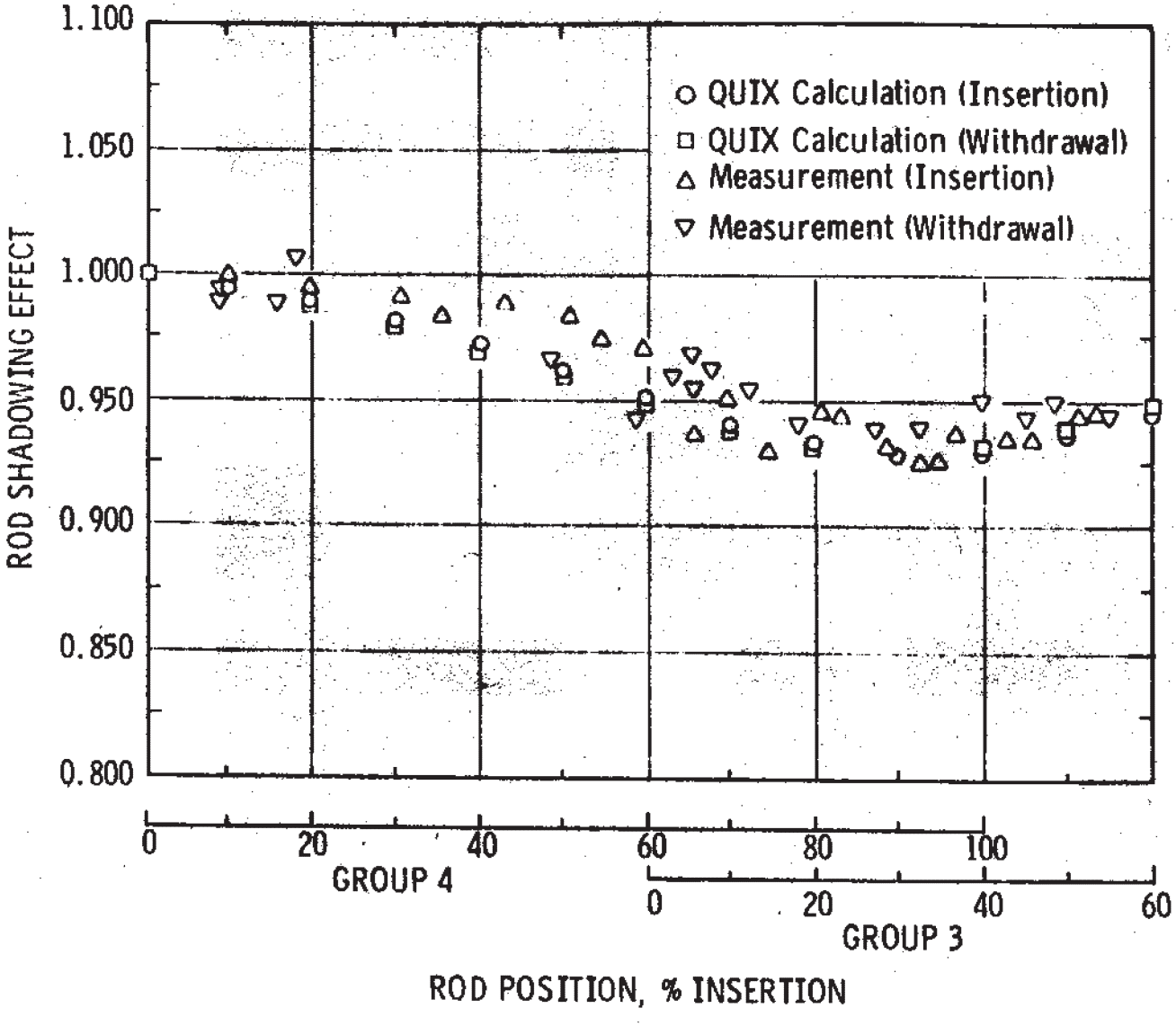

FLORIDA POWER & LIGHT COMPANY
ST. LUCIE PLANT UNIT 2

ROD SHADOWING EFFECT VS ROD POSITION FOR ROD INSERTION AND WITHDRAWAL TRANSIENTS AT PALISADES

FIGURE 4.3-46

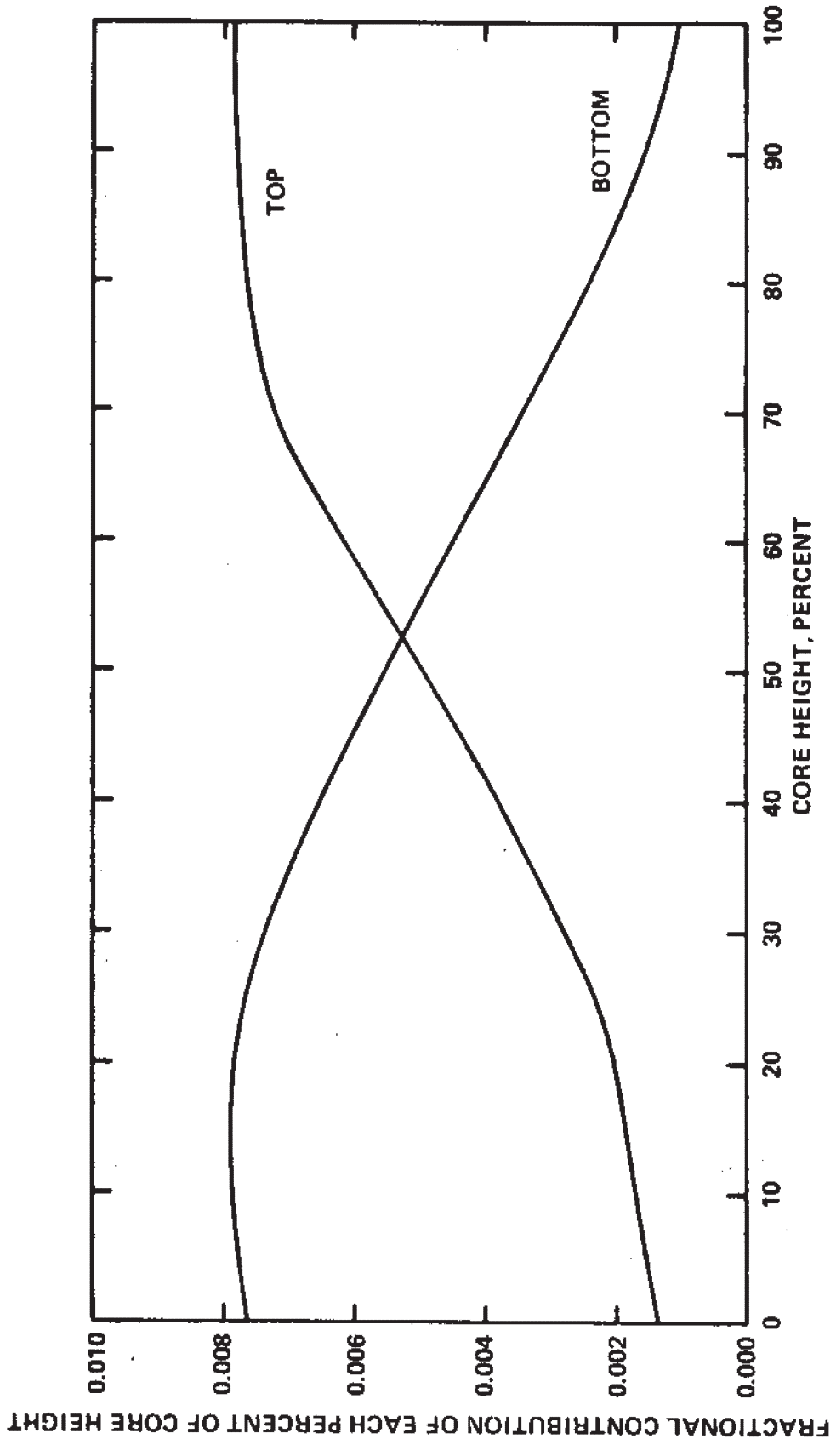

FLORIDA POWER & LIGHT COMPANY
ST. LUCIE PLANT UNIT 2

TYPICAL SHAPE ANNEALING FUNCTION, TWO SUBCHANNEL

FIGURE 4.3-47

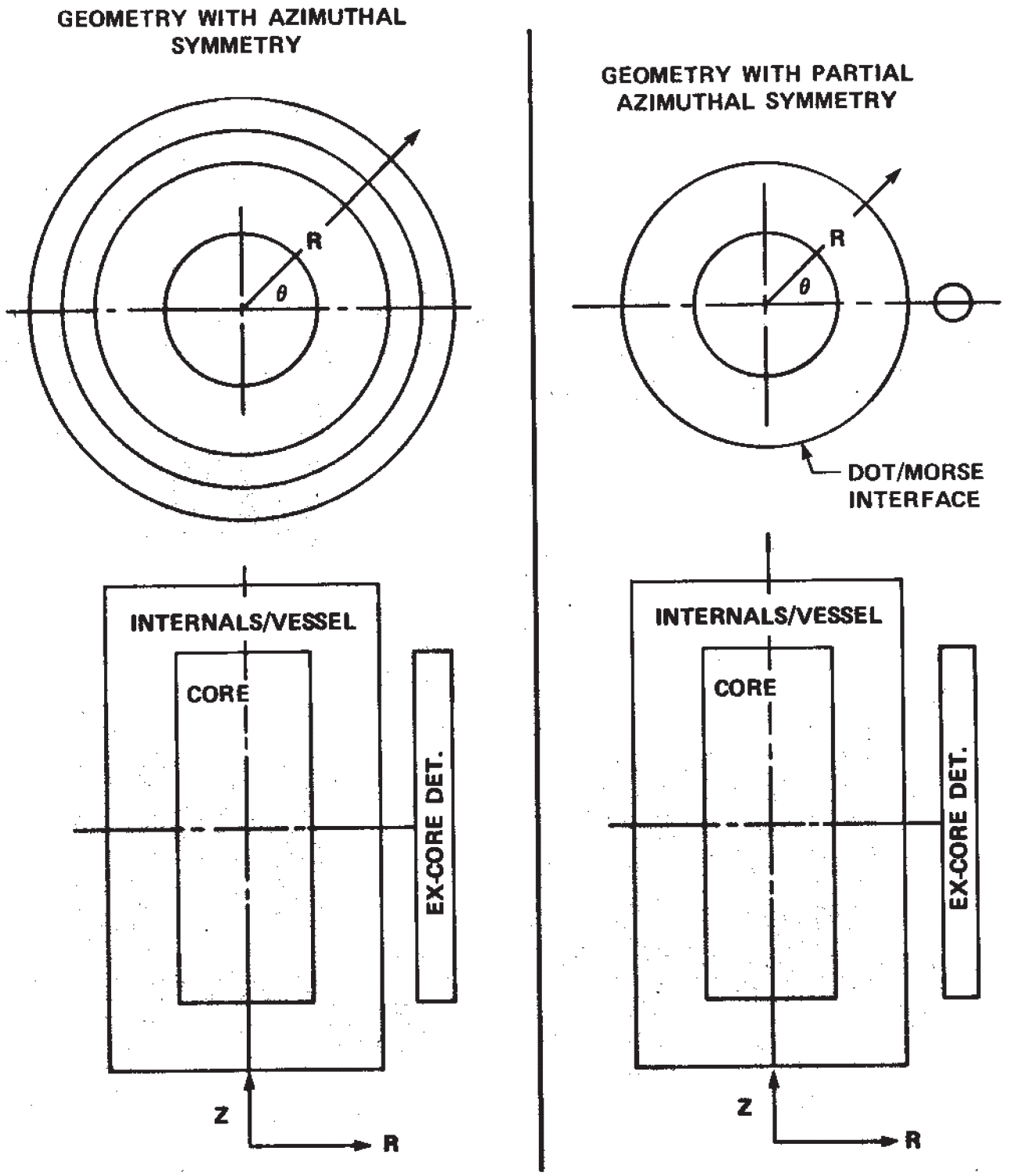

FLORIDA POWER & LIGHT COMPANY
ST. LUCIE PLANT UNIT 2

GEOMETRY WITH FULL & PARTIAL AZIMUTHAL SYMMETRY

FIGURE 4.3–48

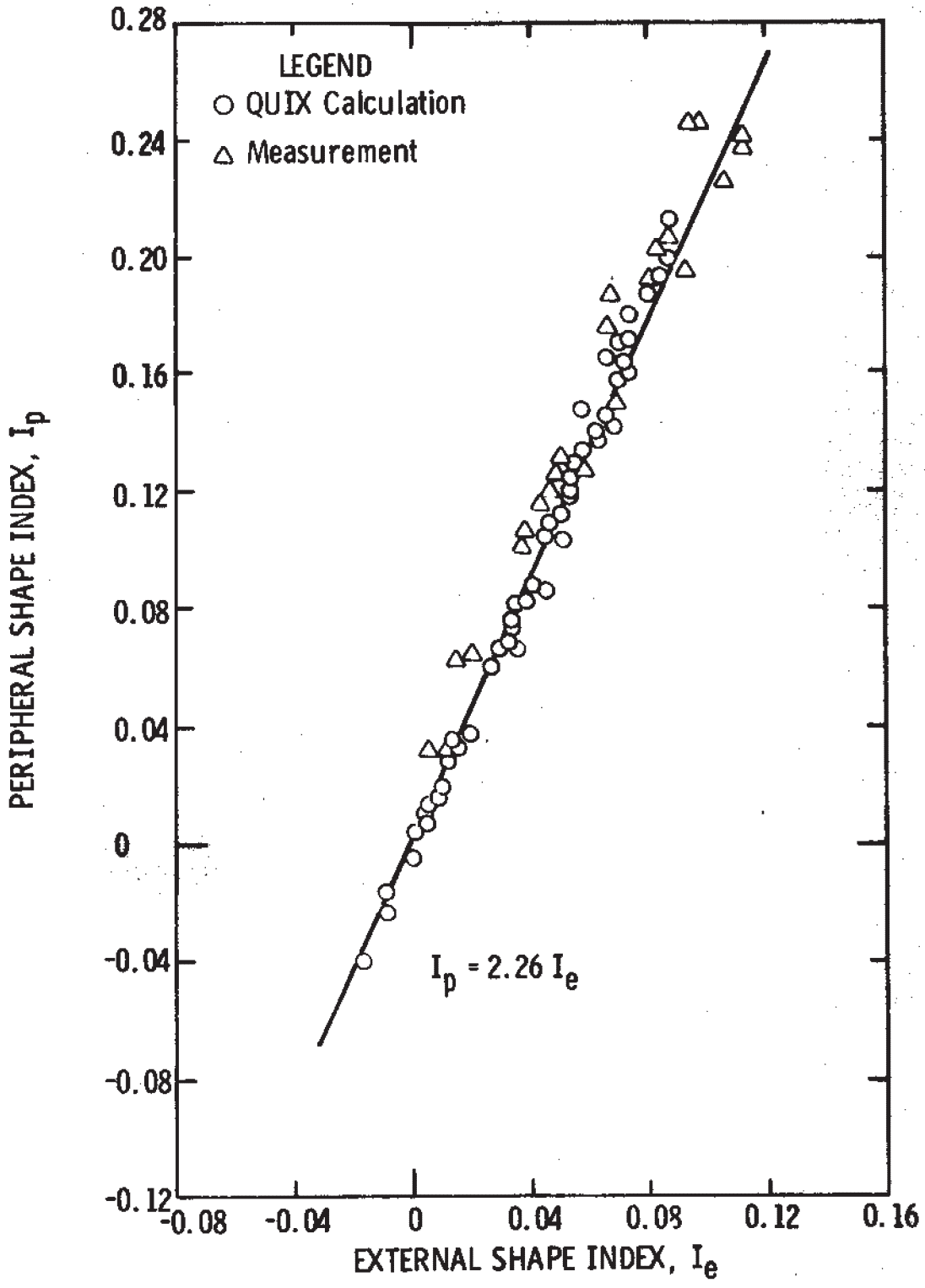

FLORIDA POWER & LIGHT COMPANY
ST. LUCIE PLANT UNIT 2

COMPARISON OF MEASURED AND CALCULATED SHAPE ANNEALING CORRECTION FOR PALISADES

FIGURE 4.3-49

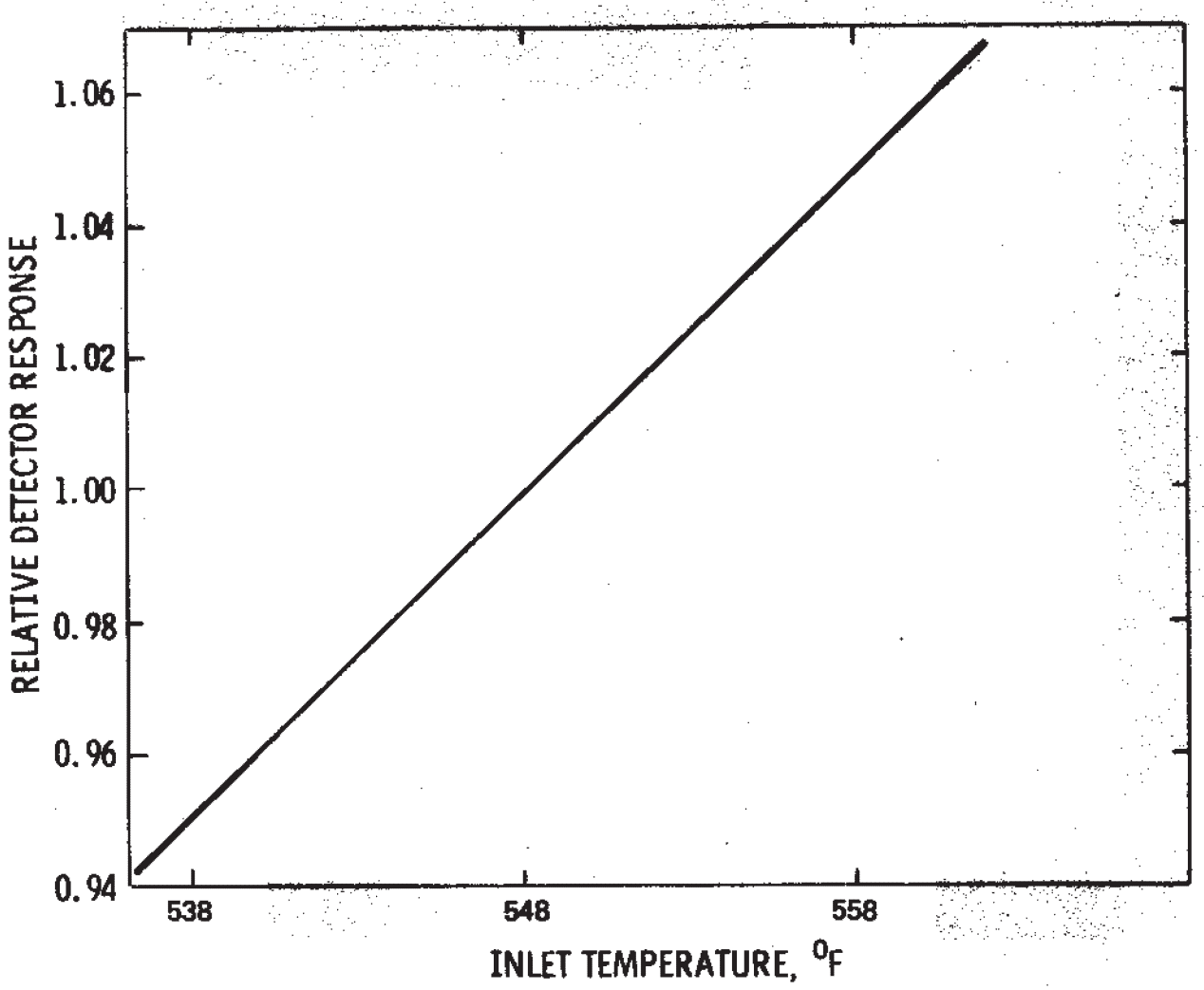

FLORIDA POWER & LIGHT COMPANY
ST. LUCIE PLANT UNIT 2

TYPICAL TEMPERATURE DEFECT
VS REACTOR INLET TEMPERATURE
FIGURE 4.3-50

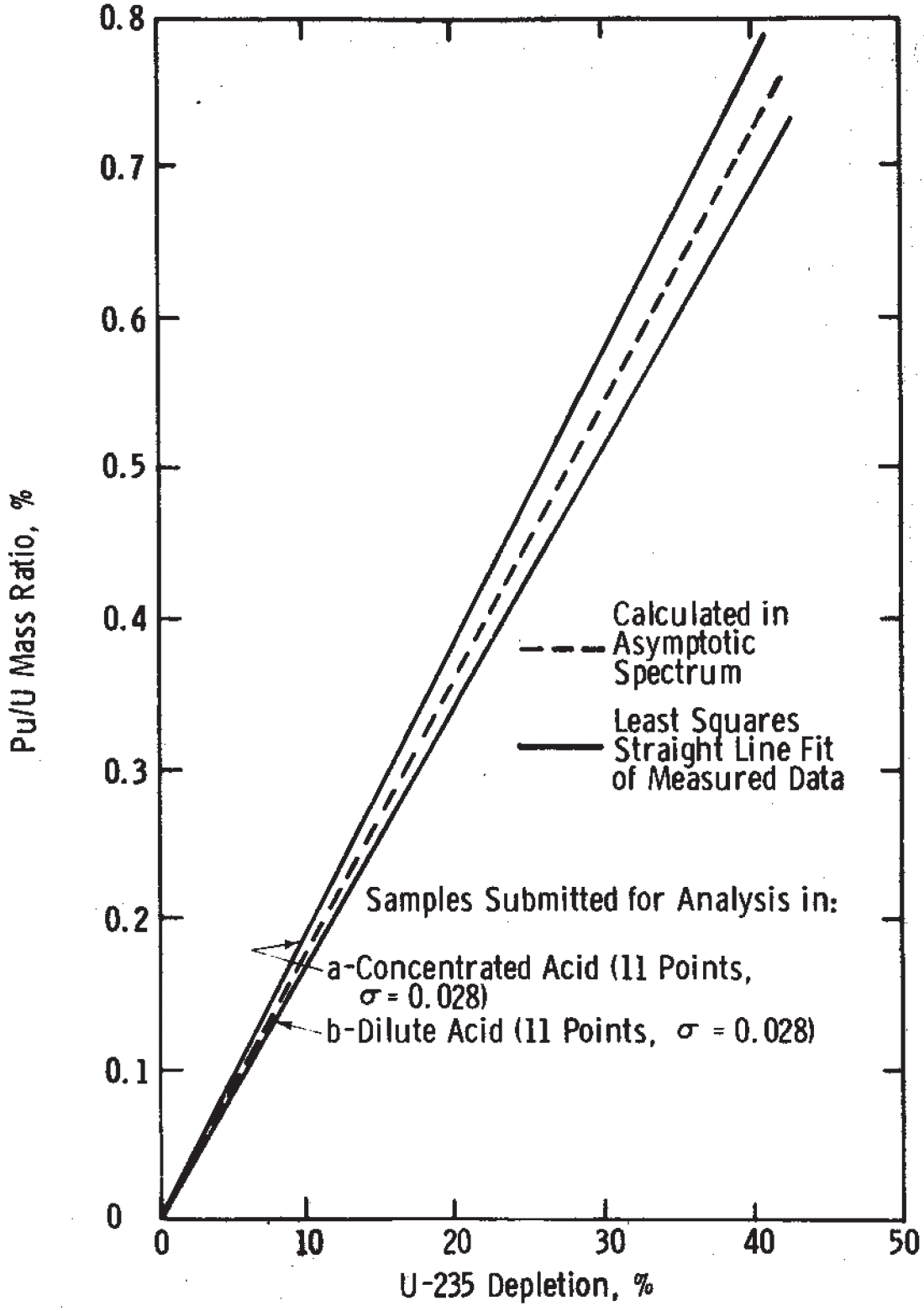

FLORIDA POWER & LIGHT COMPANY
ST. LUCIE PLANT UNIT 2

COMPARISON OF CALCULATED AND MEASURED PLUTONIUM TO URANIUM MASS RATIO IN THE ASYMPTOTIC NEUTRON SPECTRUM FOR YANKEE

FIGURE 4.3-51

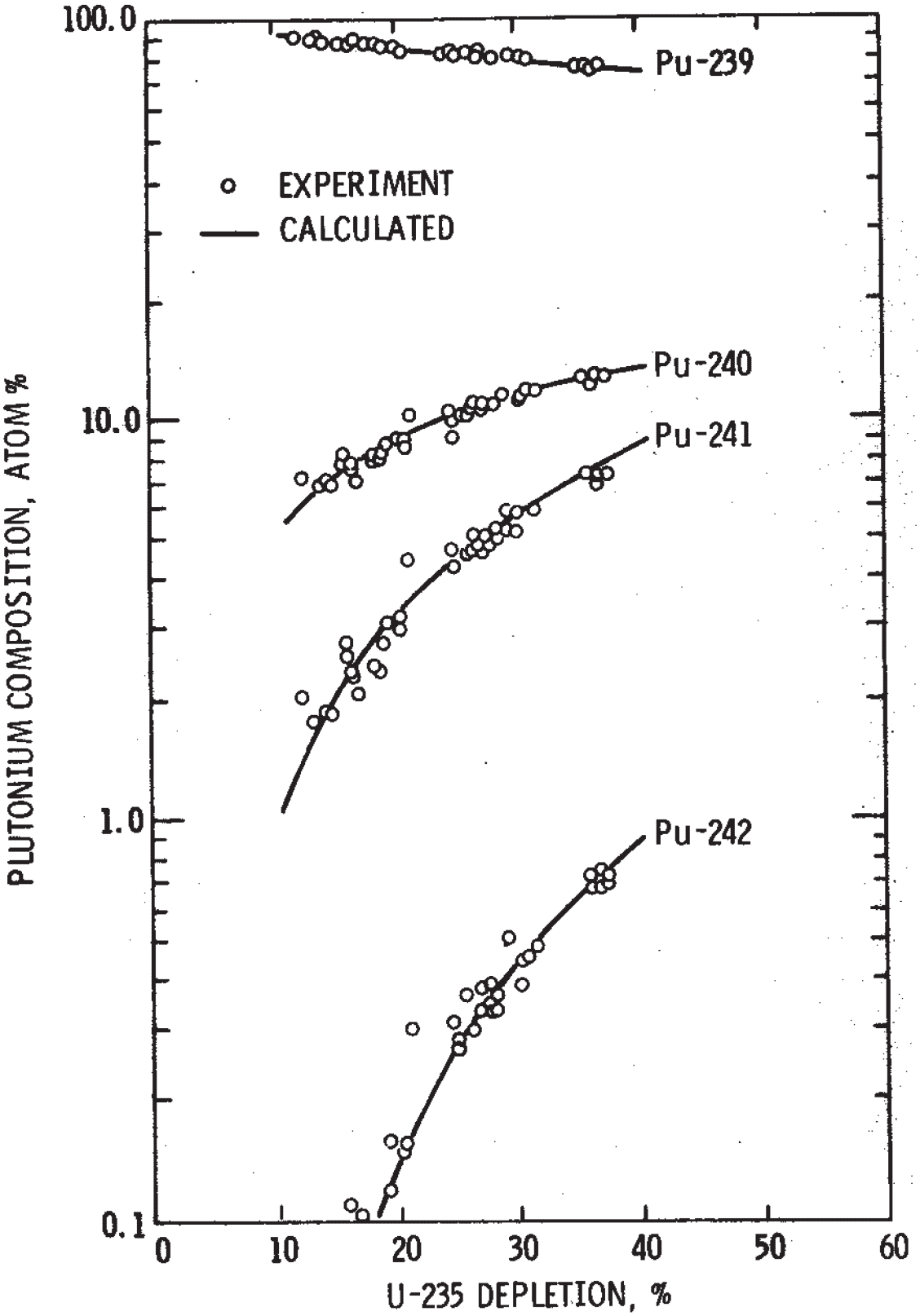

FLORIDA POWER & LIGHT COMPANY
ST. LUCIE PLANT UNIT 2

PLUTONIUM ISOTOPIC COMPOSITION VS FUEL DEPLETION IN THE ASYMPTOTIC SPECTRUM FOR YANKEE

FIGURE 4.3-52

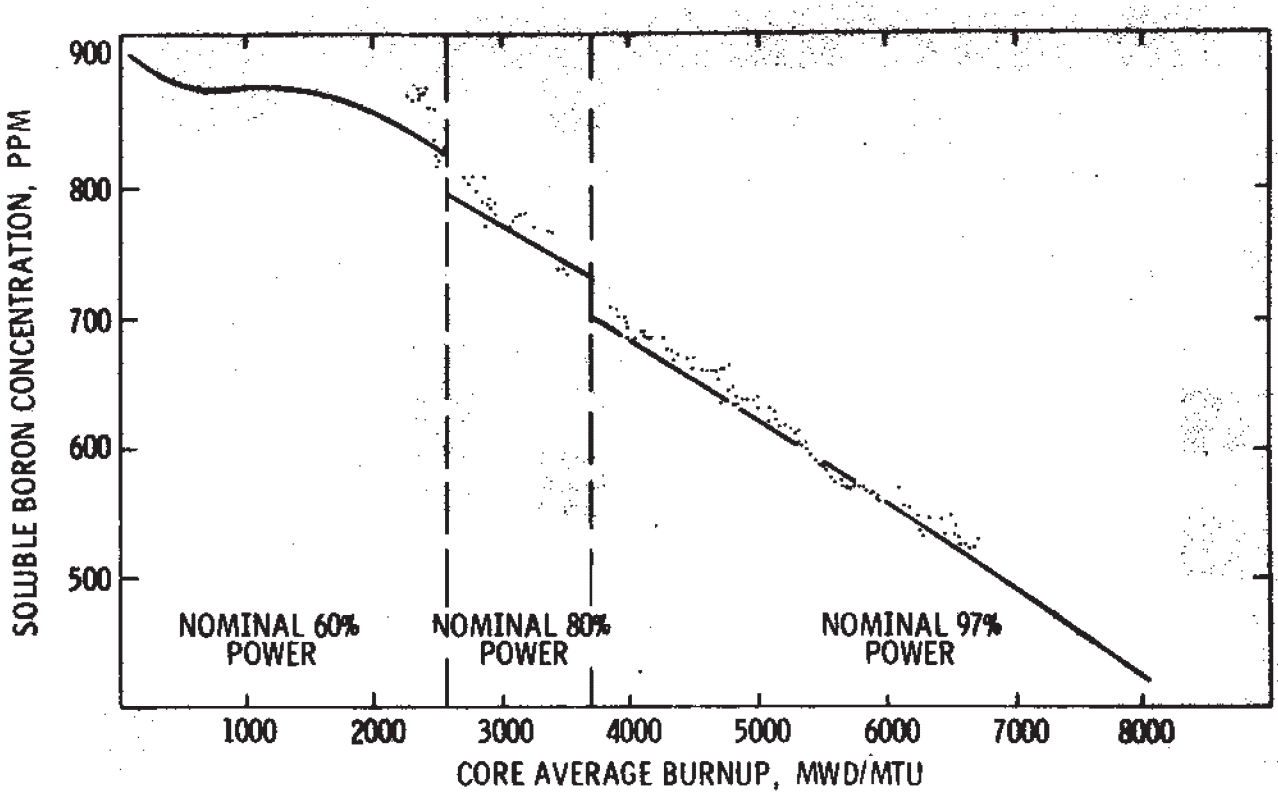

FLORIDA POWER & LIGHT COMPANY
ST. LUCIE PLANT UNIT 2

CRITICAL BORON REACTIVITY
DEPLETION OF PALISADES
FIGURE 4.3-53

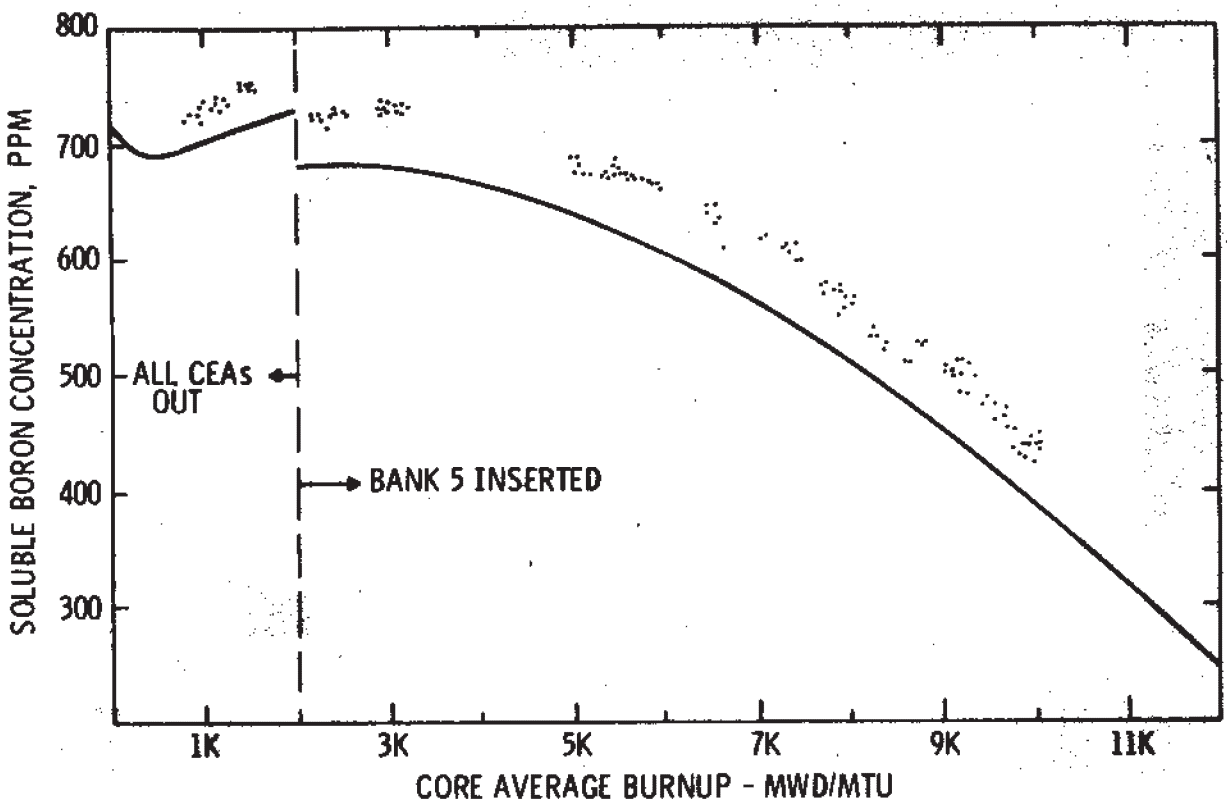

FLORIDA POWER & LIGHT COMPANY
ST. LUCIE PLANT UNIT 2

CRITICAL BORON FOR MAINE YANKEE
FIGURE 4.3-54

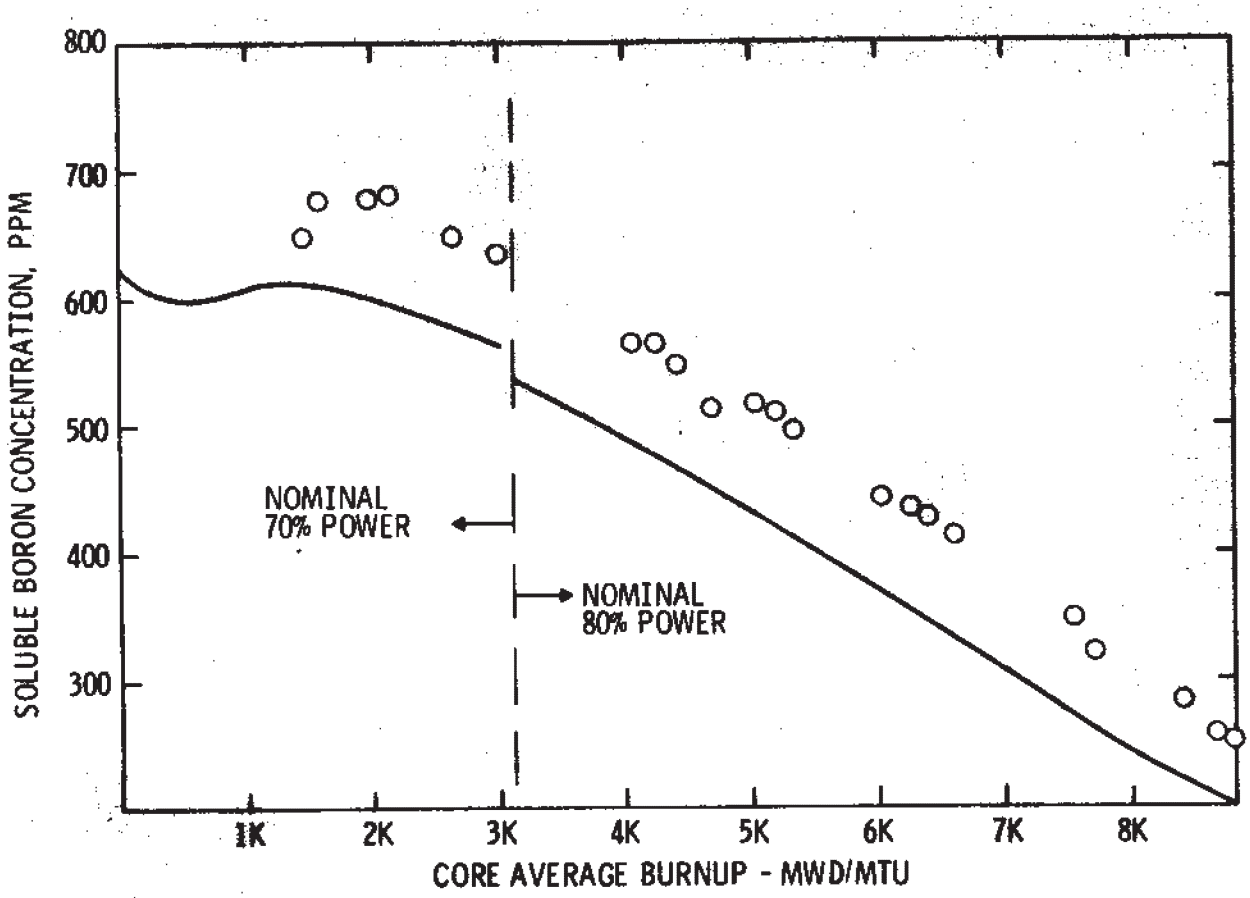

FLORIDA POWER & LIGHT COMPANY
ST. LUCIE PLANT UNIT 2

. CRITICAL BORON FOR OMAHA

FIGURE 4.3-55

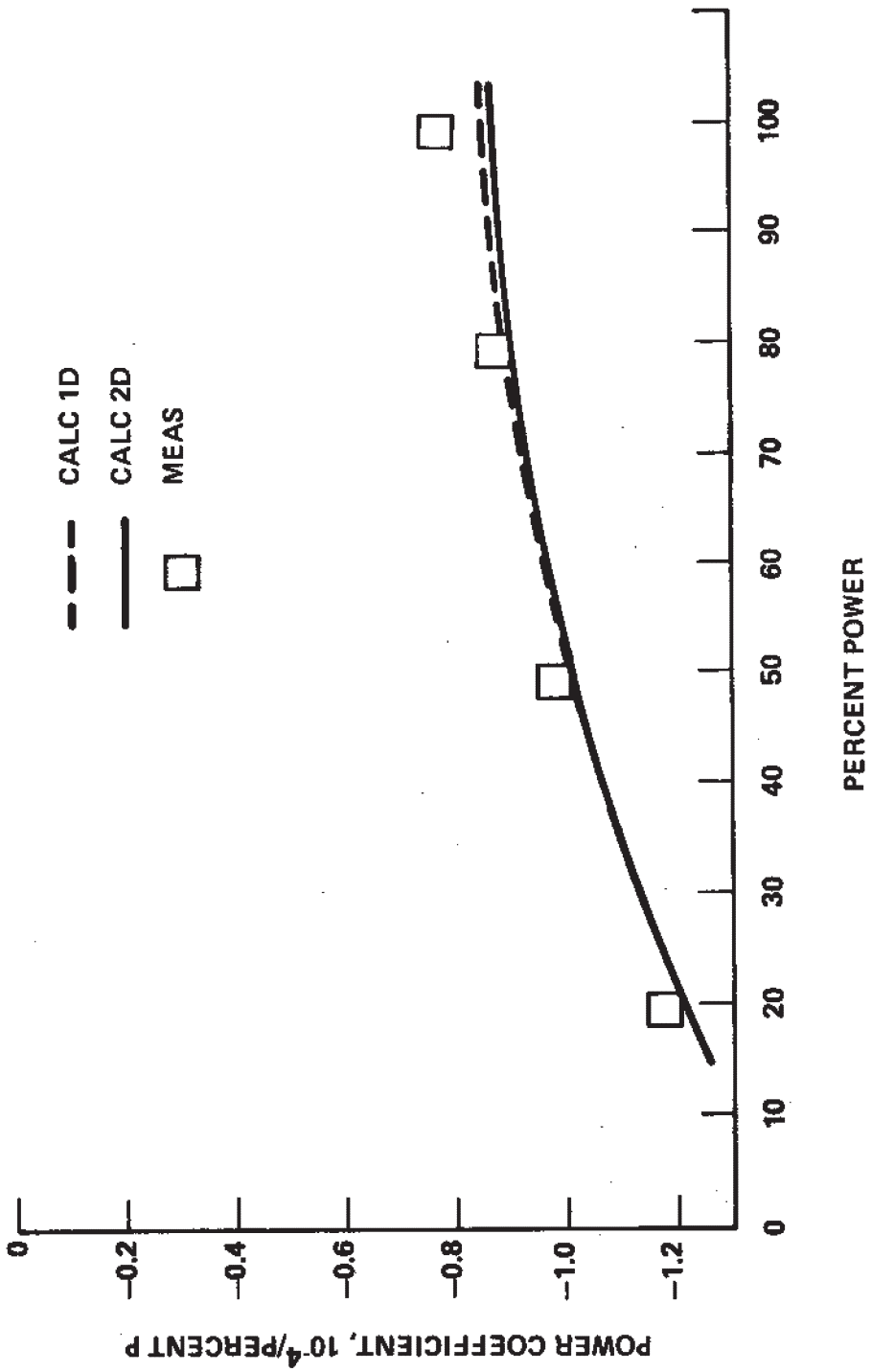

FLORIDA POWER & LIGHT COMPANY
ST. LUCIE PLANT UNIT 2

MILLSTONE UNIT 2 POWER COEFFICIENTS

FIGURE 4.3-56

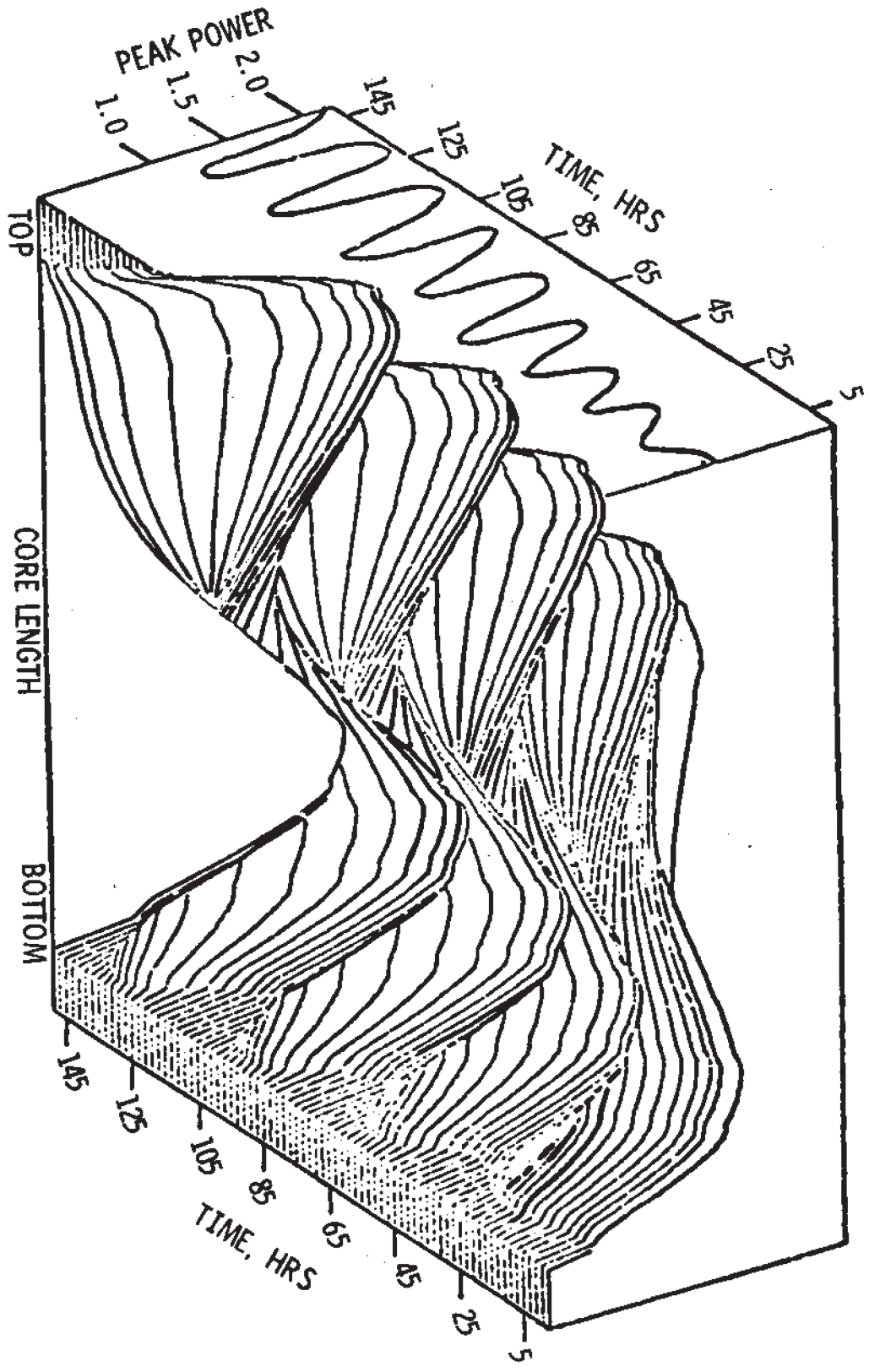

FLORIDA POWER & LIGHT COMPANY
ST. LUCIE PLANT UNIT 2

A DIVERGENT AXIAL OSCILLATION IN AN EOC CORE WITH REDUCED POWER FEEDBACK
($\alpha = 0.96 \times 10^{-4} \Delta\rho/(KW/FT)$)

FIGURE 4.3-57

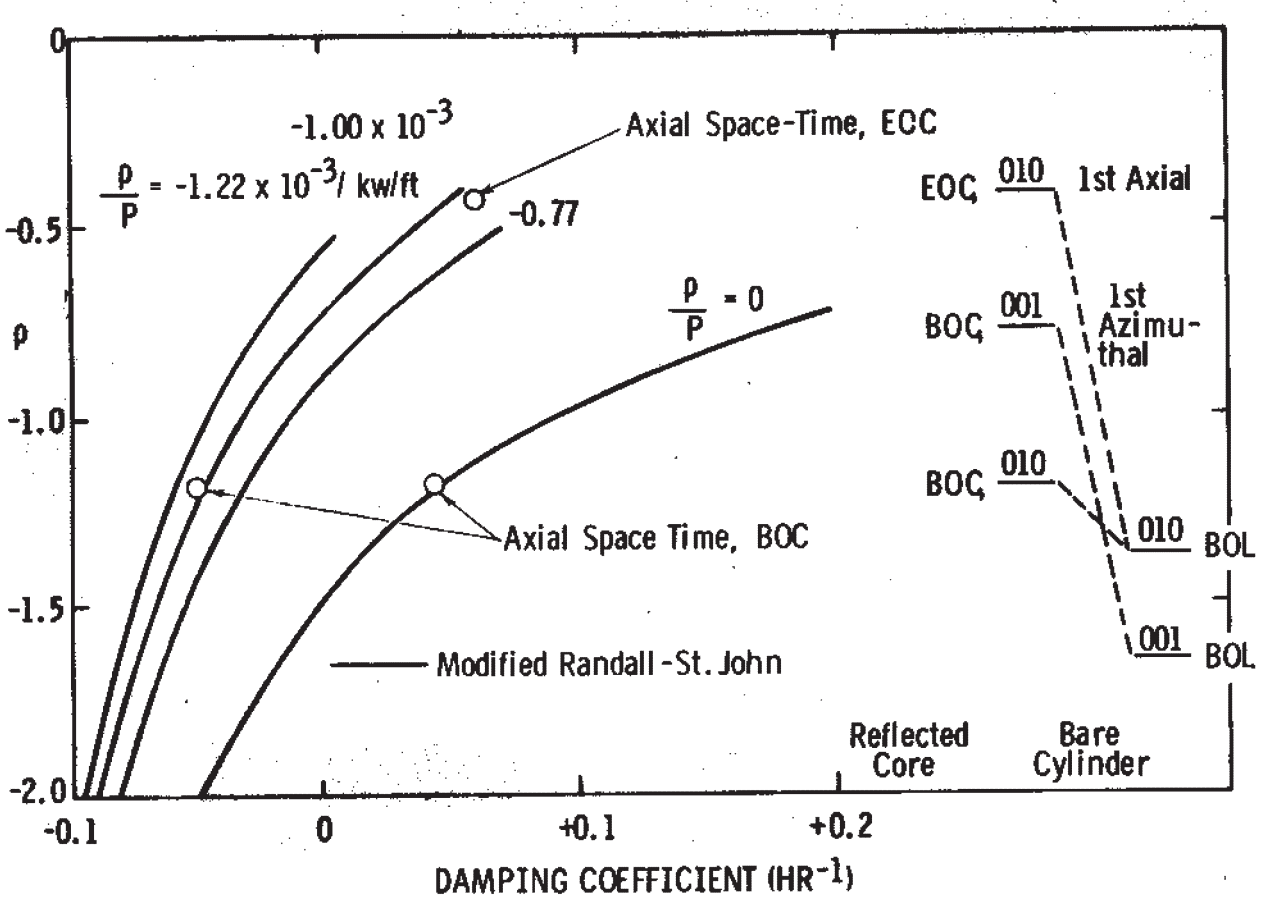

FLORIDA POWER & LIGHT COMPANY
ST. LUCIE PLANT UNIT 2

DAMPING COEFFICIENT VS REACTIVITY DIFFERENCE BETWEEN FUNDAMENTAL AND EXCITED STATE

FIGURE 4.3-58

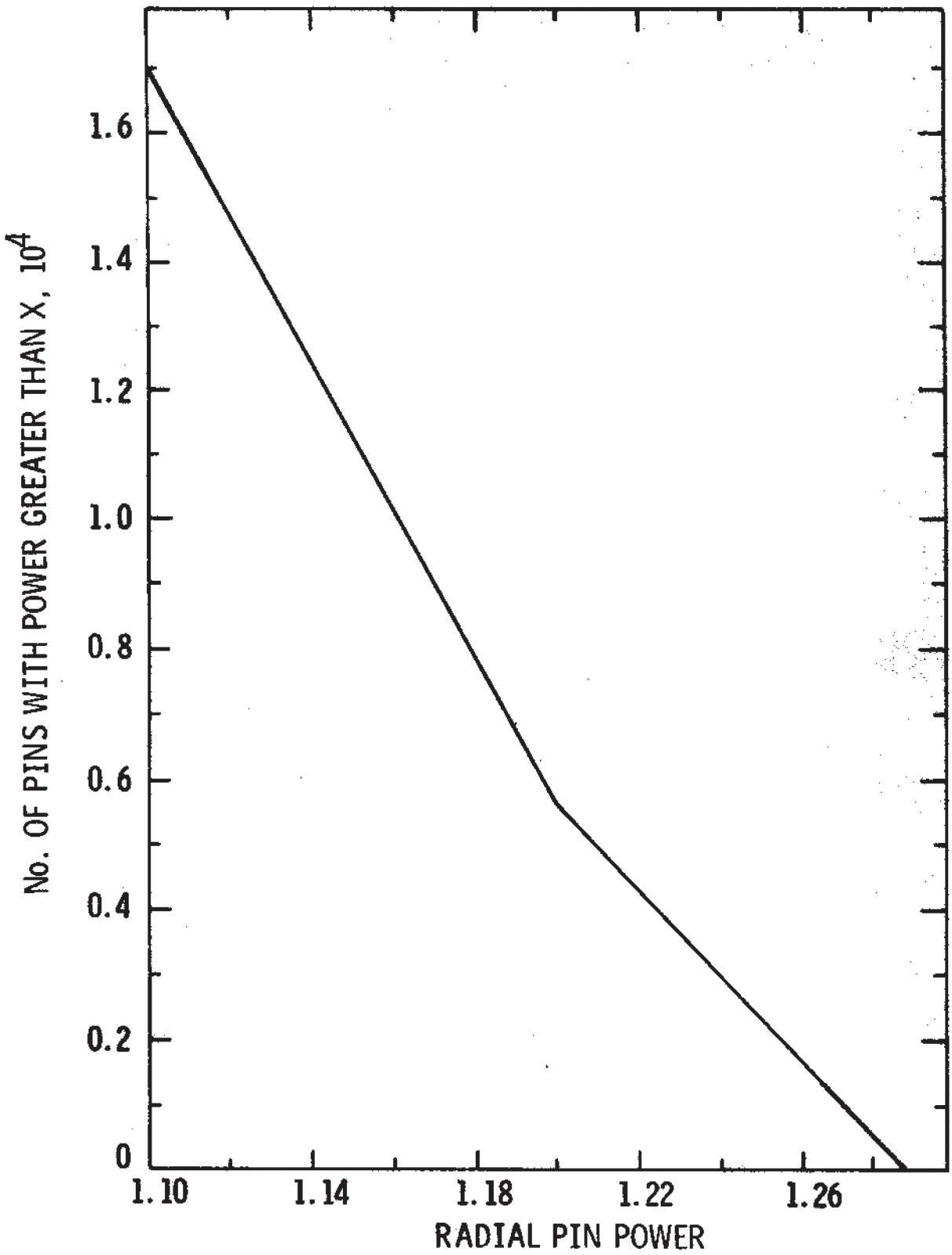

FLORIDA POWER & LIGHT COMPANY
ST. LUCIE PLANT UNIT 2

*LIMITING INTEGRAL RADIAL PIN POWER DISTRIBUTION

FIGURE 4.3-59

% INCREASE IN POWER

GAPPED ROD	(1) 4.477	(3) 1.687	(5) 0.788
(1) 4.477	(2) 3.007	(4) 1.447	(5) 0.788
(3) 1.687	(4) 1.447	(5) 0.788	
(5) 0.788	(5) 0.788		

LEGEND:

(n) ROD GROUPING INDEX FOR THE LOCATION OF UNGAPPED ROD RELATIVE TO THE GAPPED ROD

x.xxx PEAKING IN UNGAPPED ROD DUE TO A SINGLE GAP AT INDICATED LOCATION

FLORIDA POWER & LIGHT COMPANY
ST. LUCIE PLANT UNIT 2

LIMITING SINGLE GAP POWER PEAKING AND ASSOCIATED ROD LOCATION RELATIVE TO THE GAP LOCATION
FIGURE 4.3-60

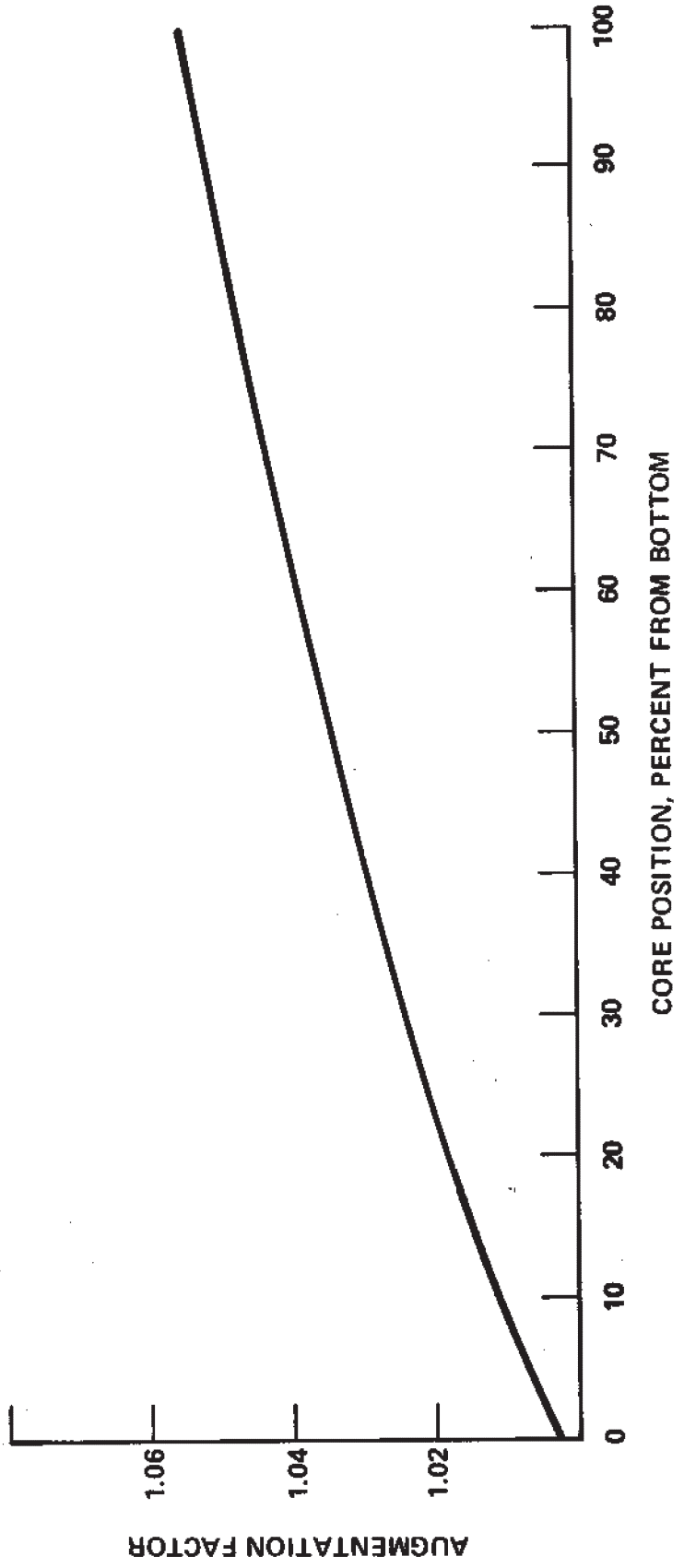

FLORIDA POWER & LIGHT COMPANY
ST. LUCIE PLANT UNIT 2

AUGMENTATION FACTOR VS AXIAL POSITION

FIGURE 4.3-61

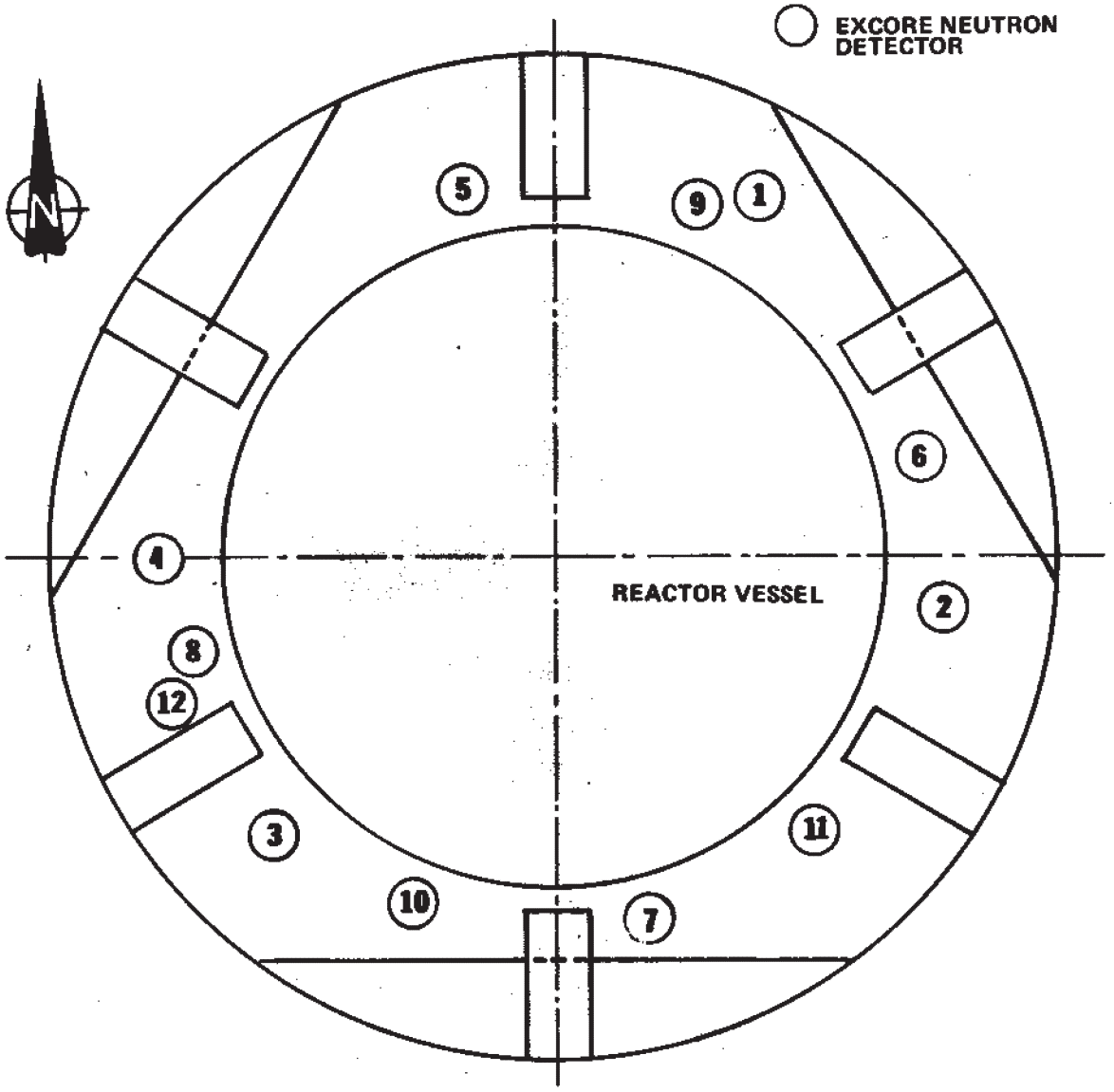

DESCRIPTION			
WELL #	CHANNEL	WELL #	CHANNEL
1	WIDE RANGE CHANNEL 1 (A)	7	LINEAR CHANNEL 3 (C)
2	START UP CHANNEL 1	8	LINEAR CHANNEL 4 (D)
3	WIDE RANGE CHANNEL 3 (C)	9	CONTROL CHANNEL 1
4	START UP CHANNEL 2	10	CONTROL CHANNEL 2
5	LINEAR CHANNEL 1 (A)	11	WIDE RANGE CHANNEL 2 (B)
6	LINEAR CHANNEL 2 (B)	12	WIDE RANGE CHANNEL 4 (D)

EXCORE NEUTRON DETECTORS ARE DESCRIBED IN CHAPTER 7
THE SAFETY SYSTEM IS COMPRISED OF LINEAR CHANNELS 1,2,3 AND 4

FLORIDA POWER & LIGHT COMPANY
ST. LUCIE PLANT UNIT 2

EXCORE DETECTOR LOCATIONS

FIGURE 4.3-62

THIS FIGURE HAS BEEN DELETED

THIS FIGURE HAS BEEN DELETED

FLORIDA POWER & LIGHT COMPANY
ST. LUCIE PLANT UNIT 2

Amendment No. 13, (05/00)

FIGURE 4.3-64

DELETED

EC287528

FLORIDA POWER & LIGHT COMPANY
ST. LUCIE PLANT UNIT 2

Figure 4.3-65

DELETED

EC287528

FLORIDA POWER & LIGHT COMPANY
ST. LUCIE PLANT UNIT 2

Figure 4.3-66

DELETED

EC287528

FLORIDA POWER & LIGHT COMPANY
ST. LUCIE PLANT UNIT 2

Figure 4.3-67

DELETED

EC287528

FLORIDA POWER & LIGHT COMPANY
ST. LUCIE PLANT UNIT 2

Figure 4.3-68

4.4 THERMAL AND HYDRAULIC DESIGN

This section presents the steady-state thermal and hydraulic analysis of the reactor core, the analytical methods, and the experimental work done to support the analytical techniques. Discussions of the analyses of anticipated operational occurrences and accidents are presented in Chapter 15. The prime objective of the thermal and hydraulic design of the reactor is to ensure that the core can meet steady-state and transient performance requirements without violating the design bases.

The St. Lucie Unit 2 UFSAR has been revised to incorporate the Bounding Cycle introduced in the Cycle 12 reload information. Historical information pertaining to Cycles 1 and Cycle 2 has been retained. Bounding Cycle modifications to the Cycles 1 and 2 Design have been incorporated where required.

The St. Lucie Unit 2 UFSAR has been revised to incorporate the reload methodology described in WCAP-9272-P-A/WCAP-9273-NP-A (Reference 41) in support of the 30% steam generator tube plugging (SGTP). The WCAP-9272 bounding cycle information has been incorporated into the appropriate sections.

The St. Lucie 2 UFSAR has been revised to incorporate the transition to the AREVA CE-16 HTP™ fuel starting with Cycle 23 as presented in Reference 48. Historical information has been retained. Details regarding the analysis of the AREVA CE-16 HTP™ Fuel Transition are provided in Section 4.4.7. EC287528

4.4.1 DESIGN BASES

Avoidance of thermally or hydraulically induced fuel damage during normal steady-state operation and during anticipated operational occurrences is the principal thermal hydraulic design bases. The design bases for accidents are specified in Chapter 15. In order to satisfy the design bases for steady-state operation and anticipated operational occurrences, the following design limits are established, but violation of these will not necessarily result in fuel damage. The Reactor Protective System (RPS) provides for automatic reactor trip or other corrective action before these design limits are violated.

The St. Lucie Unit 2 FSAR has been revised to incorporate the Extended Power Uprate (EPU) analyses. The EPU information has been incorporated into the appropriate sections and historical information has been retained. The EPU uses the same codes and methodology as the WCAP-9272 bounding analysis unless otherwise noted.

4.4.1.1 DNBR Analysis

Steady state DNBR analyses of Cycle 2 at the Stretch power level of 2700 Mwt have been performed using the TORC computer code described in Reference 6, the CE-1 Critical Heat Flux (CHF) correlation described in Reference 1, the simplified modeling methods described in Reference 10, and the CETOP code described in Reference 26.

A variation of TORC called CETOP, optimized for simplified modeling applications, was used in Cycle 2 to develop the "design thermal margin model" described generically in Reference 10. Details of CETOP are discussed in Reference 26, CETOP is used only because it reduces computer costs significantly; no margin gain is expected or credited.

Steady state DNBR analyses of the bounding cycle design at the rated power level of 2700 Mwt have been performed using the TORC computer code, the CE-1 CHF correlation, the simplified TORC modeling methods, and the CETOP code described respectively in References 1, 26, 33, 34 and 38.

Table 4.4-11 presents pertinent thermal-hydraulic design parameters for the current cycle. The reference cycle design is based on a core with all GUARDIAN™ fuel which was previously introduced in Region N. Thermal hydraulic design for transition cycles is discussed in Section 4.4.2.2.2. For the reference cycle, the Extended Statistical Combination of Uncertainties (ESCU) methodology presented in Reference 35 was applied with St. Lucie Unit 2 specific data using the calculational factors listed in Table 4.4-11 and other uncertainty factors at the 95/95 confidence/probability level to define a design limit of 1.28 on the CE-1 minimum DNBR.

The bounding cycle DNBR limit includes the following allowances:

1. NRC specified allowances for TORC code uncertainty and CE-1 CHF correlation cross validation uncertainty as discussed in Reference 36.

2. NRC specified allowances for uncertainty associated with the CE-1 CHF correlation applied to CE HID grid fuel, discussed in Reference 39.

3. Rod bow penalty as discussed in Section 4.4.4.1.

Table 4.4-11 also presents pertinent thermal-hydraulic design parameters for the WCAP-9272 bounding cycle introduced in Cycle 15. The bounding cycle design is based on a core with all GUARDIAN fuel that was previously introduced in Region N. The DNBR calculations are performed using the ABB-NV DNB correlation (References 42 and 43), Westinghouse version of the VIPRE-01 (VIPRE) code (Reference 44 and 45), and the Revised Thermal Design Procedure (RTDP) methodology Reference 46. RTDP defines a Design Limit DNBR based on St. Lucie 2 specific data using the parameters listed in Table 4.4-11 and other uncertainty factors, including the ABB-NV correlation uncertainty, at a 95 probability with a 95% confidence level (95/95).

Table 4.4-11 also presents pertinent thermal-hydraulic design parameters for the EPU. The EPU design is based on the same fuel, codes and methodology as the WCAP-9272 bounding cycle analyses.

Bounding cycle assumptions will be confirmed on a cycle by cycle basis.

4.4.1.1.1 Minimum Departure from Nucleate Boiling Ratio (DNBR)

The minimum DNBR is such as to provide at least a 95 percent probability with 95 percent confidence that departure from nucleate boiling (DNB) does not occur on a fuel rod having that minimum DNBR during steady-state operation and anticipated operational occurrences. A value of 1.13, using the CE-1 correlation coupled with the TORC code, provides at least this probability and confidence. Based on review of CENPD-162(1), the NRC requires use of a minimum DNBR of 1.19. Further adjustments to the 1.19 design DNBR limit are required by the NRC to account for the possibility of the fuel rod bowing (Reference 20) and increased grid spacing, which results in an increase in the DNBR limit from 1.19 to 1.20. These additional penalties are applied to the value of F_r^T. DNBR limit for Cycle 2 was 1.28. For the Bounding

Cycle Analyses introduced in Cycle 12, rod bowing is discussed in Section 4.4.4.1. For cycles prior to Cycle 15, ESCU was used and the DNBR limit was 1.28.

The 95/95 ABB-NV correlation DNBR limit is 1.13 coupled with either the TORC code (Reference 42) or the VIPRE code (Reference 43). For the WCAP-9272 bounding cycle analysis, the maximum RTDP Design Limit is 1.30. For the EPU analysis, the maximum RTDP Design Limit is 1.32. The rod bow penalty discussed in Section 4.4.4.1 remains applicable to the minimum DNBR predicted using the ABB NV correlation (Reference 43).

4.4.1.2 Hydraulic Stability

Operating conditions do not lead to flow instability during steady-state operation or anticipated operational occurrences.

4.4.1.3 Fuel Design Bases

a. The peak temperature of the fuel is less than the melting point (5080 F) unirradiated and reduced by 58 F per 10,000 MWD/MTU during steady-state operation and anticipated operational occurrences.

b. The fuel design bases for fuel clad integrity and fuel assembly integrity are given in Subsection 4.2.1. Thermal and hydraulic parameters that influence the fuel integrity include maximum linear heat rate, core coolant velocity, coolant temperature, clad temperature, fuel-to-clad gap conductance, fuel burnup, and UO_2 temperature. Other than the design limits already specified, no limits need be applied to these parameters directly. Conformance with the design limits specified here and conformance with the design bases specified in Subsection 4.2.1, are sufficient to ensure fuel clad integrity, fuel assembly integrity, and the avoidance of thermally or hydraulically induced fuel damage for steady-state operation and anticipated operational occurrences.

4.4.1.4 Coolant Flow, Velocity, and Void Fraction

The reactor coolant flow with all four pumps in operation is neither less than the minimum allowable nor greater than the maximum allowable. These two values for Cycle 1 are shown in Table 4.4-1

The core flow used in the thermal margin analyses is determined by subtracting the maximum core bypass flow from the minimum allowable reactor coolant flow. This is the flow rate that the four reactor coolant pumps will produce at a 97.7 percent probability. A more detailed definition of minimum allowable flow is given in Subsection 4.4.4.5.1.

The core bypass flow is the percentage of the flow entering the reactor vessel which is not effective for cooling the core.

Design of the reactor internals ensures that the coolant flow to the core such that the core is adequately cooled during steady-state operation and anticipated operational occurrences. Therefore, no specific orificing configuration is used.

Although the coolant velocity, its distribution, and the coolant voids affect the thermal margin, design limits need not be applied to these parameters because they are not in themselves

limiting. These parameters are included in the thermal margin analyses and thus affect the thermal margin to the design limits.

4.4.2 DESCRIPTION OF THERMAL AND HYDRAULIC DESIGN OF THE REACTOR CORE

4.4.2.1 Summary Comparison

The thermal and hydraulic parameters for the St. Lucie Unit 2 reactor, Cycle 1, are compared to those for St. Lucie Unit 1 in Table 4.4-1.

The principal reason for the differences is that the St. Lucie Unit 2 reactor uses 16 x 16 fuel assemblies and the St. Lucie Unit 1 reactor contains 14 x 14 fuel assemblies.

4.4.2.2 Critical Heat Flux Ratios

4.4.2.2.1 Departure from Nucleate Boiling Ratio

The margin to DNB in the core is expressed in terms of the departure from nucleate boiling ratio (DNBR). The DNBR is defined as the ratio of the heat flux required to produce departure from nucleate boiling at the calculated local coolant conditions to the actual local heat flux.

The DNB correlation used for design of the core is the CE-1 correlation. [(1)(2)] Based on statistical evaluation of the CE-1 correlation and relevant data, it is concluded that the appropriate minimum DNBR is 1.13.[(1)(2)] NRC evaluation of the uniform axial power distribution data results in their concluding that the CE-1 critical heat flux correlation (CHF), when coupled with the TORC code provides an acceptable correlation of uniform axial CHF data and that the minimum acceptable DNBR is 1.19.[(4)] Therefore, the minimum DNBR used for design is 1.19 for Cycle 1. Cycle 2 uses a DNBR of 1.28. Subsequent cycles with ESCU also use a DNBR of 1.28.

A typical DNB analysis is performed to evaluate the minimum DNBR in the core for the coolant conditions and engineering factors given in Table 4.4-1 for Cycle 1. Adverse radial and axial power distributions in Figures 4.4-1, 4.4-2 and 4.4-3 are chosen to evaluate the minimum DNBR in the core for Cycle 1. The 1.26 peak axial power distribution is chosen for the analysis since it produces the lowest DNBRs compared to the other distributions in Figure 4.4-3. The radial power distributions chosen in Figures 4.4-1 and 4.4-2 are typical adverse distributions but may not be the most limiting in the core. Table 4.4-1 gives the value of minimum DNBR for this DNB analysis.

A comparison of the minimum DNBRs computed using different correlations for the same power, flow, coolant temperature and pressure, and power distribution is presented in Table 4.4-2. The minimum DNBR values in both the limiting matrix subchannel and the limiting subchannel next to the guide tube are presented. The correlations compared are the CE-1 correlation, the original W-3 correlation,[(3)] the revised W-3 correlation[(5)] and the B&W-2 correlation.[(5)] The differences between the original and revised W-3 correlations as used here are in the C-factor and the cold wall correction factor. Further explanation of the C-factor and the cold wall correction factor can be found in References 3 and 5, respectively.

Additional comparisons are contained in CENPD-162A.[(l)] In general, the CE-1 correlation predicts lower values of critical heat flux than the B&W-2 correlation, with the differences increasing with increasing inlet subcooling. In comparison with the W-3 correlation, the CE-1

correlation tends to predict lower values of CHF with high inlet subcooling and higher values of CHF with low inlet subcooling.

The TORC computer code[6] is used to compute the local coolant conditions in the core and the minimum DNBR. For the WCAP-9272 bounding cycle analysis, the VIPRE-01 code (References 44 and 45) is used to compute the local coolant conditions in the core and the minimum DNBR. A discussion of the CE-1 DNB correlation, the ABB-NV DNB correlation and the analytical methods is presented in Subsections 4.4.4.1 and 4.4.4.5.2, respectively.

4.4.2.2.2 Application of Power Distribution and Engineering Factors

Distribution of power in the core is expressed in terms of factors that define the local power per unit length produced by the fuel relative to the core average power per unit length produced by the fuel. The method used to compute these factors, which describe the core power distribution, is discussed in Section 4.3. The energy produced in the fuel deposits in the fuel pellets, fuel cladding, and the moderator and results in the generation of heat in those places. The fraction of energy deposited in the fuel pellet and cladding is called the fuel rod energy deposition fraction. Accordingly, the core average heat flux from the fuel rods is determined by multiplying the core power by the average fuel rod energy deposition fraction and then dividing by the total heat transfer area. The energy deposition fractions used for DNB analyses for the average and the hot fuel rods are given in Table 4.4-1 for Cycle 1.

The effect on local heat flux and subchannel enthalpy rise of within tolerance deviations from nominal dimensions and specifications are included in thermal margin analyses by certain factors called engineering factors. These factors are applied to increase the local heat flux at the location of minimum DNBR and to increase the enthalpy rise in the subchannel adjacent to the rod with the minimum DNBR. Diversion crossflow and turbulent interchange mixing are not input as factors on subchannel enthalpy rise but are explicitly treated in the subchannel code analytical model.

Uncertainties in the power distribution factors are discussed in Subsection 4.4.2.9.4.

4.4.2.2.2.1 Power Distribution Factors

a. Rod Radial Power Factor

The rod radial power factor is the ratio of the average power per unit length produced by a particular fuel rod to the average power per unit length produced by the average powered fuel rod in the core. The maximum rod radial power factor is the ratio of the average power per unit length produced by the highest powered rod in the core to the average power per unit length produced by the average powered fuel rod in the core. Radial power distributions are dependent upon a variety of parameters (control rod insertion, power level, fuel exposure, etc.). The core wide and hot assembly radial power distributions used for a sample DNB analysis are shown in Figures 4.4-1 and 4.4-2.

The design maximum rod radial power factor selected is 1.70. The actual maximum rod radial power factor in the figures is 1.63. The actual maximum rod radial power factor in the core will normally be lower than the design maximum peak but it is not limited to this maximum value. The only limits are those specified in Subsection 4.4.1. The protective system ensures that those design limits are not violated.

The effects of fuel rod bowing on DNBR margin have been incorporated in the safety and setpoint analyses in the same manner as discussed in Reference 28. The value used for this analysis, 1.75% MDNBR, is valid for bundle burnups up to 30,000 MWD/MTU.

For those assemblies with an assembly average burnup in excess of 30 GWD/T, the minimum best estimate margin available, relative to more limiting peaking values present in other assemblies, exceeds the corresponding rod bow penalties based upon Reference 28. Hence, sufficient available margin exists to offset rod bow penalties for assemblies with burnup greater than 30 GWD/T.

For the Bounding Cycle Analyses introduced in Cycle 12 the effects of fuel rod bowing on DNBR margin have been incorporated in the safety and setpoint analyses in the manner discussed in References 35, 28, 39 and 40. The rod bowing penalty used for this analysis, 1.2% on minimum DNBR, is valid for bundle burnups up to 31,700 MWD/MTU. This penalty is included in the 1.28 DNBR limit. For assemblies with burnups greater than 31,700 MWD/MTU sufficient margin is available due to the reduction in radial power peaking to offset potential rod bow penalties for these higher burnup assemblies. Hence, the rod bow penalty based upon Reference 28 and methodology in References 39 and 40 for 31,700 MWD/MTU is bounding for all assembly burnups expected for the bounding cycle. The rod bow penalty of 1.2% on minimum DNBR remains applicable with the ABB-NV DNB correlation (Reference 42).

b. Axial Power Factor

The axial power factor is the ratio of the local power per unit length produced by a fuel rod to the average power per unit length produced by the same fuel rod. The maximum axial power factor is the ratio of the maximum local power per unit length produced by a rod to the average power per unit length produced by the same fuel rod. The axial power distribution directly affects DNBR.

Typically, the farther the location of the peak heat flux is from the core inlet, the lower the value of the peak heat flux needed to reach the DNBR limit. The axial power index and power density are monitored continuously and processed through the RPS such that the design basis limits are not exceeded. Section 4.3 describes the power distributions and their control. Figure 4.4-3 shows sample axial power distributions. The minimum DNBR for Cycle 1 in Table 4.4-1 is determined using the 1.26 peaked axial power distribution whereas the maximum heat fluxes are determined using 1.47 peaked axial power distributions.

c. Nuclear Power Factor

The nuclear power factor is the ratio of the maximum local power per unit length produced in the core to the average power per unit length produced by the average powered fuel rod in the core. It is conservatively calculated as the product of the maximum axial and radial power factors. The selected value for computing maximum heat fluxes for Cycle 1 is shown in Table 4.4-1. The actual value of the nuclear power factor will normally be lower throughout the cycle; but it is not limited to a maximum value shown in the table. The design limits are

those specified in Subsection 4.4.1. The protective systems assure that those design limits are not violated.

d. Total Heat Flux Factor

The total heat flux factor is the ratio of the maximum local fuel rod heat flux to the core average fuel rod heat flux. The effects of fuel densification are not included in this factor. To determine the maximum local heat flux including the effect of gaps occurring between the fuel rod pellets, the augmentation factor should be applied. From this definition, the total heat flux factor is the product of the nuclear power factor, the engineering heat flux factor, and the ratio of the hot to the average rod energy deposition fractions. The total heat flux factor for Cycle 1 is given in Table 4.4-1.

e. Augmentation Factor

The densification of the fuel may lead to axial gaps in the fuel pellets stacks and can cause increased localized power peaking. This effect is expressed in terms of the augmentation factor which is defined as the ratio of the local heat flux to the unperturbed heat flux. The axial length over which the localized power perturbation considered to occur is called the gap length. Maximum values of the augmentation factor and gap length for Cycle 1 are given in Table 4.4-1. The effect of this factor on DNBR is discussed in Subsection 4.4.2.2.3.

4.4.2.2.2.2 Engineering Factors

a. Engineering Heat Flux Factor

The effect on local heat flux due to normal manufacturing deviations from nominal design dimensions and specifications is accounted for by the engineering heat flux factor. Design variables that contribute to this engineering factor are initial pellet density, pellet enrichment, pellet diameter, and clad outside diameter.

These variables are combined statistically to obtain the engineering heat flux factor. The design value used for the engineering heat flux factor is based on deviations obtained from fuel manufacturing inspection data for over 25 batches of fuel for previous reactor cores. Similar tolerances and quality control procedures are used for the St. Lucie Unit 2 core, and as-built fuel manufacturing data are used to confirm that the Cycle 1 factors given in Table 4.4-1 is conservative. The engineering heat flux factor is applied to the rod with the minimum DNBR and increases the heat flux only for the calculation of DNBR. This factor does not affect the enthalpy rise in the subchannel; the effect on the enthalpy rise in the subchannel due to normal manufacturing deviations from normal design dimensions and specifications is accounted for by the engineering enthalpy rise factor.

b. Engineering Factor on Linear Heat Rate

The effect of deviations from nominal fuel rod design dimensions and specifications on fuel temperature is accounted for by the engineering factor on

linear heat rate. The method used to calculate this factor is described in detail in Appendix B of Reference 24. Since the final value is expected to be less than the value shown in Table 4.4-1, this is the value currently used; it is confirmed to be conservative when dimensional tolerances and specifications are established.

c. Engineering Enthalpy Rise Factor

The engineering enthalpy rise factor accounts for the effects of normal manufacturing deviations in fuel fabrication from nominal dimensions and specifications on the enthalpy rise in the subchannel adjacent to the rod with minimum DNBR. Tolerance deviations (averaged over the length of the fuel rods that adjoin the subchannel) for fuel pellet density, enrichment, and diameter contribute to this factor. As-built fuel manufacturing data will be used to confirm that the factor for Cycle 1 given in Table 4.4-1 is conservative.

The engineering ethalpy rise factor is applied by multiplying the factor times the rod radial power factor of the fuel rods adjacent to the subchannel adjoining the rod with the minimum DNBR. This increases the enthalpy rise in the subchannels which adjoin the same fuel rods.

d. Pitch and Clad Diameter Allowance and Rod Bow Penalty

The pitch and clad diameter allowance and rod bow penalty are allowances for the effect on enthalpy rise of the possible decreased flowrate in the subchannel resulting from a smaller than nominal subchannel flow area. The pitch and clad diameter allowance accounts for the systematic variation, while the rod bow penalty accounts for the random variation, in the fuel rod pitch and clad diameter.

The fractional heat deposited in the limiting subchannel adjacent to the rod with the minimum DNBR is multiplied by the pitch and clad diameter allowance. This increases the enthalpy rise in that subchannel in the same manner as does the engineering enthalpy rise factor, but does not directly affect the heat input into the surrounding subchannels. The combined effects of diversion crossflow and turbulent interchange resulting from the higher heat input and enthalpy rise are computed by the subchannel code.

The rod bow penalty is applied to the measured value of F_RT Discussion of fuel and poison rod bowing are presented in CENPD-225[20] and Subsection 4.4.4.1.

4.4.2.2.3 Fuel Densification Effect on DNBR

The perturbation in local heat flux due to fuel densification is given in Table 4.4-1 as the augmentation factor. As shown in CENPD-207(2) (see Subsection 4.4.4.1), even much larger local heat flux variations have no significant adverse effect on DNB. Therefore, no specific allowance is made or required for the effect on DNBR of local heat flux variations due to densification of the fuel.

The perturbation in core average heat flux due to fuel densification is considered by adjusting the active core length with the fuel densification factor given in Table 4.4-1. This factor reduces the active core length slightly which causes an increase in the core average heat flux.

4.4.2.3 Linear Heat Generation Rate

The core average and maximum fuel rod linear heat generation rates for Cycle 1 are given in Table 4.4-1. The maximum fuel rod linear heat generation rate is determined by multiplying the core average fuel rod linear heat generation rate by the product of the nuclear power factor, the engineering factor on linear heat rate, and the ratio of the hot to the average fuel rod energy deposition fractions. The local effects of fuel densification are not included in the maximum fuel rod linear heat generation rate presented in Table 4.4-1; although, to determine the maximum local linear heat generation rate including the effect of gaps occurring between the fuel pellets, the augmentation factor is applied.

4.4.2.4 Void Fraction Distribution

The core average void fraction and the maximum void fraction are calculated using the Maurer method[7] for Cycle 1. The void fractions discussed below are values for the reactor operating conditions and engineering factors for Cycle 1 given in Table 4.4-1, for the radial power distributions in Figures 4.4-1 and 4.4-2, and for the 1.26 peaked axial power distribution in Figure 4.4-3. For these conditions, only subcooled boiling occurs in the core.

The core average void fraction is less than 0.1 percent. The local maximum void fraction is less than 10 percent and occurs at the exit of the subchannel adjacent to the rod with the minimum DNBR. The average exit void fractions and qualities in different regions of the core are shown in Figure 4.4-4 for the core radial power distribution shown on Figure 4.4-1. The axial distribution of quality in the subchannel adjacent to the rod with the minimum DNBR is shown on Figure 4.4-5. The void fraction in that subchannel is very close to zero and therefore the axial distribution of void fraction is not shown.

4.4.2.5 Core Coolant Flow Distribution

The core inlet flow distribution is required as input to the subchannel margin code (refer to Subsection 4.4.4.5.2). The inlet flow distribution for four pump operation was determined from a 1/5 scale reactor flow model test. Descriptions of the model test and the resulting core inlet flow distribution are given in Subsection 4.4.4.2.1.

Intentional selective orificing is not used in the core design.

4.4.2.6 Core Pressure Drops and Hydraulic Loads

4.4.2.6.1 Reactor Vessel Flow Distribution

The main coolant flow path in the reactor vessel is down the annulus between the reactor vessel and the core support barrel, through the flow skirt, up through the core support region and the reactor core, through the fuel alignment plate, and out through the two reactor vessel outlet nozzles. A portion of this flow leaves the main flow path as shown schematically in Figure 4.4-6. Part of the bypass flow is used to cool the reactor internals in areas not in the main coolant flow path and to cool the CEAs. Table 4.4-3 lists the bypass flow paths and the percent of the total vessel flow that enters and leaves these paths.

The thermal margin calculations conservatively use the maximum bypass flow of 3.7 percent of the total vessel flow as compared to the calculated best estimate bypass flow shown in Table 4.4-3.

4.4.2.6.2 Reactor Vessel and Core Pressure Drops

The irrecoverable pressure losses from the inlet to the outlet nozzles are calculated using standard loss coefficient methods and information from flow model tests (Subsection 4.4.4.2).

Pressure losses (at 100 percent power, minimum allowable reactor coolant flow, and an operating pressure of 2250 psia), are listed in Table 4.4-4 together with the coolant temperature used to calculate each pressure loss. The calculated pressure losses include both geometric and Reynolds number dependent effects.

4.4.2.6.3 Hydraulic Loads on Internal Components

The significant hydraulic loads which act on the reactor internals during steady state operation are listed in Table 4.4-5. These loads are determined from analytical methods and from results of reactor flow model and components test programs (refer to Subsections 4.4.4.2.1 and 4.4.4.2.2, respectively). The design hydraulic loads consist of steady state drag and impingement loads, and the fluctuating loads induced by pump-induced pressure pulsations, vortex shedding, and turbulence.

In evaluating the design hydraulic loads, consideration is given to the particular pump operating configuration and coolant temperature that maximizes the hydraulic load for a given internal component.

All hydraulic loads in Table 4.4-5 are based on a coolant flow rate of 389,760 gpm and a coolant temperature of 500°F. Where conservative and applicable, core pressure drop is increased by six psi in the calculation of design hydraulic loads to account for the possibility of core crudding. The six psi value was chosen to provide a sufficient margin for accommodating core crudding effects. Recent experience at other CE plants indicates that any increases in core pressure drop due to crudding effects are much smaller than the six psi design value.

Finally, an uncertainty allowance of 10 percent in the resulting load is added to arrive at the final design hydraulic loads. When other coolant conditions result in more limiting loading for individual components, the loads in Table 4.4-5 are adjusted in the detailed design analysis.

The 389,760 gpm value represents the original maximum design reactor coolant flow set for the CE 2560 MWt class reactors. Subsequent startup of the first four of these reactors showed that the indicated flow rates exceeded the 389,760 gpm value due to high performance curves for the primary coolant pumps. Re-evaluation of the stress margins at the higher indicated flow rates and subsequent operating experience have shown that operation is satisfactory at those flow rate levels. In the case of St. Lucie Unit 2, the internals are identical to the CE 3400 MWt class reactor internals with the exception of the shorter core length for St. Lucie. The 3400 MWt internals have been designed to withstand hydraulic loads based on a flow rate of 475,200 gpm. This value is significantly larger than the current maximum allowable flow rate of 424,350 gpm set for St. Lucie Unit 2 and shown in Table 4.4-1. The 424,350 gpm value is also consistent with the operating experience from earlier CE 2560 MWt plants and is expected to envelope the indicated flow rates from the St. Lucie Unit 2 flow tests; see Subsection 4.4.4.5.1. The mechanical design flow rate has increased to 431,000 gpm (Reference 47). New calculations have been carried out that demonstrate the acceptability of the increased flow rate for the RSGs.

Hydraulic loads for postulated accident conditions are discussed in Subsection 3.9.2.5.

4.4.2.7 Correlations and Physical Data

4.4.2.7.1 Heat Transfer Coefficients

The correlations used to determine cladding temperatures for non-boiling forced convection and nucleate boiling are discussed here. The surface temperature of the cladding is dependent on the axial and radial power distributions, the temperature of the coolant, and the surface heat transfer coefficient.

The surface heat transfer coefficient for non-boiling forced convection is obtained from the Dittus-Boelter correlation[8] where fluid properties are evaluated at the bulk condition.

$$h_{db} = \frac{0.023k}{De}(N_R)^{0.8}(N_{pr})^{0.4}$$

where:

h_{db} = Heat transfer coefficient, Btu/h-ft^2 - F

k = Thermal conductivity, Btu/h-ft - F

De = Equivalent diameter = $4A/P_W$, ft

N_R = Reynolds number, based on the equivalent diameter and coolant properties evaluated at the local bulk coolant temperature.

N_{Pr} = Prandtl number, based on coolant properties evaluated at the local bulk coolant temperature.

A = Cross-sectional area of flow subchannel, ft^2.

P_w = Wetted perimeter of flow subchannel, ft.

No specific allowance is made or considered necessary for the uncertainties associated with the Dittus-Boelter correlation because the Dittus-Boelter correlation is not used directly in computing thermal margin, but rather plays a part in determining pressure drop and cladding temperature. The validity of the overall scheme for predicting pressure drop is shown by the excellent agreement between predicted and experimental values obtained during the DNB test program described in Subsection 4.4.4.1. The uncertainty associated with the cladding temperatures calculated for single phase heat transfer is not a major concern because the limiting fuel and cladding temperatures occur where the cladding-to-coolant heat transfer is by nucleate boiling.

The temperature drop across the surface film is calculated from:

$$T_{film} = q''/h_{db} = T_{wall_{db}} - T_{coolant}$$

where:

q" = fuel rod surface heat flux, Btu/h-ft^2

$T_{wall_{db}}$ = fuel rod surface temperature determined by Dittus-Boelter, F

$T_{coolant}$ = reactor coolant temperature, F

The maximum fuel rod heat flux is the product of the core average fuel rod heat flux and the total heat flux factor (refer to Table 4.4-1 and Subsection 4.4.2.2.2). Nucleate boiling may occur on the clad surface. In the nucleate boiling regime, the surface temperature of the cladding for Cycle 1 is determined from the Jens and Lottes correlation[9].

$$T_{wall_{JL}} = T_{sat} + 60\,(q'' \times 10^{-6})^{0.25}\,[\exp(-P/900)]$$

where:

P = Pressure, psia

q" = Defined above

$T_{wall_{JL}}$ = Fuel rod surface temperature determined by Jens and Lottes, F

T_{sat} = Saturation temperature, F

Nucleate boiling is assumed to exist if $T_{wall_{JL}}$ is less than $T_{wall_{db}}$

The cladding surface temperature is calculated by summing the temperature of the coolant at the particular location and the temperature drop across the surface film; or if nucleate boiling is occurring, it is calculated directly from the Jens and Lottes correlation.

4.4.2.7.2 Core Irrecoverable Pressure Drop Loss Coefficients

Irrecoverable pressure losses through the core result from friction and geometric changes. The pressure losses through the lower and upper end fittings were initially calculated using the standard loss coefficient method and then verified by test (refer to Subsection 4.4.4.2.2). The correlations used to determine frictional and geometric losses in the core are presented in Subsection 4.4.4.2.3.

4.4.2.7.3 Void Fraction Correlations

There are three separate void regions to be considered in boiling flow for Cycle 1. Region 1 is highly subcooled in which a single layer of bubbles develops on the heated surface and remains attached to the surface. Region 2 is a transition region from highly subcooled to bulk boiling where the steam bubbles detach from the heated surface. Region 3 is the bulk boiling regime.

The void fraction in Regions 1 and 2 is predicted using the Maurer method.[7] The calculation of the void fraction in the bulk boiling regime is discussed in Subsection 4.4.4.2.3.

4.4.2.8 Thermal Effects of Operational Transients

Design basis limits on DNBR and fuel temperature are established to assure that thermally induced fuel damage will not occur during steady-state operation and during anticipated operational occurrences. The RPS ensures that the design limits are not violated.

4.4.2.9 Uncertainties in Estimates

4.4.2.9.1 Pressure Drop Uncertainties

The reactor vessel pressure losses in Table 4.4-4 are the values calculated for the best estimate flow with standard loss coefficient methods. The uncertainties in the correlations for the loss coefficients and the dimensional uncertainties on the reactor vessel and internals are accounted for when determining maximum and minimum vessel hydraulic resistance. The uncertainties at the 2 σ level are estimated to be equivalent to approximately ±10 percent of the best estimate vessel pressure loss.

4.4.2.9.2 Hydraulic Loads Uncertainties

The design hydraulic loads are determined at the maximum allowable reactor coolant flow rate (refer to Subsection 4.4.2.6.3); the effects of uncertainties in load determination are represented by a 10 percent increase in the hydraulic loads to arrive at the final design values.

4.4.2.9.3 Fuel and Clad Temperature Uncertainty

Uncertainty in the ability to predict the maximum fuel temperature is a function of gap conductance, thermal conductivities, peak linear heat rate, and heat generation distribution. Uncertainties in gap conductance and thermal conductivity are taken into account in the analytical model.

Uncertainties in the peak linear heat rate are accounted for by including the engineering factor on linear heat rate in the analysis. This factor includes uncertainties in fuel pellet density, enrichment, and pellet diameter.

Uncertainty in predicting the cladding temperature at the location of maximum heat flux is the uncertainty in the film temperature drop, which is minimal at this location where nucleate boiling occurs.

4.4.2.9.4 DNBR Calculation Uncertainties

a. The uncertainty in the calculation of minimum DNBR is divided into:

    1. The uncertainty in the input to the core analytical model, the subchannel code. This includes the core geometry, power distribution, inlet flow and temperature distribution, exit pressure distribution, single phase friction factor constants, spacer grid loss coefficients, diversion crossflow resistance and momentum parameters, turbulent interchange constants, and hot fuel rod energy deposition fraction.

    2. The uncertainty in the analytical model to compute the actual distribution of flow and the local subchannel coolant conditions.

    3. The uncertainty in the DNB correlation to predict DNB.

b. The following paragraphs discuss the above uncertainties and the allowances for them, if needed, in the thermal margin analysis of the core.

1. Uncertainty in the input to the core analytical model:

   (a) Uncertainty in core geometry, as manifested by manufacturing variations within tolerances, is considered by the inclusion of engineering factors in the DNBR analyses; see Subsection 4.4.2.2.2.2 for a discussion of the method used to compute conservative values.

   (b) The core inlet flow distribution is obtained from flow model testing discussed in Subsection 4.4.4.2. Uncertainties in the core flow distribution are included in the design method for DNBR analyses.

   (c) Uncertainties in the core inlet temperature distribution and core exit pressure distribution are included in the design method for DNBR analyses.

   (d) The Blasius single-phase friction factor equation for smooth rods is given and shown to be valid in Subsection 4.4.4.2.3. The loss coefficient for the spacer grid is obtained from pressure drop data discussed in Subsection 4.4.4.2.3.

   (e) The value of minimum DNBR is relatively insensitive to crossflow resistance and momentum parameters.[6]

   (f) Subsection 4.4.4.1 describes the testing to determine the inverse Peclet number which is indicative of the turbulent flow interchange between subchannels. The inverse Peclet number is input to the subchannel code and is used to determine the effect of turbulent interchange on the enthalpy rise in adjacent subchannels. From the testing, a value of 0.0035 is justified.

   (g) The same fuel rod energy deposition fraction is used for the hot rod as for the average rod. The hotter the rod, the lower is the actual value of energy deposition fraction with respect to that for the average rod. A lower energy deposition fraction reduces the hot rod heat flux and thereby increases its DNBR. The use of the average rod energy deposition fraction for the hot rod is therefore conservative. See Section 4.3 for a discussion of the calculation of the energy deposition fractions.

2. Uncertainty in the analytical model:

   The ability of the TORC code to accurately predict local subchannel conditions in rod bundles is described in CENPD-161.[6] The ability of the code to accurately predict the core wide coolant conditions is described in CENPD-206.[10]

   The ability of the VIPRE code to accurately predict reactor core and local subchannel conditions in rod bundles is described in References 44 and 45.

3. Uncertainty in the DNB correlation:

The uncertainty in the DNB correlation is determined by a statistical analysis of DNB test data. For example, a value of 1.13 has been shown to provide a 95 percent probability with 95 percent confidence that DNB will not occur on a fuel rod having that minimum DNBR.[(1)(2)]

4.4.2.10 Flux Tilt Considerations

An allowance for degradation in the power distribution in the x-y plane (commonly referred to as flux tilt) is provided in the protection limit setpoints even though little, if any, tilt in the x-y plane is expected.

The tilt, along with other pertinent core parameters, is monitored during operation. The RPS actuates a trip if limiting safety system settings are reached.

The thermal margin calculations used in designing the reactor core are performed using the subchannel code, such as TORC or VIPRE. The TORC code, which is described in Subsection 4.4.4.5.2, is based on an open core analytical method for performing such calculations and treats the entire core on a three-dimensional basis. Thus, any asymmetry or tilt in the power distribution is analyzed by providing the corresponding power distribution in the TORC input.

4.4.3 DESCRIPTION OF THE THERMAL AND HYDRAULIC DESIGN OF THE REACTOR COOLANT SYSTEM (RCS)

A summary description of the RCS is given in Section 5.1.

4.4.3.1 Plant Configuration Data

An isometric view of the RCS is given in Figure 4.4-7. Dimensions are shown on the general arrangement drawings, Figures 5.1-1 and 5.1-2. Table 4.4-6 lists the valves and pipe-fittings which form part of the RCS.

Table 4.4-7 lists the design flow through each flowpath in the RCS.

Table 4.4-8 provides the volume, flowpath length, height and liquid level of each volume, bottom elevation of each volume, and minimum flow area for each component within the RCS.

The line lengths and sizes of the safety injection lines are listed in Table 4.4-9 and Figures 6.3-1a, 6.3-1b, and 6.3-1c.

Tables 4.4-10 and 5.1-1 list the thermal-hydraulic design parameters for the RCS.

4.4.3.2 Operating Restrictions on Pumps

The minimum RCS pressure for reactor coolant pump (RCP) operation at any given temperature is limited by the required net positive suction head (NPSH) for the RCPs during portions of plant heatup or cooldown. To ensure that the pump NPSH requirements are met under all possible operating conditions, an operating curve is used which gives permissible RCS pressure for RCP operation as a function of temperature (See Subsection 5.4.1.2).

The reactor coolant pump NPSH restriction on this curve is determined by using the most restrictive NPSH requirement for any combination of pump operation and correcting it for pressure and temperature instrument errors and pressure measurement location. The NPSH required versus pump flow is supplied by the pump vendor. RCP operation below this curve is prohibited. At low reactor coolant temperature and pressure, minimum RCP seal pressure may require that the minimum pressure for RCP operation versus temperature curve be above the NPSH curve.

4.4.3.3 Power-Flow Operating Map (BWR) This subsection is not applicable to St. Lucie Unit 2.

4.4.3.4 Temperature-Power Operating Map (PWR)

Reactor operation at power with one, two or three pumps operating, or while in natural circulation is not allowed. However, decay heat may be transferred to the steam generator in any of the above cases. The temperature - power operating map (temperature control program) is shown in Figure 4.4-10.

The adequacy of natural circulation for decay heat removal after reactor shutdown has been verified analytically and by tests on the Palisades reactor (Docket No. 50-255) and Calvert Cliffs I (Docket No. 50- 317). The core ΔT in the analysis has been shown to be lower than the normal full power ΔT; thus the thermal and mechanical loads on the core structure are less severe than normal design conditions. In addition, St. Lucie Unit 1 (Docket No. 50-335) successfully performed a cooldown from full power conditions using only natural circulation cooling following a reactor trip.

Heat removed from the core during natural circulation may be rejected either by dumping steam to the main condenser or to the atmosphere; the rate of heat removal may be controlled to maintain core ΔT within allowable limits.

4.4.3.5 Load Following Characteristics

The design features of the RCS influence its load following and transient response. The RCS is capable of following the normal transients identified in Subsection 3.9.1. These requirements are considered when designing the pressurizer spray and heater systems, charging/letdown system, Reactor Regulating System, turbine bypass control system, and Feedwater Regulating System. Finally, these transients are included in the equipment specification for each RCS component to ensure the structural integrity of the system.

When load changes are initiated, the Reactor Regulating System senses a change in the turbine power and positions CEAs to attain the programmed coolant average temperature. RCS boron concentration can also be adjusted to attain the appropriate coolant temperature. The turbine bypass control system senses changes in steam pressure and steam flow in order to control steam pressure following load reductions. The feedwater system employs a controller which senses changes in steam flow, feedwater flow, and water level and acts to maintain steam generator level at the desired point. The pressurizer pressure and water level control systems respond to deviations from preselected setpoints caused by the expansion or contraction of the reactor coolant and actuate the spray or heaters and the charging or letdown systems as necessary to maintain pressurizer pressure and water level.

4.4.3.6 Thermal and Hydraulic Characteristics Table

Principal thermal and hydraulic characteristics of the RCS components are listed in Table 4.4-10.

4.4.4 EVALUATION

4.4.4.1 Critical Heat Flux

The margin to critical heat flux (CHF) or DNB is expressed in terms of the DNBR. The DNBR is defined as the ratio of the heat flux required to produce DNB at the calculated local coolant to the actual heat flux.

The CE-1 correlation[(1)(2)] was used with the TORC computer code[(6)] to determine DNBR values for normal operation and anticipated operational occurrences. The CE-1 correlation was developed in conjunction with the TORC code specifically for DNB margin predictions for fuel assemblies with standard spacer grids similar to those in St. Lucie Unit 2. Topical Reports CENPD-162[(1)] and CENPD-207[(2)] provide detailed information on the CE-1 correlation and source data, and also provide comparisons with other data and correlations. In brief, the correlation is based on data from tests conducted for CE at the Chemical Engineering Research Laboratories of Columbia University. Those tests used electrically-heated 5 x 5 array rod bundles corresponding dimensionally to a portion of a 16 x 16 or 14 x 14 assembly with standard spacer grids. The test programs conducted for the 16 x 16 and 14 x 14 assembly geometries each included tests to determine the effects on DNB of the CEA guide tube, bundle heated length, axial grid spacing, and lateral and axial power distributions.

The uniform axial power CE-1 correlation[(1)] was developed from DNB data for six test sections with the following characteristics:

Fuel Assembly Geometry	No. Heated Rods	Lateral Power Distr	Heated Length (ft)	Axial Grid Spacing (in.)
16 x 16	25	Uniform	7	16.0
16 x 16	21	Nonuniform	7	18.3
16 x 16	21	Nonuniform	12.5	17.4
14 x 14	25	Uniform	7	14.3
14 x 14	21	Nonuniform	7	14.3
14 x 14	21	Nonuniform	12.5	14.3

Local coolant conditions at the DNB location were determined by using the TORC code in a manner consistent with the use of the code for reactor thermal margin calculations. The uniform axial power CE-1 correlation was developed from 731 DNB data for the following parameter ranges:

Pressure	1785 to 2415 lb/in.^{2}a
Inlet temperature	382 to 644°F
Heat flux	0.213×10^6 to 0.952×10^6 Btu/h-ft^2

Local coolant quality	-.016 to 0.20
Local mass velocity	0.87×10^6 to 3.21×10^6 lb/h-ft^2

The uniform axial power CE-1 correlation predicted the 731 source data with a mean and standard deviation of the ratio of measured and predicted DNB heat fluxes of 1.000 and 0.068, respectively. The validity of the CE-1 correlation for predicting DNB for 16 x 16 fuel assemblies was further verified by the analysis of data obtained by repeating one of the tests for the 16 x 16 assembly geometry at the Winfrith Laboratory of the UKAEA.

For nonuniform axial power distribution, the uniform axial power CE-1 correlation is modified by the F- factor[5]. The conservatism of that method of predicting DNB for 16 x 16 fuel assemblies with nonuniform axial flux shapes is demonstrated in CENPD-207[2]. CENPD-207[2] presents measured and predicted DNB heat fluxes for a series of tests using nonuniform axial power rod bundles representative of 16 x 16 or 14 x 14 fuel assemblies with standard spacer grids. Those test sections had the following characteristics:

Fuel Assembly Geometry	No. Heated Rods	Lateral Power Distr	Axial Power Distr	Heated Length (ft)	Axial Grid Spacing (ft)
16 x 16	21	Nonuniform	1.46 symmetric	12.5	14.2
16 x 16	21	Nonuniform	1.47 top peak	12.5	14.2
14 x 14	21	Uniform	1.68 top peak	12.5	17.4
14 x 14	21	Nonuniform	1.68 bottom peak	12.5	17.4

The DNB data from those tests were evaluated using the CE-1 correlation modified by the F-factor and the TORC code used in a manner consistent with the use of the code for reactor calculations. The evaluation included DNB data within the following parameter ranges:

Pressure	1745 to 2425 lb/in.^{2}a
Inlet temperatures	333 to 631°F
Local coolant quality	-0.27 to 0.20
Local mass velocity	0.81×10^6 to 3.07×10^6 lb/h-ft^2

It was found that the mean and standard deviation of the ratio of measured and predicted DNB heat fluxes were 1.229 and 0.125, respectively, for the 369 DNB data within the parameter ranges mentioned above.

Testing was also conducted with rod bundles representative of the 16 x 16 fuel assembly to determine the effect on DNB of local perturbations in heat flux. Results are presented in CENPD-207[2] for two nonuniform axial power rod bundles which were similar except that one test bundle had a heat flux spike (23 percent higher heat flux for a four in. length) at the location where DNB was anticipated. The results show that there is no significant adverse effect on DNB due to that flux spike. Therefore, it is concluded that no allowance is required for the effect on DNB or local heat flux perturbations less severe than that tested.

One important factor in the prediction of DNB and local coolant conditions is the treatment of coolant mixing or turbulent interchange. The effect of turbulent interchange on enthalpy rise in the subchannels of 16 x 16 fuel assemblies with attendant spacer grids is calculated in the TORC code by

$$\hat{P}e = \frac{\omega'}{\overline{G}D_e} = 0.0035$$

where:

$\hat{P}e$ = inverse Peclet number

ω' = turbulent interchange between adjacent subchannels lb/h-ft

D_e = average equivalent diameter of the adjacent subchannels, ft

G = average mass velocity of the adjacent subchannels, lb/h-ft^2

The value of 0.0035 for the inverse Peclet number for use with the 16 x 16 fuel assembly with standard spacer grids was originally chosen based on cold water dye mixing tests conducted for the 14 x 14 assembly and for a "prototype" of the Palisades reactor fuel assembly. The validity of the inverse Peclet number of 0.0035 for the 16 x 16 assembly with standard grids was verified with data obtained in the tests conducted at Columbia University.[(1)]

The design basis requires that the minimum DNBR for normal operation and anticipated operational occurrences be chosen to provide a 95 percent probability at the 95 percent confidence level that DNB will not occur on fuel rod having that minimum DNBR. Statistical evaluation of the CE-1 correlation and relevant data shows that the appropriate minimum DNBR is 1.13[(1)(2)]. Based on review of CENPD-162[(1)], the NRC requires use of a minimum DNBR of 1.19. CE maintains that use of the 1.19 DNBR design limit with the St. Lucie Unit 2 15.8-inch grid spacing is bounded by the 14.3-inch and 17.4-inch grid spacing CHF data. However, the NRC has required that, in the absence of specific test data on the St. Lucie Unit 2 bundle geometry, the design limit DNBR should be penalized resulting in a DNBR limit of 1.20 for Cycle 1. The DNBR limit for Cycle 2 was changed to 1.28. Subsequent cycles that used ESCU also used a DNBR limit of 1.28. Commencing with Cycle 15, RTDP (Reference 71) and a DNBR limit of 1.30 is used. The EPU DNBR limit is 1.32.

Although the illustrative DNBR analysis presented here does not include an allowance for rod bow, Reference 25 provided a method for convoluting the CE-1 DNB statistics with rod bowing statistics, which is applied. Reference 20, particularly in its supplements B and C, provides supporting data on the appropriate adjustments to the unbowed design limit DNBR, to produce a burnup dependent design limit DNBR which includes the effects of rod bow. Modifications are made to the value of F_r^T to account for fuel rod bow DNBR penalty and the additional penalty on DNBR due to increased grid spacing.

For the Bounding Cycle analyses introduced in Cycle 12 the effects of fuel rod bowing on DNBR margin have been incorporated in the safety and setpoint analyses in the manner discussed in References 35, 28, 39 and 40. The rod bowing penalty used for this analysis, 1.2% on minimum DNBR, is valid for bundle burnups up to 31,700 MWD/MTU. This penalty is included in the 1.28 DNBR limit. For assemblies with burnups greater than 31,700 MWD.MTU

sufficient margin is available due to the reduction in radial power peaking to offset potential rod bow penalties for these higher burnup assemblies. Hence, the rod bow penalty based upon Reference 28 and methodology in References 39 and 40 for 31,700 MWD/MTU is bounding for all assembly burnups expected for the bounding cycle.

For the bounding cycle analysis, the rod bowing effects are extrapolated from the 14X14 channel closure data using the L^2/I dependence as discussed in References 39 and 40. L is the span length between two adjacent grids, and I is the moment of inertia of the fuel rod cladding. A comparative analysis of design features of the 14x14 design (rod bow data in Reference 28), the Arkansas Nuclear One Unit 2 design (rod bow data in Reference 39), and St. Lucie Unit 2 with respect to factors that influence rod bow justifies use of the L^2/I dependence for St. Lucie Unit 2. The bases for that conclusion are summarized below.

The mechanism causing rods to bow is compressive axial loads on the rod induced by the spacer grids restraint of differential growth between the fuel rods and the guide tubes. With this loading, the rod behaves like a column with multiple supports.

The basic design differences pertinent to the evaluation of rod bow are the axial spacing between grids (L), the moment of inertia of the cladding (I), the number of spacer grid assemblies, and the differential growth between the fuel rods and the guide tubes. The comparative analysis evaluated the 14x14 design, the St. Lucie 2 design, and the Arkansas Nuclear One Unit 2 design with respect to these differences.

The St. Lucie 2 design was shown to represent less of an extrapolation from the 14x14 design than the Arkansas design because, relative to the Arkansas design, the St. Lucie 2 design has a longer span length; the same moment of inertia of the cladding, fewer spacer grids, and less differential growth between the fuel rods and the guide tubes. Furthermore, there have been no design or manufacturing changes introduced that increase either the as-fabricated rod bow, or the anticipated rod bow as a function of burnup, relative to the Arkansas fuel measured rod bow.

Since rod bow data has demonstrated the applicability of the L^2/I dependency for Arkansas and the St. Lucie 2 design has been shown to be conservatively represented by the Arkansas design, the L^2/I dependence has been applied in extrapolating from the 14x14 channel closure data to determine the rod bow penalty for St. Lucie 2 fuel.

For the WCAP-9272 bounding cycle analysis, the ABB-NV DNB correlation (Reference 42) was used as the primary correlation with the VIPRE code (References 44 and 45) to determine DNBR values. The ABB-NV correlation was developed for CE14x14 and CE16x16 non-mixing vane fuel designs, based on the Critical Heat Flux (CHF) test data obtained from the Heat Transfer Research facility of Columbia University. The CHF tests simulated 5x5 and 6x6 arrays of the fuel assembly geometry with or without guide tubes, uniform and non-uniform axial power shapes, and different grid designs and heated lengths. The empirical correlation includes the following variables: pressure, local mass velocity, local quality, distance from grid to CHF location, heated length and the heated hydraulic diameter of the CHF subchannel. Special geometry terms are used in the correlation to correct CHF for grid, heated length, cold wall and guide tube effects. The Tong F-factor was also optimized and applied to the correlation to account for the effects of non-uniform axial power shapes. The 95/95 DNBR limit for the ABB-NV correlation is 1.1.3 (Reference 42).

The ABB-NV correlation was developed and first applied with the TORC code. Reference 43 provides justification on use of the ABB-NV correlation with the VIPRE code and demonstrates

that VIPRE is equivalent to TORC for the DNBR calculations. The inverse Peclet number of 0.0035 for the CE16x16 fuel assembly remains unchanged with the the use of VIPRE code. The 95/95 DNBR limit for the ABB-NV correlation remains applicable with the VIPRE code under the following parameter ranges:

Pressure	1750 to 2415 psia
Local Mass Velocity	0.8 to 3/16 Mlbm/hr-ft^2
Local Quality	-0.14 to 0.22
Heated Length, Inlet to CHF Location	48 to 150 inches
Grid Spacing	8 to 18.86 inches
Heated Hydraulic Diameter Ratio	0.679 to 1.08

4.4.4.2 Reactor Hydraulics

Design reactor hydraulic parameters include the distribution of flow in the reactor core, the sum and breakdown of irreversible pressure drops, and the forces due to flow acting on various reactor internal components. These parameters are derived for steady state flow conditions from flow test measurements in reactor scale models and full-scale prototype fuel assemblies. These tests are part of the Combustion Engineering reactor development program and are instituted whenever results of prior tests cannot be extended with sufficient accuracy for evaluation of a new reactor or component design.

4.4.4.2.1 Reactor Flow Model Tests

Combustion Engineering (CE) reactor scale model flow test programs have supported the progression of seven basic geometric configurations, as follows:

Configuration	Reactor(s)	Distinguishing Hydraulic Features
1	Palisades	Four inlets, two outlets, cruciform control elements, 204 fuel assemblies.
2	Fort Calhoun	Four inlets, two outlets, 5-rod control elements, 133 fuel assemblies.
3	Maine Yankee	Three inlets, three outlets, 5-rod control elements, 217 fuel assemblies 137 inch active core.
4	2560 MWT Class: Calvert Cliffs 1 and 2, St. Lucie Unit 1 and 2, Millstone 2	Four inlets, two outlets, 5-rod control elements, 217 fuel assemblies, 137 inch active core
5	Arkansas Nuclear One (Unit 2)	Four inlets, two outlets, 5-rod control elements, 177 fuel assemblies 150 inch active core
6	3400 MWT Class: San Onofore 2 and 3 Forked River Waterford 3, Pilgrim 2	Four inlets, two outlets, 5-rod control elements, 217 fuel assemblies, 150 inch active core.
7	System 80	Four inlets, two outlets, 4-rod control elements, 241 fuel assemblies modified upper and lower plena design 150 inch active core.

Flow model tests have been conducted for configurations 1 through 4, 6 and 7. The configuration 1 and 2 tests were run under contract to Battelle Memorial Institute using air as the test medium. The configuration 3, 4, 6 and 7 tests were performed in a 15,000 gal/min cold water facility in the CE Nuclear Laboratories. All final tests have been with representation of the entire reactor; generally at 1/5 scale. The final System 80 flow model, configuration 7, was constructed at 3/16 scale. Model components for these tests were constructed geometrically to scale, with the exception of the model core, where individual fuel assemblies were represented by "core tubes".

Core tubes for configuration 1 through 4 were "closed", with a single flow metering orifice sized to represent the fuel assembly axial flow resistance. Core tubes for configurations 6 and 7 were "open", with prototypical flow redistribution permitted through holes in the double-wall boundaries between adjoining core tubes. Fuel assembly axial flow resistance in the open-core tests was represented by a series of six orifice plates.

Hydraulic design analysis methods for St. Lucie Unit 2 are based on appropriate consideration of data from all flow model tests through configuration 6. Test results most directly applicable to St. Lucie Unit 2 are those of configurations 4 and 6. The configuration 4 and 6 models have identical geometry up to the core inlet. Beyond the core inlet, configuration 6 most closely represents St. Lucie Unit 2, since St. Lucie Unit 2 has the 3400-MWT class 16 x 16 fuel rod array and outlet plenum geometry. Except for its shorter core and lower power rating, St. Lucie Unit 2 would be grouped with the 3400 MWT class reactors.

Descriptions of the 1/5 scale configuration 6 flow model, the test facility, and portions of the test information can be found in Appendix A of CENPD-206[10]. An elevation view of the flow model is shown here on Figure 4.4-11. Instrumentation was installed at several points within the reactor flow model to measure the variables of interest. The coolant flow path on the model was segmented by station numbers from inlet to outlet as shown in Figure 4.4-11. The tabulation below describes the measured variables and the location and type of instrumentation.

	Measured Variable	Model Station	Description of Instrumentation
1.	Inlet duct flowrate	Inlet ducts, upstream of station 1	Pressure differential measured across a Gentile- type flow meter in each inlet duct.
2.	Inlet nozzle static pressure	Station 1	Static pressure measured at each inlet nozzle, using four equally spaced pressure taps upstream of inlet elbows.
3.	Downcomer inlet static pressure	Station 5	Static pressure measured at each of 12 pressure taps located equally spaced around the vessel wall.
4.	Downcomer outlet static pressure	Station 7	Static pressure measured at each of 12 pressure taps locations equally spaced around the vessel wall.
5.	Core tube inlet static pressure	Station 13	Static pressure measured in each core tube with a wall static pressure tap at a position of 0.5 inches upstream of the inlet orifice plate.
6.	Core tube inlet flowrate	Station 17	Differential pressure measured across each core tube inlet orifice plate with static pressure taps 0.5 inches upstream and 0.25 inches downstream of the orifice plate.
7.	Core tube outlet static pressure	Station 18	Static pressure measured in each core tube with a wall static pressure tap at a position of 0.5 in. upstream of the outlet orifice plate. The static pressure at the core tube exit, (station 20) was calculated from static pressures measured at station 18, the measured core tube exit flow rate, and the calibrated core tube exit pressure loss coefficients.
8.	Core tube outlet flowrate	Station 18	Pressure differential measured across each core tube outlet orifice plate with static pressure taps 0.5 in. upstream and 0.25 in. downstream of the orifice plate.

9.	Outlet nozzle static pressure	Station 24	The static pressure measured at each outlet nozzle using four equally spaced pressure taps just downstream of the outlet nozzle.
10.	Outlet nozzle flowrate	Outlet ducts, downstream of station 24	Pressure differential measured with an elbow type flow meter in each outlet duct.
11.	Coolant temperature	Test loop duct	Temperature measured with an iron-constantan thermocouple.

The pressure differentials across the flow meters in the inlet and outlet ducts were set and measured with mercury filled manometers. The remaining flow model pressures and pressure differentials were measured using a system consisting of several diaphragm-type pressure transducers with a scanning valve arrangement.

4.4.4.2.1.1 Core Inlet Flow and Core Outlet Pressure Distributions

The core inlet flow distribution and core outlet pressure distribution serve as boundary conditions for TORC open-core thermal margin analysis (refer to Subsection 4.4.4.5.2). The applicable configuration 6 flow model core flow and pressure distributions are given in Appendix A of CENPD -206[10].

For application in reactor TORC analyses, the core inlet flow distribution is non-dimensionalized as the ratio of local to average fluid mass velocity. The core outlet pressure distribution is non-dimensionalized as a Euler number describing individual bundle outlet static pressure relative to the planar average. The standard error of estimate determined for the reactor core inlet flow distribution is three percent; for the reactor core outlet pressure distribution standard error of estimate is one percent.

4.4.4.2.1.2 Reactor Pressure Losses

The reactor vessel pressure losses were determined on the basis of data from the 1/5 scale configuration 6 flow model tests and from the components tests on the CE 16x16 fuel assembly (refer to Subsection 4.4.4.2.2). The flow path segments, using station numbers in Figure 4.4-11 as identification:

Region	Station Numbers
Inlet nozzle and 90° turn	1-5
Downcomer annulus	5-7
Lower plenum	7-13
Core	13-20
Upper plenum	20-24

The reactor vessel pressure loss for the core region (given in Table 4.4-4) was determined from the components test results, while the pressure losses for the remaining regions are based on the flow model results. Where appropriate, corrections were made to the flow model test results to account for differences in Reynolds number and surface relative roughness between model and reactor.

4.4.4.2.2 Components Testing

Components test programs have been conducted in support of all CE reactors. The tests subject a full- size reactor core module comprising one to five fuel assemblies, control rod assembly and extension shaft, control element, drive mechanism, and reactor internals to reactor conditions of water chemistry, flow velocity, temperature, and pressure under the most adverse operating conditions allowed by design. Two objectives of the programs are to confirm the basic hydraulic characteristics of the components and to verify that fretting and wear will not be excessive during the component's lifetime. When the reactor design is revised, a new program embodying the important aspects of the latest design is conducted.

Thus, components tests have been run on the Palisades design, with cruciform control rods, on the Fort Calhoun with CEAs and rack-and-pinion control element drive mechanisms (CEDM), on the Maine Yankee design with a dual CEA and a magnetic jack CEDM, and on the Arkansas design with a 16x16 fuel assembly, a CEA, and magnetic jack CEDM.

During the course of the tests, information is obtained on fuel rod fretting, on CEA/CEDM trip behavior, and on fuel assembly uplift and pressure drop. The first two subjects are discussed in Section 4.2. The third is discussed below.

As part of the assessment of fuel assembly margin to uplift in the reactor, measurements are made of the flow rate required to produce fuel assembly lift-off over a temperature range of 150 to 600°F at a system pressure of 350 to 2250 psia. To obtain the desired information, the point of fuel assembly lift-off is determined with load beams or lift-off conductivity probes. With the first appproach, one of the fuel assemblies of the module is mounted on the load beam so that the assembly net weight can be monitored as a function of flow rate and temperature. Fuel assembly lift-off is established when the net weight goes to zero. With the second approach, the lift-off probes are mounted to contact the bottom of the fuel assembly. When the fuel assembly is seated, the contact between the assembly and lift-off is indicated by a large step change in the circuit resistance, caused by the break in contact between the probes and the fuel assembly.

Data reduction involves the calculation of an uplift coefficient, describing the hydraulic uplift force acting on the assembly; the coefficient is defined as follows:

$$K_{up} = Wo/(\rho V^2 A/2 g_c)$$

where:

W_o = wet weight of assembly, lb.

V = flow velocity in assembly at the point of lift-off, ft/sec.

A = envelope area of assembly, ft^2

ρ = water density, lb/ft^3.

A plot of the K_{up} data shows that they can be fitted by the relation:

$$K_{up} = \alpha N_R^{-\beta}$$

where α and β are peculiar to the particular components test being run and the standard error of estimate is typically four percent including replication and instrument error.

The uplift coefficient and its associated uncertainty are employed in the analysis of the uplift forces on the fuel assemblies in the reactor. The force is determined for the most adverse assembly location for startup and normal operating conditions. Additional input to the calculation includes analytical corrections to the coefficient for the absence of the CEA, for crud formation, and for small geometrical differences among the fuel assemblies for the different reactor designs all nominally describable by the same components test.

Pressure drop measurements are also made during the components test to verify the accuracy of the calculated loss coefficients for various fuel assembly components. Direct reduction of the pressure drop data yields the loss coefficients for the lower and upper fitting regions, while the spacer grid loss is evaluated by subtracting a calculated fuel rod friction loss from the measured pressure drop across the fuel rod region.

Experience has shown that the experimental end fitting loss coefficients are essentially independent of Reynolds Number and, with their sample standard deviations, are in reasonable agreement with the predicted values used in the calculation of core pressure drop (Subsection 4.4.2.6).

Evaluation of St. Lucie Unit 2 core pressure drop and fuel assembly uplift relationships is made with components test results for Arkansas fuel. Test results reduced to individual spacer grid and end fitting loss coefficients are directly applicable to the shorter St. Lucie Unit 2 fuel. The reactor fuel assembly uplift coefficient is derived by an analytical model which is matched to test results. The analytical model, proven for the Arkansas fuel, is applicable to St. Lucie Unit 2 fuel, with adjustments for the shorter St. Lucie Unit 2 fuel and the fewer spacer grids.

4.4.4.2.3 Core Pressure Drop Correlations

The total pressure drop along the fuel rod region of the core is computed as the sum of the individual losses resulting from friction, acceleration of the fluid, the change in elevation of the fluid, and spacer grids. The individual losses are computed using the momentum equation and the consistent set of empirical correlations presented in the TORC code[6].

In the following paragraphs, the correlations used are summarized and the validity of the scheme is demonstrated with a comparison of measured and predicted pressure drops for single-phase and two-phase flow in rod bundles with CEA-type geometry.

For isothermal, single-phase flow, the pressure drop due to friction for flow along the bare rods is based on the equivalent diameter of the bare rod assembly and the Blasius friction factor:

$$f = 0.184\ N_R^{-0.2}$$

The pressure drop associated with the spacer grids is computed using a grid loss coefficient (K_{SG}) given by a correlation which has the following form:

$$K_{SG} = D_1\ (N_R)\ D_2 \pm \text{Standard Error of Estimate}$$

The constants, D_n, are determined from pressure drop data obtained for a wide range of Reynolds Numbers for isothermal flow through a CEA-type rod bundle fitted with the high impact

spacer grids. The data comes from a components test program on a 16x16 fuel assembly design (Subsection 4.4.4.2.2). The standard error of estimate associated with the loss coefficient relation includes replication and instrument error.

To compute pressure drop either for heating without boiling or for subcooled boiling, the friction factor given above for isothermal flow is modified through the use of the multipliers given in Pyle[13]. It is important to recognize that the multipliers were developed in such a way as to incorporate the effects of subcooled voids on the acceleration and elevation components of the pressure drop as well as the effect on the friction losses. Consequently, it is not necessary to compute specifically either a void fraction for subcooled boiling or individual effects of subcooled boiling on the friction, acceleration, or elevation components of the total pressure drop.

The effect of bulk boiling on the friction pressure drop is computed using a curve fit to the Martinelli- Nelson data[14] above 2000 lb/in,^{2}a or the Martinelli-Nelson correlation[14] with the modification given in Pyle[13] below 2000 lb/in^{2}a. The acceleration component of the pressure drop for bulk boiling conditions is computed in the usual manner for the case of two-phase flow where there may be a nonunity slip ratio[15]. The elevation and spacer grid pressure drops for bulk-boiling are computed as for single phase flow except that the bulk coolant density ($\overline{\rho}$) is used, where:

$$\overline{\rho} = \alpha \quad \rho_v \quad + (1 - \alpha)\, \rho_\ell$$

and

α = bulk boiling void fraction

p_v = density of saturated vapor, lb/ft^3

ρ_ℓ = density of saturated liquid, lb/ft^3

The bulk boiling void fraction used in computing the elevation, acceleration, and spacer grid losses is calculated by assuming a slip ratio of unity if the pressure is greater than 1850 lb/in^2 absolute or by using the Martinelli-Nelson void fraction correlation[14] with the modifications presented in Pyle [13] if the pressure is below 1850 lb/in^2 absolute.

To verify that the scheme described above accurately predicts pressure drop for single-phase and two-phase flow through the 16x16 assembly geometry comparisons have been made of measured pressure drop and the pressure drop predicted by TORC,[6] for the rod bundles used in the DNB test program at Columbia University (refer to Subsection 4.4.4.1). Figure 6.7 of CENPD-161[6] shows some typical results for a 21 rod bundle of the 16x16 fuel assembly geometry (5x5 array with four rods replaced by a control rod guide tube). The excellent agreement demonstrates the validity of the methods described above.

4.4.4.2.4 Hydraulic Loads on Reactor Internals Components

Hydraulic loads were estimated on the basis of both experimental data from flow model tests on reactor configurations one thorough four and by analytical means. When experimental data are used, they are first reduced to dimensionless forms of a pressure difference coefficient,

$$E = \frac{P_{local} - P_{ref}}{\rho V^2_{ref} / 2 g_c}$$

a force coefficient,

$$C_F = \frac{F}{\rho V^2_{ref} A / 2 g_c}$$

or a velocity ratio,

$$\frac{V_{local}}{V_{ref}}$$

The quantities with subscript "ref" represent appropriate reference values: for example, the average velocity or pressure at the particular flow path station of interest. These dimensionless quantities are then converted to absolute quantities by multiplying by the appropriate reference quantity (i.e., by $V^2_{ref} 2g_c$ or V_{ref}) for the reactor of interest.

Adjustment to the resulting absolute quantities are made by analytical means if there are substantial differences in geometry between the reactor configuration for which the test data were derived and the reactor configuration of interest.

4.4.4.2.5 Effect of Partial or Total Isolation of a Loop on Core Hydraulics

Power generation is only permitted with 4-pump operation and the "low flow trip" will shutdown the reactor if flow to the vessel is reduced due to a loss of one of the coolant pumps (See Section 7.2). However, part-loop operation is permitted during plant startup and shutdown. Hydraulic loads on various reactor internal components were computed for all part-loop configurations to assure the integrity of the components. These part-loop loads are included in the analysis of Subsection 4.4.2.6.3.

4.4.4.3 Influence of Power Distributions

The reactor operation is such that power distributions which are permitted to occur will have adequate margin to satisfy the design bases during anticipated operational occurrences. A discussion of the methods of controlling the power distributions is given in Subsection 4.3.2.4.2. A discussion of the expected power distributions is given in Subsection 4.3.2.2.3, and typical planar rod radial power factors and axial shapes are given in Figures 4.3-2 through 4.3-18. The full-power maximum rod radial power factor is taken as 1.63 and is used in the calculations of the core thermal margins which are given here in Section 4.4. Comparison with expected power distributions, discussed in Section 4.3, shows that this integrated rod radial power factor is at least five percent higher than all the calculated values and, therefore, is a meaningful value for thermal margin analyses.

If CEAs are inserted in the core, the same planar radial power distribution does not exist at each axial elevation of the core, nor does the same axial power distribution exist at each radial location in the core. From the analysis of many three-dimensional power distributions, the important parameters which establish the thermal margin in the core are the maximum rod power and its axial power distribution.[10] Examination of many axial power distributions shows the 1.26 peaked axial power distribution in Figure 4.4-3 to be among those giving the lowest DNBRs. The combination of that axial shape and the maximum rod radial power factor is a

meaningful combination for DNB analyses. The maximum linear heat rate at a given power is determined directly from the core average fuel rod linear heat rate and the nuclear power factor. The value of 2.5 for the nuclear power factor is selected and corresponds to the 1.7 design maximum radial power factor combined with the 1.47 peaked axial shape shown on Figure 4.4-3. The RPS monitors the maximum rod radial power factor and the axial power distribution in the core and ensures that the design limits specified in Subsection 4.4.1 are not violated.

When fuel from regions prior to Region N are present in the core, more favorable power distributions than those used in the bounding thermal-hydraulic design will compensate for the effect of a reduction in inlet flow due to the GUARDIAN™ fuel. Evaluation of power distributions will be performed each transition cycle to confirm the more favorable power distribution assumption. Therefore, the bounding design is expected to be applicable to transition cycles. If the more favorable power distributions do not entirely compensate for the reduction in inlet flow to the GUARDIAN™ fuel for a transition cycle, an additional penalty will be applied to offset the uncompensated adverse effect due to the inlet flow reduction.

4.4.4.4 Core Thermal Response

Steady-state core parameters for Cycle 1 are summarized in Table 4.4-1 for normal four-pump operation. Figure 4.4-12 shows the sensivity of the minimum DNBR to small changes in pressure, inlet temperature, and flow from the conditions specified in Table 4.4-1. The 1.26 peaked axial power distribution and 1.63 maximum rod radial power factor are used.

The response of the core to plant transients is discussed in Chapter 15.

4.4.4.5 Analytical Methods

4.4.4.5.1 Reactor Coolant System Flow Determination

Upon completion of the manufacturing and testing of the pumps, the characteristic pump head or performance curve is established. The maximum allowable, best estimate, and minimum allowable Reactor Coolant System flow rates are determined as follows:

a. Best Estimate Expected Flow

   The best estimate expected RCS flow is determined by equating the head loss around the reactor coolant flow path to the head rise supplied by the reactor coolant pumps (Subsection 5.4.1 has a description of the pumps).

b. Maximum Allowable Flow

   The maximum allowable flow is defined as the upper flow rate limit on the expected flow rate probability distribution above which the actual flow rate has only a 2.3 percent probability of existing. The expected flow rate probability distribution is determined from the statistical combination of the respective pump curve uncertainties, the system resistance uncertainties and the flow measurement uncertainties.

c. Minimum Allowable Flow

The minimum allowable flow is also determined by using the expected flow rate probability distribution discussed above. The minimum allowable flow rate is defined as the lower flow rate limit on the expected flow rate probability distribution below which the actual flow rate has only a 2.3 percent chance of existing. This minimum allowable flow is used for the thermal margin analyses. The minimum allowable reactor coolant flow rate is 369,947 gpm as given in Table 4.4-1 for Cycle 1. This value corresponds to 139.4 x 10^6 lbs/Hr at the reactor inlet coolant temperature of 548°F. The minimum design reactor coolant flow rate of 122 x 10^6 lbs/Hr given in Table 5.1-1 is based upon four times the minimum pump design capacity or 4 x 81,200 = 324,800 gpm.

Upon installation of the pumps in the Reactor Coolant System, the operating flow is determined by one or more of the following flow measurement techniques:

a. Pump casing differential pressure method, using a correlation between pump casing differential pressure and flow rate

b. Calorimetric methods

The uncertainties included in the calculation of the operating flow are those uncertainties associated with the measurement technique or techniques used above. These uncertainties are statistically combined to give the overall uncertainty in reactor coolant flow as determined from onsite tests.

Any significant formation of crud buildup is detected by continuous monitoring of the Reactor Coolant System flow. A significant buildup of crud is not anticipated however, due to maintenance of proper water chemistry.

4.4.4.5.2 Thermal Margin Analysis

Discussions of methodologies within this section are written from an historical perspective and may have been superseded by newer methods as discussed in Section 4.3, Reference 65.

Thermal margin analyses of the reactor core are performed using the TORC code or the VIPRE-01 code which is an open core analytical method based on the COBRA-IIIC code[16]. A complete description of the TORC code and application of the code for detailed core thermal margin analyses is contained in CENPD-161.[6] A simplified procedure used to apply the TORC code for design thermal margin calculations is described in detail in CENPD-206[10]. A brief description of the code and its use is given here.

The COBRA-IIIC code solves the conservation equations for mass, axial and lateral momentum, and energy for a collection of parallel flow channels that are hydraulically open to each other. The size of a channel in the model can vary from the size of one or more fuel assembly down to the size of a subchannel within a fuel assembly. Therefore, certain modifications were necessary to enable a realistic analysis of thermal-hydraulic conditions in both geometries. The principal revisions to arrive at the TORC code, which leave the basic structure of COBRA-IIIC unaltered, are in the following areas:

a. Modification of the lateral momentum equation for core wide calculations where the smallest channel size is typically that of a fuel assembly.

b. Addition of the capability for handling non-zero lateral boundary conditions on the periphery of a collection of parallel flow channels. This capability is particularly important when analyzing the group of subchannels within the hot fuel assembly.

c. Addition of the capability to handle nonuniform core exit pressure distributions.

d. Insertion of standard CE empirical correlations and the ASME fluid property relationships.

Details of the lateral momentum equations and the empirical correlations used in the TORC code are given in CENPD-161[6].

The application of the TORC code for detailed core thermal margin calculations typically involves three stages. The first stage consists of calculating coolant conditions throughout the core on a coarse mesh basis. The core is modelled such that the smallest unit represented by a flow channel is a single fuel assembly. The three-dimensional power distribution in the core is superimposed on the core coolant inlet flow and temperature distributions. The core inlet flow and core exit static pressure distribution are obtained from flow model tests discussed in Subsection 4.4.4.2, and the inlet temperature for normal four-loop operation is assumed uniform. The axial distributions of flow and enthalpy in each fuel assembly are then calculated on the basis that the fuel assemblies are hydraulically open to each other. Also determined during this stage are the transport quantities of mass, momentum, and energy which cross the lateral boundaries of each flow channel.

In the second stage, typically the hot assembly and adjoining fuel assemblies are modelled with a coarse mesh. The hot assembly is typically divided into four to five partial assembly regions. One of these regions is centered on the subchannels adjacent to the rod having the minimum DNBR. The three-dimensional power distribution is superimposed on the core coolant inlet flow and temperature distributions. The lateral transport of mass, momentum, and energy from the stage one calculations is imposed on the peripheral boundary enclosing the hot assembly and the neighboring assemblies. The axial distributions of flow and enthalpy in each channel are calculated as well as the transport quantities of mass, momentum, and energy which cross the lateral boundary of each flow channel.

The third stage involves a fine mesh modelling of the partial-assembly region which centers on the subchannels adjacent to the rod having the minimum DNBR. All of the flow channels used in this stage are hydraulically open to their neighbors. The output from the stage two calculations, in terms of the lateral transport of mass, momentum, and energy is imposed on the lateral boundaries of the stage three partial assembly region. Engineering factors are applied to the minimum DNBR rod and subchannel to account for uncertainties on the enthalpy rise and heat flux due to manufacturing tolerances. The local coolant conditions are calculated for each flow channel. These coolant conditions are then input to the DNB correlation and the minimum value of DNBR in the core is determined.

A more detailed description of this procedure with example is contained in CENPD-161[6]. This procedure is used to analyze in detail any specific three-dimensional power distribution superimposed on an explicit core inlet flow distribution. The detailed core thermal margin

calculations are used primarily to develop and to support the simplified design core thermal margin calculational scheme discussed below.

The method used for design calculations is discussed in detail in CENPD-206[10]. In summary, the method is to use one limiting hot assembly radial power distribution for all analyses, to raise or lower the hot assembly power to provide the proper maximum rod radial power factor, and to use the core average mass velocity in all fuel assemblies except the hot assembly. The hot assembly mass velocity is varied until the simplified thermal margin calculations produce DNBR results which are slightly conservative with respect to the detailed thermal margin calculations. This methodology is used in the thermal margin analyses.

The WCAP-9272 thermal margin analyses are performed using the VIPRE-01 (VIPRE) code (References 44 and 45) VIPRE is a three-dimensional subchannel code the accounts for hydraulic and nuclear effects on enthalphy rise in the core and hot channels. Conservation equations of mass, axial and lateral momentum, and energy are solved for the fluid enthalpy, axial flow rate, lateral flow and pressure drop. The NRC-approved VIPRE code is described in detail in Reference 44, including discussions on code validation with experimental data.

VIPRE modeling of a PWR core is based on the NRC-approved one-pass (or one-stage) modeling approach. In the one-pass modeling, hot channels and their adjacent channels are modeled in detail, while the rest of the core is modeled simultaneously on a relatively coarse mesh. The behavior of the hot assembly is determined by superimposing the power distribution upon inlet flow distribution while allowing for flow mixing and flow distribution between flow channels. Local variations in fuel rod power, fuel rod and pellet fabrication, and turbulent mixing are also considered in determining conditions in the hot channels. The VIPRE modeling method is discussed in Reference 45, including empirical models and correlations used.

The VIPRE core model is used with the applicable DNB correlations to determine DNBR distributions along the hot channels of the reactor core. The effect of crud on flow and enthalpy distribution in the core is not directly accounted for in the VIPRE evaluations. However, conservative treatment by the VIPRE modeling method has been demonstrated to bound this effect in DNBR calculations (Reference 45).

VIPRE is capable of transient DNB and/or fuel temperature analysis. The conservation equations in the VIPRE code contain the necessary accumulation terms for transient calculations. The VIPRE conduction rod model, as discussed in Reference 45, calculates transient temperature distributions of fuel rods and heat flux at the rod surface, based on core power and the local fluid conditions. The input to the conduction rod model includes pellet power profile, heat transfer correlations, and pellet-clad gap conductance. For post-DNB applications, heat addition due to zirconium-water reaction is also considered. The input description can include one or more of the following time-dependent parameters:

- Core inlet flow
- Core power
- Core pressure
- Core inlet temperature or enthalpy
- Core power distributions.

The VIPRE solution methods are generally fully implicit and have no time step size limitations for stability. However, solution instability could occur in transient calculations using a subcooled void model that was developed from steady state data. In order to avoid any numerical instability, appropriate time steps and axial nodes were selected in the transient DNBR calculations to ensure the Courant number greater than one when a subcooled void model is used. The Courant number is defined as:

$$Nc = u\Delta t/\Delta x$$

Where

Nc = Courant number

U = flow velocity

Δt = time step

Δx = axial node size.

4.4.4.5.3 Hydraulic Instability Analysis

Flow instabilities leading to flow excursions or flow oscillations have been observed in some boiling flow systems containing one or more closed, heated channels. Flow instability phenomena are a concern primarily because they may lead to a reduction in the DNB heat flux relative to that observed during a steady flow condition. Flow instabilities are not, however, expected to reduce thermal margin during normal operation or anticipated operational occurrences. This conclusion is based upon available literature, experimental evidence and the results of core flow stability analyses.

Review of the available information on boiling systems has resulted in the following qualitative observations. Flow instabilities which have been observed have occurred almost exclusively in closed channel systems operating at pressures low relative to PWR operating pressures. Increasing pressure has been found to have a stabilizing influence in many cases where flow instabilities have been observed[18] and the high operating pressure characteristic of PWR's minimizes the potential for flow instability. For PWR operating pressures, experimental results[19] have shown that, even with closed channel systems, operating limits due to the occurrence of critical heat flux (CHF) are encountered before the flow stability threshold is reached. It would be expected that the low resistance to coolant crossflow among subchannels of fuel assemblies would have a stabilizing effect, and that expectation is confirmed by experimental results[17][21][22] which show that flow stability in parallel heated channels is enhanced by cross connections between the channels.

Experimental evidence that flow instabilities will not adversely affect thermal margin is provided by the data from the rod bundle DNB tests conducted by CE[1][2]; many rod bundles have been tested over wide ranges of operating conditions with no evidence of premature DNB or of inconsistent data which might be indicative of flow instabilities in the rod bundle.

Analytical support for the conclusion that flow instabilities will not reduce the thermal margin is provided in Reference 23. That document presents an assessment of core flow stability. The assessment was made using the CE-HYDNA code, the CE version of the HYDNA flow stability

code presented in Reference 12. In addition to the flow stability assessment, Reference 23 contains:

a. A description of the CE-HYDNA flow stability code.

b. A user's manual and Fortran listing of the CE-HYDNA code.

c. Results of sensitivity studies and of code verification through comparison with experimental data.

The CE-HYDNA code provides the fundamental analytical tool for the assessment of flow stability. The code has the capability of analyzing transient one-dimensional flow phenomena in several groups of laterally closed channels with common entrance and exit plenums. The use of CE-HYDNA for analysis of open-array cores is conservative because the stabilizing effects of inter-channel communication[17,21,22] are neglected.

The results presented in Reference 23 are for a 3450 MWt class reactor but those results are representative for St. Lucie Unit 2. It was found that, for nominal coolant conditions, the flow is stable throughout the range of reactor power levels examined (100 percent - 250 percent rated power). Additional calculations were performed covering a wide range of operating conditions. These calculations showed that, even under severely adverse operating conditions, the flow is stable at greater than 100 percent of rated power. These results provide additional evidence that flow instabilities will not adversely affect core thermal margin during normal operation or anticipated operational occurrences.

4.4.5 TESTING AND VERIFICATION

Data descriptive of thermal and hydraulic conditions within the reactor vessel will be obtained as part of the startup program. These will include hot and cold leg temperature, loop flowrates, and core power distributions. The data will be evaluated and compared with design calculations and parameters to assure that the reactor thermal and hydraulic behavior is as predicted.

4.4.6 INSTRUMENTATION REQUIREMENTS

The incore instrumentation is used to confirm core power and temperature distributions and to perform periodic calibrations of the excore flux measurement system. Further descriptions are contained in Section 7.7.

4.4.6.1 Loose Parts Monitoring System

4.4.6.1.1 Design Bases

St. Lucie Unit 2 is provided with a loose parts monitoring system (LPMS) that is permanently installed to fulfill the in-service monitoring function during plant operation.

The LPMS monitors the reactor coolant system (RCS) for internal loose parts. The system is designed to detect a loose part striking the internal surface of RCS components with an energy level of one-half foot pound or more within 3 feet of one of the eight sensors.

4.4.6.1.2 Design and Operation

The LPMS consists of transducers, preamplifiers, a computer and readout instrumentation, including a flat panel display to automatically detect and record the occurrence of a loose part within the RCS.

Eight piezoelectric accelerometers are installed externally on the Reactor Coolant System:

a. Two at each steam generator

b. Two at the head of the reactor vessel

c. Two at the bottom of the reactor vessel

The accelerometer signals are individually processed within the containment for wire transmission to an alarm and recording console located in the control instrumentation area. When a loose part is detected, the data acquisition system automatically activates and an audible as well as visual alarm to alert the control room operator. Alarm indication for each accelerometer, and simultaneous recording of signals from all accelerometers is provided at the console. All channels can be recorded and compared to historical data.

Additionally, an alarm indication of a loose part or critical-failure of the system at the loose parts monitor console is also indicated on a control room annunciator. The system will activate the annunciator alarm channel whenever a critical failure or loose part is detected.

A training program is established to train operators in the Operations Department as well as the Instrumentation and Controls Maintenance Department in operation of the Loose Parts Monitoring System.

4.4.6.1.3 Guidelines of Regulatory Guide 1.133

The LPMS is able to detect a metallic loose part that weighs from 0.25 lb to 30 lb and impact with the kinetic energy of 0.5 ft-lb on the inside surface of the reactor coolant pressure boundary within 3 feet of a sensor. Additionally, the system employs High Pass, Low Pass and Algorithms to filter out non-metal to metal impact to minimize the alarms from vibrations that are not loose parts.

Two sensors in each location provide separate signals to one charge amp. Two separate outputs from the charge amp, located outside the Bio-Shield, are transmitted through one cable to the LPMS Cabinet. Separation is required only to a point that is accessible during full power operation which is maintained from the preamp to the sensors.

The LPMS has both an automatic and manual startup to data acquisition equipment. When a loose part is detected, the data acquisition system automatically activates an audible as well as visual alarm to alert the control room operator. This system also provides for recording of all sensor signal waveforms in digital form. Upon alarm, the system defaults to recording the alarming channel as well as the three nearest sensors. The system is capable of immediate visual and audio monitoring of all signals.

The LPMS system provides an alarm for a loose part and alert level for any noise or adverse system condition that is not a loose part. The capability of the system exceeds the Regulatory

Guide requirements by using alternate means of loose parts determination. All channels can be recorded and compared to historical data using the Waveform Software.

A test signal is provided to the preamp to initiate an alarm condition for checking operation of the system to the maximum extent practicable.

The portion of the system located inside the containment is designed for high temperature and humidity, is resistant to the effects of radiation and will function after a design basis earthquake. The processor is a heavy duty, industrial chassis built to withstand vibration and the environment of the Control Room.

The components supplied with the LPMS are of the highest quality available.

Self diagnostics that are a design feature of the LPMS assist in finding problems quickly. Access to the control room equipment is from the rear of the cabinet and any component can be repaired or replaced easily with plug in cables and rack style screw mounting. There are two sensors in each location, one is a backup for more reliable system operation since there is no access to the sensors during operation. The pre-amps are located outside the Bio-Shield which allows access under some at power conditions.

4.4.7 THERMAL AND HYDRAULIC DESIGN EVALUATIONS FOR CE-16 AREVA FUEL

4.4.7.1 Introduction

This section describes the Thermal-Hydraulic (T-H) analysis supporting the AREVA CE-16 HTP™ Fuel. The licensing basis for T-H design for normal operation and AOOs includes the prevention of DNB on the limiting fuel rod with a 95% probability at a 95% confidence level and criteria to avoid fuel centerline melting. The fuel analysis addresses the DNB performance including the effect of fuel rod bowing and bypass flow. The analyses have considered the implementation of the CE-16 HTP™ fuel design described in Section 4.2.2.6. The description of analyses presented in this section is a summary of those presented in Reference 48.

4.4.7.2 Input Parameters, Assumptions, and Acceptance Criteria EC287528

XCOBRA-IIIC is the core T-H sub-channel analysis code that was used for the AREVA fuel analysis. USNRC approval of the XCOBRA-IIIC code was issued in the safety evaluation report (SER) attached to Reference 49. For the fuel analysis, fuel-related safety and design parameters of the CE-16 HTP™ fuel design have been used. These parameters have been used in safety and design analyses discussed in this section.

Biases were applied to input parameters according to the approved methodologies in References 50, 51, and 52. For the transient analyses, uncertainties were deterministically applied. Thus, steady-state measurement and instrumentation errors were taken into account in an additive fashion to ensure a conservative analysis. For statistical DNB calculations, uncertainties were statistically treated according to the approved methodology (Reference 51).

Control grade equipment was modeled in such a way that it does not mitigate the effects of an event. For example, the pressurizer power operated relief valves and pressurizer spray system were assumed operable while the pressurizer heaters were assumed inoperable for DNBR transient events where suppressing primary side pressure is conservative.

The reactor trip setpoints and time delays modeled in the transient analyses were conservatively applied to provide bounding simulations of the plant response. To the extent that the reactor protection system and engineered safety features system is credited in the accident analyses, the setpoints have been verified to adequately protect the plant.

The reactor core is designed to meet the following limited T-H criteria:

- There is at least a 95% probability at a 95% confidence level that DNB will not occur on the limiting fuel rods during Modes 1 and 2, operational transients, or any condition of moderate frequency.

- No fuel melting during any anticipated normal operating condition, operational transients, or any conditions of moderate frequency.

The ratio of the heat flux causing DNB at a particular core location, as predicted by a DNB correlation, to the actual heat flux at the same core location is the DNBR. Analytical assurance that DNB will not occur is provided by showing the calculated DNBR to be higher than the 95/95 limit DNBR for conditions of normal operation, operational transients and transient conditions of moderate frequency.

4.4.7.3 Description of Analyses and Evaluations

The T-H analysis of the CE-16 HTP™ fuel is based on the approved methodologies for performing DNB calculations (References 50, 51, and 52). The S-RELAP5 code was used for the transient analysis. The XCOBRA-IIIC code was used to calculate minimum DNBR (MDNBR) using the HTP (Reference 53) and Biasi (Reference 54) critical heat flux (CHF) correlations. RODEX2-2A (References 55 and 56) and COPERNIC (Reference 57) were used to perform calculations for a fuel rod under normal operating conditions and during transient events. EC287528

The HTP DNB correlation is based entirely on rod bundle data and takes credit for the significant improvements in DNB performance due to the flow mixing nozzles effects. NRC acceptance of the HTP correlation for the CE-16 HTP™ fuel assemblies is documented in Reference 53. The Biasi CHF correlation (Reference 54) is used to calculate the DNBR for post-scram reactor conditions.

The ranges of parameters used in the CE-16 HTP™ design have been verified to fall within the range of applicability for these correlations. A 2% mixed core penalty is typically applied to DNBR safety limits as required by the SER in Reference 50.

The approved methodology for performing DNB calculations for Chapter 15 analyses using the XCOBRA-IIIC code is described in Reference 52. The MDNBR calculations were performed using a steady-state XCOBRA-IIIC model with core boundary conditions at the time of MDNBR from the S-RELAP5 transient analyses.

The Reference 51 topical report describes the method for performing statistical DNB analyses.

Protection against the fuel centerline melting (FCM) SAFDL is expressed as a limit on LHR allowed in the core. Due to the reduced thermal conductivity of gadolinia fuel rods, the FCM limit may be set by gadolinia fuel. A FCM limit is established for UO_2 fuel rods such that, FCM is precluded for all fuel rod types.

The approved methodology for calculating the enthalpy deposition for a control element assembly (CEA) ejection accident is given in Reference 58.

The impact of rod bowing on the MDNBR and peak LHR was evaluated using the rod bow methodology described in Reference 59. The objective was to determine the threshold burnup level at which a rod bow penalty must be applied to either the MDNBR or peak LHR results.

4.4.7.4 Results

UFSAR Chapter 15 summarizes the analysis limits and results for non-LOCA events as applicable to the fuel transition. The results of the analyses demonstrate that the event-specific acceptance criteria are met for implementation of the CE-16 HTP™ fuel design. The compliance with the acceptance criteria is verified on a cycle-by-cycle basis as part of the cycle specific reload evaluation. EC287528

4.4.7.5 Conclusions

The analyses have adequately accounted for the effects of the fuel transition on the thermal and hydraulic design and demonstrated that the design:

- Has been accomplished using acceptable analytical methods,
- Provides acceptable margins of safety from conditions that would lead to fuel damage during normal reactor operation and AOOs, and
- Is not susceptible to T-H instability.

The effects of the fuel transition on the hydraulic loads on the core and RCS components have been adequately addressed. Based on this, it is concluded that the thermal and hydraulic design will continue to meet its current licensing basis with respect to the requirements of GDCs –10 and -12 following implementation of the CE-16 HTP™ fuel design. Therefore, the proposed CE-16 HTP™ fuel transition is acceptable with respect to thermal and hydraulic design.

SECTION 4.4: REFERENCES

1. "Critical Heat Flux Correlation for C-E Fuel Assemblies with Standard Spacer Grids, Part 1, Uniform Axial Power Distribution," September, 1976, CENPD-162-P-A (proprietary), CENPD- 162-A (non-proprietary).

2. "Critical Heat Flux Correlation for C-E Fuel Assemblies with Standard Spacer Grids, Part 2, Non-Uniform Axial Power Distributions," June 1976; CENPD-207-P (proprietary), CENPD-207 (non-proprietary).

3. Tong, L. S., "An Evaluation of the Departure from Nucleate Boiling in Bundles of Reactor Fuel Rods," Nuclear Science and Engineering, Vol 33, pp. 7 to 15, 1968.

4. Letter from Olan O. Parr of NRC to A. E. Scherer of C-E dated May 5, 1976 concerning NRC review of CENPD-162.

5. Tong, L. S., "Boiling Crisis and Critical Heat Flux," AEC Critical Review Series, 1972.

6. "TORC Code: A Computer Code for Determining the Thermal Margin of a Reactor Core," July 1975; CENPD-161-P (proprietary), CENPD-161 (non-proprietary).

7. Maurer, G. W., "A Method of Predicting Steady-State Boiling Vapor Fractions in Reactor Coolant Channels," Bettis Technical Review, WAPD-BT-19, Reactor Technology, June 1960.

8. Dittus, F. W. and Boelter, L. M. K., "Heat Transfer in Automobile Radiators of the Tubular Type," University of California Publication in Engineer Vol 2, No. 13, pp 443-461, 1930.

9. Jens, W. R. and Lottes, P. A., "Analysis of Heat Transfer, Burnout, Pressure Drop, and Density Data for High Pressure Water," ANL-4627, May 1, 1951.

10. "TORC Code Verification and Simplified Modeling Methods," CENPD-206-P (Proprietary), CENPD-206 (Non-Proprietary), January, 1977.

11. "Coast Code Description," approval letter from O. Parr (NRC) to F. Stern (C-E), December 4, 1974, C-E Topical Report, CENPD-98 April 1973.

12. Currin, H. B., et al, "HYDNA-Digital Computer Program for Hydrodynamic Transient in a Pressure Tube Reactor or a Closed Channel Core," Report CVNA-77, 1961.

13. Pyle, R. S., "A Program for the Thermal Analysis of a Pressurized Water Nuclear Reactor During Steady-State Operation, STDY-3," WAPD-TM-213, June 1960.

14. Martinelli, R. C. and Nelson, D. B., “Prediction of Pressure Drop During Forced Circulation Boiling of Water," ASME Transactions, August, 1948.

15. Mendler, O. J., et al., "Natural Circulation Tests with Water at 800 to 2000 psia under Non-Boiling, Local Boiling, and Bulk Boiling Conditions," Journal of Heat Transfer, August 1961.

16. Rowe, D. S., "COBRA-IIIC: A Digital Computer Program for Steady-State and transient Thermal- Hydraulic Analysis of Rod Bundle Nuclear Fuel Elements," BNWL-1695, March 1973.

17. Veziroglu, T. N. and Lee, S. S., "Boiling-Flow Instabilities in a Cross-Connected Parallel-Channel or Flow System," ASME Paper 71-HT-12, August 1971.

18. Boure, J. A., Bergles, A. E., and Tong, L. S., "Review of Two-Phase Flow Instability," ASME Paper 71-HT-42, August 1971.

19. Kao, H. S., Morgan, C. D., and Parker, M. B., "Prediction of Flow Oscillation in Reactor Core Channel," ANS Transactions, Vol 16, P 212, 1973.

20. "Fuel and Poison Rod Bowing," Combustion Engineering Topical Report CENPD-225, October 1976.

21. Kakac, S., et al., "Transient Boiling Flow Instabilities in a Four Parallel Channel Upflow System," Proceedings of Condensed Papers of the Two-Phase Flow and Heat Transfer Symposium- Workshop, October 18-20, 1976, pp. 175-181.

22. RESAR-3S, Volume 2, Section 4.4.3.5, July 1975.

23. Letter to J. F. Stolz, USNRC, from D. H. Williams, Arkansas Power & Light Co., January 16, 1978, and enclosure, "Assessment of Core Flow Stability for C-E PWR's," CEN-64(A)-P (Proprietary and CEN-64(A), (Non-proprietary), July, 1977.

24. "C-E Fuel Evaluation Model Topical Report," Combustion Engineering, Inc., CENPD-139-A (Proprietary), CENPD-139-A (Non-Proprietary) CENPD-139 Supplement 1 (Proprietary), CENPD-139 Supplement 1, Rev. 01 (Non-Proprietary), CENPD-139-P-A (Proprietary), CENPD-139-A (Non-Proprietary) July, 1974.

25. Letter A. E. Scherer, Combustion Engineering, Inc. from D. B. Vassallo US NRC, June 12, 1978, and enclosure, "Staff Review of Fuel Rod Bowing Models".

26. CEN-191(B)-P, "CETOP-D Code Structure and Modeling Methods for Calvert Cliffs Units 1 and 2," December 1981.

27. CEN-123(F)-P, "Statistical Combination of Uncertainties Methodology," Parts 1, 2, and 3, December 1979, January 1980, February 1980, respectively.

28. CENPD-225-P-A, "Fuel and Poison Rod Bowing," June 1983.

29. CEN-124(B)-P, "Statistical Combination of Uncertainties, Part 1," January 1980.

30. CEN-124(B)-P, "Statistical Combination of Uncertainties, Part 2," January 1980.

31. CEN-124(B)-P, "Statistical Combination of Uncertainties, Part 3," March 1980.

32. CEN-371(F)-P, "Extended Statistical Combination of Uncertainties (ESCU)," July 1989.

33. CENPD-161-P-A. “TORC Code. A Computer Code for Determining the Thermal Margin of a Reactor Core,” April 1986.

34. CENPD -206-P-A. “TORC Code. Verification and Simplified Modeling Methods,” June 1981.

35. CEN-348 (B)-P-A, Supplement 1-P-A, “Extended Statistical Combination of Uncertainties,” January, 1997.

36. Letter, Robert a. Clark (NRC) to William Cavanaugh III (AP&L), “Operation of ANO-2 During Cycle 2,” July 21, 1981 (Safety Evaluation Report and License Amendment No. 26 for ANO-2).

37. NUREG-0787, Supplement 1, “Safety Evaluation Report Related to the Operation of Waterford Steam Electric Station, Unit No. 3,” Docket No. 50-382, October 1981.

38. CENPD-207-P-A, “Critical Heat Flux Correlation for C-E Fuel Assemblies with Standard Spacer Grids, Part 2, Non-uniform Axial Power Distribution,” December 1984.

39. Docket No. 50-368, CEN-289(A)-P, “Revised Rod Bow Penalties for Arkansas Nuclear One Unit 2,” December 1984.

40. Letter, Robert S. Lee (NRC) to John M. Griffin (AP&L), Enclosure 2, “Safety Evaluation by the Office of Nuclear Reactor Regulation Related to Amendment No. 66 to Facility Operating License No. NPF-6, Arkansas Power & Light Company, Arkansas Nuclear One, Unit 2, Docket No. 50-368,” May 7, 1985.

41. WCAP-9272-P-A/WCAP-9273-NP-A, “Westinghouse Reload Safety Evaluation Methodology," July 1985.

42. CENPD-387-P-A, Rev. 0, “ABB Critical Heat Flux Correlations for PWR Fuel," May 2000.

43. WCAP-14565-P-A, Addendum 1, “Addendum 1 to WCAP-14565-P-A Qualification of ABB Critical Heat Flux Correlations with VIPRE-01 Code," May 2003.

44. Stewart, C.W. et al., "VIPRE-01: A Thermal-Hydraulic Code for Reactor Cores," Volume 1-3 (Revision 3, August 1989), Volume 4 (April 1987), NP-2511-CCM-A, Electric Power Research Institute.

45. WCAP-14565-P-A/WCAP-15306-NP-A, “VIPRE-01 Modeling and Qualification for Pressurized Water Reactor Non-LOCA Thermal-Hydraulic Safety Analysis," October 1999.

46. WCAP-11397-P-A, “Revised Thermal Design Procedure," April 1989.

47. AREVA Document 77-5069878-01, Replacement Steam Generator Report for Florida Power and Light St. Lucie Unit 2, February 2007.

48. ANP-3352P, Revision 1, "St. Lucie Unit 2 Fuel Transition License Amendment Request Technical Report," November 2015.

49. XN-NF-75-21(P)(A), Revision 2, "XCOBRA-IIIC: A computer Code to Determine the Distribution of Coolant During Steady-State and Transient Core Operation," Exxon Nuclear Company, January 1986.

50. XN-NF-82-21(P)(A), Revision 1, "Application of Exxon Nuclear Company PWR Thermal Margin Methodology to Mixed Core Configurations," Exxon Nuclear Company, September 1983.

51. EMF-1961(P)(A), Revision 0, "Statistical Setpoints/Transient Methodology for Combustion Engineering Type Reactors."

52. EMF-2310(P)(A), Revision 1, "SRP Chapter 15 Non-LOCA Methodology for Pressurized Water Reactors."

53. EMF-92-153(P)(A) Revision 1, "HTP: Departure from Nucleate Boiling Correlation for High Thermal Performance Fuel," January 2005. EC287528

54. Energia Nucleare, Volume 14, No. 9, September 1967, "Studies on Burnout, Part 3 - A New Correlation for Round Ducts and Uniform Heating and Its Comparison with World Data, L. Biasi et. Al."

55. XN-NF-81-58(P)(A), Revision 2 and Supplements 1 and 2, "RODEX2 Fuel Rod Thermal-Mechanical Response Evaluation Model."

56. ANF-81-58(P)(A), Revision 2 and Supplements 3 and 4, "RODEX2 Fuel Rod Thermal-Mechanical Response Evaluation Model."

57. BAW-10231(P)(A) Revision 1, "COPERNIC Fuel Rod Design Computer Code."

58. XN-NF-78-44(NP)(A), "A Generic Analysis of the Control Rod Ejection Transient for Pressurized Water Reactors."

59. XN-75-32(P)(A), Supplements 1, 2, 3, and 4, "Computational Procedure for Evaluating Fuel Rod Bowing."

TABLE 4.4-1

THERMAL AND HYDRAULIC PARAMETERS

Reactor Parameters	St. Lucie Unit 2, Cycle 1	St. Lucie Unit 1, Cycle 3*
Core Average Characteristics at Full Power		
Total core heat output, MWt	2560	2560
Total core heat output, million Btu/h	8737	8737
Average fuel rod energy deposition fraction	0.975	0.975
Hot fuel rod energy deposition fraction	0.975	0.975
Pressurizer pressure, PSIA	2250	2250
Reactor inlet coolant temperature, F	548	542
Reactor outlet coolant temperature, F	596	590
Core exit average coolant temperature, F	598	592
Average core enthalpy rise, Btu/lbm	65.1	64.6
Minimum allowable reactor coolant flow rate, gal/min	369947	369947
Maximum allowable reactor coolant flow rate, gal/min	424350	424350
Maximum core bypass flow, % of reactor coolant flowrate	3.7	3.7
Minimum allowable core flow rate, gal/min	356,259	356,259
Hydraulic diameter of nominal sub-channel, in.	0.4714	0.5334

* Source of data: Letter from RE Uhrig (FP&L) to V Stello (US NRC) dated February 22, 1979, L-79-45, “Proposed Amendment to Facility Operating License.”

TABLE 4.4-1 (Cont'd)

Reactor Parameters	St. Lucie Unit 2, Cycle 1	St. Lucie Unit 1, Cycle 3*
Core flow area, ft^2	54.70	53.5
Core avg mass velocity, million lbm/h-ft^2	2.45	2.53
Core avg coolant velocity, ft/s	15.1	15.4
Core avg fuel rod heat flux Btu/h-ft^2 (1)	151,300	174,400
Total heat transfer area, ft^2	56,315	48,860

(1) Includes factor on fuel densification, does not include heat generated in moderator.

* Source of data: Letter from RE Uhrig (FP&L) to V Stello (US NRC) dated February 22, 1979, L-79-45, "Proposed Amendment to Facility Operating License".

TABLE 4.4-1 (Cont'd)

Reactor Parameters	St. Lucie 2 Cycle 1	St. Lucie Unit 1*
Average fuel rod linear heat rate kW/ft	4.43	6.00
Power density, kW/liter	78.7	9.3
No. of active fuel rods	49,580	36,896
Power Distribution Factors:		
Rod radial power factor	1.70	1.70
Nuclear power factor	2.50	2.71
Total heat flux factor	2.57	2.85
Maximum augmentation factor	1.05	1.06
Maximum gap length, in.	1.80	2.67
Engineering Factors:		
Engineering heat flux factor	1.03	1.05
Engineering enthalpy rise factor	1.03	1.05
Pitch and clad diameter allowance	1.05	1.065
Engineering factor on linear heat rate	1.03	1.03
Fuel densification factor	1.002	1.01
Characteristics of Rod and Channel with Minimum DNBR:		
Maximum fuel rod heat flux, Btu/h-ft^2	388,800	507,000
Maximum fuel rod linear heat rate, kW/ft	11.4	17.1
UO_2 maximum steady state temperature, ^oF	2986	3805
Outlet temperature, ^oF	622	639
Outlet enthalpy, Btu/lbm	646	674
Minimum DNBR at nominal conditions	2.64 (CE-1)	2.37 (orginal W-3)

* Source of data: Letter from RE Uhrig (FP&L) to V Stello (US NRC) dated February 22, 1979, L-79-45, Proposed Amendment to Facility Operating License".

TABLE 4.4-2

COMPARISON OF THE DEPARTURE FROM NUCLEATE BOILING RATIOS COMPUTED WITH DIFFERENT CORRELATIONS

	DNBRs for Nominal Reactor Conditions		DNBRs for Reactor Conditions Giving a 1.19 CE-1 Minimum DNBR in Matrix Subchannel	
Correlation	Matrix Subchannel	Subchannel Next to Guide Tube	Matrix Subchannel	Subchannel Next to Guide Tube
CE-1	3.06	2.64	1.19	1.15
Original W-3[3]	3.47	3.59	1.18	1.25
Revised W-3[5]	3.47	2.95	1.17	1.25
B&W-2[5]	3.79	3.94	1.47	1.71

TABLE 4.4-3

REACTOR COOLANT FLOWS IN BYPASS CHANNELS

Bypass Route	Percent of Total Reactor Flow
Outlet nozzle clearances	0.53
Alignment keyways	0.09
Core shroud annulus	0.63
Guide tubes	1.29
Total bypass	2.54

Note: Bypass flow rate calculations are based on the minimum design reactor flow.

TABLE 4.4-4

REACTOR VESSEL BEST ESTIMATE
PRESSURE LOSSES AND COOLANT TEMPERATURES

Component	Pressure Loss Psi	Temperature (F)
Inlet nozzle and 90° turn	5.0	546
Downcomer, lower plenum, and support structure	10.4	546
Fuel assembly	13.4	574
Fuel assembly outlet to outlet nozzle	6.7	600
Total Pressure Loss	35.5	

TABLE 4.4-5

DESIGN STEADY STATE HYDRAULIC LOADS
ON VESSEL INTERNALS AND FUEL ASSEMBLIES

Load Values at 500 F and at Original Maximum Design
Reactor Coolant Flow

Component	Steady State Load Description	Load Value		
1. Core support barrel	Radial pressure differential directed inward opposite inlet nozzle	58	lb/in2	
	Uplift load	744000	lb	
	Lateral load	189000	lb	
2. Upper guide structure	Uplift load	358000	lb	
	Lateral load	59000	lb	
3. Combined core support barrel and upper guide structure	Uplift load	865000	lb	
4. Flow skirt	Radial load	6000	max.	lb/ft of circ
	directed inward	2900	avg.	lb/ft of circ
	Axial load directed downward	1200	max.	lb/ft of circ
		600	avg.	lb/ft of circ
5. Bottom plate	Drag load directed upward	49000	lb	
6. Core support plate	Drag load directed upward	58000	lb	
7. Fuel alignment plate	Drag load directed upward	99000	lb	
8. Upper guide plate	Load directed downward	53000	lb	
9. Fuel assembly	Uplift load	1900	lb	
10. Core shroud	Radial pressure differential	22	lb/in^2	at bottom
	directed outward	0	lb/in^2	at top
11. CEA shrouds	Lateral drag load	4500	lb.	max tube
12. Instrumentation tube	Lateral drag load	750	lb.	max tube

TABLE 4.4-6

RCS VALVES AND PIPE FITTINGS

PRESSURE BOUNDARY VALVES

Valve	Valve No.	Size In.	Type
Pressurizer safety valves	V1200, V1201 V1202	3 x 6	Safety
Pressurizer power operated relief valves	V1402, V1404	2.5 x 4	Relief
Pressurizer power operated relief isolation valves (upstream/downstream)	V1403, V1405/ V1406, V1407	2.5/4	Gate/Gate
Pressurizer spray valves	PCV1100 E, PCV1100 F	3	Angle
Pressurizer spray bypass valves	V1453, V1454	0.75	Angle
Pressurizer spray isolation valves	V1441, V1442, V1443, V1444	3	Gate
Pressurizer spray check valves	V1248, V1249	3	Check
Pressurizer vapor space sample isolation valve	V1238	0.75	Globe
Pressurizer vent isolation valve	V1239	0.75	Globe
Pressurizer auxiliary spray line isolation valve	V2483	2	Gate
Surge line sample isolation valve	V1210	0.75	Globe
Refueling water level indicator connection isolation valve	V1214	0.75	Globe
Reactor vessel O-ring leak detector connection isolation valve	V1211	0.75	Globe
Reactor leak detector line drain valves	V1392, V1393	0.75	Globe
Reactor vessel head vent isolation valve	V1212	0.75	Globe

TABLE 4.4-6 (Cont'd)

Valve	Valve No	Size In.	Type
Hot leg sample isolation valve	V1213	0.75	Globe
Letdown line isolation valve	V2593	3	Gate
Charging line isolation valves	V2484, V2485	2	Gate
Hot leg shutdown cooling line isolation valves	V3480, V3652	10	Gate
Hot leg injection isolation valves	V3525, V3527	3	Check
Cold leg safety injection and shutdown cooling line isolation valves	V3217, V3227, V3237, V3247	12	Check
Hot leg drain isolation valves	V1215, V1247	2	Globe
Cold leg drain isolation valves	V1449, V1233, V1450, V1235	2	Globe

RCS PIPE FITTINGS

Elbows	Size (In.)	Radius (In.)	Quantity
35°	42 I.D.	63	2
45°	30 I.D.	45	4
60°	30 I.D.	45	6
90°	30 I.D.	45	4
32° 47'-25"	30 I.D.	45	2
90°	12 Sch. 160	Long Radius	2
80° 38'-4"	12 Sch. 160	Long Radius	1

TABLE 4.4-6 (Cont'd)

RCS PIPE NOZZLES

Nozzles	Size (In.)	Schedule	Quantity
Surge	12	160	1
Shutdown cooling outlet	12	160	2
Safety injection and shutdown cooling inlet	12	160	4
Pressurizer Spray	3	160	2
Charging inlet	2	160	2
Letdown	2	160	1
Drain	2	160	4
Sampling	3/4	160	2
Flow measurement	3/4	160	8
RTD penetration	--	--	23

TABLE 4.4-7

RCS FLOWRATES

Cycle 1

Flow Path	Flow (lbm/hr)*
Total RCS flow	139.4×10^6
Core bypass flow	5.1×10^6
Core flow	134.3×10^6
Hot leg flow	69.7×10^6
Cold leg flow	34.85×10^6

*T inlet = 548 F

TABLE 4.4-8

REACTOR COOLANT SYSTEM GEOMETRY

Component	Flow Path Length (ft)	Top Elevation (ft) (d)	Bottom Elevation (ft) (d)	Minimum Flow Area (ft^2)	Volume (ft^3)
Hot Leg	14.53	2.38	-1.75	9.62	139.81
Suction Leg	22.83	1.04	-7.25	4.91	112.07
Discharge Leg					
Parallel	16.39	1.25	-1.25	4.91	80.46
Non-parallel	16.42	1.25	-1.25	4.91	80.52
Reactor Coolant Pump	22.81	1.25	-1.79	4.91[f]	112
Pressurizer	-----	47.20	10.83	----	1500
Liquid level	-----	30.66	10.83	50.07[a]	800
Surge Line	54.51	10.83	1.75	0.56	29.30
Steam Generator					
Inlet nozzle (ea)	2.23	2.24	0.95[e]	9.62	21.77
Inlet plenum	4.64	6.91	0.36	61.04	342.94
Tubes (active and passive)	56.81	37.65	6.91	0.0024[c]	1247.71
Outlet plenum	5.50	6.91	0.36	61.04	337.95
Outlet nozzle (ea)	1.72	1.39	0.16[e]	4.91	8.58
Reactor Vessel					
Inlet nozzles	3.6	1.5	-1.5	4.9	78
Downcomer	20.9	1.5	-20.9	30.3	674
Lower plenum	6.4[b]	-20.9	-27.0	43.7	702
Lower support structure and inactive core	3.5	-17.4	-20.9	28.0	473
Active core	11.4	-6.0	-17.4	54.8	669
Upper inactive core	1.5	-4.5	-6.0	47.1	85
Outlet plenum	11.0[g]	2.0	-4.5	23.45	524
CEA shroud	12.2[g]	9.8	2.0	-----	430
UGS annulus, outside CEA shroud	4.5	6.5	2.0	-----	122
Top Head	-----	13.0	6.5	-----	753
Outlet nozzles	4.1	2.0	-2.0	9.62	105

TABLE 4.4-8 (Cont'd)

Notes:

(a) For the cylinder

(b) Represents a geometrical rather than an actual flow path length

(c) Flow path area per tube

(d) Reactor vessel nozzle centerline is the reference elevation; it has an elevation of 0.0 ft.

(e) Nozzle centerline

(f) RCP outlet

(g) Approximate flow path length

TABLE 4.4-9

SAFETY INJECTION LINE LENGTHS AND SIZES

(x) - (y)[a]	Length (ft.)	Size (in., nominal)
1 - 2	62	12
2 - 3	62	12
2 - 4	240	6
5 - 6	52	12
6 - 7	69	12
6 - 8	140	6
9 - 10	64	12
10 - 11	85	12
10 - 12	87	6
13 - 14	55	12
14 - 15	53	12
14 - 16	34	6
17 - 18	291	3
19 - 20	90	3
4 - 23	106	6
23 - 24	8	3
8 - 21	108	6
21 - 22	8	3
12 - 27	140	6
27 - 28	8	3
16 - 25	143	6
25 - 26	9	3
21 - 29	90	6
23 - 29	59	6

TABLE 4.4-9 (Cont'd)

(x) - (y)[a]	Length (ft.)	Size (in., nominal)
29 - 30	71	10
25 - 31	62	6
27 - 31	57	6
31 - 32	77	10
28 - 33	49	2
26 - 34	23	2
22 - 35	17	2
24 - 36	20	2
22 - 39	68	2
24 - 40	71	2
26 - 41	20	2
28 - 42	12	2
33 - 34	23	4
39 - 40	20	4
34 - 35	2	6
35 - 36	3	6
36 - 37	14	6
37 - 38	9	3
40 - 41	1.5	6
41 - 42	1.5	6
42 - 43	20	6
43 - 44	9	3
18 - 37	136	3
20 - 43	162	3
45 - 50	42	14

TABLE 4.4-9 (Cont'd)

(x) - (y)[a]	Length (ft.)	Size (in., nominal)
46 - 51	67	14
47 - 52	27	6
48 - 49	31	6
49 - 53	6	8
50 - 57	36	24
57 - 58	55	24
57 - 59	203	24
51 - 53	23	24
53 - 55	50	24
55 - 54	190	24
55 - 56	110	24
60 - 62	6	3
61 - 40	10	3

a. The designation (x) - (y) indicates the sections 1-2, 21-22, etc. for the line lengths and sizes as indicated on Figures 6.3-1a and 6.3-1b.

TABLE 4.4-10

REACTOR COOLANT SYSTEM COMPONENT THERMAL AND HYDRAULIC DATA[a]

Cycle 1

Component	Data
Reactor Vessel	
Rated core thermal power, MWt	2560
Design pressure, psia	2500
Operating pressure, psia	2250
Design temperature, F	650
Nominal Coolant outlet temperature, F	596
Nominal Coolant inlet temperature, F	548
Coolant outlet state	Subcooled
Minimum Allowable Reactor Coolant Flow, lbm/hr	139.4×10^6
Core average coolant enthalpy	
Inlet, Btu/lb	545
Outlet, Btu/lb	610
Average coolant density	
Inlet, lb/ft^3	47.0
Outlet, lb/ft^3	43.4
Steam Generators	
Number of units	2
Reactor Coolant side (tube side)	
Design pressure/temperature, psia/F	2500/650
Operating pressure, psia	2250
Design Inlet temperature, F	604
Design Outlet temperature, F	550
Design Flow rate, 10^6 lb/hr	61
Main Steam side (shell side)	
Design pressure/temperature, psia/F	1000/550
Operating pressure/temperature, psia/F (warranted)	815/520.3
Total steam flow per generator, 10^6 lb/hr	5.603

TABLE 4.4-10 (Cont'd)

Component	Data
Steam quality, %	99.8
Feedwater temperature, F	435
Design tube sheet differential pressure, psi	2250
Pressurizer	
Design pressure/temperature, psia/F	2500/700
Operating pressure/temperature, psia/F	2250/652.7
Internal volume, ft^3	1500
Operating water volume, ft^3	800
Heater capacity, KW	1500
Spray rate	
continuous, gpm	1.5
maximum, gpm	375
Reactor Coolant Pumps	
Number of units	4
Design pressure/temperature, psia/F	2500/650
Operating pressure/temperature, psia/F	2250/550
Rated capacity, gpm	81,200
Rated head (hot, 550 F), ft	310
Pump type	Centrifugal
Motor type	Squirrel cage induction
Power requirement, hp (cold)	6500 (1.15 service factor)
Reactor Coolant Piping	
Design Flow per loop, 10^6 lb/hr	
Hot leg	61
Cold leg	30.5

TABLE 4.4-10 (Cont'd)

Component	Data
Pipe size (inside diameter), in.	
Hot leg	42
Suction leg (cold leg)	30
Discharge leg (cold leg)	30
Design pressure/temperature, psia/F	2500/650
Operating pressure/temperature, psia/F	
Hot leg	2250/604
Cold leg	2250/550

a. Full power conditions

Table 4.4-11

St. Lucie Unit 2
Thermal Hydraulic Parameters at Full Power*++++@

General Characteristics	Units	EPU	30% SGTP & WCAP-9272+++	Reference++ or Bounding Cycle
Total Heat Output (Core Only)	MWt	3030	2700	2700
	10^6 Btu/hr	10339	9215	9215
Fraction of Heat Generated in Fuel Rod	--	0.975	0.975	0.975
Primary System Pressure (Nominal)	psia	2250	2250	2250
Inlet Temperature (Maximum Indicated)	°F	551	549	550
Total Reactor Coolant Flow (Minimum Steady State)	gpm	375,000	335,000	363,000
	10^6 lbm/hr	140.7	126.1	136.4
Bypass Flow (Maximum for Minimum Core Flow)	10^6 lbm/hr	5.2	4.7	5.0
Coolant Flow Through Core (Minimum)	10^6 lbm/hr	135.5	121.4	131.4
Hydraulic Diameter (Nominal Channel)	ft	0.039	0.039	0.039
Average Mass Velocity	10^6 lbm/hr-ft^2	2.47	2.21	2.40
Pressure Drop Across Core (Minimum Steady State Flow Irreversible Over Entire Fuel Assembly)	psi	14.3	11.6	13.4
Total Pressure Drop Across Vessel (Based on Nominal Dimensions And Minimum Steady State Flow)	psi	37.8	30.1	35.4
Core Average Heat Flux (Accounts for Fraction of Heat Generated in Fuel Rod and Axial Densification Factor)	Btu/hr-ft^2	173,634***	154,515**	154,723***
Total Heat Transfer Area (Accounts for Axial Densification Factor)	ft^2	58,055***	58,131**	58,055***
Film Coefficient at Average Conditions	Btu/hr-ft^2 - °F	5984	5700	5800
Average Film Temperature Difference	°F	29.0***	27.1**	26.7***
Average Linear Heat Rate of Undensified Fuel Rod (Accounts for Fraction of Heat Generated in Fuel Rod)	kw/ft	5.07***	4.52**	4.52***
Average Core Enthalpy Rise	Btu/lbm	76.3	75.9	70.1
Maximum Clad Surface Temperature	°F	656.7	656.5	656.6
Engineering Heat Flux Factor	----	1.032+	1.032+	1.032+
Engineering Factor on Hot Channel Heat Input	----	1.030+	1.030+	1.030+
Rod Pitch, Bowing and Clad Diameter Factor	----	1.05+	1.05+	1.05+
Fuel Densification Factor (Axial)	----	1.003	1.003	1.003

Table 4.4-11 (cont'd)

St. Lucie Unit 2
Thermal Hydraulic Parameters at Full Power*

Notes:

(*) Due to the statistical combination of uncertainties described in References 35 and 46, the nominal inlet temperature and nominal primary system pressure were used to calculate some of these parameters.

(**) Based on a core containing 33 non-fuel rods (12 shims in St. Lucie Unit 2 Cycle 14, and an allowance for up to 21 stainless steel rods).

(***) Based on a core containing a total of 100 shims and stainless steel rods, the maximum number supported in the St. Lucie Unit 2 reference analysis.

(+) These factors have been combined statistically with other uncertainty factors at 95/95 confidence/probability level and included in the design limit DNBR.

(++) The Bounding Cycle values were first introduced for Cycle 12.

(+++) The WCAP-9272 Bounding Cycle values account for 30% steam generator tube plugging.

(++++) The RSGs are warranted and analyzed to an upper limit of Steam Generator Tube Plugging of 20%.

(@) The 30% SGTP analyses remain the analysis of record with minimum RCS flow of 335,000 gpm. However, partial credit for flow increase from 335,000 gpm to 375,000 gpm is taken for the Locked Rotor and Pre-trip steam line break with LOOP at time = 0.

ASSY. AVG. ROD RADIAL POWER FACTOR →

ASSY. MAXIMUM ROD RADIAL POWER FACTOR →

					.8686 1.4420	1.1803 1.6311	
			.6844 1.1304	.9774 1.3627	1.1755 1.5123	1.4086 1.6185	1.2982 1.4708
		.6875 1.0678	1.0072 1.1893	1.0561 1.2350	1.1068 1.1893	1.2228 1.3900	1.1667 1.3556
	.6876 1.0679	.7655 .8901	.8474 1.0785	.9093 1.0785	1.0521 1.2356	1.0015 1.1770	1.0299 1.2410
.6845 1.1305	1.0073 1.1894	.8474 1.0230	.5320 .6628	.8589 1.0043	.7897 .8428	.9294 1.0665	.6041 .7471
.9776 1.3629	1.0362 1.2352	.9094 1.0786	.8589 1.0044	.8863 1.0460	1.0319 1.2090	.9874 1.1574	1.0171 1.2233
1.1757 1.5126	1.1070 1.2896	1.0523 1.2358	.7898 .8429	1.0319 1.2090	1.0797 1.2554	1.2182 1.3973	1.1538 1.3386
1.4089 1.6188	1.2231 1.3903	1.0017 1.1772	.9295 1.0667	.9874 1.1575	1.2182 1.3973	1.2279 1.4172	1.3429 1.4968
1.2985 1.4711	1.1670 1.3558	1.0301 1.2412	.6042 .7472	1.0172 1.2234	1.1538 1.3387	1.3429 1.4968	1.2879 1.4784

.8688
1.4423

1.1806
1.6315

AMENDMENT NO. 1 (4/86)

FLORIDA POWER & LIGHT COMPANY
ST. LUCIE PLANT UNIT 2

CORE WIDE PLANAR POWER DISTRIBUTION FOR SAMPLE DNB ANALYSIS

FIGURE 4.4-1

CYCLE 1

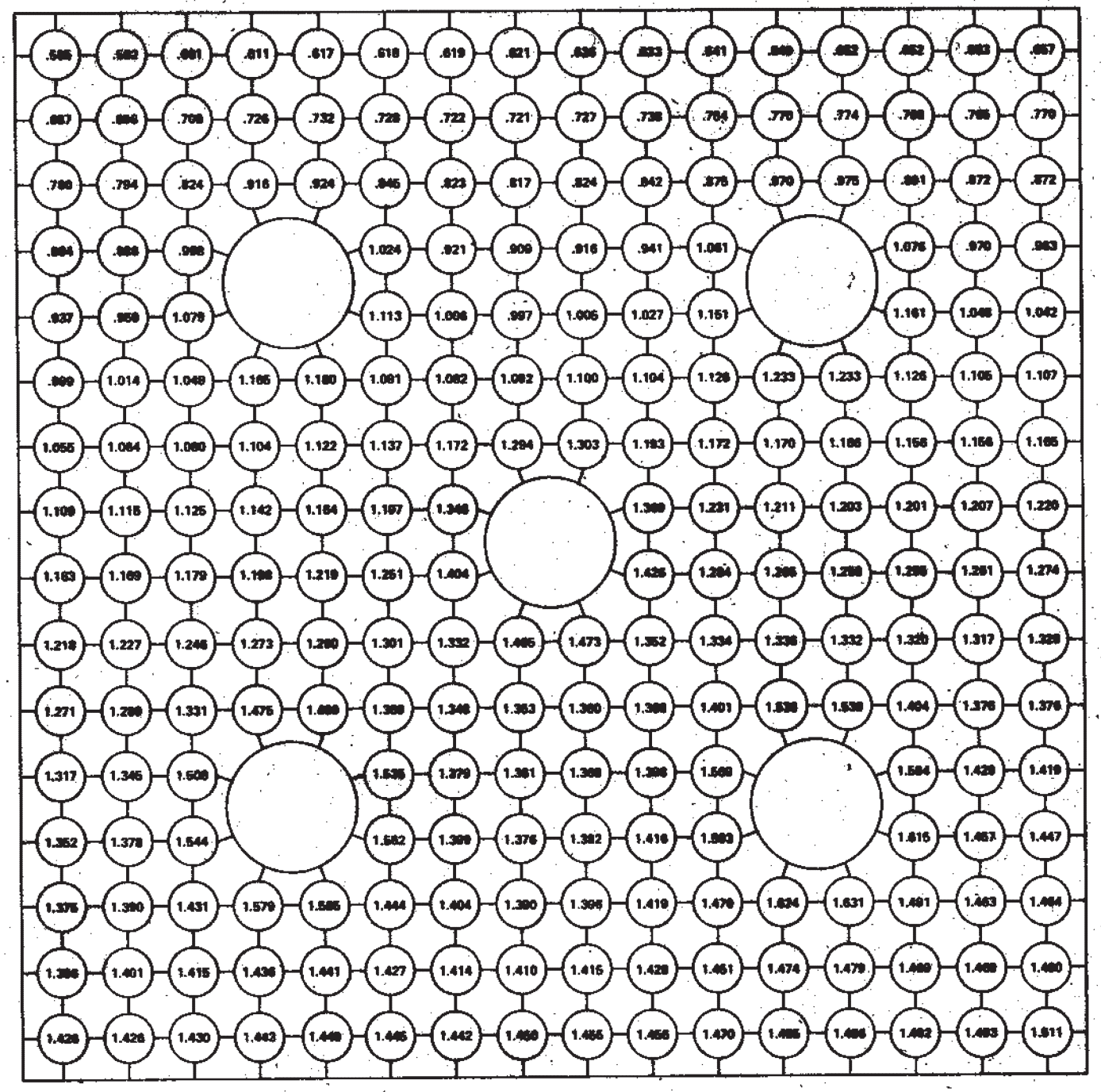

FLORIDA POWER & LIGHT COMPANY
ST. LUCIE PLANT UNIT 2

ROD RADIAL POWER FACTORS IN HOT ASSEMBLY FOR SAMPLE DNB ANALYSIS

FIGURE 4.4-2

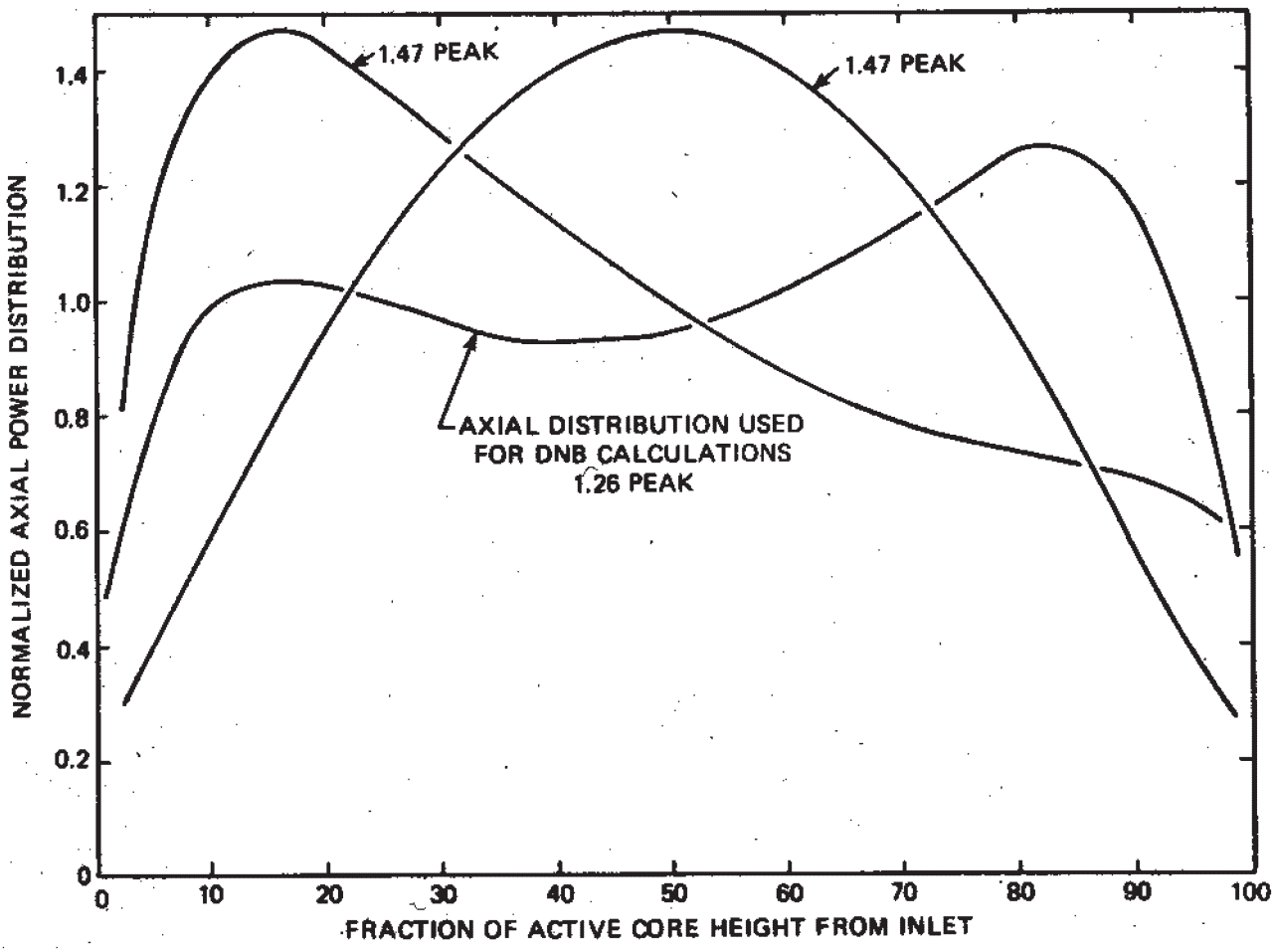

FLORIDA POWER & LIGHT COMPANY
ST. LUCIE PLANT UNIT 2

TYPICAL AXIAL POWER DISTRIBUTIONS
FIGURE 4.4-3

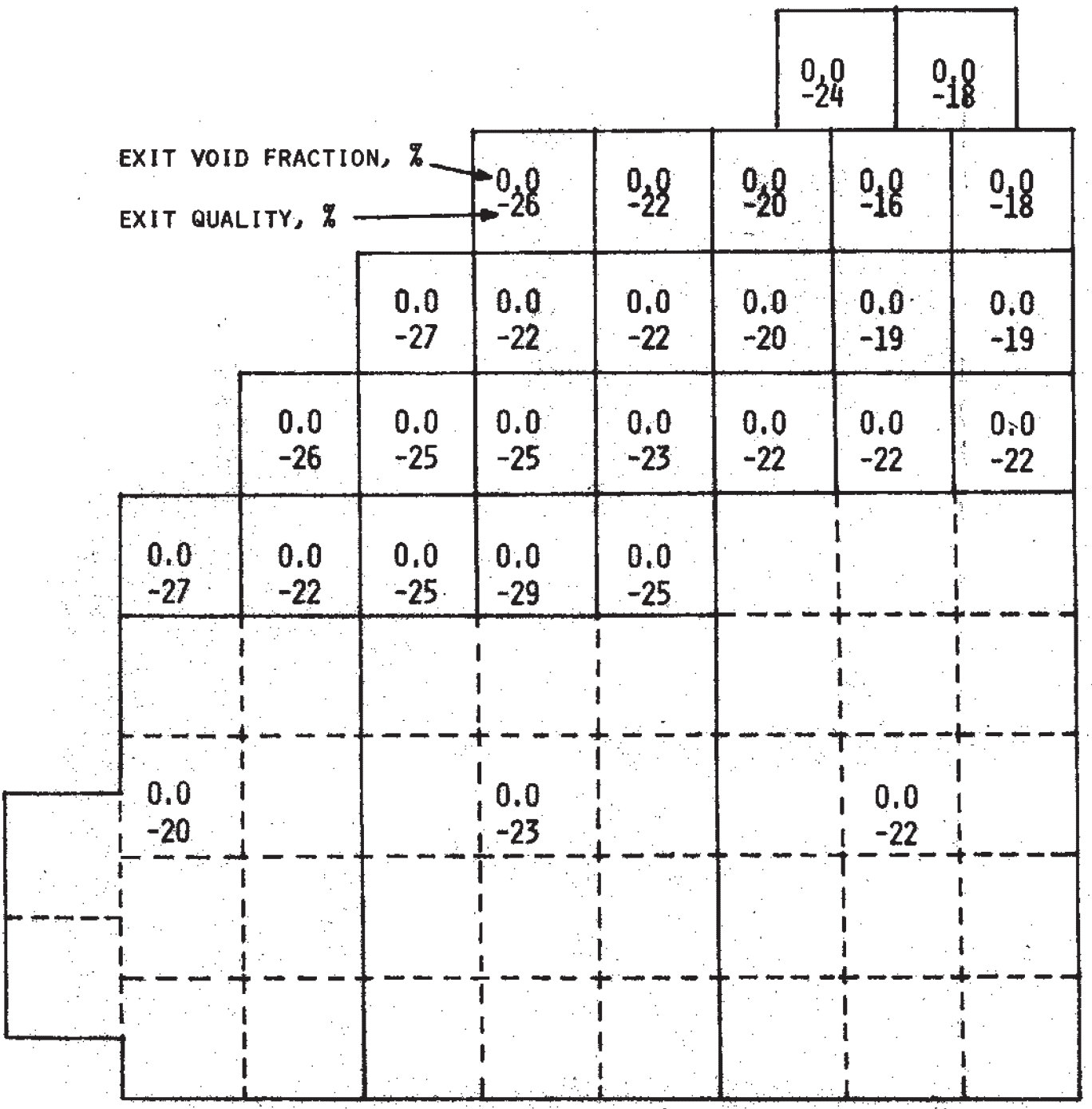

FLORIDA POWER & LIGHT COMPANY
ST. LUCIE PLANT UNIT 2

AVERAGE VOID FRACTIONS AND QUALITIES AT THE EXIT OF DIFFERENT CORE REGIONS

FIGURE 4.4-4

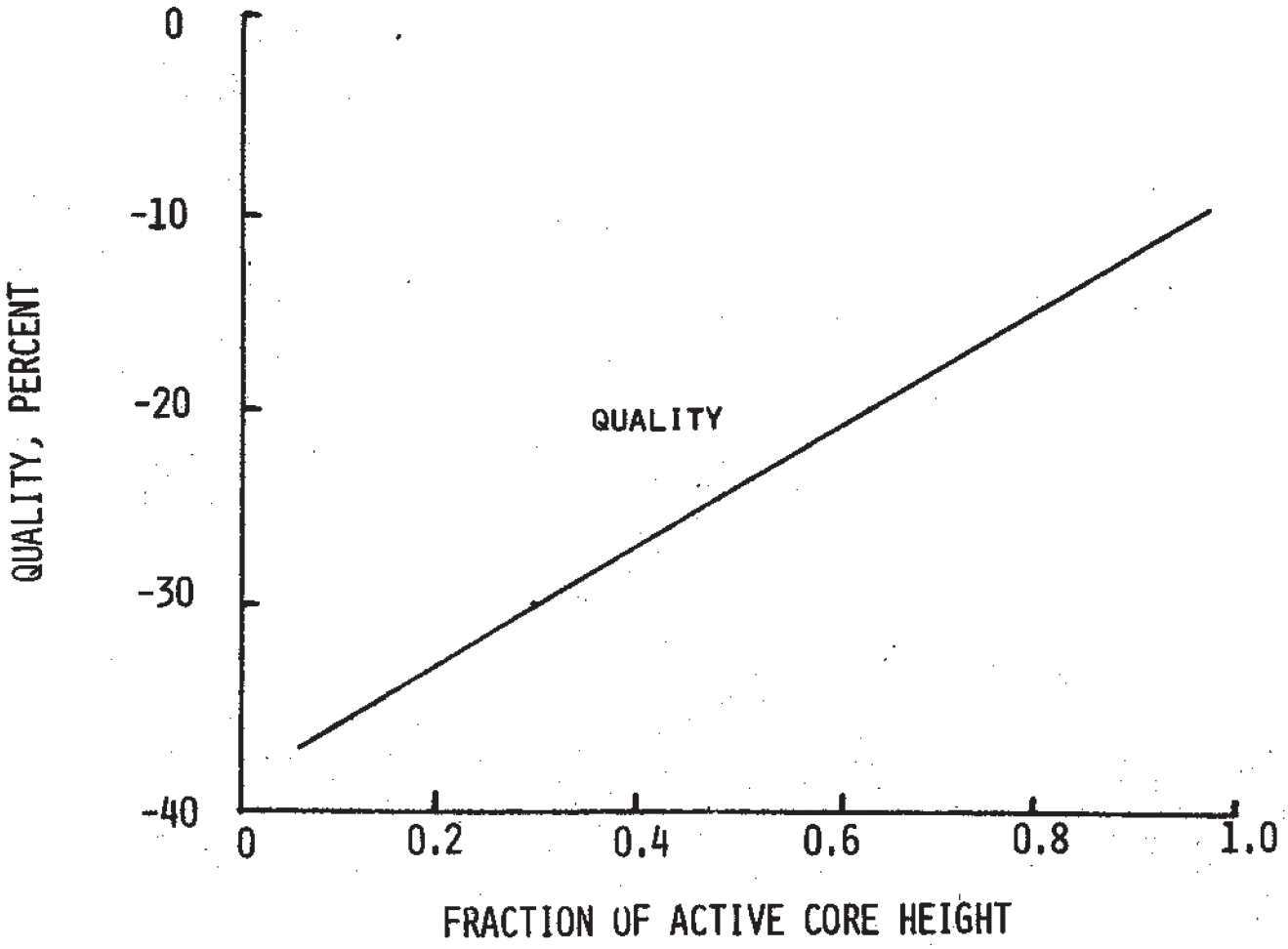

NOTE: VOID FRACTION IS ESSENTIALLY ZERO ALONG THE ENTIRE CORE HEIGHT.

FLORIDA POWER & LIGHT COMPANY
ST. LUCIE PLANT UNIT 2

AXIAL DISTRIBUTION OF VOID FRACTION AND QUALITY IN THE SUBCHANNEL ADJACENT TO THE ROD WITH MINIMUM DNBR

FIGURE 4.4-5

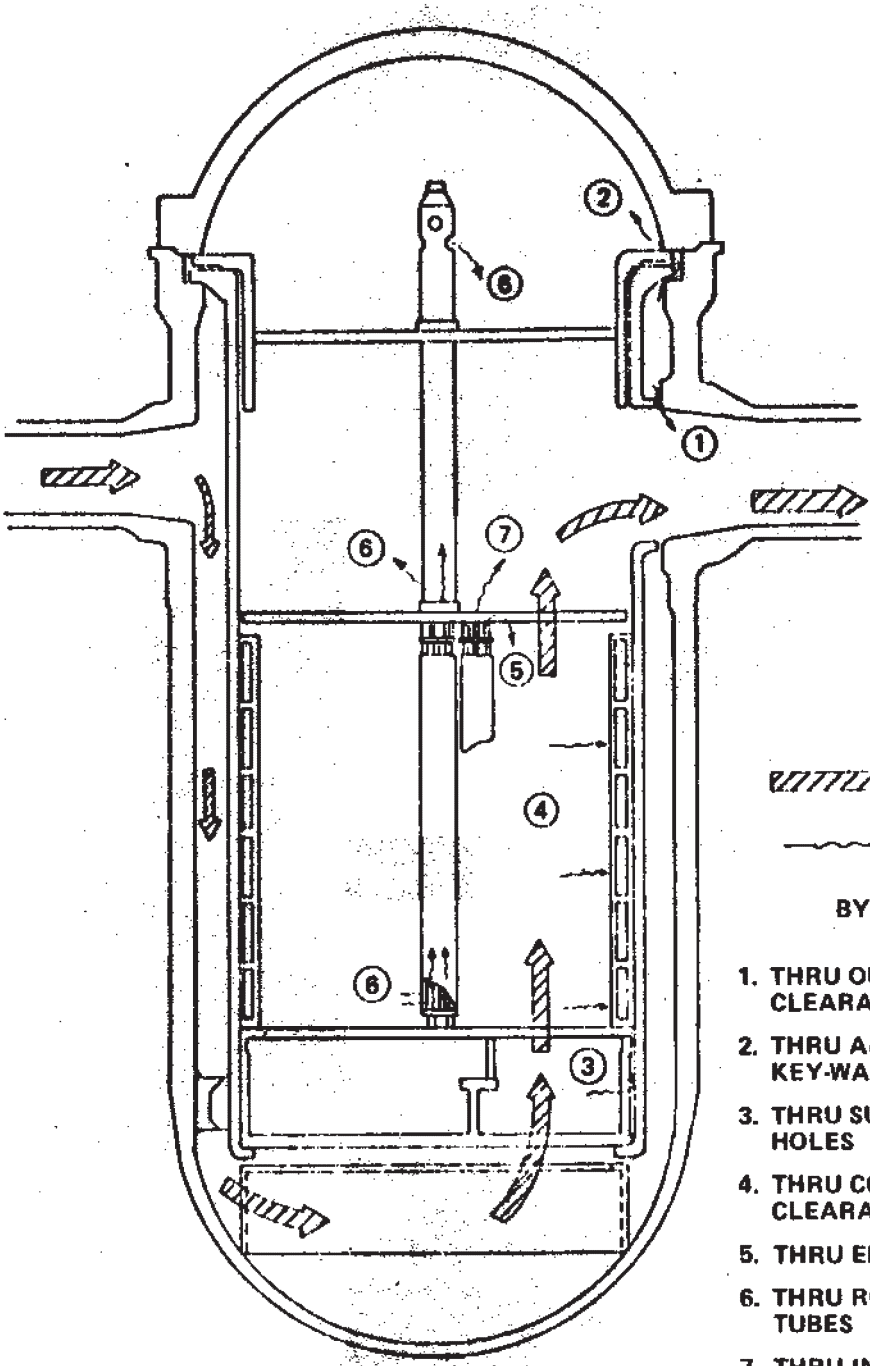

BYPASS PATHS

1. THRU OUTLET NOZZLE CLEARANCES
2. THRU ALIGNMENT KEY-WAYS
3. THRU SUPPORT CYLINDER HOLES
4. THRU CORE SHROUD CLEARANCES
5. THRU EMPTY GUIDE TUBES
6. THRU RODDED GUIDE TUBES
7. THRU INSTRUMENTED CENTER GUIDE TUBES

FLORIDA POWER & LIGHT COMPANY
ST. LUCIE PLANT UNIT 2

REACTOR VERTICAL ARRANGEMENT SHOWING BYPASS FLOW PATHS

FIGURE 4.4-6

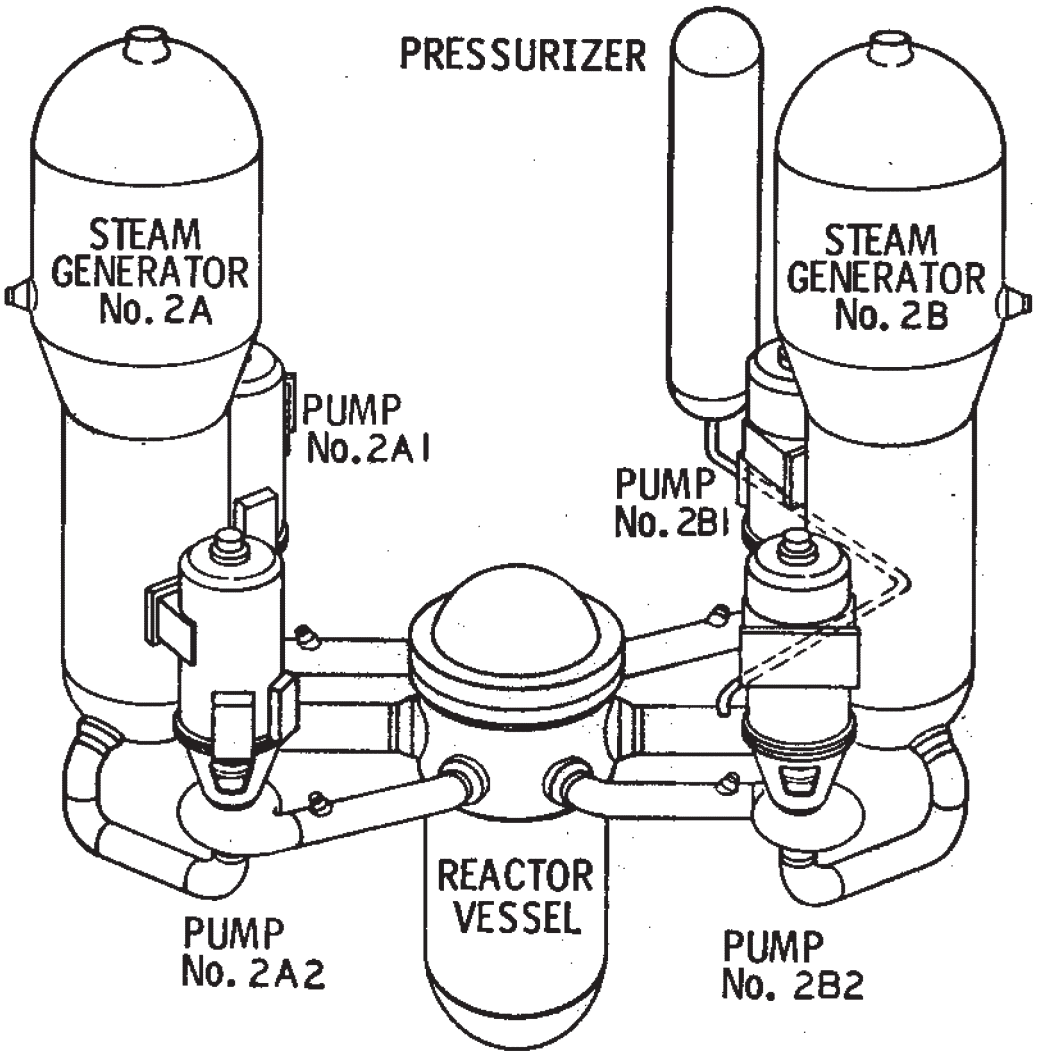

FLORIDA POWER & LIGHT COMPANY
ST. LUCIE PLANT UNIT 2

ISOMETRIC VIEW OF THE REACTOR COOLANT SYSTEM

FIGURE 4.4-7

Deleted

FLORIDA POWER & LIGHT COMPANY
ST. LUCIE PLANT UNIT 2

FIGURE 4.4-8

Deleted

FLORIDA POWER & LIGHT COMPANY
ST. LUCIE PLANT UNIT 2

FIGURE 4.4-9

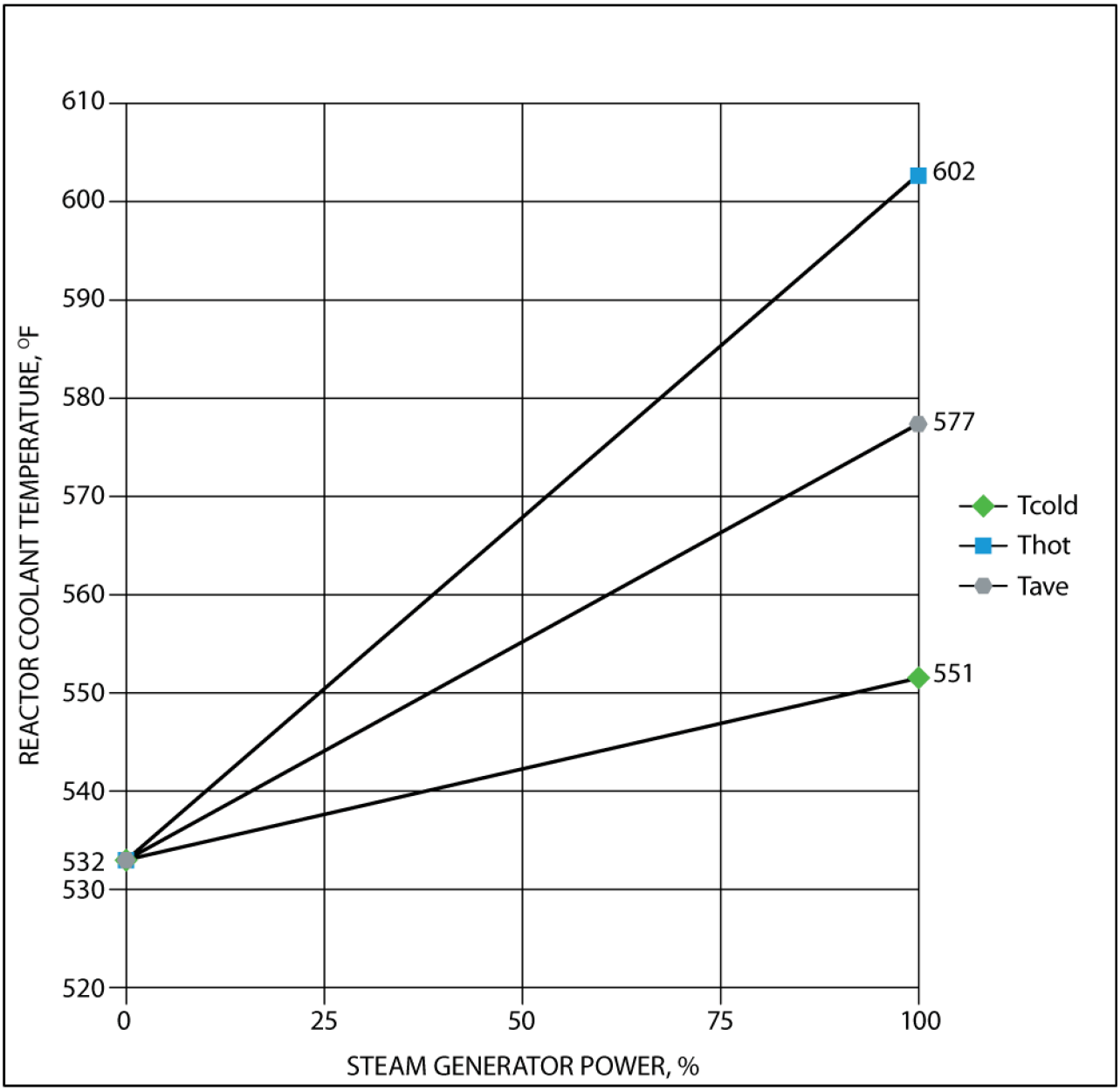

FLORIDA POWER & LIGHT COMPANY
ST. LUCIE PLANT UNIT 2

TEMPERATURE CONTROL PROGRAM

FIGURE 4.4-10

Amendment No. 21 (11/12)

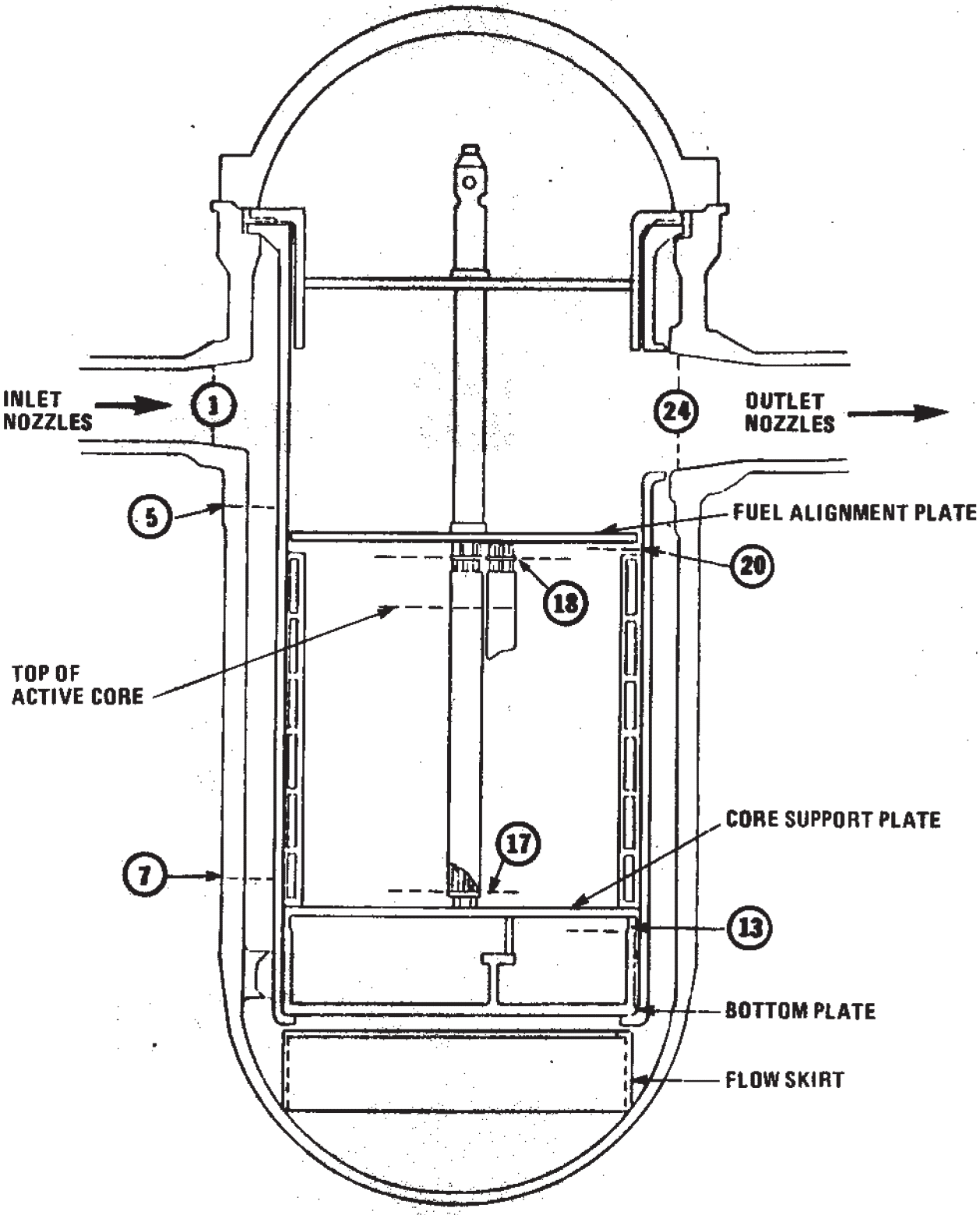

FLORIDA POWER & LIGHT COMPANY
ST. LUCIE PLANT UNIT 2

REACTOR STATIONS

FIGURE 4.4-11

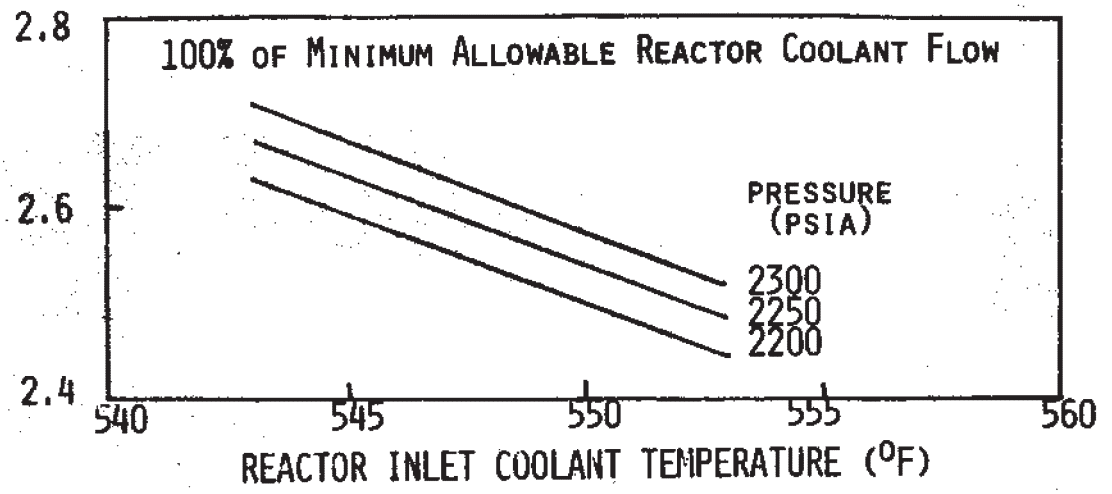

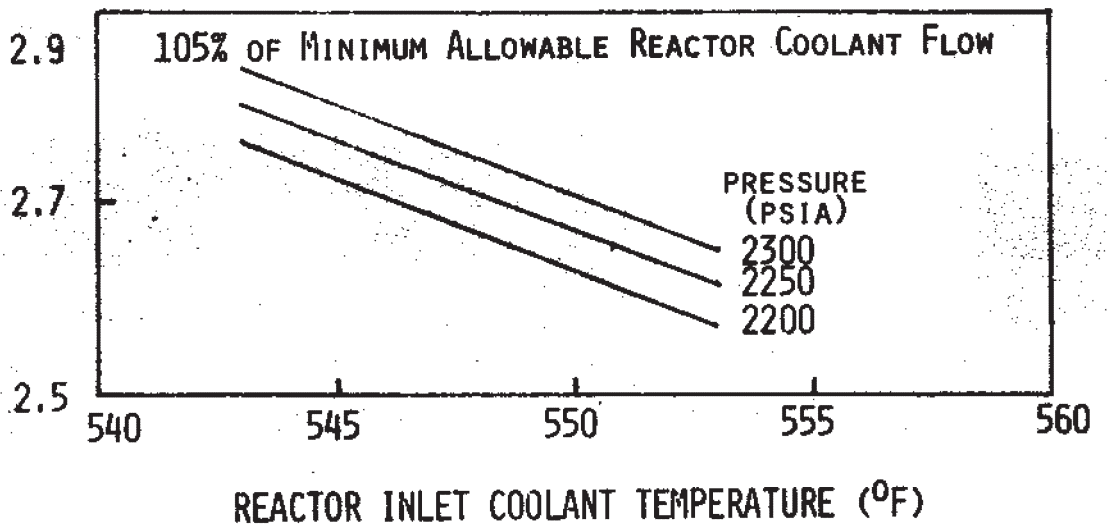

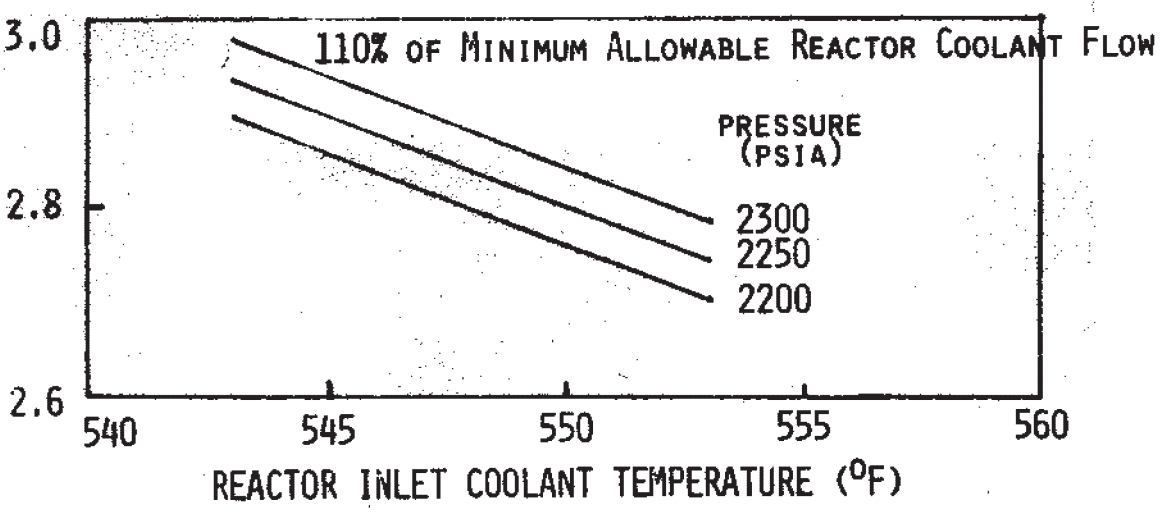

FLORIDA POWER & LIGHT COMPANY
ST. LUCIE PLANT UNIT 2

SENSITIVITY OF MINIMUM DNBR TO SMALL CHANGES IN REACTOR COOLANT CONDITIONS

FIGURE 4.4-12

4.5 REACTOR MATERIALS

4.5.1 CONTROL ELEMENT DRIVE STRUCTURAL MATERIALS

4.5.1.1 Material Specifications

a. The materials used in the control element drive mechanism (CEDM) reactor coolant pressure boundary components are as follows:

1. Motor housing assembly

   SA 182, Type 348 (austenitic stainless steel)

   SA 182, Type 403 Modified, and Code Case N-4-11 (martensitic stainless steel)

   SB 166 (Alloy 690) (nickel-chromium-iron alloy)

2. Upper pressure housing

   SA 213, Type 316 (austenitic stainless steel)

   SA 479, Type 316 (austenitic stainless steel)

   ASTM A276, Type 440 (martensitic stainless steel with yield strength greater than 90,000 lb/in.^{2})

The above listed materials with the exception of the ASTM A270, Type 440 material complay with the following ASME Code Sections and Editions:

Section II, 1998 Edition through 2000 Addenda

Section XI, 1989 Edition, No Addenda

Section XI, 1998 Edition through 2000 Addenda

The functions of the above listed components are described in Subsection 3.9.4.1.1.1.

b. The materials in contact with the reactor coolant used in the CEDM motor assembly components are as follows:

1. Latch guide tubes

   ASTM A269, Type 316 (austenitic stainless steel)

   Chrome Oxide (plasma spray treatment)

2. Magnet and spacer

   ASTM A276, Type 410 (martensitic stainless steel)

3. Latch and magnet housing

   ASTM A276, Type 316 (austenitic stainless steel)

   QQ-C-320a, Class 2B (chrome plating)

4. Spacer

   ASTM A240, Type 304 (austenitic stainless steel)

5. Alignment Button

   AMS 5643J, Type 17-4 PH (martensitic stainless steel)

6. Spring

   AMS 5698B, Inconel X-750 (nickel base alloy)

7. Pin

   Haynes Stellite No. 6B (cobalt base alloy)

8. Dowel pin

   ASTM A314, Type 410 (martensitic stainless steel)

9. Spacer and screw

   ASTM A276, Type 321 (austenitic stainless steel)

10. Stop

    ASTM A276, Type 304 (austenitic stainless steel)

11. Latch and pin

    Haynes Stellite No. 36 (cobalt base alloy)

12. Locking cup and screws

    300 Series austenitic stainless steel

The functions of the CEDM motor assembly components are described in Subsection 3.9.4.1.1.2.

c. The materials in contact with the reactor coolant used in the extension shafts are listed below:

   1. Shafts, rod, and plunger

      ASTM A276, Type 304 (austenitic stainless steel)

ASTM A264, Type 304 (austenitic stainless steel)

2. Gripper

ASTM B446 (nickel-chromium-molybdenum-columbium alloy)

QQ-C-320a, Class 2B (chrome plating)

3. Spring

AMS 5699B, Inconel X-750 (nickel base alloy)

4. Pin

304 austenitic stainless steel

The functions of the extension shaft components are described in Subsection 3.9.4.1.1.5.

d. The weld rod filler materials used with the above listed components are 308 stainless steel, 316 stainless steel and Inconel 52 or 52M.

All of the material except Alloy 690 listed in the above listings, A through D, were used in an extensively tested CEDM assembly that exceeded lifetime requirements, as described in Subsection 3.9.4.4.1. Also, all of the materials have performed satisfactorily in service in the Maine Yankee (Docket 50-309), Millstone II (Docket 50-236), Calvert Cliffs (Docket 50-317), in addition to other CE designed reactors. The CEDM assembly that was tested had Alloy 600 parts and weld material as part of the assembly. For the replacement CEDMs the Alloy 600 materials have been replaced with Alloy 690 materials. Alloy 600 materials have proven to exhibit PWSCC tendencies under some service environments. Alloy 690 materials have proven to be an acceptable material for the replacement of Alloy 600 materials because they have proven to be less susceptible to PWSCC under the same service environments. Therefore, Alloy 690 materials have become the accepted substitute for Alloy 600 materials.

4.5.1.2 Control of the Use of 90 ksi Yield Strength Material

The only control element drive structural material identified in Subsection 4.5.1.4 which has a yield strength greater than 90 ksi is ASTM A276, Type 440, martensitic stainless steel. Its usage is limited to the steel ball in the vent valve on the top of the CEDM. The ball is used as a seal and is not a primary load bearing member of the pressure boundary. This material was tested and exceeded lifetime requirements. Also, this material is presently being used in operating reactors such as Maine Yankee (Docket 50-209), Millstone II (Docket 50-236), and Calvert Cliffs (Docket 50-317) and has performed satisfactorily for the same application.

4.5.1.3 Control of the Use of Sensitized Austenitic Stainless Steel

Control of the use of sensitized austenitic stainless steel is consistent with the recommendations of Regulatory Guide 1.44, "Control of the Use of Sensitized Stainless Steel" May 1973 (R0) as described in Subsections 4.5.1.3.1 through 4.5.1.3.3, except for the criteria used to demonstrate freedom from sensitization. The ASTM A708 (Strauss Test) is used in lieu of the the ASTM A262 Method (A or E) (Modified Strauss Test) to demonstrate freedom from sensitization in

fabricated unstabilized austenitic stainless steel. The former test has shown, through experimentation, excellent correlation with the type of corrosion observed in severely sensitized austenitic stainless steel.

4.5.1.3.1 Solution Heat Treatment Requirements

All raw austenitic stainless steel, both wrought and cast, employed in the fabrication of the control element drive system structural components is supplied in the solution annealed condition as described in Subsection 4.5.2.4.2.1.

4.5.1.3.2 Material Inspection Program

Extensive testing on stainless steel mockups, fabricated using production techniques, was conducted to determine the effect of various welding procedures on the susceptibility of unstabilized 300 series stainless steels to sensitization-induced intergranular corrosion. Only those procedures and/or practices demonstrated not to produce a sensitized structure were used in the fabrication of central element drive system structural components. The ASTM Standard A708 (Strauss Test) is the criterion used to determine susceptibility to intergranular corrosion. This test has shown excellent correlation with a form of localized corrosion peculiar to sensitized stainless steels. As such, ASTM A708 is utilized as a go/no-go standard for acceptability.

4.5.1.3.3 Avoidance of Sensitization

Homogeneous or localized heat treatment of unstabilized austenitic stainless steel in the temperature range 800-1500 F is prohibited.

Weld heat affected zone sensitized austenitic stainless steel (which will fail the Strauss Test, ASTM A708) is avoided in control element drive system structural components by careful control of:

a. Weld heat input to less than 60 kJ/in.

b. Interpass temperature to 350 F maximum.

c. Carbon Content.

4.5.1.4 Control of Delta Ferrite in Austenitic Stainless Steel Welds

The austenitic stainless steel, primary pressure retaining welds in the control element drive system structural components are consistent with the recommendations MTEB 5-1, "The Interm Position of Regulatory Guide 1.31," as described in Subsection 4.5.2.4.3.

4.5.1.5 Cleaning and Contamination Protection Procedures

The procedure and practices followed for cleaning and contamination protection of the control element drive system structural components are as described in Subsection 4.5.2.4.1 and Subsection 4.5.2.5.

4.5.2 REACTOR INTERNALS MATERIALS

4.5.2.1 Material Specifications

The materials used in fabrication of the reactor internal structures are primarily Type 304 stainless steel. The flow skirt is fabricated from Inconel. Welded connections are used where feasible; however, in locations where mechanical connections are required, structural fasteners are used which are designed to remain captured in the event of a single failure. Structural fastener material is typically a high strength austenitic stainless steel; however, in the less critical applications, Type 316 stainless steel is employed. Hardfacing of Stellite material is used at wear points. The effect of irradiation on the properties of the materials is considered in the design of the reactor internal structures. Work hardening properties of austenitic stainless steels are not used.

The following is a list of the major components of the reactor internals together with their material specifications:

a. Core Support Barrel Assembly

   1. Type 304 austenitic stainless steel to the following specifications:

      (a) ASTM-A-182

      (b) ASTM-A-240

      (c) ASTM-A-479

   2. Precipitation hardening stainless steel to the following specifications:

      (a) ASTM-A-453, Grade 660

      (b) ASTM-A-638, Grade 660

b. Upper Guide Structure Assembly

   1. Type 304 austenitic stainless steel to the following specifications:

      (a) ASTM-A-182

      (b) ASTM-A-240

      (c) ASTM-A-249

      (d) ASTM-A-269

      (e) ASTM-A-479

      (f) ASTM-A-451, Grade CPF8

   2. Type 304L austenitic stainless steel to the following specification:

      (a) ASTM-A-312

c. Core Shroud Assembly

1. Type 304 austenitic stainless steel to the following specifications:

(a) ASTM-A-182

(b) ASTM-A-240

d. Holddown Ring

ASTM-A-182, modified to ASME Code Case 1747

e. Incore instrument support system

1. Type 304 austenitic stainless steel to the following specifications:

(a) ASTM-A-193

(b) ASTM-A-194

(c) ASTM-A-213

(d) ASTM-A-240

(e) ASTM-A-249

(f) ASTM-A-312

(g) ASTM-A-473

(h) ASTM-A-479 or ASTM-A-276

(i) ASTM-B-446

(j) ASTM-A-269

2. Zircaloy-4

(a) ASTM-B-351

(b) ASTM-B-353

3. Inconel 625

(a) ASTM-B-446

f. Threaded Structural Fastener and Pin Material

ASTM-A-453 and ASTM-A-638, Grade 660 material (trade name A-286) is used for bolting and pin applications. This alloy is heat treated to a minimum yield strength of 85,000 lb/in. Its corrosion properties are similar to those of the 300 series austenitic stainless steel. It is austenitic in all conditions of fabrication and

heat treatment. This alloy was used for bolting in previous reactor systems and test facilities in contact with primary coolant and has proven completely satisfactory.

g. Chrome Plating and Hardfacing

Chrome plating or hardfacing are employed on reactor internals components or portions thereof where required by function. Chrome plating complies with Federal Specification No. QQ-C-320a, Class 2B. The hardfacing material employed is Stellite 25.

All of the materials employed in the reactor internals and incore instrument support system have performed satisfactorily in operating reactors such as Palisades (Docket 50-255), Fort Calhoun (Docket 50-285), Maine Yankee (Docket 50-309).

4.5.2.2 Welding Acceptance Standards

Welds employed on reactor internals and core support structures-meet the acceptance standards delineated in article NG-5000 Section III, 1974 Edition, and control of welding has been performed in accordance with Sections III and IX of the applicable ASME Code. In addition, consistency with the recommendations of Regulatory Guides 1.31 "Control of Ferrite Content in Stainless Steel Weld Metal" May 1977 (R2) and 1.44 "Control of the Use of Sensitized Stainless Steel" May 1973 (R0) is described in Subsection 4.5.2.4.

4.5.2.3 Nondestructive Examination of Wrought Seamless Tubular Products and Fittings

Quality Group A components in the reactor internals which are wrought seamless tubular products or fittings are consistent with the recommendations of Regulatory Guide 1.66, "Nondestructive Examination of Tubular Products" (since withdrawn 9/77).

The nondestructive examination procedures used for the examination of tubular products and fittings used as elements of the reactor internals are in compliance with the Class 1 requirements of Section III of the ASME Code, 1971 issue, including 1972 Summer Addenda.

4.5.2.4 Fabrication and Processing of Austenitic Stainless Steel

The following information applies to unstabilized austenitic stainless steel as used in the reactor internals.

4.5.2.4.1 Cleaning and Contamination Protection Procedures

Specific requirements for cleanliness and contamination protection are included in the equipment specifications for components fabricated with austenitic stainless steel. The provisions described below indicate the type of procedures utilized for components to provide contamination control during fabrication, shipment, and storage.

Contamination of austenitic stainless steels of the 300 type by compounds that can alter the physical or metallurgical structure and/or properties of the material is avoided during all stages of fabrication. Painting of 300 series stainless steels is prohibited. Grinding is accomplished with resin or rubber-bonded aluminum oxide or silicon carbide wheels that have not previously been used on materials other than 300 series stainless alloys.

Internal surfaces of completed components are cleaned to the extent that grit, scale, corrosion products, grease, oil, wax gum, adhered or embedded dirt, or extraneous material are not visible to the unaided eye.

Cleaning is effected by either solvents (acetone or isopropyl alcohol) or inhibited water (30-200 ppm hydrazine). Water conforms to the following requirements:

Halides	
Chloride, ppm	<0.60
Fluoride, ppm	<0.40
Conductivity, mhos/cm	<5.0
pH	6.0-8.0
Visual clarity	No turbidity, oil or sediment

To prevent halide-induced, intergranular corrosion that could occur in an aqueous environment with significant quantities of dissolved oxygen, flushing water is inhibited via additions of hydrazine. Experiments have proven this inhibitor to be effective.[1] Operational chemistry specifications preclude halides and oxygen, (both prerequisites of intergranular attacks), and are shown in Subsections 9.3.4 and are a part of the Technical Specifications.

4.5.2.4.2 Control of the Use of Sensitized Austenitic Stainless Steel

The recommendations of Regulatory Guide 1.44 (R0), as described in Subsections 4.5.2.4.2.1 through 4.5.2.4.2.5, were followed except for the criteria used to demonstrate freedom from sensitization. The ASTM A708 Strauss Test was used in lieu of the ASTM A262 Method E Modified Strauss Test to demonstrate freedom from sensitization in fabricated unstabilized austenitic stainless steel, since the former test has shown, through experimentation, excellent correlation with the type of corrosion observed in severely sensitized austenitic stainless steel NSSS components. ASTM A262 Method E is used as the acceptance criteria for raw austenitic stainless steel method.

4.5.2.4.2.1 Solution Heat Treatment Requirements

All raw austenitic stainless steel material, both wrought and cast, employed in the fabrication of the reactor internals is supplied in the solution annealed condition as specified by the pertinent ASTM or ASME Code material specification; viz, 1900 to 2050 F for 1/2 to one hour/in. thickness and rapidly cooled to below 700 F. The time at temperature is determined by the size and type of component.

Solution heat treatment is not performed on completed or partially-fabricated components. Rather, the extent of chromium carbide precipitation is controlled during all stages of fabrication as described in Subsection 4.5.2.4.2.4.

4.5.2.4.2.2 Material Inspection Program

Extensive testing of stainless steel mockups, fabricated using production techniques, was conducted to determine the effect of various welding procedures on the susceptibility of unstabilized 300 series stainless steels to sensitization-induced intergranular corrosion. Only those procedures and/ or practices demonstrated not to produce a sensitized structure were used in the fabrication of reactor internals components. The ASTM Standard A708 (Strauss Test) is the criterion used to determine susceptibility to intergranular corrosion. This test has shown excellent correlation with a form of localized corrosion peculiar to sensitized stainless steels. As such, ASTM A708 is utilized as a go/no-go standard for acceptability.

As a result of the above tests, a relationship was established between the carbon content of Type 304 stainless steel and weld heat input. This relationship is used to avoid weld heat affected zone sensitization as described in Subsection 4.5.2.4.2.4.

4.5.2.4.2.3 Unstabilized Austenitic Stainless Steels

The unstabilized grade of austenitic stainless steel with a carbon content greater than 0.03 percent used for components of the reactor internals is Type 304. This material is furnished in the solution annealed condition. The acceptance criteria used for this material as furnished from the steel supplier is ASTM A262 Method E.

Exposure of completed or partially fabricated components to temperatures ranging from 800 to 1500 F is prohibited except as described in Subsection 4.5.2.4.2.5.

Duplex, austenitic stainless steels, containing five vol percent delta ferrite (weld metal, cast metal, weld deposit overlay), are not considered unstabilized since these alloys do not sensitize; i.e., form a continuous network of chromium-iron carbides. Specifically, alloys in this category are:

a. CF8M — Cast stainless steels (delta ferrite controlled to 5-25 volume percent)

b. CF8

c. Type 308 — Singly and combined

d. Type 309 — Stainless steel weld filler metals. (Delta ferrite controlled to 5-18 volume percent as deposited)

e. Type 312

f. Type 316

In duplex austenitic/ferrite alloys, chromium-iron carbides are precipitated at temperatures ranging from 1000-1500 F. This precipitate morphology precludes intergranular penetrations associated with sensitized 300 series stainless steels exposed to oxygenated or otherwise faulted environments.

4.5.2.4.2.4 Avoidance of Sensitization

Exposure of unstabilized austenitic 300 stainless steels to temperatures ranging from 800 to 1600F will result in carbide precipitation. The degree of carbide precipitation, or sensitization, depends on the temperature, the time at that temperature, and also the carbon content. Severe sensitization is defined as a continuous grain boundary chromium-iron carbide network. This condition induces susceptibility to intergranular corrosion in oxygenated aqueous environments, as well as those containing halides. Such a metallurgical structure will readily fail the Strauss Test, ASTM A708. Discontinuous precipitates (i.e., an intermittent grain boundary carbide network) are not susceptible to intergranular corrosion in a PWR environment.

Weld heat affected zone sensitized austenitic stainless steels were avoided (which will fail the Strauss Test, ASTM A708) by careful control of:

a. Weld heat input

b. Interpass temperature

c. Carbon content

A weld heat input of less than 60 kJ/in. is used during most fabrication states of the Type 304 stainless steel core support structure. Higher heat inputs are used in same heavy section weld joints. Freedom from weld heat-affected zone sensitization in these higher heat input weldments is demonstrated with weld runoff samples produced at the time of component welding in material having a carbon content equal to or greater than the highest carbon content of those heats of steel being fabricated. Specimens so provided are subjected to the Strauss Test, ASTM A708.

4.5.2.4.2.5 Retesting Unstabilized Austenitic Stainless Steels

Exposed to Sensitizing Temperature

Sensitization which may be susceptible to intergranular corrosion, is avoided during welding as described in Subsection 4.5.2.4.2.4. Homogeneous or localized heat treatment of unstabilized stainless steels in the temperature range 800 to 1500° F is prohibited except in the case of the core support structure. This complex substructure is thermally stabilized at 900 ± 25° F for seven hours after fabrication and prior to final machining. Such treatment produces only minor, discontinuous precipitates. In addition to thermocouple records during this heat treatment, a sample of Type 304 stainless steel having a carbon content equal to or greater than the highest carbon heat of material present in the structure is included as a monitor sample. After heat treatment, the monitor sample is subject to the Strauss Test, ASTM A708, as well as a metallographic examination to verify freedom from sensitization.

4.5.2.4.3 Control of Delta Ferrite In Welds

The recommendations of MTEB 5-1, "The Interim Position on Regulatory Guide 1.31," were followed in the following manner:

a. The analysis of the filler metal is adjusted to contain a ferrite content of at least five percent and no greater than 15 percent as determined by the modified DeLong Diagram (1973) in the as-deposited condition, and additionally by the use of a calibrated Severn Gauge (or equivalent) measurement on a weld pad.

This delta ferrite requirement is met for each heat or lot of filler metal, heat of consumable inserts, and for each combination of heat of bare electrodes and lot of dry blend of flux mix to be used for welding.

All production welds have to be capable of passing five to 15 percent by volume delta ferrite requirement as determined by a calibrated Severn (or equivalent) Gauge. The vendor performs tests on an audit basis.

4.5.2.4.4 Control of Electroslag Weld Properties

The electroslag process was not utilized to fabricate reactor internal components, and therefore Regulatory Guide 1.34 is not applicable.

4.5.2.4.5 Welder Qualification for Areas of Limited Accessibility

The specific recommendations of Regulatory Guide 1.71, "Welder Qualification for Areas of Limited Accessibility," December 1973 (R0) were not followed. However, performance qualifications, for personnel welding under condition of limited accessibility, are conducted and maintained in accordance with the requirements of ASME Code Sections III and IX. A requalification is required when:

a. Any of the essential variables of Section IX are changed
b. Authorized personnel have reason to question the ability of the welder to satisfactorily perform to the applicable requirements.

Production welding is monitored for compliance with the procedure parameters and welding qualification requirements are certified in accordance with Sections III and IX. Further assurance of acceptable welds of limited accessibility is afforded by the welding supervisor assigning only the most highly skilled personnel to these tasks. Finally, weld quality, regardless of accessibility, is verified by the performance of the required non-destructive examination.

4.5.2.4.6 Non Metallic Thermal Insulation

Nonmetallic thermal insulation is not used on the reactor internals, and therefore Regulatory Guide 1.36 is not applicable.

4.5.2.5 Contamination Protection and Cleaning of Austenitic Stainless Steel

St. Lucie Unit 2 is consistent with the recommendations of Regulatory Guide 1.37, "Quality Assurance Requirements for Cleaning of Fluid Systems and Associated Components of Water-Cooled Nuclear Power Plants," March 1973 (R0). The Quality Assurance Program for safety-related items during onsite cleaning of materials and components cleanliness control, and preoperational cleaning and layup of nuclear fluid systems is in accordance with ANSI N45.2.1-1973 as interpreted by Regulatory Guide 1.37 (R0). ASME NQA-1-1994, Subpart 2.1 was substituted for ANSI N45.2.1 as described in the FPL Quality Assurance Topical Report discussed in Section 17.2.

SECTION 4.5: REFERENCES

1. Habicht, P.R. and Bryant, P.E.C., Fluoride Induced Intergranular Corrosion of Sensitized Austenitic and Austenoferritic Stainless Steel, presented at the International Atomic Energy Authority Workshop on Stress Corrosion Cracking, San Francisco, California, March 1976.

4.6 FUNCTIONAL DESIGN OF REACTIVITY CONTROL SYSTEMS

4.6.1 INFORMATION FOR CEA CONTROL SYSTEMS

Component diagrams, descriptions, and characteristics of the Control Element Drive Mechanisms (CEDMs) are presented in Subsection 3.9.4. Figure 4.6-1 shows the reactor vessel closure head plan view detailing the CEDM layout. The instrumentation is described in Section 7.2 (Reactor Protection System) and Section 7.7 (Control System Not Required For Safety).

4.6.2 EVALUATIONS

Control element assemblies (CEAs) are inserted into the reactor core when electrical power is removed from the coils of the CEDMs by the Reactor Protective System (RPS). A failure modes and effects analysis is presented in Section 7.2 which demonstrates compliance with IEEE Standard 279-1971 and shows that no single failure can prevent electrical power from being removed from the CEDM coils when required. For the trip function, the CEDMs are essentially passive devices. When power is removed from the CEDM coils, the armature springs automatically cause the driving and housing latches to be withdrawn from the CEDM drive shaft, allowing insertion of CEAs by gravity. Actuation of trip breakers is independent of any existing control signals.

For the trip function, all CEDMs are independent of one another. That is, the failure of one CEDM to trip would have no effect on the operability of other CEDMs. Sufficient shutdown margin is always provided to assure that the safety function can be performed assuming the failure of a CEDM.

RPS design criteria are discussed in detail in Subsection 7.2.2.3.

The CEDMs are located where they are protected from common mode failure due to missiles and failure of moderate and high energy pipes. Sections 3.5 and 3.6 discuss protection of essential systems against missiles and pipe breaks. A potential source of common mode failure is loss of air cooling to the CEDM coils. Worst case analysis indicates that there would be adequate mechanical clearances, to permit CEDM trip, at temperatures well above normal operating temperatures of the reactor[1]. Testing was performed to determine the maximum CEDM temperature under conditions that simulated loss of air cooling. With the upper gripper coil energized, which is the normal operating mode, and with a reactor coolant loop temperature of 600° F, the maximum CEDM temperature was 535° F. An analysis of worst case tolerance stack-up within the CEDM indicated adequate clearances to assure scram at 650° F.

Analyses of possible malfunctions are discussed in Section 15.4.

4.6.3 TESTING AND VERIFICATION

The functional testing program for the CEDMCS is described in Subsection 3.9.4.4. (Testing of the CEAs is described in Subsection 4.2.4.4).

As discussed in Subsection 4.6.2, upon reactor trip all CEDMs are independent of one another. Thus, the worst single failure is one that prevents one CEDM from tripping. This failure mode was considered and included in the accident analysis presented in Chapter 15.

Under large break LOCA conditions (Chapter 6) where severe loads may be applied to CEAs, no credit is taken for CEDM functioning.

Testing was performed on a prototype CEDM to verify insertion time, assuming worst case plant operating conditions. Insertion time was verified by dropping the minimum effective (dry) weight of 86 pounds. This weight was calculated to be the minimum effective dry weight, assuming maximum delta-P across the core due to crudding and high reactor coolant density due to operating at a loop temperature of 475 F.

4.6.4 INFORMATION FOR COMBINED PERFORMANCE OF REACTIVITY SYSTEMS

Figures 1.2-3 through 1.2-22 provide plant and elevation layout drawings. These figures show that the CEA Control Systems, Safety Injection System (SIS), and Chemical and Volume Control System (CVCS) are located in the Reactor Building and the Reactor Auxiliary Building. The physical arrangement insures that no single occurrence can affect two or more reactivity control systems concurrently.

Table 4.6-1 lists the postulated accidents evaluated in Chapters 6 and 15 that take credit for two or more reactivity control systems for preventing or mitigating each accident. The related reactivity systems are also tabulated.

The maximum rate of reactivity addition that may be produced by the CVCS is too low to induce any significant pressure forces that might rupture the reactor coolant pressure boundary or disturb the reactor vessel internals.

Inadvertent startup of the Safety Injection System during normal plant operation would have no effect since Reactor Coolant System pressure is higher than the shutoff head of the high pressure safety injection pumps.

4.6.5 EVALUATIONS OF COMBINED PERFORMANCE

Since the CEA Control Systems and the CVCS/SIS are separated and totally diverse in design and operation, with no common link, and since the CEDMCS is protected from the effects of failure of high and moderate energy piping, there are no credible potential common mode failures that could cause the CEDMCS to fail in combination with CVCS or SIS.

Missile protection, pipe rupture and fire safety analyses are provided in Sections 3.5, 3.6 and the Fire Protection Design Basis Document (Reference 2), respectively. EC282743

SECTION 4.6: REFERENCES

1. "Review of Reactor Shutdown System (PPS Design) for Common Mode Failure Susceptability," Combustion Engineering Topical Report, CENPD-148, November 1974.

2. DBD-FP-1, Fire Protection Design Basis Document. EC282743

TABLE 4.6-1

POSTULATED EVENTS REQUIRING OPERATION
OF TWO OR MORE REACTIVITY CONTROL SYSTEMS
(Information retained for historical purposes)

Subsection*	Event Name	CEDMCS	CVCS	SIS
15.1.4.3	Loss of main steam-large, inside containment and failure to fast transfer one 6.9 kV bus	X	X	X
15.1.5.1	Loss of main steam-large, outside containment and loss of offsite power at turbine trip	X	X	
15.1.5.3	Loss of main steam, large, inside containment, and loss of offsite power at turbine trip	X	X	X
15.2.2.1	Isolation of turbine (20 percent power) and failure of one MSSV to close	X	X	X
15.2.5.2	Loss of feedwater-large, inside containment, downstream of check valve and loss of offsite power at turbine trip	X	X	X[a]
15.4.2.4	Boron Dilution	X	X	
15.4.5.3	CEA ejection and failure to fast transfer one 4.16 kV bus	X		X
15.6.2.1	Steam generator tube rupture	X	X	X
15.6.3.1	Small loss of RCS fluid-outside containment	X	X	X
6.3.3.3	Small loss-of-coolant accident	X		X
6.3.3.2	Large loss-of-coolant accident	X		X

[a] Actuated on high containment pressure but not required.

* The subsection numbers may refer to earlier FSAR Amendments and may not exist in the current amendment.

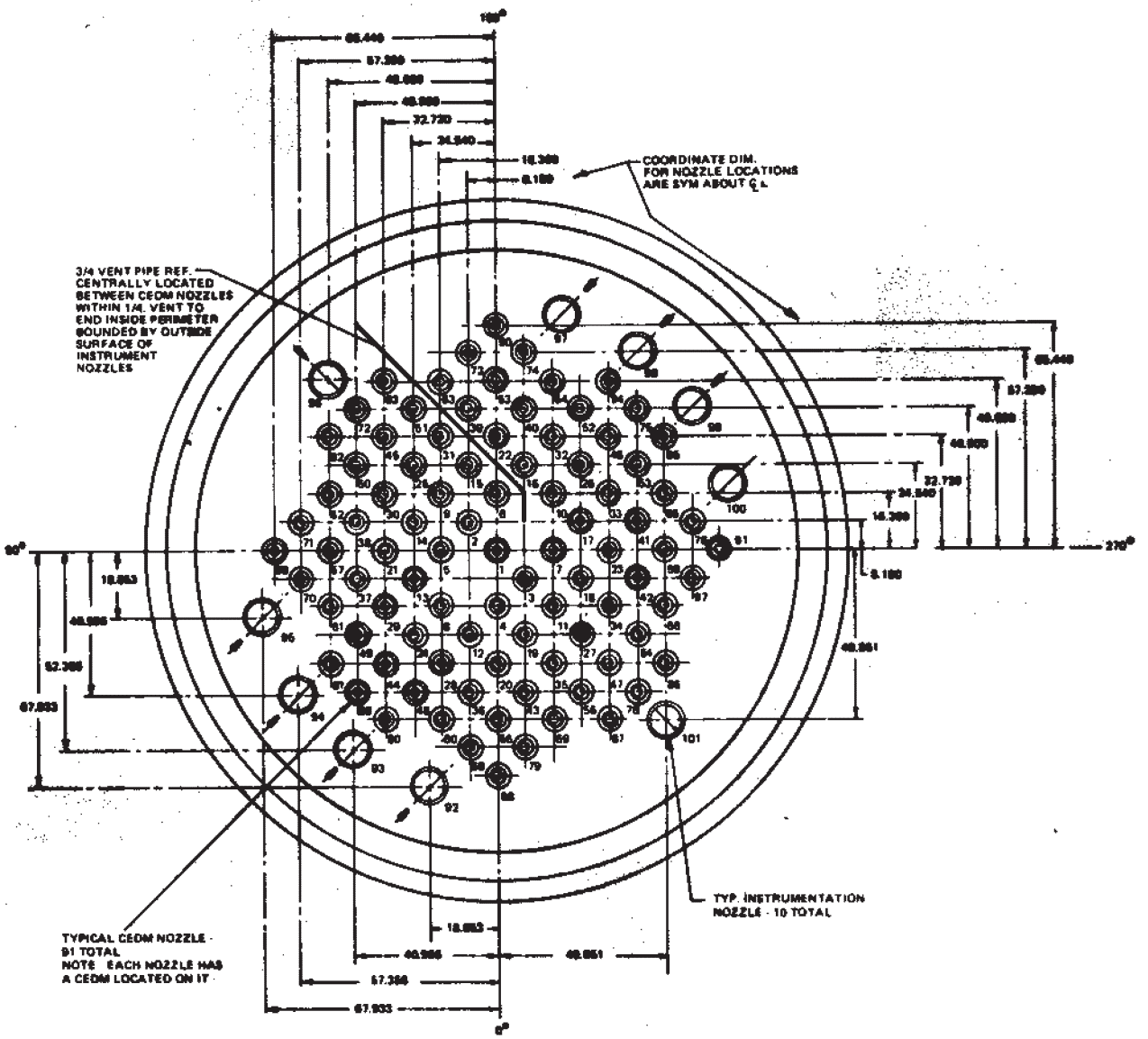

FLORIDA POWER & LIGHT COMPANY
ST. LUCIE PLANT UNIT 2

REACTOR VESSEL CLOSURE HEAD
PLAN VIEW CEDM LAYOUT

FIGURE 4.6-1